

# Drilling fluids filtration and impact on formation damage.

AMISH, M.B.

2004

*The author of this thesis retains the right to be identified as such on any occasion in which content from this thesis is referenced or re-used. The licence under which this thesis is distributed applies to the text and any original images only – re-use of any third-party content must still be cleared with the original copyright holder.*

DRILLING FLUIDS FILTRATION AND IMPACT  
ON FORMATION DAMAGE

MOHAMED BELKASEM AMISH

A thesis submitted in partial fulfilment of the requirements of  
The Robert Gordon University  
for the degree of Doctor of Philosophy

This research programme was carried out  
in collaboration with M-I SWACO, UK

July 2004



## ABSTRACT

Three major methods that the production engineer uses to quantify formation damage in terms of well performance based on the total skin factor after drilling operations are: production logging, flow measurement and well test data. The total skin factor is used in the flow equations to estimate the production rate in wells that are affected by formation damage in order to optimise the flow system to enhance productivity.

The most common source of formation damage has proved to be drilling operations. The drilling skin contributes the highest percentage of the total skin. It is however, not possible to quantify the contribution from drilling fluid to the total skin. In addition, the mechanisms of drilling fluid filtration and impact on productivity performance are not well understood. Furthermore, a satisfactory model for field applications to simulate the near-wellbore damage before drilling in terms of well performance integrated from laboratory core test analysis is still not available.

In recent times, the oil industry has shown increasing awareness towards maintaining optimum well productivity through better drilling/completion fluids design.

This thesis presents a new tool which can predict impact of drilling fluid filtration on formation damage and well performance from laboratory measurements carried out on samples of formation and drilling fluids. This tool is also capable of quantify the formation damage in terms of drilling skin ( $s_d$ ) before drilling at the design (planning stage), during drilling and post drilling (evaluation stage).

In this thesis, the results of in-depth experimental research into rheology, filtration and formation damage phenomena at elevated temperature and pressure with both water-based and oil-based fluids and the relationships between them are presented.

The experimental data combined with data analysis provide a better understanding of filtration and formation damage mechanisms under downhole conditions. They also provide the database for the semi-empirical mechanistic models that have been developed. These models have been combined and incorporated into a design and evaluation tool - the productivity tool, for predicting the effect of drilling fluid filtration on formation damage in terms of well productivity. The productivity tool is useful as a design and analysis tool for applications in the lab and in the field.

The field applications of the productivity tool based on the drilled wells studied shows it can be used to investigate the influence of many parameters such as drilling and static operational time, overbalance pressure, temperature, reservoir permeability, types of drilling fluids, rheology design, etc. on well performance. This tool is also capable of being utilised to screen different drilling fluids desired for achieving minimum formation impairment and maximum production capacity, which can reduce the overall well cost in terms of time and operations.

A number of results are presented to illustrate how the new tool can be used to evaluate the damage factor of a given fluid, specify the invaded zone skin and the depth of invasion as well as the economic implication of the skin zone on well productivity. Recommendations are also made for further work on this fascinating field of study, based on a range of new experimental techniques developed in this research.

## ACKNOWLEDGEMENTS

The author would like to express his sincere thanks and appreciation to Dr Douglas Morrison and Dr W. E. Mason (The Robert Gordon University) and Mr Mike Hodder (M-I SWACO) who provided guidance, advice, ideas and encouragement for this project.

Thanks to all the staff within the Robert Gordon University in general and the School of Engineering in particular for being helpful in different aspects.

The author is greatly indebted to the M-I SWACO Company management for their help and allocating working space within their laboratory, and for providing all routine and special equipment analysis including materials and training. Their constant help and support were really invaluable. Once again, many thanks to all the staff in research development, drilling fluids and stimulation labs, especially Mr Andrew Burn, for their help, support and encouragement. Working with them was a most pleasant and rewarding experience.

Thanks to Dr Mark Davison and Dr Peng Shuang for their suggestions and advice especially at the initiation stage of this research programme.

Thanks to the Jowfe Company for Oil Technology, Libya for sponsoring my study especially to Dr Mohamed Gebril for support and encouragement during my study.

Thanks also to all friends and colleagues in The School of Engineering for their encouragement and friendship especially Atholl Campbell.

Finally, I would like to express my appreciation to my family for standing by me all these years, especially to my wonderful children Aml, Islam, Ayman and Mariam and my dear wife Aziza Saleh Elgtanie whose understanding, patience and encouragement enabled me to complete this study.

# CONTENTS

<b>TITLE</b>	<b>Page No.</b>
<b>ABSTRACT</b>	i
<b>ACKNOWLEDGEMENT</b>	ii
<b>CONTENTS</b>	iii
<b>LIST OF FIGURES</b>	xiv
<b>LIST OF TABLES</b>	xxvii
<b>NOMENCLATURE</b>	xxxvi
 <b>CHAPTER 1</b>	
<b>INTRODUCTION</b>	
1.1 BACKGROUND	1
1.2 PROJECT OBJECTIVES	4
1.2.1 Experimental Programme	4
1.2.2 Theoretical Programme	5
1.3 PROJECT METHODOLOGY	8
1.4 SUMMARY OF ACHIEVEMENTS	10
1.5 ARRANGEMENT OF THESIS	12
 <b>CHAPTER 2</b>	
<b>HP-HT DRILLING FLUIDS FILTRATION AND FORMATION DAMAGE MECHANISMS</b>	
2.1 HP-HT DRILLING FLUIDS	15
2.1.1 High Temperature Wells Related Problems	15
2.2 FORMATION AND MUD CHEMISTRY	19
2.2.1 Formation Chemistry	19
2.2.2 Chemistry of Water Based Muds	20
2.2.3 Chemistry of Synthetic Oil Based Muds	21
2.3 INHIBITIVE MUDS	23
2.3.1 Inhibition Mechanisms	23

2.4 TYPES OF FLUIDS SELECTED	24
2.4.1 Fresh Water Lignosulphonate Mud	24
2.4.2 Oil Emulsion Mud	25
2.4.3 Synthetic Oil Mud	25
2.5 FILTRATION BEHAVIOUR OF DRILLING FLUIDS	26
2.5.1 Definition of Liquid Filtration	26
2.5.2 Borehole Filtration Mechanisms	26
2.5.2.1 Mechanisms Bridging and Invasion of Filtrate	28
2.5.2.2 Mechanisms of Flow through Filter Cake	30
2.5.3 Jamming Ratios	32
2.6 THE PROBLEMS CAUSED BY FILTRATION OF DRILLING FLUIDS	34
2.6.1 Formation Damage	34
2.6.1.1 Swelling and Migration of Clay Particles	36
2.6.1.2 Particle Plugging	36
2.6.1.3 Wettability	36
2.6.1.4 Water Blocking	37
2.6.1.5 Emulsions	37
2.6.1.6 Scale and precipitates	37
2.6.1.7 Unconsolidated Sands	38
2.6.2 Drilling Problems Associated with Filtrate Invasion	38
2.6.2.1 Pipe Sticking	38
2.6.2.2 Hole Instability	39
2.6.2.3 Logging Tool Response	39
2.6.2.4 Cementing	40
2.7 FORMATION DAMAGE MECHANISMS	40
2.7.1 Permeability Damage from Foreign Solids	40
2.7.2 Permeability Damage from Formation Fines	43
2.7.3 Drilling Fluid Selection	44

## **CHAPTER 3**

### **DRILLING FLUIDS FILTRATION MODELS**

3.1 LITERATURE REVIEW ON FILTRATION PROPERTIES	46
3.1.1 The Effect of Individual Wellbore Variables	46
3.1.1.1 The Effect of Pressure	46
3.1.1.2 The Effect of temperature	48
3.1.1.3 The Effect of Filter Medium	51
3.1.1.4 The Effect of Annular Hydraulics on Dynamic Filtration	54
3.1.1.5 The Effect of Mud Constituents and Properties	56
3.2 KEY PARAMETERS FOR FILTRATION MECHANISMS	61
3.3 FLOW THROUGH THE FILTER CAKE AND POROUS FORMATION	62
3.4 DERIVATION OF FILTRATION EQUATION	63
3.4.1 Static Filtration	63
3.4.2 Dynamic Filtration	67
3.5 APPLICATION OF THE FILTRATION EQUATION	71
3.5.1 Static Filtration	71
3.5.2 Erodability of Dynamic Deposited Cake	71
3.6 REVIEW OF DRILLING FLUIDS FILTRATION	72

## **CHAPTER 4**

### **THE EXPERIMENTAL STUDIES AND QUALITY CONTROL PROCEDURE**

4.1 MATERIAL PREPARATION AND ANALYSIS	78
4.1.1 Mud System Analysis	78
4.1.1.1 Mud System Selection	78
4.1.1.2 Mud System Composition	79
4.1.1.3 Mud System Preparation	82
4.1.1.3.1 Laboratory Mixing of Lignosulphonate Mud	82

4.1.1.3.2 Laboratory Mixing of Oil Emulsion Mud	83
4.1.1.3.3 Laboratory New Mixing Procedure of Synthetic Oil Based Mud	83
4.1.1.4 Test Results of Initial Mud	85
4.1.1.4.1 Static Sag Measurement	86
4.1.1.4.2 Dynamic Sag Measurement	87
4.1.2 Development of a New Method for Optimum Emulsifiers Selection Using the Particle Size Analyser Testing Technique	90
4.1.2.1 Brief Introduction to Emulsification Mechanisms	90
4.1.2.2 Fundamentals of Emulsion, Emulsifiers and Wettability	91
4.1.2.3 Testing Procedure and Results	94
4.1.3 Core Analysis	97
4.1.3.1 Core Preparation	97
4.1.3.2 Morphological Formation Characteristics	99
4.1.3.3 Results of Rock Characteristics	101
4.1.3.3.1 Porosity and Permeability Relationship	101
4.1.3.3.2 Tortuosity and Formation Resistivity Factor	102
4.1.3.4 Modelling Mean Pore Throat Diameter	104
4.1.3.4.1 Modelling Mean Pore Throat Diameter from Laminar Flow	104
4.1.3.4.2 Modelling Mean Pore Throat Diameter from Laminar Flow and Turbulent	108
4.1.3.5 Quality Control Tool For Formation Damage Testing Procedure	115
4.1.3.5.1 Formation Damage Evaluation	115
4.1.3.5.2 Permeability Measurement Methods	115
4.1.3.5.3 Flow in Porous Rocks	116
4.1.3.5.4 Quality Control Testing Methodology	118

4.2 FILTRATION EXPERIMENTAL STUDIES	125
4.2.1 Apparatus Description	125
4.2.2 HP-HT Filtration Testing Procedure	127
4.2.3 Analysis of Results	127
4.3 FORMATION DAMAGE EXPERIMENTAL STUDIES	128
4.3.1 Apparatus Description	128
4.3.2 Formation Damage Testing Procedure	129
4.3.2.1 Initial and Return Permeability Testing Procedure	129
4.3.3 Analysis of Results	129
4.4 RHEOLOGICAL CHARACTERISATION EXPERIMENTAL STUDIES	130
4.4.1 Apparatus Description	130
4.4.2 HP-HT Fann 70 Viscometer Testing Procedure	130
4.4.3 Analysis of Results	130
4.5 PARTICLE SIZE EXPERIMENTAL STUDIES	131
4.5.1 Apparatus Description	131
4.5.2 Basic Theory for Particle Size Analysis	131
4.5.2 Particle Size Distribution Testing Procedure	132
4.5.3 Analysis of Results	132

## **CHAPTER 5**

### **FLUID RHEOLOGY, FILTRATION AND FORMATION DAMAGE ANALYSIS**

5.1 FLUID RHEOLOGY	133
5.1.1 Rheological Characterisation of Drilling/Completion Fluids	134
5.2 NEWTONIAN FLUID	134
5.3 NON- NEWTONIAN FLUID	135
5.3.1 Review of Rheological Models	136
5.3.1.1 Bingham Plastic Model	137
5.3.1.2 Power Law Model	137

5.3.1.3 Herschel-Bulkley Model	137
5.3.2 Effective Viscosity of non-Newtonian Fluids	138
5.4 METHODOLOGY FOR CALCULATING PARAMETERS AND SELECTING THE BEST MODEL	139
5.4.1 Calculating Model Parameters	139
5.4.2 Calculating Shear Stress	141
5.4.3 Model Selection	141
5.5 PREVIOUS RESEARCH	141
5.6 RHEOLOGICAL CHARACTERISATION OF HP-HT FLUIDS	143
5.7 EXPERIMENTAL RESULTS OF STATIC FILTRATION FOR WATER AND OIL BASED MUDS	146
5.7.1 Spurt Loss and Cumulative Filtrate Volume	146
5.7.1.1 Effect of Pressure and Temperature	146
5.7.1.2 Effect of Solids Concentration	148
5.7.2 Filter Cake Thickness	150
5.7.2.1 Effect of Pressure and Temperature	150
5.7.2.2 Effect of Solids Concentration	151
5.7.3 Wet to Dry Cake Mass Ratio	151
5.7.3.1 Effect of Pressure, Temperature and Solids Concentration	151
5.8 EXPERIMENTAL RESULTS OF DYNAMIC FILTRATION FOR WATER AND OIL BASED MUDS	151
5.8.1 Spurt Loss and Cumulative Filtrate Volume	152
5.8.1.1 Effect of Shear Rate	152
5.8.2 Filter Cake Thickness	152
5.8.2.1 Effect of Pressure, Temperature and Solids Concentration	152
5.8.2.2 Effect of Shear Rate	153
5.8.3 Wet to Dry Cake Mass Ratio	153
5.8.3.1 Effect of Pressure, Temperature and	



Solids Concentration	153
5.8.3.2 Effect of Shear Rate	154
5.9 EFFECT OF FLUID LOSS ADDITIVES UPON	
STATIC AND DYNAMIC FILTRATION	154
5.9.1 Effect of Fluid Loss Additives on Spurt Loss, Cumulative	
Filtrate, Cake Mass Ratio and Cake Thickness in Static	
and Dynamic Filtration	155
5.10 PARTICLE SIZE ANALYSIS	158
5.10.1 Particle Size Analysis for Static and Dynamic Filter Cakes	158
5.11 FORMATION DAMAGE CHARACTERISATION	161
5.11.1 Experimental Results	161
5.11.2 Pore and Particle Size Distribution Analysis	167

## **CHAPTER 6**

### **DEVELOPMENT OF DRILLING FLUID RHEOLOGY, FILTRATION AND FORMATION DAMAGE PREDICTION MODELS**

6.1 DRILLING FLUID RHEOLOGY ANALYSIS	
OF WATER AND OIL BASED MUDS	170
6.1.1 Introduction to Factor Analysis Technique	171
6.1.1.1 Methodology of Data Analysis	172
6.1.2 Drilling Fluid Rheology Modelling	173
6.1.2.1 Methodology of Model Development	179
6.1.2.2 Comparison between Model Predictions and	
the Experimental Data	181
6.1.2.3 Comparison between Model Predictions and	
Validating Data	182
6.2 STATIC FILTRATION MODELLING	186
6.2.1 Methodology of Static Filtration Models	186
6.2.2 Static Filtration Model for Water based mud	187

6.2.2.1 Comparison between Model Predictions and the Experimental Data	187
6.2.3 Static Filtration Model for Oil based mud	191
6.2.3.1 Comparison between Model Predictions and the Experimental Data	191
6.3 APPLICATION OF THE EXPERIMENTAL DATA TO STATIC FILTRATION MODELS FOR WATER AND OIL BASED MUDS	195
6.3.1 Average Specific cake Resistance and Effective Filter Medium Resistance	196
6.3.1.1 Effect of Pressure and Temperature	196
6.3.1.2 Effect of Solids Concentration	196
6.3.1.3 Effect of Fluid Loss Additives	197
6.3.2 Average Filter Cake Porosity and Permeability	197
6.3.2.1 Effect of Pressure and Temperature	197
6.3.2.2 Effect of Solids Concentration	198
6.3.2.3 Effect of Fluid Loss Additives	199
6.4 DYNAMIC FILTRATION MODELLING	200
6.4.1 Methodology of Dynamic Filtration Models	201
6.4.2 Dynamic Filtration Model for Water based mud	201
6.4.2.1 Comparison between Model Predictions and the Experimental Data	202
6.4.3 Dynamic Filtration Model for Oil based mud	206
6.4.3.1 Comparison between Model Predictions and the Experimental Data	206
6.5 APPLICATION OF THE EXPERIMENTAL DATA TO DYNAMIC FILTRATION MODELS FOR WATER AND OIL BASED MUDS	210
6.5.1 Effective Filter Medium Resistance	212
6.5.1.1 Effect of Pressure, Temperature, Fluid Loss and solids Concentration	212

6.5.1.2 Effect of Shear Rate	212
6.5.2 Average Specific cake Resistance	213
6.5.2.1 Effect of Pressure, Temperature and solids	213
6.5.2.2 Effect of Shear Rate	213
6.5.2.3 Effect of Fluid Loss Additives	213
6.5.3 Average Filter Cake Permeability	214
6.5.3.1 Effect of Pressure, Temperature and solids	214
6.5.3.2 Effect of Shear Rate	215
6.5.3.3 Effect of Fluid Loss	215
6.5.4 Dynamic cake Erodability	216
6.5.4.1 Effect of Pressure Temperature	216
6.5.4.2 Effect of Solids Concentration	216
6.5.4.3 Effect of Shear Rate	216
6.5.4.4 Effect of Fluid Loss Additives	217
6.6 PRESSURE DROP ACROSS POROUS FORMATION AND FILTER CAKE MODELS	218
6.6.1 Pressure Drop in Static Filtration Process	218
6.6.2 Pressure Drop During Dynamic Filtration Process	219
6.7 DEVELOPMENT OF MODELS FOR DRILLING FLUID DAMAGE	222
6.7.1 Filter Cake Build up in Static and Dynamic Filtration	223
6.7.2 Development Models for Depth of Solids Invasion	225
6.7.3 Development Models for Depth of Filtrate Invasion	227
6.8 PRODUCTIVITY EVALUATION	
6.8.1 Linear Flow through the Core Plug	229
6.8.2 Radial Flow through Wellbore	230

## CHAPTER 7

### THE PRODUCTIVITY TOOL

7.1 BACKGROUND	234
----------------	-----

7.2 SCREENING AND UPSCALING	235
7.3 FUNCTIONS OF THE PRODUCTIVITY TOOL (PRT)	237
7.4 PRODUCTIVITY TOOL FORMULATION	237
7.5 PRODUCTIVITY TOOL STRUCTURE	238
7.6 SYSTEM ARCHITECTURE	240
7.7 USER GUIDE	241
7.7.1 Constructing the Framework for Analysis - Input Menu	241
7.7.2 Display of Results in Tabular or Graphical Form - Results Menu	242
7.8 APPLICATION OF THE PRODUCTIVITY TOOL	244
7.8.1 Evaluation Stage [simulated versus field data]	245
7.8.2 Planning Stage for Fluid Optimisation	251
7.8.2.1 Optimisation Process	252

## **CHAPTER 8**

### **CONCLUSIONS AND RECOMMENDATIONS**

8.1 INTRODUCTION	281
8.2 EXPERIMENTAL WORK	281
8.3 APPLICATION OF THE PRT	282
8.4 RECOMMENDATIONS FOR FURTHER WORK	284

<b>REFERENCES</b>	288
-------------------	-----

## **APPENDIX A**

Description of Testing Facilities	310
Tabular and Graphical Permeability Measurement	317
HP-HT Filtration Testing Procedure	320
Static and Dynamic Filtration Testing Results for WBM	321
Static and Dynamic Filtration Testing Results for OBM	328
Initial Permeability Testing Procedure	336

Return Permeability Testing Procedure	337
HP-HT Fann 70 Viscometer Testing Procedure	338
HP-HT Fann 70 Viscometer Readings for WBM and OBM	340
Particle Size Distribution Testing Procedure	342
<b>APPENDIX B</b>	
Rheological Characterisation Results for WBM and OBM	344
<b>APPENDIX C</b>	
Rheological Models Validation for WBM and OBM	349
Static and Dynamic Results for WBM and OBM	351
<b>APPENDIX D</b>	
“A Productivity Tool for Impact of Filtration on Well Performance in an HP-HT Environment”, SPE/IADC 85335, Paper Presented at the SPE/IADC Middle East Drilling Technology Conference & Exhibition held in Abu Dhabi, UAE, 20-22 October 2003	363
“Field Applications of a Productivity Tool for Improved Oil Recovery (IOR)”. Paper Presented at the Second International Symposium on Improved Oil Recovery Conference & Exhibition held in Libya, 12-16 September 2003	
CD The Productivity Tool Package	

## LIST OF FIGURES

	<b>Page No.</b>
Figure 1.1	Schematic of rig-site drilling fluid circulating system 2
Figure 1.2a	Project objective 6
Figure 1.2b	Project objective 7
Figure 1.3	Thesis arrangement 14
Figure 2.1	Schematic diagram for optimum fluid selection 16
Figure 2.2	Example of HP-HT mud gelation 18
Figure 2.3	Water hydration of calcium 21
Figure 2.4	Association of clay particles 21
Figure 2.5	Schematic diagram showing inhibition mechanisms 24
Figure 2.6	A typical plot of cumulative filtrate volume collected as a function of time for subsequential filtration 27
Figure 2.7	Filtration versus flow rate changes 28
Figure 2.8	Invasion of permeable formation by mud solids 29
Figure 2.9	Modes of particle entrapment 30
Figure 2.10	Schematic diagram for drag force on solid particles 30
Figure 2.11	Schematic diagram of important parameters in cake formation 31
Figure 2.12	Pressure drop relationships 31
Figure 2.13	Most common types of formation damage 35
Figure 2.14	Particle retention in porous media 42
Figure 2.15	Pore blocking mechanisms 43
Figure 3.1	Comparison between effect of temperature on mud filtrate, water and brine viscosities 50
Figure 3.2	Comparison of dynamic fluid loss rate with API fluid loss as a function of fluid loss additives concentration 59
Figure 3.3	Relationship between filter cake and cumulative

		Page No.
	deposited cake	69
Figure A1	LP-LT Fann-35 Viscometer	311
Figure A2	Gas Permeability Unit	312
Figure A3	Cannon-Fenske Viscometer	313
Figure A4	Retort Kit	313
Figure A5	Density Meter	314
Figure A6	Mud Balance	314
Figure A7	pH Meter	314
Figure A8	Roller Oven	315
Figure A9	Pressurised Cell	315
Figure A10	Electric Stability Tester	316
Figure A11	Silverson mixer	316
Figure A12	Conductivity meter	316
Figure A13	Precision Component Analyser	316
Figure A14	Titration Kit	321
Figure 4.1	Sag tester	88
Figure 4.2	Schematic of invert and regular emulsion	92
Figure 4.3	Contact angles in three phases	93
Figure 4.4	Relationship between emulsifier concentrations and water droplet size	96
Figure 4.5	Effect of emulsifier concentration on OBM	96
Figure 4.6	Permeability versus porosity for Clashach sandstone	103
Figure 4.7	Tortuosity versus permeability and porosity for Clashach sandstone	103
Figure 4.8	Formation resistivity factor versus permeability and porosity for Clashach sandstone	103
Figure 4.9	Formation resistivity factor versus porosity for Clashach sandstone	103
Figure 4.10	Formation resistivity factor versus porosity for	

		Page No.
	Clashach sandstone	103
Figure 4.11	Formation resistivity factor versus tortuosity and porosity	103
Figure 4.12	Resistivity model validation with external data	103
Figure 4.13	Pore throat radius versus cumulative distribution	105
Figure 4.14	Pore throat radius versus pore size distribution	105
Figure 4.15	Pore throat radius versus cumulative distribution	105
Figure 4.16	Pore throat radius versus pore size distribution	105
Figure 4.17	Pore throat radius versus cumulative distribution	105
Figure 4.18	Pore throat radius versus pore size distribution	105
Figure 4.19	Pore throat radius versus cumulative distribution	105
Figure 4.20	Pore throat radius versus pore size distribution	105
Figure 4.21	Particle diameter versus permeability and porosity	105
Figure 4.22	Pore throat diameter versus permeability and porosity	108
Figure 4.23	Pore throat diameter versus permeability and porosity	110
Figure 4.24	Pore throat diameter models validation with external data	110
Figure 4.25	Non-Darcy coefficient versus pore throat diameter	112
Figure 4.26	Non-Darcy coefficient versus porosity	112
Figure 4.27	Non-Darcy coefficient versus permeability	112
Figure 4.28	Non-Darcy coefficient versus tortuosity	112
Figure 4.29	Non-Darcy coefficient versus permeability and porosity	114
Figure 4.30	Non-Darcy coefficient models comparison	114
Figure 4.31	Flow regimes classification	118
Figure 4.32	Flow regime correlations	118
Figure 4.33	Relationship between gas and liquid permeability	119
Figure 4.34	Flow chart for the quality control procedure of formation damage evaluation	120
Figure 4.35	Flow regimes	122
Figure 4.36	Tabular and graphical display for permeability	



		Page No.
	measurement and deviation in linearity in turbulent flow regime for medium permeability	124
Figure A15 (4.37)	Tabular and graphical display for permeability measurement and deviation in linearity in turbulent flow regime for high permeability cores	317
Figure A16 (4.38)	Tabular and graphical display for permeability measurement and deviation in linearity in laminar flow regime for low permeability cores	318
Figure A17 (4.39)	Tabular and graphical display for permeability measurement and deviation in linearity in laminar flow regime for low permeability cores	319
Figure A18	Schematic diagram of the core holder	336
Figure 4.40	Schematic diagram of the apparatus for HP-HT dynamic filtration	125
Figure 4.41	Core holder and natural core	127
Figure 4.42	Paddle stirrer	127
Figure 4.43	Filtrate viscosity of water and oil based muds	128
Figure 4.44	Filtrate density of water and oil based muds	128
Figure 4.45	A schematic of the formation damage apparatus	129
Figure 4.46	HP-HT Fann-70 Viscometer	130
Figure 4.47	Malvern Mastersizer	131
Figure 5.1	Flow curves for typical drilling fluids rheology models	135
Figure 5.2	Variation of the effective viscosity of typical fluids with shear rate	136
Figure 5.3	Fitting rheogram for best fitting model for OBM	145
Figure 5.4	Fitting rheogram for best fitting model for WBM	145
Figure 5.5	Shear stress as function of temperature for OBM	145
Figure 5.6	Shear stress as function of temperature for WBM	145
Figure 5.7a	Shear stress as function of pressure for OBM	145

		<b>Page No.</b>
Figure 5.7b	Shear stress as function of pressure & temperature for OBM	145
Figure 5.8	Shear stress as function of pressure for WBM	145
Figure 5.9	Apparent viscosity as function of pressure for OBM	145
Figure 5.10	Apparent viscosity as function of pressure for WBM	145
Figure 5.11	Spurt loss as function of pressure in static filtration tests for WBM	146
Figure 5.12	Cumulative volume as function of pressure in static filtration tests for WBM	146
Figure 5.13	Cumulative volume as function of pressure in static filtration tests for OBM	147
Figure 5.14	Pressure exponent as function of temperature for WBM and OBM	147
Figure 5.15	Average filter cake permeability as function of temperature for WBM and OBM	147
Figure 5.16	Cumulative volume per unit area as function of solids concentration for WBM	149
Figure 5.17	Average filter cake permeability as function of solids concentration for WBM	150
Figure 5.18	Cumulative volume as function of solids concentration and permeability for WBM concentration for WBM	150
Figure 5.19	Cumulative volume as function of time in static filtration tests for WBM	150
Figure 5.20	Cumulative volume as function of time in static filtration tests for WBM	150
Figure 5.21	Cumulative volume as function of solids in static filtration tests for OBM	150
Figure 5.22	Cumulative volume as function of permeability in static filtration tests for OBM	150
Figure 5.23	Measured filter cake thickness as function of pressure	

		Page No.
	for WBM	151
Figure 5.24	Measured filter cake thickness as function of solids for WBM	151
Figure 5.25	Cumulative volume as function of shear rate in dynamic filtration tests for OBM	152
Figure 5.26	Equilibrium filtration rate as function of shear rate for WBM	152
Figure 5.27	Equilibrium filtration rate as function of pressure for WBM	152
Figure 5.28	Equilibrium filtration rate as function of temperature for WBM	152
Figure 5.29	Measured filter cake thickness as function of shear rate for WBM	153
Figure 5.30	Measured filter cake thickness as function of shear rate for OBM	153
Figure 5.31	Measured cake ratio as function of pressure for WBM	154
Figure 5.32	Measured cake ratio as function of temperature for WBM	154
Figure 5.33	Measured cake ratio as function of solids for WBM	154
Figure 5.34	Measured cake ratio as function of plugging agent for WBM	155
Figure 5.35	Comparison between static and dynamic filtration tests as function of (FLA) for OBM	157
Figure 5.36	Cumulative filtrate volume as function of FLA in static filtration tests for OBM	157
Figure 5.37	Cumulative filtrate volume as function of FLA in dynamic filtration tests for OBM	157
Figure 5.38	Measured filter cake thickness as function of FLA in static filtration tests for OBM	157
Figure 5.39	Measured filter cake thickness as function of FLA	

		Page No.
	in dynamic filtration tests for OBM	157
Figure 5.40	Comparison between static and dynamic filtration as function of (FLA) for WBM	157
Figure 5.41	Measured filter cake thickness as function of FLA in static filtration tests for WBM	157
Figure 5.42	Measured filter cake thickness as function of FLA in dynamic filtration tests for WBM	157
Figure 5.43	Comparison chart between particle-size distribution of 11 ppg oil base mud, static and dynamic cake	159
Figure 5.44	Chart illustrating particle size distribution of dynamic filtration cake (OBM)	159
Figure 5.45	Particle size distribution of dynamic filtration cake (OBM)	160
Figure 5.46	Mud cake and cleanup test	162
Figure 5.47	Cake rupture for WBM ad OBM	162
Figure 5.48	Return permeability for WBM and OBM	164
Figure 5.49	Particle size distribution of dynamic filtration cake (WBM)	168
Figure 6.1	Comparison between experimental and model prediction for WBM	182
Figure 6.2	Comparison between validated test data and model prediction for WBM	182
Figure 6.3	Comparison between experimental and model prediction for OBM	184
Figure 6.4	Comparison between validated test data and model prediction for OBM	184
Figure 6.5a	Comparison between model prediction and field data for OBM	184
Figure 6.5b	Comparison between model prediction and field data for OBM	184

		Page No.
Figure 6.6	Comparison between experimental and model prediction for WBM	188
Figure 6.7	Comparison between validated test data and model prediction for WBM	189
Figure 6.8	Comparison between validated test data and model prediction for WBM	191
Figure 6.9	Comparison between experimental and model prediction for OBM	192
Figure 6.10	Comparison between validated test data and model prediction for OBM	192
Figure 6.11	Comparison between validated test data and model prediction for OBM	192
Figure 6.12	Comparison between validated test data and model prediction for OBM	194
Figure 6.13	Average specific resistance as function of pressure in static filtration for OBM	196
Figure 6.14	Average specific resistance as function of temperature in static filtration tests for OBM	196
Figure 6.15	Average specific resistance as function of pressure in static filtration tests for WBM	197
Figure 6.16	Average specific resistance as function of solids in static filtration tests for WBM and OBM	197
Figure 6.17	Average specific resistance as function of FLA in static filtration tests for OBM	198
Figure 6.18	Medium resistance as function of pressure and temperature in static filtration tests for OBM	198
Figure 6.19	Medium resistance as function of FLA in static filtration tests for OBM	198
Figure 6.20	Average filter cake porosity as function of pressure	

		Page No.
	in static filtration tests for OBM	198
Figure 6.21	Average filter cake permeability as function of pressure in static filtration tests for OBM	198
Figure 6.22	Average filter cake permeability as function of temperature in static filtration tests for OBM	198
Figure 6.23	Average filter cake porosity as function of solids concentration in static filtration tests for OBM	199
Figure 6.24	Average filter cake permeability as function of rock permeability in static filtration tests for OBM	199
Figure 6.25	Average filter cake permeability as function of solids concentration in static filtration tests for WBM	199
Figure 6.26	Average filter cake porosity as function of oil concentration in static filtration tests for WBM	200
Figure 6.27	Average filter cake permeability as function of FLA in static filtration tests for OBM	200
Figure 6.28	Average filter cake permeability as function of FLA in static filtration tests for WBM	200
Figure 6.29	Comparison between experimental and model prediction for WBM	202
Figure 6.30	Comparison between validated test data and model prediction for WBM	203
Figure 6.31	Comparison between validated test data and model prediction for WBM	206
Figure 6.32	Comparison between validated test data and model prediction for WBM	206
Figure 6.33	Comparison between experimental and model prediction for OBM	207
Figure 6.34	Comparison between validated test data and model prediction for OBM	207

		Page No.
Figure 6.35	Comparison between validated test data and model prediction for OBM	210
Figure 6.36	Comparison between validated test data and model prediction for OBM	210
Figure 6.37	Medium resistance as function of pressure and temperature in dynamic filtration tests for OBM	212
Figure 6.38	Medium resistance as function of solids in dynamic filtration tests for OBM	212
Figure 6.39	Medium resistance as function of FLA in dynamic filtration tests for OBM	212
Figure 6.40	Medium resistance as function of shear rate in dynamic filtration tests for OBM	212
Figure 6.41	Medium resistance as function of shear rate in dynamic filtration tests for WBM	213
Figure 6.42	Average specific cake resistance as function of shear rate in dynamic filtration tests for OBM	214
Figure 6.43	Average specific cake resistance as function of shear rate in dynamic filtration tests for WBM	214
Figure 6.44	Average specific cake resistance as function of FLA in dynamic filtration tests for OBM	214
Figure 6.45	Average specific cake resistance as function of FLA in dynamic filtration tests for WBM	214
Figure 6.46	Average filter cake permeability as function of shear rate in dynamic filtration tests for WBM	215
Figure 6.47	Average filter cake permeability as function of solids concentration in dynamic filtration tests for OBM	215
Figure 6.48	Average filter cake permeability as function of FLA in dynamic filtration tests for WBM	215

		Page No.
Figure 6.49	Average filter cake permeability as function of FLA in dynamic filtration tests for OBM	215
Figure 6.50	Filter cake erodability as function of pressure in dynamic filtration tests for OBM	216
Figure 6.51	Filter cake erodability as function of temperature in dynamic filtration tests for OBM	216
Figure 6.52	Filter cake erodability as function of pressure in dynamic filtration tests for WBM	216
Figure 6.53	Filter cake erodability as function of solids concentration in dynamic filtration for WBM	216
Figure 6.54	Filter cake erodability as function of shear rate in dynamic filtration tests for WBM	217
Figure 6.55	Filter cake erodability as function of shear rate in dynamic filtration tests for OBM	217
Figure 6.56	Filter cake erodability as function of FLA in dynamic filtration tests for WBM	217
Figure 6.57	Filter cake erodability as function of FLA in dynamic filtration tests for OBM	217
Figure 6.58a	Experimental pressure drop across filter cake (top gauge)	220
Figure 6.58b	Experimental pressure drop across sand face (bottom gauge)	220
Figure 6.59	Static versus dynamic pressure drop for WBM	222
Figure 6.60	Static versus dynamic pressure drop for OBM	222
Figure 6.61	Comparison of pressure drops in static filtration tests for WBM and OBM	222
Figure 6.62	Comparison of pressure drops in dynamic filtration tests for WBM and OBM	222
Figure 6.63	Theoretical simulation of filter cake build-up as function of time for WBM	224
Figure 6.64	Theoretical simulation of filter cake build-up as	



		Page No.
	function of time for OBM	224
Figure 6.65	Theoretical simulation of filter cake build-up as function of shear rate for WBM	224
Figure 6.66	Theoretical simulation of filter cake build-up as function of shear rate for OBM	224
Figure 6.67	Solids invasion using X-ray Vs. model prediction for WBM	226
Figure 6.68	Solids invasion using X-ray Vs. model prediction for OBM	226
Figure 6.69	Schematic diagram for core damage	230
Figure 6.70	Near-wellbore zone: ideal and real flowing bottomhole pressure	231
Figure 6.71	Schematic diagram for near wellbore damage	232
Figure 7.1	The PRT flow chart	239
Figure 7.2	Flow chart for the PRT package	241
Figure 7.3	Best-fit model for OBM	247
Figure 7.4	Rheological characterisation for OBM	248
Figure 7.5	Wellbore pressure distribution for OBM	249
Figure 7.6	Effect of rheology on formation damage for OBM	252
Figure 7.7	Effect of rheology on formation damage for WBM	253
Figure 7.8	Effect of rheology characterisation on depth of invasion	253
Figure 7.9	Effect of rheology on depth of invasion for OBM	254
Figure 7.10	Effect of reservoir permeability	255
Figure 7.11	Effect of drilling time	255
Figure 7.12	Effect of wellbore temperature	256
Figure 7.13	Effect of overbalance pressure	256
Figure 7.14	Effect of pump rate on well performance	257
Figure 7.15	Best-fit model for OBM	260
Figure 7.16	Rheological characterisation for OBM	261
Figure 7.17	Wellbore pressure distribution for OBM	261
Figure 7.18	Filtration characteristics for OBM	262

	<b>Page No.</b>
Figure 7.19 Filtration pressure distribution for OBM	263
Figure 7.20 Filter cake characteristics for OBM	263
Figure 7.21 Formation damage characteristics for OBM	264
Figure 7.22 Formation damage characteristics for OBM	265
Figure 7.23 Well Flow performance for OBM	265
Figure 7.24 Best-fit model for WBM	267
Figure 7.25 Rheological characterisation for WBM	268
Figure 7.26 Wellbore pressure distribution for WBM	268
Figure 7.27 Filtration characteristics for WBM	269
Figure 7.28 Filter pressure distribution for WBM	269
Figure 7.29 Filter cake characteristics for WBM	270
Figure 7.30 Formation damage characteristics for WBM	270
Figure 7.31 Formation damage characteristics for WBM	271
Figure 7.32 Well Flow performance for WBM	271
Figure 7.33 Wellbore pressure distribution for OBM	272
Figure 7.34 Formation damage characteristics for OBM	273
Figure 7.35 Well flow performance for OBM	273
Figure 7.36 Wellbore pressure distribution for WBM	274
Figure 7.37 Wellbore pressure distribution for WBM	275
Figure 7.38 Formation damage characteristics for WBM	276
Figure 7.39 Well flow performance for WBM	276
Figure 7.40 Wellbore pressure distribution for WBM	277
Figure 7.41 Formation damage characteristics for WBM	278
Figure 7.42 Well flow performance for WBM	278
Figure 7.43 Wellbore pressure distribution for WBM	279
Figure 7.44 Formation damage characteristics for WBM	280
Figure 7.45 Well flow performance for WBM	280
Figure 8.1 Invasion profile in vertical and horizontal wells	286

## LIST OF TABLES

		Page No.
Table 2.1	HP-HT inhibitive drilling fluids systems	16
Table 2.2	Typical Properties for First-Generation Synthetic-Base Liquids	22
Table 2.3	Typical Properties for Second-Generation Synthetic-Base Liquids	22
Table 3.1	Viscosities of water and 6% sodium chloride	50
Table 4.1a	Composition of Lignosulphonate Water Base Mud	79
Table 4.1b	Composition of Synthetic Oil Base Mud	79
Table 4.2a	Brief Description of Lignosulphonate Water Base Mud	80
Table 4.2b	Brief Description of Synthetic Oil-Base Mud	80
Table 4.3	Order and Timing of Mixing HP-HT Lignosulphonate Water-Base Mud	83
Table 4.4	Order and Timing of Mixing HP-HT Synthetic Oil-Base Mud	85
Table 4.5a	Initial Testing of HP-HT Lignosulphonate Water-Base Mud	89
Table 4.5b	Initial Testing of HP-HT Synthetic Oil Base Mud	89
Table 4.6	Relationship between emulsifier concentration and oil droplet size for WBM	97
Table 4.7	Cementation Factor values for different minerals	100
Table 4.8	Rock description versus (m) values	101
Table 4.9	Values of <i>m</i> and <i>a</i> as function of rock type	101
Table 4.10	Comparison between Coberly, Blake-Kozeny and modified-equations for particle diameter prediction	107
Table 4.11	Comparison between experimental Blake-Kozeny and modified equations for pore throat diameter prediction	108
Table 4.12	Empirical correlations to correct non-Darcy coefficient	113
Table 4.13	Design criteria to classify the fluid flow regimes	122

		Page No.
Table A1	Effect of pressure and temperature (static filtration	
(4.14)	experimental) for WBM	321
Table A2	Effect of pressure and temperature (static filtration	
(4.15)	experimental) for WBM	321
Table A3	Effect of solids concentration (static filtration experimental)	
(4.16)	for WBM	322
Table A4	Effect of FLA plugging agent (static filtration experimental)	
(4.17)	for WBM	322
Table A5	Effect of FLA viscosifying agent (static filtration	
(4.18)	experimental) for WBM	323
Table A6	Effect of FLA coating agent (static filtration experimental)	
(4.19)	for WBM	323
Table A7	Effect of pressure and temperature (dynamic filtration	
(4.20)	experimental) for WBM	324
Table A8	Effect of pressure and temperature (dynamic filtration	
(4.21)	experimental) for WBM	324
Table A9	Effect of solids concentration (dynamic filtration	
(4.22)	experimental) for WBM	325
Table A10	Effect of FLA plugging agent (dynamic filtration	
(4.23)	experimental) for WBM	325
Table A11	Effect of FLA viscosifying agent (dynamic filtration	
(4.24)	experimental) for WBM	326
Table A12	Effect of of FLA coating agent (dynamic	
(4.25)	filtration experimental) for WBM	326
Table A13	Effect of shear rate (dynamic filtration	
(4.26)	experimental) for WBM	327
Table A14	Effect of pressure and temperature (static filtration	
(4.27)	experimental) for OBM	328
Table A15	Effect of pressure and temperature (static filtration	

		Page No.
(4.28)	experimental) for OBM	328
Table A16	Effect of filter medium (static filtration	
(4.29)	experimental) for OBM	329
Table A17	Effect of solids concentration (static filtration	
(4.30)	experimental) for OBM	329
Table A18	Effect of FLA coating agent (static filtration	
(4.31)	experimental) for OBM	330
Table A19	Effect of FLA plugging agent (static filtration	
(4.32)	experimental) for OBM	330
Table A20	Effect of FLA viscosifying agent	
(4.33)	(static filtration experimental) for OBM	331
Table A21	Effect of pressure and temperature	
(4.34)	(dynamic filtration experimental) for OBM	332
Table A22	Effect of pressure and temperature	
(4.35)	(dynamic filtration experimental) for OBM	332
Table A23	Effect of shear rate (dynamic filtration	
(4.36)	experimental) for OBM	333
Table A24	Effect of solids concentration (dynamic filtration	
(4.37)	experimental) for OBM	333
Table A25	Effect of FLA coating agent (dynamic filtration	
(4.38)	experimental) for OBM	334
Table A26	Effect of FLA plugging agent (dynamic filtration	
(4.39)	experimental) for OBM	334
Table A27	Effect of of FLA viscosifying agent (dynamic filtration	
(4.40)	experimental) for OBM	335
Table A28	HP-HT Fann 70 viscometer reading for WBM	340
(4.41)		
Table A29	HP-HT Fann 70 viscometer reading for OBM	341
(4.42)		

	<b>Page No.</b>
Table 5.1 Expressions for non-Newtonian rheological models	136
Table 5.2 Expressions for non-Newtonian viscosity for various rheological models	139
Table B1 (5.3) Rheological characterisation for WBM at 150 °F	344
Table B2 (5.4) Rheological characterisation for WBM at 200 °F	344
Table B3 (5.5) Rheological characterisation for WBM at 250 °F	345
Table B4 (5.6) Rheological characterisation for WBM at 300 °F	345
Table B5 (5.7) Rheological characterisation for OBM at 150 °F	346
Table B6 (5.8) Rheological characterisation for OBM at 200 °F	346
Table B7 (5.9) Rheological characterisation for OBM at 250 °F	347
Table B8 (5.10) Rheological characterisation for OBM at 300 °F	347
Table 5.11 Fluid loss additive mechanisms for WBM and OBM	155
Table 5.12 Results of retained permeability versus testing parameters for OBM	165
Table 5.13 Results of retained permeability versus testing parameters for WBM	165
Table 5.14 Jamming ratio analysis for WBM	169
Table 5.15 Jamming ratio analysis for OBM	169
Table 6.1 Application of multivariate analysis for WBM (low-shear rate)	175
Table 6.2 Application of multivariate analysis for WBM (high-shear rate)	176
Table 6.3 Application of multivariate analysis for OBM (low-shear rate)	177
Table 6.4 Application of multivariate analysis for OBM (high-shear rate)	178
Table 6.5 Empirical coefficients for equation (6.3)	181
Table C1 (6.6) Comparison between experimental, validation test data	

	<b>Page No.</b>
and model prediction for WBM	349
Table C2 (6.7) Comparison between experimental, validation test data and model prediction for WBM	349
Table C3 (6.8) Comparison between experimental, validation test data and model prediction for OBM	350
Table C4 (6.9) Comparison between experimental, validation test data and model prediction for OBM	350
Table 6.10a Model prediction error with field data (Gulf of Mexico Field)	184
Table 6.10b Well summary	185
Table 6.10c Predicted wellbore pressure versus field data	186
Table C5 (6.11) Regression coefficients of static filtration for WBM (model application for pressure and temperature)	351
Table C6 (6.12) Regression coefficients of static filtration for WBM (model application for solids concentration)	351
Table C7 (6.13) Regression coefficients of static filtration for WBM (model application for permeability)	352
Table C8 (6.14) Regression coefficients of static filtration for WBM (model application for permeability)	352
Table C9 (6.15) Regression coefficients of static filtration for WBM (model application for permeability)	353
Table C10 (6.16) Regression coefficients of static filtration for WBM (model application for FLA) coating materials	353
Table C11 (6.17) Regression coefficients of static filtration for WBM (model application for FLA) plugging materials	354
Table C12 (6.18) Regression coefficients of static filtration for WBM (model application for FLA) viscosifying materials	354
Table C13 (6.19) Regression coefficients of static filtration for OBM (model application for pressure and temperature)	355

Table C14 (6.20)	Regression coefficients of static filtration for OBM (model application for solids concentration)	355
Table C15 (6.21)	Regression coefficients of static filtration for OBM (model application for permeability)	356
Table C16 (6.22)	Regression coefficients of static filtration for OBM (model application for FLA) coating materials	356
Table C17 (6.23)	Regression coefficients of static filtration for OBM (model application for FLA) plugging materials	357
Table C18 (6.24)	Regression coefficients of static filtration for WBM (model application for FLA) viscosifying materials	357
Table 6.25	Comparison between model prediction error and experimental data for WBM	188
Table 6.26	Comparison between model prediction error and test data for WBM	189
Table 6.27	Comparison between model prediction error and experimental data for WBM	189
Table 6.28	Empirical constants for adapted static filtration equation (6.9) for WBM	190
Table 6.29	Comparison between model prediction error and experimental data for WBM	190
Table 6.30	Comparison between model prediction error and experimental data for OBM	192
Table 6.31	Comparison between model prediction error and test data for OBM	193
Table 6.32	Comparison between model prediction error and test data for OBM	193
Table 6.33	Empirical constants for adapted static filtration equation (6.11) for OBM	194
Table 6.34	Comparison between model prediction error and test data for OBM	194



		Page No.
Table C19	Regression coefficients of dynamic filtration for WBM	
(6.35)	(model application for pressure and temperature)	358
Table C20	Regression coefficients of static filtration for WBM	
(6.36)	(model application for solids concentration)	358
Table C21	Regression coefficients of static filtration for WBM	
(6.37)	(model application for permeability and solids)	358
Table C22	Regression coefficients of static filtration for WBM	
(6.38)	(model application for shear rate)	359
Table C23	Regression coefficients of static filtration for WBM	
(6.39)	(model application for FLA) plugging agent	359
Table C24	Regression coefficients of static filtration for WBM	
(6.40)	(model application for FLA) viscosifying agent	359
Table C25	Regression coefficients of static filtration for WBM	
(6.41)	(model application for FLA) coating agent	359
Table C26	Regression coefficients of dynamic filtration for OBM	
(6.42)	(model application for pressure and temperature)	360
Table C27	Regression coefficients of static filtration for OBM	
(6.43)	(model application for solids concentration)	360
Table C28	Regression coefficients of static filtration for OBM	
(6.44)	(model application for permeability and solids)	360
Table C29	Regression coefficients of static filtration for OBM	
(6.45)	(model application for shear rate)	360
Table C30	Regression coefficients of static filtration for OBM	
(6.46)	(model application for FLA) coating agent	361
Table C31	Regression coefficients of static filtration for OBM	
(6.47)	(model application for FLA) plugging agent	361
Table C32	Regression coefficients of static filtration for OBM	
(6.48)	(model application for FLA) viscosifying agent	361
Table 6.49	Comparison between model prediction error and	

		Page No.
	experimental data for WBM	202
Table 6.50	Comparison between model prediction error and test data for WBM	203
Table 6.51	Comparison between model prediction error and test data for WBM	204
Table 6.52	Comparison between model prediction error and test data for WBM	204
Table 6.53	Comparison between model prediction error and test data for WBM	204
Table 6.54	Empirical constants for equation (6.25) for WBM depend on type of FLA	205
Table 6.55	Empirical constants for equation (6.25) for WBM depend on solids and shear rate	205
Table 6.56	Comparison between model prediction error and test data for WBM	205
Table 6.57	Comparison between model prediction error and experimental data for OBM	207
Table 6.58	Comparison between model prediction error and test data for OBM	208
Table 6.59	Comparison between model prediction error and test data for OBM	208
Table 6.60	Comparison between model prediction error and test data for OBM	208
Table 6.61	Empirical constants for equation (6.27) for OBM depend on type of FLA	209
Table 6.62	Empirical constants for equation (6.27) for OBM depend on solids and shear rate	209
Table 6.63	Comparison between model prediction error and test data for OBM	210

		Page No.
Table 6.64	Conversion factors for equations (6.52&6.53)	225
Table C33	Shear stress acting on filter cake surface	
(6.64)	for WBM (pressure and temperature application)	362
Table C34	Shear stress acting on filter cake surface for WBM	
(6.65)	(shear rate application)	362
Table C35	Shear stress acting on filter cake surface for WBM	
(6.66)	(pressure and temperature application)	362
Table C36	Shear stress acting on filter cake surface for WBM	
(6.67)	(shear rate application)	362
Table 7.1	Well summary	244
Table 7.2	Field data for well (A1) 8.5 inch hole	246
Table 7.3	Predicted wellbore pressure distribution	
	Against field data (pump pressure)	249
Table 7.4	Formation damage predicted against field measurement	250
Table 7.5	Formation damage predicted against field measurement	251
Table 7.6	WBM&OBM rheology	252
Table 7.7	Field data for well (A1) 6 inch hole	259
Table 7.8	Field data for well (A2) 6 inch hole	266

## NOMENCLATURE

A	Cross-sectional area of filter cake Also pressure coefficient defined in equation (6.3), (6.7 to 6.15) and (6.18 to 6.27)	$[m^2]$ $[m^2/N]$
$A_c$	Constant	$[-]$
a	Constant Also empirical structure parameter in equation (4.7)	$[-]$ $[-]$
$a_1$	Static filtration coefficient	$[s/m^3]$
$a_1^t$	Constant defined in equations (6.8 & 6.13)	$[s/m^3]$
$a_2$	Static filtration coefficient	$[s/m^6]$
$a_2^t$	Constant defined in equations (6.7 & 6.12)	$[s/m^6]$
B	Dynamic filtration coefficient Also viscosity constant for Newtonian fluid defined in equation (3.62) Temperature coefficient defined in equation (6.3), (6.7 to 6.15) and (6.18 to 6.27)	$[kg/m^2s]$ $[-]$ $[1/^{\circ}C]$
b	Constant	$[-]$
C	Constant Also pressure constant defined in equation (6.3) Also temperature constant defined in equation (5.19) Also constant defined in equations (6.9 & 6.14)	$[kg/m^2]$ $[m^2/N]$ $[1/^{\circ}C]$ $[m^3/kg]$
$C_1$	Dynamic filtration coefficient Also static filtration rate defined in equation (3.61) Also conversion factor defined in equation (6.52)	$[s/m^3]$ $[m/s^{0.5}]$ $[-]$
$C_1^t$	Constant	$[s/m^3]$
$C_2$	Dynamic filtration coefficient Also static filtration volume constant	$[s]$ $[m/s^{0.5}]$

	Also conversion factor defined in equation (6.52)	[-]
$C_2'$	Constant	[s]
$C_3$	Dynamic filtration coefficient	[m <sup>3</sup> ]
	Also conversion factor defined in equation (6.53)	[-]
$C_3'$	Constant	[m <sup>3</sup> ]
$C_4$	Conversion factor defined in equation (6.53)	[-]
$C_5$	Conversion factor defined in equation (6.53)	[-]
$C_B$	Constant	[m]
$C_F$	Constant	[m <sup>6</sup> /s]
$C_w$	Constant	[m]
$C_w$	Constant	[1/m <sup>0.5</sup> ]
$D_1$	Annular inner diameter	[m]
$d$	Constant defined in equations (6.10 & 6.15)	[m <sup>3</sup> /kg]
	Also Constant defined in equations (6.20 to 6.27)	[1/m <sup>2</sup> ]
	Also Constant defined in equations (6.20 to 6.27)	[sec]
$d_1$	The diameter of drill pipe	[m]
$d_2$	The diameter of wellbore	[m]
$D_{pore}$	Pore throat diameter	[m]
$d_p$	Particle diameter	[m]
$d_{50}$	Mean particle diameter	[m]
$F$	Constant	[-]
	Also constant defined in equations (6.9 & 6.14)	[s/m <sup>6</sup> ]
	Also constant defined in equations (6.10 & 6.15)	[s/m <sup>3</sup> ]
$f$	The coefficient of internal friction of the cake surface layer	
	Also volume of cake defined in equation (3.4)	
	Also friction factor defined in equation (4.34)	[-]
$f_G$	Internal geometry	[-]

$F_R$	Resistivity formation factor	[-]
$h_{eq}$	Filter cake thickness at equilibrium stage	[m]
$h$	Constant defined in equations (6.20 & 6.25)	[s/m <sup>3</sup> ]
	Also Constant defined in equation (6.21 & 6.26)	[m/s <sup>0.5</sup> ]
	Also Constant defined in equation (6.22 & 6.27)	[m <sup>2</sup> ]
$K$	Permeability	[m <sup>2</sup> ]
	Also consistency index defined in equation (5.3)	[Ns/m <sup>2</sup> ]
$k$	Constant defined in equation (3.46)	[-]
$\bar{K}$	Average permeability	[m <sup>2</sup> ]
$K_{avg}$	The average filter cake permeability	[m <sup>2</sup> ]
$K_c$	Filter cake permeability	[m <sup>2</sup> ]
$K_d$	Permeability Damage	[m <sup>2</sup> ]
$K_f$	Formation permeability	[m <sup>2</sup> ]
$K_v$	Vertical permeability	[m <sup>2</sup> ]
$K_H$	Horizontal permeability	[m <sup>2</sup> ]
$k_L$	Constant for specific mud	[m <sup>3</sup> ]
$k_\tau$	Dynamic filtration erodability coefficient	[kg/Ns]
$k_z$	Kozeny constant	[-]
$L$	The length of filter bed	[m]
	Also filter cake thickness defined in equation (3.1)	[m]
$L$	The length of tube or rock sample	[m]
$L_a$	Actual length of rock sample	[m]
$L_c$	The length of filter cake	[m]
$L_d$	The depth of solids invasion	[m]
$L_f$	The length of filter medium	[m]
$M_w$	Constant	[m <sup>2</sup> /s]
$M_G$	Constant	[s/m <sup>6</sup> ]
$M'_G$	A number defining filter cake characteristics	[s/m <sup>6</sup> ]

m	Ratio of wet to dry cake mass	[-]
	Also constant defined in equation (3.46)	[-]
	Also cementation factor in equation (4.7)	[-]
$N_G$	Constant	[s/m <sup>3</sup> ]
n	Constant defined in equation (3.46)	[-]
	Number of cones n equation (3.66)	[-]
	Also Power Law index	[-]
P	Filtration pressure	[N/m <sup>2</sup> ]
$P_a$	Applied pressure	[N/m <sup>2</sup> ]
$P_L$	Hydraulic pressure	[N/m <sup>2</sup> ]
$P_s$	Pressure on solids	[N/m <sup>2</sup> ]
$\Delta P$	Pressure differential	[N/m <sup>2</sup> ]
$\Delta P_c$	Pressure differential across filter cake	[N/m <sup>2</sup> ]
$\Delta P_f$	Pressure drop across formation	[N/m <sup>2</sup> ]
$\Delta P_{meff}$	Pressure differential across effective filter medium	[N/m <sup>2</sup> ]
$\Delta P_T$	Total pressure drop across filter cake and formation	[N/m <sup>2</sup> ]
$PI_{actual}$	Productivity index after formation damage	[ST/Dm <sup>2</sup> /N]
$PI_{ideal}$	Productivity index before formation damage	[ST/Dm <sup>2</sup> /N]
q	Filtrate flow rate per unit area	[m/s]
$q_{eq}$	Dynamic equilibrium filtrate flow rate	[m/s]
R	Resistance	[1/m]
$R_c$	Resistance of filter cake	[1/m]
$R_L$	Ratio of filtrate volume/volume of deposited solids	[-]
$R_m$	Resistance of filter medium	[1/m]
$R_{meff}$	Effective resistance of filter medium	[1/m]
r	The internal radius of the tube	[m]
	Also the constant resistance of filter medium	
	defined in equation (3.65)	[1/m]

$r_f$	The depth of filtrate invasion	[m]
$S$	Sortivity	[m/s <sup>0.5</sup> ]
$S_0$	Specific surface of solids	[1/m]
$s$	Solids percentage concentration in the slurry	[-]
	Also a compaction function of the cake defined in equation (3.52)	[-]
$s_b$	Blockage skin	[-]
$s_c$	Solids percentage concentration in cake	[-]
$s_c$	Partial completion skin	[-]
$s_d$	Drilling skin	[-]
$s_p$	Perforation skin	[-]
$s_g$	Gravel-pack skin	[-]
$T$	Temperature	[°C]
$t$	Time	[s]
$t_{eq}$	Dynamic equilibrium time	[s]
$t_o$	Time	[s]
$t_{sp.}$	Spurt loss time	[s]
$V$	Cumulative filtrate volume	[m <sup>3</sup> ]
$V'$	Cumulative filtrate volume	[m <sup>3</sup> ]
$v$	A function of cake compressibility	[-]
	Also defined as ratio of volume of filter cake to volume of filtrate in equations (3.53) and (3.65)	[-]
$V_{ann}$	Annular mud flow velocity	[m/s]
$V_b$	Bulk volume	[m <sup>3</sup> ]
$V_p$	Pore volume	[m <sup>3</sup> ]
$V_{sp}$	Spurt loss volume	[m <sup>3</sup> ]
$W$	Cumulative deposited solids weight per unit area	[kg/m <sup>2</sup> ]
$W_c$	Filter cake weight per unit area	[kg/m <sup>2</sup> ]



$W_e$	Eroded solids weight per unit area	[kg/m <sup>2</sup> ]
$W_s$	Solids weight as laid on filter medium	[kg]
$W_1$	Weight of dry core	[kg]
$W_1$	Weight of saturated core	[kg]
$x$	Pressure exponent	[-]
	Fluid loss concentration defined in equation (6.9)	[kg/m <sup>3</sup> ]
	Also permeability constant defined in equation (6.20)	[m <sup>2</sup> ]
	Also shear rate constant defined in equation (6.20)	[rpm]

## GREEK SYMBOLS

$\alpha$	Specific filter cake resistance	[m/kg]
$\alpha_a$	Specific filter cake resistance	[m/kg]
$\alpha_{avg}$	Average specific filter cake resistance	[m/kg]
$\beta$	Non Darcy flow coefficient	[1/m]
$\gamma$	Shear rate	[1/s]
$\gamma_w$	Shear rate at wall	[1/s]
$\delta$	Dynamic filter cake thickness	[m]
$\mu$	Viscosity	[Ns/m <sup>2</sup> ]
$\mu_e$	Viscosity	[Ns/m <sup>2</sup> ]
$\mu_p$	Plastic viscosity of Bingham Plastic mud	[Ns/m <sup>2</sup> ]
$\mu_f$	Filtrate viscosity	[N.s/m <sup>2</sup> ]
$\upsilon$	Ratio of volume of filter cake to volume of filtration	[-]
$\rho$	Density	[kg/m <sup>3</sup> ]
$\rho_f$	Filtrate density	[kg/m <sup>3</sup> ]
$\rho_s$	Density of solids	[kg/m <sup>3</sup> ]
$\tau$	The shear stress on the cake surface exerted by mud stream	[N/m <sup>2</sup> ]
$\tau_o$	The yield point Bingham Plastic mud	[N/m <sup>2</sup> ]
$\tau_R$	Shear stress ratio	[-]

$\phi$	Formation porosity	[-]
$\phi_{avg}$	Average filter cake porosity	[-]
$\phi_{tr}$	The trap porosity	[-]

## ACRONYMS

AH	After hot rolling
BH	Before hot rolling
BHA	Bottom hole assembly
BCE	Base exchange capacity
CD	Compacted disc
CMC	Sodium Carboxymethyl Cellulose
DF	Damage factor
DR	Damage ratio
D1	Density of top part of the mud
D2	Density of bottom part of the mud
Do	Density of mud prior the dynamic sag
Ds	Density of mud after the dynamic sag
ECD	Equivalent circulation density
FE	Flow efficiency
FLA	Fluid loss additives
HEC	Hydroxyethyl Cellulose
HP-HT	High pressure-high temperature
HHP	Hydraulic horsepower
$K_{liquid}$	Permeability to liquid
$K_{gas}$	Permeability to gas
I.D.	Inside diameter
IO	Internal olefin
I.F	Impact force
JR	Jamming ratio
LAO	Linear alpha olefin

LP	Linear paraffin
Lb/bbl	Pounds per barrel
LP-LT	Low pressure-low temperature
md	Millidarcy
N	Total data points
OBM	Oil based mud
O.D.	Outside diameter
PAO	Paraffin alpha olefin
Ppg	Pounds per gallon
Pr	Pil price per barrel
pH	Hydrogene-ion concentration
PSD	Pore size distribution
PSA	Particle size analyser
PRT	The productivity Tool
R <sup>2</sup>	Goodness-of-fit
Re	Reynolds number
RMS	Residual of error
SCR	Schlumberger Cambridge research
SS <sub>i</sub>	Shear stress
WBM	Water based mud
x	x-coordinate
y	y-coordinate
z	z-coordinate
lbs/bbl	Pounds per barrel

## CONVERSION FACTORS

### Length:

$$1 \text{ cm} = 0.3937 \text{ inch}$$

$$1 \text{ ft} = 30.481 \text{ cm}$$

$$1 \text{ }\mu\text{m} = 10^{-6} \text{ m}$$

### Area:

$$1 \text{ m}^2 = 10.764 \text{ ft}^2$$

### Pressure:

$$1 \text{ psi} = 6894.80 \text{ N/m}^2 = 6.8948 \text{ KPa}$$

$$1 \text{ atm} = 14.696 \text{ psi}$$

### Temperature:

$$0 \text{ }^{\circ}\text{C} = 273.157 \text{ K} = 32 \text{ }^{\circ}\text{F}$$

### Volume:

$$1000 \text{ cm}^3 = 1 \text{ L} = 0.2642 \text{ gallons}$$

$$1 \text{ ft}^3 = 0.02831 \text{ m}^3 = 28.31 \text{ L}$$

### Viscosity:

$$1 \text{ cP} = 0.010 \text{ dyne sec/cm}^2 = 100 \text{ Ns/m}^2$$

### Density:

$$1 \text{ kg} = 0.00834 \text{ ppg}$$

### Flow Rate:

$$1 \text{ m}^3/\text{sec} = 35.310 \text{ ft}^3/\text{sec}$$

### Mass:

$$1 \text{ kg} = 2.205 \text{ pounds}$$

### Permeability:

$$1 \text{ Darcy} = 1000 \text{ millidarcy (md)} = 0.9869 \text{ }\mu\text{m}$$

## CHAPTER ONE

### INTRODUCTION

#### 1.1 BACKGROUND

Oil and gas, as found in nature, are trapped underground within the myriad of microscopic pores of reservoir rocks into which they migrated from source rocks over a period of millions of years. They are derived almost entirely from decayed plants and animals. These source rocks were deposited in ancient seas, rivers or lakes. Impervious sediments, deposited on top of the porous reservoir formations, sealed the reservoir underground, in many cases preventing the hydrocarbons from seeping away to the surface. To reach underground oil and gas, operators drill boreholes (i.e. wells) through subterranean rock, generally up to several thousand meters deep, making wells. The wells are completed by installing production tubing.

During drilling operations, it is necessary to pump a fluid (drilling mud) downhole through the bore of the drill-pipe and the bit nozzles. This mud then flows upwards through the drill-pipe / wellbore annulus, carrying the rock cuttings generated by the rotating bit. At the surface, the cuttings are then removed by solids control equipment before the mud is again pumped downhole [Figure 1.1].

The drill-bit can be directly connected to the drill-string or, instead, to a mud motor which in turn is connected to the drill-string. The latter configuration allows the bit to be rotated without rotating the drill-pipe and is hence often employed for drilling deviated sections of the well path. The former configuration is usually used for straight sections.

The fluid (generally called “drilling mud” because of its physical appearance), consists of base fluid (water or oil), various special chemicals and frequently a weighting element (e.g. barite).

One of the major functions of a drilling fluid is the control of formation pressure. In order to prevent formation fluids from flowing into the borehole, the hydrostatic pressure of the mud column is usually made to exceed the formation pressure. This differential pressure provides the driving force for a flow of mud movement through

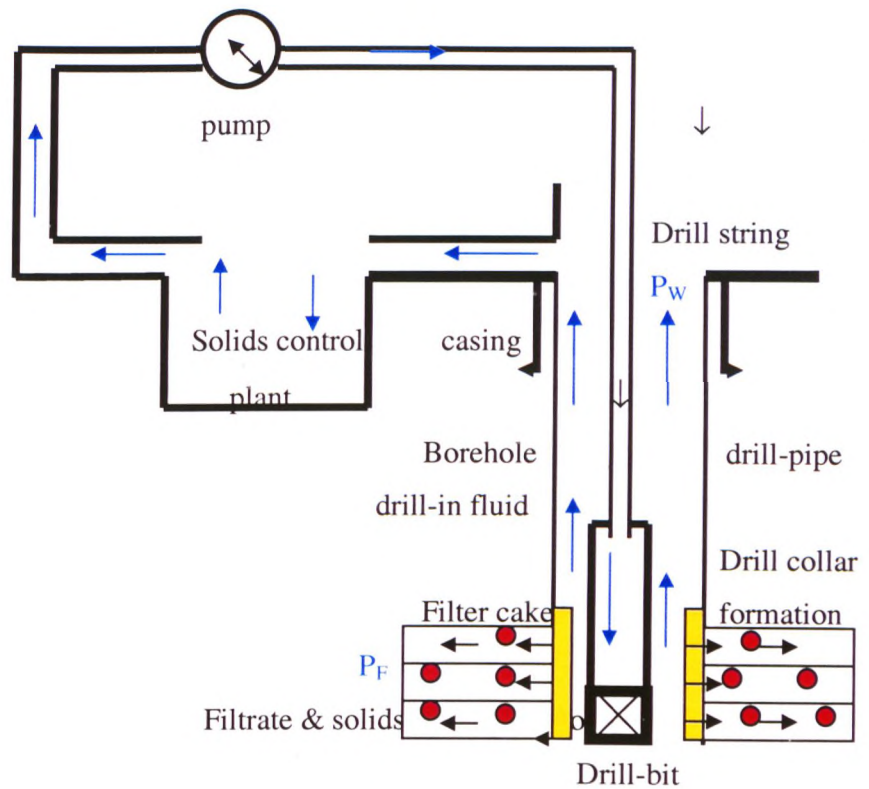


**Figure 1.1 Schematic of rig-site drilling fluid circulation system**

the borehole wall into the formation. During drilling the dynamic filtration is influenced by the equivalent circulation density which in turn is a function of fluid rheology, solids content, chemical additives, etc. The deposition of solids on the face of the formation creates a wall cake. A steady state flow regime, characterized by a constant filtrate invasion rate and a constant thickness of filter cake (dynamic equilibrium), is generally observed. Excessive loss of liquid and associated drilling mud solids can result in formation damage and contribute to borehole instability.

The formation damage depends upon a large number of parameters such as drilling fluid type, formation properties and operating conditions (overbalance pressure, shear rate, etc.). The formation damage can be characterised by the following factors: the static and dynamic fluid losses, damaged permeability in the zone occupied by internal cake, properties of external cake such as cake thickness, permeability, etc., pressure drop across cake and sand face, and the depth of solids and filtrate invasion. Drilling rigs are equipped only with static filtration cells and low pressure-low temperature (LP-LT) Viscometer. The static fluid loss test that is used in the rig site

gives only a vague indication of downhole static and dynamic fluid loss. Fluid rheological properties are strongly affected by pressure and temperature. The rheological behaviour of the drilling fluid has a major impact on pressure distribution in the wellbore and hence affects drilling overbalance pressure and thus filtration. Therefore, to adequately predict downhole filtration and impact on formation damage, it is also necessary to predict downhole fluid rheology, so that the pressure distribution can be computed and hence pressure drops across cake and sand face and filtrate and solids invasion can be calculated. However, an extensive database requires to be generated from controlled experimental studies in order to develop models to predict these factors accurately. The laboratory experimental database needs to be integrated for field application in order to quantify formation damage and evaluate the well productivity.

In recent times, the oil industry has given increasing awareness attention to maintaining optimum well productivity through better drilling/completion fluids design, since minimising filtration is beneficial to borehole stability and production. Yet the engineer is left with some ad-hoc approach and a few bench tests to guide him through decisions which may ultimately cost thousands of dollars in mud materials additives, stimulation treatments and lost production.

Overall the studies and practices to date showed limitations because:

1. They mostly concentrate on LP-LT water based muds (WBMs).
2. The effect of the rheological behaviour of the drilling fluid on filtration mechanisms and fluid invasion is still not clearly understood.
3. Addition of fluid loss additives (FLA) to the drilling fluid is based only on standard rig site static filtration tests. Filtration control with different fluid loss additives has a considerable impact on drilling fluid properties and performance, on drilling cost and well productivity.
4. Most of the existing filtration models are limited in application to LP-LT WBMs; rigs are equipped only with API HP-HT static cells and field engineers need to deduce dynamic filtration characteristics from static filtration data.



5. No consistent relationship has been established between static versus dynamic filtration.
6. Three major tools that the field engineer uses to quantify formation damage in terms of well performance after drilling operations are, production logging, flow efficiency and the total skin factor estimated from well test data. The most common source of formation damage has proved to be drilling operations. The drilling skin contributes the highest percentage of the total skin. It is however not possible to quantify the contribution from drilling fluid to the total skin. In addition, a satisfactory model for field applications to simulate the near-wellbore damage before drilling in terms of well flow performance integrated from laboratory core test analysis is still not available.

Furthermore defining the complex relationship between key operational parameters makes the situation more difficult.

The economic impacts of wellbore formation damage justify a thorough study of this problem in order to find ways to minimize its effects on well performance.

Therefore, the main aim of this study is to link laboratory measurements to field scale applications and to provide a better understanding of filtration mechanisms and impact on formation damage in order to evaluate well performance and optimise fluid selection.

## **1.2 PROJECT OBJECTIVES**

This thesis represents the results of a combined experimental and theoretical study of the fluid rheology and the filtration properties of WBM and OBM (oil base mud) in relation to formation damage (Figures 1.2a and 1.2b). The tested muds cover the most commonly used HP-HT drilling fluids, including lignosulphonate muds, emulsion muds and synthetic oil muds, both barite-weighted and unweighted.

### **1.2.1 Experimental Programme**

The experimental programme was designed to identify the effects of a number of key parameters that govern the filtration process, the fluid rheology and formation



damage mechanisms, to generate a database from controlled experimental studies at different operating conditions in order to develop theoretical models and to investigate:

- Rheological characterisation of WBM and OBM for temperatures ranging from 150 ° F- 300 ° F and pressures ranging from 15 psi-17000 psi.
- Filtration characteristics (static and dynamic) for WBM and OBM under the effect of the following factors:

Parameter	Range
Pressure, psi	200 to 900
Temperature, °F	150 to 300
Solids concentration, %	6 to 20
Permeability (natural cores, synthetic cores, and filter paper), md	40 to 4000
Shear rate, sec <sup>-1</sup>	80 to 240
FLA, lb/bbl	0 to 6

- Formation damage characteristics for WBM and OBM under the above conditions.

### 1.2.2 Theoretical Programme

The theoretical programme was designed to integrate (scale) laboratory test results to field applications which required the following models:

- Development of a rheology model to predict rheological properties under downhole conditions for WBM and OBM in order to compute wellbore pressure distribution and hence drilling overbalance pressure.
- Development of pressure drop models to predict pressure drop across formation and filter cake in order to compute depth of invasion.
- Development of a static and dynamic filtration model to predict static and dynamic filtration properties (fluid loss and filter cake) for WBM and OBM in order to compute filtrate invasion.

- Development of a dynamic filtration versus static filtration model to predict dynamic filtration from API static filtration test data.
- Development of solids and filtrate invasion models to predict depth of solids and filtrate invasion.
- Development of a productivity tool to predict the impact of drilling fluid filtration on formation damage in order to evaluate well performance and optimise fluid selection.

Extensive experimental studies need to be conducted in order to support the models predictive features at different operating conditions.

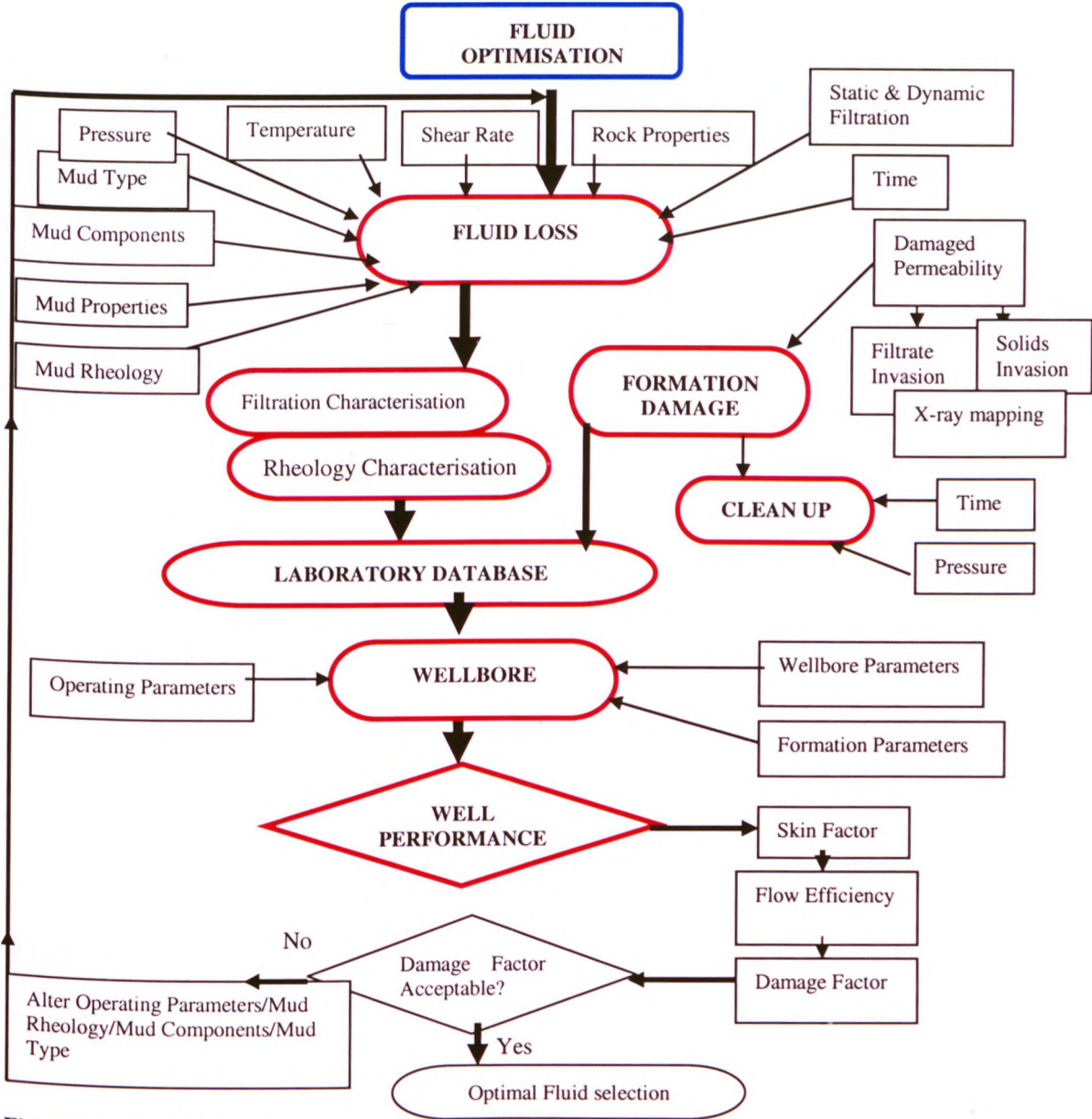
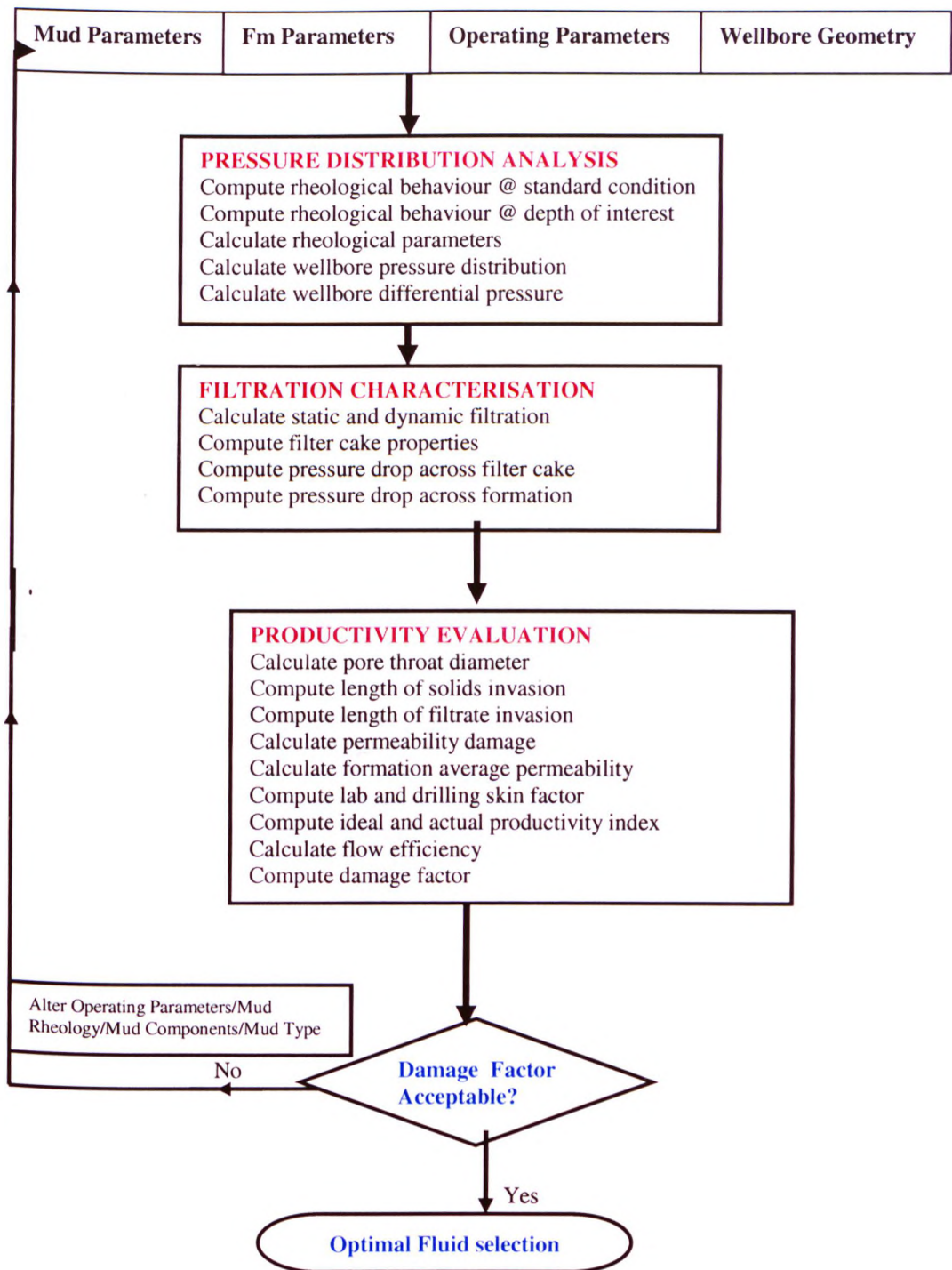


Figure 1.2a Project objectives



**Figure 1.2b Project Objectives**

### 1.3 PROJECT METHODOLOGY

To achieve the above research objectives, the following programme was undertaken:

1. Literature Search and Review: as a first step towards the provision of a thorough understanding and to build up knowledge on drilling fluids, filtration mechanisms, drilling fluids rheology, formation damage and experimental facilities and current technology an extensive literature search and review has been carried out in line with the project objectives.
2. Experimental programme: to analyse and investigate drilling fluid rheology, filtration and formation damage with respect to the main key parameters that affect the filtration mechanisms. Extensive resources of sophisticated experimental equipment have been used for this study.
3. Characterisation of filtration and formation damage:
  - (a) Sourcing and selecting common drilling fluids (WBM and OBM), each type of mud has been mixed twice in order to achieve the best fluid properties with optimum chemical concentrations.
  - (b) The chemicals used for mixing drilling fluids (WBM and OBM) were selected from the same manufacturing batch for consistent test results.
  - (c) The experimental programme was conducted using the same fluid batch for accurate test results.
  - (d) A new experimental testing technique has been developed for selecting optimum emulsifier concentrations for (WBM and OBM).
  - (e) The static and dynamic sag tests were conducted for any fluid mixed for optimum fluid design to ensure that the mud is not sagging as this could affect the accuracy of experimental results.
4. Homogenous Clashach sandstone rock samples were selected for the present work with support from the Core Analysis Company (Corex Company). The selected core samples exhibit a wide range of porosity, (10 to 28 percent), and a wide range of permeability, (from less than 50 md to few thousand md “millidarcy”).



- (a) The depth of solids invasion requires knowledge of the morphological characteristics. Therefore measurements of porosity, permeability and resistivity factor were performed.
  - (b) Pore Size Distribution studies from capillary pressure tests using mercury injection were carried out for selected samples and used for comparison against derived models.
  - (c) An attempt has been made to establish a relationship between the morphological characteristics of Clashach sandstone such as permeability, porosity, particle diameter, tortuosity, resistivity factor, average pore throat diameter, non-Darcy flow coefficient and to use these to classify flow in porous media.
5. Extended rheological characterisation has been carried out for the most common water and synthetic oil based muds used for downhole applications<sup>1</sup>:
- (a) The best rheological model to fit water and oil based muds is Herschel-Bulkley model.
  - (b) Rheological models for water and oil-based muds were developed which can predict rheological properties for a given shear rate under downhole conditions.
  - (c) The effect of rheological properties has been incorporated into the description of the filtration and formation damage mechanisms under downhole conditions.
6. Classic models of drilling fluid filtration have been sourced from the literature and modified to establish:
- (a) The classic static filtration equations for WBM and OBM, which show substantial advantages when adapted to fit static filtration data of drilling fluids (WBM and OBM).
  - (b) The dynamic filtration equations for WBM and OBM, which provided more realistic results when adapted to fit dynamic filtration data of drilling fluids (WBM and OBM).

- (c) The drilling fluid filtration models developed can predict static and dynamic filtration behaviour or dynamic from static filtration data.
  - (d) Filter cake characteristics such as average specific cake resistance and cake permeability have been predicted and described, which has been established a greater insight into filtration mechanisms.
7. The laboratory test results database has been extrapolated to field scale applications (the productivity tool).
  8. The productivity tool can predict the impact of drilling fluid filtration on formation productivity in terms of depth of solids and filtrate invasion, drilling skin, flow efficiency and loss of revenue.

#### **1.4 SUMMARY OF ACHIEVEMENTS**

Details of the attempts to analyse the impact of drilling fluid filtration on formation damage have been presented. The analysis has been based on the results of in-depth experimental research into rheology, filtration and formation damage phenomena.

The main contribution to knowledge from this work can be summarised as follows:

- Controlled Experimental studies combined with data analysis of fluid rheology, static and dynamic filtration and formation damage models provides a better understanding of filtration mechanisms under downhole conditions<sup>2</sup>. This analysis also considers different variables such as solids, shear rate, medium type and permeability, fluid loss additives, pressure and temperature.
- The experimental data also provided the database for the semi-empirical mechanistic models that were developed. These models have been combined and incorporated into a design and evaluation tool - the productivity tool (PRT), for predicting the effect of drilling fluid filtration on formation damage in terms of well productivity<sup>3</sup> (Appendix D). The productivity tool is useful as a design and analysis tool in laboratory and field scale, which can be used for predicting formation damage mechanisms caused by particulate and filtrate invasion<sup>4</sup>. The

field applications<sup>5</sup> of the productivity tool based on the drilled wells studied (Appendix D) shows it can be used to investigate the influence of many parameters such as drilling and static operational time, overbalance pressure, temperature, reservoir permeability, types of drilling fluids, rheology design, etc. on well performance.

The productivity tool can be used before drilling at the design stage (planning tool), during drilling and post drilling for evaluation and comparison tool with well test data. This predictive tool is capable of being utilised to screen different drilling fluids desired for achieving minimum impairment and maximum production capacity, which can reduce the overall well cost in terms of time and operations. As a result of this, the considerable economic implication of the skin zone on well productivity can be greatly minimised.

- A new application testing technique<sup>6</sup> has been introduced using a Particle Size Analyser for the following purposes:
  1. Selecting optimum emulsifier concentrations for water-based muds.
  2. Selecting optimum primary and secondary emulsifier concentrations for oil-based muds.
  3. A quality control tool for comparison of different types of emulsifiers.
  4. Selection and comparison of emulsifiers can be achieved in a short time, thus reducing economic impact.
  5. A backup tool for the dynamic sag test.
  6. Particle size classification analysis for static and dynamic filtration filter cakes.
- It was discovered that there exists a critical overbalance pressure zone for water-based mud where decreased permeability impairment occurs<sup>3</sup>. In this zone a minimum invasion depth was observed in the overbalance pressure range from 400 to 650 psi. This has been explained in terms of tight particle bridging, compaction and lower filter cake permeability, thereby allowing fewer particles

to move into the formation through the cake. This is an important effect, as it is common practice for oil operators to drill with lower differential pressure in the belief that this will minimise the formation permeability damage. However, contrary to this expectation it has been found that the permeability damage will be higher at lower differential pressures.

- The mixing procedure order for OBM components described in API RP 13B-2 has been modified.

## **1.5 ARRANGEMENT OF THESIS**

Chapter 2 presents HP-HT drilling fluid chemistry and inhibition mechanisms, the fundamental concepts of drilling fluid filtration, formation damage mechanisms and associated problems.

Chapter 3 presents an extensive review carried out on the experimental studies of filtration properties of drilling fluids. Previous studies on the effects of the individual parameters under downhole conditions on filtration performance are compared with the present work. This is followed by a review of classical filtration models.

Chapter 4 presents the experimental studies and quality control procedures. The API oil-based mud mixing procedure has been modified and a new major testing technique using the Particle Size Analyser for optimum emulsifiers selection has been established. Design criteria to classify the fluid flow regimes in porous media and a quality control approach has been established for formation damage testing procedures. The main experimental facilities are also described and presented.

The experimental results of the rheological, filtration and formation damage characterisation test results are presented and discussed in chapter 5.

Chapter 6 presents the development of the theoretical models to predict downhole drilling fluid rheology, static and dynamic filtration and formation damage. An attempt to validate these models using experimental, independent test and field data has been made under different applied factors and conditions. Attempts have also



been made to integrate the lab database analysis for field applications to predict the effect of drilling fluid filtration on formation damage in terms of productivity impairment.

Chapter 7 presents the insights gained into fluid rheology and filtration mechanisms and their application to the problem of formation damage productivity impairment. A number of mechanistic models developed have been combined and incorporated into a design and evaluation tool (called the productivity tool) for predicting the effect of drilling fluid filtration on formation damage in terms of formation productivity. Applications of the PRT have been carried out using field data from North African oilfields with both WBM and OBM. The PRT shows good agreement with the field measurements based on the drilled wells studied.

Chapter 8 the final chapter, summarises the findings of this research and makes recommendations for further studies Figure 1.3.

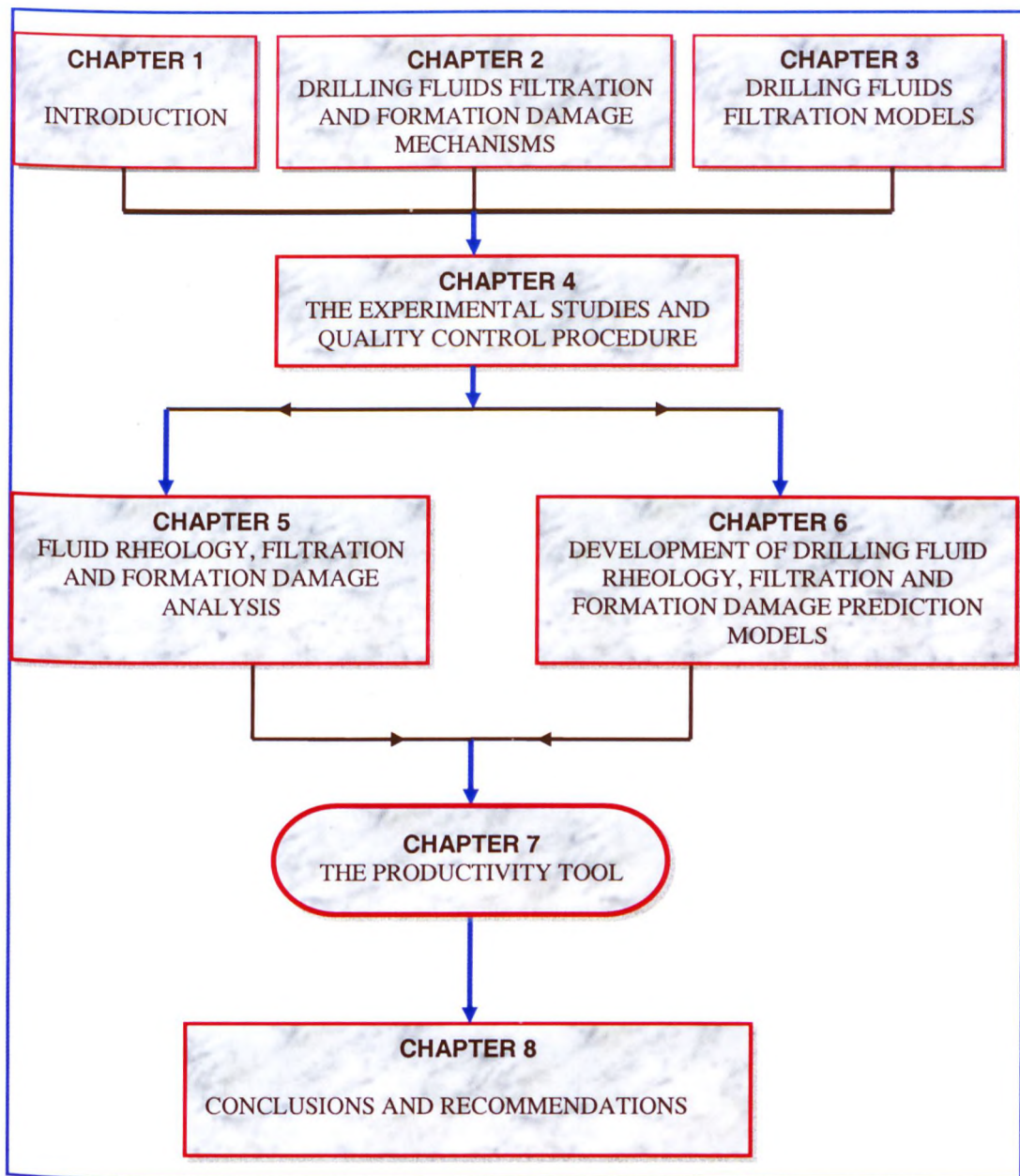


Figure 1.3 Thesis Arrangement

## **CHAPTER TWO**

# **DRILLING FLUIDS FILTRATION AND FORMATION DAMAGE MECHANISMS**

HP-HT drilling fluid chemistry and inhibition mechanisms, the fundamental concepts of drilling fluid filtration, formation damage mechanisms and associated problems are presented in this chapter.

### **2.1 HP-HT DRILLING FLUIDS**

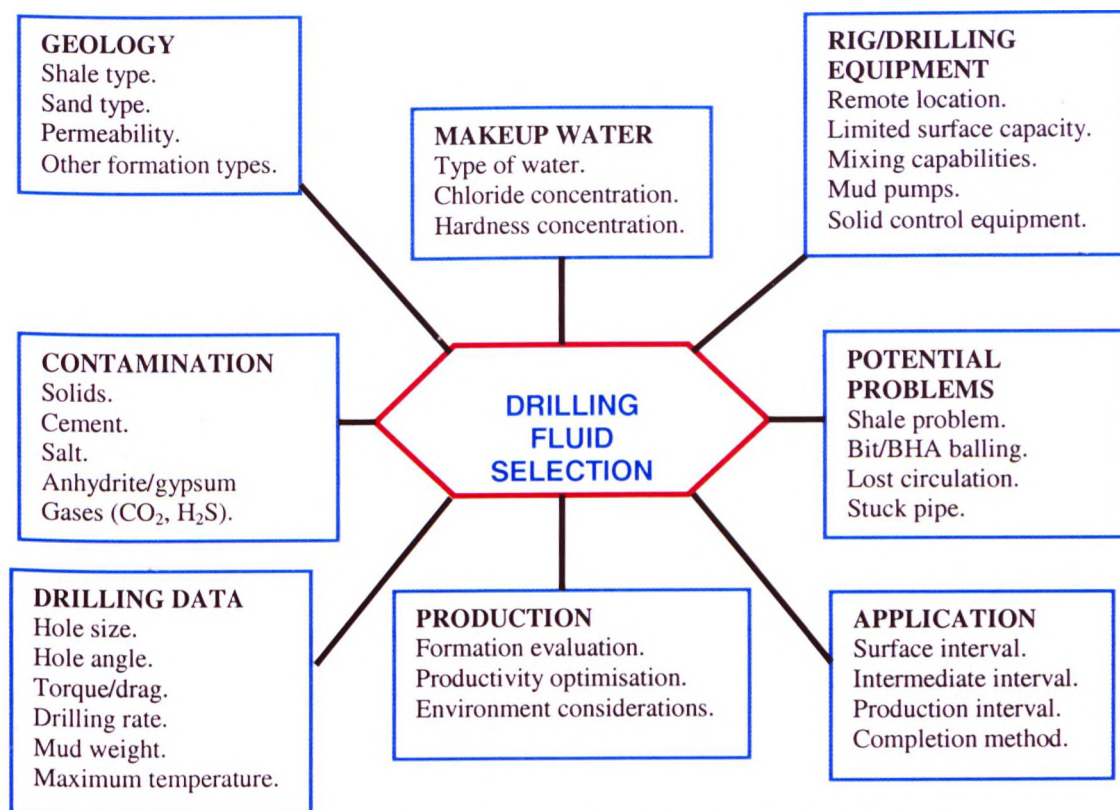
Drilling fluids are commonly classified according to their base fluid into three main groups<sup>7,8</sup>: (1) water based mud, (2) oil based mud, and (3) gaseous based mud.

Over the years a considerable number of drilling fluid formulations have been developed to suit various subsurface conditions. Selection of the best fluid to meet anticipated conditions will minimise well costs and reduce the risk of potential problems such as stuck pipe, loss of circulation and kicks. Consideration must also be given to obtaining adequate formation evaluation and maximum productivity<sup>8</sup> [Figure 2.1].

Basic drilling fluid systems are used in the initial stages of drilling usually converted to more complex inhibitive systems as the well depth increases and the wellbore temperature and/or pressure increases. The common types of HP-HT drilling fluids are listed in Table 2.1.

#### **2.1.1 High Temperature Wells Related Problems**

From the drilling fluid standpoint, high temperatures can be considered as those above which conventional drilling fluid additives begin to thermally degrade at an appreciable rate. This degradation leads to loss of product function and system maintenance becomes difficult and expensive.



❑ Figure 2.1 Schematic diagram for optimum fluid selection

Table 2.1 HP-HT inhibitive drilling fluids systems

System	Type of mud	Temperature limitation ° F	Remarks
WATER BASED MUD	Saturated saltwater	300	Extended to 350
	Potassium chloride	300	Extended to 350
	Polymer drill	300	Extended to 350
	Lignosulphonate**	350	Extended to 500
OIL BASED MUD	Diesel oil	600	
	Mineral oil	600	
	Synthetic**	600	

\*\* Mud types selected for this study

The majority of mud treatment chemicals begin to degrade at temperatures between 212 and 250 °F. However, the main problems in high temperature (HT) wells can be summarised as follows<sup>7</sup>:

1. Mud products degradation: With the exception of weight material the constituents of drilling fluids degrade with time at elevated temperatures; the higher the temperature the greater the rate of degradation. The polymers (FLA) are, however, susceptible to thermal degradation.

The two primary reactions responsible for polymer breakdown are oxidation and hydrolysis. Both temperature and the rate of degradation at that temperature must be taken into account when specifying the temperature stability of mud or mud product. The critical temperature for each mud product should be calculated or established by experience. Mud product degradation can affect all mud properties.

2. High-temperature gelation: High temperatures both disperse and flocculate bentonite suspensions. Hydration of bentonite increases with temperature and an increased number of clay platelets are split from aggregated stacks. A greater number of particles are then present in the suspension and the viscosity of the suspension increases. The split of aggregated stacks presents fresh surfaces for adsorption of hydroxyl ions producing a consequential drop in pH (hydrogen-ion concentration). A pH drop will tend to increase flocculation within the suspension. In general WBM HT-gelation is caused by clay flocculation and compounded by degradation of polymers, a drop in pH and an increase in the filtrate loss. In OBM it can be caused by interaction between colloidal particles (clay and fluid loss additives) and breakdown of emulsifiers may cause gelation [Figure 2.2].
3. Fluid loss: Regardless of the type of drilling fluid, the static and dynamic fluid losses usually increase with temperature and pressure. This is largely due to loss of product function, and to changes in filter cake compressibility with changing temperatures.



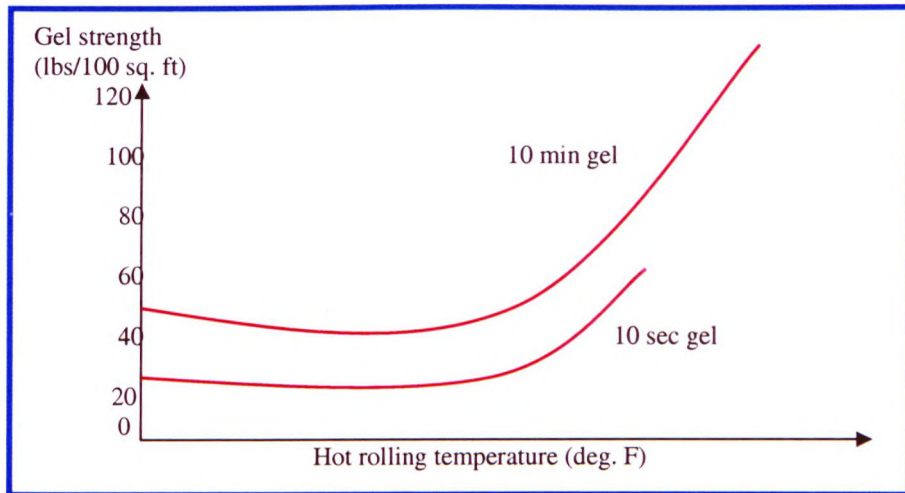


**Figure 2.2 Example of HT mud gelation**

4. **Rheological properties:** Due to mud product degradation and gelation the rheological properties are affected and cause increase in viscosity [Figure 2.2]. In commonly utilised oilfield drilling fluids all rheological properties decrease with increasing temperature. However, under downhole conditions this effect may be reduced by increased pressures (e.g. OBM's) and the viscosity may be increased by the increased hydration and flocculation of clay. Properly controlling the rheological properties in the field depends on efficient solids-control equipment and high-performance drilling fluid additives. Small increases in colloidal-sized drilled solids can rapidly escalate the fluids rheological properties, leading to unacceptable pressure losses, barite sag and drilling fluid gelation, which causes excessive swab, and surge pressures. Conversely, low rheological properties promote poor hole cleaning, barite sag (settlement of solids), and a non-uniform density profile in the annulus that can promote drilling fluid losses to the formation or potential well control problems.
5. **Density:** The mud weight can vary significantly with temperature; a decrease in density (less than 6%) with increasing temperature is due to the volumetric thermal expansion of the fluid phase. This is particularly true of oil muds as the oil continuous phase has a greater expansion than does water.

6. **Alkalinity:** Temperature rise increases the rate and the extent of most chemical reactions. The increased yield of clays results in more sites being available for reaction with ions, particularly hydroxyl ions. The end result of this is a reduction in alkalinity and an increase in flocculation.

In OBM's the increased reaction of lime with surfactants greatly increases with temperature and reductions in mud alkalinity are common, particularly after lengthy trips. Often the performance of the mud will be hindered by lack of a good excess of lime.

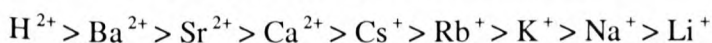
## **2.2 FORMATION AND MUD CHEMISTRY**

Understanding the formation chemistry and drilling mud interactions is crucial for selecting the type of drill-in/completion fluid (i.e. fluids used to minimise formation damage), in terms of wellbore stability and formation productivity.

### **2.2.1 Formation Chemistry**

The stability of the borehole and formation productivity depends to a large extent on interactions between the drilling fluid and the formations present.

The physiochemical properties of clays, which are of great interest to petroleum engineers, are (1) base exchange capacity "BEC", and (2) adsorption of water (swelling). Base Exchange is defined as cation exchange between the clay building unit and a solution e.g.  $K^+$  displaces  $Na^+$ . However when two ions of different valences are present, the one with the higher valence is generally adsorbed preferentially. The order of preference usually is:



The field procedure for determining cation exchange capacity is called the methylene blue capacity test.

Two swelling mechanisms are recognised: crystalline and osmotic. Crystalline swelling (sometimes called surface hydration), results when water invades the pores of a typical clay structure and forces the clay particles apart. Osmotic swelling causes

much larger increases in bulk volume than does crystalline swelling [Figure 2.3]. Remedial treatments for swollen clays are commercially available, but it is easier to prevent clay swelling by using inhibited drilling fluids than it is to reverse it (section 2.3.1).

### **2.2.2 Chemistry of Water Based Muds**

The mud system<sup>7,8</sup> consists of: (1) a continuous phase: water or oil, (2) a dispersed phase: clays (bentonite, attapulgite), (3) chemical additives: reactive such as chemicals used to control mud properties, and non-reactive chemicals such as barite. Clay minerals originate from the degradation of igneous rocks, and mostly belong to the group of silicates having layer structures. The two common members used in water based mud drilling fluid are sodium montmorillonite (bentonite) from the smectite group, which is used in fresh water muds, and sepolite from the attapulgite group, which is normally used for salt water muds.

Clay minerals, i.e., hydrous aluminium silicate [Figure 2.3], provide the colloidal base of many aqueous muds, and are also used in oil based muds.

Based on clay particle orientation there are four structure mechanisms, aggregation, dispersion, flocculation, and deflocculation [Figure 2.4].

1. Aggregation is face to face linkage leading to thicker plates. This decreases the number of particles and causes a decrease in the plastic viscosity and increased filtration volume.
2. Dispersion is the reverse of aggregation and leads to a greater number of particles and to higher plastic viscosity and gel strength.
3. Flocculation refers to edge-to-edge and/or edge-to-face association of particles. This causes an increase in viscosity, gelation and filtration volume.
4. Deflocculation is the disassociation of flocculated particles. This removes the attraction that results in edge-to-edge and/or edge-to-face bonding between clay particles and causes a decrease in the viscosity.



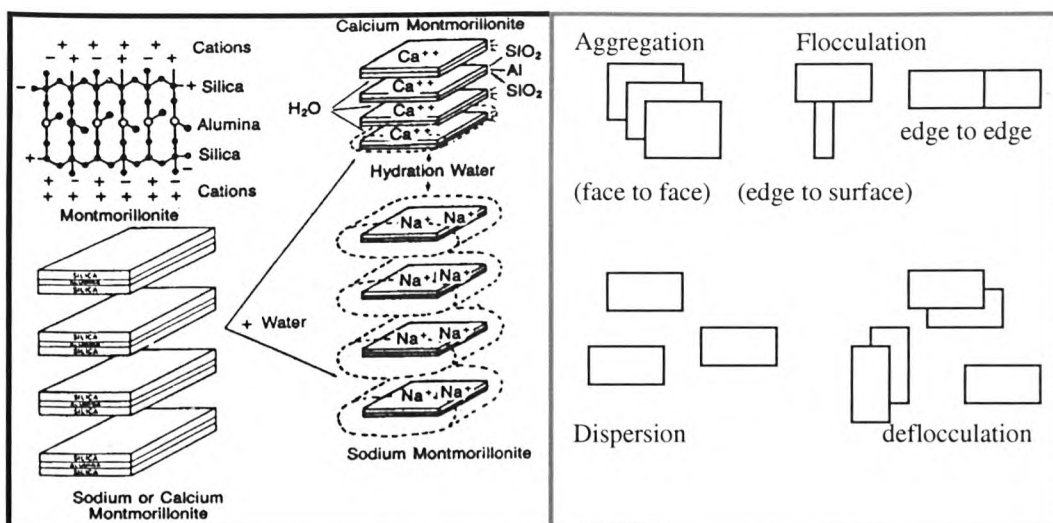


**Figure 2.3** Water hydration of calcium and sodium montmorillonite

**Figure 2.4** Association of clay particles

The fluid loss additives (FLA) can be used for more than one function. The two most frequent FLA applications are for filtration control and to build viscosity.

The filter cake properties such as permeability are affected by the type, amount and molecular size of the FLA. The FLA mechanisms can be divided into:

1. Blocking and plugging of filter cake pores creates low permeability filter cake.
2. Coating mud particulates and creating impermeable layers preventing escape of water into the formation.
3. Viscosifying the base fluid.

e.g. sodium carboxymethyl cellulose (CMC) combines the flocculation and deflocculation, creates link structure (encapsulation) which trap water in between and avoid water escape.

Clay interactions, solubility of various components, corrosion, and effectiveness of additives are all dependent on pH.

### 2.2.3 Chemistry of Synthetic Oil Based Muds

The synthetic oil based muds (SBMs) can be divided into first and second generations<sup>9</sup>. Typical physical properties for the first generation are shown in Table

2.2. Esters, ethers, and acetals contain oxygen in their structures giving an active carbon site that is susceptible to attack by either acidic or basic reactants; the result is degradation.

**Table 2.2 Typical Properties for First-Generation Synthetic-Base Liquids**

Typical properties	Ester	PAO	Ether	Acetal
Density (SG)	0.85	0.80	0.83	0.84
Viscosity @ 40 <sup>0</sup> C (Cst) **	5.0 - 6.0	5.0 - 6.0	6.0	3.50
Flash point (°C)	>150	>150	>160	>135
Pour point (°C)	<-15	<-55	<-40	<-60
Aniline point (°C)	25	108	40	-

\*\*Cst = centi-stokes = cP/SG

Second-generation base liquids: Typical physical properties of these are shown in Table 2.3. However, all the olefin products are thermally stable under HT applications and tolerate contamination well.

**Table 2.3 Typical Properties for Second-Generation Synthetic-Base Liquids.**

Typical properties	LAO	IO	LP
Density (SG)	0.77 - 0.79	0.77 - 0.79	0.77
Viscosity @ 40 <sup>0</sup> C (Cst) **	2.10 - 3.10	3.10	1.75 - 2.50
Flash point (°C)	113 - 146	137	>90
Pour point (°C)	-12 - +3	-24	-10
Aniline point (°C)	-94	-94	>93

Poly-Alpha Olefin (PAO), Linear Alpha Olefins (LAO), Internal Olefins (IO), and Linear Paraffins (LP).

## 2.3. INHIBITIVE MUDS

Inhibitive muds are defined in the “Glossary of Drilling Fluid Terms<sup>7</sup>” (API, 1974) as any drilling fluid having an aqueous phase with a chemical composition that tends to retard and even prevent (inhibit) appreciable clay hydration and dispersion through chemical and/or physical means. Several mud types fitting this description are listed in Table 2.1.

### 2.3.1 Inhibition Mechanisms

Inhibitive muds can be prepared by addition of:

1. Cation exchange - electrolytes to prevent clay swelling by addition of salts such as sodium ( $\text{Na}^+$ ) and potassium chloride (KCl) [Figure 2.5a].
2. Coating the clay or shale in an impermeable viscous shell such as Lignosulphonate (encapsulation).
3. Plugging the pore spaces to prevent water invasion by use of Alpex and Glycol.
4. Fluids having an aqueous phase with a chemical composition that tends to prevent reaction with the formation such as OBM.
5. Combination of two or more of the above.

It is interesting to summarise the inhibition mechanism of lignosulphonate water based mud because this has been selected in this study.

Browning and Perricone<sup>7</sup> have discussed the chemistry of lignosulphonates. Basically, lignosulphonate molecules are attached or adsorbed onto the clay surface creating a viscous multilayer. Lignosulphonate molecules also exhibit strong lateral attraction among themselves when adsorbed on clay surfaces, which further stabilises the viscous multilayer.

These viscous multilayers prevent flocculation of the clay particles by physically preventing them from coming close enough to each other. These results in the reduction of viscosity, yield point, and gel strength.

Water loss is reduced because the strong lateral attraction between lignosulphonate molecules results in the formation of a continuous impermeable layer when the clay particles are deposited on the formation face. Lignosulphonate molecules prevent the escape of water into the formation [Figure 2.5b], prevent hydration and also fill pore spaces that may exist between deposited clay particles.

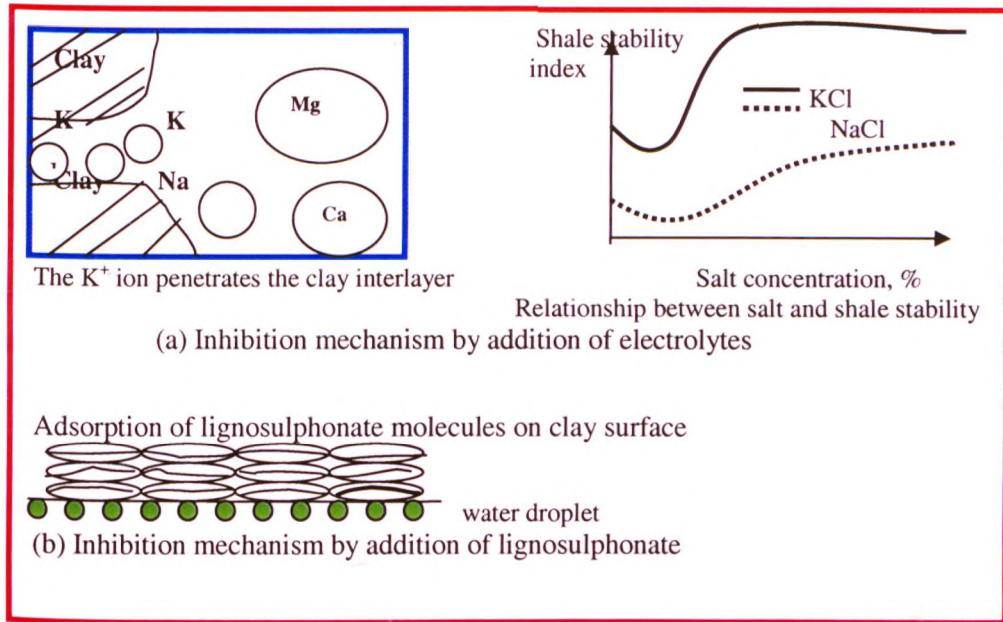


**Figure 2.5 Schematic diagram showing inhibition mechanisms**

## 2.4 TYPES OF FLUIDS SELECTED

Two common inhibitive HP-HT mud systems have been selected and used in this study, viz:

1. Fresh water lignosulphonate mud (WBM).
2. Synthetic oil based mud "linear alpha olefin, LAO" (OBM).

### 2.4.1 Fresh Water Lignosulphonate Mud

In 1955 Roy Dawson introduced the Lignosulphonate system to the oil field drilling industry and in June 1956, the first application was used successfully in West Hackberry Field, Louisiana<sup>10-12</sup>. This is the most widely used inhibitive water based

mud and was specifically designed for the following attributes: rheological stability, excellent shale inhibition, tolerance to contaminants, favourable logistics.

#### **2.4.2 Oil Emulsion Mud**

In brief<sup>13-17</sup>, the conclusion was that the emulsification of oil improved the performance of WBMs as evidenced by an increase in drilling rate, bit life, and improved productivity, which was cited as a major advantage of oil emulsion mud.

#### **2.4.3 Synthetic Oil Based Mud Description**

Commercial oil based muds became available in 1960, and higher initial oil production was usually noted<sup>18-23</sup>. Coring for reservoir information was a frequent application of oil mud<sup>24</sup>, and release of stuck drill pipe was another<sup>25,26</sup>. A new record was set in 1974 in the 1 Benevides well of Shell Oil Company and El Paso Natural Gas Company with a temperature of 555 °F measured at a depth of 23,837 feet<sup>27</sup>. The main component of the OBM is called “base oil” which is made up from<sup>28</sup>:

1. **Crude oil:** This was the first to be used but is seldom employed now because of environmental concerns.
2. **Diesel oil:** It is less expensive and still used in some cases, particularly when there are regulations that require oil mud cuttings to be processed at a disposal or treatment site.
3. **Low-aromatic mineral oil:** In early 1980s, efforts were made to reduce the environmental impact by reducing the amount of aromatic hydrocarbons present in the oil.
4. **Synthetic oils:** An environmentally acceptable substance was first seen in March 1990 with the use of a mud made from synthetic-base fluid (an ester) in the Norwegian sector of the North Sea. The first poly-Alpha Olefin (PAO) was used in May 1991. Other synthetic base fluids were introduced to the industry in the following order: Linear Alpha Olefins (LAO), Internal Olefins (IO), and Linear Paraffins (LP).



## **2.5 FILTRATION BEHAVIOUR OF DRILLING FLUIDS**

### **2.5.1 Definition of Liquid Filtration**

Filtration<sup>29</sup> is the separation of suspended particles from a fluid stream by passing the suspension through a porous substance referred to as a filter medium. As the fluid or suspension is forced through the voids or pores of the filter medium, the solid particles are retained on the surface and in the pores, while the fluid, referred to as the filtrate, passes through.

### **2.5.2 Borehole Filtration Mechanisms**

There are three types of filtration<sup>30</sup> process that can occur during drilling and completion operations:

#### **1. Filtration Beneath the Bit**

Very little filter cake forms on the bottom of the hole because the action of the mud jets leads to erosion<sup>31-34</sup>.

#### **2. Dynamic Filtration**

During circulation of drilling fluid, filtration takes place under dynamic conditions. When the surface of the rock is first exposed, the rate of filtration is very high, and the cake grows rapidly; the rate of growth decreases as time passes, until eventually it is equal to the erosion rate at the equilibrium stage. Thereafter the thickness of the cake and the flow rate are both constant and attain plateau values. During dynamic filtration the rate of cake build-up is the difference between the rate of particle deposition by filtration and the rate of particle erosion by the circulating mud. The particle deposition rate is the mass flux of particles carried toward the formation face by the fluid flowing in the direction normal to the cake surface. The erosion rate of particles from the filter cake is assumed proportional to the shear stress exerted by the circulation of the drilling fluid on the cake surface.

#### **3. Static Filtration**

Static filtration takes place when the mud is not being circulated; the thickness of the filter cake increases as filtration continues. Examples include wiper trips for bit changes, logging, etc.

[Figure 2.6] shows a typical filtration curve for a sequence of dynamic- static filtration<sup>34,36</sup>. During the initial dynamic filtration period  $T_0$  to  $T_1$ , the filtration rate and the cake thickness increase. From  $T_1$  to  $T_2$  the thickness of the cake remains constant, but the filtration rate continues to decrease, because, according to Outmans<sup>37,38</sup>, the filter cake continues to compact. (Presumably, therefore, the rate of deposition equals the rate of compaction). This suggested that the permeability of the cake decreases because of a classifying action as the mud stream erodes and redeposit particles in the cake surface, gives another explanation. At time  $T_2$  an equilibrium condition is reached, and both filtration rate and cake thickness remain constant to  $T_3$ , which depends upon the properties of the dynamically deposited filter cake. The next phase of the curve corresponds to the period of static filtration  $T_3$  to  $T_4$ . A static cake is thus laid down on top of a dynamic one, so the filtration rate decreases and the filter cake thickness increases. The third phase  $T_4$  to  $T_6$  is after circulation is resumed; the soft upper layers of the static cake are eroded, and the thickness of the cake decreases, but most of the static cake remains. This infers that upon restarting circulation the shear is insufficient to erode the static cake except for the gelatinous outer layer. This confirms the theory proposed by Ferguson and Klotz<sup>34</sup>.

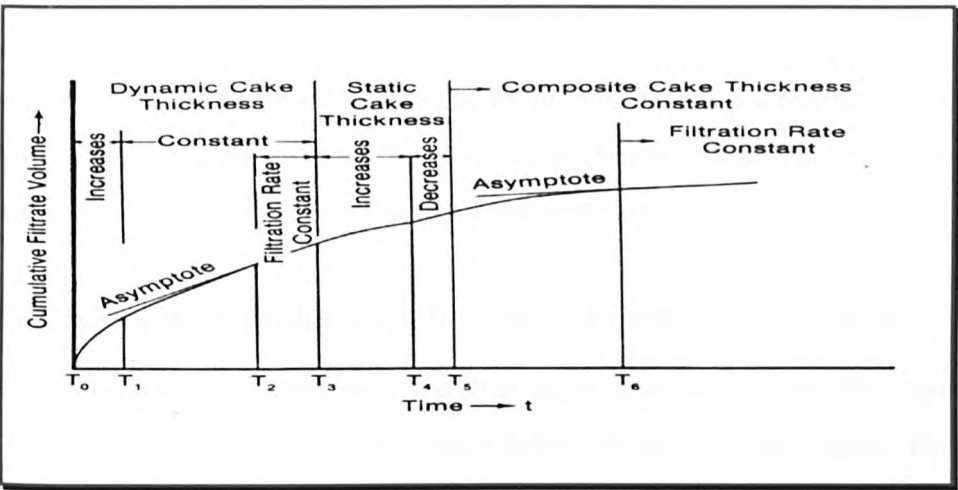
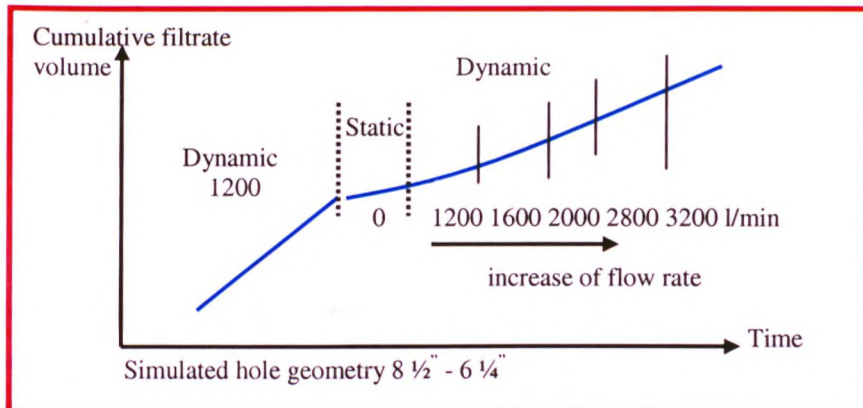


Figure 2.6 A typical plot of cumulative filtrate volume collected as a function of time for sequential filtration

The thickness of the cake again remains constant while the filtration rate decreases to a new equilibrium filtration rate. Thus the thickness of the cake increases with each dynamic-static cycle, but the amount of increase is small. However the growth of the filter cake is limited by mechanical wear when the drill string is rotating, and by abrasion when pulling or running pipe; however, these effects cannot be quantified (as discussed earlier).

Vaussard et al.<sup>39</sup> found out that the dynamic rate was reduced by a period of static filtration, but increased if the annular flow rate was increased - markedly so at the onset of turbulence, which occurred at about 1,800 l/min in their experiments [Figure 2.7].



**Figure 2.6 Filtration versus flow rate changes**

The process of drilling a well results in alternating periods, of varying duration, of dynamic and static filtration. The relative amounts of filtrate entering the formation during each of these phases will be dictated by the filtration characteristics of the mud and these will be a function of the mud composition, formation properties and operating conditions (overbalance pressure, shear rate, etc.).

### 2.5.2.1 Mechanisms of Bridging and Invasion of Filtrate into Formation

The invasion of filtrate occurs once filtration starts. It is well known that there is a mud spurt at the start of a filtration process before filtration proper begins. The mud contains particles of the size required to bridge the pores of the rock and establish a base on which the filter cake can form. Only particles of a certain size relative to the



pore size can bridge. Particles larger than the pore openings cannot enter the pore, and are swept away by the mud stream. Particles considerably smaller than the size of the pore throat can also bridge when they enter a pore throat simultaneously. But particles of a certain critical size stick at bottle-necks in the flow channels and form a bridge just inside the surface pores. Once a primary bridge is established, successively smaller particles, down to fine colloids, are trapped, an external filter cake starts to establish on the borehole wall and thereafter only filtrate invades the formation. The mud spurt period is very brief, a matter of a second or two at the most<sup>40,41</sup>.

As a result of the mechanisms just described, three invaded regions are established<sup>8</sup> in a permeable formation, which are shown in [Figure 2.8].

1. An external filter cake on the walls of the borehole;
2. An internal filter cake, extending a couple of grain diameters into the formation;
3. A zone invaded by the fine particles during the mud spurt period, which normally extends about an inch into the formation<sup>31,42-44</sup>.

Experimental results reported by Krueger and Vogel<sup>45</sup> suggest that these fine particles do not initially cause much permeability impairment, but may do so after filtration has progressed for some hours, presumably because of migration and consequent pore blocking.

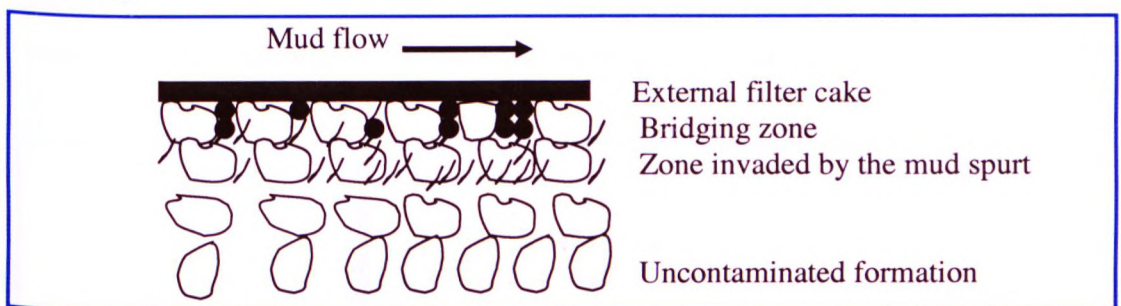


**Figure 2.8 Invasion of permeable formation by mud solids**

In 1992 Schechter<sup>46</sup> [Figure 2.9] illustrated possible modes of particle entrapment. Large particles transported to the surface of the porous medium will bridge over the surface pores and form an external filter cake (first mode). Smaller particles passing through the porous medium may adhere to the surface of the pore bodies (second

mode), resulting in little permeability impairment. Particle bridges in the pore throats (third mode) effectively plug the pores. However the relative size of the fines and the pore throats are primary factors in determining whether formation damage due to fines movement will occur.

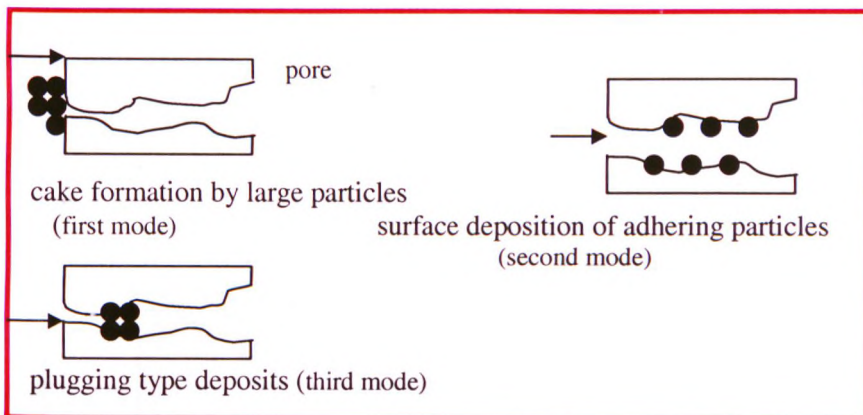


**Figure 2.9 Modes of particle entrapment**

### 2.5.2.2 Mechanism of Flow through Filter Cake

As suspended solids are deposited during cake filtration, liquid flows through the cake interstices as a result of the pressure difference over the cake. A drag force is therefore exerted on the solid particles [Figure 2.10] and since the force on each particle is transmitted to its neighbours the total drag force increases as the filter medium is approached. The compressive stress,  $P_s$ , within the particles will therefore also increase.

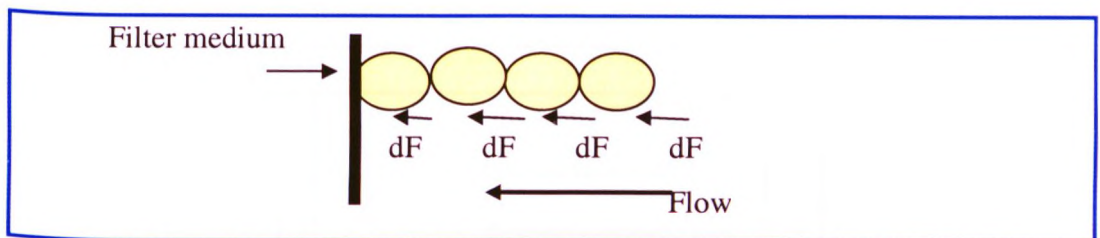


**Figure 2.10 Schematic diagram for drag force on solid particles**

If the cake is incompressible then no compaction of the solids occurs as a result of the drag pressure and the porosity is constant throughout the cake.



However, drill-in fluid filter cakes do undergo compaction of the solids as  $P_s$  increases<sup>8</sup>.

These compressible filter cakes exhibit non-linear permeability and porosity profiles, with the porosity a maximum at the cake surface (i.e., where  $x = L$ ) and a minimum at the filter medium surface (i.e., where  $x = 0$ ). The cake is dry and compacted near the medium whereas the cake surface is wet. A schematic definition of this system is illustrated in Figure 2.11.

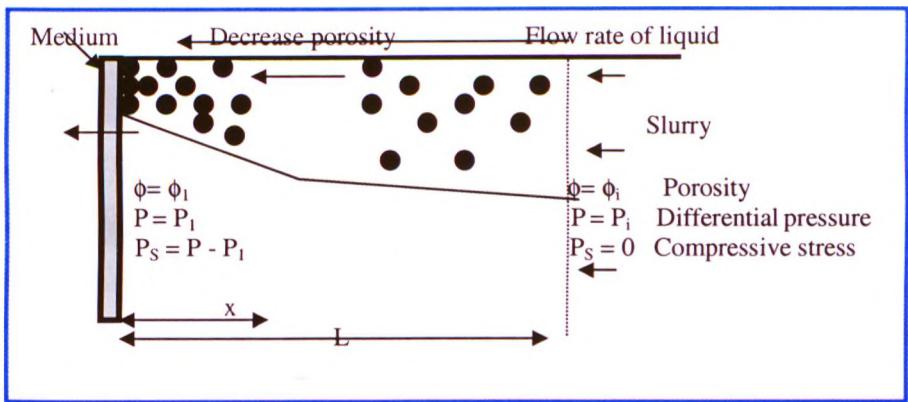


**Figure 2.11 Schematic diagram of important parameters in cake formation**

Figure 2.12 illustrates pressure relationships in which ( $P$ ) drops from the applied pressure  $P$  to  $P_1$ , the pressure required to overcome the resistance  $R_m$  of the medium.

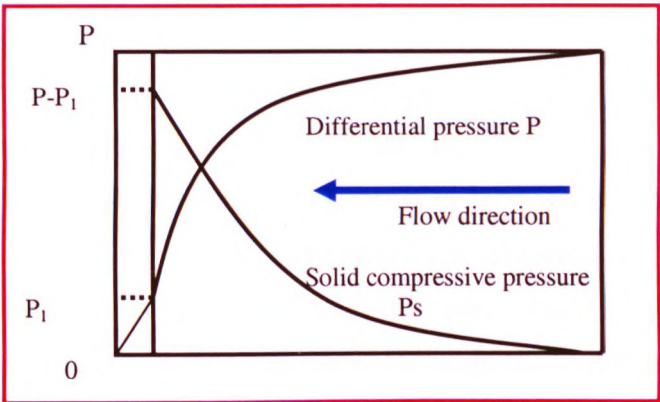


**Figure 2.12 Pressure drop relationships**

### 2.5.3 Jamming Ratios (JR)

The jamming ratio is defined as the ratio between particle size diameter ( $d_{50}$ ) and pore throat diameter ( $D_{pore}$ ). The expression for particle/pore size ratio is derived from the Carman-Kozeny equation for permeability<sup>47</sup>:

$$\text{Particle/Pore Size Ratio} = \frac{d_{50}}{0.95\sqrt{k_g}}$$

$$\text{Where } D_{pore} = \sqrt{K_g}$$

$d_{50}$  - mean particle diameter,  $\mu\text{m}$  and  $K_g$  is permeability in md

$D_{pore}$  - pore throat diameter,  $\mu\text{m}$

Basically jamming ratios cover three main aspects:

1. Solid particles: to determine particulate invasion from relationship between the mean grain size diameter and average pore throat diameter.
2. Pore size distribution: to determine the average pore throat diameter from any crushed core sample or even drilling cuttings from the shale shaker screen.
3. Selection of appropriate size for loss circulation control systems, and gravel.

#### 1. Solids Particles

The mechanism of solid particles plugging a porous medium has been studied by many researchers<sup>42-62</sup>. Abrams<sup>44</sup> proposed empirical criteria for rock permeability impairment from suspended solid particles, which can occur by one of the following mechanisms:

- (a) Particles larger than  $1/3^{\text{rd}}$  of the pore diameter can bridge the pore entrance at the formation face to form an external cake.
- (b) Particles smaller than  $1/3^{\text{rd}}$  but larger than  $1/7^{\text{th}}$  of the pore diameter invade the formation and are trapped, forming an internal filter cake.
- (c) Particles smaller than  $1/7^{\text{th}}$  of the pore diameter cause no formation impairment, because they are carried through the formation.

a. For instant bridging	b. For invasion and deposition
$d_{50} > 0.33 * D_{pore}$	$0.1 * D_{pore} < d_{50} < 0.33 * D_{pore}$

This rule was found to be unsatisfactory by several researchers<sup>53,56</sup>. New rules have been developed as follows:

Researchers	Jamming ratio
Van Velzen and Leerlooijer <sup>60</sup>	1/3-1/4
Pautz and Crocker <sup>58</sup>	1/5
Zhang and et al. <sup>59</sup>	1/8
Peden et al. <sup>62</sup>	<5

## 2. Pore Size Distribution

In many oil field applications a rule-of-thumb method is used to give an estimate of average pore throat diameter. This rule estimates the average pore diameter in microns ( $\mu m$ ) as roughly equal to the square root of the formation permeability (in md). However, in 1989 Pautz and Crocker<sup>58</sup>, extensively studied and compared both methods, capillary pressure method and rule-of thumb. They conclude that generally, the average pore throat diameter is not equal to  $\sqrt{K}$  and the ratio of particle size to laboratory measured average pore throat diameter is not a good indicator of permeability reduction.

In 1999, Cargnel and Luzardo<sup>61</sup> compared the rule-of thumb method and the SEM method. For instance, the permeability of the 10-micron porous element tested was 950 md to gas. The square root of this value is 30.80 microns, which is three times the average pore throat diameter measured by SEM.

This is because Cargnel and Luzardo<sup>61</sup> used permeability to gas, without applying gas correction factor (Klinkenberg effect), which gives a very big difference in comparison. (However in chapter 4 a relationship has been established between gas and liquid permeability).

The average pore throat size of the formation, generally computed using Coberly or Blake-Kozeny equations<sup>62</sup> defined as follows:

A. Coberly equation:

$$D_{pore} = d_{50}/6.50$$

B. Blake-Kozeny equation:

$$D_{pore} = d_{50} \phi / 3(1 - \phi) \quad \phi = \text{porosity}$$

Peden et al.<sup>62</sup> found that effective management of particulates generally requires a predicted pore size 2-3 times bigger than predicted by Coberly or Blake-Kozeny equations. (Details of analysis will be discussed in chapter 4).

## **2.6 THE PROBLEMS CAUSED BY FILTRATION OF DRILLING FLUIDS**

The problems can be classified into two categories:

1. Formation damage problems: normally discovered after drilling operations, which may lead to an expensive operational treatment or well abandonment if not successful. The main formation damage problems are: swelling and migration of clay particles, particle plugging, wettability, water blocking, emulsion, scale and precipitates, and unconsolidated sands.
2. Drilling problems: usually occurring during drilling operations, the main drilling problems can be listed as: differential sticking, hole instability, logging tool response, and cementing. These drilling problems may lead to an expensive fishing operation, if unsuccessful the well will be sidetracked or abandoned. The well plan for selecting drilling fluid will be crucial. The following gives a summary of these problems.

### **2.6.1 Formation Damage**

When filtrate enters the formation the outcome can be a number of potentially serious problems that result in substantial permeability impairment of the formation and a lower than expected hydrocarbon recovery. However formation damage generally can



be considered to be caused by physical or chemical interaction between the following:

1. The solid constituents of the invading fluid and the reservoir rock;
2. Invading fluid liquid phase and the reservoir rock constituents;
3. Invading fluid liquid phase and the reservoir fluid.

These can all lead to a reduction in the effective production capacity or injectivity of a given reservoir formation. Three basic mechanisms exist by which filtrate invasion can effect a reduction in permeability of the formation:

- (a) Reduction in the formation absolute permeability – results from plugging of pore channels by particles in the invading fluid.
- (b) Alteration in the relative permeability of the formation to a specific fluid – results from an increase in water saturation or oil wetting of the rock.
- (c) Alteration in the viscosity of the mobile fluid – results from high treating fluids (e.g. emulsifiers).

Diagnosis of formation damage problems has led to the conclusion that formation damage is usually associated with either the movement or bridging of fine solids and chemical reactions<sup>63,64</sup>. The fine solids may be introduced from wellbore fluids or generated in situ by interaction of invading fluids with rock minerals or formation fluids. Some of the important formation damage mechanisms, which related to borehole filtration are shown in Figure 2.13 and briefly discussed below.

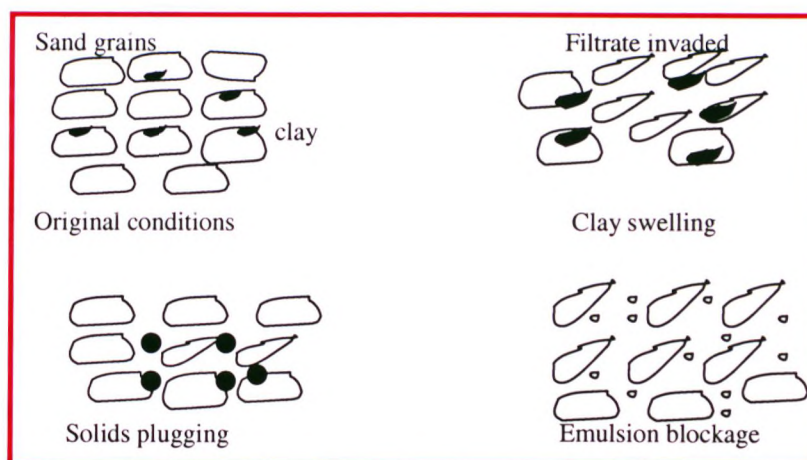


**Figure 2.13 most common types of formation damage**

Krueger<sup>64</sup>, Amaefule and Kersey<sup>65</sup>, and Economides and Nolte<sup>66</sup> provided an extensive analysis of formation damage problems. They all recognise that from the time the drill bit enters the formation until the well is put on production, invasion of mud filtrate and solids are the major causes of permeability damage.

Keelan and Koepf<sup>67</sup> identified three main types of near-wellbore permeability damage that can be evaluated by core analysis:

1. Clay hydration and swelling of clay particles, dispersion and their movement with produced or injected water.
2. Plugging of pores and pore throats by solids introduced during drilling and completion.
3. Fines production from unconsolidated sands, causing loss of well productivity.

#### **2.6.1.1 Swelling and Migration of Clay Particles**

When formation clays come in contact with drilling or completion fluids as a result of filtrate invasion, clay swelling occurs and usually causes plugging of flow channels and reduction in well productivity, and is now the subject of intensive experimental and theoretical investigations.<sup>68-74</sup>

#### **2.6.1.2 Particle Plugging**

Near-wellbore plugging occurs from the fine solids carried by wellbore fluids. As distinct from particle migration, this term refers to the entry, movement and subsequent deposition in the pore spaces or pore throats of the porous media. The size of the particles which can invade the formation will depend on the porosity, permeability and stability of the filter cake on the wall of the borehole<sup>40-45,75-78</sup>.

#### **2.6.1.3 Wettability**

The use of complex organic chemicals such as finely divided particles (e.g., asphalts), and surfactants in muds can have adverse effects on the wettability of the formation.



If reservoirs are converted from being water wet to oil wet the relative permeability may be greatly reduced in the near-wellbore region.

#### **2.6.1.4 Water Blocking**

The introduction of the water-based filtrate during drilling and completion operations into the formation can cause a reduction in reservoir productivity as a result of an increase in the water saturation of the reservoir.

Treatment to remove water blocking involves the use of surfactants and alcohols to reduce interfacial tension between the oil and water. However, if the filtrate has a very high viscosity, e.g., it contains polymers which are not completely soluble, then the impairment might be more difficult to remove.

#### **2.6.1.5 Emulsions**

The formation of an emulsion of water and oil is promoted by a high degree of turbulent mixing of the two phases and/or by the presence of chemical emulsifiers as used in oil emulsion mud systems. In the borehole filtration situation, it is unlikely that the filtration flow rate will be high enough to give rise to turbulence except may be during the spurt loss period. Chemicals which act as emulsifiers could be present, e.g., asphalt and some dissolved emulsifiers will cause emulsion blockage resulting in increased viscosity and thus impair the mobility of crude oil.

#### **2.6.1.6 Scale and Precipitates**

The formation and subsequent deposition of precipitates or scales can occur when an In situ reservoir fluid is in contact with an incompatible filtrate. The salts so formed can be insoluble such as  $\text{BaSO}_4$  or  $\text{CaSO}_4$  (Barium and calcium sulphate) and once present in the pore space they are difficult to remove.

#### **2.6.1.7 Unconsolidated Sands**

A wellbore in an unconsolidated formation is likely to be unstable, and usually leads to sand production and consequent reduction in well productivity. Increases in the drawdown also lead to the movement and production of formation sand. High drawdowns also can cause premature compaction due to sudden changes in the stress state near the well, which invariably result in caving and subsequent flow of sand into the wellbore.

#### **2.6.2 Drilling Problems Associated with Filtrate Invasion**

There are a number of drilling problems related to the use of drilling fluids, viz.:

1. Differential pipe sticking.
2. Hole instability.
3. Logging tool response.
4. Cementing.

##### **2.6.2.1 Pipe Sticking**

Thick filter cakes can cause the drill string to become mechanically stuck during tripping or pipe connection. A combination of high differential pressure and a thick filter cake is the major cause for the drill string to become stuck by a mechanism known as differential sticking which has a major impact on drilling efficiency and well cost. This phenomenon was first recognised by Hayward<sup>79</sup> in 1937, and Helmick and Longley demonstrated the mechanism<sup>80</sup> in the laboratory in 1957. Differential sticking can occur opposite permeable sections if the drill string or logging tools are left stationary in the hole or the string is not rotated (e.g. when slide drilling). It is thought to arise when the pipe becomes embedded in the dense part of the filter cake near the rock formation, such that a pressure seal exists which prevents the drilling fluid from equalising the pressure around the pipe. The excess overbalance pressure is then exerted against the pipe, holding it against the side of the well and increasing the friction between the pipe and the filter cake, preventing the pipe from being moved<sup>81</sup>.

Thick filter cakes can also contribute to excessive torque when rotating the pipe, excessive drag when pulling it, and high surge and swab pressures while tripping, with the possibility of lost circulation.

#### **2.6.2.2 Hole Instability**

The filtration properties required for the successful completion of a well depend largely on the nature of the formations to be drilled. Stable formations<sup>8</sup> with low permeability, such as dense carbonates, sandstones, can usually be drilled with little or no control of filtration properties. But many shales are water sensitive, i.e., on contact with water, they develop swelling which causes caving and hole enlargement. Sealing of incipient fractures by mud filter cake will help to control the caving, but the type of mud used and the chemical composition of its filtrate are more important factors. Optimum filtration properties are also necessary when drilling in unconsolidated sands, which will slump into the hole unless protected by the rapid formation of a filter cake.

#### **2.6.2.3 Logging Tool Response**

Many studies have been carried out to investigate the effect of the filtration properties on the logging tool response<sup>82-92</sup>. The response of many logging tools can be affected by the presence of thick filter cake and filtrate invasion, as briefly discussed below.

1. Neutron logs respond to the amount of hydrogen present in the formations containing water or oil and reflect the amount of liquid-filled porosity. The presence of polymers, and water, all of which contain large amounts of hydrogen, will affect the estimation of formation porosity.
2. The formation density log is used for identification of minerals, the detection of gas and the determination of hydrocarbon density. The problems caused by filtrate invasion are therefore similar to those found with Neutron tools. Any roughness of borehole wall from enlargement or presence of thick filter cake will affect the contact of the tool with the formation.

3. Resistivity logs can be affected by the invasion of mud (during the spurt period) and mud filtrate into the formation. As the filtrate moves into the formation it displaces the native fluids and, since the filtrate resistivity is usually different from the formation water resistivity, the resistivity of the formation changes. Accurate analysis of these logs will require information on the depth and properties of the invading filtrate.

#### **2.6.2.4 Cementing**

The nature of the mud filter cake is of central importance to a good cement job. Ravi et al.<sup>93</sup> stated that the potential outcome of primary cement jobs is mainly affected by the condition of the wellbore when the cement is pumped downhole. A successful job requires removal of both mud and filter cake by the use of casing movement, and casing scratchers prior to cement placement. A mud cake with low shear strength would appear to be the best for removability. Sherwood<sup>94</sup> has considered the formation of a cement filter cake above a pre-existing mudcake. For this reason Bannister et al.<sup>95</sup> stated that care should be taken to minimise mud fluid loss to permeable formations prior to wellbore cementing.

## **2.7 FORMATION DAMAGE MECHANISMS**

### **2.7.1 Permeability Damage from Foreign Solids**

There are many published studies related to formation damage mechanisms caused by suspended particles in injected fluids, drilling and completion fluids.

Barkman and Davidson<sup>52</sup> proposed four mechanisms of well impairment: wellbore narrowing (external cake formation), particle invasion (internal cake or deep bed filtration), wellbore fillup, and perforation plugging.

Davidson<sup>78</sup> reported that there is a relationship between particle movement through porous media and linear flow velocity.

Gruesbeck and Collins<sup>96</sup> found that there exists a critical velocity, or flow rate, below which entrainment of fines does not occur and above which the rate of entrainment increases linearly with flow rate.

Vetter et al.<sup>54</sup> provided a critical review of previous laboratory and model studies on formation damage and conducted particle filtration tests. Their results show that particles of all sizes from 0.05 through 7 microns cause formation damage.

The larger particles cause a rapid decline in permeability with the damage region being shallow. Smaller particles (in the submicron range) enter the core and cause a gradual permeability decline. The higher the linear velocity, the greater the depth of particle penetration.

Other researchers have used the jamming ratio to estimate a minimum particle size that would contribute to permeability reduction. This rule was found to be unsatisfactory by several researchers<sup>53,56</sup>.

In summary, there are three common mechanisms of foreign solids transport in porous rocks by which permeability damage can occur during filtration process:

(1) gradual pore blocking, (2) single pore blocking, and (3) cake formation.

Gruesbeck and Collins<sup>96</sup> defined gradual pore blocking as a surface-type deposition and showed that during this mechanism the rate of deposition is directly proportional to the solids concentration in the flow stream.

Previous studies on pore blocking mechanisms in sandstone cores by Wojtanowicz<sup>97</sup>, have attempted to define three distinct mechanisms [Figure 2.14] that can occur in a porous medium invaded by foreign particles, namely:

1. Gradual pore blocking mechanism: this is a phenomenon in which the particles migrate through the pore throats but deposit on walls resulting in a gradual reduction in pore size and permeability. This mechanism is characterised by:
  - a. Parabolic-type permeability reduction, and
  - b. Steady decrease in the size of invading solids. The duration of this mechanism is a function of size and concentration of solid particles in the drilling fluid.

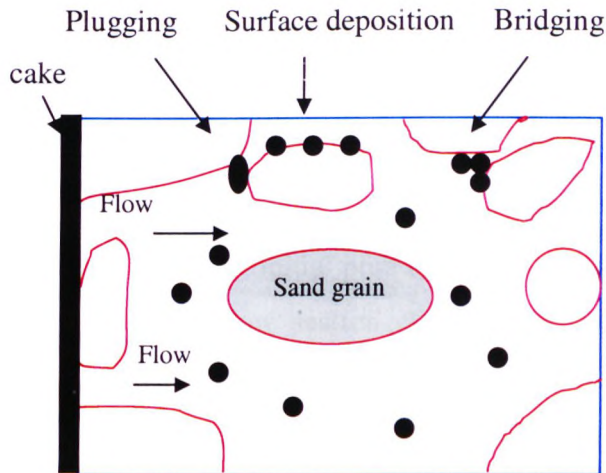


**Figure 2.14 Particle retention in porous media**

2. Single-pore blocking mechanism: this phenomenon occurs when single particles of size close to the pore throat size (critical size) instantly block individual pores, thus eliminating them from the flow system. This mechanism is characterised by:
  - a. Linear-type permeability reduction,
  - b. Deep invasion of particles, and
  - c. Single particle migration.
3. Cake-forming mechanism has two characteristics:
  - a. Hyperbolic-type permeability reduction, and
  - b. Limited invasion distance.

Yan Bingo et. al<sup>98</sup> studied the pore blocking mechanisms in gravelpacks [Figure 2.15] in order to define the permeability decline as a function of production time. Five mechanisms were identified namely:

1. No interaction ( $d_p / D_{pore} > 15$ ): represents the phenomenon in which there is free passage of fines due to very large pores existing in the gravelpack. It is characterised by a trend of constant permeability which remains unchanged with fines invasion.



2. Pore filling ( $10 < d_p / D_{pore} < 15$ ): This mechanism is associated with the phenomenon of gradual deposition of particles in the pore spaces of the gravelpack resulting mostly in a hyperbolic reduction of permeability with time.
3. Combined internal bridging and single pore blocking ( $6.5 < d_p / D_{pore} < 10$ ): The phenomenon is one of initial pore blocking followed by accelerated build-up of particles at the shallow section of the gravelpack. In this shallow zone the permeability reduction is hyperbolic.

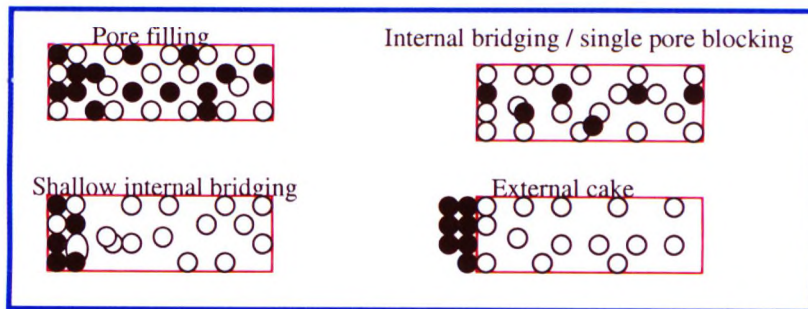


**Figure 2.15 Pore blocking mechanisms**

4. Shallow internal bridging ( $5 < d_p / D_{pore} < 6.5$ ): Particle bridging occurs at pore throats close to the gravelpack face. The particles can be easily removed by backflow.
5. No invasion ( $d_p / D_{pore} < 5$ ): When the gravelpack pores are too small to allow any invasion by the fines. External cake results without damage to the gravelpack.

## 2.7.2 Permeability Damage from Formation Fines

Formation fines may be generated as chemical precipitates from chemical reactions between the completion fluid and formation water, or released from the surface rock as the completion fluid interacts with the various clay and non-clay minerals present in the formation rock. Once mobilised, these fines can damage the permeability in a similar manner to foreign solids.



### 2.7.3 Drilling Fluid Selection

In recent times, the oil industry has made increasing efforts to maintaining optimum well productivity through better drilling/completion fluids design. However, the mechanisms of drilling fluid filtration and impact on productivity performance are not well understood.

In open hole completions the productivity losses are critical because the near-wellbore damage is not by-passed by perforations.

A key parameter in quantifying formation damage is the skin factor<sup>99</sup>. The skin factor estimated from well test data is used in the flow equations to estimate the production rate in wells that are affected by formation damage.

Generally, when rating the performance of various drill-in fluid formulations, the permeability damage evaluation is quantified through oil return permeability measurements and flow-initiation pressures performed on core samples damaged during mud filtration tests<sup>100,101</sup>.

Extensive studies of formation damage in the laboratory and several modelling efforts for prediction of formation damage have been reported in the literature. Few attempts were made to transfer these laboratory data into a near-wellbore model to evaluate the permeability damage. Liu et al.<sup>102</sup> simulated formation damage by fluid injection and mud filtration and Scott Lane<sup>103</sup> and Semmelbeck et al.<sup>104</sup> simulated filtrate invasion for improving log interpretation, but their impact on well performance was not investigated. Some workers<sup>105,106</sup> studied well performance using representative formation damage, but laboratory tests were not integrated in their studies.

Filter cake removal in open hole completions where formation impairment cannot be bypassed by perforation remains a challenge. Flow initiation pressure has been used as a measure for filter cake removal during drawdown<sup>107-113</sup>. Formation damage modelling is obviously complex. Some attempts have been made to evaluate and compare the various models<sup>54,114,115</sup> and the conclusion from these studies are as follows:

1. Most of the work has been conducted on incompressible fluids.
2. Each of these models has its own limitations.

3. Increasing the number of model parameters increases model complexity.
4. Most of the models were developed on linear core scale.
5. Lack of realistic values for particle invasion depth.

In addition, a satisfactory model for field applications to simulate the near-wellbore damage before drilling in terms of well flow performance integrated from laboratory core test analysis is still not available.

In this thesis the full process of near wellbore damage is modelled from link laboratory measurements to field scale applications. The fluid rheology, static and dynamic filtration, filter cake properties and permeability damage obtained from controlled specific laboratory measurements are used to model the formation damage for fluid optimisation and selection.

## **CHAPTER THREE**

### **DRILLING FLUIDS FILTRATION MODELS**

In this chapter, an extensive review is carried out on the experimental studies of filtration properties of drilling fluids. Previous studies on the effects of the key parameters under downhole conditions on filtration performance are compared with the present work.

The models which govern the filtration process are presented. Having such information on hand, one should be able to predict improvements in existing knowledge in filtration of drilling fluids under downhole conditions. Also a number of classical models, which are relevant to the definition of filtration phenomena in a wellbore, are reviewed.

#### **3.1 LITERATURE REVIEW ON FILTRATION PROPERTIES**

It is meaningful to identify and summarise the effects of the key variables upon the filtration process which has been used in this study and to compare some of these studies with the present work. These variables discussed below include, pressure, temperature, formation characteristics, annular hydraulics, mud constituents and properties.

##### **3.1.1 The Effect of Individual Wellbore Variables**

###### **3.1.1.1 The Effect of Pressure**

If the filter cake were of constant permeability then the volume of filtrate obtained would be proportional to the square root of the pressure differential according to Darcy's law, and a log-log plot of filtrate volume versus pressure should yield a straight line with a slope of 0.50. Actually, this condition is never met because drilling mud filter cake is to a greater or lesser extent compressible, so that the

permeability is not constant, but decreases with increase in pressure (which agrees with Larsen<sup>116</sup>).

Larsen<sup>116</sup> found that fluid loss is proportional to the one-half power of time and an exponential function of pressure. For the mud tested (WBM&OBM), the exponent varies between 0 and 0.24 and depends largely on the size and shape of the particles composing the cake (which agrees with Darley and Gray<sup>7</sup>), but is always less than 0.50.

Arthur et al.<sup>117</sup> reported that the spurt loss was a power function of pressure with exponent varying between 0.05 and 0.25. Actually it is very difficult to model spurt loss as you can do for commutative fluid loss.

Jones and Babson<sup>118</sup> and Hall and Dollarhide<sup>119</sup> observed that in going from the differential pressure of 100 to 500 psi, the pressure had a significant effect on the fluid loss and the mud cake thickness deposited was little affected the variations in pressure above 500 psi. Since the relationship between the fluid loss and pressure is a power law for compressible fluids and 500 psi is the critical pressure. Therefore increased pressure results in increased rate of compaction and the cake permeability decreases for the WBM and OBM tested.

The mud spurt increased with increase differential pressure, which might be attributed to the increase in velocity of the mud solids at the instant of application<sup>120-122</sup>. Simpson<sup>122,123</sup> found that the greatest effect of pressure was on the viscosity of oil (compared with water) and no simple calculation could be made to normalise the effect of pressure.

The effect of temperature and pressure on WBM and OBM has been studied in the current work and a model developed to predict viscosity at downhole conditions was used to describe the effect of fluid rheology on the dynamic filtration process as will be discussed (in chapter 5).

Bezemer and Havenaar<sup>124</sup> found that the erodability of the cake surface and the equilibrium rate at a constant value of shear rate was independent of the filtration pressure.

Fisk and Jamison<sup>125</sup> studied the dynamic filtration of four types of drilling fluids namely, dispersed and lime-water based muds, diesel and mineral oil based muds. They concluded that filtration pressures greater than 300 psi had a minimal effect on the dynamic filtration rates of the oil and water base fluids at all temperatures.

The formulation and properties of the WBM and OBM used by Fisk and Jamison may be questioned. First, for the WBM there is no FLA and 17 lb/bbl clay concentration was used for 16 ppg mud and this value should not exceed 8 lb/bbl to avoid mud flocculation and gelation especially at higher temperature. Second, oil based muds were formulated with high concentrations of emulsifiers (16 lb/bbl), these should not exceed 10 lb/bbl. The FLA mixed at 20 lb/bbl concentration also very high and should instead be in the range of 6 to 8 lb/bbl. Furthermore, yield point (YP = 3 to 6) is too low to avoid barite sag which affect tests results.

William<sup>126</sup> found that the equilibrium dynamic filtration rate was a function of pressure. WBM and OBM were tested in the current study and showed that increased filtration pressure and temperature increase the filter cake erodability and equilibrium filtration rate.

### 3.1.1.2 The Effect of Temperature

Larsen<sup>116</sup> studied the effect of temperature on cumulative filtrate volume and proposed that:

$$\frac{V(T_2)}{V(T_1)} = \sqrt{\frac{\mu(T_1)}{\mu(T_2)}}$$

Where V and  $\mu$  are cumulative filtrate volume and filtrate viscosity at temperature  $T_1$  and  $T_2$  respectively.

Other researchers<sup>117,127-129</sup> report filtrate volumes higher than given by Larsen's equation.

Byck<sup>130</sup> reported that no existing method would permit even an approximate determination of the filtration rate at higher temperatures from data obtained at room temperature.

Arthur et al.<sup>117</sup> reported that filtrate viscosity can be used to provide good estimates of fluid loss when test temperature is not greatly different from the temperature of interest.

These discrepancies between researchers may be explained from the tests conducted for WBM and OBM in the current work. Increase in temperature may increase the filtrate volume in several ways. Firstly, it reduces the viscosity of the filtrate. Therefore if changes in the cake structure and properties do not occur with changing temperature, then the cumulative filtrate volume will be inversely proportional to the square root of the viscosity. The viscosities of the water and 6% brine are shown over a range of temperature in Table 3.1<sup>8</sup>. It is evident that changes in temperature will have a substantial effect on filtrate volume because of changes in filtrate viscosity. However WBM and OBM filtrate viscosities have been studied and Figure 3.1 shows the comparison between Darley and Gray's<sup>8</sup> work on brine/water viscosity and the current work on filtrate viscosity.

Change in temperature may also affect filtrate volume through changes in the electrochemical equilibria which govern the degree of flocculation and aggregation of the clay particles, thus altering the permeability of the filter cake. As a result of such effects, filtrate volumes may be higher or lower than predicted from Larsen's equation<sup>116</sup> but are usually higher. Furthermore, the filter cake permeability has been tested in the current work for WBM and OBM using the Particle Size Analyser, which will be discussed in (chapter 5).

Chemical degradation of one or more components of the mud is a third mechanism by which high temperatures can affect filtrate properties. Many organic filtration control agents start to degrade significantly at temperatures above 212 °F, and the rate of degradation increases with further increase in temperature until filtration cannot be adequately maintained.

Jones et al.<sup>118</sup> found that both fluid loss and cake thickness increase with increase in temperature.

Bezemer et al.<sup>124</sup> found that the dynamic equilibrium filtration rate is independent of temperature change. The explanation is that if the temperature increases, and



accordingly the filtrate viscosity is reduced, the filtrate rate will increase giving rise to increased deposition of cake solids and increasing cake resistance (thickness).

**Table 3.1 Viscosities of Water and 6% Sodium Chloride Brine at Various temperatures<sup>8</sup>**

Temperature ( ° C)	Temperature ( ° F)	Viscosity of Water (cP)	Viscosity of Brine (cP)
0	32	1.792	-
10	50	1.308	-
20.2	68.4	1.000	1.110
30	86	0.801	0.888
40	104	0.656	0.733
60	140	0.469	0.531
80	176	0.356	0.408
100	212	0.284	-

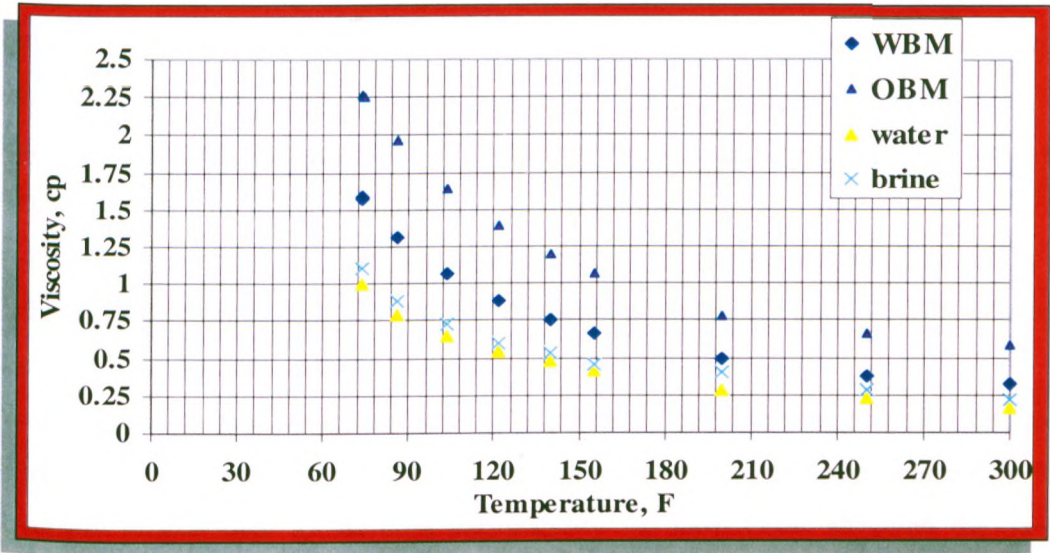


**Figure 3.1 Comparison between effect of temperature on mud filtrate, water and brine viscosities**

Accordingly the balance is maintained. It is unlikely that this will be true for all muds because the WBM and OBM tests show that increased in temperature increases the



dynamic filter cake erodability and equilibrium filtration rate. However Byck<sup>131</sup> found that, of six muds tested, the permeability of the cakes increased correspondingly, from  $2.2$  to  $4.5 \times 10^{-3}$  md (an increase of over 100%) and the permeability of the cakes for another three muds remained constant.

Hence the static and dynamic filtration models reported in this thesis take into account filter cake properties, filtrate viscosity and mud constituents and can be used to predict static and dynamic filtration under downhole conditions; Larsen's equation should be ignored.

### **3.1.1.3 The Effect of the Filter Medium**

The researchers on this subject have reached conflicting conclusions. Williams and Cannon<sup>132</sup> concluded that the filtration properties of muds are governed by the amount and size of solids in the mud, and therefore independent of formation permeability.

Larsen<sup>116</sup> published data in support of his claim that the filtration rates he obtained were independent of the filter bed materials used, namely compressed sand, natural sandstone, and filter paper.

Byck<sup>131</sup> measured fluid loss and the permeability of cake deposited on a range of filter materials with different muds, and concluded that:

1. Filter cake permeability does not depend upon the formation permeability.
2. Fluid loss does not depend upon the formation permeability but does depend upon the amount and nature of the mud solids.

Nowak and Krueger<sup>40</sup> suggested that it is primarily particle plugging that controls filtrate flow. Their results indicated that the cumulative volume seemed to be inversely proportional to the core permeability for most cases although the exact behaviour depends on the mud type. In some cases, this was due to higher spurt loss and in others to higher filtration rates. These experiments were performed with dynamic filtration. In addition, for static filtration using cores within a permeability

range of 744 md to 896 md, both spurt loss and cumulative filtrate were inversely proportional to core permeability.

Beeson and Wright<sup>120</sup> reported that although the type of filter paper used did not affect the fluid loss, it was greatly increased when sand cores acted as the filter medium. The following results were concluded:

1. The mud might give a negligible loss on filter paper, but give a large one on a permeable formation downhole.
2. The difference between the fluid loss on filter paper and on sand indicated that mud particles entered the pore channels prior to and during formation of the cake in the sand media.

Glenn and Slusser<sup>42</sup> concluded that the spurt loss increases with sample permeability and from the experimental volume-time data obtained during exposure of filter paper or a consolidated porous medium to a mud under differential pressure that there could be three stages involved in an experiment, viz.:

1. Mud spurt period – An initial period when mud particles bridged pores inside porous medium and initiated filter cake formation. Filtration rates were very high.
2. Non-uniform cake thickness period – An intermediate period during which filter cake build-up inside porous medium occurs and the differential pressure across the cake increases. Additional particles were “piled-up” behind the bridging particle or particles so that a “filter cake” was rapidly built up. Filtration rates were in continuous decline.
3. Constant pressure filtration period – A later stage in which pressure drop across the filter becomes constant. Filtration rates were constant.

Shremp and Johnson<sup>129</sup> divided the filtration process into two steps:

Step1: Bridging of openings in the filter medium.

Step 2: Filtration of fluid through the filter cake that developed on the filter medium as filtration takes place.

Horner et al.<sup>32</sup> measured fluid loss beneath the bit and found that it was dependent upon formation permeability since a permanent filter cake does not exist, and this was confirmed by Young and Gray<sup>31</sup>.

Ferguson and Klotz<sup>34</sup> reported that mud particle bridging and plugging limit the flow of filtrate to the formation even beneath the bit where no mud cake exists.

Simpson<sup>122</sup> simulated downhole conditions and observed higher dynamic fluid loss with low permeability cores (0.5 md) than with high permeability cores (500 md), which suggested an internal cake was deposited limiting filtration in high permeability cores. Meanwhile the thin sheet of filter paper used in the API test does not provide pore spaces where internal filter cake might start.

Peden et al.<sup>133</sup> reported that the filtrate loss is highly dependent upon core permeability for dynamic filtration.

Young and Gray<sup>31</sup> found that the filtration was independent of rock permeability, except in the case of synthetic media<sup>39</sup>.

Hall and Dollarhide<sup>119</sup> found that increasing rock permeability resulted in an increased spurt loss but the final filtration rates remained the same.

Dickey and Bryden<sup>134</sup> observed internal bridging by semi colloidal particles which were transported into the pore space where they bridged thus plugging pore throats and preventing further filtration.

The discrepancies were probably due to different experimental conditions used by individual researchers. The experimental results from the current work for WBM and OBM tested show that increasing permeability of natural cores will decrease filtration due to deposition of an internal cake limiting filtration, whereas increasing the permeability of synthetic cores increased the dynamic fluid loss, as also concluded by others<sup>40,132,135</sup>. However synthetic cores should be ignored for filtration experimental evaluation.

Therefore, the relationship between the pore size distribution of the filter medium and the particle size distribution in the mud will control, to a large extent, the amount of particle invasion into the filter and the time taken for a surface filter cake to be initiated. If the particle size in the mud is such that particles are capable of flowing

into the porous rock resulting in plugging, then the filtrate loss may be lower in a high permeability formation. However in low permeability formations, in which this cannot occur, an external filter cake will only be formed due to bridging and the fluid loss increases. If the particle size distribution of the mud is such that it provides good bridging for all permeabilities then the fluid loss will appear to be independent of filter medium permeability.

#### **3.1.1.4 The Effect of Annular Hydraulics on Dynamic Fluid Loss**

Although a number of researchers have studied dynamic filtration, few have attempted to evaluate the relationship between the hydraulics in the annular space and dynamic fluid loss. The following variables are involved in this relationship:

1. Annular fluid circulation velocity.
2. Fluid shear rate/shear stress on the surface of the cake.
3. Reynolds numbers in the annulus, which cover turbulent or laminar flow regimes in the annulus.

Larsen<sup>116</sup> reported that fluid loss is independent of circulation rate, provided it was not sufficient to remove the filter cake.

Williams<sup>126</sup> concluded that the dynamic filtration rate was proportional to the square root of the volumetric flow rate, and this was confirmed by Ferguson and Klotz<sup>34</sup>. They added that for cake erosion to occur, the hydrodynamic shear of the circulating mud must exceed the cake shear strength.

Prokop<sup>38</sup> concluded that the dynamic fluid loss was greater than static fluid loss. The reduction of dynamic filter cake thickness, due to erosion action of the flowing mud, leads to increased filtration rates compared with static filtration. He also indicated that the rate of cake erosion was approximately proportional to the square of the circulation velocity for turbulent flow.

Ferguson and Klotz<sup>34</sup> found that the initial dynamic filtration rate starts high, about the same as the rate of static filtration and thereafter the dynamic filtration rate becomes constant, whereas the static rate continues to decrease.

William<sup>126</sup> observed that the value of the equilibrium filtration rate was related to a constant thickness filter cake, which resulted from equilibrium between the deposition and the erosion of solids. This value is a function of mud circulation rate<sup>136</sup>.

Havenaar<sup>137</sup> reported the following:

1. A state of equilibrium was eventually reached, i.e., both cake thickness and filtration rate attained constant values.
2. The rate of shear at the cake surface is a good measure of the effect of mudflow on dynamic filtration.
3. The equilibrium filtration rate was found to be linearly proportional and the equilibrium cake thickness inversely proportional to the shear rate at the cake surface.

Peden et al.<sup>121,133</sup> reported that the statically deposited filter cake could be largely eroded during mud circulation. Also they observed that dynamic filtration rates decreased with increase in annular velocity when circulating KCL polymer mud. They suggest that the reason was that high annular velocities tended to erode the coarser particles and increase the deposition of the polymer chains, thus decreasing the permeability of the filter cake. This conclusion may only be restricted to Kcl polymer mud which was formulated without bentonite.

Bizanti<sup>138</sup> found that an increase in Reynolds number increased dynamic fluid loss. The dynamic filtration rate decreases if the rate of circulation is reduced.<sup>36</sup>

There appears to be no correlation between the API static filtrate and dynamic filtrate under borehole conditions.<sup>32,34,121,122,139-143</sup>

Fordham<sup>143</sup> reported the fluid loss in the dynamic phase varies with the tested mud systems at approximately the 0.60 power of shear rate.

WBM and OBM have been tested in the current study and the results show that with increasing shear rate, the dynamic fluid loss and dynamic filter cake erodability increases, while the cake thickness decreases for OBM significantly more than WBM.

### 3.1.1.5 The Effect of the Mud Constituents and Properties

Most of the published research in this area has been directed at understanding the relationship between the size distribution of the particulates in muds and the control of filtration through the establishment of a low permeability filter cake.

It appears that the permeability of the filter cake is the key parameter that controls both static and dynamic filtration. It more truly reflects downhole filtration behaviour than does any other parameter.

Cake permeability is, however, influenced by the kind of colloid as well as by the amount and size of particles. For instance, filter cakes of bentonite suspensions in fresh water have exceptionally low permeability because of the flat, filmy nature of the clay platelets, which enables them to pack tightly normal to the direction of filtrate flow.

Williams et al.<sup>132</sup> and Fisk et al.<sup>140</sup> indicated that drilling fluids containing clay form compressible filter cakes.

Larsen<sup>116</sup> reported that fluid loss was increased by calcium ion flocculation of the mud.

A wide range of particle sizes with a high percentage of colloids is conducive to fluid loss<sup>126,127,133,136</sup>. However a range of particle sizes sufficient to plug off the surface of the formation, limit particle invasion and initiate a filter cake of low permeability is also needed.

The degree of dispersion/flocculation and hydration of the clays present has considerable influence on filter cake permeability<sup>35,116,126,128,144,145</sup>. Clay flocculation results in more permeable filter cakes and hence increased filtration rates.

Bo et al.<sup>145</sup> concluded that cake porosity was affected by particle size and size distribution in a way analogous to the effect on permeability reported above. Minimum porosity was obtained when there was an even gradation of particle sizes, because the smaller particles then packed in the pores between the larger particles.



Early investigators of filtration behaviour measured cake permeability. Williams and Cannon et al.<sup>132</sup> obtained values between  $0.2$  and  $0.6 \times 10^{-3}$  md at 8-atmosphere pressure for Gulf Coast field muds, and  $72 \times 10^{-3}$  md for a West Texas mud.

Byck<sup>130</sup> measured permeabilities between  $0.46$  and  $7.42 \times 10^{-3}$  md at 34-atmosphere pressure with California muds. It was shown that the filtration rates depend only on the permeability of the filter cake.

Di Jio et al.<sup>142</sup> reported that oil based mud filter cakes consist primarily of water droplets stabilised by colloidal particles and emulsifiers. The results achieved in this current work show that OBM filter cakes have less resistance to shear than WBM. This is due to the fact that the filter cake structure is made from water droplets hence has less solids concentration, and is less resistant to shear rate than WBM cakes. New applications have been developed by the author using Particle Size Analyser which shows that the water droplet size  $< 4$  micron.

Gates and Bowie<sup>127</sup> measured the permeability of 20 field muds and 40 laboratory muds, and obtained values from  $0.31$  to over  $250 \times 10^{-3}$  md at 6.8-atmosphere pressure (100 psi). They correlated mud filtration properties against the particle size distribution in the mud and reported the following results:

1. The best filtration control was provided by mud composed of 65% colloids, 30% silt-size particles and 5% sand-size particles.
2. The poorest filtration control was observed in muds having a very low concentration of colloids.

This point, regarding the contribution of colloids to fluid loss control, was earlier suggested by Sawdon<sup>146</sup>, and Krubien et al.<sup>147</sup>

Prokop<sup>38</sup> reported that the filter cake deposited during continuous circulation would gradually decrease in permeability as long as the experiment continued. This was shown by a continual decrease in filtration rate after the filter cake had reached a constant thickness.

Glenn and Slusser<sup>42</sup> reported that the initiation of filter cake deposition and the consequent control of spurt loss are dependent upon mud particulate bridging against the pore throats of the porous medium. This bridge can take place inside or outside



the porous media. The bridging phenomenon and the presence of particles in the filtrate indicated that the spurt loss depends upon the particle size distribution of the mud and the pore entry size distribution of the porous medium.

Darley<sup>41</sup>, who confirmed the significance of the colloidal fraction on fluid loss control, has suggested from experimental measurements that this initial bridging process is accomplished in less than a second for many drilling fluids. Meanwhile he suggested that there was a crucial size range for bridging in the surface pores.

The rapid control of the fluid loss has been attributed to the presence of the bridging particles in the drilling fluid by several authors<sup>41,148,149</sup>. They investigated the effect of addition of sized particles to the mud to control spurt loss for rocks in the permeability range of 70-350 md and fluid particle sizes in the range of 1-6  $\mu\text{m}$  were effective.

The bridging process and spurt loss will therefore be characterised by the relationship between the mud particle and mean formation pore size as indicated by the results of Beeson and Wright<sup>120</sup>. Darley<sup>41</sup>, in a paper discussing productivity impairment, suggests that presence of a mixture of particle sizes with a range 2-150  $\mu\text{m}$  will bridge most formations. It has been reported that invasion due solely to the spurt loss period can extend to a depth of one inch in consolidated sandstone.

In addition McGuire et al.<sup>150</sup> questioned the validity of the 1/3 bridge rule when applied to  $\text{CaCO}_3$  / HEC suspensions. This rule was also found unsatisfactory by several other researchers.<sup>53-56</sup>

Wyant et al.<sup>134</sup> studied dynamic fluid loss measurement of oil mud additives for low-toxicity mineral oil. They found that the optimum fluid loss additives (FLA) at a concentration of 4 lb/bbl decreased static and dynamic fluid loss, while higher concentrations of polymer-based FLA increase dynamic fluid loss.

Fisk et al.<sup>140</sup> reported that the soluble FLA increases attractive forces during dewatering and makes the filter cake hard to erode under shear rate force.

Krueger<sup>36</sup> investigated the effect of several WBM fluid loss additives on API static fluid loss and compared results with the dynamic fluid loss volumes. The results

showed that there are various relationships between dynamic filtration rate and API static fluid loss for the different type of FLA [Figure 3.2]. Furthermore, the API fluid loss decreased continuously with an increase of all the fluid additives, but the dynamic rates decreased to a minimum, and then increased and there is no reason given.

The effect of three FLA mechanisms on WBM and OBM has been studied extensively in the current work and the results show that the difference between the effect of FLA on static and dynamic filtration depends on the type of FLA mechanism and concentration. This is due to the fact that dynamic fluid loss decreased then increased with increase FLA due to increase filter cake permeability and filter cake erodability at certain fluid loss concentration as will be discussed in chapter 5.

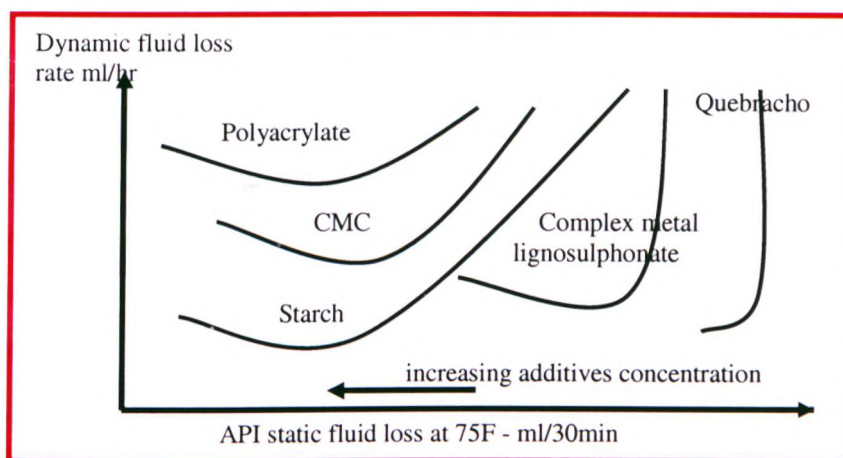


**Figure 3.2 Comparison of dynamic fluid loss rate with API fluid loss as a function of fluid loss additives concentration<sup>36</sup>**

Larsen<sup>116</sup> reported that fluid loss was inversely proportional to the one-half power of the filtrate viscosity.

Horner et al.<sup>32</sup> found no correlation between the rheology of the mud and the dynamic fluid loss. Fisk and Jamison<sup>125</sup> found that decrease in fluid rheology increased dynamic filtration rates for WBM and OBM. This discrepancy arose because Horner et al.<sup>32</sup> plotted rheology and dynamic filtration of different types of fluids (WBM and

OBM) and was trying to find trends between them. Actually each drill-in fluid has different rheological behaviour and should each be correlated separately in order to determine trends.

Prokop<sup>38</sup> suggested that the rheology is significant and that it influences the flow regime in the annulus for dynamic filtration.

The addition of diesel oil into water-based mud decreased the API static filter loss<sup>36,144,151,152</sup>, but increases the dynamic fluid loss.<sup>36,145,152</sup>

The addition of 3 to 13 % by volume oil to WBM has been tested in the current work and led to decreases of the static and dynamic fluid loss. These discrepancies may be because the rheology of the mud mixed by the other researchers is very low which could affect the results achieved.

Peden et al.<sup>121,133</sup> found that the presence of barite in the mud results in more permeable, less compressible filter cakes, reduction in fluid loss and increase in cake thickness.

Sharma et al.<sup>144</sup> and Black et al.<sup>152</sup> reported that increased concentration of barite and other weighted material in the mud results in more permeable, less compressible filter cakes and increased fluid loss and cake thickness.

These discrepancies are probably because of different experimental conditions used by various researchers. Peden et al.<sup>121,133</sup> used WBM with solids concentration of 10% and other researchers used WBM with solids concentration ranging from 4 to 20% by volume.

However, WBM has been tested in the current work with solids concentration ranges from 6 to 20 % by volume and it was found that the results agree with Sharma et al.<sup>144</sup> and Black et al.<sup>151</sup>. Furthermore a critical solids concentration of 11% was observed where cake permeability and fluid loss increases. OBM shows that increase in solids concentration decreases cake permeability. Furthermore, from practical experience there is a critical ratio between clay and barite concentrations for WBM; above this ratio the mud properties and the fluid loss increase.

Plank et al.<sup>139</sup> reported that the starch polymer forms characteristic bridges within filter cake pores. PAC polymer is absorbed into the edge of clay platelets and forms

few bridges. Furthermore, synthetic HT-polymer was imaged extending into the pore space.

The potential use of the Scanning Electron Microscope technique for evaluating filter cakes has been reported<sup>151</sup>. However the use of such a technique has highlighted the complex structure of both mud additives and filter cake properties.<sup>139,141,153-157</sup>

### **3.2 KEY PARAMETERS FOR FILTRATION MECHANISMS**

The key parameters that govern filtration mechanisms under downhole conditions are as follows:

1. Cake characteristics:
  - a. Filter cake thickness
  - b. Cake mass ratio
  - c. Filter cake porosity
  - d. Filter cake permeability
  - e. Density of cake solids
  - f. Filter cake pore size (function of size, shape, and distribution)
2. Viscosity of filtrate
3. Density of filtrate
4. Shear rate and shear stress

The shear rate and shear stress are functions of hole size, mud viscosity, mud type, etc. under downhole conditions. However a specific rheological model of mud type should be determined under existing application conditions.

5. Mud constituents and properties:
  - a. Mud type and mud density
  - b. Mud particle (function of size, shape, and distribution)
  - c. Fluid loss additives (FLA) mechanisms
6. Time
7. Temperature

8. Differential pressure (function of mud weight and pore pressure)
8. Filter medium characteristics:
  - a. Formation type
  - b. Morphological characteristics (including permeability, porosity, pore size distribution, etc).
  - c. Filtration area

In order to achieve a better understanding for filtration mechanisms therefore, the best filtration models which take all these parameters into account and develop the functional relationships between time, flow rate, pressure, temperature, mud constituents and shear rate will be selected.

### 3.3 FLOW THROUGH THE FILTER CAKE AND POROUS FORMATION

A simplified model of cake filtration is the handling of the permeability of a bed of porous material. While cake filtration is concerned with the passage of liquid through a porous medium with continually increasing thickness, permeability deals with the passage of liquid through a porous bed of fixed dimensions. Most of the existing mathematical models of the filtration were adapted from the basic Darcy's law equation.

The linear flow Darcy<sup>158</sup> equation is given as:

$$q = \frac{KA\Delta P}{\mu L} \quad (3.1)$$

Where:

- q - flow rate of fluid
- A - cross-sectional area
- $\Delta P$  - differential pressure over filter bed
- $\mu$  - fluid viscosity
- K- permeability of porous rock
- L - length of filter bed



### 3.4 DERIVATION OF FILTRATION EQUATION

#### 3.4.1 Static Filtration

Using Darcy's law for flow through a porous bed, Sperry<sup>159</sup> showed that the filtration resistance consists of two parts in series (the cake and the medium). Ruth<sup>160,161</sup> first recognised the parabolic nature of the filtrate volume against time plot and the assumption that the cake resistance is directly proportional to the amount of cake solids deposited and yields the so-called "classical" static filtration equation (3.2).

$$t = \frac{\mu \alpha \rho_f s}{2(1 - ms) A^2 \Delta P} V^2 + \frac{\mu R_m}{A \Delta P} V \quad (3.2)$$

Where:

$t$  – time,  $V$  = volume of filtrate,  $\mu$  - filtrate viscosity,  
 $\Delta P$  - differential pressure,  $m$  - ratio of mass of wet cake to mass of dry cake,  
 $\alpha$  - specific cake resistance,  $R_m$  - filter medium resistance  
 $s$  - mass fraction of solids in the slurry,  $\rho_f$  - filtrate density  
 $A$  - cross-sectional area of filter cake

This equation is only valid on condition that the filter cake is incompressible and the differential pressure across the cake is constant. In fact, in drilling engineering the filter cake formed from the mud is compressible. It is understood that the pressure differential across the cake at the initial stage of the filtration process increases from zero to maximum while the pores of the filter medium are plugged and bridged and/or the first layer of the filter cake is forming. It is clear therefore that the assumption of constant pressure filtration is approximate. The equation needs to be modified before it can be used for predicting drilling fluid filtration under downhole conditions.

Since cake permeability is defined as the ease with which liquid is passed, cake resistance is conversely defined as the difficulty with which liquid is passed. Thus

$$K = \frac{1}{R} = \frac{1}{\alpha}$$



The modified Darcy equation is:

$$\frac{dV}{dt} = \frac{K A P}{\mu L} = \left(\frac{1}{\alpha}\right)\left(\frac{A P}{\mu L}\right) \quad (3.3)$$

Where  $\alpha$  is the cake resistance. If it is assumed that each layer of cake as deposited is identical, then  $L$  may be replaced as follows: cake volume =  $LA = f V$  where  $f$  is the volume of cake produced per unit volume of filtrate,  $A$  is the cross sectional area and  $V$  is total of filtrate.

$$\text{Then } L = \frac{fV}{A} \quad \text{and} \quad (3.4)$$

Substitute  $L$  in equation (3.4) into (3.3), then:

$$\frac{dV}{dt} = \frac{A^2 P}{\alpha \mu f V} \quad (3.5)$$

For a constant pressure filtration, we may rearrange and integrate, thus

$$t = \frac{\alpha \mu f}{2PA^2} V^2 \quad (3.6)$$

This is the equation for a parabola. Early attempts to use this equation to correlate time- volume filter discharge data met with little success because the equation fails to take into account the resistance of the filter medium. Assuming that the filtration resistance consists of two parts in series (the cake and the medium), both of which follow the Darcy equation, the following was derived:

$$\frac{dV}{dt} = \frac{PA^2}{\mu(\alpha fV + R_m A)} \quad (3.7)$$

Here  $R_m$  is the resistance of the filter medium while  $\alpha$  is the resistance of the cake.

Integration at constant pressure gives:

$$t = \frac{\alpha \mu f}{2PA^2} V^2 + \frac{\mu R_m}{PA} V \quad (3.8)$$

Or

$$\frac{t}{V} = \left( \frac{\alpha \mu f}{2PA^2} \right) V + \frac{\mu R_m}{PA} \quad (3.9)$$

Equation (3.9) has been arranged to conform with the standard equation for a straight line,  $y = mx + b$ . Thus when  $\frac{t}{V}$  is plotted versus  $V$ ,  $\alpha\mu f / 2PA^2$  may be equated with the slope,  $m$  to evaluate  $\alpha$  and  $\mu R_m / PA$  with the  $y$  intercept,  $b$ , to evaluate filter medium resistance,  $R_m$ . In rearranged equation form:

$$\alpha = 2mPA^2 / \mu f \quad (3.10)$$

and

$$R_m = bPA / \mu \quad (3.11)$$

The Sperry filtration rate equation adequately relates the principal variables in a cake filtration and is valid only for incompressible filter cakes.

The assumption of equation (3.4) could be obtained from a macroscopic mass balance: Weight of Slurry = Weight of Wet Filter Cake + Weight of Filter

Or symbolically:

$$\frac{W_s}{s} = \frac{W_s}{s_c} + \rho_f V \quad (3.12)$$

Where:  $W_s$  - solids weight as laid on filter medium

$\rho_f$  - the density of filtrate

$s, s_c$  - the solids fraction in slurry and filter cake respectively

Comparing equation (3.4) with equation (3.12), then

$$f = \frac{\rho_f s}{1 - ms} \quad (3.13)$$

Where:

$m = 1/s_c$  the ratio of weight of wet filter cake to dry filter cake.

Then equation (3.9) becomes:

$$t = \frac{\mu \alpha \rho_f s}{2(1 - ms)A^2 \Delta P} V^2 + \frac{\mu R_m}{A \Delta P} V \quad (3.14)$$

For compressible filter cake the basic filtration equation can be modified to allow for variation in  $\alpha_{avg}$  and  $\phi_{avg}$  in the initial stages of filtration. The above equation is then rewritten to include a correction term yielding:

$$t = \frac{\mu\alpha_{avg}\rho_f s}{2(1-ms)A^2\Delta P}V^2 + \frac{\mu R_m}{A\Delta P}V + t_0 \quad (3.15)$$

The spurt volume and spurt time can be subtracted from the data of cumulative filtrate volume versus time. Filtration then commences with solids already deposited in the pores and on the surface of the filter medium.

$$t - t_{sp} = \frac{\mu\alpha_{avg}\rho_f s}{2(1-ms)A^2\Delta P}(V - V_{sp})^2 + \frac{\mu}{A\Delta P}(R_m + R_{sp})(V - V_{sp}) + t_0 \quad (3.16)$$

Where  $V_{sp}$  is the spurt volume and  $R_{sp}$  is the resistance of solids deposited during the spurt period of duration  $t_{sp}$ .

Putting:

$$t - t_{sp} = t' \quad a_1 = \frac{\mu}{A\Delta P}(R_m + R_{sp}) \quad (3.17)$$

$$V - V_{sp} = V' \quad a_2 = \frac{\mu\alpha_{avg}\rho_f s}{2A^2(1-ms)\Delta P} \quad (3.18)$$

$$\text{Gives:} \quad t' = a_2 V'^2 + a_1 V' + t_0 \quad (3.19)$$

This is the modified static filtration equation can be used for drilling fluids.

The modified static filtration equation is then used to fit experimental data points  $V - t$  and by using the least squares second order polynomial method the values of the static filtration coefficients  $t_0$ ,  $a_1$  and  $a_2$  are obtained and the static filter cake characteristics can be described for lignosulphonate and synthetic oil based muds as will be discussed in (chapter 6).

From the modified static filtration equation then the cake characteristics can be described as follows:

1. Average specific cake resistance:

$$\alpha_{avg} = \frac{2\Delta PA^2(1-ms)}{\mu\rho_f s} a_2 \quad (3.20)$$

2. Effective filter medium resistance:

$$R_{meff} = \frac{\Delta PA}{\mu} a_1 \quad (3.21)$$

3. Average cake porosity ( $\phi_{avg}$ ):

$$\phi_{avg} = \frac{(m-1)}{(m-1) + \frac{\rho_f}{\rho_s}} \quad (3.22)$$

4. Average cake permeability ( $k_{avg}$ ):

$$K_{avg} = \frac{1}{\rho_s (1 - \phi_{avg}) \alpha_{avg}} \quad (3.23)$$

The above equations can be used to determine the average cake porosity and average cake permeability based on the ratio of wet to dry filter cake mass, average filter cake resistance, the density of the filtrate and solids, which can be obtained experimentally chapter 6.

### 3.4.2 Dynamic Filtration Equation

The modelling of drilling fluid filtration mechanisms is based on the following assumptions:

1. The weight of eroded solids from the cake is proportional to the duration of circulation, the filter cake area, and the shear stress on the filter cake surface if the mud is circulated.

2. Filter cake build-up is a continual process of deposition and erosion, and these actions occur simultaneously.
3. Flow through the filter cake is laminar, which implies that Darcy's law applies.
4. The filter medium resistance is constant through out the whole filtration process.

In Figure 3.3, if the eroded mass of solids is expressed in terms of equivalent filter cake mass, the external mass balance can also be used:

$$W = W_c + W_e \quad (3.24)$$

Where:

$W_c$  = Filter cake weight per unit area ( $\text{Kg/m}^2$ )

$W_e$  = Eroded solid weight per unit area ( $\text{Kg/m}^2$ )

$W$  = cumulative deposited solids (filter cake) weight per unit area ( $\text{Kg/m}^2$ )

According to the above assumption, we may express  $W_e$  as:

$$W_e = K_\tau \tau t \quad (3.25)$$

Or:

$$W_e = B t \quad (3.26)$$

Where:

$t$  – time,  $B$  - dynamic filtration coefficient

$\tau$  - shear stress on filter cake surface,  $K_\tau$  - dynamic filtration erodability coefficient

$K_\tau$  - is defined as the eroded solid mass per unit of shear stress on a unit of filter cake surface area.

Writing the external mass balance:

$$\frac{W}{s} = \frac{W}{s_c} + \rho_f \frac{V}{A} \quad (3.27)$$

Solving equation (3.27) for  $W$ , we obtain:

$$W = \frac{\rho_f s}{1 - ms} \frac{V}{A} \quad (3.28)$$

Where:  $m = \frac{1}{s_c}$

Substituting  $W_e$  in equation (3.26) and equation (3.28) for  $W$  , then  $W_c$  in equation (3.24), becomes:

$$W_c = \frac{\rho_f s}{1 - ms} \frac{V}{A} - K_r \tau t \quad (3.29)$$

Or  $W_c = \frac{\rho_f s}{1 - ms} \frac{V}{A} - Bt \quad (3.30)$

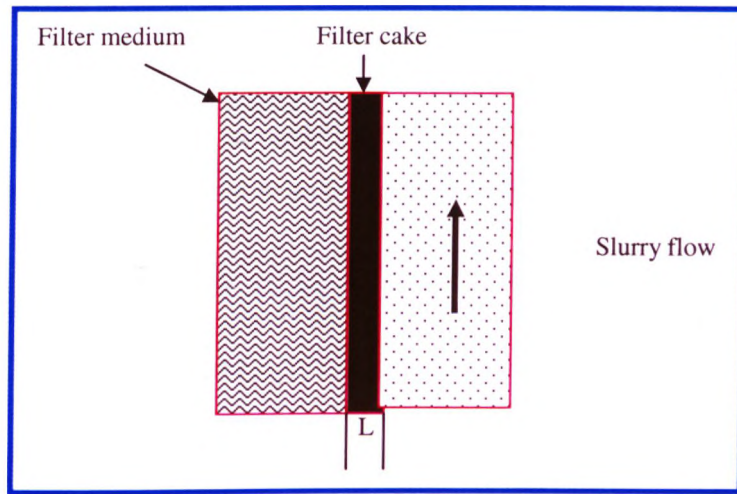


Figure 3.3 Relationship between filter cake and cumulative deposited cake

Applying Darcy's law:

$$q = \frac{\Delta P}{\mu R} = \frac{\Delta P}{\mu(R_c + R_m)} \quad (3.31)$$

The filter cake resistance  $R_c$  is defined as:

$$R_c = \alpha W_c \quad (3.32)$$



Where  $\alpha$  is the specific cake resistance. Therefore, combining equation (3.30) and equation (3.32) for  $R_c$  and inserting into equation (3.31) and by rearrangement, we get:

$$\frac{dt}{dV} = \frac{\mu \alpha \rho_f s}{\Delta P A^2 (1 - ms)} V - \frac{\mu \alpha K_\tau \tau}{\Delta P A} t + \frac{\mu R_m}{\Delta P A} \quad (3.33)$$

This equation is a first order non-homogeneous linear differential equation, if all the terms on the right handside, except  $t$  and  $V$ , are assumed to be constant with time. Solving for  $t$  versus  $V$  with the boundary condition  $V = 0$  when  $t = 0$ , we can get:

$$t = C_1 V - C_2 (1 - e^{-C_3 V}) \quad (3.34)$$

Peng<sup>162</sup> gave the details of solution of equation (3.34).

However, equation (3.34) should be modified before it can be used. The spurt volume and spurt time should be subtracted from cumulative filtrate volume vs. time. Then it becomes:

$$t' = C_1 V' - C_2 (1 - e^{-C_3 V'}) + t_0 \quad (3.35)$$

$$\text{Where: } C_1 = \frac{\rho_f s}{(1 - ms) A K_\tau \tau} \quad (3.36)$$

$$C_2 = \frac{\Delta P \rho_f s}{(1 - ms) \mu \alpha K_\tau^2 \tau^2} - \frac{R_m}{\alpha K_\tau \tau} \quad (3.37)$$

$$C_3 = \frac{\mu \alpha K_\tau \tau}{\Delta P A} \quad (3.38)$$

By fitting the dynamic filtration experimental data points  $V$  vs.  $t$  to equation (3.35) and using the least squares non-linear regression method then the dynamic filtration coefficients  $C_1$ ,  $C_2$ ,  $C_3$ , and  $t_0$  are obtained and dynamic filter cake characteristics can be described for lignosulphonate and synthetic oil based muds as will be discussed in chapter 6.

### 3.5 APPLICATION OF THE FILTRATION EQUATION

#### 3.5.1 Static Filtration Equation

Equation (3.33) is the general equation of filtration, which applies to both static and dynamic filtration. It is apparent that if  $\tau = 0$ , then equation (3.33) can be integrated, then:

$$t = a_2 V^2 + a_1 V \quad (3.39)$$

This is the classic static filtration equation.

#### 3.5.2 Erodability of Dynamically Deposited Cake

Differentiating equation (3.34) on both sides with respect to time:

$$1 = C_1 \frac{dV}{dt} - C_2 C_3 e^{-C_3 V} \frac{dV}{dt} \quad (3.40)$$

By rearranging the above equation:

$$\frac{dV}{dt} = \frac{1}{C_1 - C_2 C_3 e^{-C_3 V}} \quad (3.41)$$

When  $t \rightarrow \infty$ ,  $V \rightarrow \infty$ , then  $e^{-C_3 V} \rightarrow 0$ ,  $\left. \frac{dV}{dt} \right|_{eq} = \left. \frac{dV}{dt} \right|_{\substack{t \rightarrow \infty \\ V \rightarrow \infty}} \rightarrow \frac{1}{C_1}$ , therefore:

$$q_{eq} = \frac{1}{A} \left. \frac{dV}{dt} \right|_{eq} = \frac{1}{AC_1} = \frac{(1 - ms)B}{\rho_f s} \quad (3.42)$$

$q_{eq}$  is defined as the dynamic equilibrium filtration rate.

By combining equation (3.25) and equation (3.26), it is obtained:

$$B = K_\tau \tau \quad (3.43)$$

Inserting equation (3.43) into equation (3.42), we obtain:

$$q_{eq} = \frac{(1 - ms)K_\tau \tau}{\rho_f s} \quad (3.44)$$

Equation (3.44) represents the relationship between the dynamic equilibrium filtration rate and shear stress on the filter cake surface. From equation (3.44), we can get:

$$K_r = \frac{\rho_f s}{(1 - ms)\tau AC_1} \quad (3.45)$$

The static and dynamic filtration equations (3.19) and (3.35) combine all the most important parameters that governing the static and dynamic filtration processes. These two equations have been modified in an empirical form in chapter 6 to predict static and dynamic filtration under downhole conditions. An attempt has also been made to predict dynamic filtration from static filtration data. Since the modified filtration equations can predict the static and dynamic filtration coefficients such as ( $a_1, a_2, C_1, C_2$ , and  $C_3$ ) therefore the filter cake characteristics such as cake resistance, permeability, porosity, etc. can be computed and described for the WBM and OBM.

### 3.6 REVIEW OF DRILLING FLUIDS FILTRATION

Earlier published papers on cake filtration, in which the investigators concentrated their efforts to obtain relationships between flow rate, applied pressure, and mud constituents for compressible filter cakes, will now be briefly reviewed.

Almy and Lewis<sup>163</sup> derived from experiments a formula of filtration for any particular fluid:

$$q = \frac{1}{A} \frac{dV}{dt} = k \frac{P_a^m}{V^n} \quad (3.46)$$

Where:  $k, m$ , and  $n$  - constant for any experiment

$dV/dt$  - the rate of discharge of liquid through the cake

$m$ - an exponent of  $P$  varying with nature of the solids

$n$ - an exponent of  $V$  depending upon the solids

Flow rate is proportional to  $P^m$ . The superscript  $m$  was defined as the compressibility coefficient, having values from zero to 0.50. Incompressible fluids have  $m = 0.50$  while for compressible fluids, the value is less than 0.50.

Baker<sup>164</sup> reported an equation called “the fundamental law of filtration” of the form:

$$\frac{dV}{dt} = \frac{C A^2 P_a^m}{V^n} \quad (3.47)$$

Where:

$C$  is proportionality constant, depending upon the nature of the sludge

Wiber and Harshey<sup>165</sup> produced the rate equation of the form:

$$q = \frac{1}{A} \frac{dV}{dt} = \frac{P_a A}{\alpha \mu C V} \quad (3.48)$$

Carman<sup>166</sup> modified Kozeny's equation in the form:

$$q = \frac{1}{A} \frac{dV}{dt} = \frac{\phi^3}{(1-\phi)^2 k_z S_0^2} \frac{\Delta P}{\mu L} \quad (3.49)$$

Where:  $\phi$  - porosity of the filter cake,  $k_z$  - Kozeny's constant

$S_0$  - specific surface area of solids, i.e., surface area per unit volume of solid

According to Darcy's law, the permeability coefficient should be:

$$K = \frac{\phi^3}{(1-\phi)^2 k_z S_0^2} \quad (3.50)$$

Williams and Cannon<sup>20</sup> predicted the static filtration of drilling fluids.

$$\frac{V}{A} = \sqrt{M_w t + C_w^2 - C_w} \quad (3.51)$$

Where:

$$M_w = \frac{2 \Delta P_c^{1-s}}{\mu \nu R (1-s)} \quad (3.52)$$

$$C_w = \frac{A \rho f (\Delta P_c)}{\nu R \Delta P_c^s} \quad (3.53)$$

Where:  $w$  - subscript represents Williams

$s$  - a compaction function of the cake,  $R$  - a function of resistivity of the cake

$\Delta P_c$  - pressure drop across cake

$v$  - ratio of volume of filter cake to volume of filtrate

$\rho f(P)$  - a function of the resistance of the filtration medium

$\rho$  - resistance coefficient of filtration medium and sludge contained therein

Williams found that filtration rate during dynamic conditions became constant after a short time and this constant rate attained in any particular test depended on the pressure, rate of mud circulation, and mud properties. The equilibrium filtration rate:

$$q_{eq} = \frac{1}{A} \frac{dV}{dt} \Big|_{eq} = C_w \sqrt{QM_w} \quad (3.54)$$

Where:  $Q$  - mud flow rate,

$C_w$  - empirical constant

$M_w$  - determined in equation (3.52)

Williams also extended equation (3.51) for borehole radial filtration as:

$$V = \frac{2\pi L \Delta P_c^{1-s}}{\mu R (1-s)} \quad (3.55)$$

Larsen<sup>116</sup> developed a static filtration equation for incompressible cake from Darcy's

law: 
$$V = k_L \sqrt{\frac{P R_L t}{\mu}} \quad (3.56)$$

Where:  $R_L = \frac{V_{filtrate}}{V_{cake}}$  Ratio of filtrate volume/volume of deposited solid;

$k_L$  - Constant for specific mud

Larsen<sup>116</sup> further investigated the validity of the above equation by varying the applied differential pressure. It can be seen from equation (3.56) that  $V$  should be proportional to the square root of the differential pressure; however, the experimental results showed that the following relationship was valid:

$$V = k_L P^x \quad (3.57)$$

Where  $x < 0.5$  and could be evaluated from the log-log plot of volume versus pressure. Further, Larsen also studied the effect of temperature on the cumulative filtrate volume and proposed that:

$$\frac{V(T_2)}{V(T_1)} = \sqrt{\frac{\mu(T_1)}{\mu(T_2)}} \quad (3.58)$$

Where  $V$  and  $\mu$  are the cumulative filtrate volume and filtrate viscosity at temperature  $T_1$  and  $T_2$  respectively.

Glenn and Slusser<sup>42</sup> used the classic static filtration equation to evaluate the filtration characteristics of drilling muds in the form:

$$\frac{t}{V} = M_G V + N_G \quad (3.59)$$

Where:

$M_G$  - a coefficient defined by physical characteristics of the mud filter cake and conditions imposed during filtration

$N_G$  - a constant defined by the fluid flow characteristics of filter medium

They considered that the septum resistance is very small compared to cake resistance.

It was then neglected without appreciable error. Then equation (3.59) becomes:

$$\frac{t'}{V'} = M_G V' \quad (3.60)$$

Hassen<sup>167</sup> proposed a series of equations to predict the filtration as follows:

$$q = C_1 t^{0.5} \quad (3.61)$$

Where:  $q$  - filtrate flow rate per unit area

$C_1$  - static filtration rate constant

Equation (3.61) represents filtration under constant temperature and pressure conditions. In order to include the effect of temperature, it is compensated for by a factor as shown in equation (3.62):

$$q_2 = q_1 \exp \left[ \frac{B(T_2 - T_1)}{2T_2 T_1} \right] \quad (3.62)$$



Where:  $B$  – viscosity constant for Newtonian fluid

He believed that the effect of temperature is caused by the change of filtrate viscosity.

The effect of pressure on filtrate flow rate considered is described by equation (3.63):

$$q_2 = q_1 \left( \frac{\Delta P_2}{\Delta P_1} \right)^p \quad (3.63)$$

Where:  $p$  – pressure correction exponent for filter cake.

If the filter cake is incompressible,  $p$  is 0.5. In fact, in most cases,  $p$  is less than 0.5.

Bezemer and Havenaar<sup>124</sup> reported the relationship between equilibrium filtration rate and rate of shear at the cake surface could be given by:

$$\left. \frac{1}{A} \frac{dV}{dt} \right|_{eq} = q_{eq} = C_B \gamma \quad (3.64)$$

Where:  $eq$  – subscript referring to equilibrium conditions

$C_B$  - constant for specific mud,  $\gamma$  - rate of shear at the cake surface

$$\frac{Pt}{V/A} = \left( \frac{\mu \alpha}{2} \right) V/A + \mu r \quad (3.65)$$

Plotting  $(Pt)/(V/A)$  vs.  $(V/A)$  should yield a straight line an intercept of  $(\mu r)$  and slope of  $(\mu \alpha/2)$ .

Havenaar<sup>168</sup> derived the following equation for filtration through the bottom of the hole while drilling:

$$Q = \frac{\pi D^2}{4} \sqrt{\left( \frac{nm}{C} \right)} \quad (3.66)$$

Where:

$Q$  - filtration rate in  $\text{cm}^3/\text{sec}$ ,

$D$  - annulus diameter

$n$  - the number of cones on a bit rotating at,  $m$ , times per second and  $C$  can be determined from equation (3.67)

$$C = \frac{2 K P Q_w}{\mu \mu Q_c} \quad (3.67)$$

Where:

$Q_c$  = volume of cake,

$Q_w$  = volume of filtrate

He compared the filtration rates calculated by this equation. The poor correlation obtained with oil-base mud is probably because cakes of oil-base muds are easily eroded and also equation (3.66) neglects erosion by mud jets.

Martins et al.<sup>169</sup> recently proposed the following equation to predict the static filtration as follows:

$$t = \left( \frac{h}{k_f} V + \frac{V^2}{2AK_c} \left( \frac{1-s}{s} \right) \left( \frac{1}{1-\phi} \right) \right) \frac{\mu}{\Delta PA} \quad (3.68)$$

Where:

$K_f$  – formation permeability

$K_c$  – cake permeability

## **CHAPTER FOUR**

### **THE EXPERIMENTAL STUDIES AND QUALITY CONTROL PROCEDURES**

The experimental programme was designed to identify the effects of a number of key parameters that govern the fluid rheology, the filtration process, and formation damage mechanisms, to generate a database from controlled experimental studies at different operating conditions in order to develop theoretical models.

This chapter presents material analysis, which includes brief descriptions of mud system selection, composition, mud testing procedures, results and quality control testing techniques. The API oil-based mud mixing procedure has been modified and new major testing technique using Particle Size Analyser for optimum emulsifier selection and particle size classification for filter cakes has been established. The main experimental facilities are also described and presented. Core preparation and extensive experimental analysis has been carried out on Clashach sandstone morphological characteristics and a number of approximate correlations have been established and validated with experimental and external field data. These correlations have been incorporated into design criteria to classify the fluid flow regimes in porous media and a quality control approach has been established for formation damage testing procedures.

#### **4.1 MATERIALS PREPARATION AND ANALYSIS**

##### **4.1.1 Mud System Analysis**

###### **4.1.1.1 Mud System Selection**

Two commonly used types of HP-HT inhibitive drilling fluids have been selected and tested, viz:

1. Synthetic oil-based mud (oil/water ratio of 75/25).
2. Lignosulphonate water-based mud.

OBM and WBM were formulated with 9, 11 and 13 ppg (pounds per gallon) mud weight in each case and loaded with drilling solids of 35 lbs/bbl (pounds per barrel) in

order to represent the typical wellbore conditions, mixed in a Silverson mixer and tested using API Standards<sup>170-172</sup> and developed modified methods.

#### 4.1.1.2 Mud System Composition

The compositions of the two HP-HT muds used are listed in Tables 4.1a and 4.1b.

The main components and their function are presented in Tables 4.2a and 4.2b.

Emulsion-based mud prepared by the addition of diesel to the lignosulphonate mud was also tested.

**Table 4.1a Composition of Mud System 1: Lignosulphonate Water Base Mud**

COMPONENT (9.2, 11, 13 PPG MUD WEIGHT)	BRAND	CONCENTRATION (LBS/BBL)
Fresh Water	-	322.46, 298.86, 273.01
Non Treated Bentonite	BENTONITE	15
Caustic Soda	CAUSTIC SODA	1.5
HT-Fluid Loss Agent	RESINEX	3
High Viscosity-PAC	POLYPAC-R	1
Weighting Agent	BARITE	20, 100.32, 210.21 respectively
Thinner	SPERSENE	4
HT-Stabiliser	LIGNITE	4
Drilled Solids	DRILLED SOLIDS	35

**Table 4.1b Composition of Mud System 2: Synthetic Oil Base Mud**

COMPONENT (9, 11, 13 PPG MUD WEIGHT)	BRAND	CONCENTRATION (LBS/BBL)
Base Oil	NOVATEC-B	172.79, 156.57, 140.34
HT-Clay	VERSAGEL-HT	7
Brine (water + calcium chloride)	Brine (water + calcium chloride)	(77.06+27.86), (70.23+25.39), (63.40+22.9)
Primary Emulsifier	NOVATEC-P	6
Secondary Emulsifier	NOVATEC-S	3
Lime	LIME	5.5
Fluid Loss Agent	NOVATEC-F	3
Weighting agent	BARITE	41.07, 150.79, 260.51
Drilled Solids	DRILLED SOLIDS	35

**Table 4.2a Brief Description of HP-HT Mud Component**  
**Mud System 1: Lignosulphonate Water Base Mud**

COMPONENT	DESCRIPTIONS
WYOMING BENTONITE	Mainly sodium montmorillonite clay used primarily to impart rheological properties to the mud and to control fluid loss by the formation of filter cakes of low permeability
CAUSTIC SODA	Sodium hydroxide used for increasing pH to activate chemicals functions
POLYTEMP*	Polymeric dispersant of sodium salt, HT-fluid loss control as viscosifying agent
RESINEX*	Synthetically formed sulfonated lignite with resin used as HT-fluid loss control, coating agent and rheology stabiliser
POLYPAC-R	Polyanionic cellulose polymer, a more refined cellulose which gives viscosity and fluid loss control
BARITE	Barium sulphate used for increasing density
SPERSENE *	Thinner, shale inhibitor, fluid loss control, emulsifier and an excellent rheology stabiliser at HT
CHROM-LIGNITE*	HT-fluid loss, thinner and rheology stabiliser at HT
DRILLED SOLIDS	75 micron sized calcium carbonate and OCMA clay

\*Trademark of M-I L.L.C

**Table 4.2b Brief Description of HP-HT Mud Components**

**Mud System 2: Synthetic Oil Base Mud**

COMPONENT	DESCRIPTIONS
NOVATEC-B*	LAO base liquid, continuous phase (Linear Alpha Olefin $C_{14}C_{16}$ )
NOVATEC-P*	Modified calcium salts of higher organic acids, used as primary emulsifier of water in oil
NOVATEC-S*	Oil soluble surfactant, used for primary oil wetting of solids and emulsion stability
CALCIUM CHLORIDE	Water phase activity ( $CaCl_2$ )
LIME	Calcium hydroxide, used as a source of alkalinity and to activate primary and secondary emulsifiers
NOVATEC-F*	Surfactant blend in organic solvent, used for primary fluid loss control as particle coating agent
GILSONITE*	Organophylic lignite colloidal particle, used for primary fluid loss control as plugging agent
ECOTROL*	Methyl styrene acrylate resin, used for primary fluid loss control as viscosifying agent
VERSAGEL-HT*	High performance blended clay, used for primary viscosifying to impart HT-rheological properties and to control fluid loss by the formation of filter cakes of low permeability
DRILLED SOLIDS	75 micron sized calcium carbonate and OCMA clay

\*Trademark of M-I L.L.C



#### 4.1.1.3 Mud System Preparation

To maintain high quality testing results the following steps have been followed:

1. Mix the required mud volume from the same chemical-manufacturing batch.
2. Mix the required mud volume in one mixing batch.
3. Ensure that the quality control testing procedure has been applied.

All the muds were mixed in batches of 1400 ml (4 “lab barrels”), and because large volumes were required, separated batches were mixed and combined before testing.

Mixing was undertaken in a 2 litre conical metal jug in a standard Silverson mixer fitted with a high shear square hole screen. A cold water bath was used throughout to prevent excessive heating (maximum 150 °F). The mixing heads were positioned appropriately to ensure adequate mixing at height of 1-2 inches above the base of the container, being raised if required such as during the addition of barite. The mixer speed was maintained at 6000 rpm throughout the mixing, checking it at intervals with a tachometer.

##### 4.1.1.3.1 Laboratory Mixing of Fresh Water Lignosulphonate Mud

The list of components in Table 4.3 is the order in which the chemicals were added over a total time interval of 1 hour and the following is a summary of the procedure:

1. Add WYOMING BENTONITE gradually to the fresh water whilst stirring with a Silverson mixer. The mixture then can be left for 16 hours to allow the bentonite to pre-hydrate.
2. Mix for 5 minutes and adjust pH to 10.5 with caustic soda.
3. Add POLYPAC-R and RESINEX slowly over a 4-minute period, ensuring that all polymers were completely dispersed and that none adheres to the sides of the mixing vessel or the mixer shaft. Mix for a further 6 minutes.
4. Add the weighting material (BARITE) gradually over a 2-minute period. Mix for a further 8 minutes.
5. Add dispersants (SPERSENE and LIGNITE) slowly over a 5-minute period. Mix for a further 5 minutes. Adjust pH to 10.5 with caustic soda if necessary.

6. Add the simulated drilled solids (CALCIUM CARBONATE and CLAY) over a 2-minute period.
7. Continue to mix the whole mud during the remaining time in the hour (13-minutes).

**Table 4.3 Order and Timing of Mixing HP-HT Drilling Fluids**

**Mud System 1: Lignosulphonate Water Base Mud**

Order	Addition of Chemicals	Add after time (min)	Addition time (min)	Mix time (min)	Component
1	Prehydrated Gel	0	-	5	Wyoming Bentonite
2	pH	5	1	4	Caustic Soda
3	Black Powder	10	2	3	Resinex
4	Polymeric additives	15	2	3	Polypac-R
5	Weighting Agent	20	2	8	Barite
6	Dispersant	30	2	8	Spersene & Lignite
7	pH Adjustment	40		5	a.a
8	Drilled Solids	45	2	13	Calcium Carbonate & OCMA Clay

4.1.1.3.2 Laboratory Mixing of Fresh Oil Emulsion Mud

The mud was prepared by addition of diesel oil to the same fresh water lignosulphonate mud mixed above. Emulsification was achieved by mechanical agitation using a high shear rate mixer and also by substances already present in the mud, such as lignosulphonate. Three samples of mud were tested with commonly used diesel percentages (as a percentage of the total volume of mud) of 3, 8 and 13%.

4.1.1.3.3 Laboratory New Mixing Procedure of Synthetic Oil-Based Mud

The mixing order for OBM components described in API<sup>171</sup> RP 13B-2 has now been modified. API RP 13B-2 recommended mixing in a sequential order, i.e. oil,

emulsifier, lime, brine, clay, wetting agent and barite. This procedure makes the brine to be tightly emulsified in oil and therefore the clay will have difficulty to react with water to yield properly. Consequently, the mud properties will be very low and barite sag could occur. The new procedure developed makes the clay to react with brine and yield properly before the addition of emulsifiers. The list of components in Table 4.4 represents the new mixing order in which the chemicals were added for a total time interval of 1 hour and the following is a summary of the new procedure:

1. Pour synthetic base oil in the Silverson cup and add organophillic clay gradually over a 1-minute period. Mix for a further 4-minutes.
2. Add the brine phase (pre-dissolved calcium chloride in water) slowly over a 2-minute period. Mix for a further 8 minutes.
3. Add primary and secondary emulsifiers gradually over a 1-minute period and mix for a further 4 minutes. Add lime and mix for 5-minutes.
4. Add fluid loss additives gradually over a 1-minute period. Mix for a further 4 minutes.
5. Add the weighting material (barite) slowly over a 2-minute period. Mix for a further 8-minutes.
6. Add the simulated drilled solids (calcium carbonate and clay) over a 2-minute period.
7. Continue to mix the whole mud during the remaining time in the hour (13-minutes).

**Table 4.4 Order and Timing of Mixing HP-HT Drilling Fluids**

**Mud System 2: Synthetic Oil Base Mud**

Order	Addition of Chemicals	Add after time (min)	Addition time (min)	Mix time (min)	Component
1	Base Oil	0	-	-	Synthetic Oil
2	HT-Clay	5	1	4	HT-Clay
3	Brine	15	2	8	Calcium Chloride
4	Emulsifier /Wetting Agent	20	1	4	Novatec -P/ Novatec-S
5	Lime	25	1	4	Lime
6	Fluid Loss Additives	30	1	4	Novatec-F,Gilsonite, Truflo-100
7	Weighting Agent	35	2	8	Barite
8	Drilled Solids	45	2	13	Calcium Carbonate and OCMA Clay

**4.1.1.4 Test Results for Initial Mud**

Upon completion of the mixing procedure all the sample batches were blended together to ensure uniformity before commencement. The mud was initially tested using the techniques described in API RP<sup>170-172</sup> and the results obtained are given in Tables 4.5a and 4.5b.

Test technique (API RP)

1. Density at ambient temperature-70 ° F measured using pressurised mud balance.
2. 6 speed rheology (600, 300, 200, 100, 6, 3 rpm), at 120 ° F using Fann-35 Viscometer and thermostatically controlled Viscometer Cup.
3. Electric stability at 120 ° F for oil based mud using Electric Stability Meter.
4. HP-HT fluid loss at 300 ° F and 500-psi differential pressure using HP-HT Filter Press.

5. The initial muds were hot rolled using the 350 ml cell pressurised to 100 psi and then submitted for hot roll (8 hours for WBM and 16 hours for OBM) at 300° F using Heat Roller Oven.
6. A pressurised 350-ml mud bomb was placed vertically in the oven for static ageing to measure static sag factor at high temperature. The static and dynamic sag measurements are summarised in (section 4.1.1.4.1 and 4.1.1.4.2).

The purpose of conducting static and dynamic sag tests is to ensure the absence of barite sagging during experimental work as the presence of it could affect test results. After the ageing period the samples of mud were again blended together to ensure uniformity and homogeneity. They were mixed for 15 minutes prior to testing using the techniques described in API RP. Testing for this particular mud, static and dynamic filtration was carried out taking into account complete rheological properties and electric stability.

Descriptions of routine testing equipment are given in Appendix A [Figures A1 to A14].

#### 4.1.1.4.1 Static Sag Measurement

The sag factor is a measurement of the amount of sag or settlement of solids during a static ageing test and is an important test to ensure that the mud during HT static filtration test is not sagging as this could affect the accuracy of experimental results.

##### Measurement Procedure

After cooling the bombs Appendix A [Figure A9] , carefully open the valve and note the release pressure, if no pressure release occurs, it is likely that the bomb has leaked and the test should be repeated.

1. Carefully extract any free water (or free oil) from the top of the cell using a syringe. Record volume of free liquid.
2. Weigh a clean 10-ml syringe, then sample the top part of the bomb, and ensure that the mud sample contains no air. Record the volume and reweigh the syringe to calculate the weight of mud sample and hence the density (D1).

3. Carefully remove the remaining mud with a syringe leaving 20-40 ml in the bottom of the bomb. Note any hard solids settlement.
4. Sample the mud remaining at the bottom of the bomb. Record the density of the bottom portion of the mud as (D2).
5. The syringes used for measuring the initial and final densities of the mud are accurate if care is taken to eliminate trapped air.
6. Calculate the sag factor as: Density of bottom portion / (Density of top portion + Density of bottom portion).

In general the closer the sag factor is to 0.50, the better the result. The water and oil-based muds show 0.51.

#### 4.1.1.4.2 Dynamic Sag Measurement

The dynamic sag tester shown in Figure 4.1 is a new device developed by Schlumberger Cambridge Research (SCR), which is designed to measure dynamic sag at low shear rate. The sag test followed a standard period of 30 minutes, under ambient conditions, to ascertain the dynamic barite sag potential of the mud.

#### Measurement Procedure

1. Weigh the 5 ml empty syringe and re-weigh with 2.5 ml mud and inject into the bottom of the sag tester. Ensure that the mud sample contains no air.
2. Fill the space inside the sag tester with mud using the 10 ml syringe then rotate the bob at 6 rpm (which is equivalent to  $10.20 \text{ sec}^{-1}$  shear rate) and start the clock.
3. After 30 minutes, stop the rotation and draw out 2.5 ml plus syringe of mud, exactly level it to 2.5 ml and weigh.
4. From the weights of the syringes, calculate the density of mud prior and after the sagging (Do and Ds respectively). For a 2.5-ml syringe, the density is given by:  

$$400 \times (\text{weight of full syringe (g)} - \text{weight of empty syringe (g)}) \text{ kg/m}^3$$
5. Calculate the excess density as:  $(D_o - D_s) \text{ kg/m}^3$ . The higher the excess density, the more it is prone to sagging. The factor 400 in the equation



above is obtained by dividing 1000 by 2.5 (volume of mud weighed). Dynamic sag for WBM and OBM is about 0.52.

6. The syringes used for measuring the initial and final densities of the mud are accurate if care is taken to eliminate trapped air.

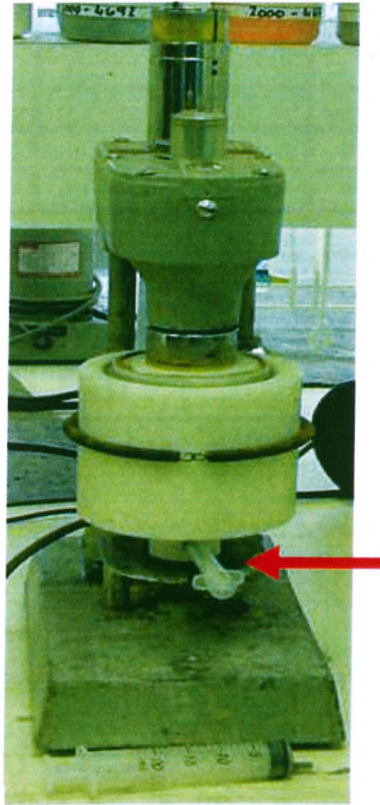


Figure 4.1 Sag tester

**Table 4.5a Initial Testing of HP-HT Drilling Fluids**

**Mud System 1: Synthetic Oil Base Mud**

RPM	Reading  BF*150 ° F @ 14.70 psi	MUD SG =  150 ° F @ 15 psi	1.321 AH*  150 ° F 3000 psi	200 ° F 6000 psi	250 ° F 10000 psi	300 ° F 12000 psi
600	50	49	59	55	51	50
300	30	29	39	36	35	34
200	25	24	32	30	29	25
100	19	18	23	22	22	21
6	11	9	12	11	12	10
3	10	8	10	10	11	10
Gel strength	12/18	10/17	11/16	10/17	10/16	10/17
O/W	75/25	75/25				
W.P.S	181,151	181,151				
Electric stability	510	950				
Static sag Factor	0.51	0.51				
Dynamic sag Factor	0.52	0.52				

**Table 4.5b Mud System 2: Fresh Water Lignosulphonate Mud**

RPM	Reading  BF*150 ° F @ 14.70 psi	Mud SG=  150 ° F @ 15 psi	1.321 AH*  150 ° F 3000 psi	200 ° F 6000 psi	250 ° F 10000 psi	300 ° F 12000 psi
600	85	82	92	62	49	40
300	51	49	56	37	28	22
200	39	38	43	27	22	18
100	25	24	26	19	16	13
6	7	6	6	5	5	4
3	6	5	5	4	4	3
Gel strength	11/18	10/16	10/15	9/13	8/11	7/11
pH	10.50	10.50				
Static sag Factor	0.51	0.51				
Dynamic sag Factor	0.52	0.52				

\*BF- Before hot rolling

\*AH- after hot rolling

#### **4.1.2 Development of a New Method for Optimum Emulsifier Selection Using the Particle Size Analyser Testing Technique**

The new method developed can be used for:

1. Selection of optimum emulsifier concentration for water-based mud.
2. Selecting optimum primary and secondary emulsifier concentrations for oil-based mud.
3. A quality control tool for comparison of different types of emulsifiers.
4. The selection and comparison of emulsifiers can be achieved with minimum time of testing, thus reducing economic impact.
5. A backup tool for dynamic sag test.
6. Measure particle size classification for filter cakes (chapter 5).

##### **4.1.2.1 Brief Introduction to Emulsification Mechanisms**

The occurrence of barite sag has been recognised, but it is a poorly understood phenomenon in the drilling industry. Problems such as lost circulation, well control and stuck pipe have resulted from the occurrence of barite sag. Invasion of filtrate includes excess emulsifiers, which may result in altering the rock wettability.

In recent times, the oil industry has shown increasing awareness of borehole instability and formation damage. Optimum drill-in/completion fluid design and selection are essential to the control of these problems.

Oil-in-water and water-in-oil based muds require additional emulsifiers to maintain emulsion stability. However it has become crucial to find a technique for optimum emulsifier concentration and performance.

The oil-in-water emulsion drilling fluid is prepared by adding 5 to 15% by volume oil to WBMs. Emulsification of oil takes place by the addition of surfactants using an ad-hoc approach.

OBMs are essentially water-in-oil emulsions with an aqueous dispersed phase (water) varying from 10 to 40 percent.

OBM chemicals are more expensive than WBM. Emulsifiers are common to oil mud systems, which aid to drilling mud stability; however when filtrates from such muds

invade, they may include some of these emulsifiers and result in an altering of rock wetting characteristics<sup>28</sup>.

Nigel et al.<sup>173</sup> described a method to characterise emulsifier performance. Several studies<sup>174,175</sup> concluded that low shear rate viscosity is a rheological parameter of importance in determining the capacity of a drilling fluid to minimize or prevent the occurrence of barite sag, particularly dynamic sag. They correspond to “low shear rate” at the 3 rpm dial reading ( $5.1 \text{ s}^{-1}$ ), corresponding to the lowest operating speed of the Fann 6-speed viscometer.

The frequency of problems associated with barite sag is higher with invert emulsions, compared to water-based systems, when drilling highly deviated wells<sup>174</sup>.

Up to now, there is no accepted method to select optimum emulsifier concentration. Drilling fluid performance has a significant economic impact on the petroleum industry, and justifies a thorough study of this problem.

#### **4.1.2.2 Fundamentals of Emulsion, Emulsifiers and Wettability<sup>176</sup>**

An emulsion is formed between two liquids by lowering the interfacial surface tension of one liquid with an emulsifier, or surfactant, to enable that liquid to form a stable dispersion of fine droplets in the other liquid.

In most regular emulsions, the oil phase is dispersed as fine droplets in the continuous or aqueous phase. This is commonly known as in oil-in-water (O/W) emulsion. Water based mud, containing oil as the internal phase is an example of this type of emulsion. In an invert emulsion, the aqueous phase is the dispersed phase and the oil phase is the continuous phase. This is known as a water-in-oil (W/O) emulsion. The present state-of-the-art OBMs are invert-drilling fluids.

Invert emulsions may contain as much as 40% by volume water. This water is broken up into small droplets and uniformly dispersed in the oil phase. The more water present in an emulsion, the distance between droplets is decreased, thereby the greater the chances of the water droplets coming together and coalescing.

To emulsify water-in-oil, there must be sufficient chemical emulsifier to completely form a film around each water droplet [Figure 4.2].



If there is insufficient emulsifier, the emulsion will be unstable. From the standpoint of stability, the smaller the droplet the more stable the emulsion. Large droplets will coalesce more easily than smaller droplets. To obtain small droplets, energy or work must be applied in the form of shear. This is done through agitation by the high shear units, bit jets, mud guns or centrifuge pumps.

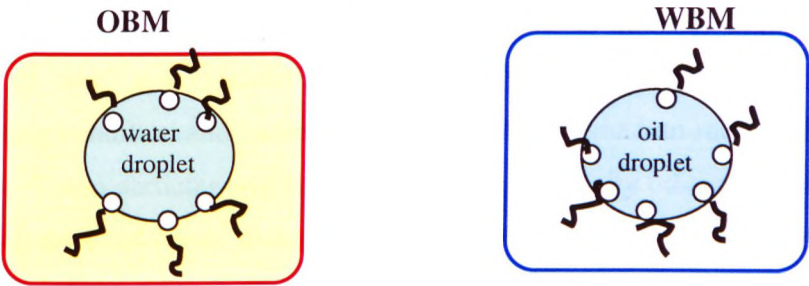


**Figure 4.2 Schematic of invert and regular emulsion**

The water droplets aid in the reduction of fluid loss in invert muds (they plug filter cake pores). In addition, the droplet size also contributes to the rheological properties of drill-in fluid.

When oil (continuous phase) is added, the emulsion becomes more stable because the distance between droplets is greater. The reverse is also true, additional of water will decrease stability because the distance between water droplets is less. The addition of oil decreases viscosity while addition of water increases viscosity.

The inclusion of solids into a water-in-oil emulsion may have either positive or negative effects depending upon the manner in which they become wetted. Figure 4.3 illustrates the five principal states of wetting that can occur in three-phase systems (solid/liquid/liquid) such as oil-based mud. Each condition is contingent upon the angle contact formed between each liquid and the solid. By definition, if the angle,  $\theta$ , formed by a liquid and a solid is less than  $90^\circ$  the solid is said to be preferentially wetted by the liquid. Thus, in Case 1 [Figure 4.3], when the angle  $\theta_w$  formed by the water and solid is less than  $90^\circ$  then the solid is said to be preferentially water wet. If the contact angle,  $\theta$ , becomes  $0^\circ$ , the solid is said to be totally wetted by the liquid, Cases 4 and 5 illustrate the concept of total wetting of a solid by a liquid.

Oil mud systems contain certain surfactants which alter the contact angle (wettability) of the solid/liquid interface. These chemicals will cause a solid to become preferentially oil wet or totally oil wet if used in excess.

In an oil mud system it is necessary to maintain the solids in a preferentially oil-wet condition. Solids, which become preferentially or totally water wet, will cluster together and settle out of suspension. Settling of this type is characterised by soft settling or “sag” as it is sometimes described. Additions of wetting agents will alter the wetting condition and cause these clusters to disperse into more easily suspended particles. These particles will then exist in a preferentially oil-wet condition whereby clustering does not occur. Solids which have become totally oil-wet, may settle into a very compacted hard type of settling.

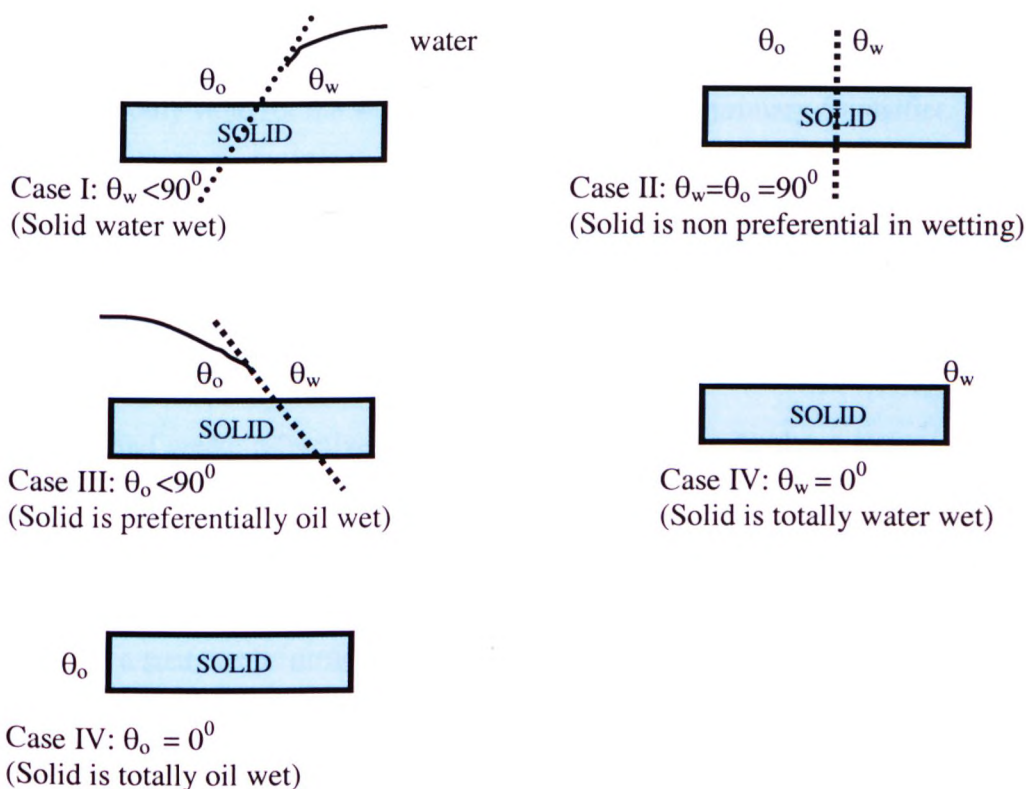


**Figure 4.3 Contact angles in three phases**

The measurement of contact angles is difficult, imprecise, and not practical in an oil mud drilling fluid. Several simple tests have been developed which indicate the need



to change the wettability of the solids from water wet to a preferentially oil wet condition.

In the past, it had been advised that adequate amount of emulsifiers should be added and at the same time over-treatment avoided. The word “adequate” was often used in the drilling engineering mud programme to avoid any problems. In practice, however, there were no definite guidelines for the optimum level of treatment. As a rule of thumb, the electrical stability and traces of water in the HP-HT filtration were used as an indicator of the emulsion quality. However, Erhu et al.<sup>177</sup> have developed a method for optimum wetting agent (secondary emulsifier) selection using dynamic sag equipment. They found that the plastic viscosity (PV) reduces dramatically until reaching a certain plateau level. Thereafter a further increase in the concentration of wetting agent has little effect on the PV and no explanation has been given for these phenomena. This procedure shows two major limitations:

1. It is only valid for the wetting agent but not for the primary emulsifier.
2. Over treatment with primary emulsifier could occur.

However this study shows an alternative and better method has been developed using Particle Size Analyser based on water droplet size.

#### **4.1.2.3 Testing Procedure and Results**

Modify and create refractive index (RI) for Particle Size Analyser to measure oil-in-water and water-in-oil particle size.

Basically, pilot mud should be mixed (base oil, brine, and lime) using a Silverson mixer at 6000 rpm without emulsifiers and weighting material. Then the mud sample can be tested with different emulsifier concentrations and at each additional concentration the water droplet size can be measured with a Particle-size Analyser. One can observe a dramatic decrease in water droplet size and an optimum level of emulsifier can be selected when there is no further decrease. After the addition of a wetting agent sample testing can be started and again the water droplet size will decrease smoothly until a point is reached where there is no further reduction in water

droplet size. This can be used also as an optimum level of wetting agent as shown in Figure 4.4 for synthetic oil-based mud.

This method can also be used for selection of optimum emulsifier concentration for water-based mud when addition of oil is required. Oil droplet size can be measured and dramatically reduced when emulsifier is added. Therefore the optimum emulsifier concentration can be selected when there is no further reduction in oil droplet size as shown in Table 4.6.

Furthermore, electric stability and Fann-Viscometer readings can also be determined and used, if other results are required during this particle-size analysis and again one can observe the same trends as discussed above for monitoring reduction of water or oil droplet size. Electric stability as an example will increase sharply with the addition of emulsifier and it becomes steady when the optimum level of emulsifier is achieved. The addition of a wetting agent increases electric stability until it reaches a steady value, which indicates that the optimum level is achieved [Figure 4.5]. As a guideline, with the addition of emulsifiers, the filtration volumes and rheology of drilling fluids decrease until they reach steady values. Electric stability also increases until it reaches a steady state.

OBM filter cake<sup>178</sup> consists of fine water droplets, clay and barite. The new application technique developed in this study shows that the water droplet size is less than 4 microns.

However, this interesting method need further study for comparing the performance of different emulsifiers or designing different fluid formulations. The technique can be also applied with same manner to de-emulsifiers selection and performance.

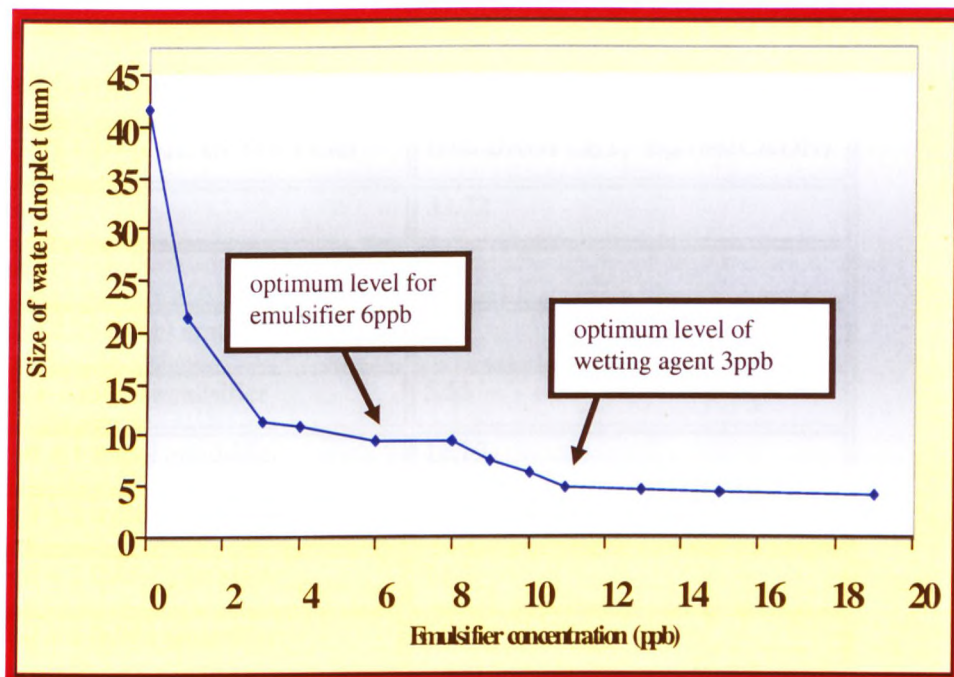


Figure 4.4 Relationship between emulsifier concentration and water droplet size

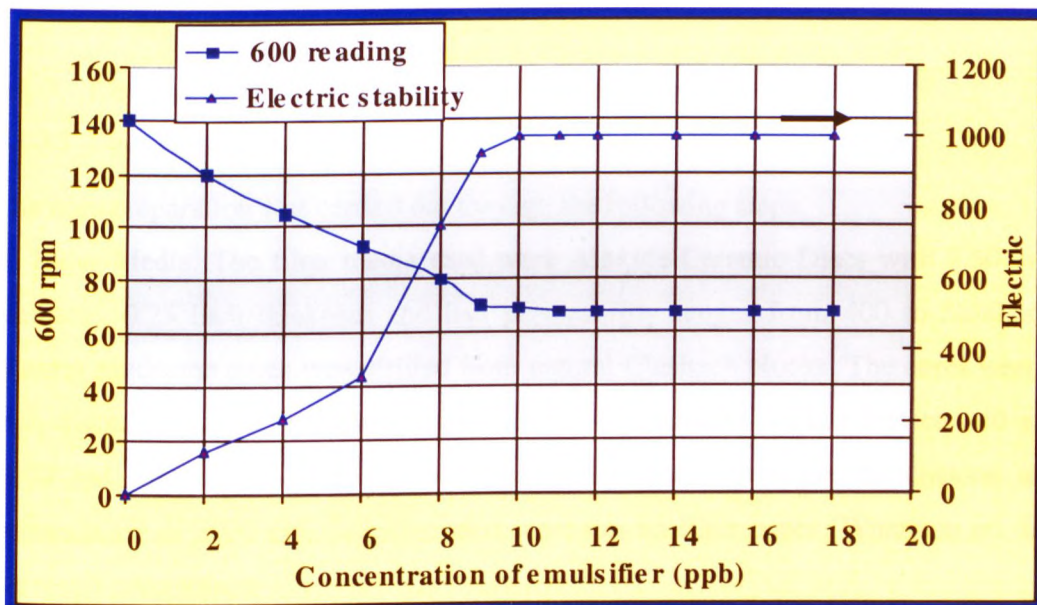


Figure 4.5 effect of emulsifier concentration on OBM

**Table 4.6 Relationship between emulsifier concentration and oil droplet size for WBM**

<b>BASE FLUID (OIL IN WATER)</b>	<b>OIL DROPLET, <math>D_{50}</math> (MICRON)</b>
1% oil	33.72
3% oil	35
5% oil +0.25 lb/bbl emulsifier	6.65
8% oil + 1 lb/bbl emulsifier	5.55
13% oil + 1 lb/bbl emulsifier	12.79
13% oil + 2 lb/bbl emulsifier	7.59
16% oil + 2 lb/bbl emulsifier	7.80
16% oil + 3 lb/bbl emulsifier	5.80
16% oil + 4 lb/bbl emulsifier	2.47
16% oil + 8 lb/bbl emulsifier	2.44
16% oil + 12 lb/bbl emulsifier	2.44

### 4.1.3 Core Analysis

#### 4.1.3.1 Core Preparation

The core preparation was carried out through the following steps:

- (i) Filter Media: The filter media used were Aloxide Ceramic Discs with 2.50 inch diameter, 0.25 inch thickness and had permeability ranges from 400 to 5000 md. Natural sandstone cores were drilled from natural Clashach blocks. The cores were 1 inch diameter, about 1.20 inch length and had permeability values between 40 and 4000 md. Selective synthetic cores were used with the same dimensions and permeability of 3000 md. Selective tests were run on filter paper (Whatman no. 50) for result comparison.
- (ii) Core Samples: The petroleum industry has standard porous media for formation damage laboratory experiments, and uses several quarried sandstone and carbonate

rocks. The data obtained from these tests are usually compared to similar reservoir cores. These rocks are chosen because they are relatively inexpensive, readily available and relatively homogenous. They are also outcrops of producing subsurface formations. The most commonly used “rock standard” includes Clashach and Berea sandstone and Baker carbonates. The cores were measured for their exact length and diameter using a Vernier gauge. The core weights were also measured accurately using a highly sensitive digital mass balance. (When not in use the cores were stored in a dessicator).

(iii) Core saturation: All the cores and Aloxide Discs were vacuum saturated in brine for WBM and in base oil for OBM filtered on 0.45-micron filter paper. A vacuum pump was used and the brine ( $\text{NaCl}_2$  45,000 PPM and  $\text{CaCl}_2$  4,500 PPM), which is mostly similar to the formation water was then allowed to flow through the core or Disc. Once saturation was completed, the outer valve was then closed for 10 minutes and samples removed after venting the pressure. Saturation was carried out before each single filtration test for experimental confidence.

The core weights were measured accurately and porosity calculated using equation

$$(4.1): \quad \phi = \frac{V_p}{V_b} = \frac{\text{Pore Volume}}{\text{Bulk Volume}} \quad (4.1)$$

$$\text{Where} \quad V_b, \text{Bulk volume} = \pi r^2 L, \text{ cm}^3 \quad (4.2)$$

$$V_p, \text{Pore Volume} = \frac{W_2 - W_1}{\rho}, \text{ cm}^3 \quad (4.3)$$

$\phi$ = porosity, fraction	$\rho$ = specific gravity of saturated fluid, gm/cm <sup>3</sup>
$W_1$ = weight of dry core, gm	$W_2$ = weight of saturated core, gm
$r$ = core radius, cm	$L$ = core length, cm

(iv) Core permeability: Using Nitrogen Gas Permeameter unit (90101) the permeability to gas was measured for selected natural and synthetic cores. Meanwhile initial (liquid) permeability has been measured for all the natural Clashach sandstone cores using core holder equipment.



#### 4.1.3.2 Morphological Formation Characteristics

The formation characteristics have been investigated in depth in order to:

1. Study Clashach sandstone formation characteristics such as permeability, porosity, etc.
2. Establish a general model to predict mean pore throat diameter.
3. Compare model predictions against experimental data and validate with external field data.
4. Compare model prediction with classic jamming ratios.
5. Set up design criteria of formation damage testing procedure for quality control assurance.
6. The depth of solids invasion requires the knowledge of the formation morphological characteristics such as permeability, porosity, tortuosity etc.

However in order to achieve the above objectives some empirical correlations need to be first defined<sup>179</sup>. The tortuosity factor,  $\tau$ , is defined by:

$$\tau = \left(\frac{L_a}{L}\right)^2 \quad (4.4)$$

Where  $L$  is the length of the rock sample, and  $L_a$  is the actual length of the flow path. Different methods can be used to measure tortuosity such as CT Scan, SEM and Precision Component Analyser. Therefore, tortuosity has been defined in terms of other quantities that can be measured in laboratory. Formation factor ( $F_R$ ) using Precision Component Analyser (Appendix A) and porosity ( $\phi$ ) can be used as follows: The general expression for tortuosity in porous media can be calculated from:

$$F_R = \frac{\tau}{\phi} \quad (4.5)$$

$$\tau = \phi F_R \quad (4.6)$$

Archie's<sup>179</sup> formula can be approximated by:

$$F_R = \frac{a}{\phi^m} \quad (4.7)$$



Where  $m = 1.70$ , which is referred to as the “cementation” factor, as defined by Guyod<sup>180</sup>, structure parameter ( $a$ ) is function of the shape and distribution of pores. It is determined from a plot of the formation resistivity factor versus porosity on log-log graph. A straight line having slope  $m$  generally can approximate such a plot. The general form to estimate the formation factor can be expressed as:

$$F_R = \frac{1}{\phi^m} \quad (4.8)$$

Doveton<sup>181</sup> concluded from a study of morphological characteristics of sands of varying shape and size distribution that the exponent ( $m$ ) is a function of pore shape, and ( $a$ ) is a function of both pore size and pore shape.

Unalmiser and Funk<sup>182</sup> concluded that the structure parameter ( $a$ ) is a tortuosity factor, is usually close to unity, but normally lies between 0.5 to 1.50.

Typical values for ( $m$ ) for various minerals and porous media as given by Hilchie<sup>183</sup> are shown in Table 4.7.

**Table 4.7 Cementation Factor values for different minerals**

MINERALS AND SOLIDS	$m$	MINERALS AND SOLIDS	$m$
Na, montmorillonite	3.28	Carbonates	2.0
Ca, montmorillonite	2.70	Shell Fragments	1.90
Muscovite	2.46	Kaolinite	1.87
Attapulgit	2.46	Cemented sand	1.80
Mediterranean clays	2.40	Natural sand	1.60
Sandstone	2.15	Platy sand	1.52
Illite	2.11	Rounded quartz sand	1.40

Table 4.8 permits the selection of the approximate values of ( $m$ ) from a lithological description of the core of interest summarised by Pirson<sup>184</sup>.

**Table 4.8 Rock description versus (*m*) values**

ROCK DESCRIPTION	<i>m</i> VALUES
Unconsolidated	1.30
Very slightly cemented	1.40-1.50
Slightly cemented	1.60-1.70
Moderately cemented	1.80-1.90
Highly cemented	2.0-2.20

The Archie equation has been studied widely and proposed in many different forms for different types of sandstone, carbonates and other rock types. Table 4.9 indicates different coefficient and exponents summarised by Asquith.<sup>185</sup>

**Table 4.9 Values of *m* and *a* as function of rock type**

$F_R = 1 / \phi^2$	for carbonates (limestone, dolomites)
$F_R = 0.81 / \phi^2$	for consolidated sandstone
$F_R = 0.62 / \phi^{2.15}$	for consolidated sandstone (Humble equation)
$F_R = 1.65 / \phi^{1.33}$	for shaly sands
$F_R = 1.45 / \phi^{1.70}$	for calcareous
$F_R = 2.45 / \phi^{1.08}$	for Pliocene sands (California)
$F_R = 1.97 / \phi^{1.29}$	for unconsolidated Miocene sands (US Gulf Coast)
$F_R = 1 / \phi^{(2.05\phi)}$	for clean granular formations

#### 4.1.3.3 Results of Rock Characteristics

##### 4.1.3.3.1 Porosity and Permeability Relationship

Clashach sandstone is brownish to yellow in colour, and mostly well sorted, medium- to coarse grained with well-rounded quartz grains and silica cemented. The selected

core samples exhibit a wide porosity range, which varied from 10 to 28 percent and permeability from less than 50 to a few thousand millidarcy. Figure 4.6 clearly demonstrated strong correlation between porosity and permeability. The permeability appears to increase with increasing porosity.

#### 4.1.3.3.2 Tortuosity and Formation Resistivity Factor

Figure 4.7 demonstrates the relationship between tortuosity, permeability and porosity. Figure 4.8 shows the non-linear relationship between formation resistivity factor versus porosity and permeability.

Figure 4.9 shows a plot of the formation resistivity factor versus porosity on log-log graph and  $(m)$  can be approximated from the slope of such a plot.

Figures 4.10 and 4.11 show the best morphological characteristics relationship with formation resistivity factor. Figure 4.10 clearly demonstrated that the formation resistivity factor has a non-linear relationship with porosity. Parameters  $a$  and  $m$  for Clashach sandstone formation used in the present work can be approximated by equation (4.9), which agrees closely with the Humble formula<sup>184</sup> and can be expressed as:

$$F_R = \frac{0.65}{\phi^{2.10}} \quad (4.9)$$

Figure 4.11 shows the relationship between formation resistivity factor, tortuosity and porosity, which agrees with equation (4.5). However equation (4.9) for Clashach sandstone formation has been correlated with external field data from two Middle Eastern carbonate reservoirs (Dixon 1990)<sup>186</sup> [Figure 4.12]. Equation (4.10) shows the best fit for carbonate reservoirs.

Parameters  $a$  and  $m$  for carbonate formations can be expressed as:

$$F_R = \frac{0.89}{\phi^{2.0}} \quad (4.10)$$

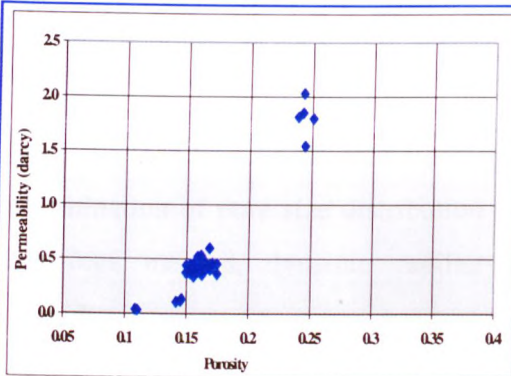


Figure (4.6) Permeability Vs. Porosity for Clashach sandstone cores

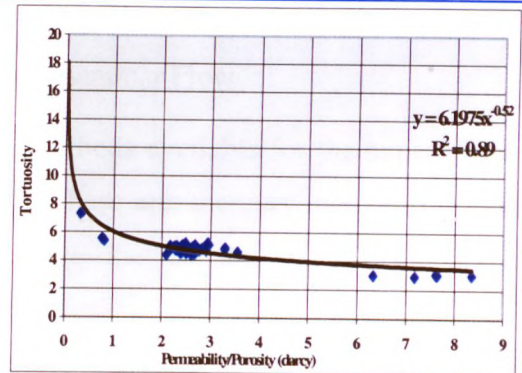


Figure (4.7) Tortuosity Vs. Permeability over Porosity

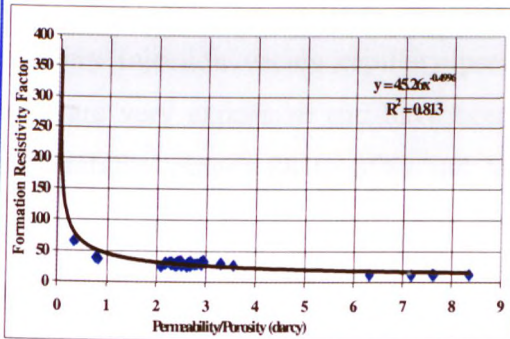


Figure (4.8) Formation Resistivity Factor Vs. Permeability over Porosity

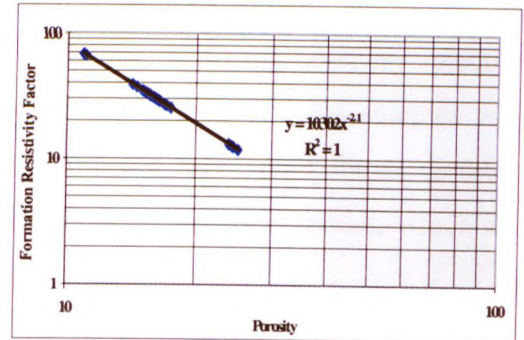


Figure (4.9) Formation Resistivity Factor Vs. Porosity

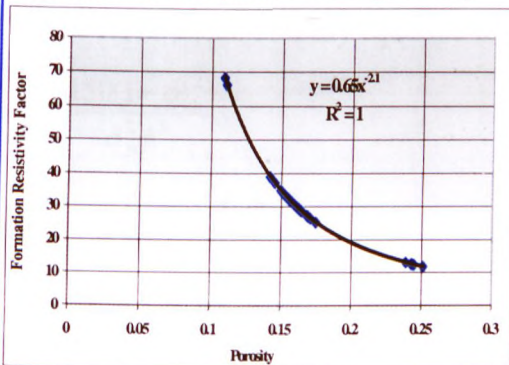


Figure (4.10) Formation Resistivity Factor Vs. Porosity for sandstone cores

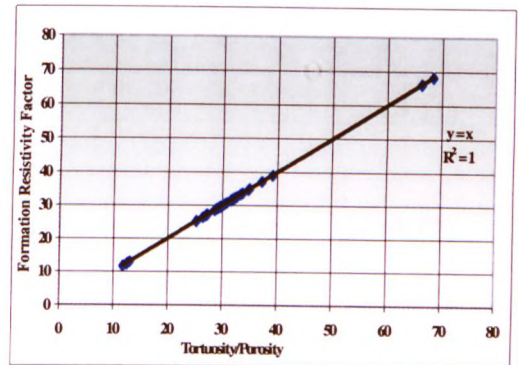


Figure (4.11) Formation Resistivity Factor Vs. Tortuosity over Porosity

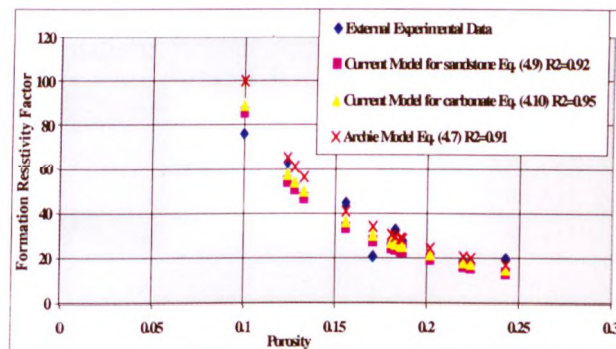


Figure (4.12) Validation Archie Model for Resistivity Formation Factor With External Data

#### 4.1.3.4 Modelling Mean Pore Throat Diameter ( $D_{pore}$ )

##### 4.1.3.4.1 Modelling Pore Throat Diameter from Laminar Flow

There are four basic quantitative description methods available for the experimental determination of pore size distribution (PSD). These are: mercury injection method, centrifuge method, dynamic capillary pressure method and porous diaphragm method.

In the present work, the mercury injection method was used. The basis of this method is to inject mercury into the test sample at incremental pressures and derive the mercury injection versus capillary pressure relations. However, mercury injection tests are very expensive and have been carried out on four selected samples with permeability ranges 88 to 3982 md to determine the mean pore throat diameter ( $D_{pore}$ ) [Figures 4.13 to 4.20]. In order to establish an empirical model, which can predict  $D_{pore}$  in terms of morphological characteristics and compare the results with experimental data, four common models from literature have been used.

1. The Blake-Kozeny equation for laminar flow:

$$\frac{1}{K} = \frac{150(1-\phi)^2}{d_p^2 \phi^3} \quad (4.11)$$

and  $D_{pore} = \frac{d_p \phi}{3(1-\phi)} \quad (4.12)$

2. Coberly equation:

$$D_{pore} = \frac{d_p}{6.50} \quad (4.13)$$

3. Poiseuille's equation:

$$q = \left( \frac{n \pi r^4}{8\mu} \right) \frac{\Delta P}{L} \quad (4.14)$$

4. Darcy's equation:

$$q = \left( \frac{kA}{\mu} \right) \frac{\Delta P}{L} \quad (4.15)$$



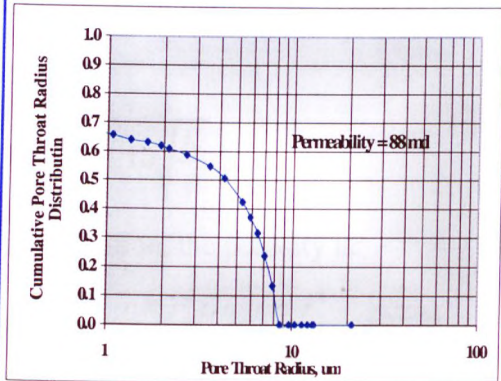


Figure (4.13) Pore Throat Radius Vs. Cumulative Distribution

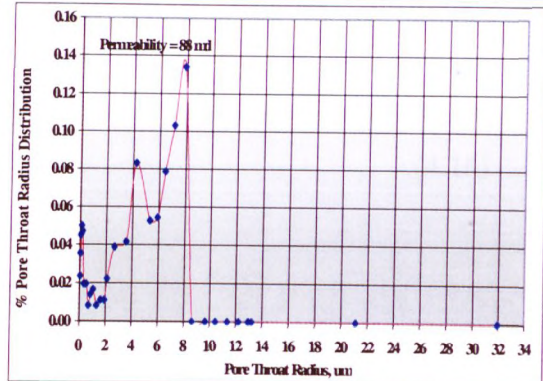


Figure (4.14) Pore Throat Radius Vs. Pore Size Distribution

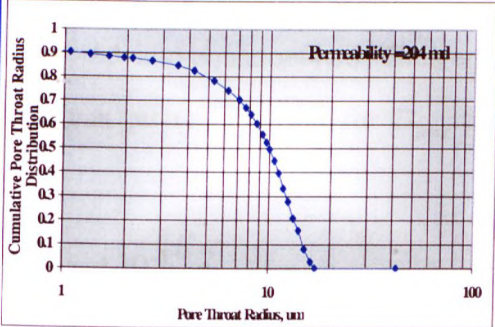


Figure (4.15) Pore Throat Radius Vs. Cumulative Distribution

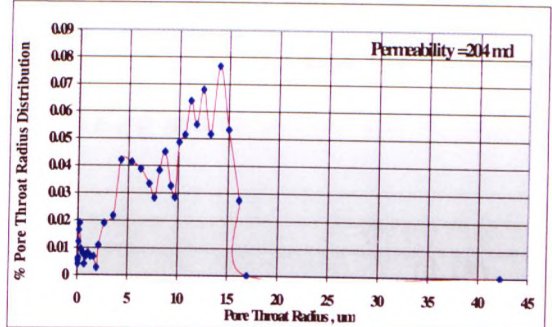


Figure (4.16) Pore Throat Radius Vs. Pore Size Distribution

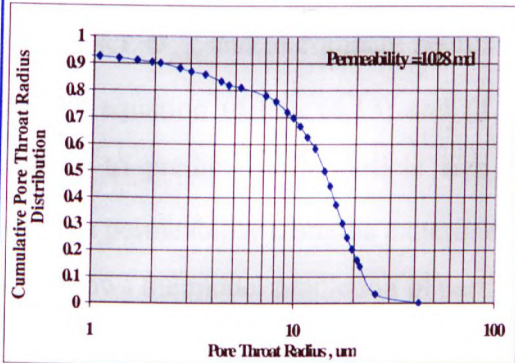


Figure (4.17) Pore Throat Radius Vs. Cumulative Distribution

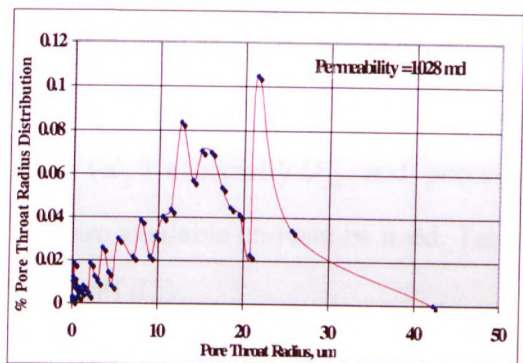


Figure (4.18) Pore Throat Radius Vs. Pore Size Distribution

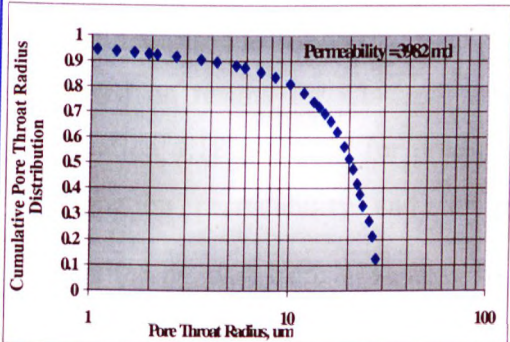


Figure (4.19) Pore Throat Radius Vs. Cumulative Distribution

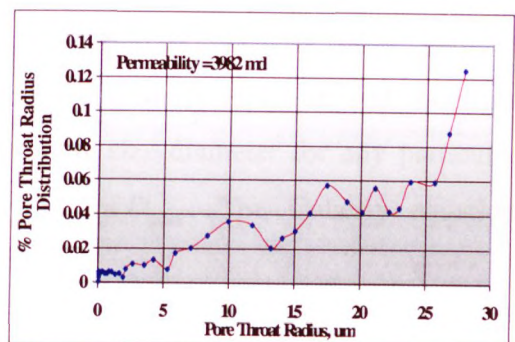


Figure (4.20) Pore Throat Radius Vs. Pore Size Distribution



Comparing equation (4.11) and (4.12), we can get a relationship for  $D_p$  in terms of  $k$  and  $\phi$ :

$$D_{pore} = 4.10 \sqrt{\frac{K}{\phi}} \quad (4.16)$$

By definition, the porosity is:

$$\phi = \frac{V_p}{V_b} = \frac{n\pi r^2 L}{AL} = \frac{n\pi r^2}{A} \quad (4.17)$$

Substituting  $L_a = L\sqrt{\tau}$  from equation 4.4 into equation 4.14 and Substituting  $A = n\pi r^2 / \phi$  into equation 4.15. Then equating equations 4.14 and 4.15 and solving for  $k$ , we can get a relationship for  $D_{pore}$  in terms of  $K$ ,  $\phi$  and  $\tau$ :

$$D_{pore} = 4.10 \sqrt{\frac{K \tau}{\phi}} \quad (4.18)$$

To predict  $D_{pore}$  and to compare results with experimental  $D_{pore}$ , the validity of these models equation (4.12), (4.13) and (4.18) was tested first. The models have been utilised to predict mean particle size diameter ( $d_p$ ) especially  $D_{pore}$  and porosity whereas permeability from the experimental data are available and can be used. Table 4.10 shows the model prediction of particle diameter ( $d_p$ ).

This comparison required particle size diameter from sieve analysis to be compared with model predictions of both equations with experimental data. The main results can be summarised as follows:

1. Based on results for Clashach sandstone the Coberly equation and modified equation 4.18 are valid for prediction particle size diameter for any particular formation permeability and for prediction of  $D_{pore}$ . The Coberly equation requires  $d_p$  data from sieve analysis.

2. Blake-Kozeny equation may be considered to be accurate for predicting particle diameter for typical reservoir permeabilities (less than 1000 md) [Table 4.10].
3. An empirical correlation for Clashach sandstone has been established to predict mean particle size diameter ( $d_p$ ) in equation (4.19) as shown in [Figure 4.21] and mean pore throat diameter  $D_{pore}$  in equation (4.20) as shown in [Figure 4.22] in terms of K and  $\phi$ .

$$d_p = a \sqrt{\frac{K}{\phi}} \quad K = \text{darcy}, \quad d_p = \text{micron} \quad a = 65.0 \quad (4.19)$$

$$D_{pore} = a \sqrt{\frac{K}{\phi}} \quad D_{pore} = \text{micron} \quad a = 10.0 \quad (4.20)$$

Dividing equation (4.19) by equation (4.20) the result will be the Coberly equation (4.13).

4. Comparison between experimental and Blake-Kozeny equation and modified equation 4.18 has been tested to predict  $D_{pore}$  [Figure 4.22] and the results are given in Table 4.11.

The result shows that modified equation 4.18 gives reliable prediction of  $D_{pore}$  only if the tortuosity  $\tau$  can be measured.

**Table 4.10 Comparison between Coberly, Blake-Kozeny and modified equations for particle diameter prediction**

Permeability (darcy)	Porosity fraction	$D_{pore}$ micron	$d_p$ Coberly micron	$d_p$ Modified eq.(4.18) micron	$d_p$ Blake-Kozeny micron
88	0.12	8.52	5.54E+01	5.53E+01	1.73E+02
204	0.14	19.40	1.26E+02	7.63E+01	3.35E+02
1028	0.16	28.20	1.83E+02	1.59E+02	4.28E+02
3982	0.26	38.30	2.49E+02	2.51E+02	3.17E+02

**Table 4.11 Comparison between experimental Blake-Kozeny and modified equations for pore throat diameter prediction**

Permeability (md)	Porosity fraction	$D_{pore}$ (experiment) (micron)	$D_{pore}$ Modified eq. (4.18) calculated micron	$D_{pore}$ Blake-Kozeny calculated micron
88	0.12	8.52	8.52	2.07
204	0.14	19.40	11.10	5.30
1028	0.16	28.20	21.80	8.41
3982	0.26	38.30	27.20	16.20

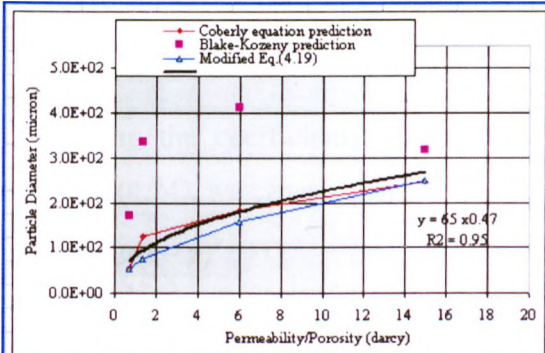


Figure (4.21) Particte Diameter Vs. Permeability over Porosity

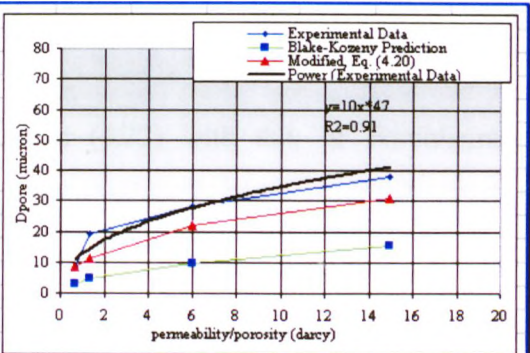


Figure (4.22) Pore Throat Diameter Vs. Permeability over Porosity

4.1.3.4.2 Modelling Pore Throat Diameter from Laminar and Turbulent Flow

In order to find the relationship between  $\beta$  and the formation characteristics to establish a predictive model for pore throat diameter from laminar and turbulent flow equations, an attempt has been made to combine four common equations namely:

1. Blake-Kozeny equation for laminar flow:

$$\frac{\Delta P}{L} = \frac{150\mu V(1-\phi)^2}{d_p^2\phi^3} \tag{4.21}$$

2. Burke-Plummer equation for turbulent flow:

$$\frac{\Delta P}{L} = \frac{1.75\rho V^2(1-\phi)}{d_p\phi^3} \tag{4.22}$$

3. Ergun equation combined Equations 4.21 and 4.22:

$$\frac{\Delta P}{L} = \frac{150\mu V(1-\phi)^2}{d_p^2 \phi^3} + \frac{1.75\rho V^2(1-\phi)}{d_p \phi^3} \quad (4.23)$$

Equation 4.23 accounts for laminar, transitional and turbulent flow regimes.

In laminar flow, viscous forces dominate and the pressure drop described by the left hand term of equation 4.23.

In turbulent flow, inertia forces dominate and the pressure drop described by the right hand term of equation 4.23.

In transitional flow both viscous and inertia forces are significant and the pressure drop described by the complete Ergun equation 4.23.

4. Forchheimer equation<sup>187</sup> can be defined as:

$$\frac{\Delta P}{L} = \frac{\mu}{k}V + \beta\rho V^2 \quad (4.24)$$

Comparing the coefficients of Ergun equation (4.23) with that of Forchheimer equation (4.24), we can see that:

$$\frac{\mu}{K} = \frac{150\mu(1-\phi)^2}{d_p^2 \phi^3} \quad (4.25) \quad \text{and}$$

$$\beta\rho = \frac{1.75\rho(1-\phi)}{d_p \phi^3} \quad (4.26)$$

Comparing equations (4.12), (4.25) and (4.26) and, the relationship between  $\beta$  in terms  $D_{pore}$ ,  $K$  and  $\phi$  can be obtained:

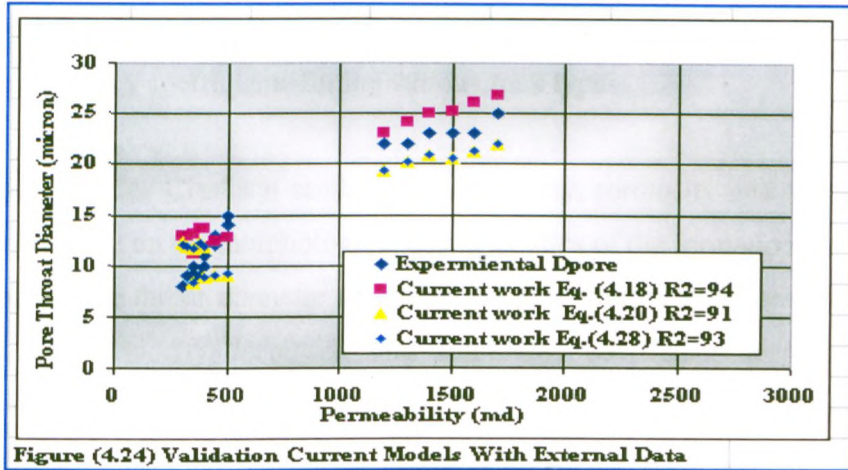
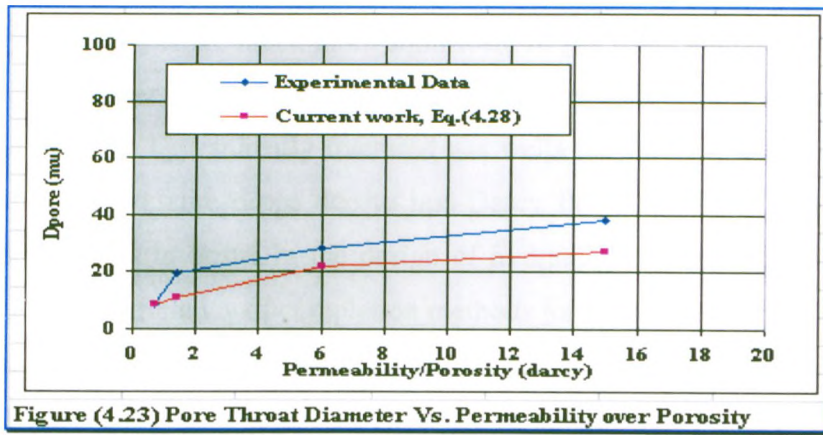
$$\beta = \frac{0.035}{K} \frac{D_{pore}}{\phi} \quad (4.27)$$

$$D_{pore} = \frac{\beta K \phi}{0.035} \quad (4.28)$$

This is a general equation to predict the mean pore throat diameter  $D_{pore}$ , which is derived from the laminar and turbulent flow equations. Figure 4.23 clearly demonstrated agreement between experimental and theoretical values for  $D_{pore}$ .



Furthermore, predicted pore throat correlation equations (4.18), (4.20) and (4.28) has been validated with external field data obtained from three selected sandstones: the Berea, from (a quarry in Ohio), Noxie and Cleveland both from Bartlesville, Oklahoma<sup>188</sup>. The ranges of porosity is 0.16 to 0.27, permeability ranges from 300 to 1700 md and a wide range of pore throat diameter ranges from 6 to 30 microns. Figure 4.24 clearly shows agreement between predicted correlations with external validated data.



In equation 4.27 substitute for  $D_{pore}$  from equation (4.18), and then evaluate:

$$\beta = \frac{0.143\tau^{0.50}}{K^{0.50}\phi^{1.50}} \quad (4.29)$$

This is an empirical model for the non-Darcy flow coefficient of a porous rock.

In general the relationship between morphological characteristics of Clashach sandstone has been correlated to  $K/\phi$  and it can be concluded that:

- I. The mean particle size diameter and mean pore throat diameter are directly proportional to  $K/\phi$ .
- II. The formation resistivity factor, tortuosity and non-Darcy coefficient are inversely proportional to  $K/\phi$ .

Non-Darcy flow effects are much more significant in gas wells than oil wells, chiefly because of the higher flow velocities as a result of the much lower viscosity of the gas. Furthermore, in hydraulically fractured gas wells the velocity can be very high, resulting in large pressure drops due to non-Darcy flow. Failure to consider these pressure drops leads to errors in the design of hydraulic fracturing treatments, etc., which reduces the efficiency of completion methods for these reservoirs.

In the past several years many empirical correlations have been established<sup>189-200</sup> to calculate the non-Darcy coefficient  $\beta$ . These are summarised in Table 4.12.

Based on extensive experimental work conducted on sandstone, limestone and dolomite cores, Janicek and Katz<sup>197</sup> concluded there is no significant difference between non-Darcy coefficients for the various rock types.

Based on results for Clashach sandstone the porosity, tortuosity and the non-Darcy coefficient depend on the morphological characteristics of the formation.

As the mean pore throat diameter increases the permeability increases, the porosity increases, the tortuosity decreases, and non-Darcy coefficient decreases sharply [Figures 4.25 and 4.28].



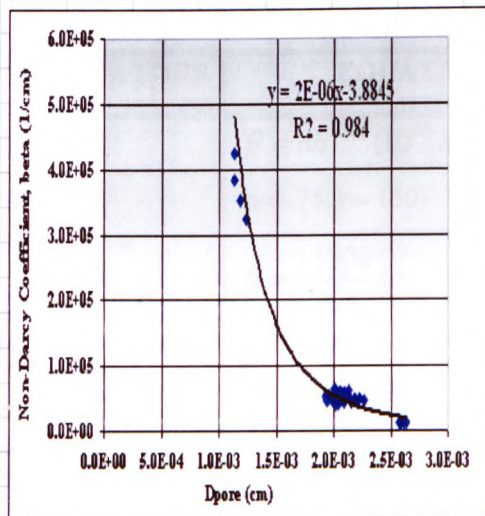


Figure (4.25) Non-Darcy Coefficient Vs. Pore Throat Diameter

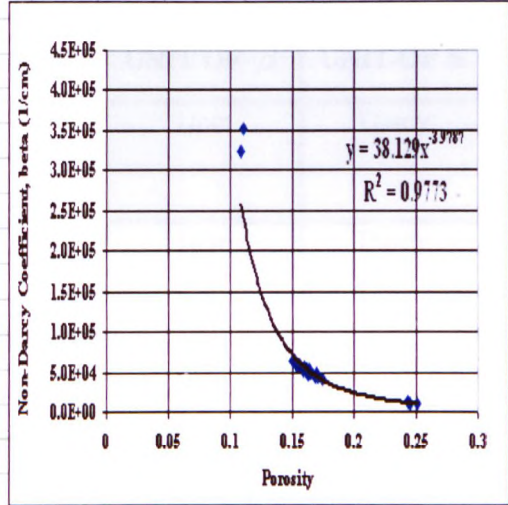


Figure (4.26) Non-Darcy Coefficient Vs. Porosity

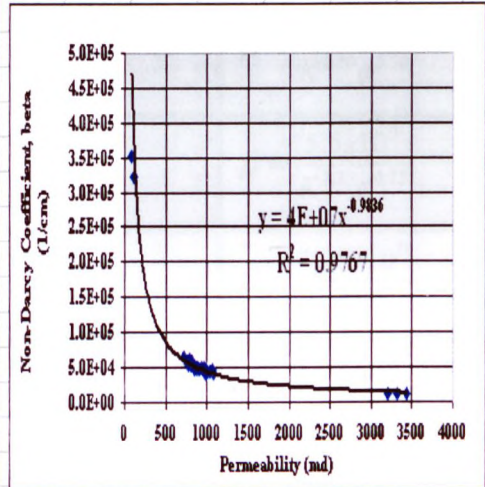


Figure (4.27) Non-Darcy Coefficient Vs. Permeability

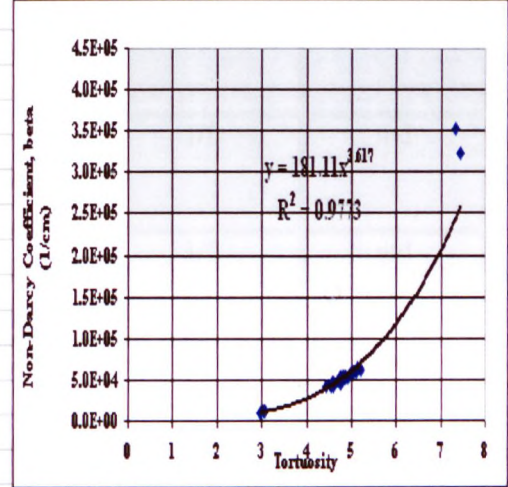


Figure (4.28) Non-Darcy Coefficient Vs. Tortuosity

**Table 4.12 Empirical correlations for the non-Darcy coefficient ( $\beta$ )**

INVESTIGATORS	EQUATION	UNIT OF $\beta$	UNIT OF K
Ergun <sup>189</sup>	$\beta = ab^{-1/2} (10^{-8} K)^{-1/2} \phi^{-3/2}$ (a=1.75, b= 150)	1/cm	Darcy
Dacun et al. <sup>190</sup>	$\beta = \frac{11500}{K\phi}$	1/cm	Darcy
Jones <sup>191</sup>	$\beta = \frac{6.15 \times 10^{10}}{K^{1.55}}$	1/ft	md
Noman et al. <sup>192</sup>	$\beta = \frac{1.12 \times 10^{11}}{K^{1.06}}$	1/ft	md
Geertsma <sup>193</sup>	$\beta = \frac{4.85 \times 10^4}{K^{0.50} \phi^{5.50}}$	1/ft	md
Tek et al. <sup>194</sup>	$\beta = \frac{5.5 \times 10^9}{K^{1.25} \phi^{0.75}}$	1/ft	md
Katz et al. <sup>195</sup>	$\beta = \frac{4.20 \times 10^{10}}{K^{1.35}}$	1/ft	md
Coles et al. <sup>196</sup>	$\beta = \frac{1.07 \times 10^{12} x \phi^{0.449}}{K^{1.88}}$	1/ft	md
Janicek <sup>197</sup>	$\beta = \frac{1.82 \times 10^8}{K^{1.25} \phi^{0.75}}$	1/cm	md
Liu et al. <sup>198</sup>	$\beta = \frac{8.91 \times 10^8 \tau}{K \phi}$	1/ft	md
Thauvin et al. <sup>199</sup>	$\beta = \frac{1.55 \times 10^4 \tau^{3.35}}{K^{0.98} \phi^{0.29}}$	1/cm	md
Cooper et al. <sup>200</sup>	$\beta = \frac{10^{-3.25} \tau^{1.943}}{K^{1.023}}$	1/cm	cm <sup>2</sup>

For all equations:  $\phi$  = porosity as a fraction,  $\tau$  = tortuosity (dimensionless), and K = permeability

We can see all the correlations for  $\beta$  exhibit a lot of scatter.

Figure 4.29 shows that the best relationship between the non-Darcy coefficient and the morphological characteristics of the formation and can be approximated by:

$$\beta = 16.56 \times 10^3 \left( \frac{\tau}{\sqrt{\frac{K}{\phi}}} \right)^{1.50} \quad (4.30)$$

Therefore the Forchheimer equation (4.24) can be written approximately as follows:

$$-K \frac{\Delta P}{\Delta L} = \mu v + 16.56 \times 10^3 \left[ \frac{\tau}{\sqrt{\frac{K}{\phi}}} \right]^{1.50} \rho v^2 \quad (4.31)$$

Furthermore, screening all of the non-Darcy models in Table 4.12 and the best-models to the established model equation (4.30) has been plotted in Figure 4.30.

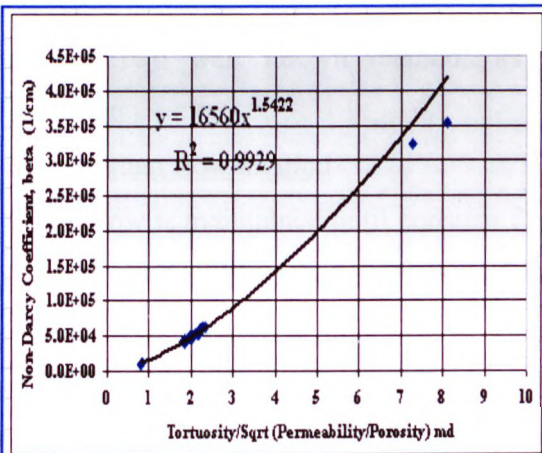


Figure (4.29) Non-Darcy Coefficient Vs. Tortuosity, Permeability over Porosity

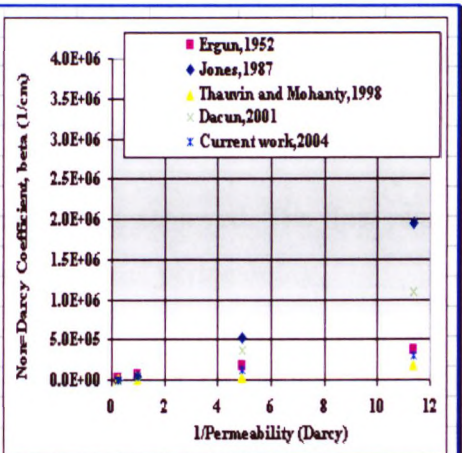


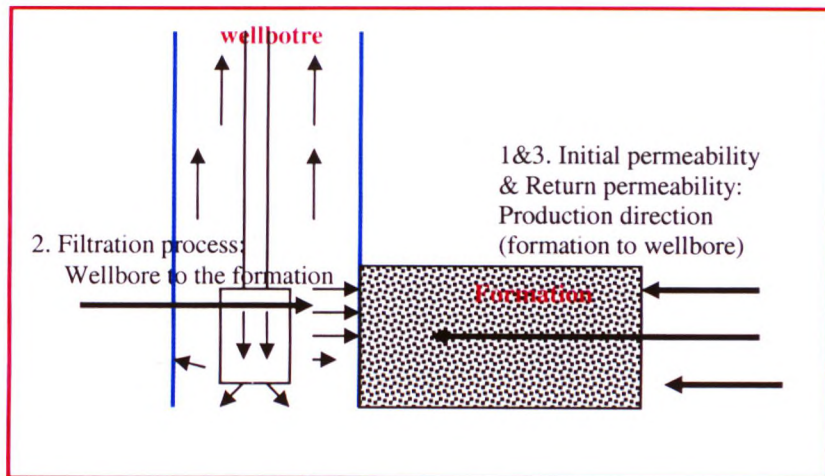
Figure (4.30) Non-Darcy Coefficient Models Comparison

#### 4.1.3.5 Quality Control Tool for Formation Damage Testing Procedure

##### 4.1.3.5.1 Formation Damage Evaluation

Normally evaluation of formation damage from drilling and completion fluids is undertaken in three stages as follows:

1. Initial permeability measurement in the formation to wellbore direction.
2. Static and dynamic filtration process in the wellbore to the formation direction.
3. Return permeability measurement as production direction.



##### 4.1.3.5.2 Permeability Measurement Methods

Basically two well known methods as follows can determine the production simulation:

###### 1.Constant flow method

The flow is maintained until constant flow stability is achieved. The flow rate for return permeability is the same as used during the initial permeability.

###### 2.Constant pressure method

A constant differential pressure to simulate drawdown conditions should be maintained until stable flow is achieved. The return permeability can be determined using the same constant pressure and procedure as used in the initial permeability determination.



In recent years there has been considerable interest in the development and standardisation of recommended practice for formation damage testing from several oil companies, drilling fluid companies and core analysis laboratories which will allow good levels of repeatability and reproducibility. Meanwhile the testing procedure submitted to all the oil companies, and the test materials (plugs, muds, oil and brine) are as uniform as possible. The result of these studies shows that the goal has not been achieved and significant variations are obtained, both between and within laboratories<sup>201,202</sup>. A major factor, which limits this practice, there is no standard procedure exists for this type of testing.

The general guidelines, which have been used in the current work as a quality assurance technique for formation damage testing procedures, are:

1. Mix all the required volume of drilling fluid to be tested in one batch.
2. To prevent imbibition all the cores should be saturated in the base fluid (water or oil) as base mud mixed.
3. Establish design criteria to characterise flow regimes in porous media in order to eliminate formation fines migration during flow measurement in the transition or turbulent flow regimes (see section 4.1.3.5.3).

#### 4.1.3.5.3 Flow in Porous Rocks

In flow of fluids in porous rock, it is important to know if the flow is laminar or turbulent. The laminar flow regime is dominant if the fluid particles move along smooth streamlines parallel to the wall of the pore throat passage. The velocity of the flowing fluid is virtually constant with time during laminar flow. The turbulent flow regime is dominant if the fluid velocity at any point in the pore throat passage varies randomly with time. In 1883, Osborne Reynolds<sup>179</sup> first investigated the differences between these two flow regimes. His experimental and theoretical work showed that the nature of the flow regime in pipes depends on the Reynolds number ( $Re=Dv\rho/\mu$ ), where  $D$  is the pipe inside diameter,  $\rho$  and  $\mu$  are the density and viscosity of the fluid respectively.

In a similar manner the Reynolds number of a porous rock (the ratio of inertial to viscous forces) can be defined in terms of rock parameters  $K$ ,  $\phi$  and  $\tau$ :

$$Re = \frac{D_{pore} V \rho}{\mu} \quad (4.32)$$

Substitute for  $D_{pore}$  in equation (4.18), then evaluate:

$$Re = 4 \sqrt{\frac{K \tau}{\phi}} \frac{V \rho}{\mu} \quad (4.33)$$

From analysis of the experimental studies (Clashach sandstone) it was possible to develop a correlation between the friction factor ( $f$ ) and the Reynolds number ( $Re$ ) of a porous rock. Figures 4.31 and 4.32 show three regions:

I.  $Re < 400$ , flow is in the laminar region viscous forces dominate (Darcy flow).

$$f = \frac{5}{Re^{1.20}} \quad (4.34)$$

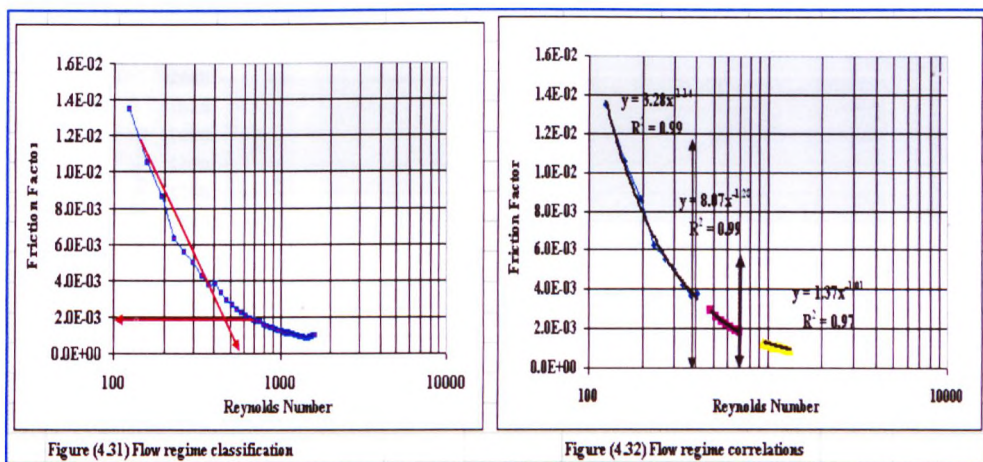
II.  $400 < Re < 600$ , the nature of the flow regime is transitional, i.e., the flow is in a region in which both viscous and inertia forces are significant.

$$f = \frac{10}{Re^{1.30}} \quad (4.35)$$

III.  $Re > 600$ , the flow is fully turbulent (inertia forces dominate).

$$f = \frac{1.50}{Re} \quad (4.36)$$





#### 4.1.3.5.4 Quality Control Tool Testing Methodology

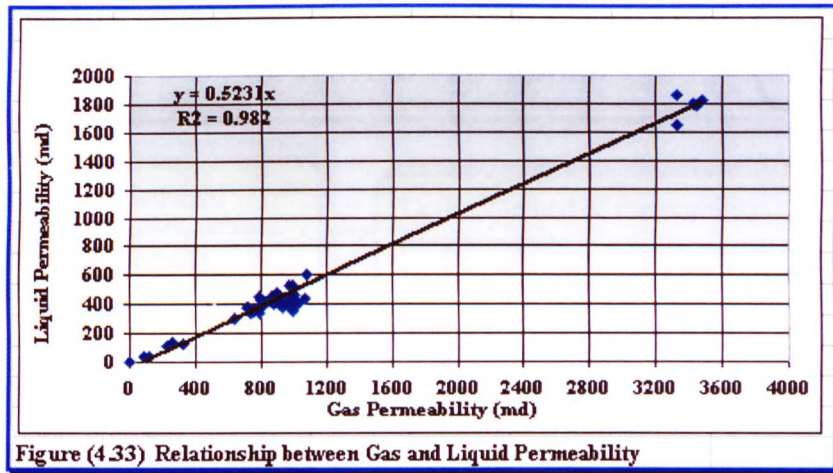
Based on the formation morphological characteristics the fluid flow through a porous medium has been characterised in terms of the Reynolds number and the friction factor for the porous rock, as in equations (4.34), (4.35) and (4.36). Therefore, the testing procedure for formation damage evaluation has been established as shown in Figure 4.34.

Table 4.13 shows an example of the criteria chosen to classify the fluid flow regimes in a porous medium.

With reference to the draft recommended practice for formation damage testing<sup>201</sup> the following method may be adopted:

1. Core preparation, characterisation, and fluid preparation can be carried out as recommended<sup>201</sup> with the following additions:
  - (a) An attempt has been made to establish a correlation equation 4.37 between gas permeability and liquid permeability as shown in Figure 4.33. Because the company supplying the cores (Corex) did not use the gas correction factor (Klinkenberg effect) for obtaining the core permeability.

$$K_{\text{liquid}} = 0.523 K_{\text{gas}} \quad (4.37)$$



- (b) The core plug should be saturated in brine for water-based mud or same base oil for oil based mud. The saturation fluid should be filtered to  $0.45 \mu m$ .
  - (c) The core plug should be installed on the core holder cell where all the measurement will take place.
  - (d) The pressure transducer should be selected with a maximum pressure of 100 psi and measurements taken to 3 decimal places for accuracy.
2. Initial permeability measurement:
- (a) Establish Excel spread sheet to set the criteria for flow regimes using Reynolds number (Re) and the friction factor of a porous rock to identify laminar and turbulent regimes as shown in Table 4.13. Tables 4.14 to 4.16 are given in Appendix A [Tables A1 to A3].
  - (b) The core plug should be flooded at laminar flow conditions with a minimum of fifty pore volumes and stability should be achieved before any measurements are undertaken.
  - (c) The flow should be maintained between  $Re = 200 - 400$  with fifty pore volumes and the pressure should be maintained until a constant flow rate is achieved.



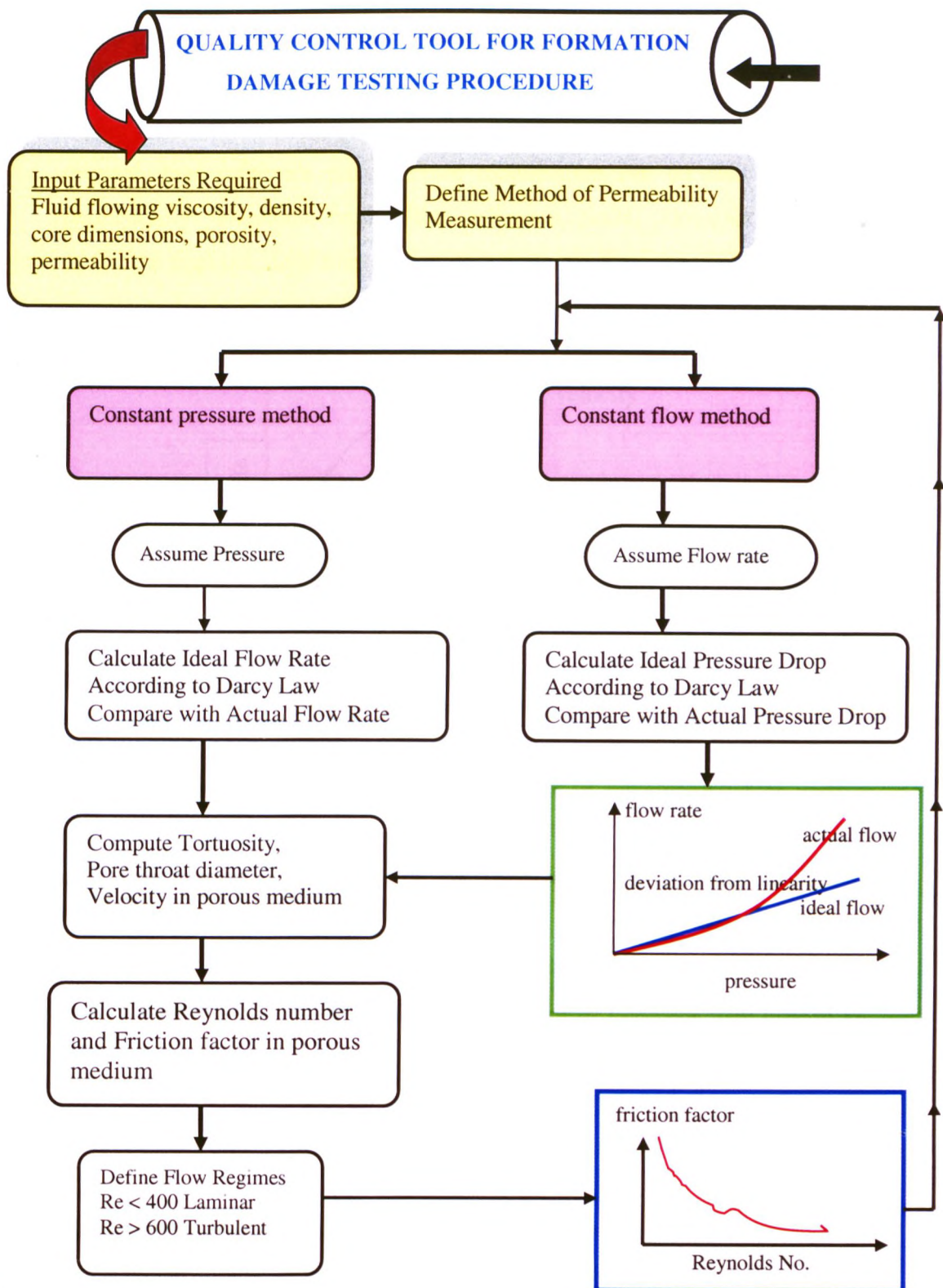
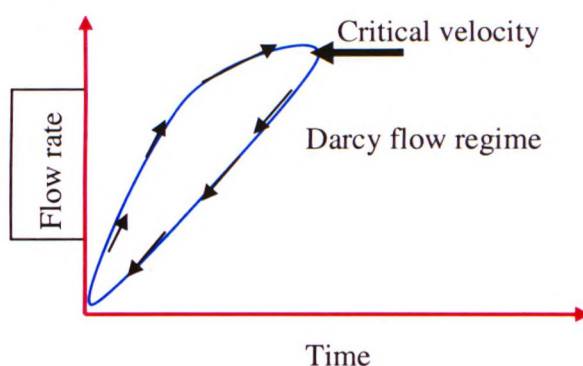


Figure 4.34 Flow chart for the quality control procedure of formation damage evaluation

- (d) Three points in the Darcy flow regime can be taken as references for initial permeability measurement [Figure 4.35]. The core plug can be flooded at higher flow rates (turbulent regime), and then the flow can be decreased to the original three reference points. Fines mobilisation can be distinguished if permeability decreases before the reference point. However Clashach sandstone does not show fines migration.



**Figure 4.35 Flow Regimes**

3. Dynamic filtration measurement can be followed as recommended or until a minimum of one pore volume filtrate is obtained.
4. Return permeability measurement is undertaken with the following recommendations:
  - (a) Clean the mud from the cell without disturbance to the filter cake.
  - (b) Flow initiation and cake-lift off pressures should be recorded with respect to time.
  - (c) After a minimum of fifty pore volumes has flowed and flow stability is achieved the return permeability can be recorded at the initial three reference points.
  - (d) The core plug should then be flooded with a minimum fifty pore volumes in the turbulent regime then the return permeability can be measured again for comparison with the above.



Porosity	Permeability	K, um	D pore, m	Area, m2					
0.17	530	0.52	9.92E-06	7.73E-11					
Formation resistivity factor = 29.33 Tortuosity = 4.98 Actual flow path = 7.07 cm									
Table 4.13 Criteria to classify the fluid flow regimes									
fr.f	volume, m3/sec	pore area, m2	velocity, m/sec	density, kgm-3	diameter, m	visc, kgm-ls-1	Reynold no.	Actual, pressur, psi	Ideal, pressure, psi
1.6E-01	2.29E-10	7.73E-11	2.96E+00	780	9.92E-06	0.0014	16.38	1	
3.1E-02	7.29E-10	7.73E-11	9.43E+00	780	9.92E-06	0.0014	52.14		1
1.9E-02	1.23E-09	7.73E-11	1.59E+01	780	9.92E-06	0.0014	87.90		
1.4E-02	1.73E-09	7.73E-11	2.24E+01	780	9.92E-06	0.0014	123.65	2	
1.1E-02	2.23E-09	7.73E-11	2.88E+01	780	9.92E-06	0.0014	159.41		2
8.7E-03	2.73E-09	7.73E-11	3.53E+01	780	9.92E-06	0.0014	195.17	3	
6.3E-03	3.23E-09	7.73E-11	4.18E+01	780	9.92E-06	0.0014	230.93		3
5.6E-03	3.73E-09	7.73E-11	4.82E+01	780	9.92E-06	0.0014	266.69		
5.0E-03	4.23E-09	7.73E-11	5.47E+01	780	9.92E-06	0.0014	302.45	4	
4.2E-03	4.73E-09	7.73E-11	6.12E+01	780	9.92E-06	0.0014	338.21		4
3.7E-03	5.23E-09	7.73E-11	6.76E+01	780	9.92E-06	0.0014	373.97		
3.8E-03	5.73E-09	7.73E-11	7.41E+01	780	9.92E-06	0.0014	409.72	5	5
3.4E-03	6.23E-09	7.73E-11	8.06E+01	780	9.92E-06	0.0014	445.48		
2.9E-03	6.73E-09	7.73E-11	8.70E+01	780	9.92E-06	0.0014	481.24		6
2.6E-03	7.23E-09	7.73E-11	9.35E+01	780	9.92E-06	0.0014	517.00	6	
2.4E-03	7.73E-09	7.73E-11	1.00E+02	780	9.92E-06	0.0014	552.76		
2.2E-03	8.23E-09	7.73E-11	1.06E+02	780	9.92E-06	0.0014	588.52		7
2.1E-03	8.73E-09	7.73E-11	1.13E+02	780	9.92E-06	0.0014	624.28	7	
1.9E-03	9.23E-09	7.73E-11	1.19E+02	780	9.92E-06	0.0014	660.04		8
1.8E-03	9.73E-09	7.73E-11	1.26E+02	780	9.92E-06	0.0014	695.79		
1.8E-03	1.02E-08	7.73E-11	1.32E+02	780	9.92E-06	0.0014	731.55	8	9
1.7E-03	1.07E-08	7.73E-11	1.39E+02	780	9.92E-06	0.0014	767.31		
1.6E-03	1.12E-08	7.73E-11	1.45E+02	780	9.92E-06	0.0014	803.07		
1.5E-03	1.17E-08	7.73E-11	1.52E+02	780	9.92E-06	0.0014	838.83	9	10
1.4E-03	1.22E-08	7.73E-11	1.58E+02	780	9.92E-06	0.0014	874.59		
1.4E-03	1.27E-08	7.73E-11	1.65E+02	780	9.92E-06	0.0014	910.35		11
1.3E-03	1.32E-08	7.73E-11	1.71E+02	780	9.92E-06	0.0014	946.11	10	
1.2E-03	1.37E-08	7.73E-11	1.78E+02	780	9.92E-06	0.0014	981.86		12
1.2E-03	1.42E-08	7.73E-11	1.84E+02	780	9.92E-06	0.0014	1017.62		
1.2E-03	1.47E-08	7.73E-11	1.91E+02	780	9.92E-06	0.0014	1053.38	11	
1.1E-03	1.52E-08	7.73E-11	1.97E+02	780	9.92E-06	0.0014	1089.14		13
1.1E-03	1.57E-08	7.73E-11	2.03E+02	780	9.92E-06	0.0014	1124.90	12	
1.1E-03	1.62E-08	7.73E-11	2.10E+02	780	9.92E-06	0.0014	1160.66		14
1.1E-03	1.67E-08	7.73E-11	2.16E+02	780	9.92E-06	0.0014	1196.42		
1.0E-03	1.72E-08	7.73E-11	2.23E+02	780	9.92E-06	0.0014	1232.18		
9.7E-04	1.77E-08	7.73E-11	2.29E+02	780	9.92E-06	0.0014	1267.93	13	15
9.5E-04	1.82E-08	7.73E-11	2.36E+02	780	9.92E-06	0.0014	1303.69		
9.1E-04	1.87E-08	7.73E-11	2.42E+02	780	9.92E-06	0.0014	1339.45		
8.9E-04	1.92E-08	7.73E-11	2.49E+02	780	9.92E-06	0.0014	1375.21	14	
8.5E-04	1.97E-08	7.73E-11	2.55E+02	780	9.92E-06	0.0014	1410.97		
8.4E-04	2.02E-08	7.73E-11	2.62E+02	780	9.92E-06	0.0014	1446.73		
8.2E-04	2.07E-08	7.73E-11	2.68E+02	780	9.92E-06	0.0014	1482.49	15	
8.9E-04	2.12E-08	7.73E-11	2.75E+02	780	9.92E-06	0.0014	1518.25		
9.0E-04	2.17E-08	7.73E-11	2.81E+02	780	9.92E-06	0.0014	1554.00		
9.6E-04	2.22E-08	7.73E-11	2.88E+02	780	9.92E-06	0.0014	1589.76	20	
9.6E-04	2.27E-08	7.73E-11	2.94E+02	780	9.92E-06	0.0014	1625.52		20
1.0E-03	2.32E-08	7.73E-11	3.00E+02	780	9.92E-06	0.0014	1661.28		25
1.1E-03	2.37E-08	7.73E-11	3.07E+02	780	9.92E-06	0.0014	1697.04	25	

Open the cell and visually observe the filter cake; if this is completely removed then the test is completed otherwise it is manually removed and the return permeability measurement is repeated. Therefore the fluid design can be discussed or a suitable cake clean-up procedure can be proposed.

The design criteria established has been used as predictive criteria for formation testing procedure and it shows interesting results, which can be summarised as follows:

1. Fluid flow behaviour in medium and high permeability formations shows that the deviation from Darcy linearity occurs in the turbulent regime as expected [Figure 4.36]. Figure 4.37 is given in Appendix A (A15).
2. Fluid flow behaviour in low permeability formations shows that deviation from Darcy linearity can occur in the laminar regime which is different from expected range ( $\sim Re < 400$ ) as shown in Figures 4.38 and 4.39 in Appendix A (A16 and A17).



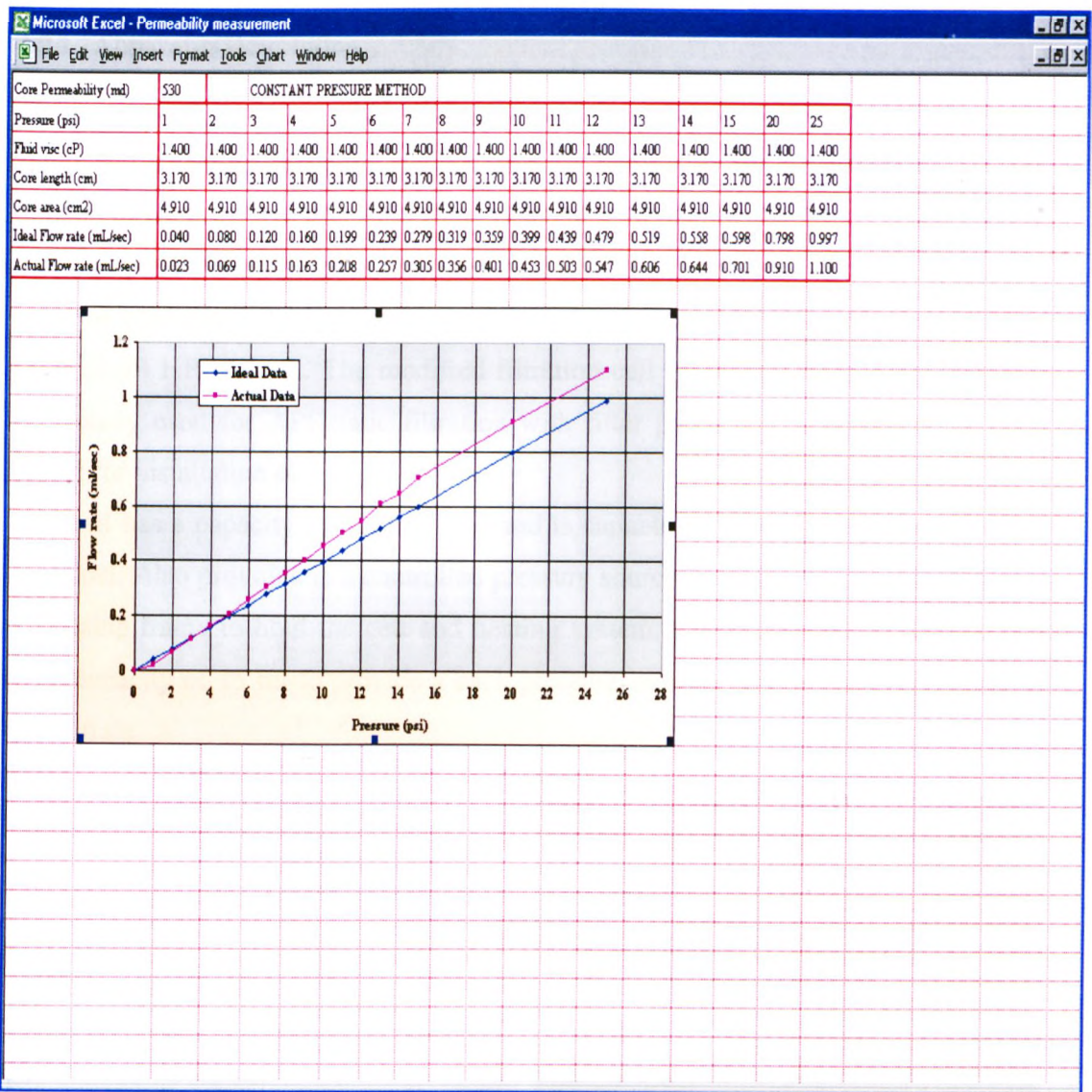


Figure 4.36 Tabular and graphical display for permeability measurement and deviation in linearity in the turbulent flow regime

## 4.2 FILTRATION EXPERIMENTAL STUDIES

### 4.2.1 Apparatus Description

The equipment, designed and built by Schlumberger Cambridge Research (SCR) for static and dynamic filtration studies, permits testing to be completed at realistic temperatures, pressures and fluid shear rates under dynamic conditions [Figure 4.40]. The equipment consists of a core holder [Figure 4.41] containing the plug (natural core) or modified cell containing a ceramic disc is placed in one end of a modified (elongated) HP-HT cell. The modified filtration cell originated from a cell that was previously used for API static filtration with filter paper and modified to be open ended for installation of a porous disc.

The cell has a capacity of 160 ml mud and is capable of working at pressures up to 3200 psi. Also provided is a controlled pressure source, a system for heating the cell, a suitable frame to hold the cell and heating system, and pressurised collection cell with capacity of 15 ml to provide a back pressure in order to prevent evaporation of the filtrate.

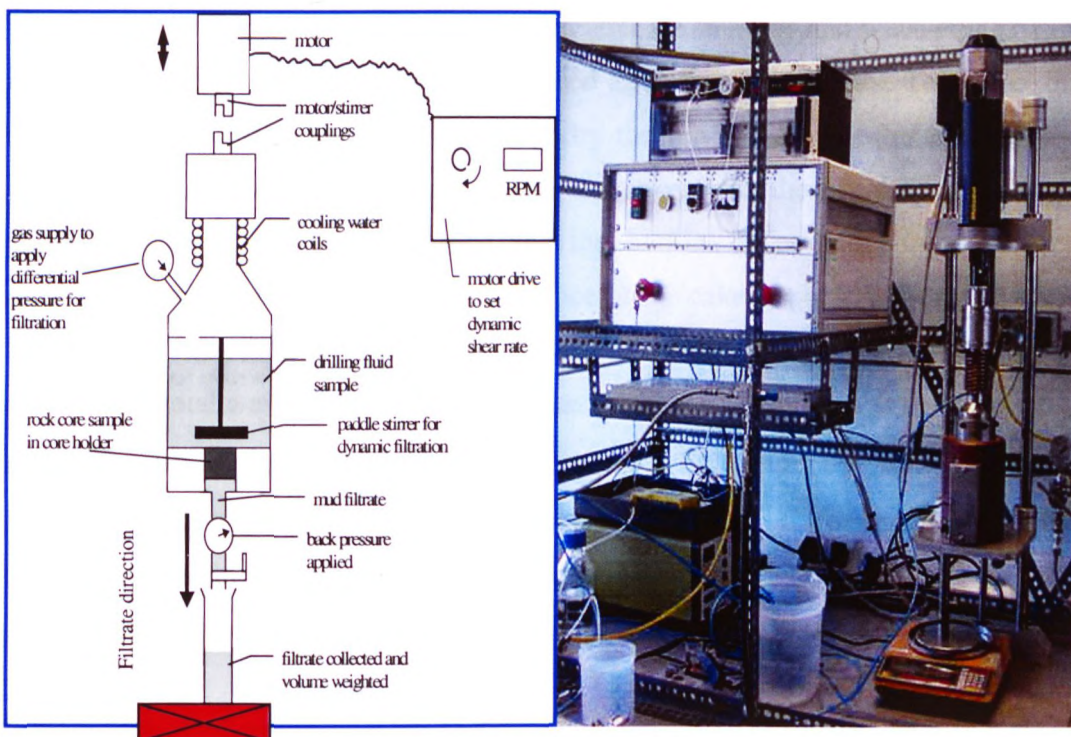


Figure 4.40 Schematic diagram of the apparatus for HP-HT dynamic filtration

A shim measuring 500  $\mu\text{m}$  is placed on the core and the paddle adjusted so that it touches the shim. The shim is then removed and the fluid to be tested added. This method ensures that the paddle is a standard distance from the core face for all the experimental tests. The paddle is rotated via a motor drive connected to a stirrer [Figure 4.42]. The paddle speed is controlled by means of a control unit, which allows a maximum speed of 1000 rpm. An accurate rotation speed is displayed on the digital display. Whilst waiting for the test cell to heat up, a pressure of 100 psi was applied from the top valve.

The bottom valve stem was closed and the mud stirred at a low shear rate to ensure fluid homogeneity. The filtrate volume was collected, weighed and recorded for each core plug tested. Due to equipment limitations the maximum temperature used was 300 °F and 900 psi differential pressure.

The spurt loss was measured at 20 seconds. The filtration weight was measured manually with respect to time due to the restriction at the bottom valve when used above 200 °F.

The first filtration test conducted was stopped after seven hours and when equilibrium was achieved, dynamic filtration was recorded after about two hours. Thereafter the bottom valve was initially closed followed by the top valve and after cooling, the pressure was then carefully released. The top cover was then removed, the mud drained off, the bolts were loosened and the bottom cover and core were then removed. Any excess mud lying on the surface of the cake, especially from the static filtration test, was then gently scraped and the filter cake thickness was measured by caliper. The total weight of the wet filter cake was recorded and it was then placed in a heated oven at 90 °C for two days to dry out. To ensure the cake was dried completely the oven temperature was then raised to 120 °C for another day. No decrease in weight was recorded after this second drying period. Finally, the cell was cleaned carefully and dried with pressurised air.





**Figure 4.41 Core holder and natural core**

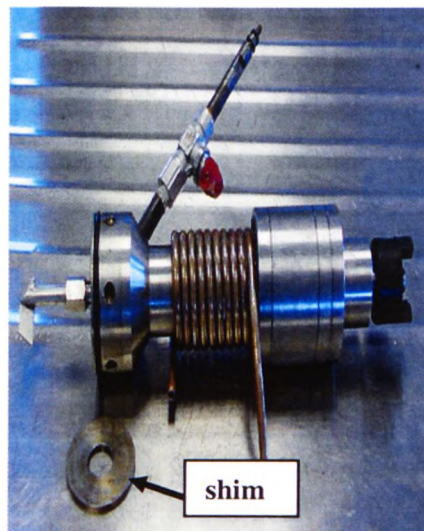


**Figure 4.42 Paddle stirrer**

#### **4.2.2 HP-HT filtration Testing Procedure**

The HP-HT filtration testing procedure is given in Appendix A (A4.2.2).

#### **4.2.3 Analysis of Results**

The static and dynamic filtration results for WBM and OBM are given in Appendix A [Tables 4.14 (A1) to 4.40 (A27)]. The analysis of the results is discussed in Chapter 5.

Oil-and water-based mud filtrate viscosities and densities were measured using a Cannon-Fenske Glass Capillary Viscometer (no.25763) and Density Meter. Results are presented in Figures 4.43 and 4.44 respectively.

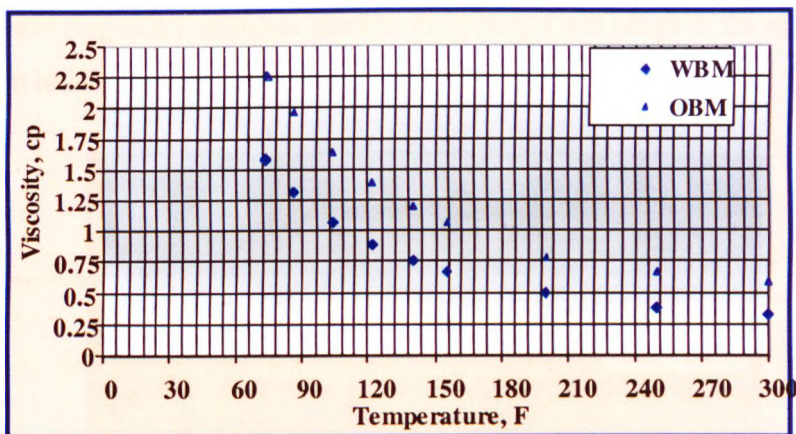


Figure 4.43 Filtrate viscosity of water and oil based muds

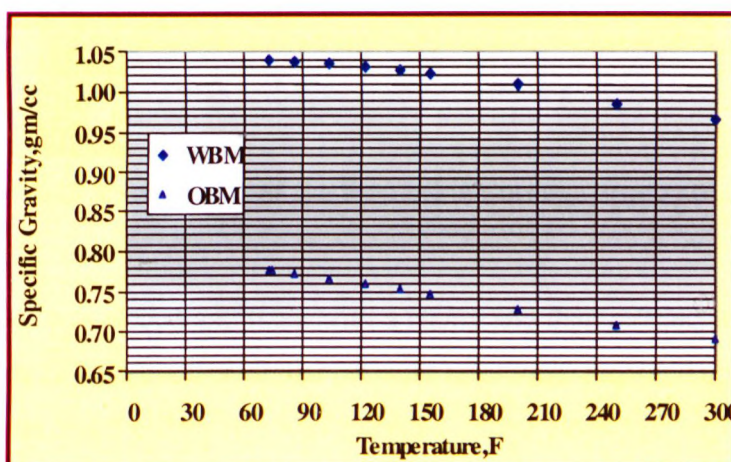


Figure 4.44 Filtrate density of water and oil based muds

### 4.3 FORMATION DAMAGE EXPERIMENTAL STUDIES

#### 4.3.1 Apparatus Description

The formation damage apparatus [Figure 4.45] is designed to measure initial and return permeabilities after the rock core has been exposed to a drilling fluid, or any other fluid which comes into contact with the reservoir.

The equipment consists of an HP/HT filtration cell, sample cell holder as shown in Figure 4.41, a base plate, a rubber Hassler sleeve (2mm wall thickness), a stainless



steel pressure ring and a stainless steel locking ring. Core plugs of 25 mm in diameter and 30 mm in length were used.

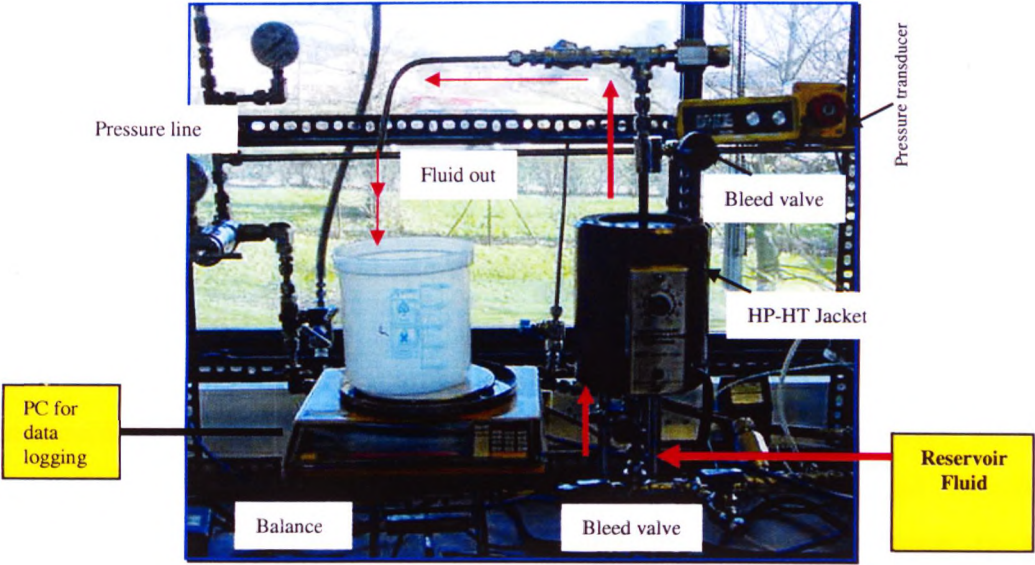


**Figure 4.45 A schematic of the formation damage apparatus**

The core holder was placed and fixed with a clamp and then connected to a reservoir delivering brine or base oil. The digital pressure transducer recorded up to 60 psi. The pressure was set and the flow rate was recorded on the electronic balance connected to a PC running the data logging software.

### 4.3.2 Permeability Measurement Method

The constant pressure method has been used in the current study.

#### 4.3.2.1 Initial and Return Permeability Testing Procedure

The formation damage testing procedure is given in Appendix A (A4.3.2.1).

### 4.3.3 Analysis of Results

The analysis of the results is discussed in Chapter 5.



## **4.4 RHEOLOGICAL CHARACTERISATION EXPERIMENTAL STUDIES**

### **4.4.1 Apparatus Description**

The Fann-70 HP-HT Viscometer (Figure 4.46) is a sophisticated apparatus capable of measuring the rheology of fluids using 6-speed dial reading, at conditions up to 500 °F and 20,000 psi and is only available in research labs.

The dial reading measurements are undertaken at rotor speeds of 600, 300, 200, 100, 6, and 3 rpm respectively. For the fluid to be homogeneous, constant temperature was maintained and pressure varied up to 17000 psi. Temperature was increased in steps from 150 °F up to 300 °F.

The time duration for one particular test varies depends on the number of measurements but could take a minimum of four hours including preparation, testing, re-installation and cleaning. This equipment was used for fluid rheology characterisation under downhole conditions because of its relevance to the programme objectives of this research work.



**Figure 4.46 HP-HT Fann-70 Viscometer**

### **4.4.2 HP-HT Fann-70 Rheometer Testing Procedure**

The testing procedure is given in Appendix A (A4.4.2).

### **4.4.3 Analysis of Results**

The results are listed in Tables 4.41 and 4.42, given in Appendix A (Tables A28 and A29). The analysis of results is discussed in Chapter 5.

## 4.5 PARTICLE SIZE EXPERIMENTAL STUDIES

### 4.5.1 Apparatus Description

The Malvern Mastersizer Micro Plus (Model No. MAF-5001) analyser is shown in Figure 4.47. The instrument (computer controlled) is capable of measuring particle-size distribution over the range of  $0.05\ \mu\text{m}$  to  $550\ \mu\text{m}$ , which is adequate for most oil field applications. The equipment has been used to measure particle size distribution for WBM and OBM. It has been adapted by the author to measure:

1. Particle size distribution for static and dynamic filter cakes.
2. Particle size of water and oil droplets to achieve optimum emulsifier concentration for water and oil based muds.
3. A quality control tool for comparison of different types of emulsifiers.

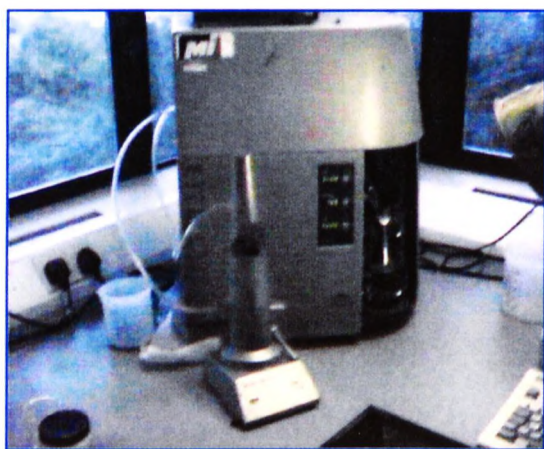


**Figure 4.47 Malvern Mastersizer**

### 4.5.2 Basic Theory for Particle Size Analysis (PSA)

The Malvern Mastersizer instrument uses the main technique, namely, laser diffraction. With the laser diffraction technique, an "equivalent sphere" is the sphere which would produce the same scattering intensities as the particle being examined and characterised by a single linear dimension, the diameter or radius. That is, it is a sphere of approximately equal volume. When light is scattered by the presence of particles in a beam of light, the pattern of light intensity shows variations with angle.

Small particles scatter at large angles and conversely large particles scatter at small angles. The light scattered from the distribution of particles is measured by a series of detectors and the data subsequently processed to give an estimate of the initial size distribution relative to the volumetric distribution of particle sizes present. This is done by using a mathematical model (Mie theory) which takes into account the Refractive Index (R.I.) of the medium, R.I. of the particle and relative R.I. of absorption, thus giving a better prediction of the equivalent volume diameters of the particles.

#### **4.5.3 Particle Size Distribution Testing Procedure**

The Malvern Master-sizer Micro Plus particle size analyser measurement procedure is given in Appendix A (A4.5.2).

#### **4.5.4 Analysis of Results**

The analysis of the results is discussed in Chapter 5.

## **CHAPTER FIVE**

### **FLUID RHEOLOGY, FILTRATION AND FORMATION DAMAGE CHARACTERISATION**

This chapter presents the experimental results of the rheological, filtration and formation damage characterisation studies, which extend the rheological, filtration and formation damage characterisation data available under different applied factors and conditions for the most common HP-HT drilling fluids. The effect of rheological properties has been incorporated into the description of the filtration mechanism under dynamic conditions. It was found that a critical overbalance pressure zone for water based mud exists where decreased permeability impairment occurs. A new application testing technique developed for the Particle Size Analyser to measure particle size distribution for static and dynamic filter cakes is also presented.

#### **5.1 FLUID RHEOLOGY**

##### **Background**

Rheology is an extremely important aspect of drilling fluids, completion fluids and cements. In drilling operations, the term rheology refers to the significance of the shear stress, shear rate, and time relationships of drilling fluids. The shear rate is determined by the flow rate of the fluid through a particular geometrical configuration. Resistance of the fluid to the applied rate of shear is called the shear stress, which is related to the pump pressure for the circulating system.

The accurate description of the fluid rheological properties is fundamental to specific applications such as:

1. The prediction of pressure drops and equivalent circulating density in the wellbore which can minimise fluid loss and avoid fracture of the formations crossed due to the under estimation of the annular pressure drop.
2. The design of optimum hydraulics for effective wellbore cleanup and stability.



3. The determination of optimum operating conditions such as pumping rate and circulation pressure.
4. The detection of unexpected changes of the stand pipe pressures due to a change in the hydraulic drilling circuit and decisions on action to restore the original conditions.
5. The suspension and transport of solids including cuttings and milled tools.
6. The design for the concentration and type of chemical additives for optimum fluid formulation.

Consequently, mud rheology is monitored on a continuous basis during drilling and adjusted with additives or dilution to meet the needs of the operation.

### **5.1.1 Rheological Characterisation of Drilling/Completion Fluids**

It is essential to use a minimum of 6-speeds in a viscometer to characterise drilling and completion fluids. The common multi-speed instrument is the six-speed Fann model<sup>176</sup> 35A. The operating speeds are 600, 300, 200, 100, 6 and 3 rpm. At the rig site the rheological properties of drilling fluids are measured at ambient pressure and at elevated temperature, usually 120 or 150 °F. Rotational viscometers exist for the measurement of rheological properties at elevated temperatures and pressures, which reflects downhole conditions. Costly devices such as HP-HT Fann-70 viscometer are only used in the laboratory for specialist studies, such as the present work.

## **5.2 NEWTONIAN FLUIDS<sup>203</sup>**

Fluids in which the shear stress is directly proportional to the shear rate are called Newtonian. Water, brine and diesel oil are some examples of Newtonian fluids. The viscosity of Newtonian fluids, i.e. the ratio of the shear stress to shear rate is a constant for any given temperature and pressure. In Figure 5.1 the flow curve for the Newtonian fluid passes through the origin, i.e. at zero shear rate there is zero shear stress. The equation defining a Newtonian fluid is:

$$\tau = \mu(\dot{\gamma}) \quad (5.1)$$

where  $\tau$  is the shear stress,  $\mu$  the viscosity and  $\gamma$  the shear rate.

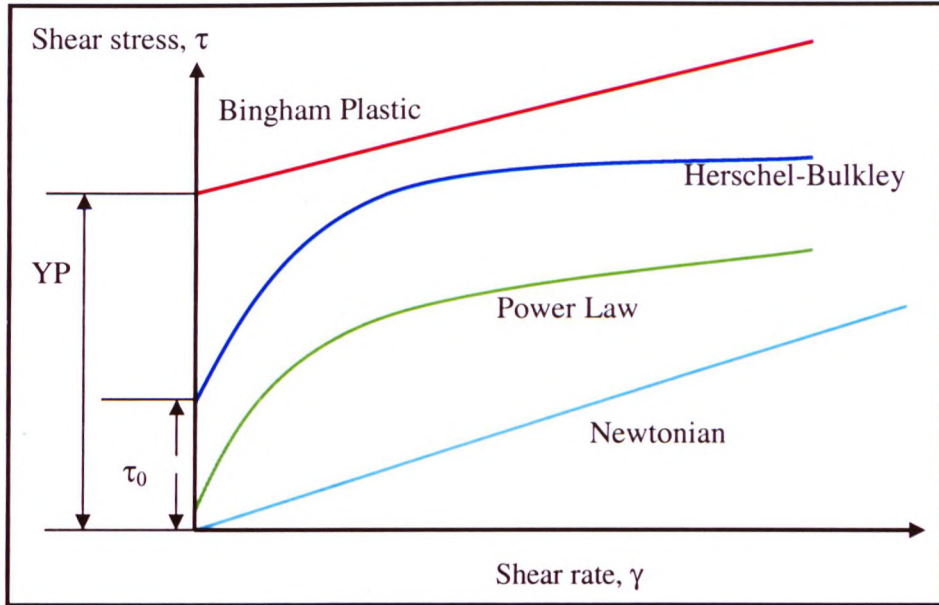


**Figure 5.1 Flow curves for typical drilling fluids rheology models**

### 5.3 NON-NEWTONIAN FLUID<sup>203</sup>

The viscosities of most drilling fluids change with shear rate and thus they do not behave as Newtonian fluids. A fluid with a viscosity which is dependent on shear rate is called non-Newtonian. The multitude of functions performed by a drilling fluid are most often not met satisfactorily by a fluid having a constant viscosity at all shear rates. It is desirable for a drilling fluid to have a very low viscosity around the bit for better penetration rate and bottom hole cleaning, a relatively low viscosity in the pipe to minimise pressure losses in the drill string and higher viscosity in the annulus for hole cleaning. A fluid whose viscosity decreases as the shear rate increases - a so-called shear thinning fluid - meets these requirements. The variation of viscosity with shear rates for typical drilling fluids are shown in Figure 5.2.

A large number of rheological models (a minimum of 15 models) have been proposed which relate the shear stress to shear rate. Rather than describing the stress-rate relationship with one constant (the viscosity) as for a Newtonian fluid, two or more



constants are required for non-Newtonian fluids. The complexity of the model and its application increases as the number of constants increase. The two-and three-parameter models, which have found considerable use in the drilling industry for describing the rheological behaviour of drilling fluids[Figure 5.1], are discussed in section 5.3.1.

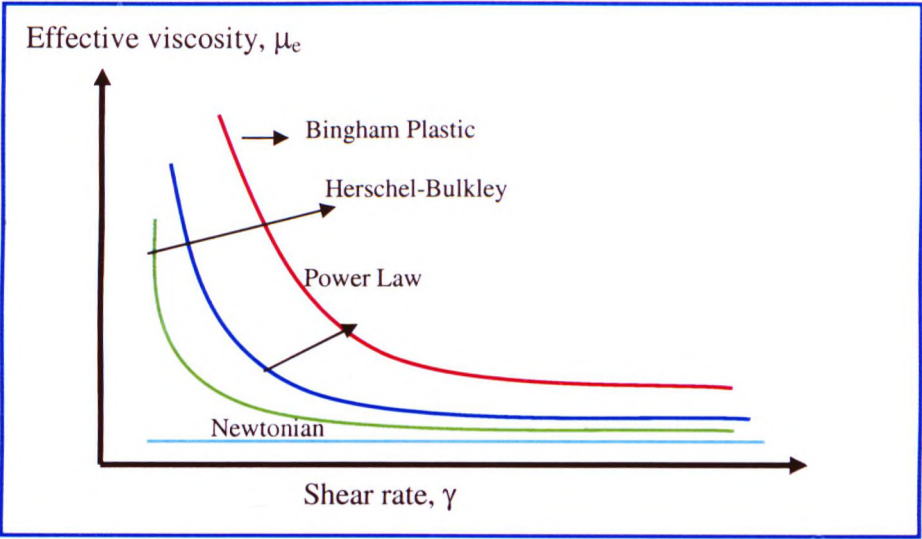


**Figure 5.2** Variation of the effective viscosity of typical drilling fluids with shear rate

### 5.3.1 A Review of Rheological Models

Non-Newtonian fluid flow behaviour is characterised by a number of rheological models. Five models are listed in Table 5.1.

**Table 5.1** Expressions for non-Newtonian rheological models

Basic Expression				
Bingham-Plastic <sup>204</sup>	Power-Law <sup>205</sup>	Herschel-Bulkley <sup>206</sup>	Robertson-Stiff <sup>209</sup>	Casson <sup>210</sup>
$\tau = YP + PV(\gamma)$	$\tau = K(\gamma)^n$	$\tau = \tau_0 + K(\gamma)^n$	$\tau = (\gamma_0 + \mu_0 \gamma)^n$	$\tau = [(\tau_0 + \mu_0 \gamma)^{0.5}]^2$

Where:  $\tau$ - shear stress

$\gamma$ - shear rate

PV-Bingham plastic viscosity

K- consistency index

$\tau_0$ - true yield stress

$\gamma_0$ - shear rate intercept

YP- Bingham yield point

n- flow behaviour index

$\mu_0$ -high shear rate viscosity

#### 5.3.1.1 Bingham Plastic Model

In the early 1900s, E.C. Bingham<sup>204</sup> first recognised that some fluids exhibited a linear shear stress - shear rate behaviour after an initial shear stress threshold has been reached. Plastic viscosity (PV) is the slope of the line and yield point (YP) is the threshold stress. The Bingham Plastic model is one of the simplest non-Newtonian models used for describing drilling fluids and can be expressed mathematically as follows:

$$\tau = YP + PV (\gamma) \quad (5.2)$$

The two parameters PV and YP are used extensively in the drilling fluids industry due to the relative ease in calculating these parameters. Plastic viscosity is used as an indicator of the size, shape, distribution and quantity of solids, and the viscosity of the liquid phase. The Bingham yield point is a measure of electrical attractive forces in the drilling fluid under flowing conditions.

#### 5.3.1.2 Power Law Model

The Power Law model<sup>205</sup> is traditionally used to represent the fluids whose viscosity decreases as shear rate increases. This shear-thinning phenomenon can be described mathematically as follows:

$$\tau = K (\gamma)^n \quad (5.3)$$

#### 5.3.1.3 Herschel-Bulkley Model (Modified Power Law)

The rheological behaviour of the Herschel Bulkley<sup>206</sup> model at low shear rate often falls below the Bingham Plastic model and above the Power Law. On the other hand,

a procedure suitable for field use has been proposed for the Herschel-Bulkley model<sup>207</sup>. Not surprisingly, the Herschel-Bulkley model is rapidly gaining importance in industry as a more accurate description of drilling fluid than the two traditional models, namely Bingham Plastic and Power Law models<sup>208</sup>.

The reason for this is that the Herschel-Bulkley model is a three-parameter model and thereby offers greater flexibility in matching viscometer data. The Herschel-Bulkley model can be described mathematically as follows:

$$\tau = \tau_0 + K (\dot{\gamma})^n \quad (5.4)$$

The three parameters:  $\tau_0$ ,  $K$  and  $n$  are the true yield stress, the consistency factor and the behaviour index respectively.

If the exponent  $n$  is equal to one, equation (5.4) reduces to Bingham Plastic model. If the yield stress  $\tau_0$  is zero, equation (5.4) reduces to the power Law model. If  $n = 1$  and  $\tau_0 = 0$ , then equation (5.4) describes a Newtonian fluid with a viscosity of  $K$ .

### 5.3.2 Effective Viscosity of non-Newtonian Fluids

The effective viscosity, ( $\mu_e$ ), is defined as the ratio of the shear-stress to the shear-rate and can be described mathematically by:

$$\mu_e = \tau / \dot{\gamma} \quad (5.5)$$

The expressions for the effective non-Newtonian viscosity ( $\mu_e$ ) for the five rheological models discussed are given in Table 5.2.

The variation of the effective non-Newtonian viscosity,  $\mu_e$  with shear-rate,  $\dot{\gamma}$  is depicted for the Bingham Plastic, Power Law and Herschel-Bulkley models in Figure 5.2. It can be observed that the non-Newtonian viscosity,  $\mu_e$  is characterised by high values at low shear-rates, drops rapidly with increasing shear, and levels off at high shear - rates.

**Table 5.2 Expressions for non-Newtonian viscosity for various rheological models**

Expressions for non-Newtonian viscosity				
Bingham-Plastic	Power-Law	Herschel-Bulkley	Robertson-Stiff	Casson
$\frac{YP}{\gamma} + PV$	$K\gamma^{n-1}$	$\frac{\tau_0}{\gamma} + K\gamma^{n-1}$	$\frac{(\gamma_0 + \mu_0\gamma)^n}{\gamma}$	$\left[ \left( \frac{\tau_0}{\gamma} \right)^{0.5} + \mu_0^{0.5} \right]^2$

**5.4 METHODOLOGY FOR CALCULATING PARAMETERS  
AND SELECTING THE BEST MODEL**

Most of the relevant literature provides expressions for parameter estimation for Bingham Plastic, Power Law, and Herschel-Bulkley fluids. These parameter estimation procedures were developed for quick, field computation. Representative rheological model selection can only be performed through the evaluation of relative model performance against measured viscometer data. The problem of recent work<sup>7,8,211</sup> is that the fluid characterisation for the whole flowing system is based on an assumption that the fluid can be characterised based on readings at high shear rates (typically  $\theta_{600}$  and  $\theta_{300}$ ), where  $\theta_{600}$  represent the actual reading taken at 600 rpm and  $\theta_{300}$  is the same for 300 rpm. This results in poor fluid characterisation for low shear rates. The author agrees with the work of Bailey et al.<sup>212</sup> and others<sup>213</sup> who conclude that the fluid characterisation should take into account both low and high shear rates.

**5.4.1 Calculating Model Parameters**

This section outlines a simple analytical method for model parameter calculation and defines the correct approach for selecting the most suitable rheological model. Direct parameter solution refers to the method of rheological solution using rotational viscometer readings to solve a set of equations derived from the rheological model

itself. The computation of a simple parameter solution for the standard Fann Viscometer can be made as follows:

$$\text{Shear rate } \gamma, \text{ sec}^{-1} = 1.7032 \times \text{RPM}$$

$$\text{Shear stress } \tau, \text{ dynes/cm}^2 = 5.1 \times \theta_{300}$$

### 1. Bingham Plastic

The API method uses readings directly from the Fann viscometer as follows:

$$\text{PV} = \theta_{600} - \theta_{300} \quad \text{cP} \quad (5.6)$$

$$\text{YP} = \text{PV} - \theta_{300} \quad \text{lbs/100ft}^2 \quad (5.7)$$

Where  $\theta_{600}$  and  $\theta_{300}$  represent the actual readings taken at 600 rpm and 300 rpm respectively.

### 2. Power Law

$$n = 0.50 \log_{10} (\theta_{300}/\theta_3) \quad (5.8)$$

$$K = (100 \times \theta_{300} / 511^n) \quad \text{cP} \quad (5.9)$$

### 3. Herschel-Bulkley - Simple Parameter Estimation Procedure

$$\tau_0 = (2 \times \theta_3) - \theta_6 \quad \text{lb/100ft}^2 \quad (5.10)$$

Where  $\theta_6$  and  $\theta_3$  are respectively the readings at 6 rpm and 3 rpm.

$$\tau'_{300} = (\tau_{300}) - \tau_0 \quad (5.11)$$

$$\tau'_3 = (\tau_3) - \tau_0 \quad (5.12)$$

Where  $\tau_{300}$  and  $\tau_3$  represents the shear stresses at 300 rpm and 3 rpm respectively.

$$n = 0.50 \log_{10} (\tau'_{300} / \tau'_3) \quad (5.13)$$

$$K = (100 \times \tau'_{300} / 511^n) \quad (5.14)$$



### 5.4.2 Calculating Shear Stress

The shear stress for each particular shear rate can be calculated using equations (5.2) to (5.4) for the Bingham Plastic, Power Law and Herschel-Bulkley models respectively.

### 5.4.3 Model Selection

Goodness-of-fit criteria have been used to compare measured and calculated shear stress and the most suitable rheological model selected. Statistical measures of goodness-of-fit are necessary to determine appropriate rheological models to be employed<sup>214,215</sup>.

#### Residual of Error Method (RMS):

It is standard practice to analyse residuals of error in order to detect the inadequacies of a model as:

$$\text{Percentage of Error} = \sqrt{\frac{\sum_{i=1}^N \left( \frac{SS_{i \text{ predicted}} - SS_{i \text{ measured}}}{SS_{i \text{ predicted}}} \right)^2}{N}} \times 100 \quad (5.15)$$

where:

$SS_{i \text{ predicted}}$  shear stress predicted from the model

$SS_{i \text{ measured}}$  shear stress from experimental data

$N$  total data points

## 5.5 PREVIOUS RESEARCH

A number of publications have dealt with the behaviour of drilling fluids at various combinations of temperature and pressure using common rheological models namely, Bingham Plastic, Power Law, and Herschel-Bulkley models.

McMordie et al.<sup>216</sup> concluded that the Power Law model gave the best mathematical description of the viscosity of an invert oil base mud at constant temperature and

pressure. However, the Power Law constants for each mud must be determined experimentally. DeWolfe et al.<sup>217</sup> in a study of lower toxicity base oils found the Herschel-Bulkley model fitted their data very well. Politte<sup>218</sup> chose to model invert oil base mud as a Bingham plastic fluid. Bailey et al.<sup>219</sup> used the Bingham model to describe the rheology of low toxicity oil base mud, but noted that at higher temperatures the data departs from this model. Rheological behaviour of the drilling fluid may change at different temperature and pressure, therefore the methodology for calculating parameters and selecting the best model (section 5.4.1) should be tested at several different pressures and temperatures. Houwen et al.<sup>220</sup> investigated invert oil base mud and found the Herschel-Bulkley model fitted the data very well.

Studies of water based muds have also attempted to fit rheological models to experimentally determined rheograms. Gucuyener<sup>221</sup> studied weighted bentonite fluids and found the Casson model fitted the data. Wanneng et al.<sup>222</sup> studied the high shear rate viscosity at the bit nozzle for low solids bentonite fluids and found that the Casson model gave the best fit. Alderman et al.<sup>223</sup> studied bentonite polymer fluids and found the rheograms best fitted using the Herschel-Bulkley model. Davison et al.<sup>224</sup> studied invert and synthetic oil base fluids and water base fluids to evaluate the impact of cold temperature rheology on the equivalent circulation density and found the Herschel-Bulkley model fitted their data very well.

The correct selection of a rheological model to describe drilling fluid rheology is very important for engineering hydraulics calculations such as hole cleaning, equivalent circulation density, etc. However, for wells with small margins (narrow drilling window) between pore and fracture pressure, careful evaluation and analysis of effects of temperature and pressure on wellbore hydraulics and kick probability is essential for management of bottom-hole pressure.<sup>177,225,226</sup>

Overall the studies and practices to date showed limitations because:

1. Most of the existing models are limited in application and rigs are equipped only with the LP-LT Fann viscometer which is inadequately for a field engineer to predict fluid rheology accurately under downhole conditions.

2. The effect of the rheological behaviour of the drilling fluid on filtration mechanisms and formation damage is still not clearly understood.

The rheological behaviour of the drilling fluid has a major impact on the pressure distribution profile in the wellbore, hence affecting drilling overbalance pressure and in turn drilling fluid filtration and formation damage mechanisms. Therefore, to adequately predict impact of downhole filtration on formation damage, it is also necessary to predict downhole fluid rheology.

The current increase in HT developments presents unique challenges for drilling fluid design and application. Therefore drilling fluid studies should be extended to include HP-HT drilling fluids such as lignosulphonate water based mud and synthetic oil based mud as new applications.

## **5.6 RHEOLOGICAL CHARACTERISATION OF HP-HT DRILLING FLUIDS**

The rheological characterisation of the freshwater lignosulphonate and synthetic oil based muds was investigated using HP-HT Fann 70 measurements at temperature values of 150, 200, 250 and 300 °F and pressure values from 15 to 17000 psi. In Appendix B the results are given in Tables B1 (5.3) to B4 (5.6) (for WBM) and in Tables B5 (5.7) to B8 (5.10) are (for OBM).

The rheological behaviour of water and oil based muds were described using the three most common rheological models, namely, the Bingham Plastic, Power Law, and Herschel-Bulkley models.

Figures 5.3 to 5.10 show the rheological behaviour of water and oil based muds as functions of temperature and pressure. The experimental data clearly demonstrates the following trends:

- Figures 5.3 and 5.4 show the range of temperature and pressure conditions used in this study. The Herschel-Bulkley model most accurately describes the water and oil based muds (see section 5.3.1.3). The reason for this is that the Herschel-

Bulkley model has three-parameters and thereby offers greater flexibility when calibrated against viscometer data.

- The shear stress for a given shear rate decreases significantly as the temperature increases from 150 ° F to 300 ° F [Figures 5.5 and 5.6].
- The shear stress for a given shear rate increases with increasing pressure. This increase is more pronounced at high shear rates than at low shear rates for OBM [Figure 5.7 to 5.10].
- The shear stress for a given low shear rate is less dependent on pressure and temperature than the shear stress at higher shear rates.

Temperature and pressure affects the behaviour and interactions of water or oil, clay, polymers and solids in mud. The effect of increasing the temperature of a liquid is to reduce the cohesive forces while simultaneously increasing the rate of molecular interchange. The former effect tends to cause a decrease of shear stress, while the latter causes it to increase. The net result is that liquids show a reduction in viscosity with increasing temperature.

The effect of increasing the pressure on OBM is to increase the cohesive forces, which tends to increase the viscosity.

Also the following differences were recognised between water and oil based muds:

- Pressure dependence was much more pronounced for oil based mud compared with water based mud.
- Effect of pressure is nearly equal to the effect of temperature for oil based muds [Figure 5.7b].
- For water based mud, the pressure effect was much smaller than the temperature effect.



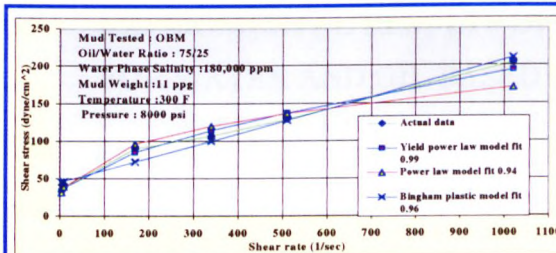


Figure (5.3) Fitting Rheogram for Best Fitting Model for OBM

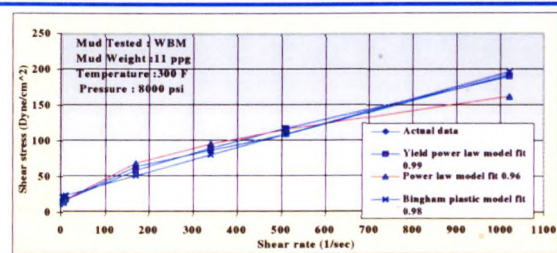


Figure (5.4) Fitting Rheogram for Best Fitting Model for WBM

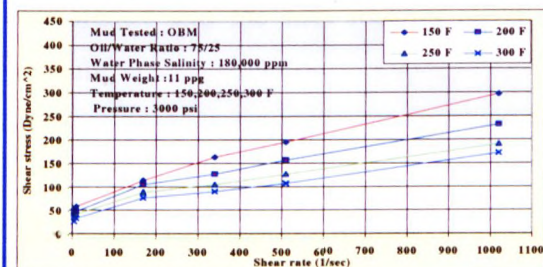


Figure (5.5) Shear Stress as Function of Temperature for OBM

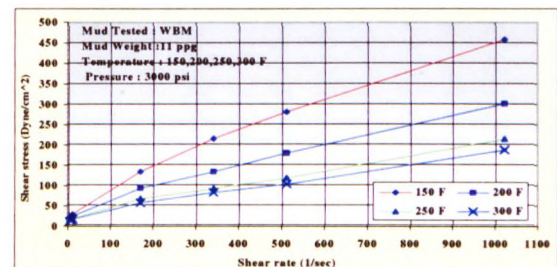


Figure (5.6) Shear Stress as Function of Temperature for WBM

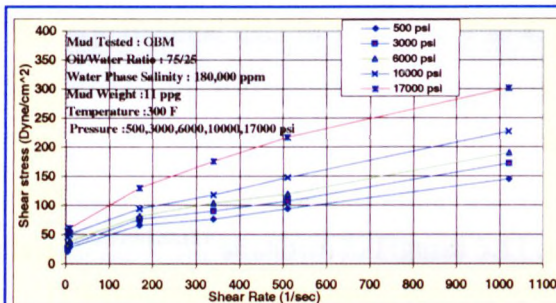


Figure (5.7a) Shear Stress as Function of Pressure for OBM

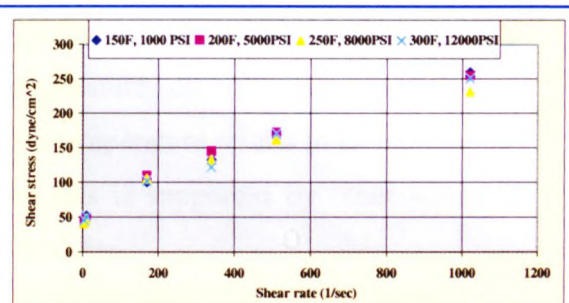


Figure (5.7b) Shear Stress as Function Temperature and Pressure for OBM

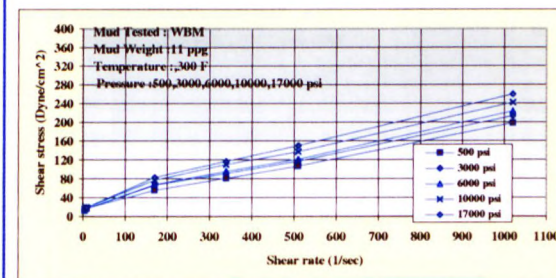


Figure (5.8) Shear Stress as Function of Pressure for WBM

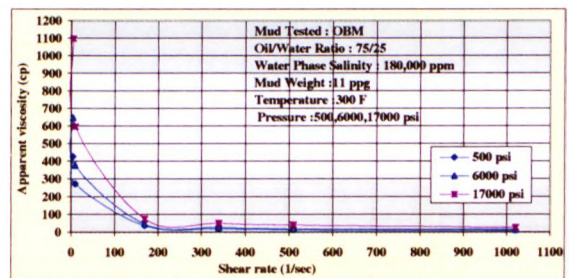


Figure (5.9) Apparent Viscosity as Function of Pressure for OBM

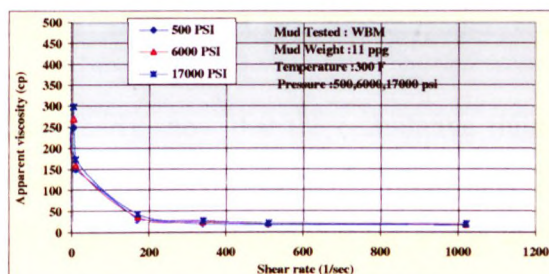


Figure (5.10) Apparent Viscosity as Function of Pressure for WBM



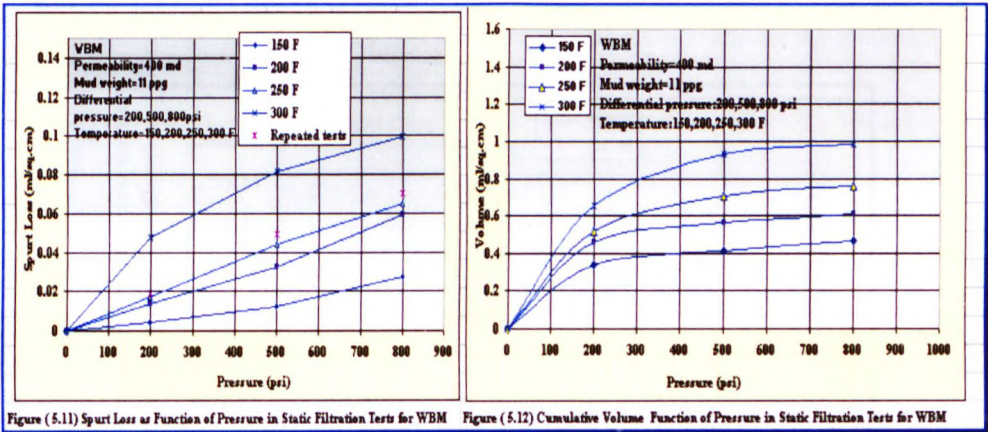
5.7 EXPERIMENTAL RESULTS OF STATIC FILTRATION FOR WATER AND OIL BASED MUDS

The average value for the 95% confidence limits for some repeated tests is reasonable and reflects the inaccuracy in measuring the spurt loss volume due to variation in: a) the rate at which the outlet valve was opened, b) the exact time at which stopwatch was started and the first reading taken, c) the degree of saturation of the filter medium.

5.7.1 Spurt Loss and Cumulative Filtrate Volume

5.7.1.1 Effect of Pressure and Temperature

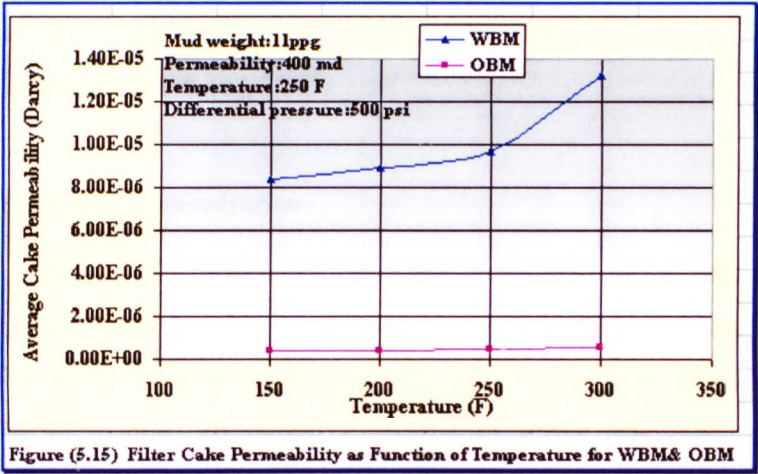
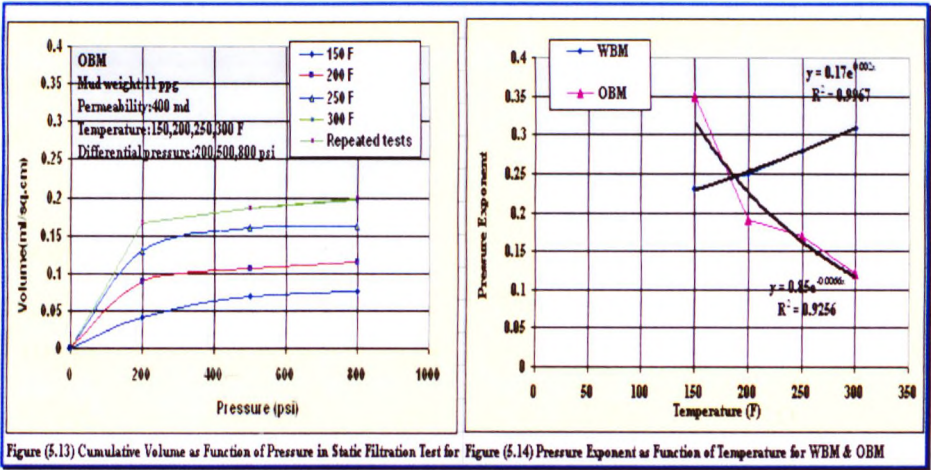
The experimental data in Tables 4.17 to 4.29 [Appendix A] clearly demonstrate that the effects of differential pressure and temperature on filtration process are significant. Generally an increase in pressure and temperature results in an increase in spurt loss and cumulative filtrate volume, and this is supported by other workers data<sup>38,42,116,120,121</sup> as shown in Figures 5.11 and 5.12.



The experimental data clearly show that the cumulative fluid loss is an exponential function of pressure, which agrees with Larsen<sup>116</sup> [Figures 5.12 and 5.13].

Figures 5.14 and 5.15 clearly demonstrate that for WBM an increase in temperature corresponds to an increase in the pressure exponent. This implies a decrease in filter

cake compressibility and hence an increase in filter cake permeability and a significant increase in fluid loss. Meanwhile increasing temperature for OBM shows a decrease in pressure exponent, implying an increase in filter cake compressibility, no significant effect on filter cake permeability and hence only a slight increase in fluid loss. Therefore the pressure exponent (equation 5.18) is directly proportional to temperature effects for WBM and inversely proportional for OBM. These differences probably reflect the different dominating media in the WBM and OBM filter cakes, namely bentonite and brine droplets respectively.



Larsen<sup>116</sup> present the relationship between the fluid loss ( $V_{cum.}$ ) and the differential pressure ( $\Delta p$ ) in the form:

$$V_{cum.} = a\Delta P^x \quad (5.16)$$

where:

a = constant for specific mud

x = pressure exponent < 0.50

This general equation (5.16) has been modified to include the effect of temperature on the pressure exponent (x). The pressure exponent has been predicted from a plot of filtrate volume versus pressure at each temperature tested for WBM and OBM. Then the pressure exponent (x) has been correlated with temperature as shown in Figure 5.14. Therefore the pressure exponent and temperature relationship can be written in the form:

$$x = be^{CT} \quad (5.17)$$

where:

b = constant for specific mud

C = temperature coefficient, 1/°F

T = temperature (°F)

For: WBM                      b = 0.17                      and                      C = 0.002

OBM                              b = 0.85                      and                      C = - 0.0066

The relationship reported by Arthur et al.<sup>103</sup> (using filter paper as a filter medium) in which the spurt loss is an exponential function of pressure for LP-LT WBM was not found in this study [Figure 5.11].

#### 5.7.1.2 Effect of Solids Concentration

Three typical oilfield solids concentrations were considered in the studies (6, 12 and 19%). For WBM, Figure 5.16 shows that an increase in solids concentration (in this case barite) by up to 12% by volume results in a decrease in cumulative filtrate volume, while an increase in solids concentration above this range results in an increase in cumulative filtrate volume. This is because at higher mud weights (solids concentration) the filter cake becomes less compressible and this increases both filter cake permeability [Figure 5.17] and cumulative filtrate volume.



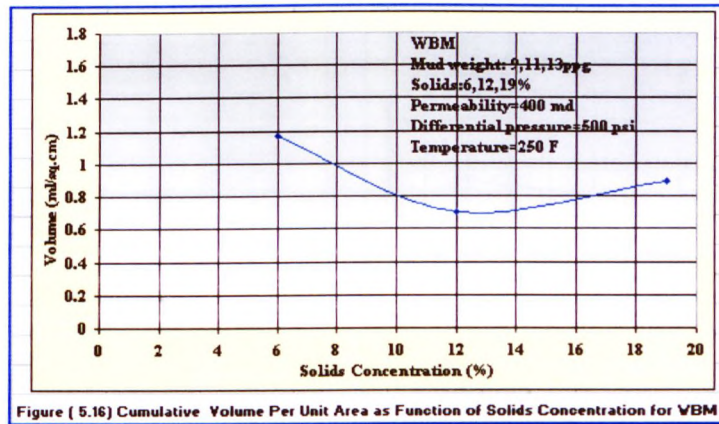


Figure 5.18 shows the relationship between cumulative filtrate volume, filter medium and amount of solids in the drilling fluid. At lower solids concentrations (<6% by volume) spurt loss and cumulative filtrate volume are directly proportional to medium permeability, while at higher solids concentrations cumulative volume is inversely proportional to medium permeability, which agrees with Nowak et al.<sup>40</sup>.

Figures 5.19 and 5.20 show a comparison between filter paper and natural core as filter media. Figure 5.19 shows that in using filter paper, an increase in solids concentration results in a decrease in cumulative filtrate volume, which gives misleading results when compared with Figure 5.20, which is based on natural core as a filter medium. This is due to the fact that the filter paper does not provide pore spaces where internal filter cake might start to form (unlike natural cores), and these findings agree with those of others<sup>120,122</sup>.

The spurt loss and cumulative filtrate volumes of OBM are expected to be lower than those of WBM. An increase in solids concentration results in a decrease in cumulative filtrate volume [Figures 5.21 and 5.22]. Primarily, water emulsion droplets and organophillic clay form the filter cake in OBM where barite is absorbed on the surface of the water droplets and prevents coalescence<sup>178</sup>. In this study the new application using the particle size analyser (see section 4.1.2) showed that the size of these water droplets is less than four microns.

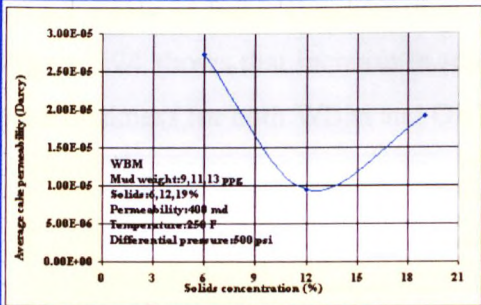


Figure (5.17) Average Filter Cake Permeability as Function of Solids % for WBM

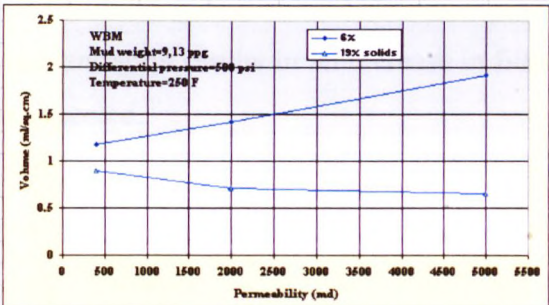


Figure (5.18) Cumulative Volume as Function of Solids Concentration & Permeability for WBM

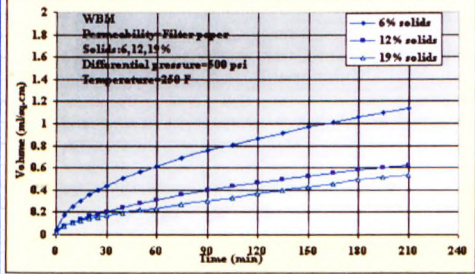


Figure (5.19) Cumulative Filtration as Function of Time in Static Filtration Tests for WBM

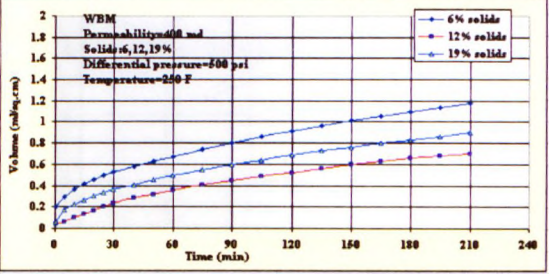


Figure (5.20) Cumulative Volume as Function of Time in Static Filtration Tests for WBM

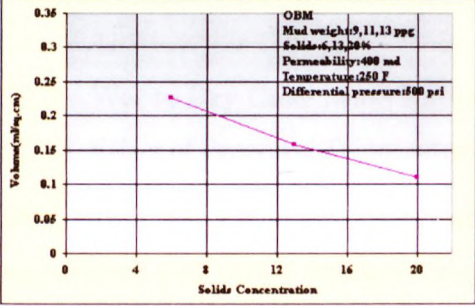


Figure (5.21) Cumulative Volume as Function of Solids in Static Filtration Tests for OBM

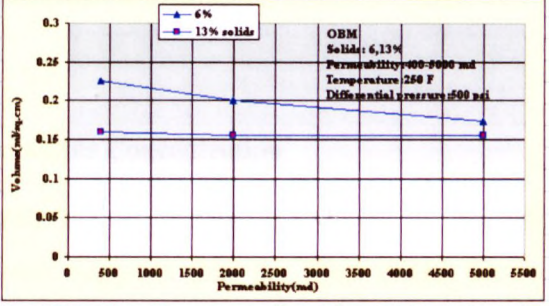


Figure (5.22) Cumulative Volume as Function of Permeability in Static Filtration Tests for OBM

## 5.7.2 Filter Cake Thickness

### 5.7.2.1 Effect of Pressure and Temperature

In general, an increase in temperature and pressure is expected to lead to an increase in the filter cake thickness. The driving force and the rate of filtration increases more slowly than the rate at which the pressure increases. The effect of pressure has two opposing actions. One increases the filter cake thickness by piling up solid particles; the other decreases the filter cake thickness by compacting. The two actions tend to compensate for each other, resulting in a small change in filter cake thickness with increase in pressure [Figure 5.23]. The result is largely in agreement with the findings of other researchers<sup>118,121</sup>.



5.7.2.2 Effect of Solids Concentration

Figure 5.24 shows that increase in solids concentration results in an increase in filter cake thickness for both WBM and OBM as expected.

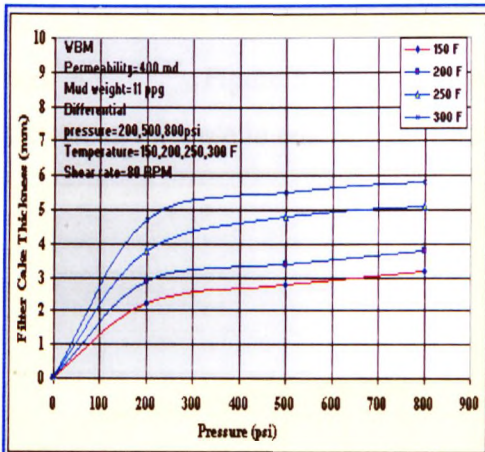


Figure (5.23) Measured Filter Cake Thickness as Function of Pressure for WBM

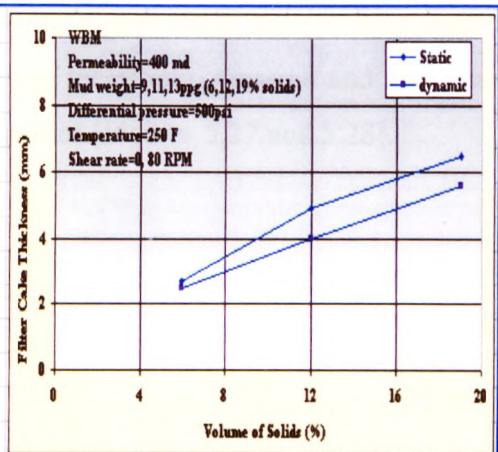


Figure (5.24) Filter Cake Thickness as Function of Solids Concentration for WBM

5.7.3 Wet to Dry Cake Mass Ratio (m)

5.7.3.1 Effect of Pressure, Temperature and Solids Concentration

Generally it was found that cake mass ratio (m) declined with increase in pressure, temperature and solids concentration, which suggests that the filter cakes formed under downhole conditions are more compressible for OBM than for WBM.

5.8 EXPERIMENTAL RESULTS OF DYNAMIC FILTRATION FOR WATER AND OIL BASED MUDS

The dynamic equilibrium filtration rate was attained between 2-3 hours for all muds tested. Specifically, the time to reach equilibrium for OBM was less than that for WBM tested under the same conditions.

5.8.1 Spurt Loss and Cumulative Filtrate Volume

5.8.1.1 Effect of Shear Rate

A reduction in effective viscosity due to increased shear rate and temperature was found to result in an increase in filtrate volume. The mud stream can continuously

erode the freshly deposited cake and under this condition the cumulative filtrate volume will increase until equilibrium is attained. However under higher shear rates, the erosion rate will decrease the time to reach equilibrium [Figure 5.25], the mud cake is thin and equilibrium filtrate rate is higher, and this is supported by others<sup>36,126,136,178</sup> [Figure 5.26]. Additionally, an increase in pressure and temperature results in an increase in equilibrium filtration rates [Figures 5.27 and 5.28].

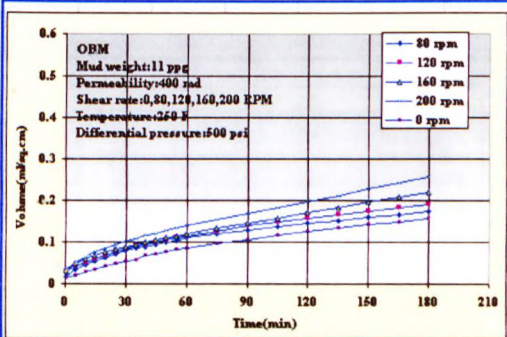


Figure (5.25) Cumulative Volume as Function of Shear Rate in Dynamic Filtration for OBM

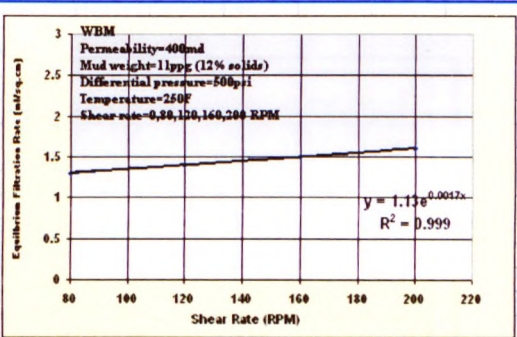


Figure (5.26) Equilibrium Filtration Rate as a Function of Shear Rate for WBM

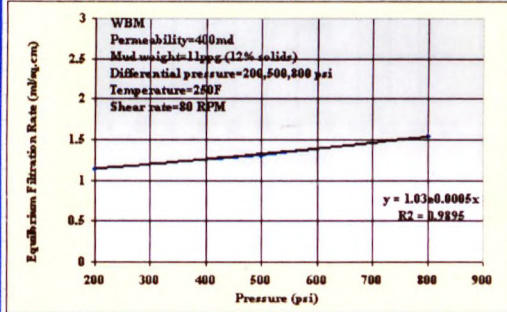


Figure (5.27) Equilibrium Filtration Rate as a Function of Pressure for WBM

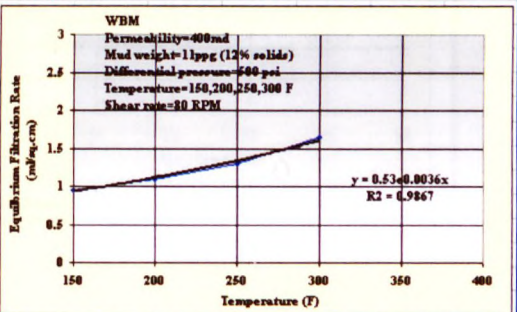


Figure (5.28) Equilibrium Filtration Rate as a Function of Temperature for WBM

## 5.8.2 Filter Cake Thickness

### 5.8.2.1 Effect of Pressure, Temperature and Solids Concentration

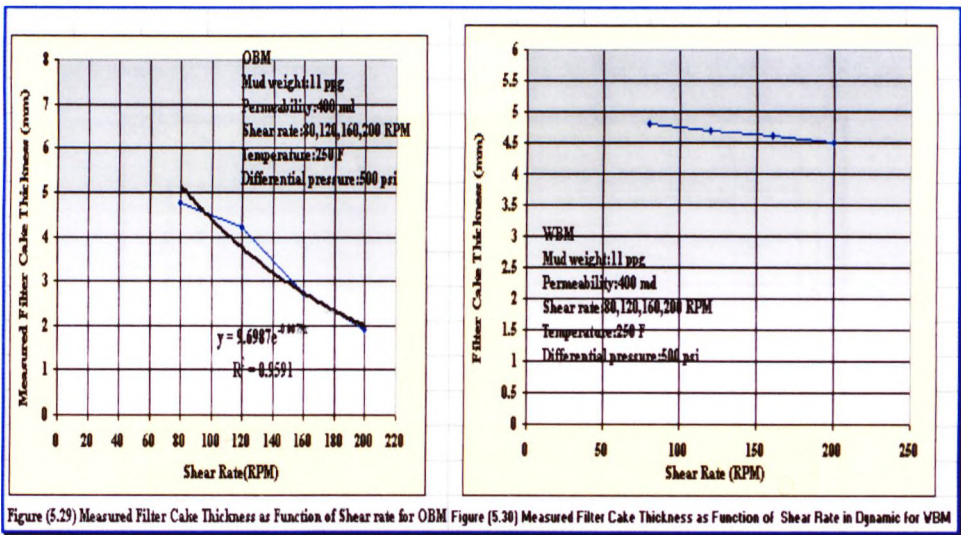
In general, the effect of temperature, pressure and solids concentration on the filter cake was found to be the same as obtained under the static conditions but with smaller cake thickness due to effect of shear rate, which agrees with others<sup>34,36</sup>.

### 5.8.2.2 Effect of Shear Rate

The effect of shear rate on filter cake is considered to lead to process of erosion and sorting, leading to a more compacted filter cake. An increase in shear rate was found



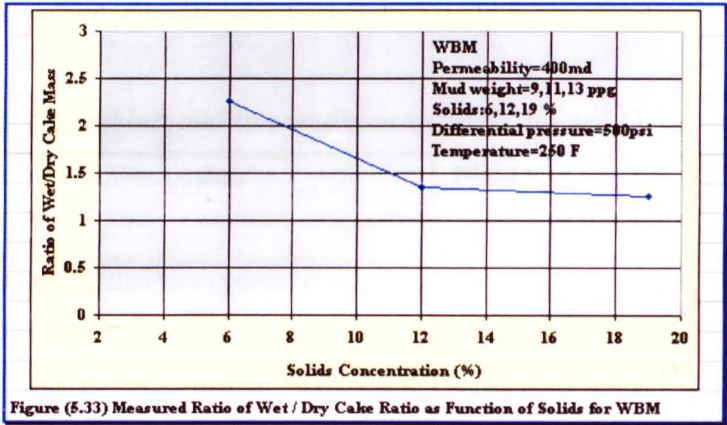
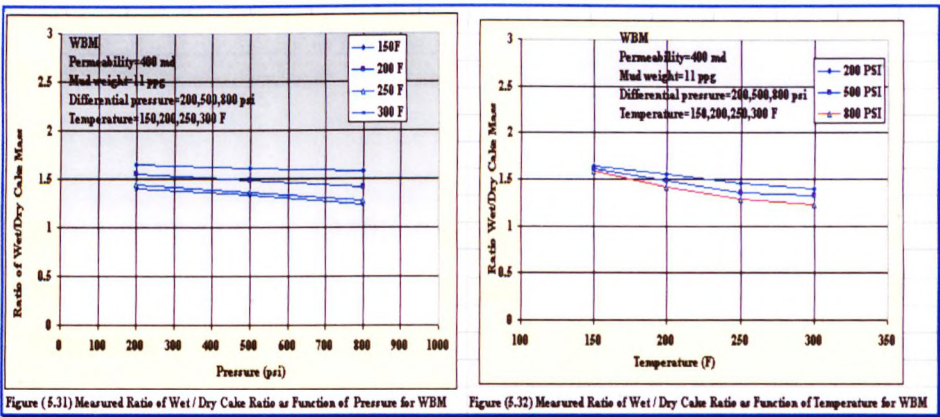
to lead to significant decrease in filter cake thickness for OBM as shown in Figure 5.29. This is due to the fact that the filter cake structure is largely made from water droplets, less solids content which are less resistant to shear rate. Figures 5.30 shows that there was no significant effect on filter cake thickness for WBM, because the filter cake contains higher solids content and is hence harder and highly resistant to shear rate.



### 5.8.3 Wet to Dry Cake Mass Ratio (m)

#### 5.8.3.1 Effect of Pressure, Temperature and Solids Concentration

Figures 5.31 and 5.33 show the measured wet to dry cake mass ratio (m) as a function of pressure, temperature and solids concentration; and was found to be similar to that obtained under static conditions but with lower values due to the effects of shear rate and compaction.



### 5.8.3.2 Effect of Shear Rate

Generally,  $m$  was found to decline with increase in shear rate. This is due the fact that during dynamic conditions the particle size selection, sorting, and compaction will cause more fluids to be squeezed from the pore space and create lower  $m$  values compared with static filter cakes.

## 5.9 EFFECT OF FLUID LOSS ADDITIVES (FLA) UPON STATIC AND DYNAMIC FILTRATION

Generally, fluid loss can be controlled with different types of additives and the rate of filtration will depend on type and concentration of each additive. Such additives include Gilsonite, Resinex, etc. Different filtration mechanisms for these additives

have been studied by different investigations, a summary of which is presented in Table 5.11.

### 5.9.1 Effect of Fluid Loss Additives (FLA) on Spurt Loss, Cumulative Filtrate Volume, Cake mass Ratio and Cake Thickness in Static and Dynamic Filtration

Generally, an increase in the concentration of fluid loss additives (FLA) results in a decreases in spurt loss, cumulative filtrate volume, filter cake mass ratio, and cake thickness in both static and dynamic filtration [Figure 5.34].

Table 5.11 Fluid loss additive mechanisms for WBM and OBM

Type of Mechanism	Fluid loss additive for WBM	Fluid loss additive for OBM
Blocking and plugging filter cake pores creates low permeability filter cake	Oil agent	Gilsonite agent
Coating mud particulate and creating impermeable layer preventing escape of water into the formation	Resinex agent	Novaec-F agent
Viscosifying base fluid	Poly-temp agent	Truflo-100 agent

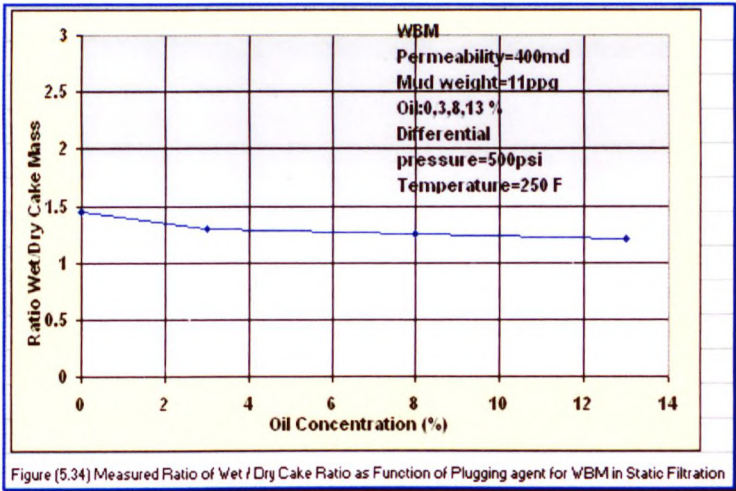


Figure (5.34) Measured Ratio of Wet / Dry Cake Ratio as Function of Plugging agent for WBM in Static Filtration



For OBM, Figure 5.35 clearly demonstrates that an increased concentration of viscosifying and plugging agents results in a significant decrease in static and equilibrium dynamic filtration. Meanwhile, increasing the coating agent results in a more smooth decrease in static filtration and a sharp decrease in equilibrium dynamic filtration. Figures 5.36 and 5.37 demonstrate that an increase in FLA could be more beneficial for static than for dynamic filtration. Furthermore, an increase in viscosifying and plugging agents results in a decrease in filter cake thickness more than for a coating agent in both static and dynamic filtration [Figures 5.38 and 5.39]. For WBM Figure 5.40 clearly shows that an increase in concentration of viscosifying and plugging agents significantly decreases both static and equilibrium dynamic filtration and filter cake thickness. Furthermore, the addition of coating agent shows a much less significant decrease in static and equilibrium dynamic filtration and filter cake thickness [Figures 5.41 and 5.42].

From the above evaluation, it can be concluded that the selection of fluid loss additives (FLA's) should be based on performance under both static and dynamic filtration conditions.

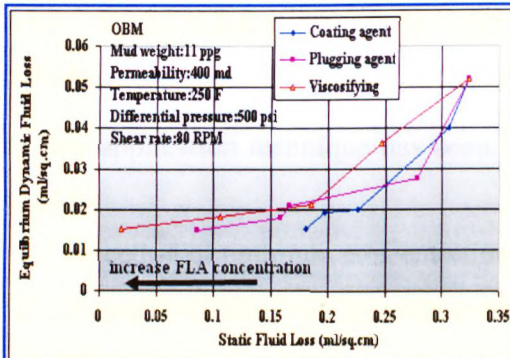


Figure (5.35) Comparison between static and dynamic filtration as function of (FLA) for OBM

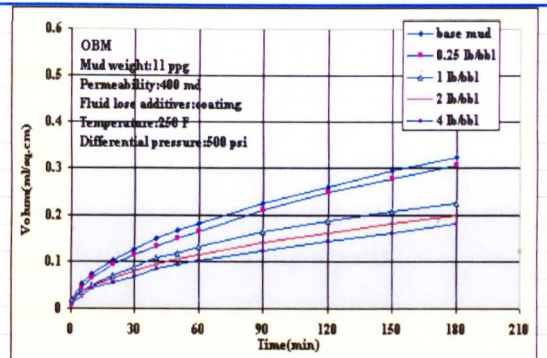


Figure (5.36) Cumulative Filtrate Volume as Function of FLA in Static Filtration for OBM

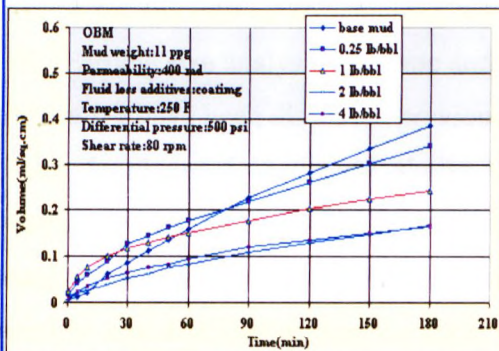


Figure (5.37) Cumulative Filtrate Volume as Function of FLA in Dynamic Filtration for OBM

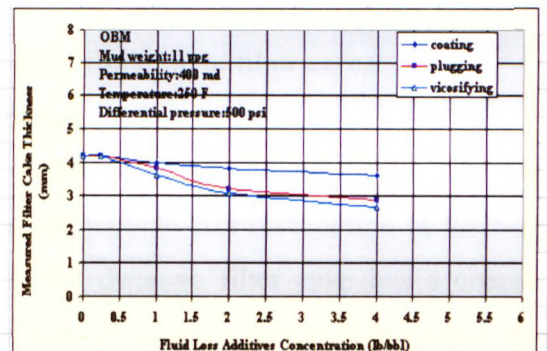


Figure (5.38) Measured Filter Cake Thickness as Function of FLA in Static Filtration for OBM

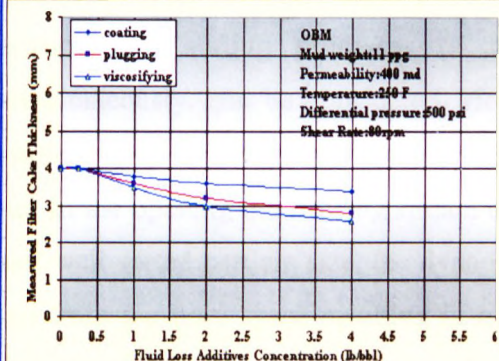


Figure (5.39) Measured Filter Cake Thickness as Function FLA in Dynamic Filtration for OBM

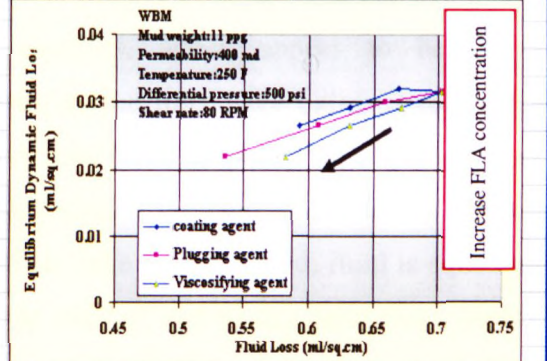


Figure (5.40) Comparison between static and dynamic filtration as function of (FLA) for WBM

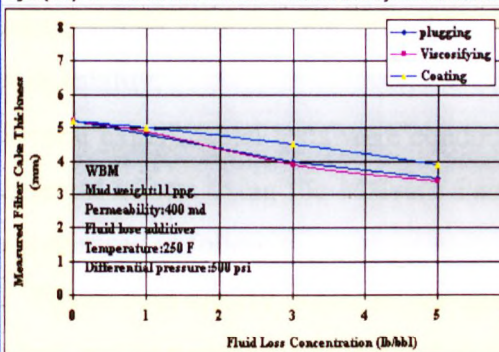


Figure (5.41) Measured Filter Cake Thickness as Function of FLA in Static Filtration for WBM

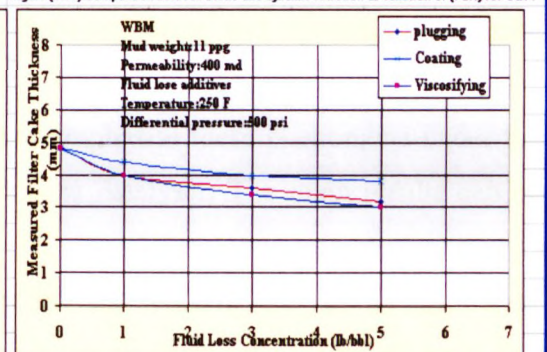


Figure (5.42) Measured Filter Cake Thickness as Function FLA in Dynamic Filtration for WBM

## **5.10 PARTICLE SIZE ANALYSIS**

### **5.10.1 Particle Size Analysis for Static and Dynamic Filter Cakes**

A new application technique has been introduced for a Particle Size Analyser to be used for:

1. Selection of optimum concentration of emulsifier and wetting agents.
2. A quality control tool for comparison of different types of emulsifiers.
3. Minimum time of testing and cost.
4. A backup tool for dynamic sag test.
5. Particle size analysis for static and dynamic filtration of filter cakes.

Points 1-4 have been discussed previously in chapter 4 (section 4.1.2).

Point 5: Figure 5.43 clearly shows that under static conditions the particle-size distribution of the filter cake is the same as the particle-size distribution of the base mud. However, under dynamic conditions, the dynamic filter cake has a coarser particle-size distribution than the static filter cake. Because in dynamic conditions the “size-classification cycle” takes place under the effect of shear rate, the two-action erosion and sorting processes of the particles, which appear to be active simultaneously, can be considered. However, as the filter cake builds it requires a particle of specific size to fill each opening or pore throat. The deposited particle does not fit the opening the flowing stream quickly sweeps it away. As a result of erosion and well-sorted particle size, the dynamic filter cake is compacted; fluid is squeezed out from the pore space resulting in a lower ratio of wet to dry cake mass. Hence dynamic filter cakes have lower cake permeability and porosity than static filter cakes, which explains the big difference between static and dynamic filter cake permeability.

Several experimental tests were conducted to emphasise these phenomena under the different effects using the Malvern Particle Size Analyser. The main results can be summarised as follows:

1. Figure 5.43 clearly demonstrates that an increase in shear rate has no significant effect on the particle size distribution of the dynamic filter cakes. This suggests that selection of a suitable shear rate could cause the particles to be deposited in a well-



sorted manner with improved plugging to give a more compacted and higher resistance filter cake.

- Figures 5.44 and 5.45 show the particle size distribution of the top, middle and bottom layers of a dynamic filter cake. Finer particle sizes are found towards the top surface.

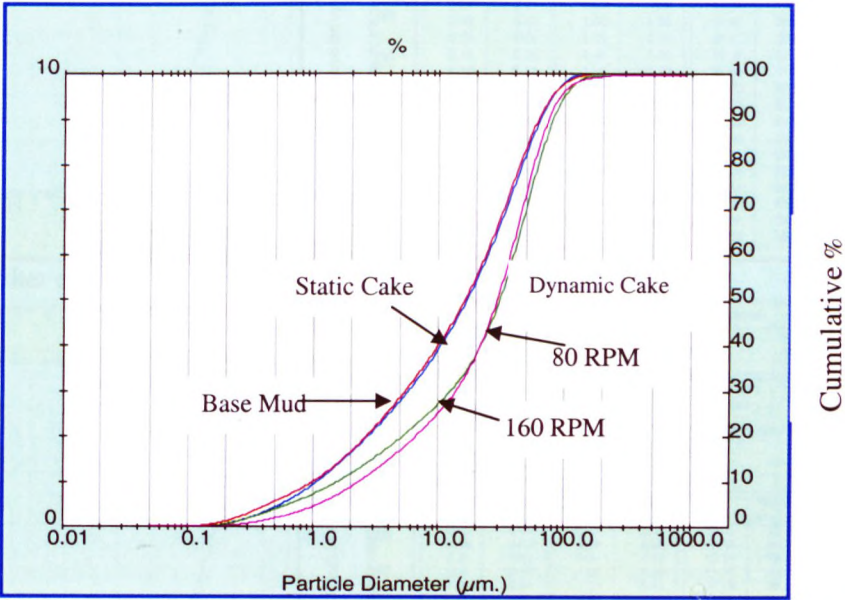


**Figure 5.43 Comparison chart between particle-size distributions of 11 ppg OBM, static and dynamic filter cakes**

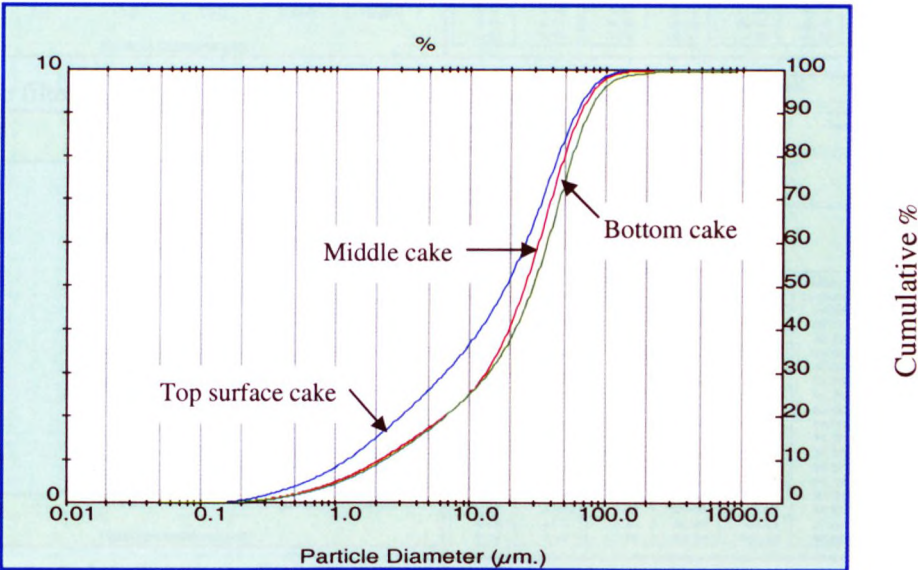
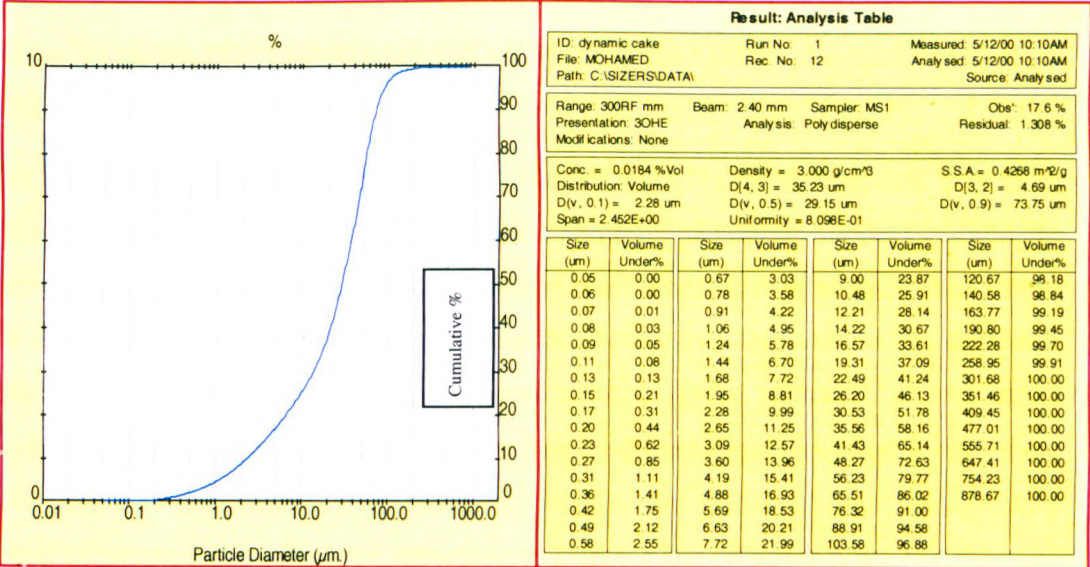
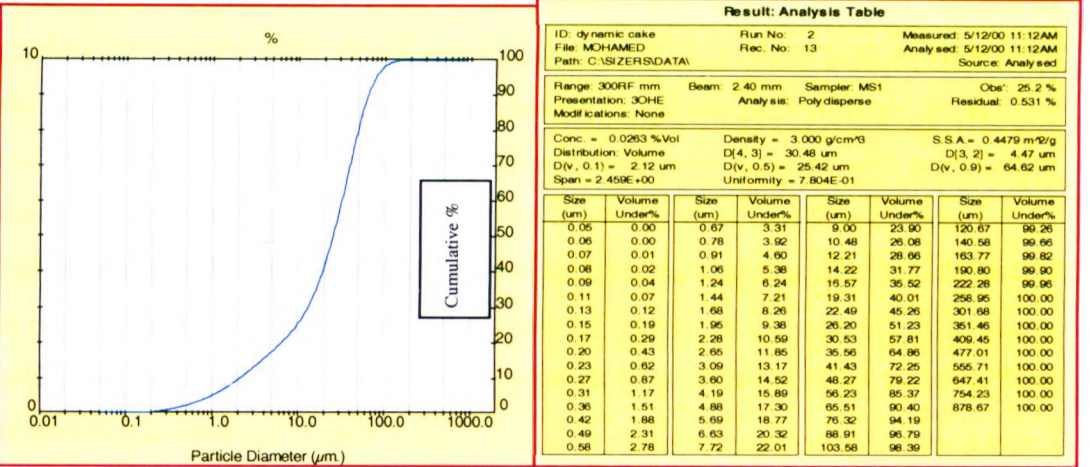


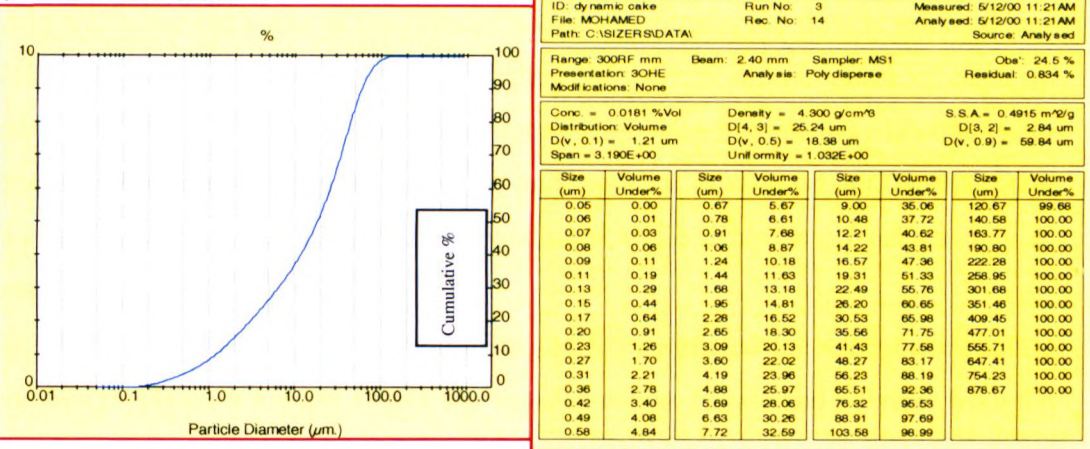
**Figure 5.44 Particle size distribution of dynamic filter cake (OBM)**



(a) Bottom filter cake



(b) Middle filter cake



(c) Surface filter cake

Figure 5.45 Particle size distribution of dynamic filter cake (OBM)



## 5.11 FORMATION DAMAGE CHARACTERISATION

### 5.11.1 Experimental Results

The data logging programme records the volumes from the balance against time in an Excel spreadsheet. These data were plotted on a graph of volume versus time and the best straight line fit obtained with a regression coefficient close to unity. The equation for the straight line was obtained. The coefficient for this line will be the flow rate (ml/sec). For greater accuracy multi-point method (three reference points) three coefficients were plotted and final straight line coefficient has been used as flow rate. Using the core dimensions, fluid viscosity, pressure and measured flow rate, the core initial permeability is calculated according to Darcy's law of linear flow.

As back flow is imposed, a peak in the pressure was observed which appears to correlate with cake rupture. Some authors have used this pressure peak as an explicit value to signify the reservoir drawdown needed to initiate flow through the drilling fluid filter cake. Others have used the difference in peak pressure with equilibrium flowing pressure in damaged core and define this as the flow initiation pressure.

Two pressure peaks can be recognised during flow back procedure. One represents the initial peak for flow initiation and the second represents the cake lift-off pressure peak. Flow is maintained until a steady-state flow is recorded from which a final permeability is obtained [Figure 5.46].

During back flow two phases may be distinguished in the clean up process. First, the flows will scour out some of the invaded solids and filtrate. As flow is initiated part of the filter cake separates from the core plug (lift-off). A second phase of clean up occurs when flow increases so the cake rupture takes place and the cake is completely removed [Figure 5.47] from the core plug and more solids scoured out. Furthermore, flow initiation occurs at laminar flow conditions while cake-lift off occurs only in turbulent flow regime for WBM.

For OBM one phase can be recognised as the flow initiated the filter cake rupture (pinholing) [Figure 5.47] and scours any invaded solids, filtrate and polymer from the core plug. This is associated with a maximum flow initiation pressure.

Furthermore, flow initiation and cake pinholing occur in the Darcy laminar flow regime for OBM.

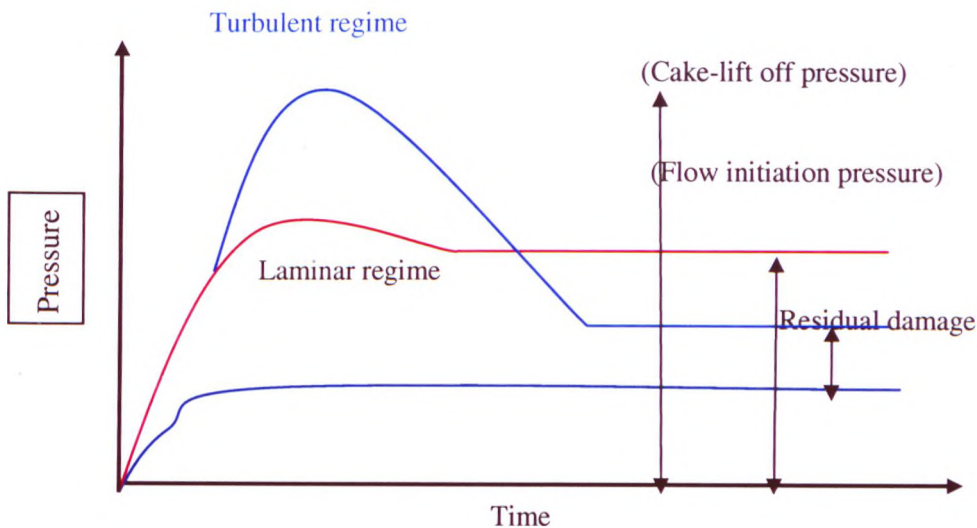


Figure 5.46 Mud cake and cleanup test

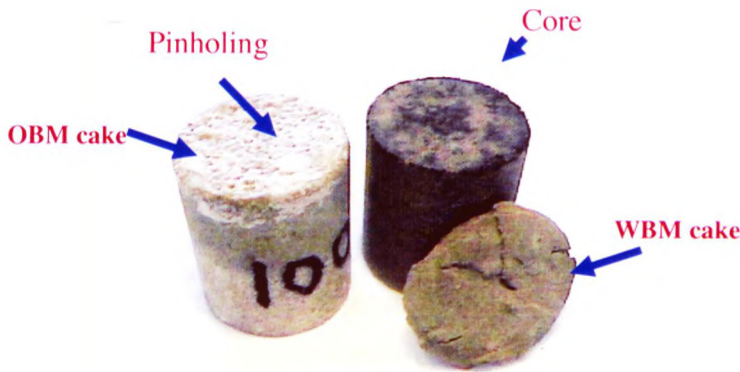


Figure 5.47 Cake rupture for WBM and OBM

Table 5.12 clearly demonstrates that for all the testing conditions the OBM shows the main damage represented by filter cake and very high reversible permeability achieved and can also be shown in Figure 5.48.

Table 5.13 clearly demonstrates that the main factor that governs permeability impairment for WBM is the overbalance pressure.

One would expect an increase in depth of invasion with increasing differential pressure in the sense that higher pressures would force the mud particles and the filtrate to penetrate deeper into the formation. However, contrary to this expectation, the experimental results for WBM indicate that at lower pressures the permeability damage increases and then as pressure increases from 400 to 650 psi the permeability damage decreases. But, as the pressure increases further the permeability damage increases in line with the expectations.

For WBM Figure 5.48 shows three pressure zones: in the first zone, representing pressures of 100 to 300 psi, return permeability decreases significantly. This is because at lower pressures the deposition is uncompacted forming loose particles and unconsolidated filter cake. Permeable filter cake allows filtrate and fine particles to pass resulting in deeper migration. This zone is characterised by lower return permeability. In the second zone, as differential pressure increases to 650 psi, the particles form tight bridging, compacted and lower cake permeability, thereby allowing less particles through them to move into the formation. This is seen by the higher return permeability achieved.

The third zone, representing increases in pressure beyond 650 psi results in deeper particle invasion and lower return permeability.

Therefore a critical pressure zone exists for WBM where decreased permeability impairment occurs. This is an important effect, as it is common practice for oil operators to drill with lower differential pressure in the belief that this will minimise the formation permeability damage. However, contrary to this expectation it has been found that the permeability damage will be higher at lower differential pressures.

Khan et al.<sup>227</sup> investigated the depth of invasion using x- ray mapping and found that minimum depth of invasion occurs at pressures between 300 and 500 psi; below or above this range the depth of invasion increases.

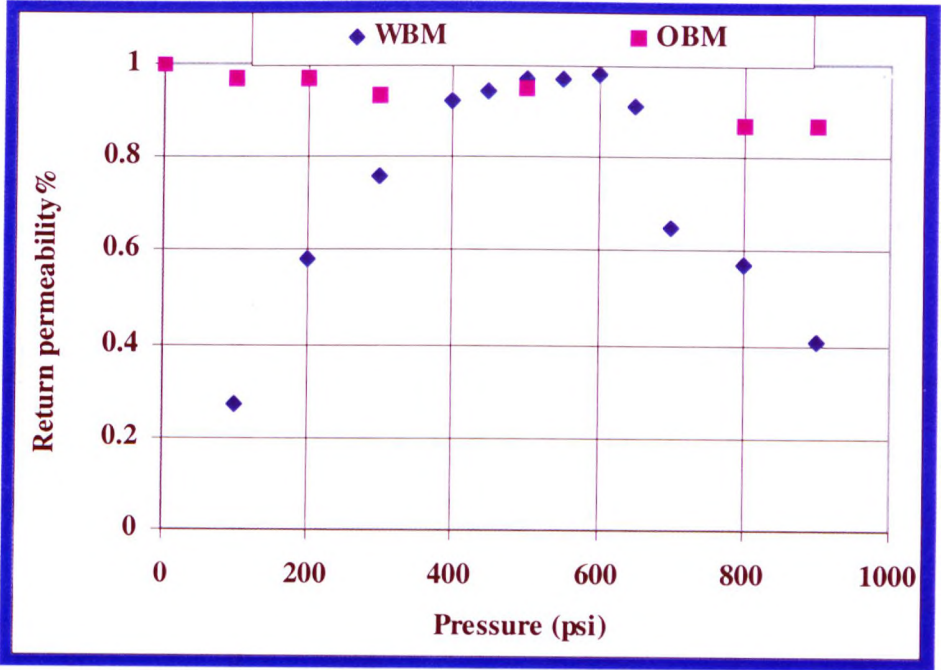


Figure 5.48 Return permeability for WBM and OBM

**Table 5.12 Results of returned permeability versus testing parameters for OBM**

1. Pressure (psi)	Gas Perm. (md)	Fluid Perm. (md)	Return Perm. (%)
100	804	424	97
200	852	425	97
300	874	454	93R
500	896	480	95
800	901	464	87
900	885	485	89
2. Temperature (F)			
150	800	450	97
200	852	425	97
250	737	345	96
300	761	355	Failure
300	845	421	94
3. Shear Rate (rpm)			
0	974	525	97
40	985	399	95
80	996	355	95
120	998	367	93R
160	1001	534	92
200	1003	403	91
240	1073	442	Failure
240	1083	600	95R
4. Permeability (md)			
13.90% solids	3323	1550	98
6.60% solids	3325	1856	91
6.60% solids	114	41	94
3.85% solids	3200	2000	89R
3.85% solids	260	132	93
3.85% solids	90	36	95R

R – repeated test



**Table 5.13 Results of returned permeability versus testing parameters for WBM**

1. Pressure (psi)	Gas Perm. (md)	Fluid Perm. (md)	Return Perm. (%)
100	805	377	27
200	848	426	58R
300	795	375	76
400	794	359	92
450	817	377	94
500	883	408	97
550	835	392	97
600	725	378	98
650	766	351	91
700	778	377	65
800	716	371	57
900	780	369	41R
2. Temperature (F)			
150	815	405	95
200	795	385	97
250	883	408	97
300	825	395	94
@ 500 psi			
3. Shear Rate (rpm)			
0	914	455	59
80	848	426	58
160	893	442	47
240	913	440	47
@ 200 psi			
4. Shear Rate (rpm)			
0	936	427	97R
80	883	408	97
160	933	383	96
@ 500 psi			
5. Permeability (md)			
12%	223	110	47
@ 200 psi	848	426	58
	3475	1819	72
6. Permeability (md)			
5%	971	457	55R
@ 200 psi	3430	1803	52

R – repeated test

### 5.11.2 Pore and particle Size Distribution Analysis

In many field applications an ad-hoc approach is used to estimate the average pore throat diameter. This rule estimates average pore diameter in micron ( $\mu\text{m}$ ) as roughly equal to the square root of the formation permeability (md). Over the years, another rule of thumb has been used called the “Jamming ratio”, which is defined as the ratio between pore throat diameter and particle size diameter. Previous work shows different jamming ratio ranges from 1/3-1/7, 1/5, 1/8 and 1/3-1/4.

However, a jamming ratio analysis has been carried out according to the  $1/3 D_{\text{pore}} < d_p < 1/7 D_{\text{pore}}$  rule discussed in chapter two and the results calculated from Figure 5.49 are summarised in Tables 5.14 and 5.15. The average pore throat diameter has been computed based on correlations developed in chapter 4.

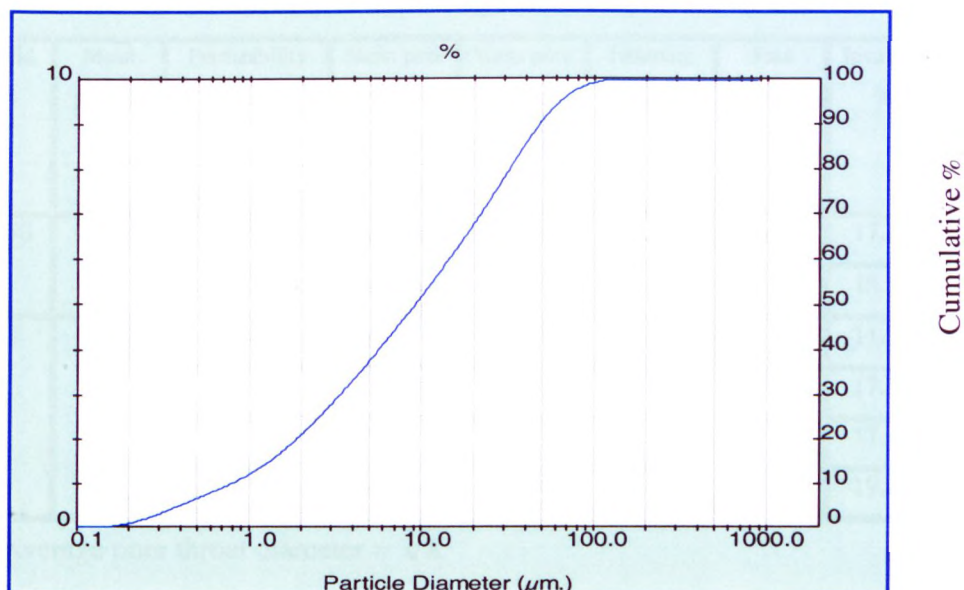
For example, in Table 5.14, the particle size range for the core with a 22.05  $\mu\text{m}$  pore throat average diameter falls between  $7.35 < d_p < 3.15$ . The WBM has a  $d_p = 9.13 \mu\text{m}$ , a cumulative size of 54.64% greater than 7.35 (bridging), a cumulative size of 17.11% between 3.15  $\mu\text{m}$  and 7.35  $\mu\text{m}$  (invasion), and the rest 28.25% pass through the core.

The bridging % represents the percentage of particle size in the remaining mud and the particle size that bridges the pore entrances at the formation face forming an external filter cake. The invasion % represents the percentage of the particle size invading the formation and bridging at some pore throat, forming an internal filter cake.

Pass through core % represents the smaller particle size carried through the formation.

The conclusions from the analysis are:

1. Generally, the average pore throat diameter is not equal to  $\sqrt{K}$ .
2. The ratio of particle size to measured average pore throat diameter is not a good indicator of permeability reduction and inconsistent with any of the existing jamming ratio values.



Result: Histogram Table

ID: 11'ppg base mud  
File: ALI  
Path: C:\SIZERS\DATA\

Run No: 3  
Rec. No: 2

Measured: 6/29/00 3:18PM  
Analysed: 6/29/00 3:18PM  
Source: Analysed

Range: 300RF mm  
Presentation: 3OHD  
Modifications: None

Beam: 2.40 mm  
Analysis: Poly disperse

Sampler: MS17  
Obs': 14.3 %  
Residual: 0.790 %

Conc. = 0.0075 %Vol  
Distribution: Volume  
D(v, 0.1) = 0.79 um  
Span = 5.212E+00

Density = 4.250 g/cm<sup>3</sup>  
D[4, 3] = 18.09 um  
D(v, 0.5) = 9.13 um  
Uniformity = 1.633E+00

S.S.A. = 0.6839 m<sup>2</sup>/g  
D[3, 2] = 2.06 um  
D(v, 0.9) = 48.38 um

Size (um)	Volume Under %	Size (um)	Volume Under %	Size (um)	Volume Under %	Size (um)	Volume Under %
0.055	0.00	0.635	8.40	7.31	45.36	84.15	98.23
0.061	0.00	0.700	9.11	8.06	47.38	92.79	98.87
0.067	0.01	0.772	9.85	8.89	49.43	102.3	99.34
0.074	0.02	0.851	10.64	9.80	51.50	112.8	99.70
0.082	0.03	0.938	11.50	10.81	53.59	124.4	99.89
0.090	0.05	1.03	12.43	11.91	55.71	137.2	99.99
0.099	0.08	1.14	13.44	13.14	57.85	151.3	100.00
0.109	0.12	1.26	14.54	14.49	60.03	166.8	100.00
0.121	0.18	1.39	15.74	15.97	62.25	183.9	100.00
0.133	0.27	1.53	17.04	17.62	64.52	202.8	100.00
0.147	0.39	1.69	18.42	19.42	66.84	223.6	100.00
0.162	0.55	1.86	19.89	21.42	69.22	246.6	100.00
0.178	0.77	2.05	21.44	23.62	71.67	271.9	100.00
0.196	1.05	2.26	23.06	26.04	74.17	299.8	100.00
0.217	1.40	2.49	24.74	28.72	76.74	330.6	100.00
0.239	1.84	2.75	26.48	31.66	79.33	364.6	100.00
0.263	2.36	3.03	28.25	34.92	81.93	402.0	100.00
0.290	2.96	3.34	30.05	38.50	84.49	443.3	100.00
0.320	3.60	3.69	31.88	42.45	86.95	488.8	100.00
0.353	4.27	4.07	33.74	46.81	89.26	539.0	100.00
0.389	4.95	4.48	35.61	51.62	91.39	594.3	100.00
0.429	5.63	4.94	37.51	56.92	93.28	655.4	100.00
0.473	6.31	5.45	39.43	62.76	94.91	722.7	100.00
0.522	7.01	6.01	41.38	69.21	96.27	796.9	100.00
0.576	7.70	6.63	43.36	76.32	97.37	878.7	100.00

Figure 5.49 Particle size distribution of WBM

**Table 5.14 Jamming ratio analysis for WBM**

Solid %	Mean particle size ( $\mu m$ )	Permeability (md)	Mean pore size Calculated ( $\mu m$ )	Mean pore size rule of thumb** ( $\mu m$ )	Jamming ratio	Pass through core %	Invasion %	Bridging %
5.50	9.13	971	22.05	31.16	0.39	28.23	17.11	54.64
		3430	26.45	58.56	0.34	31.88	15.50	52.62
12	11.27	223	11.87	14.93	0.94	13.76	11.57	74.67
		761	20.40	27.58	0.55	20.25	17.51	62.24
		914	19.61	30.23	0.57	20.25	17.51	62.24
		3475	26.81	58.94	0.42	23.06	19.24	57.70

\*\* Average pore throat diameter =  $\sqrt{K}$

**Table 5.15 Jamming ratio analysis for OBM**

Solid %	Mean particle size ( $\mu m$ )	Permeability (md)	Mean pore size calculated ( $\mu m$ )	Mean pore size rule of thumb** ( $\mu m$ )	Jamming ratio	Pass through core %	Invasion %	Bridging %
3.85	8.88	90	9.72	9.48	0.91	15.70	11.70	72.60
		260	12.82	16.12	0.69	18.03	14.78	67.19
		3525	26.81	59.37	0.33	30.88	20.07	49.05
6.60	12.88	114	10.63	10.67	1.21	19.07	9.88	71.05
		3325	26.04	57.66	0.49	28.05	14.95	56.55
13.90	16.76	737	18.76	27.14	0.89	20.12	12.09	67.71
		1003	20.54	31.67	0.81	20.16	13.70	66.14
		1001	20.52	31.63	0.81	20.16	13.70	66.14
		1083	21.34	32.90	0.78	21.37	12.49	66.14
		3323	26.35	57.64	0.63	23.87	13.31	62.82

\*\* Average pore throat diameter =  $\sqrt{K}$

## **CHAPTER SIX**

# **DEVELOPMENT OF DRILLING FLUID RHEOLOGY, FILTRATION AND FORMATION DAMAGE PREDICTION MODELS**

In this chapter the theoretical models used to predict downhole drilling fluid rheology, static and dynamic filtration and formation damage are developed using a data base generated from controlled experimental studies. These models were developed for a typical synthetic oil based mud (OBM) and a typical lignosulphonate water based mud (WBM). Based on the models developed, the filter cake characteristics such as average specific cake resistance, cake permeability and erodability can be calculated and described. The developed models provide more reliable results and substantial advantages when used to fit and describe static and dynamic filtration mechanisms under different applied factors and conditions. An attempt to validate the model predictions using experimental, independent test and field data has been made under different applied factors and conditions.

Attempts have also been made to integrate the lab database analysis for field applications to predict the effect of drilling fluid filtration on formation damage in terms of productivity impairment.

### **6.1 DRILLING FLUID RHEOLOGY ANALYSIS OF WATER AND OIL BASED MUDS**

Drilling fluid rheology has been investigated in depth in order to:

1. Characterise drilling fluid rheology under downhole conditions.
2. Develop a pressure and temperature dependent model, which can predict downhole rheology.
3. Relate fluid rheology to the fluid filtration and formation damage mechanisms.

Rheological characterisation for both water and oil based muds has been carried out using the Fann-70 HP-HT viscometer. Factor analysis technique has been applied to



analyse the data in order to identify the dominant parameters affecting drilling fluid rheology.

### 6.1.1 Introduction to Factor Analysis technique

Factor analysis is a multivariate statistical analysis technique used for the analysis of data that is both descriptive and predictive. There are at least four distinct ways in which the technique is useful.<sup>228, 229</sup> These are:

1. Factorisation of a set of variables into a smaller number of dimensions.
2. Factorisation of a group of objectives, rather than a set of variables.
3. Factor analysis can be used as a device for determining which of a large group of potential explanatory variables should be include in a regression.
4. Factor analysis can be used for summarisation of a complex set of potential explanatory variables in yet another way. Instead of using the estimated factor loading for identification of relevant variables, it is possible to find values for the factors themselves and then use them as inputs to the multiple regression analysis.

A factor is a linear combination of the observed variables. In other words,

$$F = a_1x_1 + a_2x_2 + a_3x_3 + ..... + a_nx_n$$

where (x) is the variable and (a) is the correlation coefficient of the variable.

The observed variables are grouped in such a manner that more than one factor is obtained e.g:

$$F_1 = a_1x_1 + a_2x_2 + a_3x_3$$

$$F_2 = \qquad \qquad \qquad a_4x_4 + a_5x_5$$

$$F_3 = \qquad \qquad \qquad a_6x_6 + a_7x_7$$

Each factor has, in fact, coefficients for all variables in the analysis but that these may be zero or close to zero for all variables other than those grouped in that factor.

Therefore in factor analysis each individual is assigned a **factor score**. Thus

$$F_1 = a_1x_1 + a_2x_2 + a_3x_3 + ..... + a_nx_n$$

When the factor score is correlated with the observed score on each variable, the resultant correlation is called a factor loading.

If we square the loading of each factor and sum it, we get a “sum of squares” which is technically called the eigenvalue “variance” of that factor. Each eigenvalue summarises a fraction of total variance related to the number of variables in that factor.

The variance of each variable summarised by each factor is called communality, and when the communality values are close to one (unity) this indicates that all the variables are well presented by these factors.

When the data result is very difficult to interpret the factor analysis technique may provide “new” factors from initial results by the methods of rotation. A rotation is something like staining a microscope slide; different stains reveal different structures in the tissues. However the most common is the varimax rotation, this criterion strives to maximise the variance of the square of the loading in each column in the factor pattern.

#### **6.1.1.1 Methodology of Data Analysis**

Since it is observed that the fluid rheology at higher and lower shear rates behave differently at different temperature and pressure levels, the factor analysis is applied separately for lower shear rates (5.1, 10.2 sec<sup>-1</sup>) and higher shear rates (170.2, 340.40, 510.60, and 1021.20 sec<sup>-1</sup>). The procedure for data analysis is as follows:

1. Select MINITAB statistical software programme<sup>230</sup> for data analysis.
2. Set up worksheet with input data for four columns of raw data including a total of forty sets of viscometer measurements at different pressures, temperatures and shear rates.
3. Perform factor analysis with the raw data:  
Choose Stat → Multivariate → Factor Analysis.
4. Enter the measurement data in the variable column for each condition.

5. Specify the number of factors to extract. Using principal component, the default number is the number of variables, i.e. 3.
6. Select type of rotation as varimax rotation.
7. Click Results, sort Loadings and click OK twice.

### **Interpreting the Results**

The factor analysis results for WBM and OBM are shown in Tables 6.1 to 6.4. Each table comprise three subtables showing loading and communalities: unrotated, rotated, and sorted rotated.

#### **(A). Results from unrotated Factor Loading and Commuality**

The rows and columns represent linear combinations of variables and factors respectively. Examine the proportional of variability by output line % Variance and communality values. The unrotated factors explain 99.0% of the data variability and the communality values, which is close to 1.0 indicating that all variables are well represented by these factors. The result from unrotated three factors is very difficult to interpret. Therefore varimax rotation has been applied.

#### **(B). Results from rotated Factor Loading and Commuality**

Varimax rotation where applied gives factors from initial results. Three factors describe the significant effects of temperature, pressure and shear rate on shear stress for WBM and OBM accurately.

The loadings are distributed between the factors, and the results are easier to interpret. Tables 6.1 to 6.4 for WBM and OBM show variations in the factors (1, 2 and 3) loading distribution with respect to shear rate, temperature and pressure.

#### **(C). Results from Sorted rotated Factor Loadings and Commuality**

Sorted and rotated results showing variables that have their highest absolute loading (correlation coefficient) with respect to factors are printed first and the other

next, in sorted order as shown in Tables 6.1 and 6.2 for WBM. The tables show in order loadings of shear rate, temperature and pressure and their effects on shear stress. It was found that there is no significant effect of pressure on shear stress for WBM.

Tables 6.3 and 6.4 for OBM show in order loadings of shear rate, pressure and temperature and their effects on shear stress.

The following is a summary of the analysis:

1. It is interesting to estimate the effect of pressure, temperature, and shear rate on fluid rheology, which is clearly demonstrated by the factor loading for each variable and its effect on shear stress as shown in Tables 6.1 to 6.4.
2. The pressure dependence was more pronounced for OBM compared to WBM.
3. The pressure dependence was much smaller than the temperature effect for WBM.
4. There is a balance between the effects of pressure and temperature on OBM as can be observed in Factors 2 and 3, rotated factor loadings, Table 6.4.

The factor analysis results show that the drilling fluid rheology is highly affected by two dominant factors, temperature and pressure.

However, according to the analysis above, OBM and WBM can be utilised within a single empirical model, with specific coefficients for temperature and pressure to predict downhole rheology (section 6.2.1).

**Table 6.1 Application of Multivariate Analysis for WBM Rheology  
(Low-Shear Rate)**

**Factor Analysis**

PRINCIPAL COMPONENT FACTOR ANALYSIS OF THE CORRELATION MATRIX				
a. Unrotated Factor Loadings and Communalities				
Variable	Factor 1	Factor 2	Factor 3	Communality
Pressure	0.230	0.804	-0.547	0.999
Temperature	-0.826	0.456	0.310	0.986
Shear Rate	0.494	0.384	0.777	0.995
Shear Stress	0.990	0.002	-0.002	0.980
Variance	1.9589	1.0022	0.9990	3.9601
% Var	0.490	0.251	0.250	0.990
b. Rotated Factor Loadings and Communalities (Varimax Rotation)				
Variable	Factor 1	Factor 2	Factor 3	Communality
Pressure	0.046	0.001	0.998	0.999
Temperature	-0.987	0.091	0.052	0.986
Shear Rate	0.083	0.994	-0.007	0.995
Shear Stress	0.876	0.419	0.190	0.980
Variance	1.7521	1.1723	1.0357	3.9601
% Var	0.438	0.293	0.259	0.990
c. Sorted Rotated Factor Loadings and Communalities				
Variable	Factor 1	Factor 2	Factor 3	Communality
Temperature	-0.987	0.091	0.052	0.986
Shear Stress	0.876	0.419	0.190	0.980
Shear Rate	0.083	0.994	-0.007	0.995
Pressure	0.046	0.001	0.998	0.999
Variance	1.7521	1.1723	1.0357	3.9601
% Var	0.438	0.293	0.259	0.990
Factor Score Coefficients				
Variable	Factor 1	Factor 2	Factor 3	
Pressure	-0.053	-0.048	0.976	
Temperature	-0.629	0.263	0.128	
Shear Rate	-0.131	0.892	-0.054	
Shear Stress	0.447	0.214	0.098	



**Table 6.2 Application of Mutivariate Analysis for WBM Rheology  
(High-Shear Rate)**

**Factor Analysis**

PRINCIPAL COMPONENT FACTOR ANALYSIS OF THE CORRELATION MATRIX				
a. Unrotated Factor Loadings and Communalities				
Variable	Factor 1	Factor 2	Factor 3	Communality
Pressure	0.110	0.734	0.670	1.000
Temperature	-0.606	0.583	-0.532	0.990
Shear Rate	0.770	0.353	-0.516	0.983
Shear Stress	0.986	0.001	-0.001	0.973
Variance	1.9445	1.0026	0.9979	3.9449
% Var	0.486	0.251	0.249	0.986
b. Rotated Factor Loadings and Communalities (Varimax Rotation)				
Variable	Factor 1	Factor 2	Factor 3	Communality
Pressure	0.018	0.003	1.000	1.000
Temperature	-0.055	-0.993	0.009	0.990
Shear Rate	0.989	-0.069	-0.021	0.983
Shear Stress	0.808	0.558	0.093	0.973
Variance	1.6340	1.3024	1.0085	3.9449
% Var	0.409	0.326	0.252	0.986
c. Sorted Rotated Factor Loadings and Communalities				
Variable	Factor 1	Factor 2	Factor 3	Communality
Shear Rate	0.989	-0.069	-0.021	0.983
Shear Stress	0.808	0.558	0.093	0.972
Temperature	-0.055	-0.993	0.009	0.990
Pressure	0.018	0.003	1.000	1.000
Variance	1.6340	1.3024	1.0085	3.9449
% Var	0.409	0.326	0.252	0.986
Factor Score Coefficients				
Variable	Factor 1	Factor 2	Factor 3	
Pressure	-0.026	-0.025	0.994	
Temperature	0.186	-0.826	0.035	
Shear Rate	0.683	-0.280	-0.057	
Shear Stress	0.415	0.287	0.049	

**Table 6.3 Application of Multivariate Analysis for OBM Rheology  
(Low-Shear Rate)**

**Factor Analysis**

PRINCIPAL COMPONENT FACTOR ANALYSIS OF THE CORRELATION MATRIX				
a. Unrotated Factor Loadings and Communalities				
Variable	Factor 1	Factor 2	Factor 3	Communality
Pressure	0.750	-0.646	0.101	0.989
Temperature	-0.627	-0.765	-0.120	0.993
Shear Rate	0.154	0.027	-0.988	1.000
Shear Stress	0.991	0.001	0.000	0.982
Variance	1.9601	1.0030	0.9999	3.9630
% Var	0.490	0.251	0.250	0.991
b. Rotated Factor Loadings and Communalities (Varimax Rotation)				
Variable	Factor 1	Factor 2	Factor 3	Communality
Pressure	0.993	-0.054	0.024	0.999
Temperature	-0.042	-0.995	-0.012	0.986
Shear Rate	0.023	0.009	-0.999	0.995
Shear Stress	0.783	0.593	-0.129	0.980
Variance	1.6015	1.3452	1.0163	3.9630
% Var	0.400	0.336	0.254	0.991
c. Sorted Rotated Factor Loadings and Communalities				
Variable	Factor 1	Factor 2	Factor 3	Communality
Pressure	0.993	-0.054	0.024	0.989
Shear Stress	0.783	0.593	-0.129	0.982
Temperature	-0.042	-0.995	-0.012	0.993
Shear Rate	0.023	0.009	-0.999	1.000
Variance	1.6015	1.3452	1.0163	3.9630
% Var	0.400	0.336	0.254	0.991
Factor Score Coefficients				
Variable	Factor 1	Factor 2	Factor 3	
Pressure	0.701	-0.272	0.072	
Temperature	0.200	-0.810	-0.052	
Shear Rate	-0.037	-0.036	-0.990	
Shear Stress	0.399	0.303	-0.065	

**Table 6.4 Application of Multivariate Analysis for OBM Rheology  
(High -Shear Rate)**

**Factor Analysis**

PRINCIPAL COMPONENT FACTOR ANALYSIS OF THE CORRELATION MATRIX				
a. Unrotated Factor Loadings and Communalities				
Variable	Factor 1	Factor 2	Factor 3	Communality
Pressure	0.522	0.696	0.483	0.990
Temperature	-0.473	0.720	-0.500	0.992
Shear Rate	0.683	-0.033	-0.718	0.983
Shear Stress	0.982	-0.000	0.002	0.964
Variance	1.9270	1.0030	0.9986	3.9285
% Var	0.482	0.251	0.250	0.982
b. Rotated Factor Loadings and Communalities (Varimax Rotation)				
Variable	Factor 1	Factor 2	Factor 3	Communality
Pressure	0.033	-0.994	-0.011	0.990
Temperature	-0.037	-0.002	-0.995	0.992
Shear Rate	0.989	0.047	-0.049	0.983
Shear Stress	0.722	-0.498	0.442	0.964
Variance	1.5019	1.2384	1.1883	3.9285
% Var	0.375	0.310	0.297	0.982
c. Sorted Rotated Factor Loadings and Communalities				
Variable	Factor 1	Factor 2	Factor 3	Communality
Shear Rate	0.989	0.047	-0.049	0.983
Shear Stress	0.722	-0.498	0.442	0.964
Pressure	0.033	-0.994	-0.011	0.990
Temperature	-0.037	-0.002	-0.995	0.992
Variance	1.5019	1.2384	1.1883	3.9285
% Var	0.375	0.310	0.297	0.982
Factor Score Coefficients				
Variable	Factor 1	Factor 2	Factor 3	
Pressure	-0.152	-0.866	-0.122	
Temperature	0.131	-0.115	-0.892	
Shear Rate	0.748	0.214	-0.197	
Shear Stress	0.374	-0.259	0.230	

### 6.1.2 Drilling Fluid Rheology Modelling

It is highly recommended to compute the rheology of the actual mud system under downhole conditions prior to drilling operations. If such computation has not been done (due the drilling rig being only equipped with a Fann-viscometer working at temperature up to 180 °F and 15 psi pressure), the next choice is to use empirical models that can predict the pressure and temperature dependence of mud rheology.

Several studies of the rheology of water and oil based muds have been reported by other investigators. Some of these references include many mathematical expressions that are subjective. Politte<sup>218</sup> presented a multi-term equation with 13 numerical constants to model the viscosity of diesel oil at 1000 psi. Houwen et al.<sup>220</sup> presented several equations to model rheological parameters, e.g. viscosity, plastic viscosity or yield point. API Bulletin<sup>170</sup> presented two equations, to calculate temperature and pressure constants.

However in the present work a different procedure has been adopted. Shear stress at standard conditions has been multiplied by a correction factor that depends on pressure and temperature. Then the rheological behaviour and parameters can be calculated from the shear stress predicted at temperature and pressure of interest.

A comparison between the experimental data and rheological model predictions has been made in an attempt to validate the models. An OBM rheological model is also used to analyse field data from Gulf of Mexico. Specific case studies to illustrate the interpretation of the rheological models have been carried out using actual field data (from North Africa). The rheological models developed show the agreement of the experimental data and the field data within an average error of 4 %.

#### 6.1.2.1 Methodology of Model Development

The procedure for analysis is as follows:

1. Set up two-database worksheet for drilling fluid rheology measurement for WBM and OBM.



2. Select twenty-eight sets of shear stress data (one set = 6 shear stress values) at pressures of 15, 1000, 3000, 6000, 10000, 12000 and 17000 psi for temperature values between 150 and 300 °F.
3. Use twelve sets of data as independent test data for model validation.
4. Obtain the shear stress ratio by dividing each measured shear stress by shear stress at standard condition (150 F° and 15 psi).
5. Obtain the pressure coefficient (C) and the fluid constant (A) by correlating shear stress ratio with the pressure at constant temperature. The relationship between shear stress ratio and pressure can be expressed as:

$$\tau_R = A \exp CP \quad (6.1)$$

6. Obtain the temperature coefficient (B) by correlating fluid constant (A) with the temperature at constant pressure. The relationship between fluid constant and temperature can be expressed as:

$$A = A_c \exp BT \quad (6.2)$$

Equations (6.1) and (6.2) can be combined empirically as:

$$\tau_i = \tau_s [A_c \exp(BT + CP)] \quad (6.3)$$

where:

$\tau_i$ - Shear stress of interest, dyne/cm <sup>2</sup>	$\tau_s$ - Shear stress at standard conditions
$\tau_R$ - Shear stress ratio	A- Fluid constant
C- Pressure coefficient, 1/psi	P- Pressure, psi
$A_c$ - Constant	B- Temperature coefficient, 1/°F
T- Temperature, °F	

The term within the square brackets in equation (6.3) is also called the shear stress correction factor.

In this empirical model equation (6.3) the shear stress at standard conditions is multiplied by an exponential term where the exponent includes the coefficients that depend on pressure and temperature.



Table 6.5 tabulates empirical coefficients for both OBM and WBM taken for pressure values from 15 to 17000 psi and temperature values from 150 to 300 °F. Using the results obtained from equation (6.3) the rheological behaviour and rheological parameters can then be calculated.

**Table 6.5 Empirical coefficients for equation (6.3)**

<b>OIL BASED MUD</b>	<b>WATER BASED MUD</b>
$A_c = 1.95$	$A_c = 2.74$
$B = -0.0038$	$B = -0.0064$
$C = 0.50 \times 10^{-4}$	$C = 0.10 \times 10^{-4}$

#### 6.1.2.2 Comparison between Model Predictions and the Experimental Data

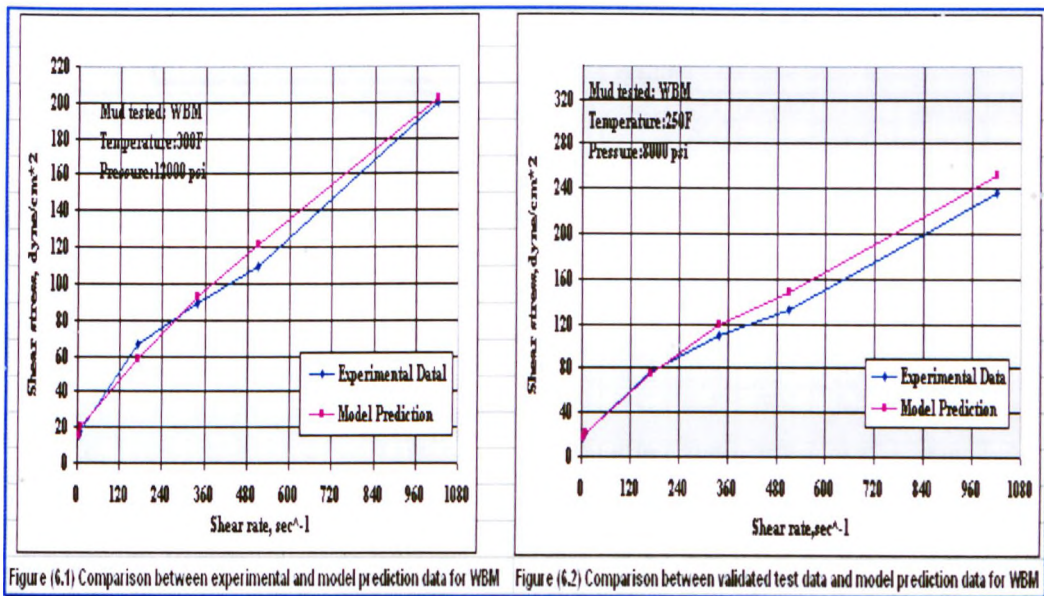
The most obvious approach to verifying the rheological models is to compare the experimental data against model predictions. The rheological models were used to predict drilling fluid rheology corresponding to each of the experimental conditions. The measured drilling fluid rheology is compared with the predicted rheology for WBM and OBM in Figures 6.1 and 6.2 respectively. From these figures it can be seen that in general, the predicted models are shown to be representative of the experimental data. The relative error can be represented by the following expression:

$$\text{Percentage of Error} = \sqrt{\frac{\sum_{i=1}^N \left( \frac{SS_{i \text{ predicted}} - SS_{i \text{ measured}}}{SS_{i \text{ predicted}}} \right)^2}{N}} \times 100 \quad (6.4)$$

where:

- $SS_{i \text{ predicted}}$  shear stress predicted from the model
- $SS_{i \text{ measured}}$  shear stress from experimental data
- $N$  total data points

The average error in the entire population of results for the prediction models for WBM is 2.69 % and for OBM is 1.77 % [Tables 6.6 to 6.8 in Appendix C].



### 6.1.2.3 Comparison between Model Predictions and Validating Data

Validation of rheological models using independent test data and field data was carried out. In Appendix C the results are given in Tables C1 (6.6) and C2 (6.7) (for WBM) and in Tables C3 (6.8) to C4 (6.9) are (for OBM).

The results show that the average error in twelve sets of WBM test data is 2.82% and 2.38 % in the case of OBM test data [Tables 6.7 and 6.8] [Figures 6.3 and 6.4].

Gulf of Mexico Field data (for OBM) provided by the M-I Company has been used for comparison between model prediction and field data. The average error of the entire population [Table 6.10a] of results for the prediction model is 4.14 % [Figure 6.5].

Therefore it is concluded that the experimental and validating data shows substantial agreement with rheology models predictions.



Table (6.6) Comparison between HP-HT model predictions,experimental and test data validation data for WBM

														coefficients		
														A=	2.74	
														B =	-0.0064	
														C =	1E-05	
$\tau_i = \tau_s [\mathcal{A}_c \exp(BT + CP)]$																
Temp	Pressure	S.S 600	prediction	S.S 300	prediction	S.S 200	prediction	S.S 100	prediction	S.S 6	prediction	S.S 3	prediction	% Error		
150	15	408		244.8		188.7		117.3		25.5		20.4				
150	1000	433.50	432.35	265.20	259.41	204.00	199.96	127.50	124.30	25.50	27.02	20.40	21.62	0.48		
150	3000	459.00	441.08	280.50	264.65	214.20	204.00	132.60	126.81	28.05	27.57	21.42	22.05	2.04		
150	5000	469.20	449.99	285.60	269.99	219.30	208.12	137.70	129.37	28.05	28.12	21.42	22.50	2.15		
150	6000	474.30	454.51	288.15	272.71	219.30	210.21	137.70	130.67	28.05	28.41	21.42	22.73	1.99		
150	8000	479.40	463.69	290.70	278.22	224.40	214.46	142.80	133.31	28.05	28.98	21.42	23.18	1.76		
150	10000	484.50	473.06	293.25	283.84	229.50	218.79	145.35	136.01	28.05	29.57	21.42	23.65	1.43		
150	12000	489.60	482.62	295.80	289.57	234.60	223.21	147.90	138.75	28.05	30.16	21.42	24.13	1.09		
150	15000	499.80	497.32	298.35	298.39	238.17	230.01	150.45	142.98	28.05	31.08	21.42	24.87	0.42		
150	17000	504.90	507.36	300.90	304.42	239.70	234.66	153.00	145.87	28.05	31.71	21.42	25.37	0.05		
200	500	285.60	312.38	163.20	187.43	122.40	144.48	81.60	89.81	28.05	19.52	15.30	15.62	4.25		
200	1000	293.25	313.95	168.30	188.37	127.50	145.20	86.70	90.26	22.95	19.62	17.85	15.70	3.27		
200	3000	300.90	320.29	178.50	192.17	132.60	148.13	91.80	92.08	22.95	20.02	17.85	16.01	2.50		
200	5000	304.47	326.76	181.05	196.06	132.60	151.13	93.84	93.94	25.50	20.42	20.40	16.34	2.60		
200	6000	308.55	330.04	183.09	198.03	134.64	152.65	96.90	94.89	25.50	20.63	20.40	16.50	2.40		
200	8000	311.10	336.71	183.60	202.03	137.70	155.73	96.90	96.80	25.50	21.04	20.40	16.84	2.91		
200	10000	317.22	343.51	187.68	206.11	142.80	158.87	99.45	98.76	25.50	21.47	20.40	17.18	2.79		
200	12000	321.81	350.45	192.27	210.27	144.84	162.08	99.45	100.76	25.50	21.90	20.40	17.52	3.04		
200	15000	326.40	361.13	196.86	216.68	147.90	167.02	102.00	103.82	25.50	22.57	20.40	18.06	3.53		
200	17000	335.07	368.42	201.45	221.05	149.94	170.39	103.02	105.92	25.50	23.03	20.40	18.42	3.54		
														Average error		2.01
														Comparison between validation test data and model predictions		2.38



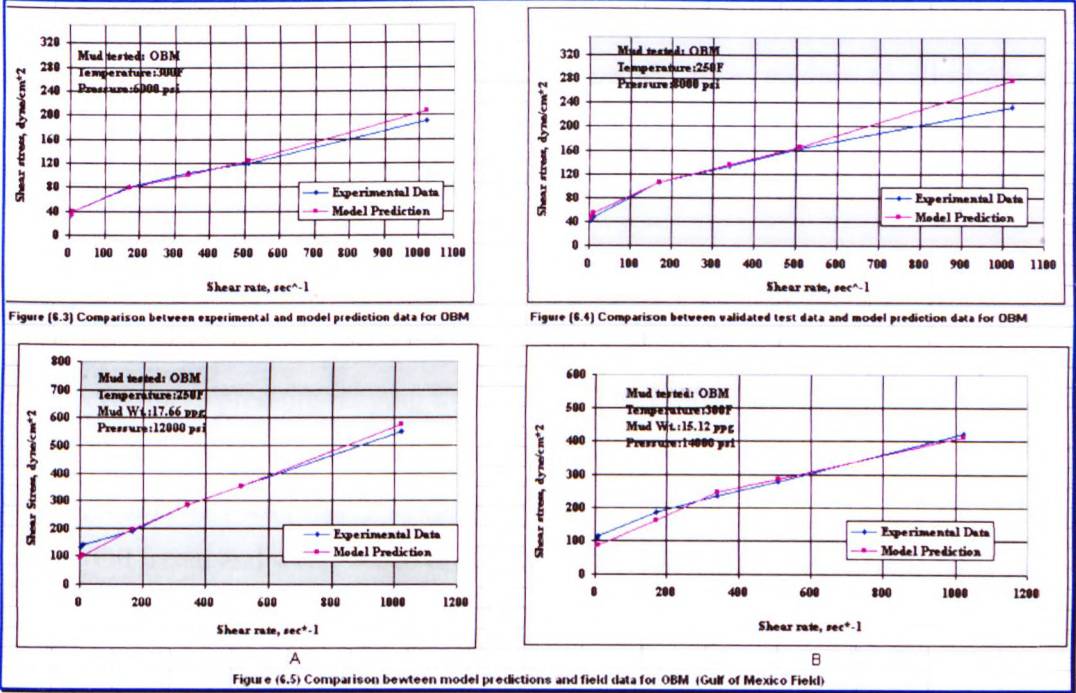


Table 6.10a Model prediction error with field data (Gulf of Mexico Field)

Mud Weight, ppg	Data Sets	% Error
15.6	15	2
17.6	15	3
14.35	20	6
11.5	15	4
16.25	24	3.8
15.12	20	1
13.75	23	4
17.3	23	5
12.67	9	3
15.83	21	3
15.63	18	3
16.22	36	5
16.8	25	6
13.40	21	7
16.59	21	7
16.74	20	2
15.91	26	5
15.20	27	3
14.30	25	6

Average error = 4.14%

## Case Studies

**Application of the Rheological Models.** Specific case studies to illustrate the practical interpretation of the rheological models have been carried out using actual field data. The data are collected from three oil companies in North Africa [Table 6.10b] and can be summarised as follows:

1. Six wells with the total well depth ranging from 10045 ft to 14580 ft.
2. Reservoir sections drilled in 5.87, 6 and 8.50 inch holes.
3. Wellbore pressure ranging from 5000 psi to 12800 psi.
4. Bottom hole temperature ranging from 240 °F to 330 °F.
5. Reservoir permeability ranging from 50 md to 400 md.
6. Oil based and water based drill-in fluids.

**Table 6.10b Well summary**

COMANY	FIELD	WELL NO.	TVD (FT)	TEMP. (°F)	FLUID TYPE	HOLE SECTION (INCH)
1	A	A1	13790	315	OBM	8.50
		A1	14580	330	OBM	6
		A2	14500	322	WBM	6
2	B	B1	13528	320	OBM	5.875
		B2	13175	305	WBM	8.50
		B2	13390	314	WBM	5.875
		B3	12245	280	WBM	5.875
3	C	C1	10045	240	WBM	8.50

The application of the models has been used as evaluation stage: The rheological models simulated results have been evaluated against field data (post drilling):

Predicted total wellbore pressure distribution versus field data (pump pressure).

The total pressure drop in the drilling hydraulic circuit consists of the sum of the pressure drop in the following parts:

- A surface circuit: composed of stand pipe, rotary hose, swivel and kelly.
- A circular section (inside drill string).
- An annular section (inside the gap between the drill string and borehole or casing).



➤ Drilling bit.

[Table 6.10c] illustrates the predicted total wellbore pressure distribution versus field data (pump pressure). The prediction shows agreement with field data.

**Table 6.10c Predicted wellbore pressure distribution versus field data (pump pressure)**

Company	Well Number	Total Depth (ft)	Hole Section (inch)	BHTemp. (°F)	Criteria	← Pump Pressure (psi) →	
						Field Data (Psi)	PRT Prediction (Psi)
1	A1	13790	8.50	315	*IF	2575	2466
		14580	6	330	IF	1780	1670
	A2	14500	6	322	IF	1700	1695
2	B1	13528	5.875	320	IF	2000	2032
		12175	8.50	305	**HHP	2600	2820
	B2	13390	5.875	314	IF	2000	2083
	B3	12245	5.875	280	IF	1500	1566
4	C1	10045	8.50	240	HHP	1950	2092

\*IF: Maximum impact force at the bit

\*\*HHP: Maximum hydraulic horse power at the bit

Note: the analysis will be discussed in [chapter 7].

## 6.2 STATIC FILTRATION MODELLING

The classic static filtration equation (6.5) was adapted to predict static filtration and filtration coefficients at different pressures and temperatures. Hence filter cake characteristics for WBM and OBM can be described. A comparison between the experimental data and independent test data and the model predictions is made to validate the model predictions.

### 6.2.1 Methodology of Static Filtration Models

1. Set up a database worksheet for static filtration experimental data.
2. Fit experimental data points (V and t) to the static filtration equation (6.5).
3. Use the least squares second order polynomial method to obtain the values of coefficients  $a_1$  and  $a_2$  in equation (6.5). In Appendix C the regression coefficients

for static experimental data are given in Tables C5 (6.11) to C12 (6.18) (for WBM) and in Tables C13 (6.19) to C18 (6.24) are (for OBM).

[The polynomial model is the most widely used nonlinear form because it can be transformed in such a way that the principle of least of squares may be used. In addition, the polynomial model provides the best fit to a set of filtration data].

$$t = a_2 V^2 + a_1 V \quad (6.5)$$

4. Set up a database worksheet for twenty-four coefficients.
5. Select twenty-one coefficients for model development and three coefficients to use for model validation as independent test data.
6. Correlate filtration coefficients to the pressure (at constant temperature), to obtain pressure coefficient (A).
7. Correlate pressure coefficient (A) with the temperature (at constant pressure), to obtain temperature coefficient (B) and constant ( $a_1'$  or  $a_2'$ ).
8. Verify static filtration models by comparing experimental data and independent test data against the model predictions.

### 6.2.2 Static Filtration Model For Water Based Mud

Equation (6.5) can be modified using methodology described (section 6.2.1) to get the model for WBM in the form of:

$$t = a_2 V^2 + a_1 V \quad (6.6)$$

where:

$$a_2 = a_2' \exp[AP + BT] \quad (6.7)$$

$$a_1 = a_1' \exp[AP + BT] \quad (6.8)$$

The following values ( $a_1'$ ,  $a_2'$ , A and B) are taken for the range of experimental conditions (pressure from 200 to 800 psi and temperature values from 150 to 300 °F):

$$a_2' = 30 \quad P = \text{pressure}$$

$$a_1' = 80 \quad T = \text{temperature}$$

$$A = -0.0010 \quad B = -0.012$$

6.2.2.1 Comparison between Model Predictions and the Experimental Data

The static filtration model was used to predict drilling fluid static filtration corresponding to the experimental conditions. The results obtained are shown in Figure 6.6. The average error is 1.79 % [Table 6.25].

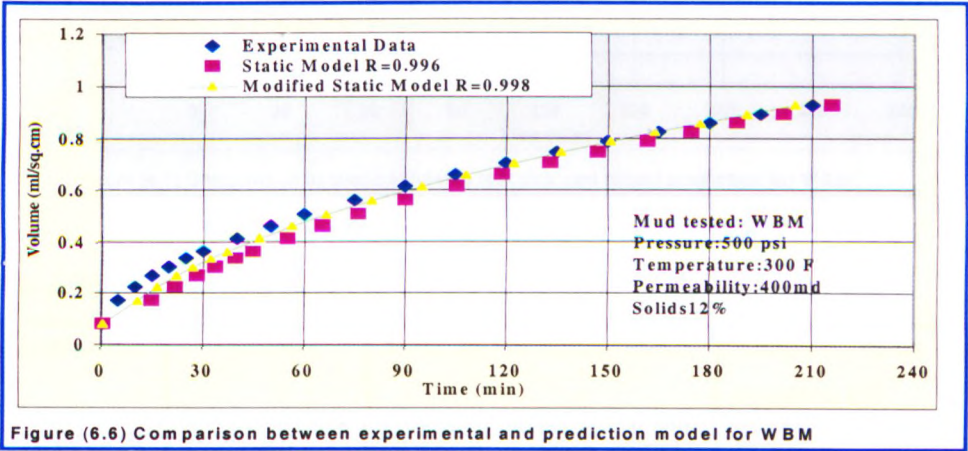


Table 6.25 Comparison between model prediction error and experimental data

Temperature	Pressure	Static model equation 6.5		Adapted static model equation 6.6	
( <sup>0</sup> F)	(psi)	% Error	Data points	% Error	Data points
150	200, 500	1.42	38	2.26	38
200	200, 800	1.95	38	1.68	38
250	200, 500, 800	1.58	228	1.60	228
300	500, 800	1.67	38	1.63	38
Average Error	=	1.65		1.79	

The model prediction has been validated with independent test data [section 6.2.1] [Figure 6.7] and shows an average error of 1.53 % [Table 6.26]. Hence the predicted model is shown to be representative of the experimental data.

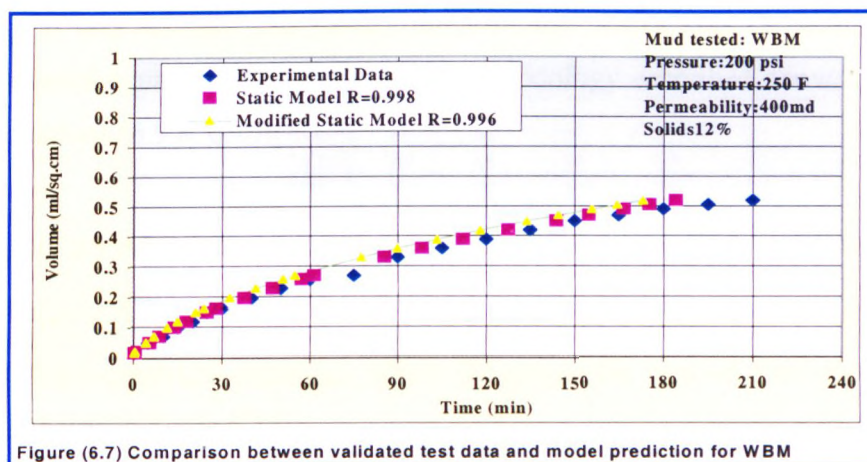


Figure (6.7) Comparison between validated test data and model prediction for WBM

Table 6.26 Comparison between model prediction error and test data

Temperature (°F)	Pressure (psi)	Static model equation 6.5		Adapted static model equation 6.6	
		% Error	Data points	% Error	Data points
150,200,300	800,500, 200 respectively	1.51	57	1.53	57

However, it is worth examining the conditions under which the model may deviate from the experimental data. Table 6.27 shows the difference between the model prediction and the experimental data, which occurs as a result of the type of FLA mechanisms used. The average error of this difference is 19 %.

Table 6.27 Comparison between model prediction error and test data

Additive type	Static model equation 6.5		Adapted static filtration model equation 6.6	
	% Error	Data points	% Error	Data points
Plugging	1.25	38	16	38
Viscosifying	2.30	38	22	38
Coating	2.65	38	18	38
Average Error	2.03		19	



Therefore it was necessary to modify the filtration coefficients ( $a_1$  and  $a_2$ ) in the existing model equation (6.6) using same methodology described above to general model equations (6.9 & 6.10):

$$a_2 = F \exp[Cx + AP + BT] \tag{6.9}$$

$$a_1 = F \exp[dx + AP + BT] \tag{6.10}$$

F, C and d are empirical constants, which depend on the type of fluid loss additive (FLA) as shown in Table 6.28.  
x = FLA concentration.

**Table 6.28 Empirical constants for adapted static filtration equations (6.9& 6.10)**

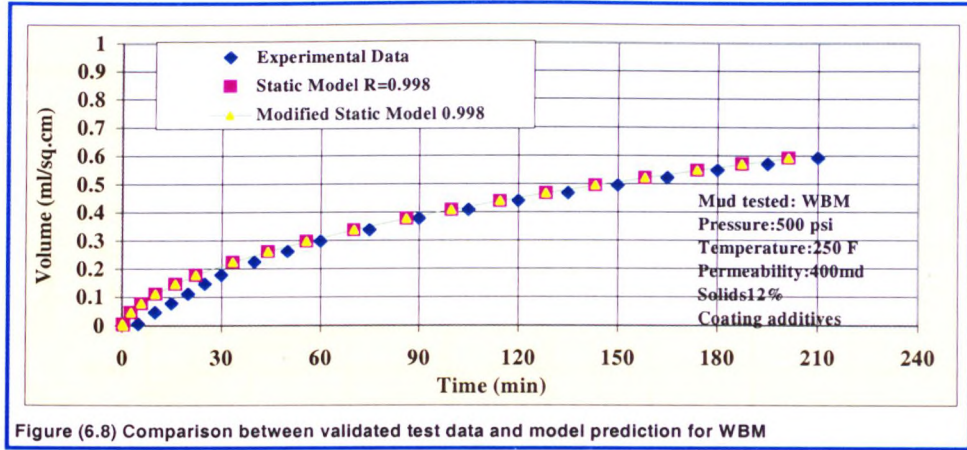
Coefficients	Coating additive	Plugging additive	Viscosifying additive
F	36	36	36
C	0.12	5.70	0.14
d	- 0.20	- 2.50	- 0.55

Table 6.29 shows that the average error between modified model and validated test data is 2.10 % [Figure 6.8].

**Table 6.29 Comparison between model prediction error and test data**

Additive type	Adapted model equations 6.9 & 6.10	
	% Error	Data points
Plugging	1.22	38
Viscosifying	2.88	38
Coating	2.12	38
Average Error	2.10	





### 6.2.3 Static Filtration Model for Oil Based Mud

Equation (6.5) can be modified using the methodology described (section 6.2.1) to get the model for OBM in the form of:

$$t = a_2 V^2 + a_1 V \quad (6.11)$$

where:

$$a_2 = a_2^t \exp[AP + BT] \quad (6.12)$$

$$a_1 = a_1^t \exp[AP + BT] \quad (6.13)$$

The following values ( $a_1^t$ ,  $a_2^t$ , A and B) are taken for the range of experimental conditions (pressure from 200 to 800 psi and temperature values from 150 to 300 °F):

$$a_2^t = 4.30 \times 10^2 \quad P = \text{pressure}$$

$$a_1^t = 3.00 \times 10^2 \quad T = \text{temperature}$$

$$A = -0.0005 \quad B = -0.011$$

#### 6.2.3.1 Comparison between Model Predictions and the Experimental Data

The measured static filtration against the predicted static filtration is shown in Figure 6.9. Table 6.30 shows that the average error is 1.50 %. Hence the predicted model is shown to be representative of the experimental data.

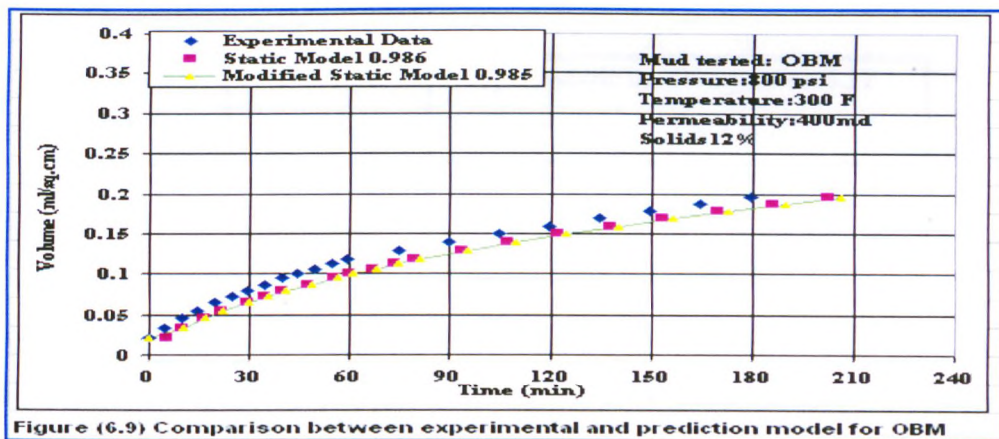


Table 6.30 Comparison between model prediction error and experimental data

Temperature ( <sup>0</sup> F)	Pressure (psi)	Static model equation 6.5 % Error    Data points	Adapted static model equation 6.11 % Error    Data points
150	200, 500	1.39        38	1.62        38
200	200, 800	1.65        38	1.68        38
250	200, 500, 800	1.42        228	1.25        228
300	500, 800	1.52        38	1.46        38
Average Error	=	1.50	1.50

The model prediction has been validated with independent test data [section 6.2.1] (Figures 6.10 and 6.11) and shows an average error of 1.57 % [Table 6.31].

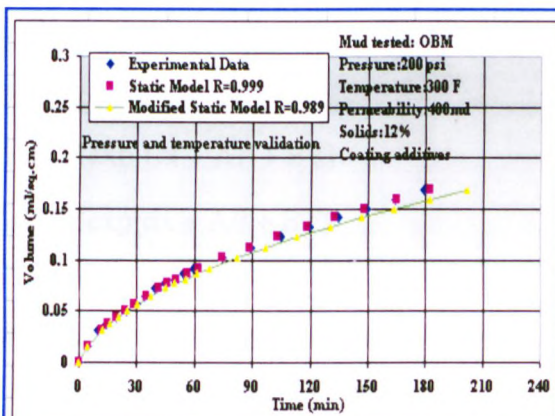


Figure (6.10) Comparison between validated test data and model prediction for OBM

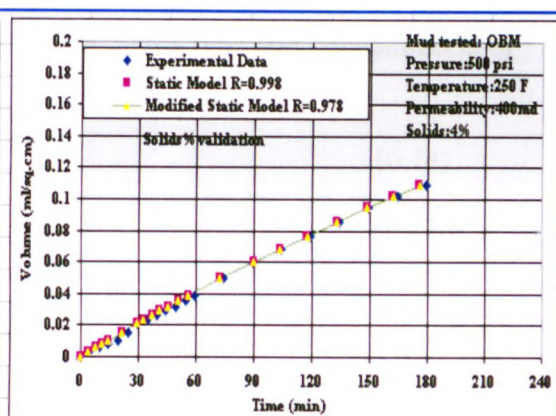


Figure (6.11) Comparison between validated test data and model prediction for OBM

**Table 6.31 Comparison between model prediction error and test data**

Temperature (°F)	Pressure (psi)	Adapted static model equation 6.11	
		% Error	Data points
150,200,300	800,500, 200 respectively	1.57	57

However, it is worth examining the conditions under which the model may deviate from the experimental data. Table 6.32 shows the difference between the model prediction and the experimental data, which occurs as a result of the type of FLA mechanisms used. The average error of this difference is 14 %.

**Table 6.32 Comparison between model prediction error and test data**

Additive type	Static model equation 6.5		Adapted static model equation 6.11	
	% Error	Data points	% Error	Data points
Plugging	2.15	38	13	38
Viscosifying	1.95	38	11	38
Coating	2.35	38	18	38
Average Error =	2.15		14	

Therefore it became necessary to modify the filtration coefficients ( $a_1$  and  $a_2$ ) in the existing model equation (6.10) using the same methodology described (section 6.2.1) to general model equations (6.14 & 6.15) depending on the type and concentration of fluid loss additives:

$$a_2 = F \exp[Cx + AP + BT] \quad (6.14)$$

$$a_1 = F \exp[dx + AP + BT] \quad (6.15)$$

F, C and d are empirical constants, which depend on the type of fluid loss additive (FLA), and are given in Table 6.33.

x = FLA concentration.



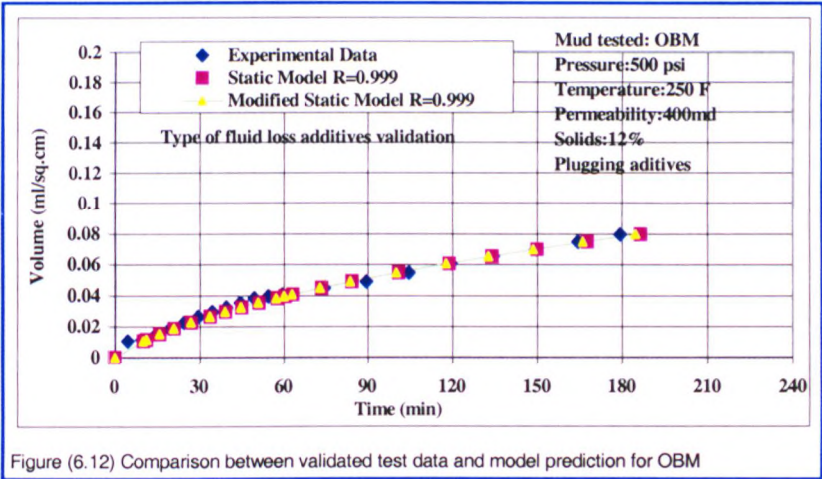
Table 6.33 Empirical coefficients for equations 6.14 & 6.15

Coefficients	Coating additive	Plugging additive	Viscosifying additive
F	110.00	110.00	110.00
C	0.26	0.53	0.85
d	0.16	0.43	0.58

Table 6.34 shows that the average error between the modified model and validated test data Figure [6.12] is 1.80 %.

Table 6.34 Comparison between model prediction error and test data

Additive type	Adapted static model equations 6.14 & 6.15	
	% Error	Data points
Plugging	1.15	38
Viscosifying	1.59	38
Coating	2.65	38
Average Error =	1.80	



### 6.3 APPLICATION OF THE EXPERIMENTAL DATA TO STATIC FILTRATION MODELS FOR WATER AND OIL BASED MUDS

In order to provide a better understanding of filtration mechanisms to minimising the filtration the coefficients ( $a_1$  and  $a_2$ ) from the modified static filtration equation can be determined and the cake characteristics such as average cake resistance, porosity and cake permeability can be calculated and described for OBM & WBM [reference equations 3.20, 3.21, 3.22 and 3.23].

Equations 3.22 and 3.23 can be used to determine the average cake porosity and average cake permeability, based on the ratio of wet to dry filter cake mass, the average filter cake resistance, and the density of the filtrate and solids. The filtrate density can be determined by a density meter. It is important to determine the solids density accurately because the filter cake is made up of several types of solids, such as bentonite, barite, drilling solids, and fluid loss additives. An example of the calculation method for true solids density ( $\rho_s$ ) and solids of fraction in slurry ( $s$ ) of WBM is as follows:

The composition of water based mud as listed in Chapter 5. First we use the following densities:

Bentonite	2300 kg/m <sup>3</sup> ,	Barite	4300 kg/m <sup>3</sup>
Drilling solids	2700 kg/m <sup>3</sup> ,	Spersene	1300 kg/m <sup>3</sup>
XP-20	1800 kg/m <sup>3</sup> ,	Resinex	1400 kg/m <sup>3</sup>
Polypac	1600 kg/m <sup>3</sup>		

Many investigators<sup>117,138,156</sup> have shown that all the above additives exist in the filter cakes. The density of solids of the WBM can be calculated as follows:

$$\rho_s = \frac{15}{82} 2300 + \frac{20}{82} \times 4300 + \frac{35}{82} \times 2700 + \frac{4}{82} \times 1300 + \frac{4}{82} \times 1800 + \frac{3}{82} \times 1400 + \frac{1}{82} \times 1600$$

$$\rho_s = 2843.10 \text{ kg/m}^3$$

According to the definition of solids fraction in slurry ( $s$ ):

$$s = \frac{\text{Mass of Solid in slurry}}{\text{Mass of Slurry}} \quad (6.16)$$



$$s = \frac{(15 + 20 + 35 + 4 + 4 + 3 + 1) \text{ lbs / bbl } \times 1.0 \text{ bbl}}{9.30 \text{ lbs / gal } \times 1.0 \text{ bbl}} = 0.209$$

### 6.3.1 Average Specific Cake Resistance and Effective Filter Medium Resistance

#### 6.3.1.1 Effect of Pressure and Temperature

Figures 6.13 to 6.15 clearly demonstrate that the average specific cake resistance increases as the pressure increases and declines as temperature increases for WBM and OBM. The average specific cake resistance for OBM is greater than that of WBM, which support the conclusion that fluid loss for OBM is lower than WBM.

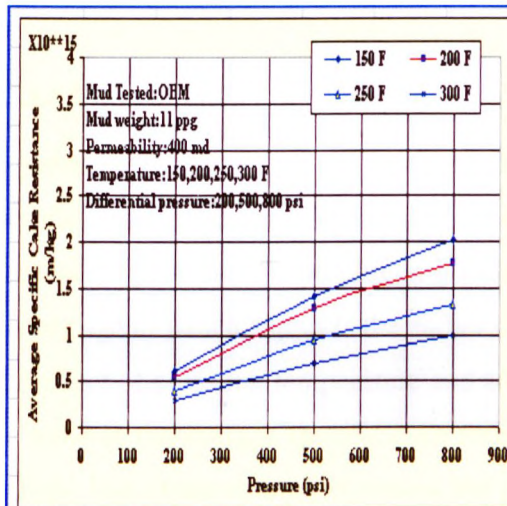


Figure (6.13) Average Cake Resistance as Function of Pressure in Static Filtration for OBM

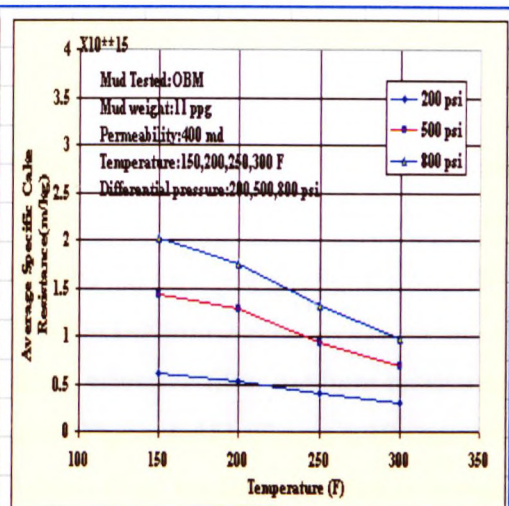


Figure (6.14) Average Cake Resistance as Function of Temperature in Static Filtration for OBM

#### 6.3.1.2 Effect of Solids

Figure 6.16 shows that as solids concentration increases the average specific cake resistance declines for WBM and increases for OBM and decreases cake permeability and hence the fluid loss. Therefore cake compressibility for WBM is dependent on solids concentration and practically independent of solids concentration for OBM. This is to be expected since the OBM cake is mostly water.

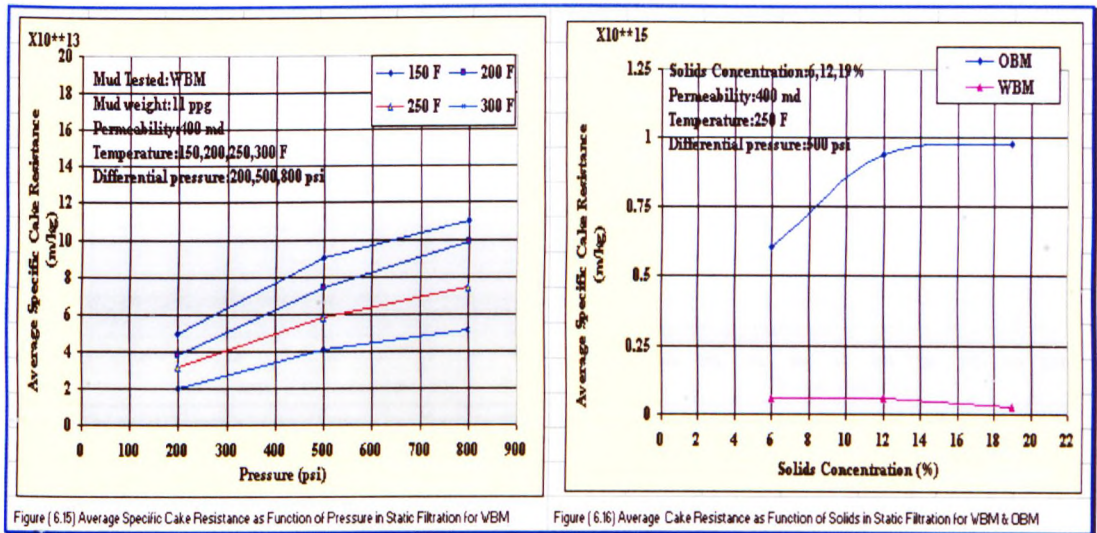


Figure ( 6.15) Average Specific Cake Resistance as Function of Pressure in Static Filtration for WBM

Figure ( 6.16) Average Cake Resistance as Function of Solids in Static Filtration for WBM & OBM

### 6.3.1.3 Effect of Fluid loss Additives

In general an increase in fluid loss concentration resulted in an increase in the average specific cake resistance. Figure 6.17 shows that the average specific cake resistance increases significantly from plugging and viscosifying FLA compared to the effect of coating agent, which supports the earlier discussion (section 5.9.1).

The effect of pressure, temperature and solids on effective filter medium resistance is the same as the average specific cake resistance [Figure 6.18]. Figure 6.19 shows that as fluid loss concentration increases the effective filter medium resistance increases for plugging and viscosifying additives compared to the coating agent.

## 6.3.2 Average Filter Cake Porosity and Permeability

### 6.3.2.1 Effect of Pressure and Temperature

Figures 6.20 to 6.22 show that the average filter cake permeability and porosity decrease as pressure increases and increase as temperature increases.



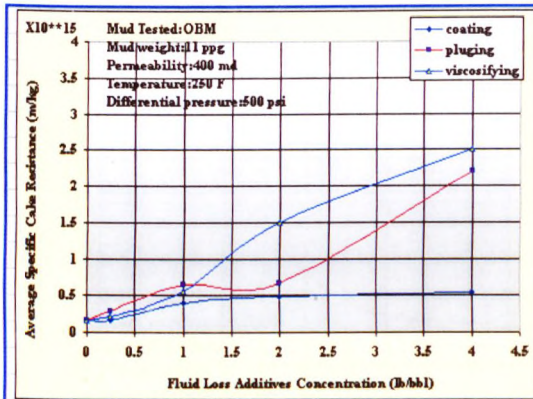


Figure (6.17) Average Cake Resistance as Function of Additives in Static Filtration for OBM

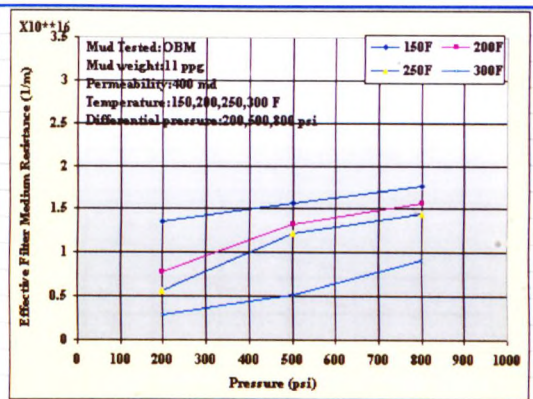


Figure (6.18) Medium Resistance as Function of Pressure & Temperature in Static Filtration for OBM

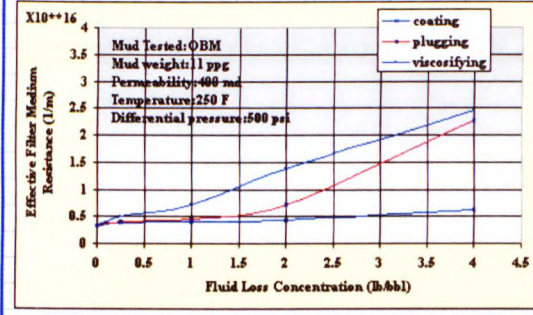
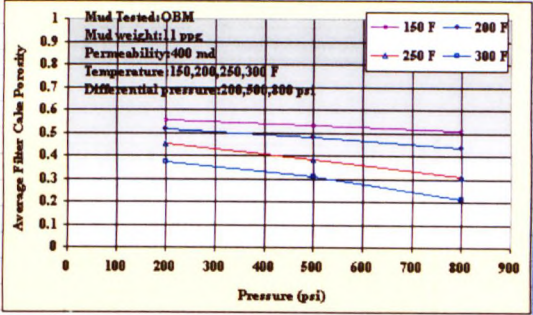


Figure (6.19) Medium Resistance as Function of Fluid Loss Additives in Static Filtration for OBM



Figure(6.20) Average Filter Cake Porosity as Function of Pressure in Static Filtration for OBM

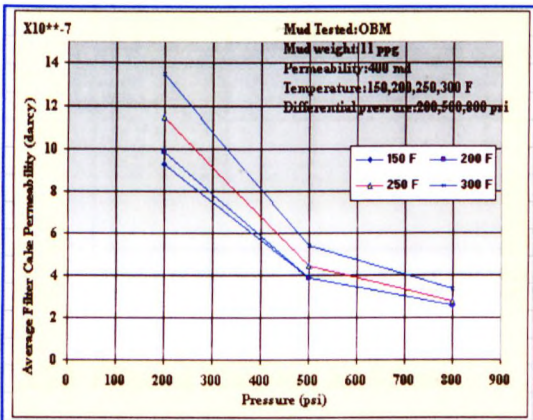


Figure (6.21) Average Cake Permeability as Function of Pressure in Static Filtration for OBM

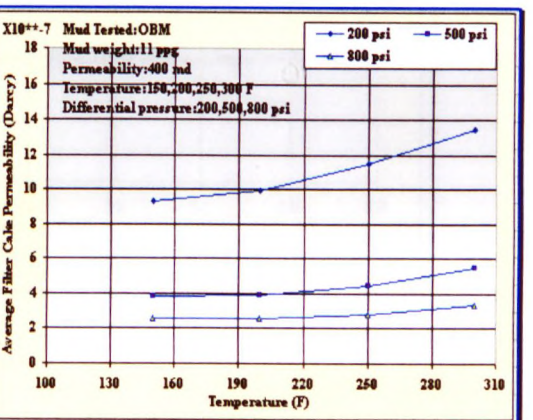


Figure (6.22) Average Cake Permeability as Function of Temperature in Static Filtration for OBM

### 6.3.2.2 Effect of Solids

Figures 6.23 to 6.25 show that increasing solids concentration will decrease filter cake permeability and porosity and hence the fluid loss for OBM, and increase filter cake permeability and porosity and hence the fluid loss for WBM, which supports the earlier discussion (section 5.7.1.2).

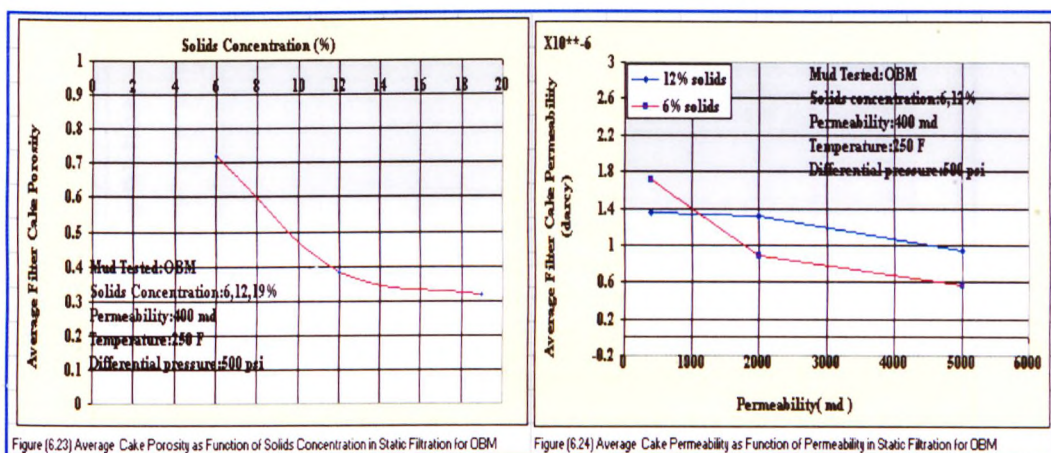


Figure (6.23) Average Filter Cake Porosity as Function of Solids Concentration in Static Filtration for OBM

Figure (6.24) Average Filter Cake Permeability as Function of Permeability in Static Filtration for OBM

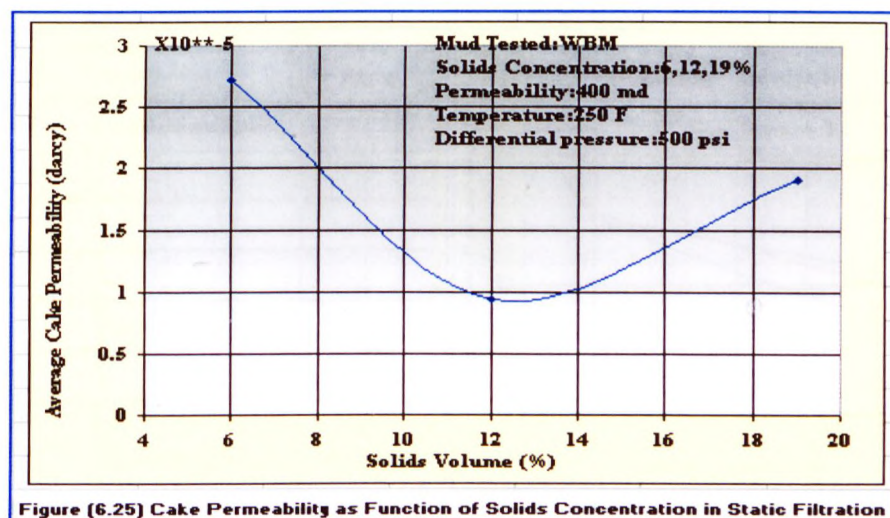


Figure (6.25) Cake Permeability as Function of Solids Concentration in Static Filtration

### 6.3.2.3 Effect of Fluid loss Additives

In general an increase in concentration of fluid loss additives results in a decrease in average cake permeability and porosity and also shows that the plugging and viscosifying additives have a more significant effect on permeability reduction than coating additives [Figures 6.26 to 6.28], which supports the earlier discussion (section 5.9.1).

Consequently the filter cake characteristics analysis results (from the application of the experimental data to static filtration model) show substantial agreement and supports the earlier discussion in chapter 5.



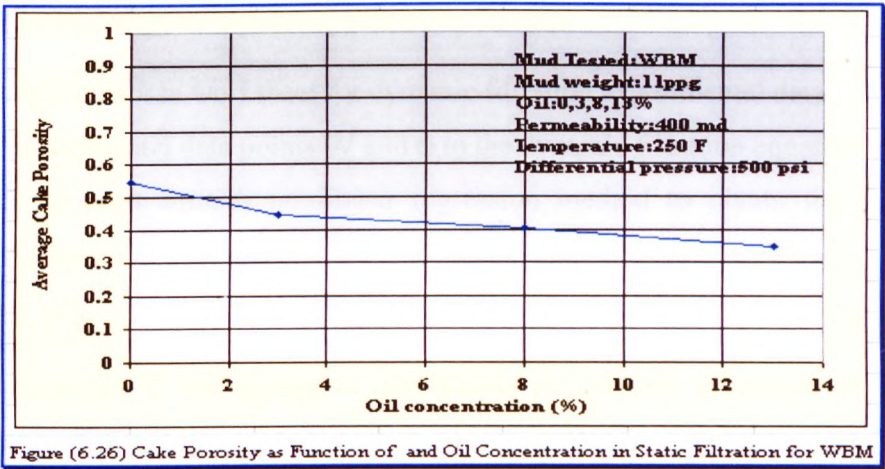


Figure (6.26) Cake Porosity as Function of and Oil Concentration in Static Filtration for WBM

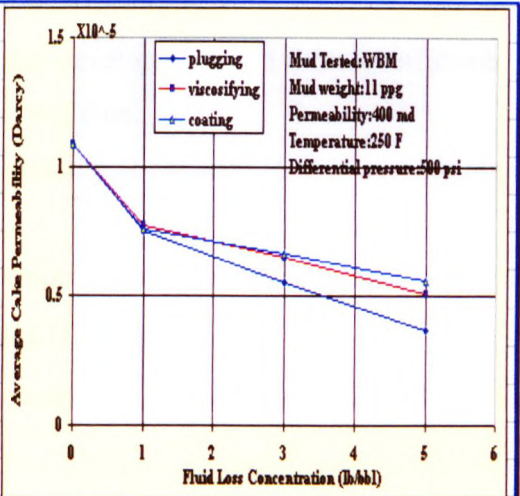
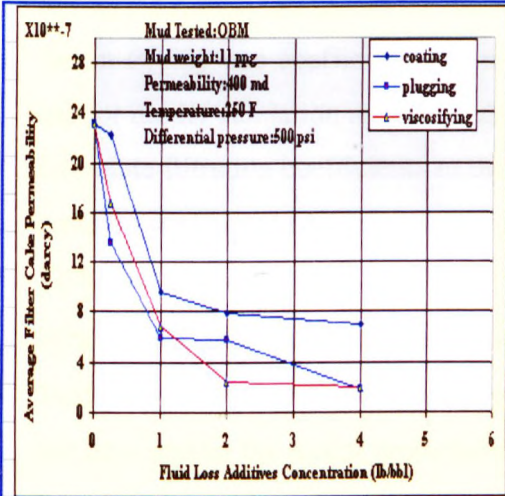


Figure (6.27) Cake Permeability as Function of Fluid Loss Additives in Static Filtration for OBM Figure (6.28) Cake Permeability as Function of Fluid Loss Additives in Static Filtration for WBM

#### 6.4 DYNAMIC FILTRATION MODELLING

The dynamic filtration equation has been adapted to predict dynamic filtration and dynamic filtration from static filtration data for WBM and OBM. The dynamic filtration coefficients can be predicted under downhole conditions and the filter cake characteristics can be described. A comparison between the experimental data and the model predictions is made in an attempt to validate the model predictions.



#### 6.4.1 Methodology of Dynamic Filtration Models

1. Set up a database worksheet for dynamic filtration experimental data.
2. Fit experimental data points (V and t) to the dynamic filtration equation (6.17).
3. Use the least squares non-linear regression method to obtain the values of coefficients  $C_1$ ,  $C_2$ , and  $C_3$ .

$$t = C_1 V - C_2 (1 - e^{C_3 V}) \quad (6.17)$$

4. In Appendix C the regression coefficients of dynamic experimental data are given in Tables C19 (6.35) to C25 (6.41) (for WBM) and in Tables C26 (6.42) to C32 (6.48) are (for OBM).
5. Set up a database worksheet for twenty-four coefficients.
6. Select twenty-one coefficients for model development and three coefficients to use for model validation as independent test data.
7. Correlate filtration coefficients to the pressure at constant temperature, to obtain pressure coefficient (A).
8. Correlate pressure coefficient to the temperature at constant pressure, to obtain temperature coefficient (B) and constants ( $C_1'$  or  $C_2'$ ).
9. Verify dynamic filtration models by comparing experimental and independent test data against the model predictions.

#### 6.4.2 Dynamic Filtration Model for Water Based Mud

Equation (6.17) can be modified to the form:

$$C_1 = C_1' \exp[AP + BT] \quad (6.18)$$

$$C_2 = C_2' \exp[AP + BT] \quad (6.19)$$

The following values ( $C_1'$ ,  $C_2'$ ,  $C_3$ , A and B) are taken for the range of experimental conditions (pressure from 200 to 800 psi and temperature values from 150 to 300 °F):

$$C_1' = 1.520 \times 10^3, \quad C_2' = 21.00 \times 10^3, \quad \text{and} \quad C_3 = 5.50 \times 10^{-2}$$

$$A = -0.0020$$

$$P = \text{pressure}$$

$$B = -0.010$$

$$T = \text{temperature}$$

These empirical constants are valid for solids concentrations above 6% and less than 80 rpm shear rate.

### 6.4.2.1 Comparison between Model Predictions and the Experimental Data

The dynamic filtration model has been used to predict drilling fluid dynamic filtration corresponding to each of the experimental conditions. The measured dynamic filtration against the predicted dynamic filtration is shown in Figure 6.29. From Table 6.49 the average error is 3.38 %. Hence the predicted model is shown to represent the experimental data with good accuracy.

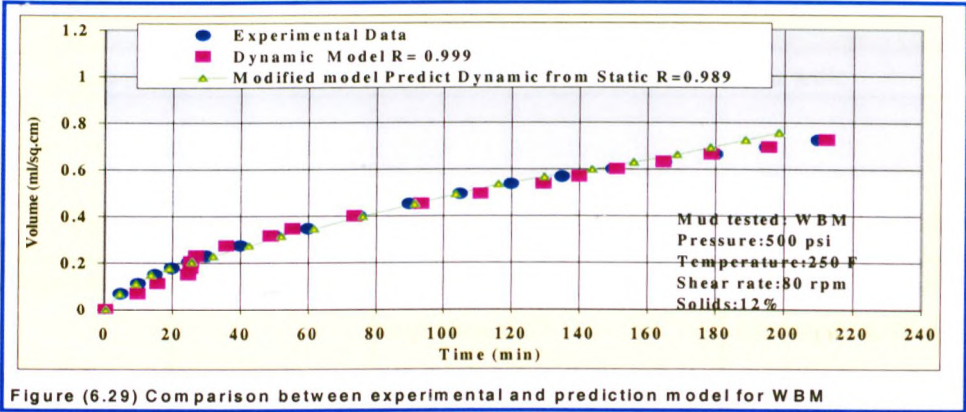
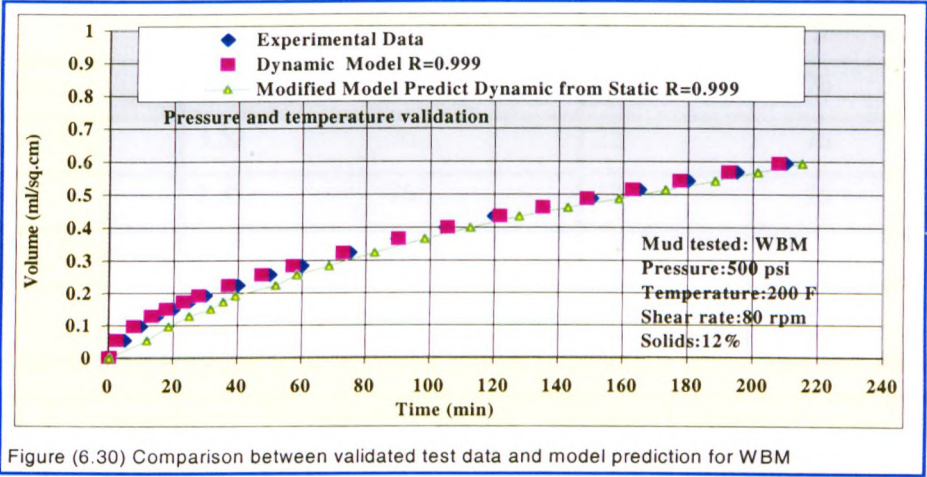


Figure (6.29) Comparison between experimental and prediction model for WBM

Table 6.49 Comparison between model prediction error and experimental data

Temperature  (°F)	Pressure  (psi)	Dynamic model equation 6.17		Adapted dynamic model equations 6.18 & 6.19	
		% Error	Data points	% Error	Data points
150	200, 500	3.50	38	3.77	38
200	200, 800	3.66	38	3.55	38
250	200, 500, 800	3.54	228	3.25	228
300	500, 800	3.46	38	2.96	38
Average Error =		3.54		3.38	

The model prediction has been validated with independent test data (section 6.4.1) [Figure 6.30] and shows an average error of 3.30 % [Table 6.50].



**Table 6.50 Comparison between model prediction error and test data**

Temperature	Pressure	Dynamic filtration model equation 6.17		Adapted filtration model equations 6.18 & 6.19	
(°F)	(psi)	% Error	Data points	% Error	Data points
150,200,300	800,500, 200 respectively	3.72	57	3.30	57

It is worth examining the conditions under which the model may deviate from the experimental data. The difference between the model predictions and the experimental data are expressed as a function of the major parameters affecting the dynamic filtration. Tables 6.51 to 6.53 shows that the difference between the model prediction and the experimental data occurs as a result of FLA mechanisms, solids concentrations less than 4 % and the use of shear rates greater than 80 rpm. The average error of this difference is 19 %.

**Table 6.51 Comparison between model prediction error and test data**

Additive type	Dynamic model equation 6.17		Adapted dynamic model equations 6.18 & 6.19	
	% Error	Data points	% Error	Data points
Plugging	4.25	76	16	76
Viscosifying	3.52	76	22	76
Coating	2.35	76	19	76
Average Error =	3.37		19	

**Table 6.52 Comparison between model prediction error and test data**

Solids (%)	Permeability (md)	Dynamic model equation 6.17		Adapted model equations 6.18 & 6.19	
		% Error	Data points	% Error	Data points
< 4	400 - 5000	4.50	57	18	57

**Table 6.53 Comparison between model prediction error and test data**

Shear rate, rpm	Dynamic model equation 6.17		Adapted dynamic model equations 6.18 & 6.19	
	% Error	Data points	% Error	Data points
> 80	6.65	57	11	57

Therefore it was necessary to modify the filtration coefficients in the existing model equations (6.18 & 6.19) using the same methodology as described above to give a general model equations (6.20, 6.21 and 6.22).

$$C_1 = h \exp[dx + AP + BT] \quad (6.20)$$

$$C_2 = h \exp[dx + AP + BT] \quad (6.21)$$

$$C_3 = h \exp[dx + AP + BT] \quad (6.22)$$

Tables 6.54 to 6.55 show that the empirical coefficients are dependent on the type and concentration of fluid loss additives, solids concentration and shear rate.



x = concentration of FLA

**Table 6.54 Empirical coefficients for equations 6.20, 6.21 &6.22 depend on type of FLA**

	C <sub>1</sub>			C <sub>2</sub>			C <sub>3</sub>		
Additive	h	&	d	h	&	d	h	&	d
Plugging	1.520	$\times 10^3$	1.70	31.5	$\times 10^3$	- 2.50	1.50		4.75
Viscosifying	1.520	$\times 10^3$	- 0.12	31.5	$\times 10^3$	- 0.52	1.50		0.40
Coating	1.520	$\times 10^3$	- 0.13	31.5	$\times 10^3$	- 0.65	1.50		0.46

**Table 6.55 Empirical coefficients for equations 6.20, 6.21 &6.22 depend on solids and shear rate**

	C <sub>1</sub>			C <sub>2</sub>			C <sub>3</sub>		
Condition	h	&	d	h	&	d	h	&	d
Solids <4% x=permeability	4.70	$\times 10^2$	0.13	13.50	$\times 10^2$	0.607	1.50		0.065
Shear rate >80 rpm x = rpm	4.70	$\times 10^2$	0.0075	13.50	$\times 10^2$	0.020	10.0		- 0.012

Table 6.56 shows that the average error between modified model and validated test data is 3.68 % [Figures 6.31 and 6.32].

**Table 6.56 Comparison between model prediction error and test data**

Condition	Adapted dynamic model equations 6.20, 6.21 & 6.22	
	% Error	Data points
Fluid loss additives	3.13	228
Solids <4%	4.25	57
Shear rate>80rpm	3.65	57
Average Error =	3.68	



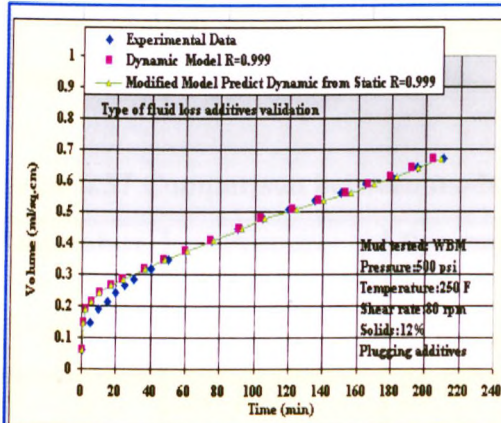


Figure (6.31) Comparison between experimental and prediction model for WBM

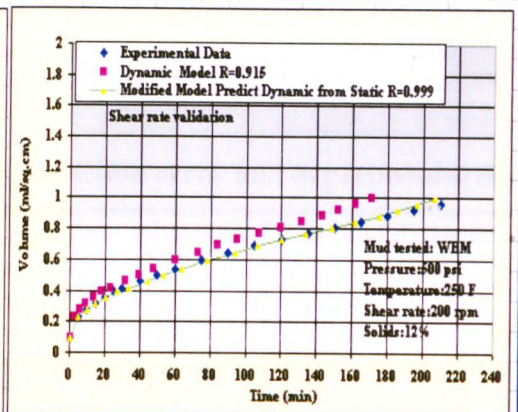


Figure (6.32) Comparison between validated test data and model prediction for WBM

### 6.4.3 Dynamic Filtration Model for Oil Based Mud

Equation (6.17) can be modified using the methodology described above to get the filtration model for OBM in the form:

$$C_1 = C_1' \exp[AP + BT] \quad (6.23)$$

$$C_2 = C_2' \exp[AP + BT] \quad (6.24)$$

The following values ( $C_1'$ ,  $C_2'$ ,  $C_3$ , A and B) are taken for the range of experimental conditions (pressure from 200 to 800 psi and temperature values from 150 to 300 °F): where:

$$C_1' = 2.50 \times 10^3, \quad C_2' = 21.00 \times 10^3, \text{ and} \quad C_3 = 9.90 \times 10^{-2}$$

$$A = -0.0020 \quad P = \text{pressure}$$

$$B = -0.0050 \quad T = \text{temperature}$$

These empirical constants are valid for shear rate < 80 rpm.

#### 6.4.3.1 Comparison between Model Predictions and the Experimental Data

The dynamic filtration model has been used to predict drilling fluid dynamic filtration corresponding to each of the experimental conditions. The measured dynamic filtration against the predicted dynamic filtration is shown in Figure 6.33. From Table

6.57 the average error is 2.35 %. Hence the predicted model is shown to be representative of the experimental data.

Table 6.57 Comparison between model prediction error and experimental data

Temperature  (°F)	Pressure  (psi)	Dynamic model equations 6.17		Adapted dynamic model equations 6.23 & 6.24	
		% Error	Data points	% Error	Data points
150	200, 500	2.42	38	1.96	38
200	200, 800	2.90	38	2.55	38
250	200, 500, 800	3.15	228	2.25	228
300	500, 800	2.25	38	2.65	38
Average Error =		2.68		2.35	

The model prediction has been validated with independent test data (section 6.4.1) [Figure 6.34] and shows an average error of 3.55 % [Table 6.58].

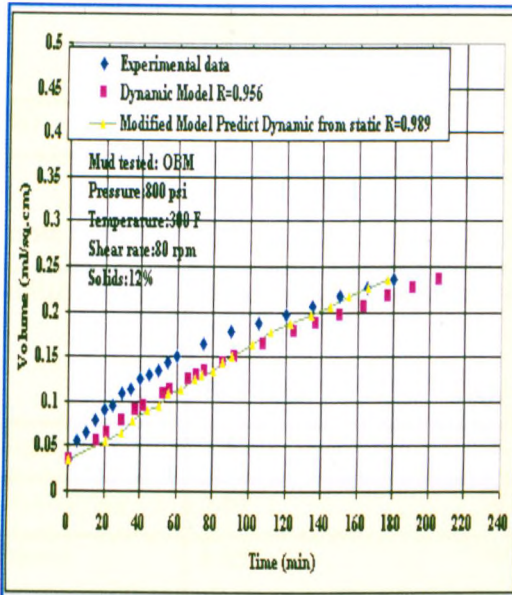


Figure (6.33) Comparison between experimental and model prediction for OBM

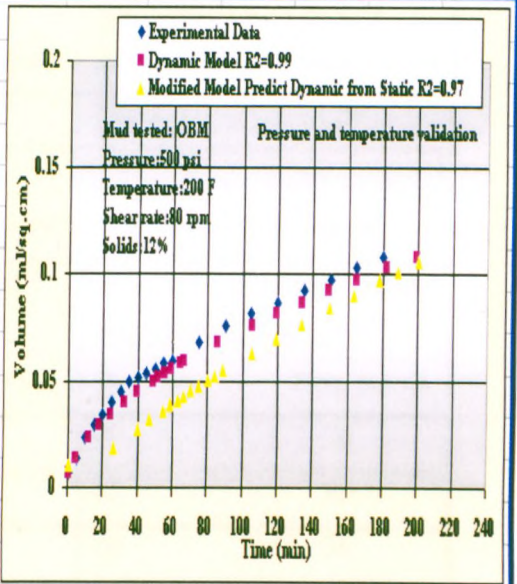


Figure (6.34) Comparison between validated test data and model prediction for OBM

**Table 6.58 Comparison between model prediction error and test data**

Temperature (°F)	Pressure (psi)	dynamic model equation 6.17		Adapted filtration model equations 6.23 & 6.24	
		% Error	Data points	% Error	Data points
150,200,300	800,500, 200 respectively	2.35	57	3.55	57

However, it is worth examining the conditions under which the model may deviate from the experimental data. The difference between the model predictions and the experimental data are expressed as a function of the major parameters affecting the dynamic filtration. Tables 6.59 and 6.60 shows that the difference between the model prediction and the experimental data occurs as a result of the type of FLA mechanisms used and shear rates greater than 80 rpm. The average error of this difference is 21 %.

**Table 6.59 Comparison between model prediction error and test data**

Shear rate (rpm)	dynamic model equation 6.17		Adapted dynamic model equations 6.23 & 6.24	
	% Error	Data points	% Error	Data points
> 80	4.25	57	17	57

**Table 6.60 Comparison between model prediction error and test data**

Additive type	dynamic model equations 6.17		Adapted dynamic model equations 6.23 & 6.24	
	% Error	Data points	% Error	Data points
Plugging	3.45	76	19	76
Viscosifying	3.65	76	25	76
Coating	4.25	76	22	76

Therefore it was necessary to modify the filtration coefficients in the existing model equations (6.23 & 6.24) using the same methodology described (section 6.4.1) to a general model equations (6.25, 6.26 and 6.27).

$C_1 = h \exp[dx + AP + BT]$  (6.25)

$C_2 = h \exp[dx + AP + BT]$  (6.26)

$C_3 = h \exp[dx + AP + BT]$  (6.27)

Tables 6.61 and 6.62 show that the empirical coefficients are dependent on the type and concentration of fluid loss additives (x) and the shear rate:

**Table 6.61 Empirical coefficients for equations 6.25 & 6.26  
depend on type of FLA**

	C <sub>1</sub>			C <sub>2</sub>		
Mechanism	h	&	d	h	&	d
Coating	6.0 x10 <sup>-2</sup>		0.42	3.0 x10 <sup>-3</sup>		0.60
Plugging	6.0 x10 <sup>-2</sup>		0.50	3.0 x10 <sup>-3</sup>		0.58
Viscosifying	6.0 x10 <sup>-2</sup>		0.57	3.0 x10 <sup>-3</sup>		0.55

**Table 6.62 Empirical coefficients for equations 6.25 to 6.27  
depend on solids and shear rate**

	C <sub>1</sub>			C <sub>2</sub>			C <sub>3</sub>		
Condition	h	&	a	h	&	a	h	&	a
Shear rate >80rpm x = rpm	35.0X10 <sup>-2</sup>		-0.014	40.0X10 <sup>-4</sup>		- 0.032	0.032		0.023

Table 6.63 shows that the average error between modified model and validated test data is 3.35 % [Figures 6.35 and 6.36].



Table 6.63 Comparison between model prediction error and test data

Condition	Adapted dynamic model equations 6.25 to 6.27	
	% Error	Data points
Fluid loss additives	4.21	228
Shear rate>80rpm	3.65	57

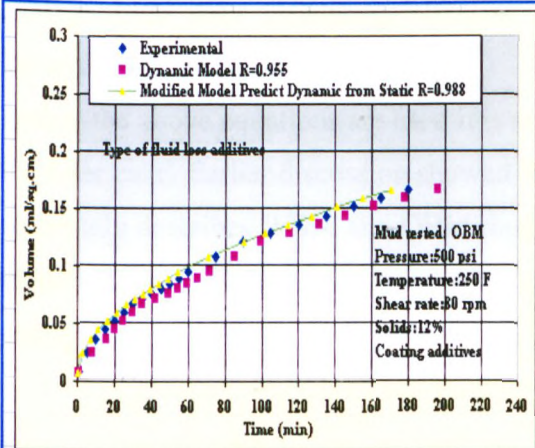


Figure (6.35) Comparison between validated test data and model prediction for OBM

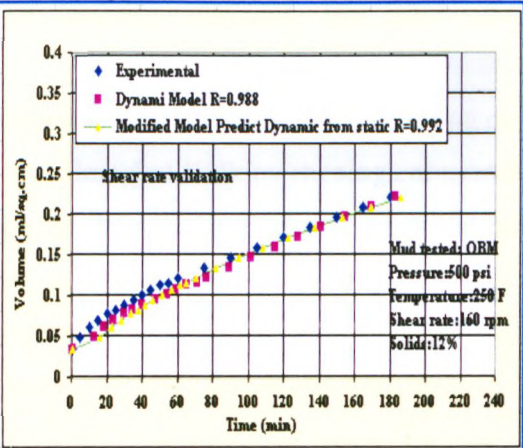


Figure (6.36) Comparison between validated test data and model prediction for OBM

### 6.5 APPLICATION OF THE EXPERIMENTAL DATA TO DYNAMIC FILTRATION MODELS FOR WATER AND OIL BASED MUDS

In order to provide a better understanding of filtration mechanisms to minimising the filtration the coefficients ( $C_1$ ,  $C_2$  and  $C_3$ ) from the modified dynamic filtration equation can be determined and the cake characteristics can be calculated and described for OBM & WBM using the following equations:

$$\alpha_{avg} = \frac{(1 - ms) \Delta p A^2 C_1 C_3}{\mu \rho_f s} \tag{6.28}$$

$$R_m = \frac{\Delta P A}{\mu} (C_1 - C_2 C_3) \tag{6.29}$$



$$B = \frac{\rho_f s}{(1 - ms) A C_1} \quad (6.30)$$

$$K_\tau = \frac{\rho_f s}{(1 - ms) \tau A C_1} \quad (6.31)$$

Equations (6.28) to (6.31) are then used for filter cake characteristics to obtain average filter cake resistance, effective filter medium resistance, and filter cake dynamic erodability respectively.

Before the above equations are used it is necessary to clarify the shear stress acting on the filter cake. Earlier discussion showed that the Herschel-Bulkley rheological model accurately describes WBM and OBM rheology, so their rheological properties can be modelled by:

$$\tau = \tau_0 + K\gamma^n \quad (6.32)$$

Using equation (6.32) to calculate the actual shear stress acting on the filter cake. The yield stress, power law index and consistency index were used for calculating the shear stress.

In SI units equation (6.32) can be written:

$$\tau = \tau_0 * 0.4788 + K * 1.0 * 10^{-3} * \gamma^n \quad (6.33)$$

where:

$\tau$  -Shear stress (N/m<sup>2</sup>),  $\tau_0$  -Yield stress (lb/100 ft<sup>2</sup>)

K-Consistency index (cP), n-Power Law index, dimensionless

$\gamma$  -Shear rate (s<sup>-1</sup>),

$\tau_0 = (\text{lb}/100 \text{ ft}^2) \times 0.4788 = (\text{N}/\text{m}^2)$

$K = (\text{cP}) \times 10^{-3} = (\text{Ns}/\text{m}^2)$

n Appendix C the shear stress values acting on the filter cake surface based on rheological behaviour of the testing fluids are given in Tables C33 (6.49) and C34 (6.50) (for WBM) and in Tables C35 (6.51) and C36 (6.52) are (for OBM).

6.5.1 Effective Filter Medium Resistance

6.5.1.1 Effect of Pressure, Temperature, Fluid Loss and Solids Concentration

In general, the effect of pressure, temperature, fluid loss additives and solids is the same as for static filtration but with higher filter medium resistance values and it is greater for OBM than that of WBM [Figures 6.37 to 6.39].

6.5.1.2 Effect of Shear Rate

The effect of the shear rate upon the medium resistance is also very significant. However, Figures 6.40 and 6.41 show that increased shear rate sharply increases filter medium resistance for OBM, while there is no clear trend observed for WBM, which may be indicate that a very narrow shear rate range has been used for WBM. The effective filter medium resistance for dynamic filter cake consists of the filter medium resistance, the resistance of internal cake (formed inside the pore space of the core surface) and the resistance of the first layer of the filter cake deposited on the core surface during the spurt time.

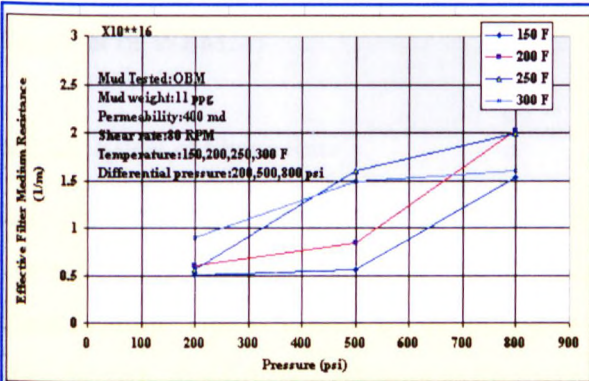


Figure (6.37) Medium Resistance as Function of Pressure and Temperature in Dynamic Filtration for OBM

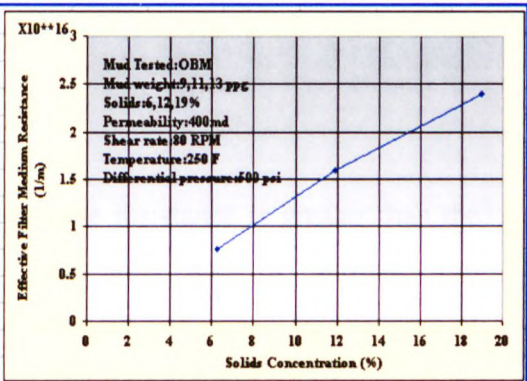


Figure (6.38) Medium Resistance as Function of Solids in Dynamic Filtration for OBM

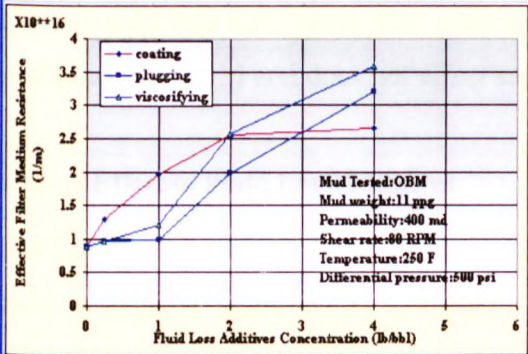


Figure (6.39) Effective Filter Medium Resistance as Function of Additives in Dynamic Filtration for OBM

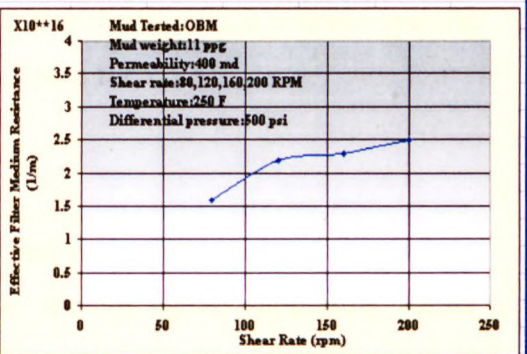


Figure (6.40) Medium Resistance as Function of Shear rate in Dynamic Filtration for OBM

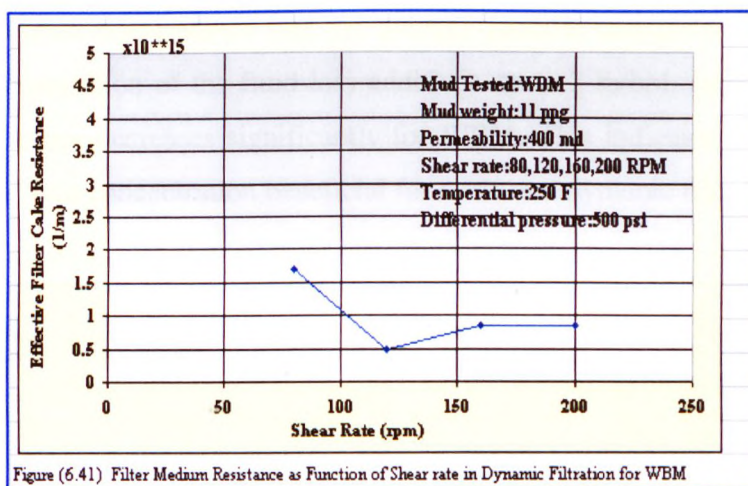


Figure (6.41) Filter Medium Resistance as Function of Shear rate in Dynamic Filtration for WBM

## 6.5.2 Average Specific Cake Resistance

### 6.5.2.1 Effect of Pressure, Temperature and Solids Concentration

The average specific cake resistance is a function of pressure, temperature, and solids concentration, which is the same as static filtration, but with higher values for OBM than that of WBM.

### 6.5.2.2 Effect of Shear Rate

It is clear that the average specific dynamic filter cake resistance is greater than the corresponding average specific static cake resistance due to particle size classification. This is caused by the plugging of the cake pore space by particles of specific size, that fill each opening as they move across the cake surface.

Figures 6.42 and 6.43 show that increase shear rate decreases the average specific resistance for OBM and does not affect cake resistance for WBM.

### 6.5.2.3 Effect of Fluid Loss Additives

For OBM [Figure 6.44] shows that the plugging and viscosifying agents increased the cake resistance significantly compared to the coating agent, supporting earlier discussion.



For WBM [Figure 6.45] shows that the average specific resistance increases with increased concentration of the fluid loss additives up to 3 lb/bbl. Beyond this value the cake resistance decreases significantly for WBM. This indicates that there is an optimum fluid loss concentration beneficial for static and dynamic filtration.

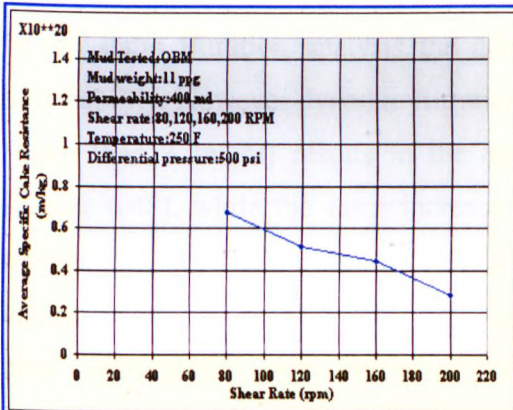


Figure (6.42) Cake Resistance as Function of Shear rate in Dynamic Filtration for OBM

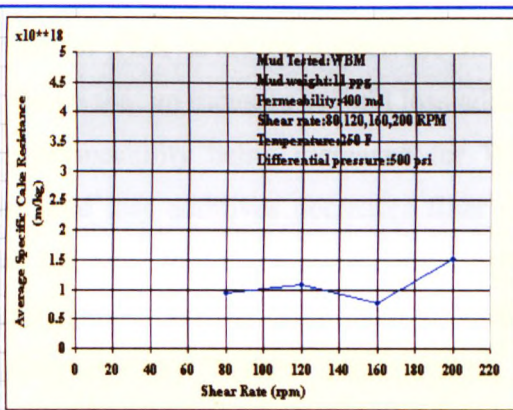


Figure (6.43) Average Cake Resistance as Function of Shear rate in Dynamic Filtration for WBM

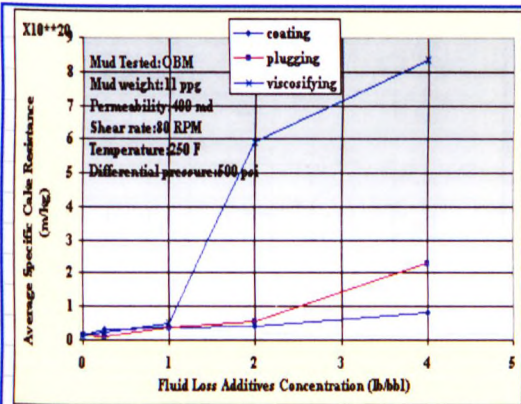


Figure (6.44) Cake Resistance as Function of Fluid Lose Additives in Dynamic Filtration for OBM

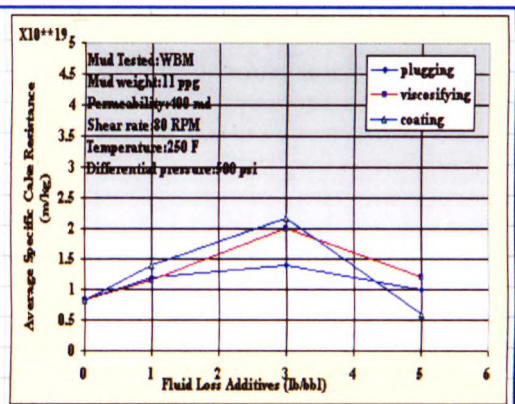


Figure (6.45) Average Cake Resistance as Function of Fluid Loss Additives in Dynamic Filtration for WBM

### 6.5.3 Average Filter Cake Permeability

#### 6.5.3.1 Effect of Pressure, Temperature and Solids Concentration

The effect of pressure, temperature, and solids on average filter cake permeability is the same as on static filter cake but with smaller values for OBM than WBM due to the effect of shear rate on particle size classification.

6.5.3.2 Effect of Shear Rate

Figures 6.46 and 6.47 clearly demonstrate that increase in shear rate does not affect cake permeability for WBM, but results in an increase of cake permeability for OBM.

6.5.3.3 Effect of Fluid Loss Additives

In the static filtration analysis the addition of FLA leads to a decrease in cake permeability. However dynamic filtration shows that an increase in fluid loss additive (more than 3 lb/bbl) results in the cake permeability being increased for WBM [Figure 6.48], while the same increase in fluid loss additives decreases filter cake permeability for OBM [Figure 6.49]. This indicates that there is an optimum fluid loss concentration beneficial for static and dynamic filtration. Additionally, the filter cake permeability was decreased significantly by higher concentrations of viscosifying and plugging additives compared to coating agent.

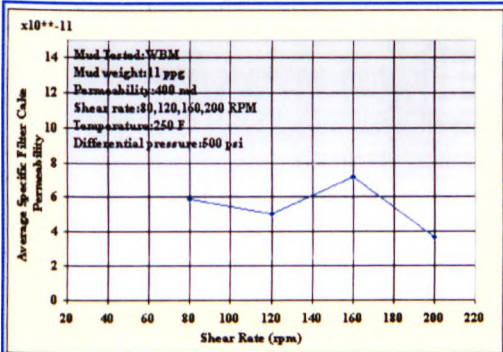


Figure (6.46) Average Filter Cake Permeability as Function to Shear Rate in Dynamic Filtration for WBM

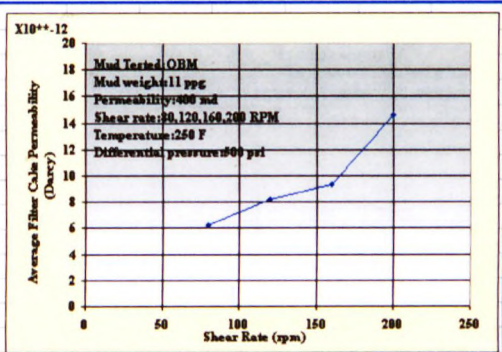


Figure (6.47) Average Cake Permeability as Function to Shear Rate in Dynamic Filtration for OBM

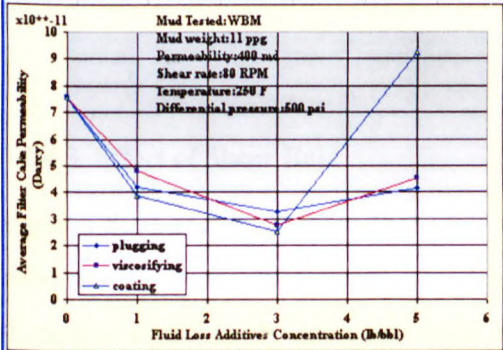


Figure (6.48) Average Filter Cake Permeability as Function of FLA in Dynamic Filtration for WBM

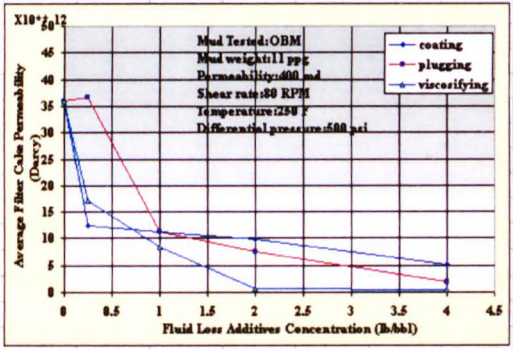


Figure (6.49) Average Cake Permeability as Function to FLA in Dynamic Filtration for OBM



6.5.4 Dynamic Cake Erodability

6.5.4.1 Effect of Pressure and Temperature

Figures 6.50 to 6.52 clearly demonstrate that the erodability of dynamic filter cake increases as the pressure and temperature increase. This effect is about ten fold less for OBM than WBM.

6.5.4.2 Effect of Solids Concentration

Figure 6.53 show that the erodability of dynamic cake decreases as solids concentration increases for WBM.

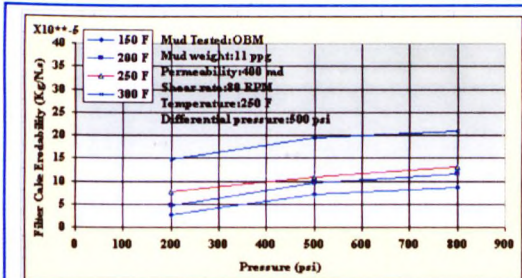


Figure (6.50) Filter Cake Erodability as Function of Pressure in Dynamic Filtration for OBM

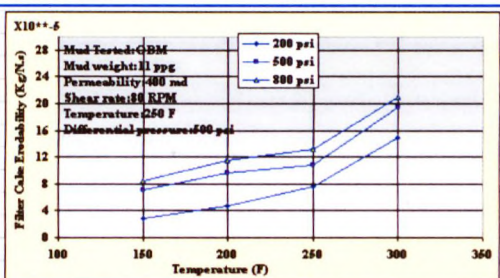


Figure (6.51) Cake Erodability as Function of Temperature in Dynamic Filtration for OBM

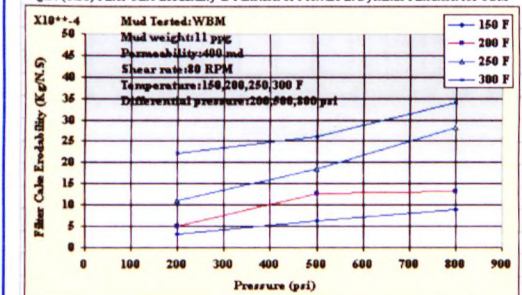


Figure (6.52) Filter Cake Erodability as Function of Pressure in Dynamic Filtration for WBM

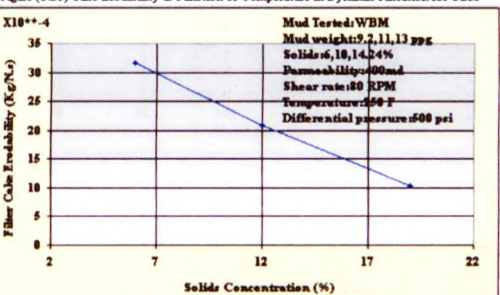


Figure (6.53) Filter Cake Erodability as Function of Solids in Dynamic Filtration for WBM

6.5.4.3 Effect of Shear Rate

Figures 6.54 and 6.55 show that with increasing shear rate, erodability of dynamic cake decreases for WBM and increases for OBM. This shows that the filter cake thickness significantly decreases with increasing shear rate for OBM, but shear rate has little effect on cake thickness for WBM.

6.5.4.4 Effect of Fluid Loss Additives

Figures 6.56 and 6.57 clearly demonstrate the erodability of dynamically deposited cake, which can be divided into two zones. In the first zone, for OBM the dynamic erodability decreases significantly as the fluid loss agents increase to 2 lb/bbl and in the second zone any further addition of agents causes the erodability to increase smoothly. For WBM in the first zone, the addition of fluid loss agents show almost no effect on erodability, and in the second zone the dynamic erodability decreases significantly.

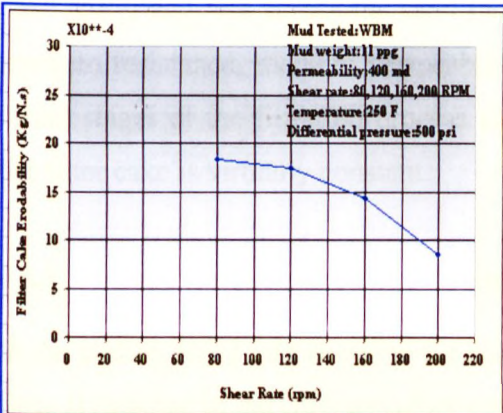


Figure (6.54) Filter Cake Erodability as Function of Shear rate in Dynamic Filtration for WBM

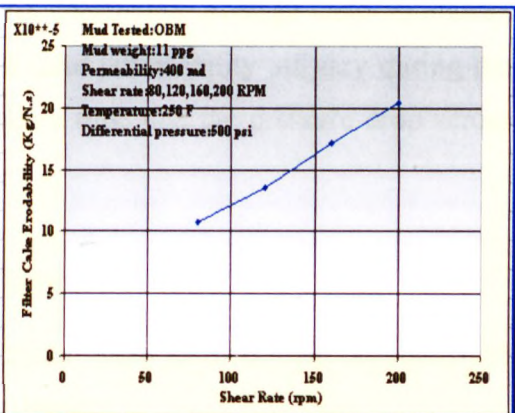


Figure (6.55) Cake Erodability as Function of Shear Rate in Dynamic Filtration for OBM

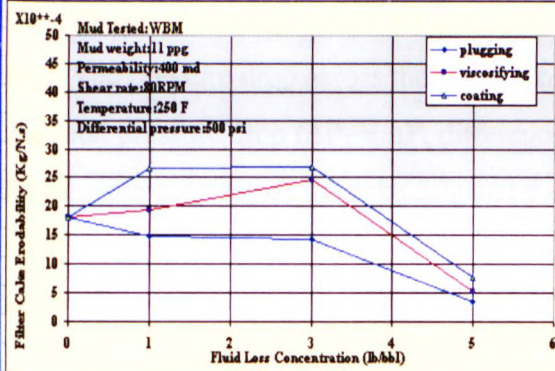


Figure (6.56) Filter Cake Erodability as Function of FLA in Dynamic for WBM

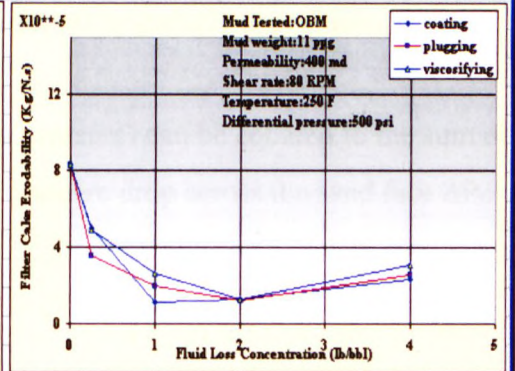


Figure (6.57) Cake Erodability as Function of FLA in Dynamic Filtration for OBM

## 6.6 DEVELOPMENT OF MODELS FOR PRESSURE DROP ACROSS POROUS FORMATION AND FILTER CAKE

The pressure distribution in the wellbore can be computed from the downhole rheology prediction models developed [section 6.1.2] hence the differential pressure and filtration volume can be computed. The pressure profile dissipated across the formation and filter cake therefore needs to be modelled in static and dynamic filtration process. This will permit the calculation of the filter cake characteristics, solids and filtrate invasion, permeability damage, and drilling skin.

At the start of the filtration, the total pressure drop ( $\Delta P_T$ ) occurs across the sand face, but as filter cake builds up, more of the pressure drop is dissipated across the filter cake ( $\Delta P_C$ ) and less across the sand face ( $\Delta P_f$ ). Meanwhile average cake resistance, medium resistance, medium permeability and cake permeability all vary during the initial stages of the filtration process until such a time that the pressure drop across the filter cake is virtually constant.

### 6.6.1 Model for Pressure Drop in Static Filtration Process

In the conventional rate equation for cake filtration there are two main resistances to flow giving rise to the corresponding pressure drops:

$\Delta P_f$  - The pressure drop across the sand face affected by particle deposition.

$\Delta P_C$  - The pressure drop across the filter cake.

The total pressure drop ( $\Delta P_T = \Delta P$ , differential pressure) can be equated to the sum of the pressure drop across the cake  $\Delta P_C$  and the pressure drop across the sand face  $\Delta P_f$ :

$$\Delta P_T = \Delta P_C + \Delta P_f \quad (6.34)$$

The conversion of Darcy's law to filtration conditions is readily accessible in filtration literature<sup>31,35,164-166</sup> and the differential pressure across the formation takes the form:

$$\Delta P_f = \mu q R_f \quad (6.35)$$



where:  $q = V/A$  (6.36)

$\Delta P_f$  - differential pressure across the sand face

$\mu$  - filtrate viscosity

$q$  - filtrate flow rate

$V$  - filtrate volume

$R_f$  - sand face resistance

$A$  - cross sectional area of the porous medium

Using the classic static filtration equation:

$$t' = a_2 V'^2 + a_1 V' \quad (6.37)$$

Differentiation of both sides with respect to  $V'$  in equation (6.37) and re-arrangement gives:

$$q = \frac{1}{A} \frac{dV'}{dt} = \frac{1}{A} \frac{1}{2a_2 V' + a_1} \quad (6.38)$$

Where:

$$R_f = \frac{\Delta P A}{\mu} a_1 \quad (6.39)$$

Inserting  $q$  from equation (6.38) and  $R_f$  from equation (6.39) into equation (6.35) and rearranging, the actual pressure drop across the sand face can be calculated as:

$$\Delta P_f = \mu \frac{1}{A} \frac{1}{2a_2 V' + a_1} \frac{\Delta P A}{\mu} a_1 = \frac{a_1}{2a_2 V' + a_1} \Delta P \quad (6.40)$$

Hence the pressure drop across the filter cake is given by:

$$\Delta P_c = \Delta P_T - \Delta P_f = \frac{2a_2 V'}{2a_2 V' + a_1} \Delta P \quad (6.41)$$

Consequently, by combining equation (6.40) and (6.41), the pressure drops across the sand face and the filter cake can be calculated at any instant of filtration as a function of time.

### 6.6.2 Model for Pressure Drop during Dynamic Filtration Process

In a similar way, we can determine the pressure drop across the sand face and the filter cake under dynamic conditions.

$$t' = C_1 V' - C_2 \left( 1 - e^{-C_3 V'} \right) \quad (6.42)$$



Differentiation of both sides with respect to  $V^t$  and re-arrangement gives:

$$q^t = \frac{1}{A} \frac{dV^t}{dt^t} = \frac{1}{A} \frac{1}{C_1 - C_2 C_3 e^{-C_3 V^t}} \quad (6.43)$$

Where:

$$R_f = \frac{\Delta P A}{\mu} (C_1 - C_2 C_3) \quad (6.44)$$

Inserting  $q^t$  from equation (6.43) and  $R_f$  from equation (6.44) into equation (6.35) gives:

$$\Delta P_f = \mu \frac{1}{A} \frac{1}{C_1 - C_2 C_3 e^{-C_3 V^t}} \frac{\Delta P A}{\mu} (C_1 - C_2 C_3) = \frac{C_1 - C_2 C_3}{C_1 - C_2 C_3 e^{-C_3 V^t}} \Delta P \quad (6.45)$$

Therefore the pressure drop across the filter cake is given by:

$$\Delta P_c = \Delta P_T - \Delta P_f = \frac{C_2 C_3 (1 - e^{-C_3 V^t})}{C_1 - C_2 C_3 e^{-C_3 V^t}} \Delta P \quad (6.46)$$

Consequently, combining equations (6.45) and (6.46), we can calculate the pressure drop across the filter cake and filter medium at any instant of filtration as a function of time under dynamic conditions.

The pressure drop models have been used to predict the pressure drop corresponding to each of the experimental conditions. In general, a comparison between pressure drops from experimental observation [Figure 6.58] and model prediction across the filter cake and the sand face shows agreement with less than 7 % error.

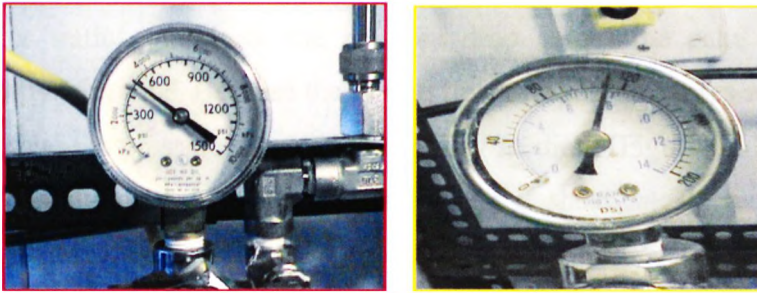


Figure 6.58a Experimental pressure drop across filter cake (top gauge) Figure 6.58b pressure drop sand face (bottom gauge)

The predicted pressure drop distribution profiles across the filter cake and the sand face during the static and dynamic filtration are shown in Figures 6.59 and 6.60 for

WBM and OBM. From the general comparison between pressure drops for the two mud systems [Figures 6.61 and 6.62], we can conclude the following:

Water based mud (WBM)

1. In static filtration, the percentage of pressure drop across the filter cake to the total applied pressure reached 96% [Figure 6.61].
2. In dynamic filtration, the percentage of pressure drop across the cake to the total applied pressure smoothly decreased to 87% compared to static condition [Figure 6.62].

Oil based mud (OBM)

1. In static filtration, the percentage of pressure drop across the filter cake to the total applied pressure reached about 97% of the total applied pressure [Figure 6.61].
2. In dynamic filtration, the percentage of pressure drop across the filter cake to the total applied pressure rapidly approaches almost a constant value of about 95%, which indicate that the resistance is maintained in dynamic filtration [Figure 6.62].

Furthermore, for oil based mud the pressure drops across the filter cake and filter medium rapidly reached a plateau while water based mud shows a more gradual hyperbolic trend [Figure 6.62]. The OBM has a lower pressure drop across the sand face than WBM. This is because OBM has lower filtrate volume in static and dynamic conditions compared to WBM [Figure 6.61].

Finally, under static conditions, the pressure drop across the cake continues to increase slightly with time. Because the filtrate flow rate still decreases with time, this leads to a decrease in pressure drop across the filter medium [Figure 6.61]. In the case of dynamic conditions at about two hours (or less if shear rate increases), [Figure 6.62] results clearly demonstrate that a constant pressure drop occurs across the filter cake. This represents equilibrium dynamic flow rate conditions, and clarifies the difference between static and dynamic filtration.

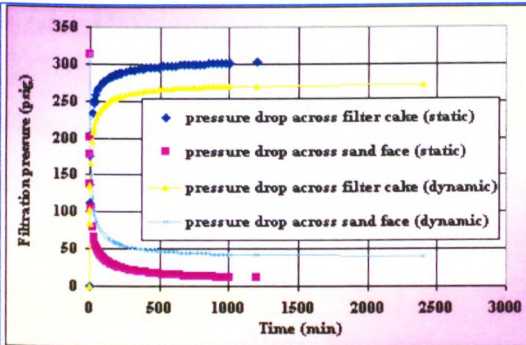


Figure 6.59 Static versus dynamic pressure drop for WBM

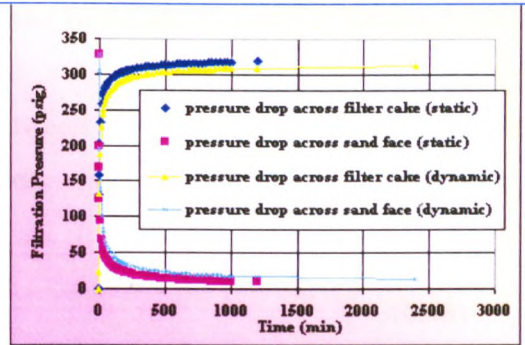


Figure 6.60 Static versus dynamic pressure drop for OBM

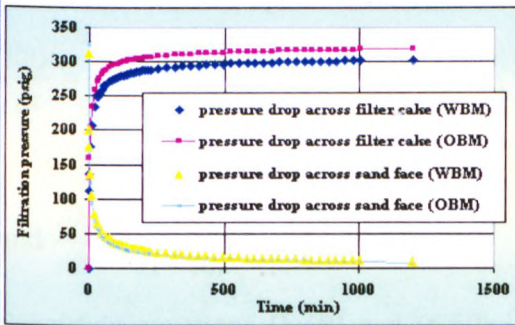


Figure 6.61 Comparison pressure drop in static filtration for WBM & OBM

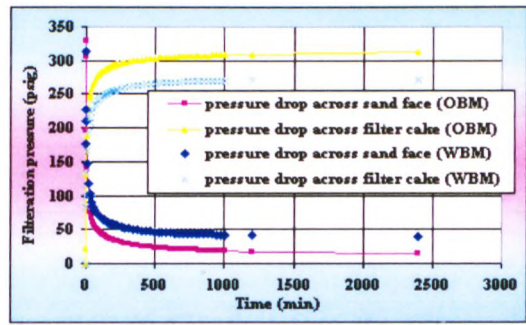


Figure 6.62 Comparison pressure drop in dynamic filtration for WBM & OBM

## 6.7 DEVELOPMENT OF MODELS FOR DRILLING FLUID DAMAGE

Formation damage mechanisms have been studied extensively<sup>62,98,231,232</sup> but a satisfactory model for field applications to simulate the near-wellbore damage in terms of well flow performance integrated from laboratory core test analysis still is not available. However, the formation damage can be characterised by the following factors: the static and dynamic fluid losses, damaged permeability in the zone occupied by internal cake, properties of external cake such as cake thickness, permeability, etc., pressure drop across cake and sand face, and the depth of solids and filtrate invasion. The first three factors can be obtained from controlled laboratory measurements and used to predict the other factors in order to simulate the full process of near wellbore damage. However, three main damaging mechanisms, which have been studied, are filter cake, particulate invasion during initial filtration period, and filtrate invasion through filter cake.



### 6.7.1 Development of Model for Filter Cake Build up in Static and Dynamic Filtration

Filter cake thickness,  $dh_c$  is the difference between the deposited cake  $dh_d$ , and eroded cake  $dh_e$  and can be obtained:  $dh_c = dh_d - dh_e$  (6.47)

$$\frac{dh_d}{dt} = \frac{W(\text{total deposited solids})}{(1-\phi)\rho_s} \quad (6.48)$$

Substitute for W in equation (3.28), we obtain:

$$\frac{dh_d}{dt} = \frac{\rho_f s V}{(1-\phi)\rho_s (1-ms)} \quad (6.49)$$

$$\text{and } \frac{dh_e}{dt} = \frac{K_\tau \tau}{(1-\phi)\rho_s} \quad (6.50)$$

Substitute equations (6.49) and (6.50) in equation (6.47), therefore the filter cake thickness can be calculated as:

$$\frac{dh_c}{dt} = \frac{\rho_f s V - K_\tau \tau}{(1-ms)} \quad (6.51)$$

where (s) is the solids concentration and (m) the ratio of wet to dry cake. The shear stress ( $\tau$ ) should be calculated from Equation (6.3).

If the mud is not circulated then the shear stress is zero and the filter cake becomes thicker as static filtration continues.

The static and dynamic filter cake build up has been simulated, based on the modified static and dynamic filtration equations which are themselves based on experimental tests conditions. These tests were conducted at pressure of 500 psi and temperature 250° F. Figures 6.63 to 6.66 show the relationship of filter cake thickness in static and dynamic conditions as a function of time for WBM and OBM.

In these figures the line labelled “cumulative cake” models the behaviour assuming no erosion. The line labelled “eroded cake” models the amount of erosion that takes



place. Thus dynamic cake plus eroded cake equal cumulative cake. The curve defined by squares was produced by assuming that the filter cake thickness is build up under the static condition where the shear stress on the filter cake is zero.

Figure (6.63) shows agreement between the experimental data, model predictions and an alternative filter cake model proposed by Liu et al<sup>102</sup> with a relative error of 2 %.

Comparing Figure (6.63) and Figure (6.64), we can see that the rate of erosion (and hence deposition) is significantly higher for WBM than for OBM. Filter cake build up has been simulated for WBM and OBM as a function of shear rate as shown in Figures (6.65 and 6.66). The figures show that the WBM filter cake is less affected by shear rate than the OBM cake and is also thicker; this is consistent with experimental observation as discussed in section 6.5.

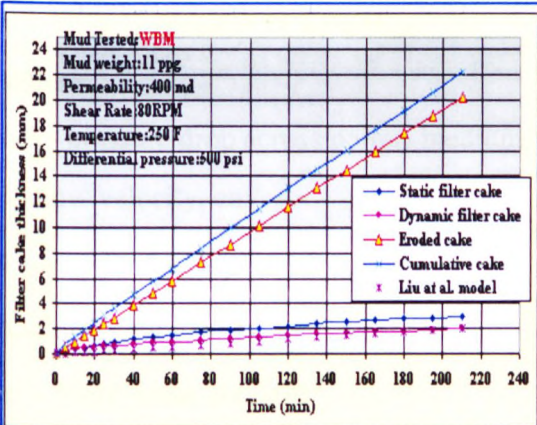


Figure (6.63) Simulation of Filter Cake Build-up as Function of Time for WBM

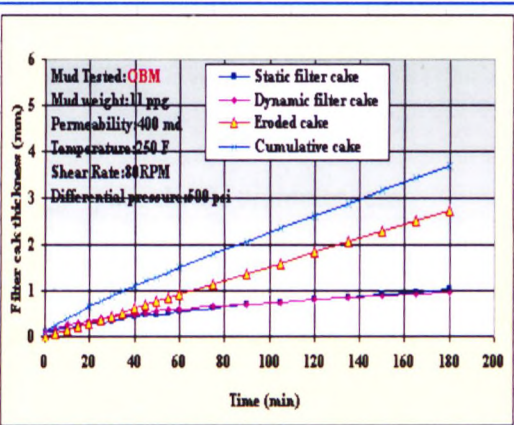


Figure (6.64) Simulation of Filter Cake Build-up as Function of Time for OBM

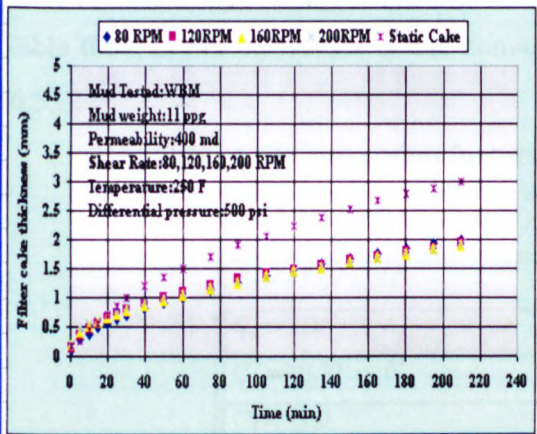


Figure (6.65) Simulation of Filter Cake Build-up as Function of shear rate for WBM

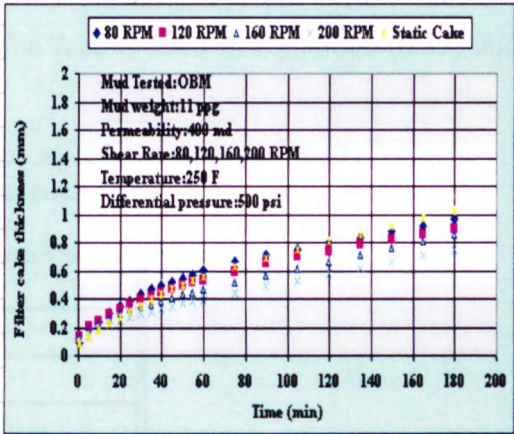


Figure (6.66) Simulation of Filter Cake Build-up as Function of shear rate for OBM

6.7.2 Development of Models for Depth of Solids Invasion

Solids invasion occurs mainly during initial filtration period. It is primarily a function of mud particle size distribution and the pore throat diameter of the formation. Empirical equations have been adapted for predicting the depth of solids invasion. These models are based on pressure drop in pipes<sup>211</sup> and assume that the solids bridge the pores of the rock and therefore involve the rheological behaviour of the drilling fluid. For Herschel Bulkley and Power Law fluids the model has been computed as:

$$L_d = \frac{C_1 \Delta P_f D_{pore}^{(1+n)}}{KV^n (C_2 \frac{3n+1}{n})^n} \tag{6.52}$$

For Bingham Plastic fluids the equation is:

$$L_d = C_3 \Delta P_f \frac{D_{Pore}^2}{(C_4 \mu_p V + C_5 \tau_y D_{Pore})} \tag{6.53}$$

Where:

- $\Delta P_f$  - pressure drop across porous medium, psi

V-flow velocity, cm/sec

$L_d$  -depth of solids invasion, cm

K-Consistency index, cP

$\tau_y$  - Yield point, lb/100ft<sup>2</sup>
- $D_{pore}$  - pore throat diameter, cm

n - Power Law index, dimensionless

$\mu_p$  - Plastic viscosity, cP

Table 6.64 shows the values of the conversion factors used in equations (6.52) and (6.53).

Table 6.64 Conversion factors for equations (6.52) and (6.53)

CONVERSION FACTORS
$C_1 = 43.89 \times 10^4$
$C_2 = 1.26$
$C_3 = 13.71 \times 10^4$
$C_4 = 3.00$
$C_5 = 20.00$



As it can be observed from the above models, determination of the depth of solids invasion requires knowledge of the formation morphological characteristics such as permeability, porosity, tortuosity etc. which have been described in chapter 4.

It is clear that the depth of solids invasion increases with increasing permeability and increasing pressure drop. As can be seen from the equations (6.52) and (6.53), the depth of solids invasion is related to the formation pore throat diameter. The depth of solids invasion depends on (a) rheological properties, (b) shear rate and fluid velocity, (c) differential pressure, and (d) the extent of invasion of the particulates with relation to pore throat diameter.

An increase in overbalance pressure during the filtration process may increase the internal formation damage as observed for water based mud. This is due to a large force pushing the particles into the pore spaces in the core during the initial stage of the filtration. However for oil based mud a high overbalance pressure expedites mud cake build-up with lower permeability thus reducing solids invasion and will result in a higher-pressure drop across the filter cake as discussed in chapter 5 and 6.

X-ray mapping has been used in the current work to investigate the depth of solids invasion for WBM and OBM and an agreement has been found with model prediction with relative error of < 8% [Figures 6.67 and 6.68].

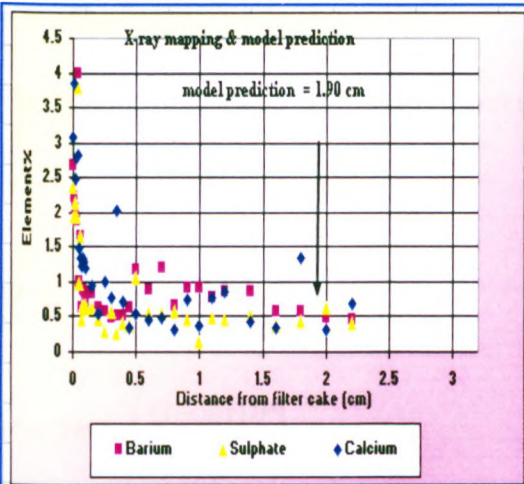


Figure 6.67 Solids invasion using X-ray Vs. model prediction for OBM

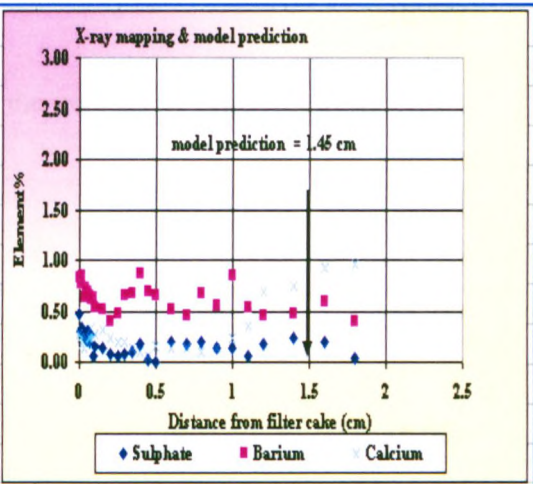


Figure 6.68 Solids invasion using X-ray Vs. model prediction for WBM

### 6.7.3 Development Models for Depth of Filtrate Invasion

The most common source of formation damage has proved to be drilling operations<sup>233</sup>. Drilling mud filtrate will invade the formation to a greater depth than drilling mud particulates. The depth of filtrate invasion depends upon many parameters such as formation characteristics, type, composition, filtration and rheological characteristics of the drilling fluid and the operating conditions (overbalance pressure, temperature, etc.). As filtrate enters the formation, a filter cake of drilling mud solids is built up on the formation face, decreasing the rate of filtrate invasion. However, the shear stress exerted by the drilling fluid will also erode the filter cake. The dynamic filtration rate ( $q$ ) accounts for this balance between filter cake formation and erosion in terms of shear stress ( $\tau$ ) effect on filter cake surface can be expressed as:

$$q = \frac{(1 - ms)K_\tau \tau}{\rho_f s} \quad (6.54)$$

$$\text{Or } q = \frac{(1 - ms)B}{\rho_f s} \quad (6.55)$$

$$\text{Where } B = K_\tau \tau \quad (6.56)$$

The filtrate flux at the wellbore per unit thickness of formation is simply the flux multiplied by borehole circumference. Then equation (6.55) become:

$$q = 2\pi r_w \frac{(1 - ms)B}{\rho_f s} \quad (6.57)$$

The volume of filtrate is then the integral of the volumetric rate with time:

$$V = \int_0^t q dt \quad (6.58)$$

$$V = \int_0^t 2\pi r_w \left( \frac{(1 - ms)B}{\rho_f s} \right) dt \quad (6.59)$$

$$V = 2\pi r_w t \left( \frac{(1 - ms)B}{\rho_f s} \right) \quad (6.60)$$



The volume of filtrate injected per unit thickness is related to the depth of penetration of the filtrate:

$$V = \pi\phi(r_d^2 - r_w^2) \quad (6.61)$$

Equating V from equation (6.60) and (6.61), then the depth of filtrate invasion  $r_d$  during dynamic condition can be expressed as:

$$r_d = \sqrt{r_w^2 + \frac{2r_w t (1 - ms)B}{\phi \rho_f s}} \quad (6.62)$$

The depth of filtrate invasion during static filtration can be calculated using equation (6.5) in the form of parabola equation:

$$q = -a_1 + \frac{\sqrt{a_1^2 - 4a_2 t}}{2a_2} \quad (6.63)$$

The filtrate flux at the wellbore per unit thickness of formation is just the flux multiplied by borehole circumference. Then equation (6.63) becomes:

$$q = 2\pi r_w \left( -a_1 + \frac{\sqrt{a_1^2 - 4a_2 t}}{2a_2} \right) \quad (6.64)$$

The volume of filtrate is then the integral of the volumetric rate with time:

$$V = \int_0^t q dt \quad (6.65)$$

$$V = \int_0^t 2\pi r_w \left( -a_1 + \frac{\sqrt{a_1^2 - 4a_2 t}}{2a_2} \right) dt \quad (6.66)$$

The volume of filtrate injected per unit thickness is related to the depth of penetration of the filtrate:

$$V = \pi\phi(r_d^2 - r_w^2) \quad (6.67)$$

Equating V from equation (6.66) and (6.67), then the depth of filtrate invasion  $r_d$  during static condition can be expressed as:

$$r_d = \sqrt{r_w^2 + \frac{2r_w}{\phi} \left( \frac{-a_1 t}{2a_2} + \frac{(a_1^2 + 4a_2 t)^{1.50}}{12a_2} - \frac{a_1^3}{12a_2} \right)} \quad (6.68)$$

## 6.8 PRODUCTIVITY EVALUATION

The insights gained into fluid rheology, filtration and formation damage mechanisms will now be applied to the problem of formation damage productivity impairment for field applications.

Well performance is reduced when near-wellbore formation is damaged. A key parameter in quantifying the formation damage or the reduction of the well productivity will be the skin factor or the flow efficiency<sup>233</sup> calculation.

### 6.8.1 Linear Flow through the Core Plug

The average permeability ( $\bar{k}$ ) Figure 6.69 can be computed from the pressure drop across the formation model (6.45) using the following equation:

$$\bar{K} = \frac{q\mu L_c}{A\Delta P_f} \quad (6.69)$$

Where:

q- flow rate

$\mu$  -fluid viscosity

$L_c$ -core length

A-cross sectional area

$\Delta P_f$  - pressure drop across core

$\bar{K}$  - average permeability

$K_f$  -formation permeability

The permeability damage  $K_d$  can be calculated using equation (6.70):

$$K_d = L_d / \left( \frac{L_c}{\bar{K}} - \frac{(L_c - L_d)}{K_f} \right) \quad (6.70)$$

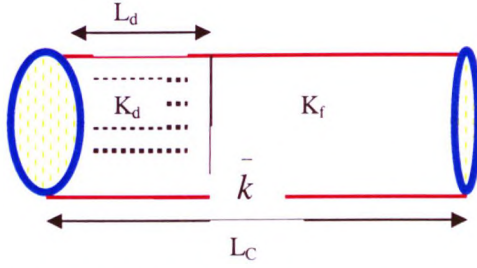


Figure 6.69 Schematic Diagram for Core Damage

$L_d$  can be calculated from equation (6.52 or 6.53). Then the lab skin factor ( $s$ ) due to filtrate invasion can be calculated as follows:

$$s = \frac{k\Delta P_f}{q\mu L_c} \quad (6.71)$$

### 6.8.2 Radial Flow through Wellbore

The radial flow equation is obtained by substituting for the cross-sectional area,  $A$ , in the Darcy equation using  $A = 2\pi rh$ :

$$P_e - P_w = \frac{q\mu}{7.08Kh} \ln \frac{r_e}{r_w} \quad (6.72)$$

Where:  $q$  - flow rate, stb/day

$K$  - formation permeability, md

$\mu$  - oil viscosity, cP

$h$  - formation thickness, ft

$P_e, P_w$  - reservoir and well flow pressure respectively, psi

$r_e, r_w$  - reservoir drainage radius and wellbore radius respectively, ft

Van Everdingen and Hurst<sup>99</sup> quantified the condition of the near-wellbore region with the introduction of the concept of the skin effect ( $s$ ) [Figure 6.70].

The total skin effect for a well,  $s$ , consists of a number of components. Generally these can be added together, and therefore:

$$s = s_d + s_p + s_c + s_b + s_g \quad (6.73)$$

Where:

$s_d$  - drilling skin

$s_p$  - perforation skin

$s_c$  - partial completion skin

$s_b$  - blockage skin

$s_g$  - gravel-pack skin

The drilling skin ( $s_d$ ) contributes the highest percentage of the total skin and need to be predicted.

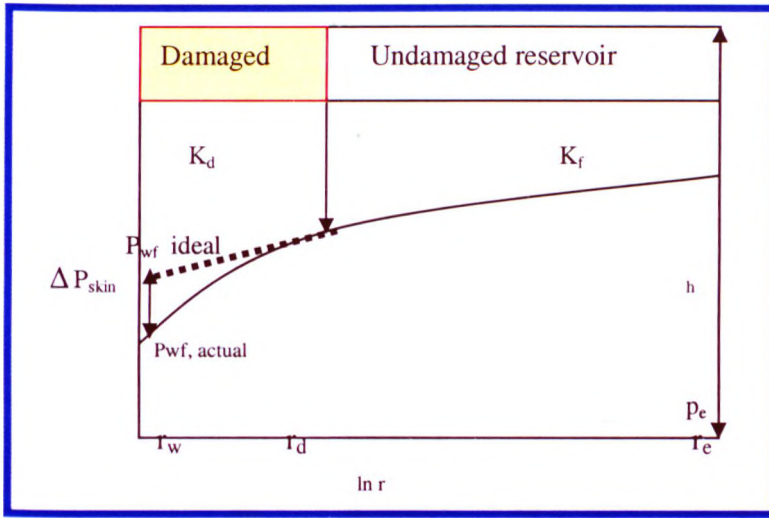


**Figure 6.70 Near-wellbore zone. ideal and real flowing bottomhole pressures**

Positive skin effects can be created by “mechanical” causes such as a partial completion. A negative skin effect can be created by stimulation operations (causing the near-wellbore permeability to exceed the natural value), and hydraulic fracturing.

This drilling skin effect result in an additional pressure drop ( $\Delta P_s$ ), given by:

$$\Delta P_s = \frac{q\mu}{7.08Kh} s \quad (6.74)$$

Equation (6.74) can be added to the pressure drop in the reservoir, thus equation (6.72) becomes:

$$P_e - P_w + \Delta P_s = \frac{q\mu}{7.08Kh} \ln \frac{r_e}{r_w} \quad (6.75)$$



$$\text{Or } P_e - P_w = \frac{q\mu}{7.08Kh} \left( \ln \frac{r_e}{r_w} + s \right) \quad (6.76)$$

$$\text{Or } P_e - P_w = \frac{q\mu}{7.08 \bar{K} h} \ln \frac{r_e}{r_w} \quad (6.77)$$

Rearranging equation (6.77) the average radial flow permeability Figure 6.71 can be expressed as:

$$\bar{K} = \frac{q\mu}{7.08h\Delta P_f} \ln \frac{r_e}{r_w} \quad (6.78)$$

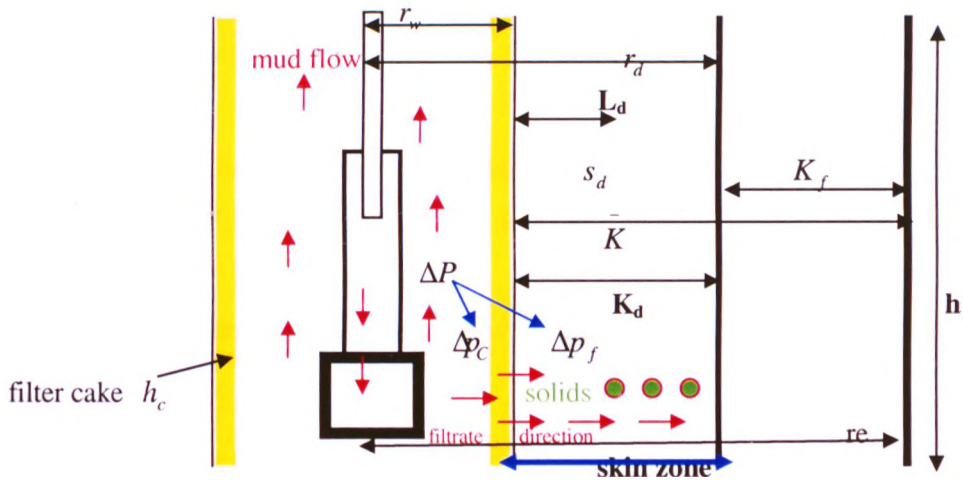


Figure 6.71 Schematic Diagram for near wellbore Damage

Equation (6.79) can be used to calculate permeability damage as:

$$(\ln r_e / r_w) / \bar{K} = (\ln r_d / r_w) / K_d + (\ln r_e / r_d) / K_f \quad (6.79)$$

$$K_d = (\ln r_d / r_w) / \left( (\ln r_e / r_w) / \bar{K} - (\ln r_e / r_d) / K_f \right) \quad (6.80)$$

The drilling skin factor can be quantified using equation (6.78):

$$\frac{q\mu(\ln r_e / r_w + s_d)}{7.08K_f h} = \frac{q\mu(\ln r_d / r_w)}{7.08K_d h} + \frac{q\mu(\ln r_e / r_d)}{7.08K_f h} \quad (6.81)$$

Note  $q\mu/7.08h$  is constant, then equation (6.81), becomes:

$$s_d = \left(1 - \frac{K_f}{K_d}\right) \ln r_w / r_d \quad (6.82)$$

Using a well productivity index (PI) to represents well performance we have:

$$PI_{ideal} = \frac{Kh}{141.20B\mu \ln(r_e / r_w)} \quad (6.83)$$

$$PI_{actual} = \frac{Kh}{141.20B\mu (\ln(r_e / r_w) + s_d)} \quad (6.84)$$

Where:

$PI_{actual}$  - productivity index after formation damage

$PI_{ideal}$  - productivity index before formation damage

Therefore, well efficiency (FE) due to near wellbore damage can be calculated as:

$$FE = \frac{PI_{actual}}{PI_{ideal}} = \frac{\ln(r_e / r_w)}{\ln(r_e / r_w) + s_d} \quad (6.85)$$

The damage ratio (DR) is defined as:  $DR = 1 - FE \quad (6.86)$

Then the damage factor (DF) from the drilling operation can be computed from reciprocal of the well flow efficiency as:

$$DF = 1 / FE \quad (6.87)$$

The economic implication of formation damage can be presented by the annual revenue loss (ARL) as:  $ARL = 365 qP_r DR \quad (6.88)$

$P_r$  – oil price per barrel

*[Note: The field applications of the models developed above will be presented in chapter seven].*

## **CHAPTER SEVEN**

### **THE PRODUCTIVITY TOOL**

In this chapter, the insights gained into fluid rheology and filtration mechanisms will be applied to the problem of formation damage productivity impairment.

A number of the mechanistic models developed have been combined and incorporated into a design and evaluation tool - the productivity tool (PRT), for predicting the effect of drilling fluid filtration on formation productivity for the vertical wells. The productivity tool is useful as a design and analysis tool for applications in the lab and in the field. This tool is also capable of being utilised to screen different drilling fluids in order to achieve minimum impairment and maximum production capacity. Two key functions are relevant to optimum fluid selection and management in addition to well test data interpretation. Applications of the PRT have been carried out using field data from North African oilfields with both WBM and OBM. The PRT shows good agreement with the field measurements based on the drilled wells studied.

#### **7.1 BACKGROUND**

Permeability is a characteristic of the formation, and can be altered by solids and mud filtrate invasion during drilling operations. Drilling mud filtrate will invade the formation to a greater depth than drilling mud particles. The decrease in permeability caused by filtrate invasion (formation damage), results in a decrease of well productivity<sup>64,231</sup>. The formation damage depends upon many parameters such as formation characteristics, type, composition, filtration and rheological characteristics of the drilling fluid and the operating conditions (overbalance pressure, temperature, etc.).

Three major methods that the production engineer uses to quantify formation damage in terms of well performance based on the total skin factor after drilling operations are production logging, flow measurement and well test data. The total skin factor is

used in the flow equations to estimate the production rate in wells that are affected by formation damage in order to enhance productivity.

The most common source of formation damage has proved to be drilling operations. The drilling skin contributes the highest percentage of the total skin. It is however not possible in general to quantify the contribution from drilling fluid to the total skin. In addition, a satisfactory model for field applications to simulate the near-wellbore damage before drilling in terms of well performance integrated from laboratory core test analysis is still not available.

In recent times, the oil industry has attached increasing importance to maintaining optimum well productivity through better drilling/completion fluids design.

This PRT is a new tool linking laboratory and field scale which can be used to evaluate well performance and quantify the formation damage in terms of drilling skin ( $s_d$ ) before drilling at the design (planning stage), during drilling and post drilling (evaluation stage).

## 7.2 SCREENING AND UPSCALING

Screening studies compare the formation damage expected to result from two or more options that may be candidates for a particular drilling operation. Options may be related to drilling fluid alternatives, different reservoir formations or critical operational parameters (e.g. overbalance pressure, pump rates, drilling time, etc.). It is essential that these screening studies include the following tests and analyses:

- 1) As a minimum requirement to upscale formation damage measurement to the field case, analyses on the core scale (laboratory tests) including measurements of fluid filtration, cake properties, viscosity and density of filtrate should be performed;
- 2) A complete formation damage analysis performed in order to clarify the causes of damage so that the suitable action can be taken, e.g. reformulation or system re-design;



- 3) Formation characteristics such as porosity and permeability and drilling fluid rheology are necessary for experimental design and evaluations.

**Upscaling.** The analysis of formation damage simulations results should be translated from the laboratory to the scale of drilling and well operations. This should be done by a systematic up-scaling process. The up-scaling process may include the following steps:

- 1) The study considered different operational parameters which make the case more complex therefore some assumptions for up-scaling are required such as:
  - (i) Formation is homogenous and isotropic,
  - (ii) The lab test data are use to define the filter cake properties such as cake permeability which will be considered the same for the radial flow simulation,
  - (iii) Filter cake thickness is defined by the solids concentration and the invasion filtrate volume,
  - (iv) The solids invasion occurs during initial filtration period is affected by the rheological properties of the fluid,
  - (v) Once a primary bridge is established, there is no particle movement through porous media,
  - (vi) The filtrate rheological behaviour is Newtonian,
  - (vii) The simulation process considers two formation damage mechanisms: filtrate and solids invasion.
- 2) Up-scaling of the effect and the extent of formation damage to the near-wellbore geometry.
- 3) Potential impact on well performance and economic implications of the selected alternative.
- 4) Relevance of observed formation damage mechanisms on field scale and selection of potential solutions for formation damage reduction.

### **7.3 FUNCTIONS OF THE PRODUCTIVITY TOOL (PRT)**

The productivity tool was constructed to link laboratory studies and field scale and to provide a design and analysis package, which can be used to perform under downhole conditions the following key functions:

1. To use the lab results of filtration and formation damage to scale fluid applications to downhole conditions. The linking establishes correlations between laboratory and field formation damage measurements (Well Test Analysis and Production Logging).
2. To analyse wellbore pressure distribution and filtration pressure across the formation and the filter cake.
3. To analyse the response of the fluid to static and dynamic filtration.
4. To characterise the rheology and filtration of the selected fluids.
5. To quantify the level and depth of formation damage.
6. To quantify the drilling skin.
7. To determine the impact of the selected fluid on formation productivity.
8. To screen appropriate drilling fluids in order to achieve minimum formation impairment and maximum formation productivity.
9. To determine relevance of formation damage mechanisms on field scale and determine the best operating drilling conditions.

A copy of the PRT package is supplied on a compact disc (CD) in Appendix D.

### **7.4 PRODUCTIVITY TOOL FORMULATION**

In order to perform the above functions (section 7.3) the productivity package incorporates a number of mechanistic models which have been developed earlier (chapter 6). The models include:

- 1) Rheology prediction models.
- 2) Static and dynamic filtration prediction models.
- 3) Filter cake build-up on sand face evaluation model.
- 4) Prediction models for filtration pressure drops across the sand face and the cake.

- 5) Formation morphological characteristics.
- 6) Prediction models for depth of solids and filtrate invasion.
- 7) Models for skin factor and flow efficiency prediction.

The models have been developed from the input of selected data generated from the extensive controlled experimental studies into fluid rheology, filtration and formation damage phenomena described in chapters 5 and 6. All the analyses carried out on laboratory core tests were conducted under linear flow conditions, and integrated into radial flow conditions, for near-wellbore damage caused by particulate and filtrate invasion.

## 7.5 PRODUCTIVITY TOOL STRUCTURE

In order to simulate the impact of drilling fluid filtration on formation damage in terms of well performance, a computer package with the above models is required. The structure of the calculation is described as follows:

1. Input the data required for the models under downhole conditions, which are: wellbore parameters at the depth of interest (hole geometry, casing size, etc), operating parameters (overbalance pressure, pump rate, etc), drill-in fluid parameters (mud type, rheology, etc) and formation parameters (permeability, porosity, etc).
2. Compute the rheological behaviour of the fluid at surface condition (assumed to be temperature of 120 °F and pressure 15 psi) and depth of interest.
3. Compute the rheological parameters and calculate the wellbore pressure distribution and filtration pressure across the formation and filter cake.
4. Compute the static and dynamic filtration and calculate filter cake properties.
5. Calculate the pressure drop across filter cake and sand face.
6. Quantify level of damage results by computing depth of particulate and filtrate invasion, average permeability and permeability damage.
7. Evaluate the results of well performance by computing the drilling skin factor, ideal and actual productivity index, flow efficiency and damage factor.

8. Alter the operational parameters as required to achieve minimum damage and maximum well productivity and select optimum drilling fluid.

Figure 7.1 shows the flow chart on which the productivity tool has been developed.

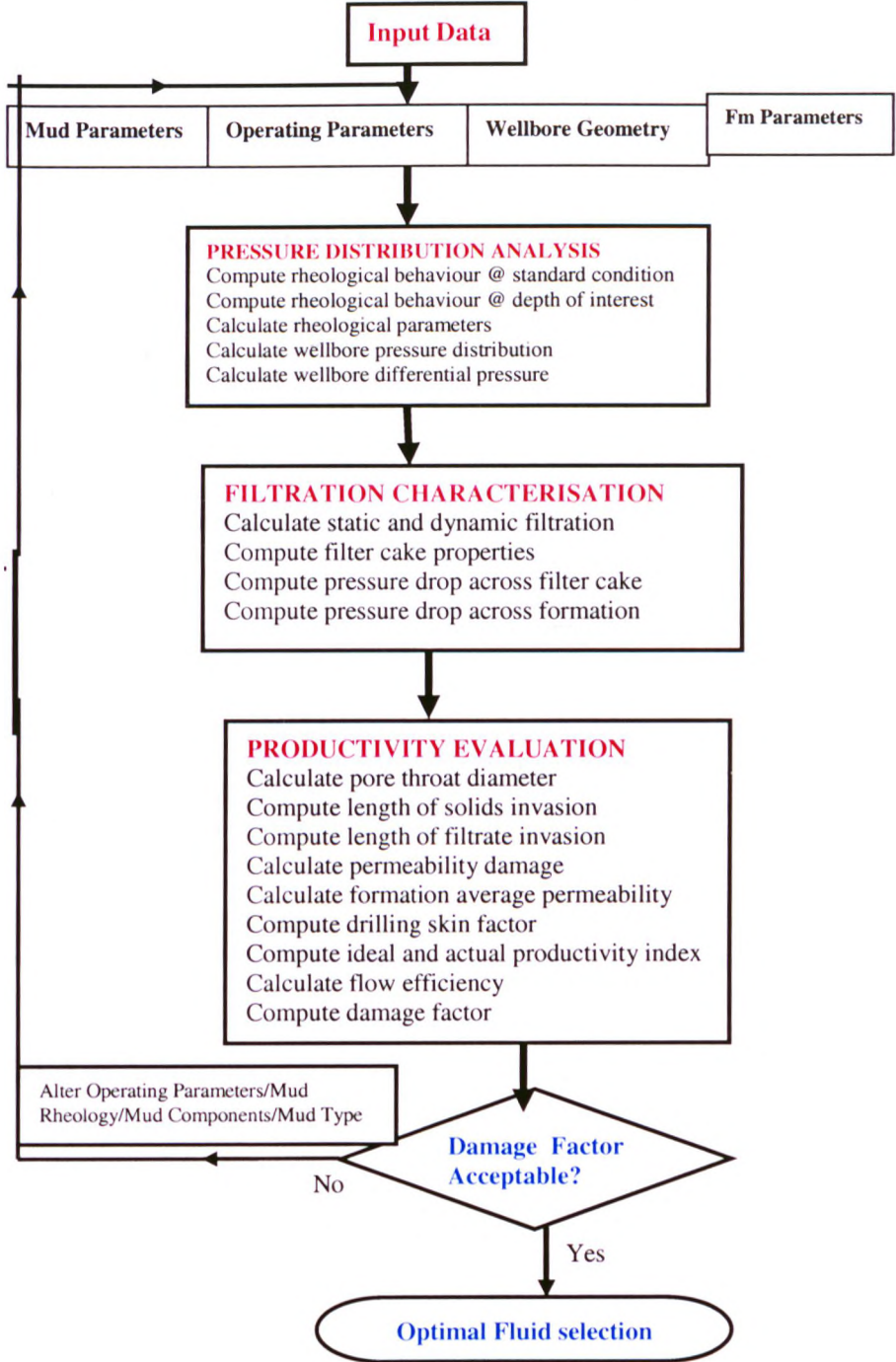


Figure 7.1 The PRT Flow chart



## 7.6 SYSTEM ARCHITECTURE

The productivity tool system architecture is made up of five user menus as shown in the flow chart in Figure 7.2. The main menus are as follows:

1. File Menu - It contains the file management facilities namely: Open, Close, New, Save, Save as, Print setup, Print, and Exit. This Menu allows the user to open both old and new files, to save current files, to print calculated results and exit the package.
2. Input Menu - This menu is designed for the user to input all operating parameters required for the calculation in S.I. or Field units.
3. Results Menu - This menu enables the user to display the results of all calculations performed. Results are presented in both tabular and graphical format.
4. Features Menu - This Menu allows the user to Zoom in/out to enable clearer viewing of the screen.
5. Home Menu - this menu takes the user back to the start screen of the program.

The platform for operation of the software is Microsoft Excel, with Visual Basic Macro routines.

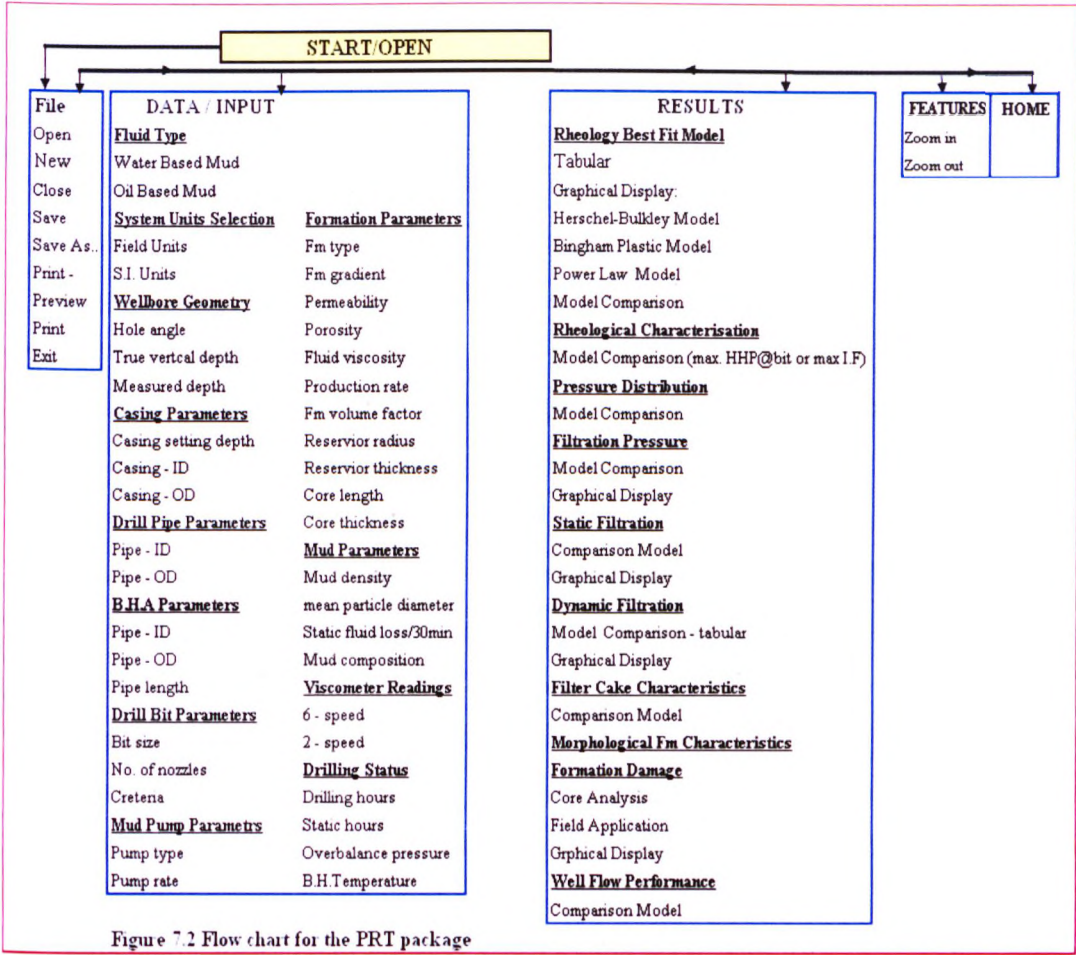


Figure 7.2 Flow chart for the PRT package

## 7.7 USER GUIDE

The purpose of the user guide is to provide the PRT operator with an easy to follow guide in which to:

1. Construct the framework for all the analysis.
2. Display results in tabular or graphical form.

### 7.7.1 Constructing the Framework for Analysis - Input Menu

Having selected the units in which the PRT analysis is to take place the user must input all the values sequentially as per DATA / INPUT menu bar otherwise

inaccurate modelling may result. However a message flag provides help to the user with this information.

- Type of Mud - select WBM or OBM.
- Input Units - select S.I. or Field units.
- Wellbore Geometry Parameters- characterise the well including: hole angle, true vertical depth and measured depth.
- Casing Parameters - input casing setting depth, external and internal diameter.
- Drillpipe parameters - input the drillpipe external and internal diameter.
- B.H.A. Parameters - allows the user to input the bottom hole assembly components.
- Drill Bit Parameters - input bit diameter and number of nozzles required. The user is required to specify the criteria for optimising the hydraulic horsepower.
- Mud Pump Parameters - input the optimum pump rate and pump efficiency.
- Formation Parameters - the user is required to input formation type, formation pressure gradient, permeability, porosity, reservoir fluid viscosity, thickness, radius and production rate. Input of the core length and thickness is also required.
- Mud Parameters - input the mud density, mud mean particle diameter ( $d_{50}$ ), static fluid loss over 30 minutes, mud composition and Fann viscometer readings at standard conditions. Selection is made from either 2 or 6-speed Fann viscometers.
- Drilling Status Parameters - the user is requested to input drilling and static times, overbalance drilling pressure and bottom hole temperature.

### **7.7.2 Display of Results in Tabular or Graphical Form - Results Menu**

1. Rheology Best-Fit Model - the option is provided within the software to give a tabular and graphical display of the rheological model which best describes the drilling fluid behaviour at standard and downhole conditions. The option is also

to allow the user to view non-Newtonian models individually namely: Herschel-Bulkley model, Bingham Plastic model and Power Law model.

2. Rheology Characterisation - provides information in a tabular form on rheological parameters for the model which best describes the drilling fluid behaviour. The option is also to allow the user to view other non-Newtonian models.
3. Pressure Distribution - provides information on the pressure distribution in the wellbore in tabular form. Here again, the facility is open to the user to view the pressure distribution across the whole system for each of the non-Newtonian models (as above) in a tabular form with the option of a tabular comparison between them.
4. Filtration Pressure - provides information on wellbore differential pressure, pressure drop across the sand face and the mud filter cake in a tabular and graphical form for each of the non-Newtonian models.
5. Static Filtration - provides information in a tabular form on static filtration cumulative volume during static operation for each of the non-Newtonian models. The option provides graphical display for static filtration.
6. Dynamic Filtration - provides information in a tabular and graphical form on dynamic filtration cumulative volumes during dynamic operation for each of the non-Newtonian models. The option provides graphical comparison between static and dynamic filtration volumes.
7. Filter Cake Characteristics - provides information on the filter cake characteristics in a tabular form for the best-fit rheological model with the option of a tabular form for other non-Newtonian models.
8. Formation Damage - provides information on formation damage characteristics such as average reservoir permeability, permeability damage, depth of solids and filtrate invasion and drilling skin factor in linear flow (lab) and radial flow (field application) with the option of a tabular form for other non-Newtonian models. The option provides graphical form for formation damage characteristics.



9. Well Flow Performance - provides information on well flow performance such as ideal and damaged productivity index, flow efficiency and damage factor with the option of a tabular form for other non-Newtonian models.

## 7.8 APPLICATION OF THE PRODUCTIVITY TOOL

Specific case studies to illustrate the interpretation and practical usefulness of the productivity tool have been carried out using actual field data. The data were collected from three oil companies in Libya [Table 7.1] and can be summarised as follows:

1. Six wells with total well depths ranging from 10045 ft to 14580 ft.
2. Reservoir sections drilled in 5.87, 6 and 8 inch holes.
3. Open hole and cased hole completions.
4. Wellbore pressure ranging from 5000 psi to 12800 psi.
5. Bottom hole temperature ranging from 240 °F to 330 °F.
6. Reservoir permeability ranging from 50 md to 400 md.
7. Oil based and water based drill-in fluids.

**Table 7.1 Well summary**

Company	Field	Well Number	Total Depth (ft)	B.HTemp. (°F)	Fluid Type	Hole Section (inch)	Completion
1	A	A1	13790	315	OBM	8.50	- cased
			14580	330	OBM	6	
		A2	14500	322	WBM	6	cased
2	B	B1	13528	320	OBM	5.875	Openhole
		B2	12175	305	WBM	8.50	- Openhole
			13390	314	WBM	5.875	
		B3	12245	280	WBM	5.875	Openhole
3	C	C1	10045	240	WBM	8.50	cased

The field application of the productivity tool has been used in two ways:

1. Evaluation Stage: The PRT simulated results have been evaluated against field data (post drilling):
  - (i) Predicted total wellbore pressure distribution versus field data (pump pressure).
  - (ii) Predicted well performance in terms of formation damage against field measurements (depth of invasion from well logging and skin factor from well test data).
2. Planning stage: The PRT has been used for fluid optimisation and selection against different operating parameters such as fluid type, rheology, pressure, etc.

#### **7.8.1 Evaluation Stage [simulated versus field data]**

Table 7.2 shows the input parameters for The PRT from well A1 using oil-based mud in order to evaluate the wellbore pressure distribution in the 8.50 inch section.

Company Name 1  
 Field Number A  
 Well Number A1  
 Hole Section 8.5 inch  
 Type of Mud : Oil Based Mud

MUD PUMP PARAMETERS			
Pump Rate		325	gpm
Pump Pressure		2575	psi

BIT PARAMETERS			
Bit Diameter		8.5	inches
No. of Nozzles		3x14	-

maximum impact force at the bit

WELLBORE GEOMETRY			
True Vertical Depth		13790	ft
Measured Depth		-	ft

CASING PARAMETERS			
Casing Setting Depth		11530	ft
Casing O.D.		9.63	inches
Casing I.D.		8.85	inches
Linear casing Setting Depth			ft
Casing O.D.		-	inches
Casing I.D.		-	inches

DRILLPIPE PARAMETERS			
Drillpipe O.D.		5	inches
Drillpipe I.D.		4.275	inches

Roughness 0.00041

BOTTOM HOLE ASSEMBLY			
Component	Length/ft	I.D./ inch	O.D. / inch
Drill collar	628	3.25	6.25
HW Dp	-	-	-

Roughness 0.0005

DRILLING STATUS			
Drilling Time		66	hours
Static Time		28	hours
B.H.Temperature		315	F

MUD COMPOSITION		
Component	Name	Lbs/bbl
1	emulsifier	8
2	wetting	6
3	HT-clay	2
4	polymer	3
5	barite	533
6	solids	35
7	-	-
8	-	-

MUD PARAMETERS		
Mud Density	17.50	ppg
API Static Filtration	3	cc

Viscometer Readings	
RPM	Reading
600	105
300	60
200	50
100	39
6	12
3	10

FORMATION PARAMETERS		
Formation Type	shale&salt	

Table 7.2 Field Data for Well (A1) (wellbore pressure distribution evaulation)



Company Name: 1  
 Field Number: A  
 Well Number: A1  
 Hole Section: 8.50 inch (Intermediate section)  
 Type of Fluid: Oil based mud  
 Display of results in tabular or graphical form - Results Menu

1. Sub menu - Rheology Best Fit Model

The results are presented in both tabular and graphical form. The information provided in Figure 7.3 shows that the best-fit rheological model is the Herschel Bulkley model at both standard conditions and 7 inch casing setting depth (13790 ft). The PRT also allows the user to view graphical results of other non-Newtonian models individually for both Bingham Plastic and Power Law models.

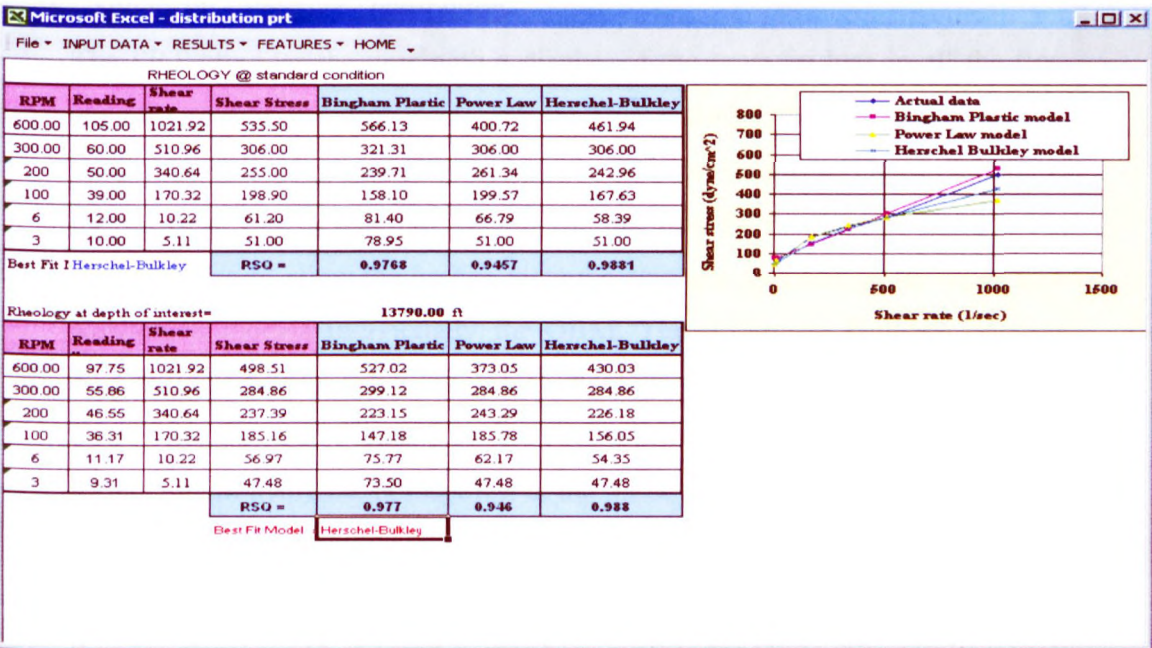


Figure 7.3 Best-fit model for OBM

2. Sub menu - Rheology Characterisation

The rheological parameters and apparent viscosity are presented in Figure 7.4 as a comparison between the actual rheological model and other non-Newtonian models.



RHEOLOGICAL CHARACTERISATION			
Best Fit Model	Herschel-Bulkley	Power Law	
Rheological Parameters			
True Yield	36	-	lb/100ft <sup>2</sup>
Flow Index	0.66	0.39	
Consistency Index	401	2516.93	cP
Apparent Viscosity			
In annulus	77	124	cP
In pipe	77.73	127.47	cP
RHEOLOGICAL CHARACTERISATION			
Best Fit Model	Bingham Plastic		
Rheological Parameters			
Plastic Viscosity	42	cP	
Yield Point	13.96	lb/100ft <sup>2</sup>	
Apparent Viscosity			
In annulus	116	cP	
In pipe	96.62	cP	

Figure 7.4 Rheological characterisation for OBM

### 3. Sub menu - Pressure Distribution

The PRT provides the user with a display of the pressure loss in all the flow conduits within the drillstring system. This includes the pressure loss both within the drillstring assembly and across the annular space. Figure 7.5 shows the pressure loss across the system for the best fit rheological model. The option is also to allow the user to view the pressure distribution for other non-Newtonian models individually for OBM. The difference between pressure distribution analysis using the actual rheological model and other models is clearly illustrated in Figure 7.5. The PRT allows the user to select the criteria for maximum hydraulic horsepower at the bit or maximum impact force. In this case an 8.50 inch hole has been drilled using maximum impact force at the bit. The results show that the Herschel Bulkley model has a lower pressure loss than the Bingham Plastic and Power Law models for OBM. The total pressure loss from the PRT is 2466 psi compared with actual field data 2575 psi.

Microsoft Excel - distribution.ppt

File - INPUT DATA - RESULTS - FEATURES - HOME

**Maximum Impact Force at the Bit**

PRESSURE DISTRIBUTION				
Bit Model Fit	Herschel-Bulkley	Bingham Plastic	Power Law	
Hydrostatic Pressure	12548.90	12548.90	12548.90	psi
Bottom Hole Circulation Pressure	12765.09	13030.37	12929.96	psi
Equivalent Circulation Density	17.80	18.17	18.03	PPG
Through the BHA	120.23	147.32	130.88	psi
Across the BHA	35.03	34.71	51.32	psi
Through the Pipe	970.56	1029.12	1049.34	psi
Across Pipe	10.24	133.79	31.67	psi
Across Casing	170.93	312.96	298.07	psi
Bit Pressure Loss	1159.02	1470.22	1384.53	psi
Total Pressure Loss	2466.00	3128.13	2945.80	psi
HHP	492	624	588	-
Total Flow Area (TFA)	0.455	0.404	0.416	in <sup>2</sup>
Size of Nozzles	J1	14	13	13
	J2	14	13	13
	J3	14	13	13
	J4	-	-	-
	J5	-	-	-
	J6	-	-	-

Figure 7.5 Wellbore pressure distribution for OBM

Table 7.3 summarises the predicted total wellbore pressure distribution versus field data (pump pressure) for all of the field data (6 wells). The PRT prediction shows agreement with field data within an average error of less than 5%.

Table 7.3 Predicted wellbore pressure distribution versus field data (pump pressure)

Company	Well Number	Total Depth (ft)	Hole Section (inch)	BHTemp. (°F)	Criteria	← Pump Pressure (psi) →	
						Field Data (Psi)	PRT Prediction (Psi)
1	A1	13790	8.50	315	*IF	2575	2466
		14580	6	330	IF	1780	1670
	A2	14500	6	322	IF	1700	1695
2	B1	13528	5.875	320	IF	2000	2032
	B2	12175	8.50	305	**HHP	2600	2820
		13390	5.875	314	IF	2000	2083
	B3	12245	5.875	280	IF	1500	1566
3	C1	10045	8.50	240	HHP	1950	2092

\*IF: Maximum impact force at the bit

\*\*HHP: Maximum hydraulic horse power at the bit

Table 7.4 shows predicted depth of invasion compared with field data. The PRT prediction shows agreement with field data (depth of invasion measurement from well logging) within an average error of 25 %.



Table 7.4 Formation damage (measured & predicted)

Company	Well Number	Total Depth (ft)	Hole Section (inch)	BHTemp. (°F)	Depth of Invasion (inch)	
					Field Data	PRT Prediction
1	A1	13790	8.50	315	-	-
		14580	6	330	40	34.79
	A2	14500	6	322	60	77.73
2	B1	13528	5.875	320	60	45.43
	B2	13390	5.875	314	70	92.73
	B3	12245	5.875	280	70	90.81
3	C1	10045	8.50	240	40	48.69

The field measurement from the well test data gives the total skin and the PRT predicts the drilling skin ( $s_d$ ). The analyses have been carried out based on standard assumptions<sup>233,234</sup> to calculate both the partial completion skin ( $s_c$ ), the perforation skin ( $s_p$ ) and the gravel pack skin ( $s_g$ ) and add these to the drilling skin predicted from the PRT, in order to enable comparison with field test data. Table 7.5 shows agreement between the PRT predicted total skin and field measurement within an average error of 15 %. It must be mentioned that there is also a margin of error from field measurements with well logs<sup>235</sup> with less than 10%. In addition, the PRT prediction is based on measurements solely from Clashach sandstone cores, and comparison with different lithologies (actual reservoir rocks) may also yield a margin of error.

Table 7.5 Skin factor (measured & predicted)

Company	Well Number	Total Depth (ft)	Hole Section (inch)	Field Data (Total skin)	PRT Prediction (Drilling skin, $s_d$ )	Calculated $s_c+s_p+s_g$	Total skin (PRT)
1	A1	13790	8.50	-	-		-
		14580	6	9.00	4.11	3.10	7.21
	A2	14500	6	12.0	5.24	3.32	8.56
2	B1	13528	5.875	10.0	4.00	5.24	9.24
	B2	13390	5.875	10.0	5.87	6.0	11.87
	B3	12245	5.875	10.0	5.63	5.24	10.87
3	C1	10045	8.50	8.00	3.62	2.61	6.23

Current industry practice involves running a well test after the drilling operations in order to determine the skin factor (due to formation damage) and to subsequently enhance productivity by means of flow system optimisation. The typical cost of such

an operation is \$ 95,000. This includes operational charges, equipment charges and crew charges.

The economic implication of the skin zone on well productivity can be evaluated by calculating the annual revenue loss due to skin damage using equation 6.83 (chapter 6). For example, the damage ratio for well A1 is 0.307, the oil price in 1995 was approximately \$30 per barrel and assuming the well was producing 1000 barrels per day, the result indicated an average of \$ 3,361,650 annual revenue loss due to formation damage per well drilled.

The PRT can be used to predict skin factor before drilling to optimise fluid selection and while drilling to monitor the operational parameters in order to minimise formation damage and maximise production, which can reduce the overall well cost in terms of time and operations.

### **7.8.2 Planning Stage for Fluid Optimisation**

The analysis have been carried out for fluid optimisation and selection against a large number of parameters such as nature and characteristics of the drilling fluid, formation properties and different operating parameters such as temperature, overbalance pressure, rheology, etc. The selected input data are from well number (A1) for a 6 inch hole section under downhole conditions and the choice was made during the planning stage to select the best drilling fluid to drill this well with minimum formation damage. The types of the drilling fluids used for evaluation were WBM and OBM. The mud composition and fluid rheology data for these types of mud have been used from field data for six wells drilled by various oil companies.

The simulation process considers three formation damage mechanisms: solids invasion, filtrate invasion and permanent permeability damage.

Figures 7.6 to 7.14 illustrate the effects of different parameters such as rheological behaviour, drilling time, temperature, overbalance pressure and reservoir permeability on the flow efficiency of well (A1) comparing different types of drill-in fluids WBM and OBM.



Three different rheological properties for both OBM and WBM [Table 7.6] have been used for fluid selection of this particular well (A1).

Temperature: 150 F

Mud Type

OBM1

n

K

Ys

0.66

226

24

Viscometer Readings

RPM	Reading
600	53
300	32
200	25
100	17
6	7
3	6

OIL BASED MUD RHEOLOGY DATA

OBM2

0.66

255

34

Viscometer Readings

RPM	Reading
600	61
300	40
200	30
100	21
6	10
3	9

OBM3

0.66

430

38

Viscometer Readings

RPM	Reading
600	105
300	60
200	50
100	39
6	12
3	10

Temperature: 150 F

Mud Type

Lignosuphonate

n

K

Ys

0.56

215

19

WBM1

Viscometer Readings

RPM	Reading
600	33
300	23
200	18
100	12
6	6
3	5

WATER BASED MUD RHEOLOGY

WBM2

0.56

227

24

Viscometer Readings

RPM	Reading
600	45
300	32
200	25
100	16
6	7
3	6

WBM3

0.59

469

33

Viscometer Readings

RPM	Reading
600	68
300	44
200	35
100	26
6	11
3	9

Table 7.6 WBM & OBM rheology

### 7.8.2.1 Optimisation Analysis

Effect of Rheological Parameters. The PRT shows that the best-fit rheological model is the Herschel Bulkley model at both standard conditions and total well depth (14580 ft) for six types of mud used in the evaluation. The PRT computed the rheological properties at depth of interest 14580 feet (temperature of 330 <sup>0</sup>F and pressure of 7582 psi). Figures 7.6 & 7.7 show that an increase in rheological parameters (yield stress Ys, and consistency index, K) and the drilling time results in an increase in depth of filtrate invasion due to increased wellbore pressure and hence an increase in damage factor which is greater for WBM than OBM.

Effect of Rheological Characterisation. Figure 7.8 shows the depth of invasion profile for WBM and OBM. The figure also shows the accurate description of the rheological behaviour of the drill-in fluid required to accurately predict the depth of invasion. Figure 7.8 illustrates effect of rheological behaviour on formation damage characterisation. A comparison has been made between the actual fluid rheological behaviour models, i.e. Herschel-Bulkley, Power Law and Bingham Plastic models. The figure shows that the Bingham model predicts higher formation damage than the

actual model. The Herschel-Bulkley model best represents actual fluid rheology, lower wellbore pressure, hence lower formation damage than the other models. The depth of invasion was found to be greater for WBM than OBM.

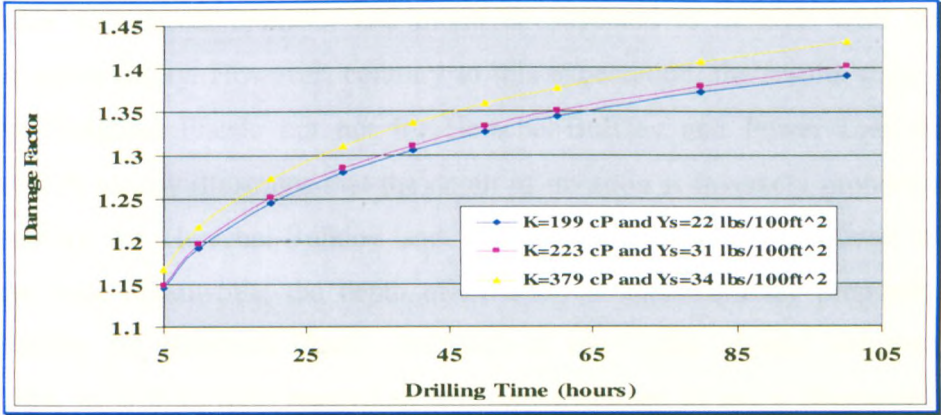


Figure 7.6 Effect of Rheology on Formation Damage for OBM

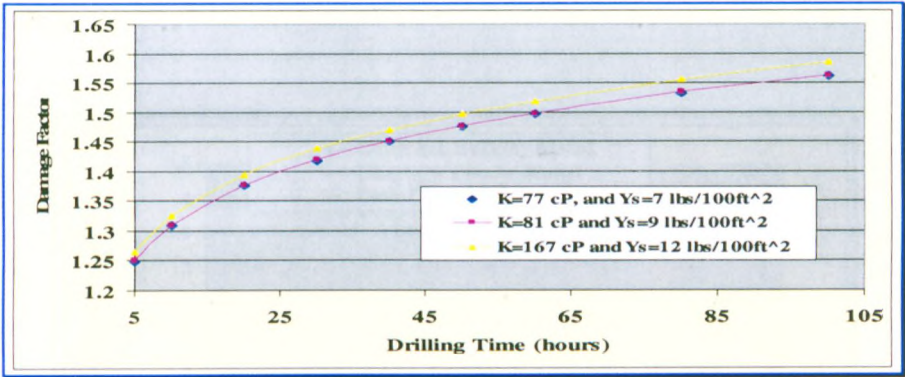


Figure 7.7 Effect of Rheology on Formation Damage for WBM

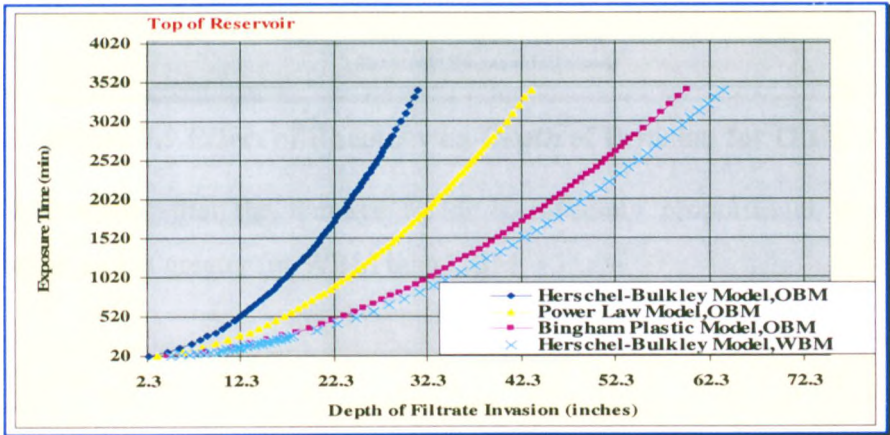


Figure 7.8 Effect of Rheology Characterisation on Depth of Invasion (invasion profile)



Effect of Reservoir Permeability. One would expect an increase in depth of invasion with increasing permeability and increasing pressure drop. As can be seen from equations (6.48 and 6.49 chapter 6), the depth of solids invasion is related to the formation pore throat diameter and might be expected to increase with the core sample permeability. However, contrary to this expectation, the results show this is line for Bingham Plastic but not for Herschel-Bulkley and Power Law models. [Figure 7.9] clearly illustrates that the depth of invasion is inversely proportional to permeability for Herschel-Bulkley and Power Law fluids due to lower annular pressure loss. Meanwhile, the depth of invasion is approximately proportional to permeability for Bingham Plastic fluid due to the higher annular pressure loss. Therefore, in drilling tight reservoirs, it is recommended to use a Bingham Plastic fluid and in drilling high permeability reservoirs it is recommended to use a Herschel Bulkley fluid.

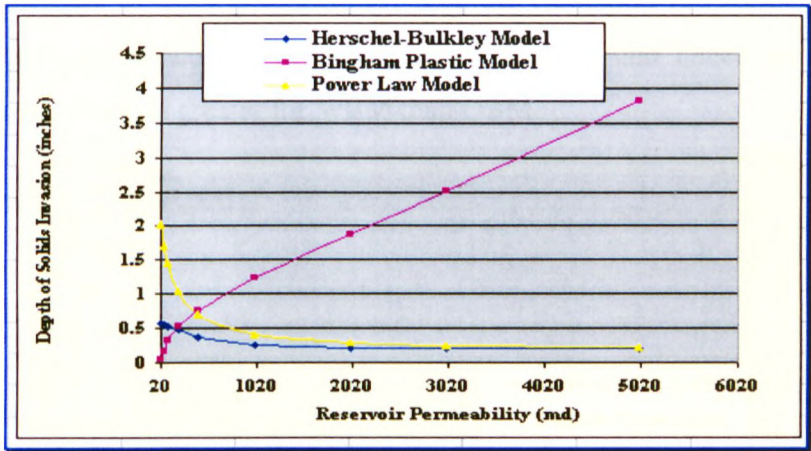


Figure 7.9 Effect of Rheology on Depth of Invasion for OBM

Figure 7.10 shows that the damage factor is inversely proportional to reservoir permeability, and is greater for WBM than OBM.

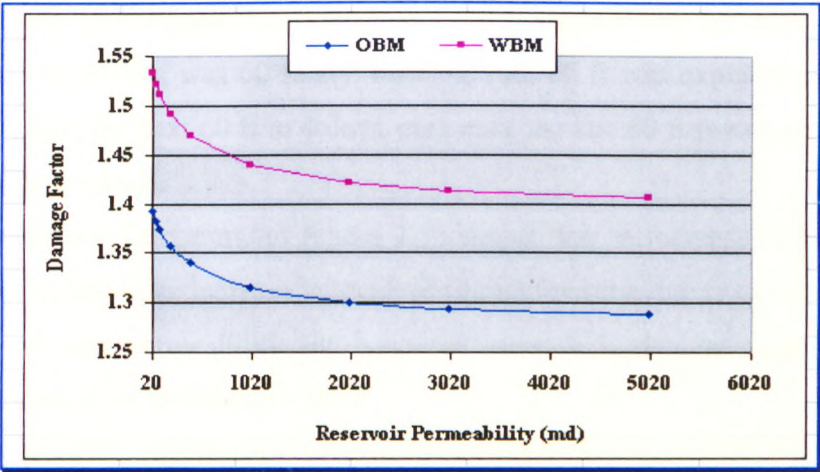


Figure 7.10 Effect of Reservoir Permeability

Effect of Exposure Time. The time the formation is exposed to drilling mud affects the extent of the formation damage and the depth of invasion in overbalance drilling. Figure 7.11 represent overbalance drilling with five days exposure time. The figure shows an increase in drilling operational time the formation is exposed to drilling mud results in an increase in depth of filtrate invasion and hence an increase in damage factor, which is greater for WBM than OBM.

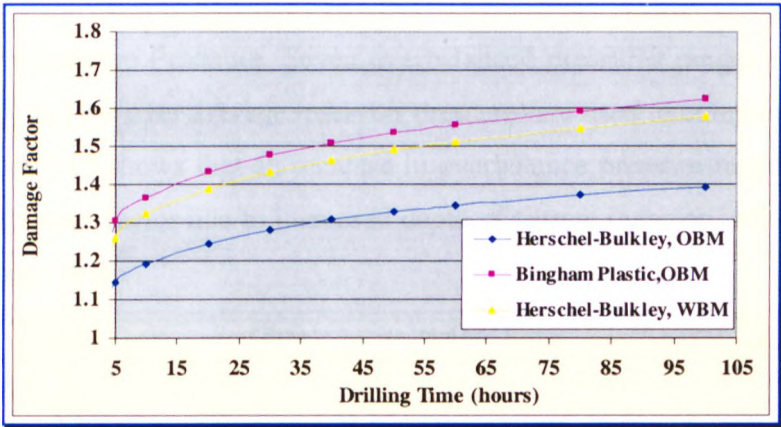


Figure 7.11 Effect of Drilling Time

During the drilling of a vertical well, it was assumed that the filtrate invasion would be larger near the top of the reservoir section and then decrease linearly to a minimum value at the bottom of the well. This assumption is based on the formation exposure



time to drilling fluid. Figure 7.8 shows that a 310 ft vertical well has been drilled and that the rate of drilling was 60 ft/day, then the first 60 ft was exposed to 5 days of filtrate invasion, the next 60 ft to 4 days, etc., until the last 60 ft is exposed to only 1 day of filtrate invasion.

Effect of Wellbore Temperature. Figure 7.12 shows that an increase in bottom hole temperature results in an increase in depth of filtrate invasion due to decreased filtrate viscosity and cake permeability and hence an increase in damage factor, which is more pronounced for WBM than OBM.

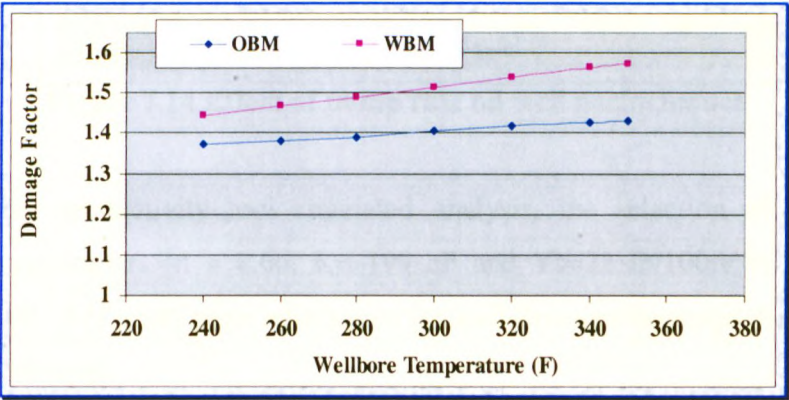


Figure 7.12 Effect of Wellbore Temperature

Effect of Overbalance Pressure. Seven overbalanced pressures ranges from (170 to 880 psi – 4% to 19% over average reservoir pressure) are used to compare OBM with WBM. Figure 7.13 shows that an increase in overbalance pressure results in a sharp increase in damage factor due to increased depth of filtrate invasion, which is greater for WBM than OBM.

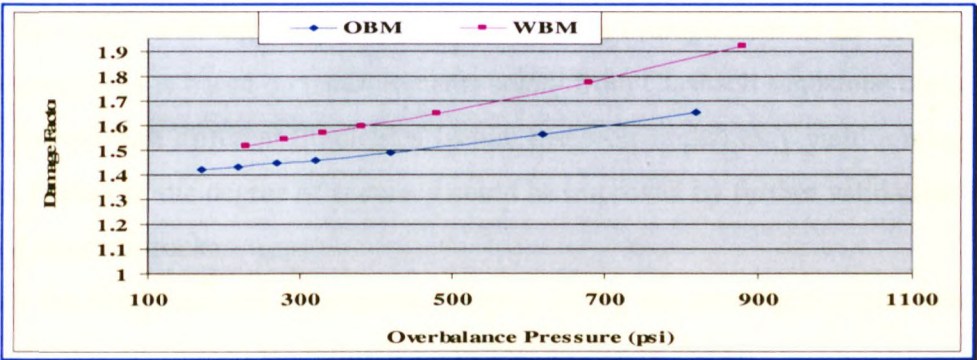
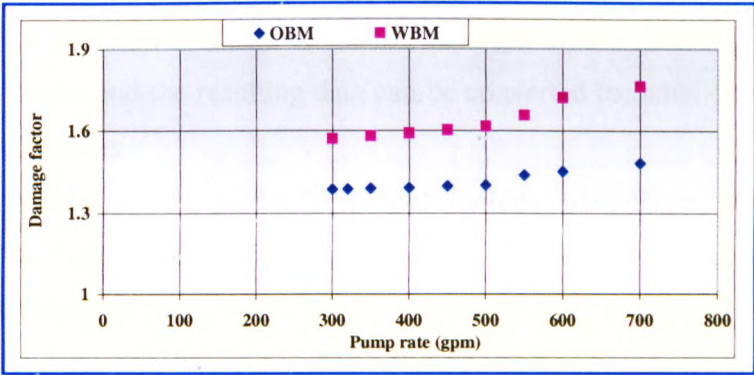


Figure 7.13 Effect of Overbalance Pressure

Figure 7.14 shows that an increase in pump rate results in an increase in damage factor which is greater for WBM than OBM.



**Figure 7.14 Effect of pump rate on well performance**

Based on the productivity tool simulated analysis, the selection of OBM with rheological parameters [ $n = 0.66$ ,  $K= 199$  cP and  $Y_s=22$  lb/100ft<sup>2</sup>] to drill this particular well (A1) gives more advantages for well flow performance than for WBM or other OBM types.

The field applications of the productivity tool based on the drilled wells studied show it can be used to investigate the influence of many parameters on well flow performance.

The PRT wellbore pressure distribution prediction shows good agreement with field data (pump pressure) with less than 5 % error.

The PRT depth of filtrate invasion and skin prediction show agreement quit variable with field data (well logging and well test) within an average error of 20 %. Since the PRT prediction is based on measurements solely from Clashach sandstone cores, and comparison with different lithologies (actual reservoir rocks) may yield a margin of error. However, the degree of accuracy could be improved by further validation using actual reservoir rocks.

Under the conditions and assumptions adopted during this investigation and based on the drilled wells studied the following conclusions can be drawn:

The productivity tool package developed is useful as a design and analysis tool for the simulation and prediction of the impact of drilling fluid filtration on formation productivity for vertical wells.

The productivity tool can evaluate formation damage in the laboratory based on linear-flow core tests and the resulting data can be converted to radial-flow geometry for oil field applications.

Input requirements for this productivity tool include parameters such as hole geometry, BHA configuration, mud type and composition, rheology data and formation characteristics.

The productivity tool can be used before drilling at the design (planning stage), during drilling and post drilling (evaluation stage) and also as comparison tool with well test data interpretation.

The productivity tool is capable of being utilised to screen different drilling fluids with the aim of achieving minimum impairment and maximum production capacity, which can reduce the overall well cost in terms of time and operations. As a result of this, the considerable economic implication of the skin zone on well productivity can be greatly minimised.

*[Analysis from the PRT are attached]*



Company Name 1  
Field Number A  
Well Number A1  
Hole Section 6 inch  
Type of Mud : Oil Based Mud

MUD PUMP PARAMETERS			
Pump Rate	265	gpm	
Pump Pressure	1780	psi	

BIT PARAMETERS		
Bit Diameter	6	inches
No. of Nozzles	3x12	-
maximum impact force at the bit		
WELLBORE GEOMETRY		
True Vertical Depth	14580	ft
Measured Depth	-	ft

CASING PARAMETERS		
Casing Setting Depth	11230	ft
Casing O.D.	9.63	inches
Casing I.D.	8.85	inches
Linear casing Depth	13795	ft
Casing O.D.	7.00	inches
Casing I.D.	6.27	inches

DRILLPIPE PARAMETERS			
Drillpipe O.D.	5	inches	
Drillpipe I.D.	4.275	inches	
Drillpipe O.D.	3.5	inches	
Drillpipe I.D.	2.76	inches	
Roughness	0.00064	-	

BOTTOM HOLE ASSEMBLY			
Component	Length/ft	I.D./ inch	O.D. / inch
Drill collar	712	2.50	4.75
Roughness	0.0007	-	

DRILLING STATUS		
Drilling Time	57	hours
Static Time	28	hours
B.H.Temperature	330	F

PRODUCTION PARAMETERS			
Depth of Filtrate Invasion	40	inches	logs
Skin Factor	9	-	well test

MUD COMPOSITION		
Component	Name	Lbs/bbl
1	emulsifier	6
2	wetting	4
3	HT-clay	3
4	polymer	5
5	barite	150
6	solids	35
7	-	-
8	-	-

MUD PARAMETERS		
Mud Density	10.00	ppg
API Static Filtration	5	cc

Viscometer Readings	
RPM	Reading
600	53
300	32
200	25
100	17
6	7
3	6

FORMATION PARAMETERS		
Formation Type	sandstone	
Permeability	200	md
Porosity	0.14	-
Production Rate	-	pbd
Oil Viscosity	1.12	cP
FmVolume Factor	2.03	-
Reservior Radius	2700.00	ft
Reservior Thickness	310	ft

Table 7.7 Field Data for Well (A1) (Formation damage evaluation)



Company Name: 1  
Field Number: A  
Well Number: A1  
Hole Section: 6 inch (Reservoir section)  
Type of Fluid: Oil based mud  
Display of results in tabular or graphical form - Results Menu

1. Sub menu - Rheology Best Fit Model

The results are presented in both tabular and graphical form. The information provided in Figure 7.15 shows that the best-fit rheological model is the Herschel Bulkley model at both standard conditions and total well depth (14580 ft). The PRT also allows the user to view graphical results of other non-Newtonian models individually for both Bingham Plastic and Power Law models.

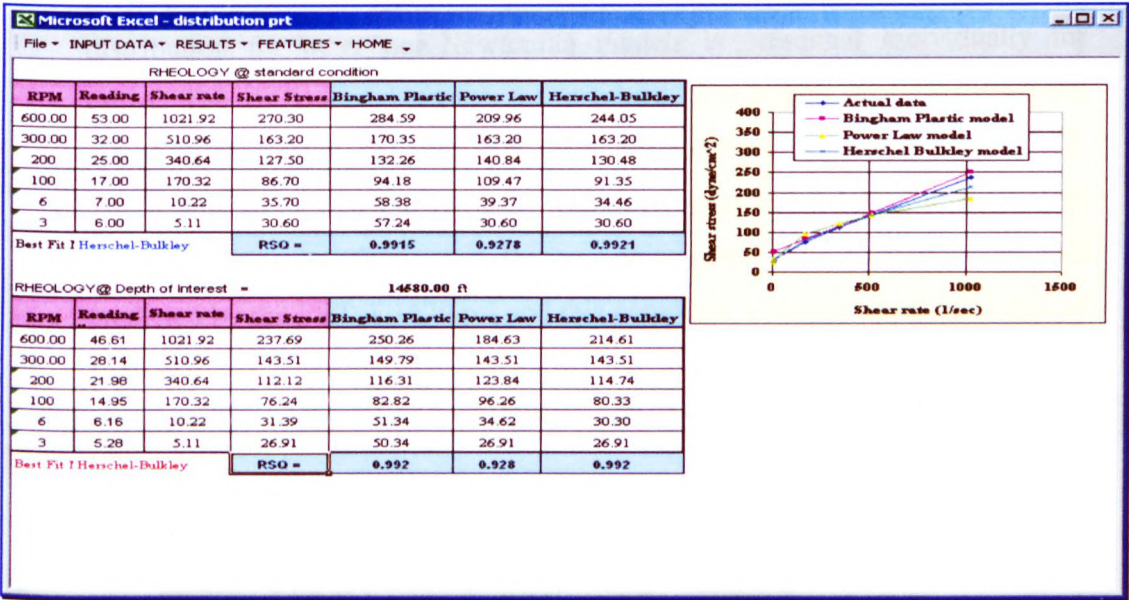


Figure 7.15 Best-fit model for OBM

2. Sub menu - Rheology Characterisation

The rheological parameters and apparent viscosity are presented in Figure 7.16 as a comparison between the actual rheological model and other non-Newtonian models.

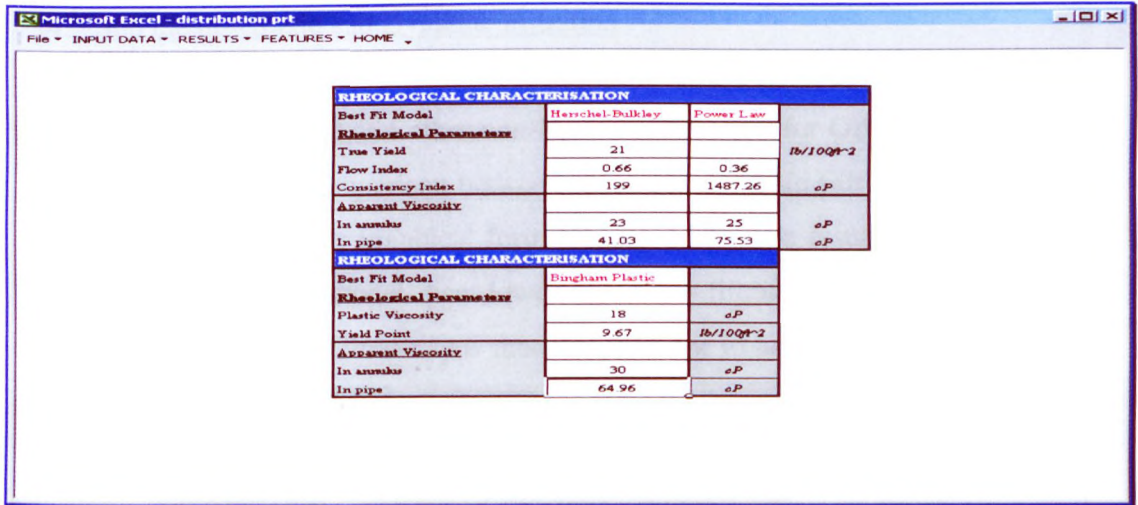


Figure 7.16 Rheological characterisation for OBM

### 3. Sub menu - Pressure Distribution

Figure 7.17 shows the pressure loss across the system for the best fit rheological model using maximum impact force at the bit. The pressure distribution for other non-Newtonian models is presented individually for OBM. The difference between the pressure distribution analysis using the actual rheological model and other models is clearly illustrated in Figure 7.17. The results show that the Herschel Bulkley model has a lower pressure loss than the Bingham Plastic and Power Law models. The total pressure loss predicted by the PRT is 1670 psi and this compares with the actual field data of 1780 psi.

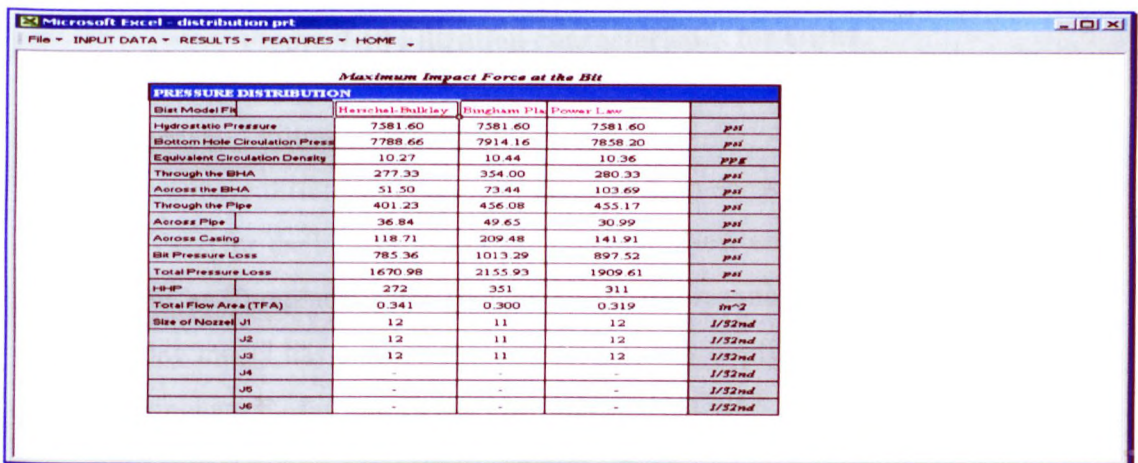


Figure 7.17 Wellbore pressure distribution for OBM



4. Sub menu – Static and Dynamic Filtration

The dynamic filtration cumulative filtration volume during dynamic operations for the best-fit model and other non-Newtonian models for OBM are presented in Figure 7.18. A comparison between static and dynamic filtration volume for OBM is presented in graphical form [Figure 7.18]. The results show that the Herschel Bulkley model has lower dynamic filtration volumes than the Bingham Plastic and Power Law models OBM due to lower pressure loss.

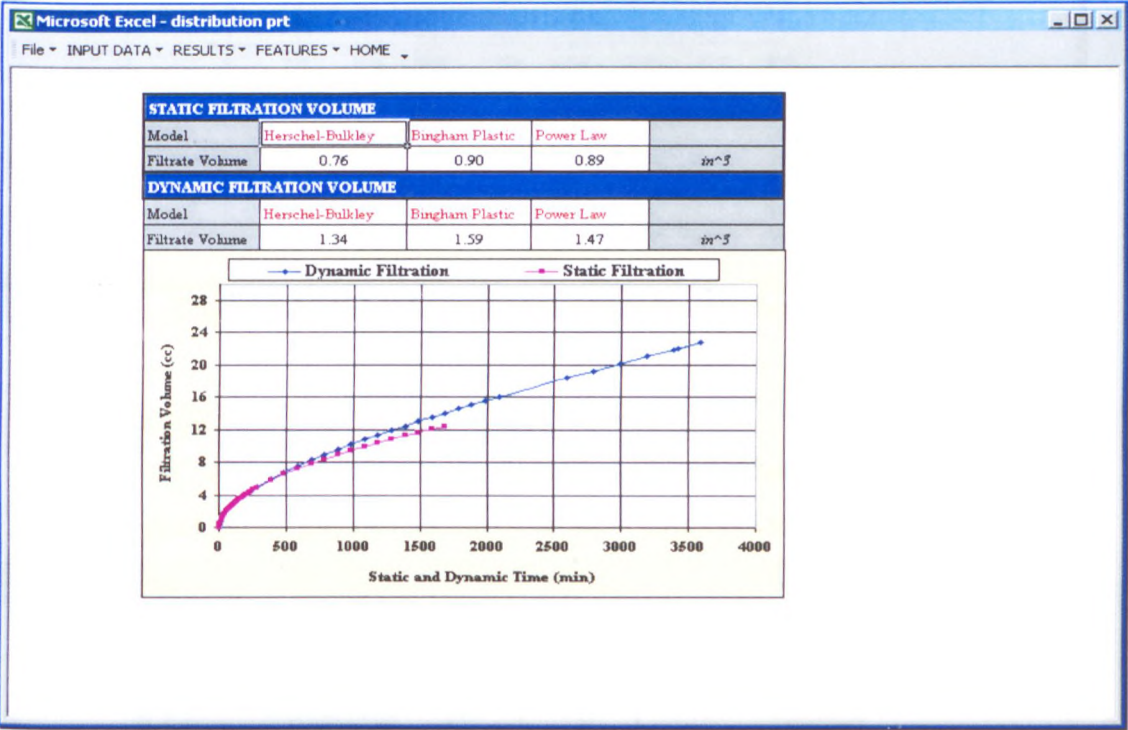


Figure 7.18 Filtration characteristics for OBM

5. Sub menu - Filtration Pressure

The wellbore differential pressure, pressure drop across the sand face and mud filter cake for the best-fit model and other non-Newtonian models are shown in tabular and graphical form [Figure 7.19]. The results show that the Herschel Bulkley model has a lower pressure drop across the filter cake as compared to the Bingham Plastic and Power Law models for OBM.

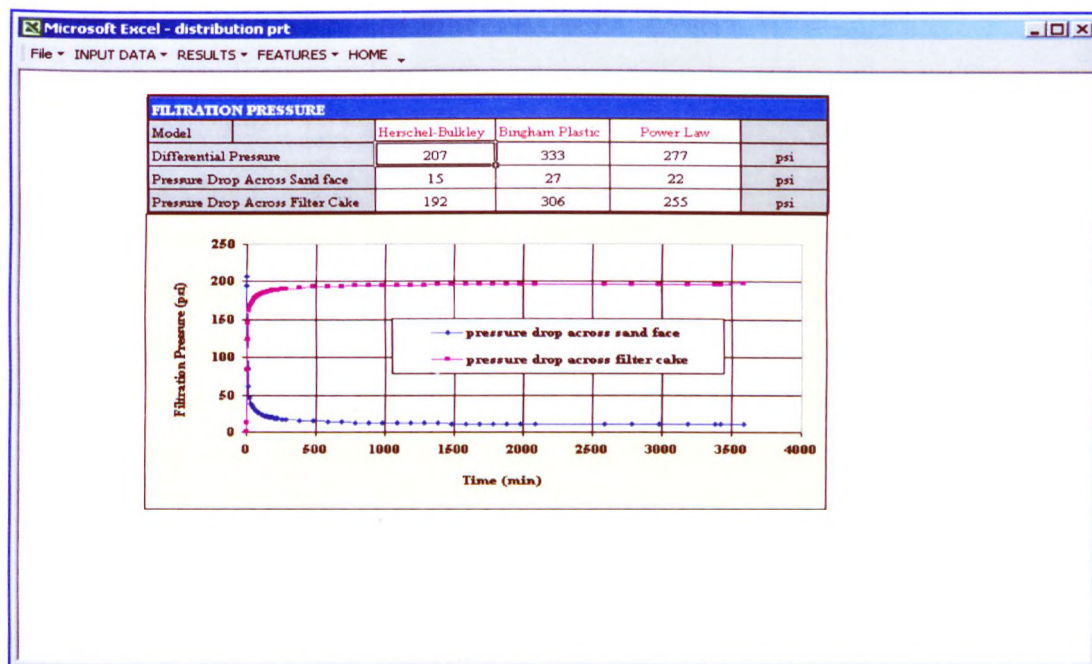


Figure 7.19 Filtration pressure distribution for OBM

#### 6. Sub menu Filter Cake Characteristics

The filter cake characteristics are presented in a tabular form for the best-fit rheological model and also for the other non-Newtonian models [Figure 7.20].

FILTER CAKE CHARACTERISTICS				
Model	Herschel-Bulkley	Bingham Plastic	Power Law	
Pressure Drop Across Filtercake	192	305.99	255	psi
Cake mass ratio	1.47	1.43	1.05	-
Density of solids	31.00	31.00	31.00	PPE
Solids Fraction	0.41	0.41	0.41	-
Density of filtrate	5.56	5.52	5.52	PPE
Filtrate Viscosity	0.53	0.53	0.53	cP
Dynamic Filtrate Coefficient	2.15E-03	1.28E-02	4.11E-03	lb/ft <sup>2</sup> s
Filter Cake Erodability	1.67E-05	5.82E-05	2.21E-05	lb/dyn s
Erosional Filter Cake	32.76	109.41	23.08	in
Filter Cake Thickness	0.01	0.01	0.004	in
Cumulative Deposited& Eroded	32.77	109.42	23.08	in
Cake Resistance	3.88E+21	5.03E+21	6.50E+21	m/lb
Medium Resistance	4.76E+16	5.94E+16	5.53E+16	1/in
Cake Porosity	0.55	0.53	0.16	-
Cake Permeability	1.88E-11	1.39E-11	5.98E-12	Darcy

Figure 7.20 Filter cake characteristics for OBM



Display of results in tabular or graphical form - Results Menu

7. Sub menu Formation Damage

Figures 7.21 and 7.22 show the formation damage characteristics simulated for radial flow (field application), for the best-fit rheological model and other non-Newtonian models in tabular form for OBM. The results are also provided in graphical form for the formation damage characteristics. The PRT results shows the depth of filtrate invasion is 34.79 inches with a skin factor (drilling skin) of 4.11; this compares with the actual field data where the depth of filtrate invasion was 40 inches and total skin factor (including perforation and completion) was 9.

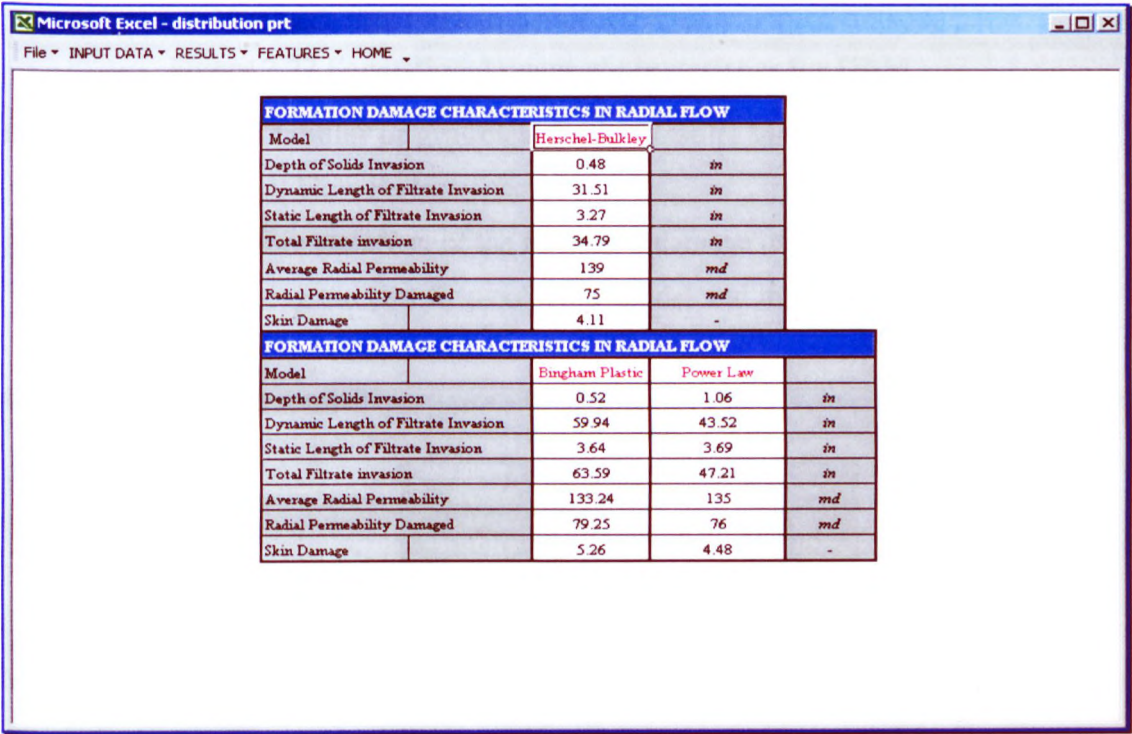


Figure 7.21 Formation damage characteristics for OBM

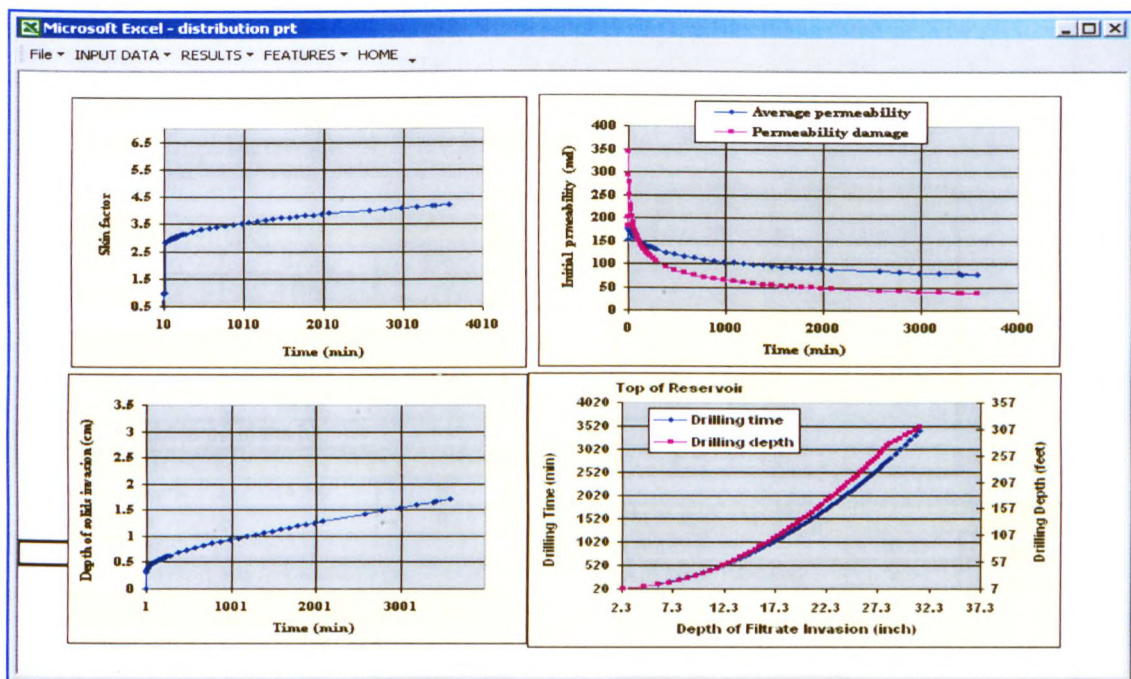


Figure 7.22 Formation damage characteristics for OBM

## Display of results in tabular or graphical form - Results Menu

### 8. Sub menu Well Flow Performance

Figure 7.23 shows the effect of the formation damage using OBM on well flow performance using the best-fit rheological model and the other non-Newtonian models.

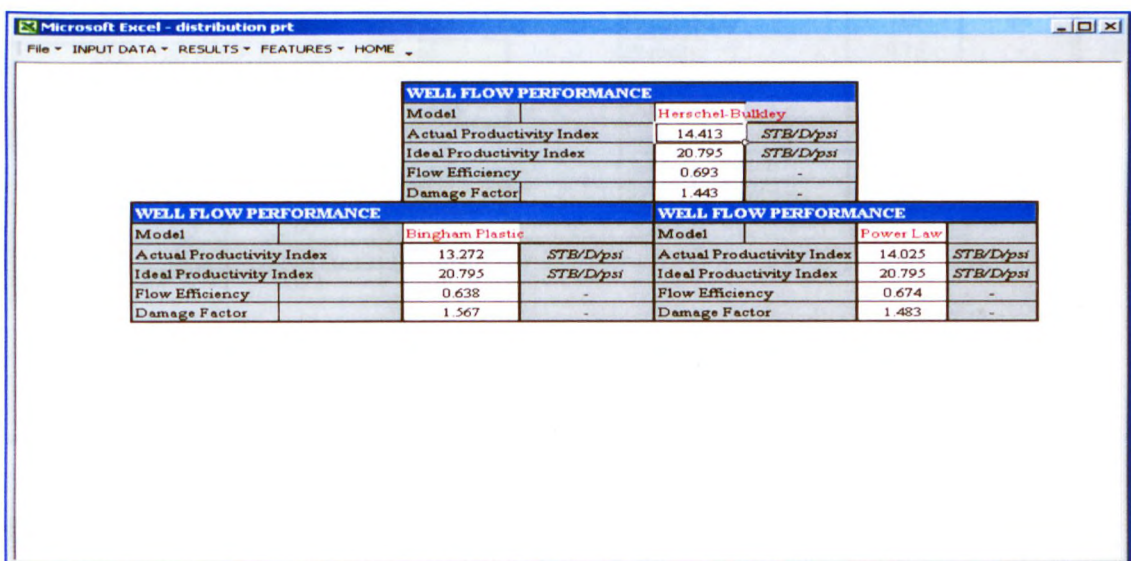


Figure 7.23 Well Flow performance for OBM



Company Name	1		
Field Number	A		
Well Number	A2		
Hole Section	6 inch		
Type of Mud :	Lignosulphonate Water Based Mud		

MUD PUMP PARAMETERS			
Pump Rate	270	gpm	
Pump Pressure	1700	psi	

BIT PARAMETERS			
Bit Diameter	6	inches	
No. of Nozzles	3x12	-	
maximum impact force at the bit			

WELLBORE GEOMETRY			
True Vertical Depth	14500	ft	
Measured Depth	-	ft	

CASING PARAMETERS			
Casing Setting Depth	12412	ft	
Casing O.D.	9.63	inches	
Casing I.D.	8.85	inches	
Linear casing Depth	13890	ft	
Casing O.D.	7.00	inches	
Casing I.D.	6.28	inches	

DRILLPIPE PARAMETERS			
Drillpipe O.D.	5	inches	
Drillpipe I.D.	4.275	inches	
Drillpipe O.D.	3.5	inches	
Drillpipe I.D.	2.76	inches	
Roughness	0.00064	-	

BOTTOM HOLE ASSEMBLY			
Component	Length/ft	I.D./ inch	O.D. / inch
Drill collar	754	2.50	4.75
Roughness	0.0007		

DRILLING STATUS			
Drilling Time	60	hours	
Static Time	38	hours	
B.H.Temperature	322	F	

PRODUCTION PARAMETERS				
Depth of Filtrate Invasion	60	inches	logs	
Skin Factor	12	-	well test	

MUD COMPOSITION		
Component	Name	Lbs/bbl
1	bentonite	10
2	HT-polymer	6
3	Dispersant	4
4	HT-stabliser	4
5	barite	150
6	solids	35
7		
8		

MUD PARAMETERS		
Mud Density	10.20	ppg
API Static Filtration	3.6	cc

Viscometer Readings	
RPM	Reading
600	59
300	37
200	29
100	21
6	9
3	7

FORMATION PARAMETERS		
Formation Type	sandstone	
Permeability	180	md
Porosity	0.13	-
Production Rate	-	pbd
Oil Viscosity	1.12	cP
Fm Volume Factor	2.03	-
Reservior Radius	2570	ft
Reservior Thickness	285	ft

Table 7.8 Field Data for Well (A2)

Company Name: 1  
 Field Number: A  
 Well Number: A2  
 Hole Section: 6 inch (Reservoir section)  
 Type of Fluid: Lignosulphonate water based mud

Display of results in tabular or graphical form - Results Menu

1. Sub menu - Rheology Best Fit Model

The results are presented in both tabular and graphical form as comparison with common non-Newtonian models Herschel Bulkley, Bingham Plastic and Power Law models. The information provided in Figure 7.24 shows that the best-fit rheological model is the Herschel Bulkley model at both standard conditions and total well depth (14500 ft).

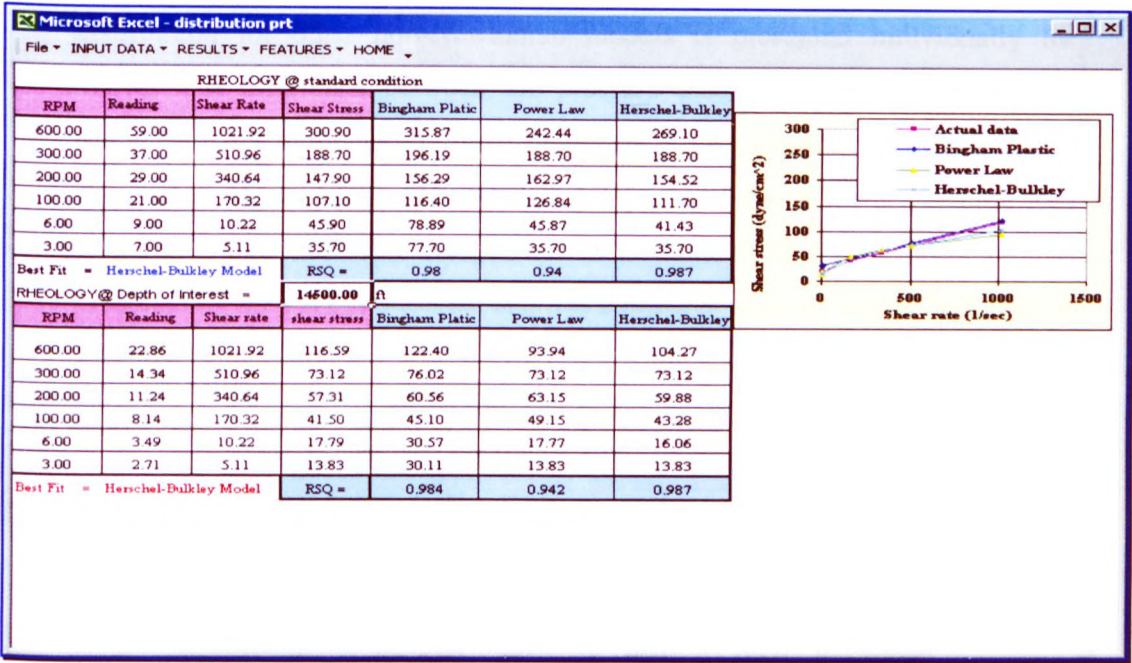


Figure 7.24 Best-fit model for WBM

2. Sub menu - Rheology Characterisation

The rheological parameters and apparent viscosity are presented in Figure 7.25 as a comparison between the actual rheological model and other non-Newtonian models.



Microsoft Excel - distribution prt

File INPUT DATA RESULTS FEATURES HOME

RHEOLOGICAL CHARACTERISATION				
Model		Herschel Bulkley	Power Law	
Rheological Parameters				
True Yield		9		$lb/100q^{n-2}$
Flow Index		0.57	0.36	-
Consistency Index		179	767.02	cP
Apparent Viscosity				
In annulus		30	12	cP
In pipe		24.10	37.69	cP

RHEOLOGICAL CHARACTERISATION				
Model		Bingham Plastic		
Rheological Parameters				
Plastic Viscosity		22		cP
Yield Point		15.00		$lb/100q^{n-2}$
Apparent Viscosity				
In annulus		31		cP
In pipe		35.45		cP

Figure 7.25 Rheological Characterisation for WBM

### 3. Sub menu - Pressure Distribution

Figure 7.26 shows the pressure loss across the system for the best fit rheological model using maximum impact force at the bit. The pressure distribution for other non-Newtonian models is presented individually for WBM. The difference between the pressure distribution analysis using the actual rheological model and other models is clearly illustrated in Figure 7.26. The results show that the Herschel Bulkley model has a lower pressure loss than the Bingham Plastic and Power Law models. The total pressure loss predicted by the PRT is 1695 psi and this compares with the actual field data of 1700 psi.

Microsoft Excel - distribution prt					
File - INPUT DATA - RESULTS - FEATURES - HOME					
Maximum impact force at the bit					
<b>PRESSURE DISTRIBUTION</b>					
Model		Herschel-Bulkley	Bingham Plastic	Power Law	
Hydrostatic Pressure		7917.00	7917.00	7917.00	psi
Bottom Hole Circulation Pressure		8116.81	8254.61	8146.58	psi
Equivalent Circulation Density		10.76	10.95	10.80	PPG
Through the BHA		255.22	304.01	249.78	psi
Across the BHA		56.30	62.01	62.08	psi
Through the Pipe		443.77	551.72	430.18	psi
Across Pipe		0	0	0	psi
Across Casing		143.51	290.60	158.50	psi
Bit Pressure Loss		797.05	1058.24	806.57	psi
Total Pressure Loss		1695.86	2251.57	1716.12	psi
Hydraulic Horsepower		283	376	287	-
Total Flow Area (TFA)		0.360	0.260	0.298	in <sup>2</sup>
Size of Nozzles	J1	13	11	11	1/32nd
	J2	13	11	11	1/32nd
	J3	13	11	11	1/32nd
	J4	-	-	-	1/32nd
	J5	-	-	-	1/32nd
	J6	-	-	-	1/32nd

Figure 7.26 Wellbore Pressure Distribution for WBM

4. Sub menu – Static and Dynamic Filtration

The dynamic filtration cumulative filtration volume during dynamic operations for the best-fit model and other non-Newtonian models for WBM are presented in Figure 7.27. A comparison between static and dynamic filtration volume for WBM is presented in graphical form [Figure 7.27]. The results show that the Herschel Bulkley model has lower dynamic filtration volumes than the Bingham Plastic and Power Law models WBM due to lower pressure loss.

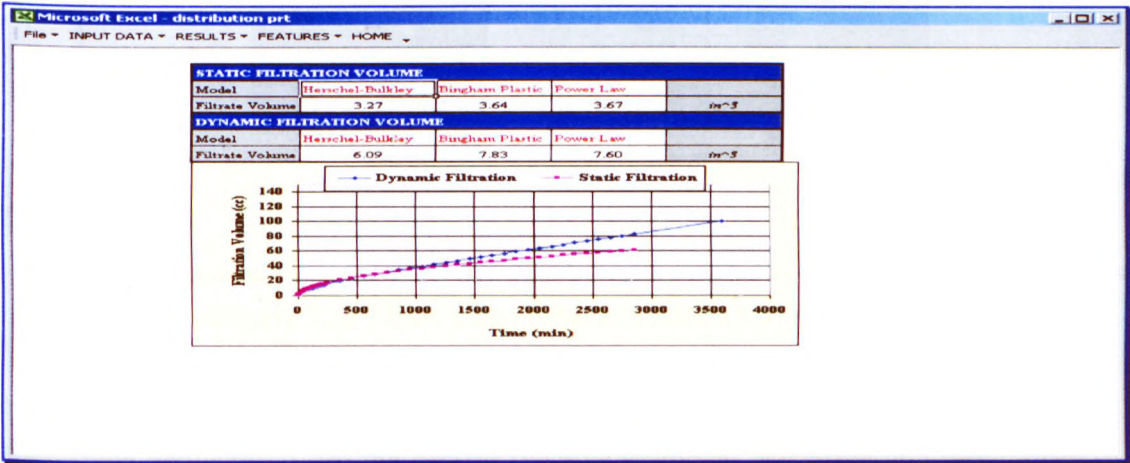


Figure 7.27 Filtration Characteristics for WBM

5. Sub menu - Filtration Pressure

The wellbore differential pressure, pressure drop across the sand face and mud filter cake for the best-fit model and other non-Newtonian models are shown in tabular form [Figure 7.28]. The results show that the Herschel Bulkley model has a lower pressure drop across the filter cake as compared to the Bingham Plastic and Power Law models for WBM.

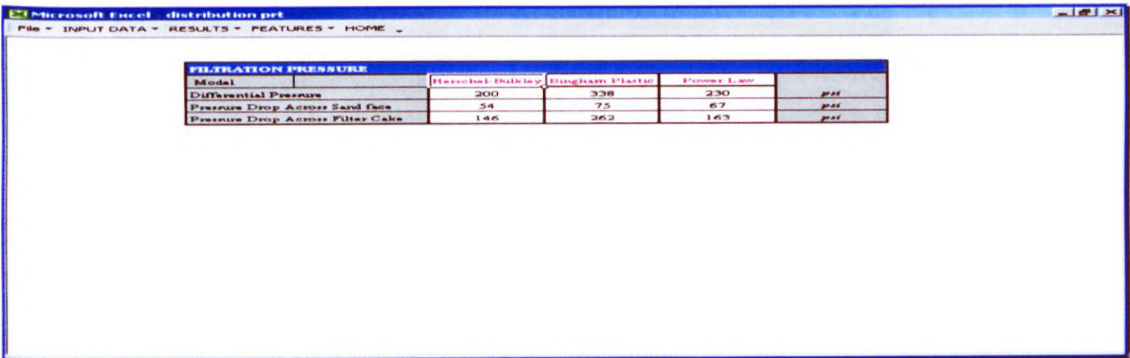
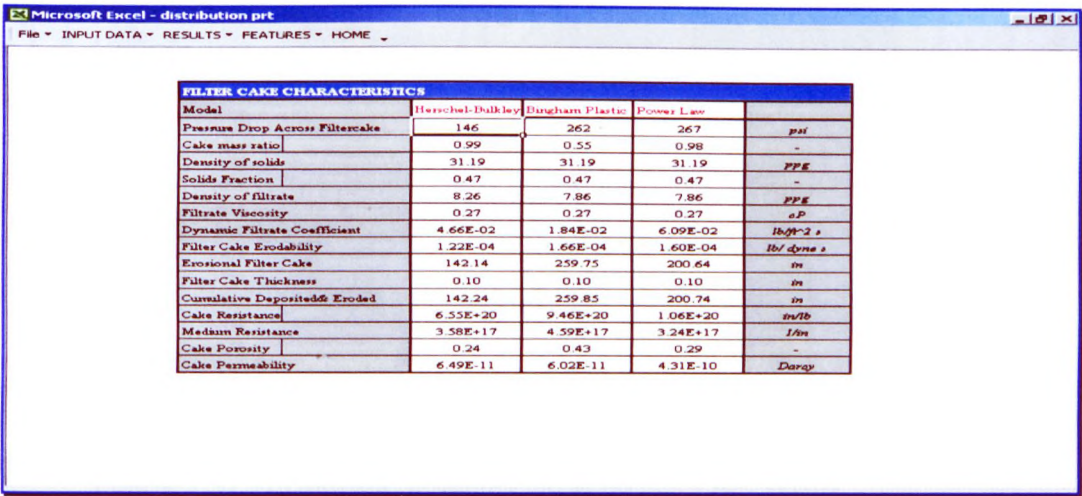


Figure 7.28 Filter Pressure Distribution for WBM



6. Sub menu Filter Cake Characteristics

The filter cake characteristics are presented in a tabular for the best-fit rheological model and also for the other non-Newtonian models [Figure 7.29].

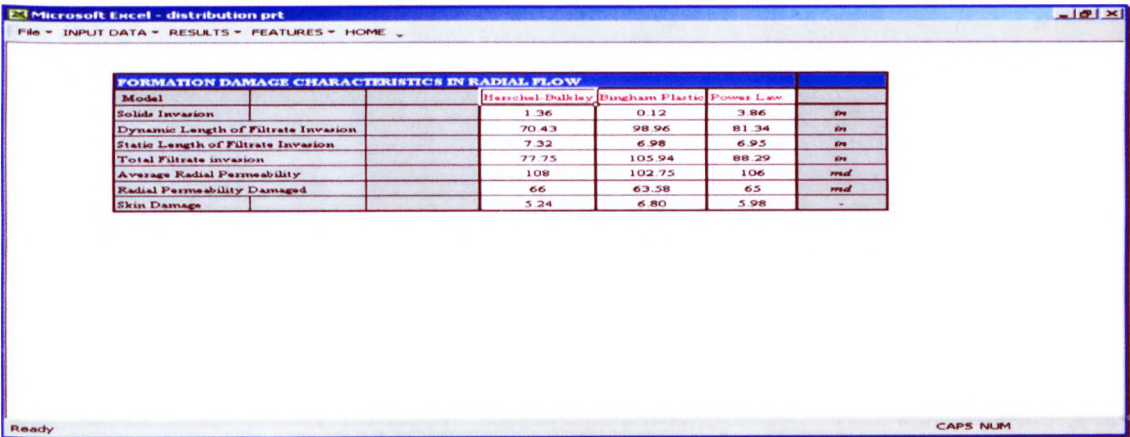


FILTER CAKE CHARACTERISTICS				
Model	Herschel-Bulkley	Bingham Plastic	Power Law	
Pressure Drop Across Filtercake	146	262	267	psi
Cake mass ratio	0.99	0.55	0.98	-
Density of solids	31.19	31.19	31.19	PPE
Solids Fraction	0.47	0.47	0.47	-
Density of filtrate	8.26	7.86	7.86	PPE
Filtrate Viscosity	0.27	0.27	0.27	cP
Dynamic Filtrate Coefficient	4.66E-02	1.84E-02	6.09E-02	lb/ft <sup>2</sup> s
Filter Cake Erodability	1.22E-04	1.66E-04	1.60E-04	lb/dyne s
Erosional Filter Cake	142.14	259.75	200.64	in
Filter Cake Thickness	0.10	0.10	0.10	in
Cumulative Deposited& Eroded	142.24	259.85	200.74	in
Cake Resistance	6.55E+20	9.46E+20	1.06E+20	in/lb
Medium Resistance	3.58E+17	4.59E+17	3.24E+17	1/in
Cake Porosity	0.24	0.43	0.29	-
Cake Permeability	6.49E-11	6.02E-11	4.31E-10	Darcy

Figure 7.29 Filter Cake Characteristics for WBM

Sub menu Formation Damage

Figures 7.30 and 7.31 show the formation damage characteristics simulated for radial flow (field application), for the best-fit rheological model and other non-Newtonian models in tabular form for OBM. The results are also provided in graphical form for the formation damage characteristics. The PRT results shows the depth of filtrate invasion is 77.73 inches with a skin factor (drilling skin) of 5.24; this compares with the actual field data where the depth of filtrate invasion was 60 inches and total skin factor (including perforation and completion) was 12.



FORMATION DAMAGE CHARACTERISTICS IN RADIAL FLOW				
Model	Herschel-Bulkley	Bingham Plastic	Power Law	
Solids Invasion	1.36	0.12	3.86	in
Dynamic Length of Filtrate Invasion	70.43	98.96	81.34	in
Static Length of Filtrate Invasion	7.32	6.98	6.95	in
Total Filtrate invasion	77.75	105.94	88.29	in
Average Radial Permeability	108	102.75	106	md
Radial Permeability Damaged	66	63.58	65	md
Skin Damage	5.24	6.80	5.98	-

Figure 7.30 Formation damage characteristics for WBM

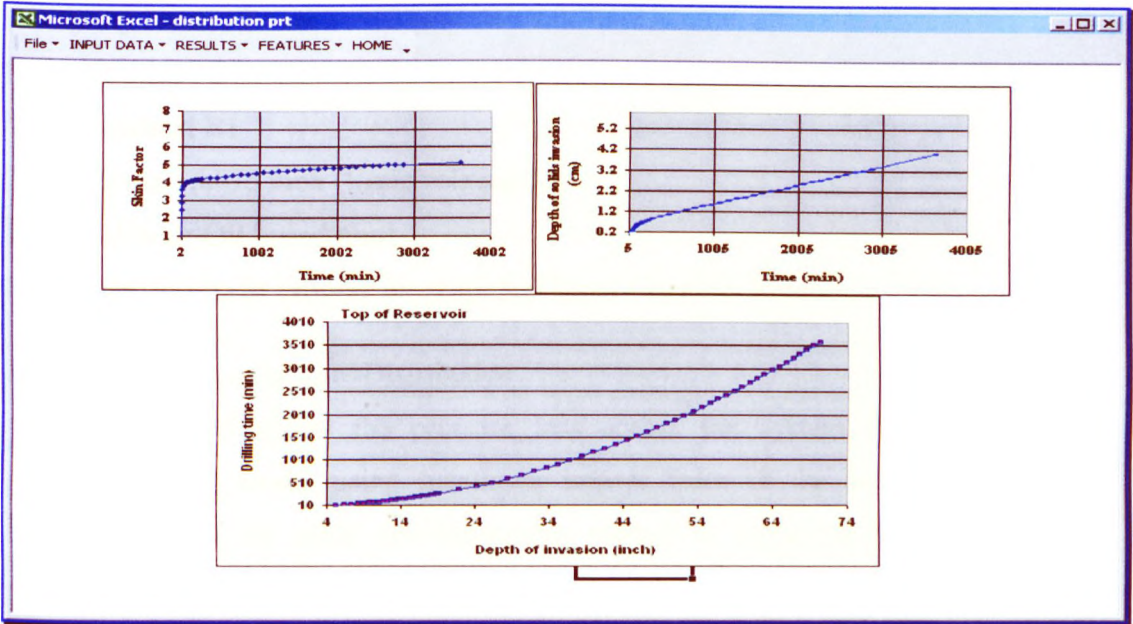


Figure 7.31 Formation damage characteristics for WBM

7. Sub menu Well Flow Performance

Figure 7.32 shows the effect of the formation damage using WBM on well flow performance using the best-fit rheological model and other non-Newtonian models.

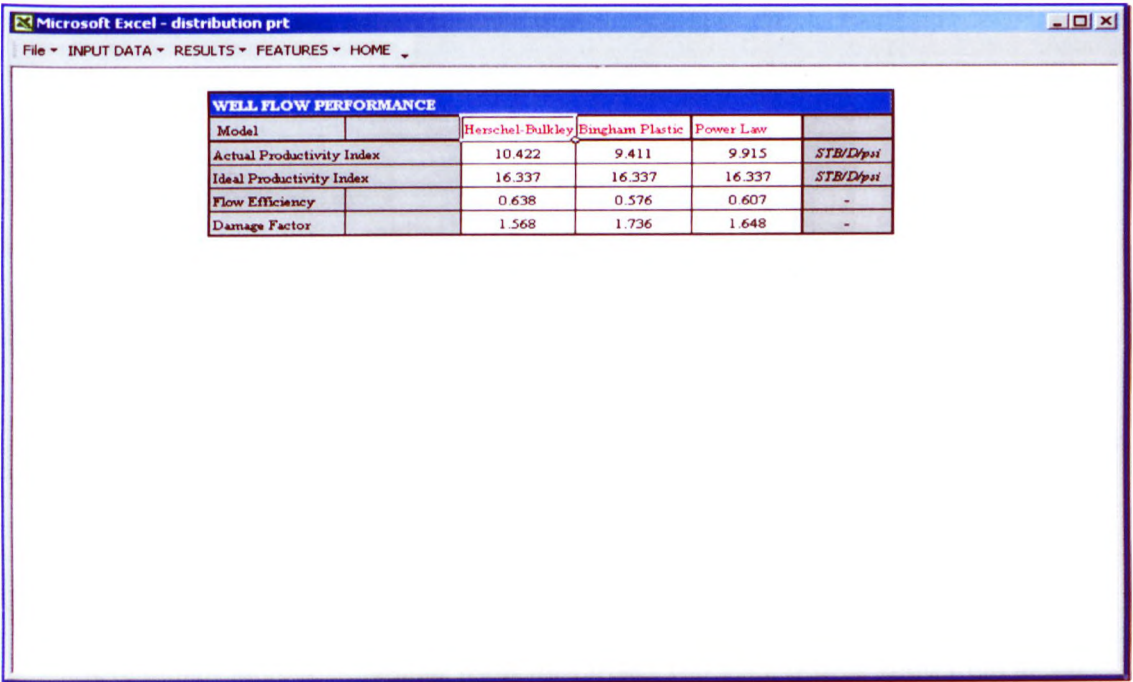


Figure 7.32 Well Flow performance for WBM



Company Name: 2  
Field Number: B  
Well Number: B1  
Hole Section: 5.875 inch (Reservoir section)  
Type of Fluid: Oil based mud  
Display of results in tabular or graphical form - Results Menu

1. Sub menu - Pressure Distribution

Figure 7.33 shows the pressure loss across the system for the best fit rheological model using maximum impact force at the bit. The pressure distribution for other non-Newtonian models is presented individually for WBM. The difference between the pressure distribution analysis using the actual rheological model and other models is clearly illustrated in Figure 7.33. The results show that the Herschel Bulkley model has a lower pressure loss than the Bingham Plastic and Power Law models. The total pressure loss predicted by the PRT is 2032 psi and this compares with the actual field data of 2000 psi.

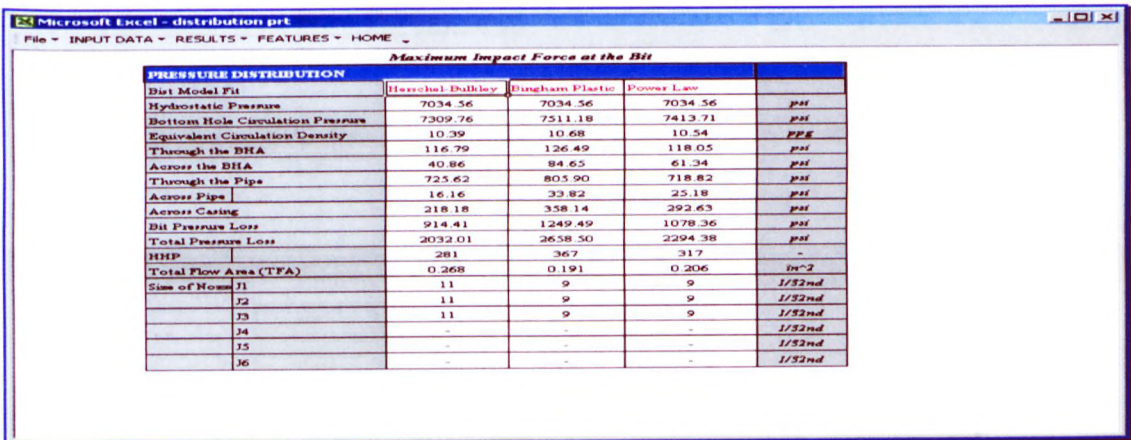


Figure 7.33 Wellbore Pressure Distribution for OBM

2. Sub menu Formation Damage

Figures 7.34 shows the formation damage characteristics simulated for radial flow (field application), for the best-fit rheological model and other non-Newtonian models in tabular form for OBM. The PRT results shows the depth

of filtrate invasion is 45.43 inches with a skin factor (drilling skin) of 4.0; this compares with the actual field data where the depth of filtrate invasion was 60 inches and total skin factor (including open hole completion) was 12.

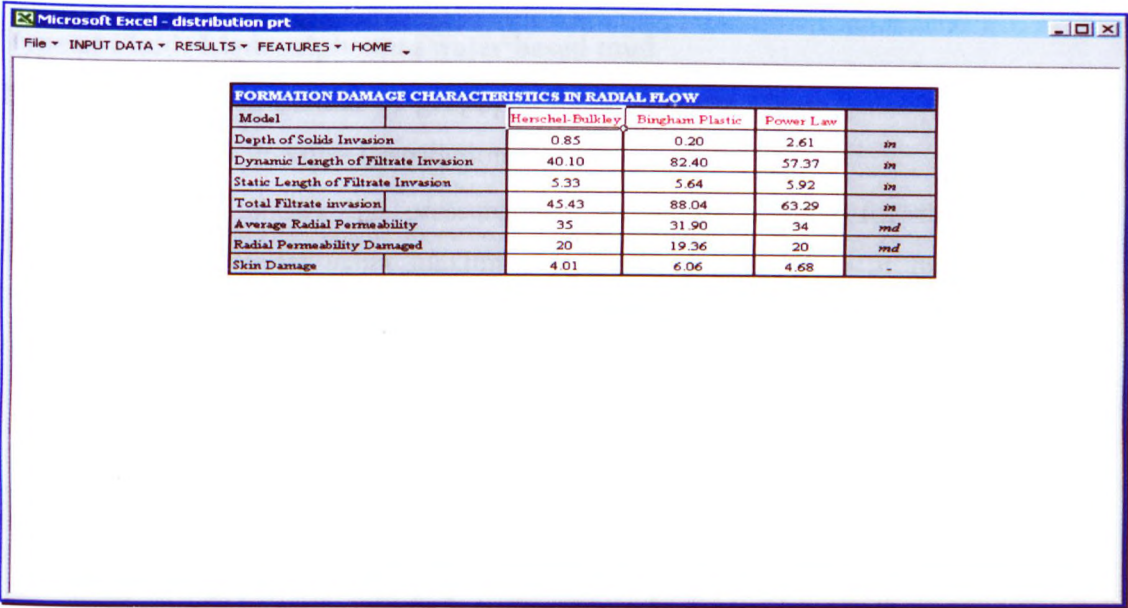


Figure 7.34 Formation damage characteristics for OBM

3. Sub menu Well Flow Performance

Figure 7.35 shows the effect of the formation damage using OBM on well flow performance using the best-fit rheological model and other non-Newtonian models.

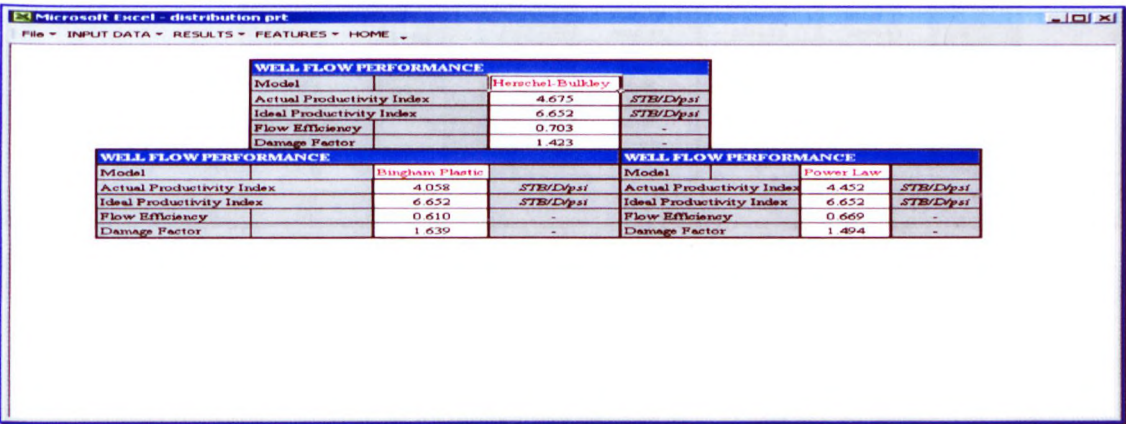


Figure 7.35 Well Flow Performance for OBM



Company Name: 2

Field Number: B

Well Number: B2

Hole Section: 8.50 inch (Intermediate section)

Type of Fluid: Lignosulphonate water based mud

Display of results in tabular or graphical form - Results Menu

1. Sub menu - Pressure Distribution

Figure 7.36 shows the pressure loss across the system for the best fit rheological model using maximum hydraulic horse power at the bit. The pressure distribution for other non-Newtonian models is presented individually for WBM. The difference between the pressure distribution analysis using the actual rheological model and other models is clearly illustrated in Figure 7.36. The results show that the Herschel Bulkley model has a lower pressure loss than the Bingham Plastic and Power Law models. The total pressure loss predicted by the PRT is 2820 psi and this compares with the actual field data of 2600 psi.

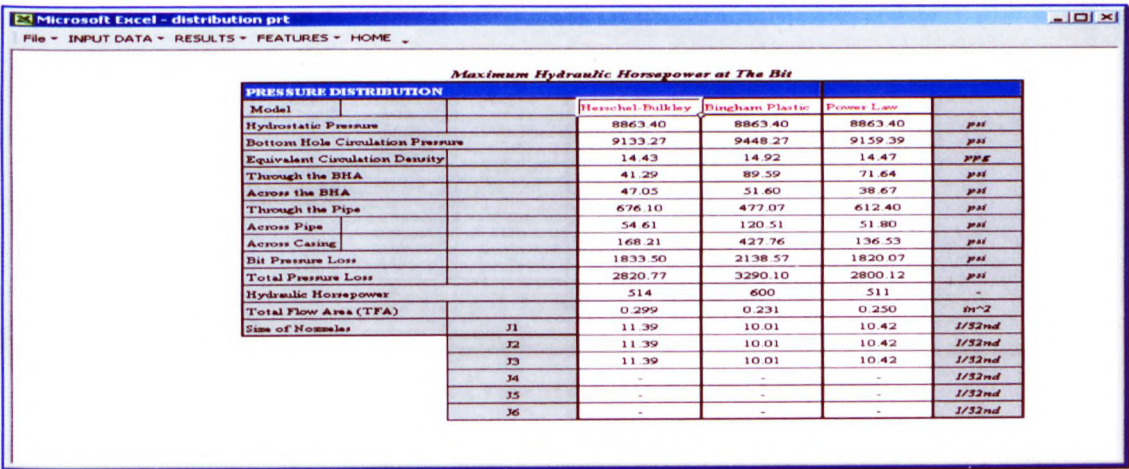


Figure 7.36 Wellbore Pressure Distribution for WBM

Company Name: 2

Field Number: B

Well Number: B2

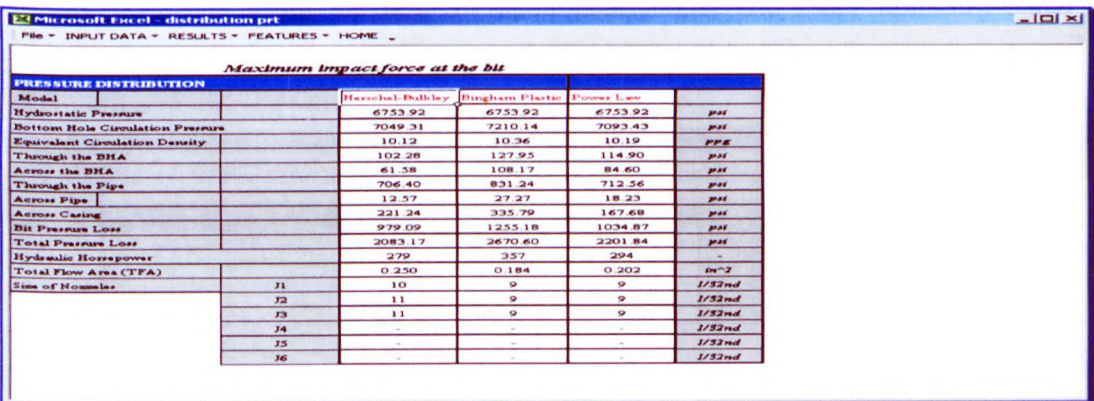
Hole Section: 5.875 inch (Reservoir section)

Type of Fluid: Lignosulphonate water based mud

Display of results in tabular or graphical form - Results Menu

1. Sub menu - Pressure Distribution

Figure 7.37 shows the pressure loss across the system for the best fit rheological model using maximum impact force at the bit. The pressure distribution for other non-Newtonian models is presented individually for WBM. The difference between the pressure distribution analysis using the actual rheological model and other models is clearly illustrated in Figure 7.37. The results show that the Herschel Bulkley model has a lower pressure loss than the Bingham Plastic and Power Law models. The total pressure loss predicted by the PRT is 2083 psi and this compares with the actual field data of 2000 psi.



Maximum Impact force at the bit					
PRESSURE DISTRIBUTION					
Model		Herschel-Bulkley	Bingham Plastic	Power Law	
Hydrostatic Pressure		6753.92	6753.92	6753.92	psi
Bottom Hole Circulation Pressure		7049.31	7210.14	7093.43	psi
Equivalent Circulation Density		10.12	10.36	10.19	PPE
Through the BHA		102.28	127.95	114.90	psi
Across the BHA		61.38	108.17	84.60	psi
Through the Pipe		706.40	831.24	712.56	psi
Across Pipe		12.57	27.27	18.23	psi
Across Casing		221.24	335.79	167.68	psi
Bit Pressure Loss		979.09	1255.18	1034.87	psi
Total Pressure Loss		2083.17	2670.60	2201.84	psi
Hydraulic Horsepower		279	357	294	-
Total Flow Area (TFA)		0.250	0.184	0.202	in <sup>2</sup>
Size of Nozzle	J1	10	9	9	1/32nd
	J2	11	9	9	1/32nd
	J3	11	9	9	1/32nd
	J4	-	-	-	1/32nd
	J5	-	-	-	1/32nd
	J6	-	-	-	1/32nd

Figure 7.37 Wellbore Pressure Distribution for WBM

2. Sub menu Formation Damage

Figures 7.38 shows the formation damage characteristics simulated for radial flow (field application), for the best-fit rheological model and other non-Newtonian models in tabular form for WBM. The PRT results shows the depth of filtrate invasion is 92.73 inches with a skin factor (drilling skin) of 5.87; this



compares with the actual field data where the depth of filtrate invasion was 70 inches and total skin factor (including open hole completion) was 10.

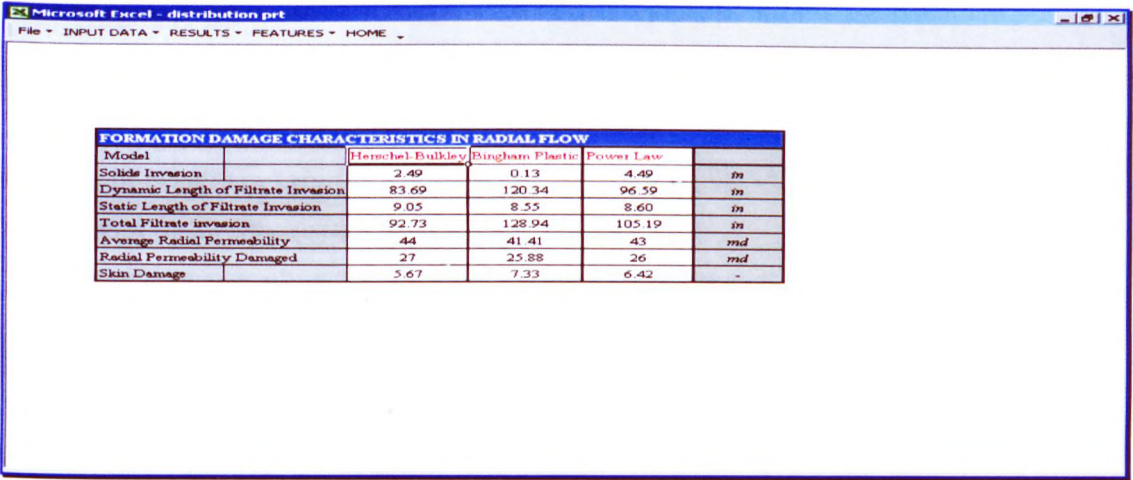


Figure 7.38 Formation damage characteristics for WBM

3. Sub menu Well Flow Performance

Figure 7.39 shows the effect of the formation damage using WBM on well flow performance using the best-fit rheological model and other non-Newtonian models.

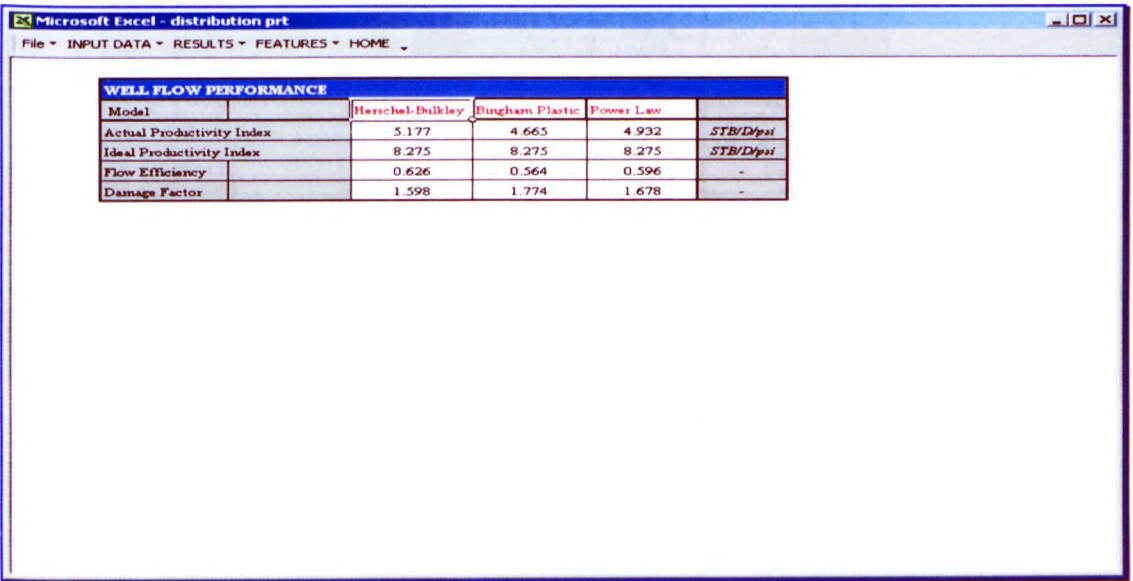


Figure 7.39 Well Flow Performance for WBM

Company Name: 2

Field Number: B

Well Number: B3

Hole Section: 5.875 inch (Reservoir section)

Type of Fluid: Lignosulphonate water based mud

Display of results in tabular or graphical form - Results Menu

1. Sub menu - Pressure Distribution

Figure 7.40 shows the pressure loss across the system for the best fit rheological model using or maximum impact force at the bit. The pressure distribution for other non-Newtonian models is presented individually for WBM. The difference between the pressure distribution analysis using the actual rheological model and other models is clearly illustrated in Figure 7.40. The results show that the Herschel Bulkley model has a lower pressure loss than the Bingham Plastic and Power Law models. The total pressure loss predicted by the PRT is 1566 psi which compares with the actual field data of 1500 psi.

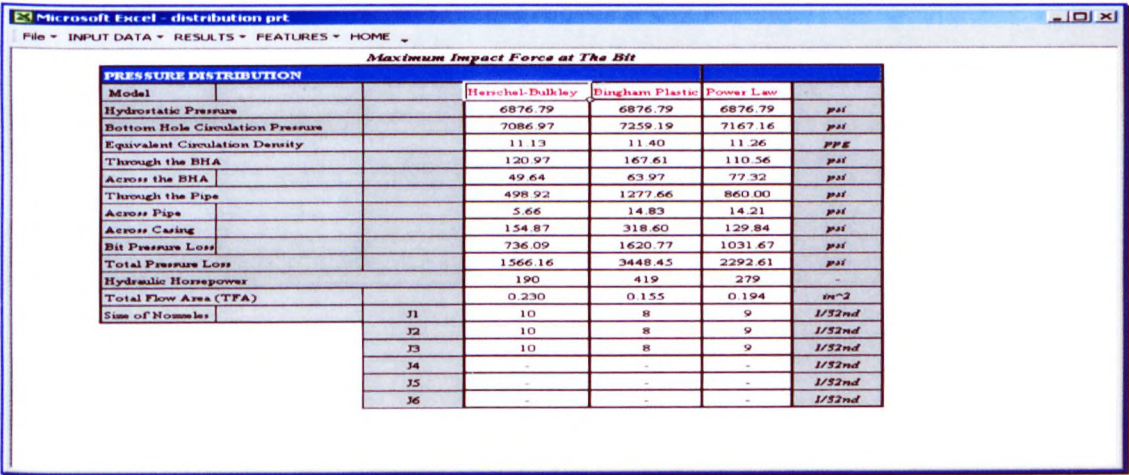
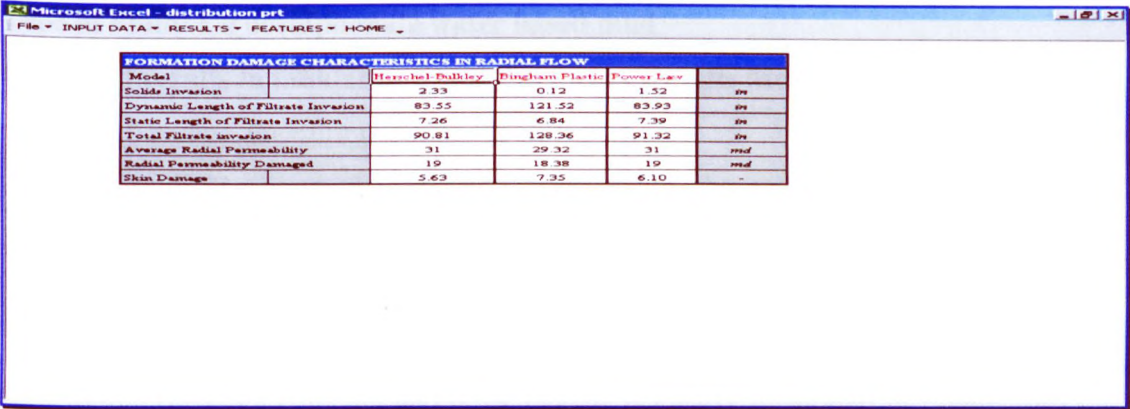


Figure 7.40 Wellbore Pressure Distribution for WBM

2. Sub menu Formation Damage

Figures 7.41 shows the formation damage characteristics simulated for radial flow (field application), for the best-fit rheological model and other non-

Newtonian models in tabular form for WBM. The PRT results shows the depth of filtrate invasion is 90.81 inches with a skin factor (drilling skin) of 5.63 which compares with the actual field data where the depth of filtrate invasion was 70 inches and total skin factor (including open hole completion) was 10.



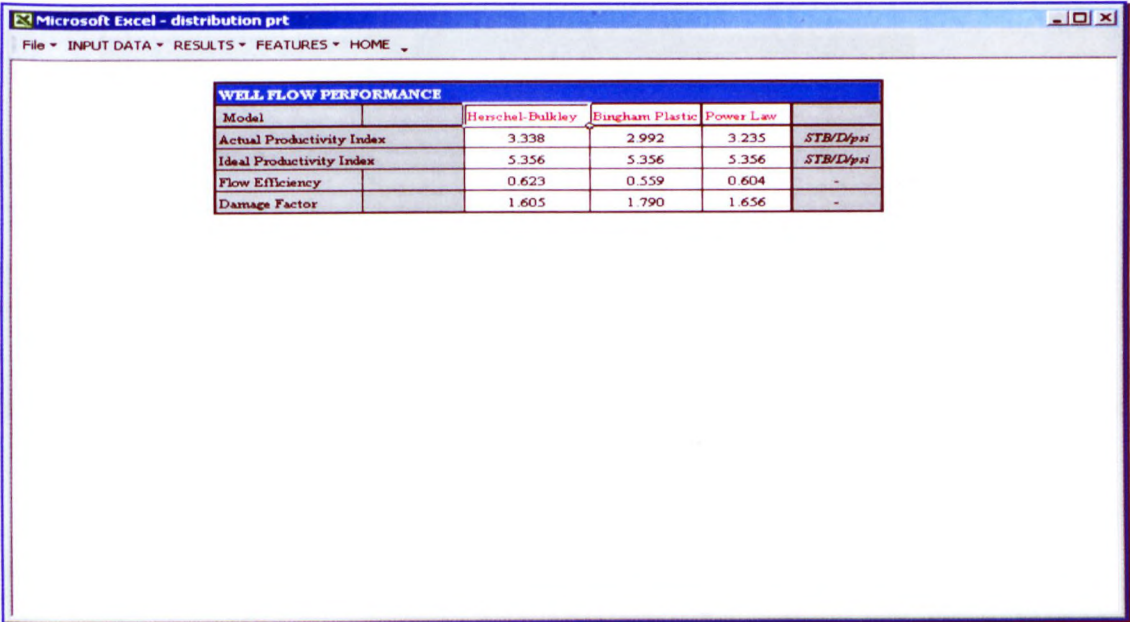
The screenshot shows a Microsoft Excel window titled "Microsoft Excel - distribution prt". The menu bar includes "File", "INPUT DATA", "RESULTS", "FEATURES", and "HOME". The main content area displays a table titled "FORMATION DAMAGE CHARACTERISTICS IN RADIAL FLOW". The table has five columns: "Model", "Herschel-Bulkley", "Bingham Plastic", "Power Law", and an empty column. The rows include "Solid Invasion", "Dynamic Length of Filtrate Invasion", "Static Length of Filtrate Invasion", "Total Filtrate invasion", "Average Radial Permeability", "Radial Permeability Damaged", and "Skin Damage".

Model	Herschel-Bulkley	Bingham Plastic	Power Law	
Solid Invasion	2.33	0.12	1.52	in
Dynamic Length of Filtrate Invasion	83.55	121.52	83.93	in
Static Length of Filtrate Invasion	7.26	6.84	7.39	in
Total Filtrate invasion	90.81	128.36	91.32	in
Average Radial Permeability	31	29.32	31	md
Radial Permeability Damaged	19	18.38	19	md
Skin Damage	5.63	7.35	6.10	-

Figure 7.41 Formation damage characteristics for WBM

3. Sub menu Well Flow Performance

Figure 7.42 shows the effect of the formation damage using WBM on well flow performance using the best-fit rheological model and other non-Newtonian models.



The screenshot shows a Microsoft Excel window titled "Microsoft Excel - distribution prt". The menu bar includes "File", "INPUT DATA", "RESULTS", "FEATURES", and "HOME". The main content area displays a table titled "WELL FLOW PERFORMANCE". The table has five columns: "Model", "Herschel-Bulkley", "Bingham Plastic", "Power Law", and an empty column. The rows include "Actual Productivity Index", "Ideal Productivity Index", "Flow Efficiency", and "Damage Factor".

Model	Herschel-Bulkley	Bingham Plastic	Power Law	
Actual Productivity Index	3.338	2.992	3.235	STB/D/psi
Ideal Productivity Index	5.356	5.356	5.356	STB/D/psi
Flow Efficiency	0.623	0.559	0.604	-
Damage Factor	1.605	1.790	1.656	-

Figure 7.42 Well Flow Performance for WBM



Company Name: 4  
Field Number: C  
Well Number: C1  
Hole Section: 8.50 inch (Reservoir section)  
Type of Fluid: Lignosulphonate water based mud  
Display of results in tabular or graphical form - Results Menu

1. Sub menu - Pressure Distribution

Figure 7.43 shows the pressure loss across the system for the best fit rheological model using maximum hydraulic horse power at the bit. The pressure distribution for other non-Newtonian models is presented individually for WBM. The difference between the pressure distribution analysis using the actual rheological model and other models is clearly illustrated in Figure 7.43. The results show that the Herschel Bulkley model has a lower pressure loss than the Bingham Plastic and Power Law models. The total pressure loss predicted by the PRT is 2092 psi which compares with the actual field data of 1950 psi.

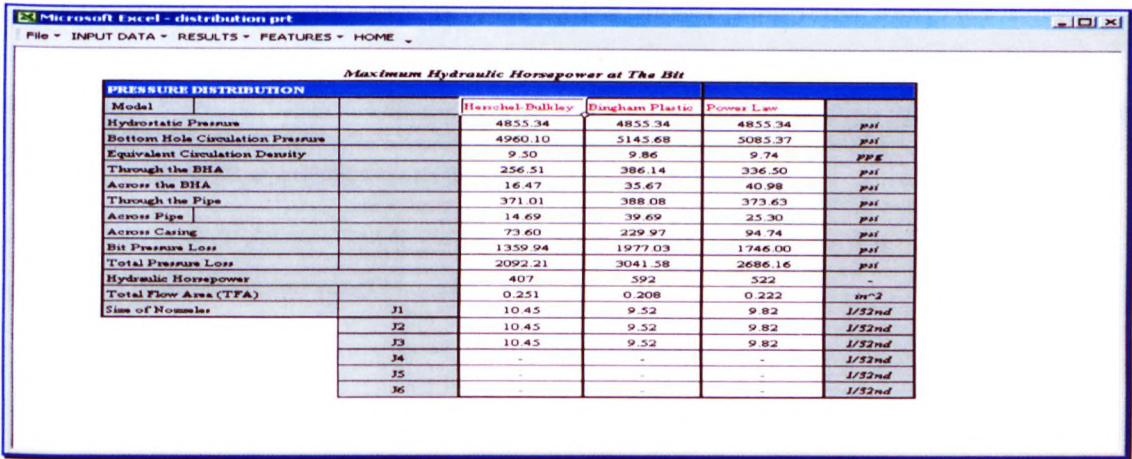


Figure 7.43 Wellbore Pressure Distribution for WBM

2. Sub menu Formation Damage

Figures 7.44 shows the formation damage characteristics simulated for radial flow (field application), for the best-fit rheological model and other non-Newtonian models in tabular form for WBM. The results are also provided in



graphical form for the formation damage characteristics. The PRT results shows the depth of filtrate invasion is 48.69 inches with a skin factor (drilling skin) of 3.62 and compares with the actual field data where the depth of filtrate invasion was 40 inches and total skin factor (including perforation and completion) was 8.

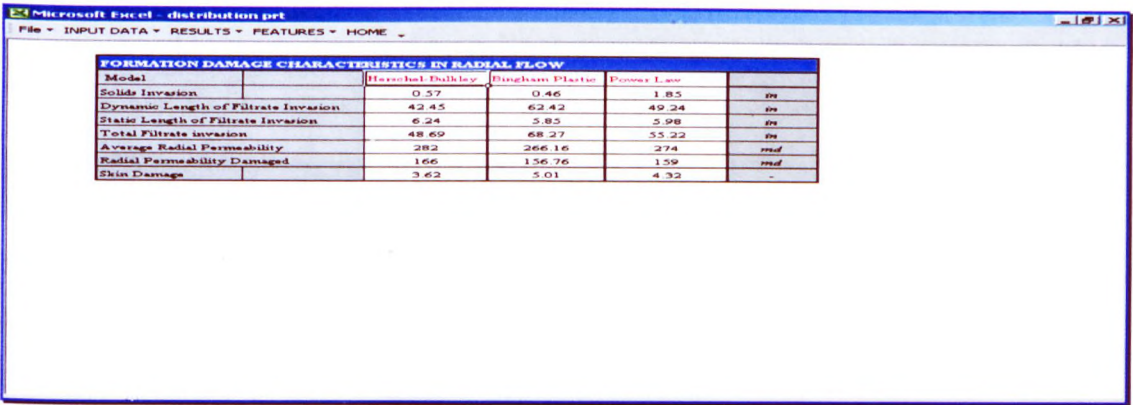


Figure 7.44 Formation damage characteristics for WBM

3. Sub menu Well Flow Performance

Figure 7.45 shows the effect of the formation damage using WBM on well flow performance using the best-fit rheological model and other non-Newtonian models.

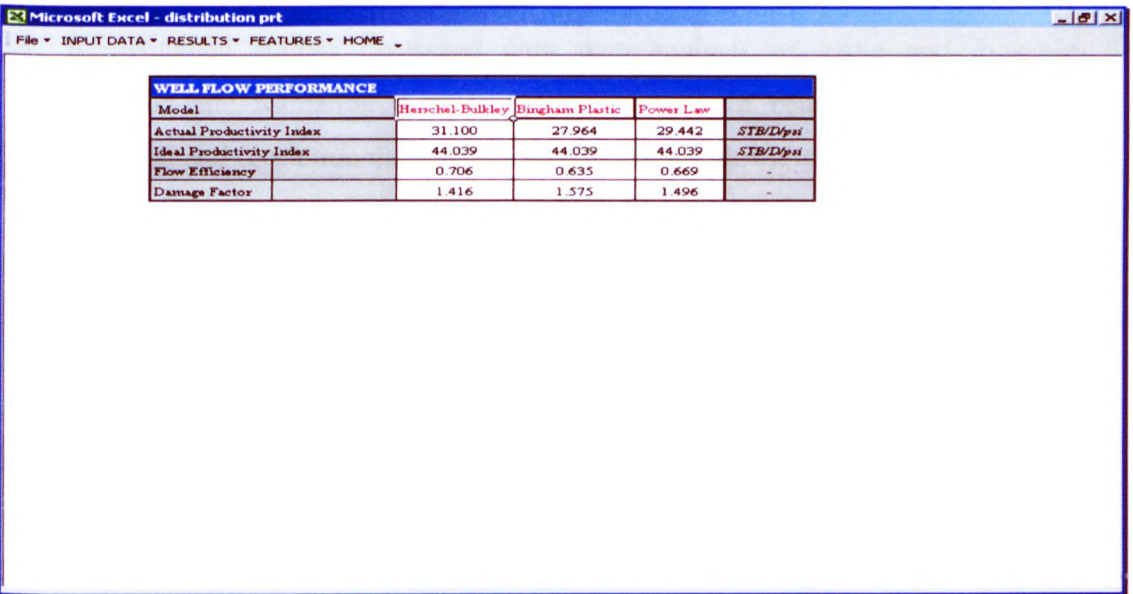


Figure 7.45 Well Flow Performance for WBM

## **CHAPTER EIGHT**

### **CONCLUSIONS AND RECOMMENDATIONS**

#### **8.1 INTRODUCTION**

In essence, this thesis has sought to present a detailed analysis of drilling fluid filtration and its impact on formation damage in terms of well performance. The present work is divided in two main parts: the experimental work and theoretical work. The theoretical work was conducted based on the use of a database generated from controlled experimental studies. Contributions to knowledge on key subjects came from both approaches.

The conclusions on different aspects of the experimental and theoretical work are closely connected and combined into a design management tool to link laboratory measurements to field scale applications, and represent the main finding of the present work which is called the productivity tool (PRT).

#### **8.2 EXPERIMENTAL WORK**

A summary of the main results is as follows:

- Experimental studies combined with data analysis of static and dynamic filtration and formation damage models provides a better understanding of filtration and formation damage mechanisms under downhole conditions<sup>2,5</sup>. This analysis also considers different variables such as solids, shear rate, medium type and permeability, fluid loss additives, pressure and temperature.
- A new application testing technique<sup>6</sup> has been introduced using a Particle Size Analyser for the following purposes:
  - (a) Selecting optimum emulsifier concentrations for water-based muds.
  - (b) Selecting optimum primary and secondary emulsifier concentrations for oil-based muds.

- (c) A quality control tool for comparison of different types of emulsifiers.
  - (d) Speeding up selection and comparison of emulsifiers, thus reducing economic impact.
  - (e) A backup tool for dynamic sag test.
  - (f) Particle size classification analysis for static and dynamic filtration filter cakes.
- It was discovered for water-based mud that there exists a critical overbalance pressure zone where decreased permeability impairment occurs<sup>3</sup>. In this zone a minimum invasion depth was observed in the overbalance pressure range from 400 to 650 psi (Chapter 5). This effect has been explained in terms of tight particle bridging, compacted and lower filter cake permeability, thereby allowing fewer particles through the cake into the formation. This is an important effect, as it is common practice for oil operators to drill with lower differential pressure in the belief that this will minimise the formation permeability damage. However, contrary to this expectation it has been found that the permeability damage will be higher at lower differential pressures.
  - The mixing procedure order for OBM component described in API RP 13B-2 has been modified.

### **8.3 APPLICATION OF THE PRT**

Using a database generated from controlled experimental studies a number of models have been developed for WBM and OBM and can be summarised as follows:

1. Rheology prediction models.
2. Static and dynamic filtration prediction models.
3. Filter cake build-up on sand face evaluation model.
4. Prediction models for Filtration pressure drops across the sand face and the filter cake.
5. Formation morphological characteristics.

6. Prediction models for depth of solids and filtrate invasion.
7. Models for skin factor and flow efficiency prediction.

A productivity tool has been developed which incorporates all of the above models. This tool is useful as a design and analysis tool, which can be used for predicting formation damage mechanisms caused by particulate and filtrate invasion<sup>3</sup> (Appendix D). The productivity tool can be used for the following tasks:

- (a) To use the laboratory results of fluid rheology, filtration and formation damage to scale fluid applications to downhole conditions. The link establishes correlations between laboratory and field pressure distribution and formation damage measurements (Well Test Analysis and Production Logging).
- (b) To analyse wellbore pressure distribution and filtration pressure across the formation and across the filter cake.
- (c) To analyse the response of the fluid to static and dynamic filtration.
- (d) To characterise the rheology and filtration of the selected fluids<sup>1,2</sup>.
- (e) To quantify the level and depth of formation damage.
- (f) To quantify the drilling skin.
- (g) To determine the impact of the selected fluid on formation productivity.
- (h) To screen appropriate drilling fluids desired for achieving minimum formation impairment and maximum formation productivity.
- (i) To determine relevance of formation damage mechanisms on field scale and determine the best operating drilling condition.

The field applications of the productivity tool based on the drilled wells studied shows it can be used to investigate the influence of many parameters such as drilling and static operational time, fluid type, etc. on well performance<sup>4</sup> (Appendix D).

The PRT wellbore pressure distribution prediction shows good agreement with field data (pump pressure) within an average error of 5 %.



The PRT depth of filtrate invasion and skin prediction show agreement with field data (well logging and well test) within an average error of 25 %. Since the PRT prediction is based on measurements solely from Clashach sandstone cores, and comparison with different lithologies (actual reservoir rocks) may yield a margin of error. However, the degree of accuracy could be improved by further validation using actual reservoir rocks.

The productivity tool can be used before drilling at the design stage (planning tool), during drilling and post drilling for evaluation and comparison with well test data. This predictive tool is capable of being utilised to screen different drilling fluids in order to achieve minimum formation impairment and maximum production capacity, which can reduce the overall well cost in terms of time and operations. As a result of this, the considerable economic impact of the skin zone on well productivity can be greatly minimised (section 7.8.1).

#### **8.4 RECOMMENDATIONS FOR FURTHER WORK**

The results of in-depth controlled experimental research into rheology, filtration and formation damage phenomena and the relationships between them are presented. They also provide the database for empirical mechanistic models that have been developed, combined and incorporated into a design and evaluation tool - the productivity tool, for predicting the effect of drilling fluid filtration on formation productivity for vertical wells.

This experimental database has been based on laboratory application results for common types of HP-HT drilling fluids namely, lignosulphonate water based mud and synthetic oil based mud on Clashach sandstone cores. The degree of accuracy of the PRT results could be improved by further validation using other drilling fluids and formation types.

Based on the equipment limitations, the experimental programme was carried out at a maximum temperature of 300 °F. The database results have then been extrapolated up

to 350 °F based on the rheological behaviour of the drill-in fluids used. The degree of accuracy of the PRT results could be improved with further validation with other tests at higher temperatures. However, as was observed in chapter 5, the main difference between OBM and WBM are the effects of pressure, which are more pronounced for OBM than WBM. For WBM the effect of pressure was very small but was highly affected by temperature increase. Therefore, the degree of accuracy of the PRT results at higher temperature applications (above 350 °F) will be expected to be higher for OBM and lower for WBM.

The investigation and development of the PRT in this research is applied to the drilling of vertical wells. However, it is envisaged that the developed PRT can be extended to study impact of fluid filtration on well inflow performance in horizontal wells. This extension is important because the drilling of horizontal wells is becoming more and more frequent throughout the world. Horizontal wells are much more susceptible to damage than their vertical counterparts due to a number of reasons, these being<sup>233,234,236</sup>:

1. Substantially longer contact time with the drilling fluid. Generally, in a vertical well drilling fluid will only be in the pay zone a matter of few days while in a horizontal well the time may be measured in weeks.
2. Most horizontal wells are not cased and remain as open hole completions, which remains a major source of permeability reduction.
3. Stimulation of horizontal wells is extremely difficult and expensive. Thus once formation damage occurs, it is usually permanent in its nature and effects.
4. In a horizontal well Figure 8.1, due to the frequent anisotropy of horizontal versus vertical permeability in many reservoir systems, the invasion pattern will be elliptical in nature, with the direction of the primary axis of the invasion ellipsoid being oriented in the direction of highest permeability.

Therefore, during the drilling of a horizontal well, it was assumed that the filtrate invasion would generate a truncated cone with the larger base near the vertical section (heel of the well), and then decrease linearly to a minimum value at the toe of the well. This assumption is based on formation exposure time to drilling fluid.

Assuming that a 2000-ft horizontal well is to be drilled and that the rate of drilling is 100-ft/day, then the first 100 ft would be exposed to 20 days of filtrate invasion, the next 100 ft to 19 days, etc., until the last 100 ft is exposed to only 1 day of filtrate invasion.

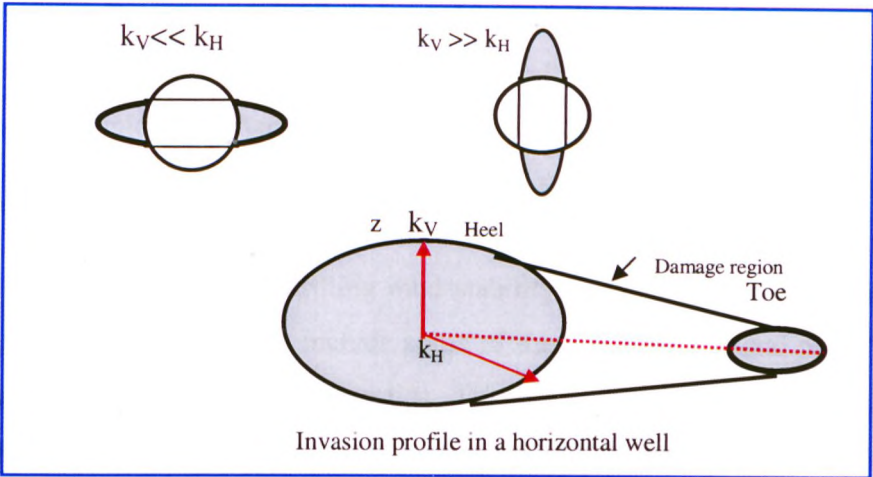


**Figure 8.1 Invasion profile in vertical versus horizontal well**

The base of this cone would be radial in the case of permeability isotropy ( $k_H = k_V$ ) and elliptical in all other cases. If the vertical permeability,  $k_V$ , were to be much smaller than the horizontal permeability,  $k_H$ , (typical anisotropy), then the cone would be elliptical, with the larger axis of the ellipse being horizontal. In the rare case when the vertical permeability may be larger, then the larger axis of the ellipse would be vertical as shown in Figure 8.1.

Further research is recommended to extend the database, which should be directed toward the improvement of the productivity tool design based on the findings of this research. The following areas are recommended for future experimental and theoretical studies:

- Natural (actual reservoir) cores with different types of lithology.
- Other types of HP-HT drilling fluids.
- Temperatures higher than 300 °F.

- Extend the PRT to incorporate the horizontal well inflow performance in terms of:
  1. Filtrate invasion profile.
  2. The shape and damage distribution profile.
  3. Estimating the damage skin factor.
- External and internal filter cakes are used to minimise fluid loss and solids invasion to a formation from drilling and completion fluids. Subsequently, the cake must be removed to increase flow area and minimise skins, especially for openhole completion. Therefore the mechanism of filter cake removal during flowback and cleanup processes requires further study on HT applications.
- OBM chemicals are more expensive than WBM. Emulsifiers are common to oil mud systems, which aid to drilling mud stability; however when filtrates from such muds invade, they may include some of these emulsifiers and result in an altering of rock wetting characteristics. Therefore, the Particle Size Analyser testing technique developed (chapter 4) requires further study for comparing the performance of different emulsifiers or designing different fluid formulations with different water droplet sizes and effects on the filtration process and de-emulsifier selection.



## REFERENCES

1. "Rheological Characterisation of HP-HT Drilling Fluids" [under Review]
2. "Characterisation of Drilling Fluid Filtration under Downhole Conditions" [under Review]
3. Mohamed B. Amish: "A Productivity Tool for Impact of Filtration on Well Performance in an HP-HT Environment", SPE/IADC 85335, Presented at the SPE/IADC Middle East Drilling Technology Conference & Exhibition held in Abu Dhabi, UAE, 20-22 October 2003
4. Mohamed B. Amish and M. B. Oyeneiyin (The Robert Gordon University) and M. H. Hodder (M-I L.L.C.): "Field Applications of a Productivity Tool for Improved Oil Recovery (IOR)", Presented at the Second International Symposium on Improved Oil Recovery Conference & Exhibition held in Libya, 12-16 September 2003
5. "Mechanisms of Formation Damage under Downhole Conditions" [under Review]
6. "Development Technique for Emulsifiers Optimisation" [under Review]
7. Chailingarian, George V and Vorabutr P.: "Drilling and Drilling Fluids" Elsevier Scientific Pub. Co, Amsterdam (New York), 1983
8. Darley, G. C. H. and Gray, G. R.: "Composition and Properties of Drilling and Completion Fluids". Fifth Edition, Gulf Publishing Company, 1988
9. "Drilling Fluid Module", Univation RGU, 2002
10. King, E. G., in personal communication to G. R. Gray, Dec. 15, 1976.
11. Gill, J. A and Carnicom, W. M.: "Offshore Louisiana New Muds and Techniques Improve Drilling Practices". World Oil, April, 1959, pp. 194-206
12. Simpson, J. P. and Sanchez, H. V.: "Inhibited Drilling Fluids-Evaluation and Utilisation". Paper 801-37C, API Pacific Coast Dist. Meeting, Los Angeles, May 11-12, 1961
13. Cartwright, R. S.: "Rotary Drilling Problems". Trans. AIME, Vol. 82, 1928, pp. 9-29

14. Lummus, J. L., Barrett, H. M. and Allen, H.: "The Effects of Use of Oil in Drilling Muds". API Drilling and Production Practice, 1935, pp. 135-145
15. Van Dycke, O. W.: "Oil Emulsion Drilling Mud". World Oil, Nov. 1950, pp. 101-106
16. Weichert, J. P. and Van Dycke, O. W.: "Effect of Oil Emulsion Mud on Drilling". Petrol. Eng., 1950, pp. B16-B38
17. Perkins, H. W.: "Oil Emulsion Drilling Fluids". API Drilling and Production Practice, 1951, pp. 349-354
18. Alexander, W. A.: "Oil Base Drilling Fluids Often Boost Production". Oil Weekly, Sept. 4, 1944, pp. 36-44
19. Dawson, R. D. and Huisman, P. H.: "Nonaqueous Drilling Fluid". U.S. Patent No. 2,223,027, Nov. 26, 1940
20. Cannon, G. E. and Williams, M.: "Weighted Nonaqueous Drilling Fluid". U.S. Patent No. 2,239,498, April 22, 1941
21. Miller, G.: "New Oil Base Drilling Fluid Facilitates Well Completion". Petrol. Eng., Sept. 1942, pp. 104-106
22. Kerston, G. V.: "Results and Use of Oil Base Drilling Fluids in Drilling and Completing Wells". API Drilling and Production Practice, 1946, pp. 61-68
23. Stuart, R. W.: "Use of Oil Base Mud at Elk Hills Naval Petroleum Reserve Number One". API Drilling and Production Practice, 1946, pp. 69-73
24. Edinger, W. M.: "Interpretation of Analysis Results on Oil or Oil-Base Mud Cores". World Oil, Dec., 1949, pp. 145-150
25. Miller, G.: "Use of Oil Base Mud to Free Stuck Pipe". Petrol. Eng., June, 1949, pp. B54-B64
26. Wright, C. C.: "Oil-Base Emulsion Drilling Fluids". Oil Gas J., March 29, 1954, pp. 88-90
27. Ives, G.: "How Shell Drilled a Super-Hot, Super-Deep Well". Petrol. Eng., March, 1974, pp. 70-78
28. Steve Devereux: "Practical Well Planning and Drilling Manual". 1998



29. Cheremisinoff, N.P.: "Liquid Filtration". Second Edition, 1998.
30. Peden, J. M.: "Reducing Formation Damage by Better Filtration Control". Offshore Services and Technology, Jan., 1982, pp. 26-28
31. Young, F.S. and Gray, K.E.: "Dynamic Filtration during Microbit Drilling". JPT, Sept. 1967, pp. 1209-1224
32. Horner, V., White, M.M., Cochran, C.d. and Deily, F.H.: "Microbit Dynamic Filtration Studies". Pet.Trans. of AIME. Vol. 210, 1957, pp. 183-189
33. Cunningham, R. A. and Eenick, J.G.: "Laboratory Study of effect of Overburden, Formation and mud Column Pressures on Drilling Rate of Permeable Formations". Pet Trans. of AIME. Vol. 216, 1959, pp. 9-17
34. Ferguson, C. K. and Klotz, J.A.: "Filtration from Mud during Drilling". JPT, Feb., Pet. Trans. of AIME. Vol. 201, 1954, pp. 29-42
35. Chelton, H. M.: "Darcy 's Law Applied to Drilling Filtration". SPE 1649, 1967
36. Krueger, R. F.: "Evaluation of Drilling Fluid Filter Loss Additives under Dynamic Conditions". JPT, Jan. 1963, pp. 90-98
37. Outmans, H. D.: "Mechanics of Static and Dynamic Filtration in Borehole". SPEJ, Sept. 1963, pp. 236-244
38. Prokop, C. L.: "Radial Filtration of Drilling Muds". Pet. Trans. of AIME. Vol. 195, 1952, pp.5-10
39. Vaussard, A., Martin, M. and Patroni, J. M.: "An Experimental Study of Drilling Fluids Dynamic Filtration". SPE 15412 Presented at the 61<sup>st</sup> Annual Technical Conference and Exhibition of the Society of Petroleum Engineers held in New Orleans. LA Oct. 5-6, 1986
40. Nowak, T. J. and Krueger, R.F.: "The Effect of Mud Filtrates and Mud Particles upon the Permeabilities of Cores". API Drilling and Production Practice, 1951, pp.164-181
41. Darley, H. C. H.: "Designing Fast Drilling Fluids". JPT, April 1965, pp. 465-470

42. Glenn, E. E., Slusser, M. L. and Huitt, J.L.: "Factors Affecting Well Productivity-I. Drilling Fluid Filtration". Pet. Trans. of AIME. Vol. 210, 1957, pp. 63-68
43. Darley, H. C. H.: "Prevention of Productivity Impairment by Mud Solids". Sept., 1975, pp. 102-110
44. Abrams, A.: "Mud Design to Minimise Rock Impairment Due to Particle Invasion". JPT, May 1977, pp. 586-592
45. Krueger, R. F., and Vogel, L.C.: "Damage to Sandstone Cores by Particle from Drilling Fluid". API Drilling Production Practice., 1954, pp. 158-171
46. Schechter, R. S.: "Oil Well Stimulation". Prentice Hall, Englewood Cliffs, NJ, 1992
47. Carman, P. C.: "Fluid Flow through Granular Beds". Transaction Institute of Chemical Engineers, V. 15, 1937, pp. 150-166
48. Maroudas, A.: "Particles Deposition in Granular Filter Media-2". Filtration and Separation, V. 3, No. 2, Mar/Apr. 1966, pp. 115-121
49. Muecke, T. W.: "Formation Fines and Factors Controlling Their Movement in Porous Media". Soc. Petrol. Eng. JPT, Feb. 1979, pp. 144-150
50. Donaldson, E. C., B. A. Baker.: "Particle Transport in Sandstone" SPE 6905 Presented at 52<sup>nd</sup> Annual Technical Conference of SPE, Denver, CO., Oct. 9-12, 1977
51. Herzig, J. P., D. M. Leclerc, and P. Legoff.: "Flow of Suspension through Porous Media Application to Deep Filtration". Sixth State-of-the-Art Symposium, sponsored by Industrial and Engineering Chemistry and the American Chemical Society, Washington, DC, June 9-11, 1969, pp. 129-157
52. Barkman, J. H. and Davidson, D. H.: "Measuring Water Quality and Predicting Well Impairment". JPT, July 1972, pp. 865-873
53. Eylander, J. G. R.: "Suspended Solids Specifications of Water Injection from Core flood Tests". SPE 16256 Presented at SPE International Symposium on Oilfield Chemistry, SanAntonio, TX, Feb. 4-6, 1987



54. Vetter, O. T., V. Kandarpa, M. Stratton and E. Veith.: "Particle Invasion into Porous Medium and Related Injectivity Problems". SPE 16255 Presented at SPE International Symposium on Oilfield Chemistry, San Antonio, TX, Feb. 4-6, 1987, pp. 101-120
55. Reg, S. D. and H. S. Fogler.: "Network Model for Straining Dominated Particle Entrapment in Porous Media". Chemical Eng. Science, V. 42, No. 7, 1987, pp. 1553-1564
56. Kumar, T. and A. C. Todd.: "A New Approach for Mathematical Modelling of Formation Damage due to Invasion of Solid Suspensions". SPE 18203 Presented at the 63<sup>rd</sup> Annual Technical Conference of SPE, Houston, TX, Oct. 2-5, 1988
57. Ershaghi, I., R. Hashemi, S. C. Coathien, and D. Abdassah.: "Injectivity Losses under Particle Cake Build-up and Particle Invasion". SPE 15073 Presented at the 56<sup>th</sup> California Regional Meeting of SPE, Oakland, Apr. 2, 1986
58. Pautz, J. F. and Crocker, M. E.: "Relating Water Quality and Formation Permeability to Loss of Injectivity". SPE 18888, 1989
59. Zhang, N. S., Somerville, J. M., and A. C. Todd.: "An Experimental Investigation of the Formation Damage Caused by Produced Oily Water Injection". SPE 26702, 1993
60. Van Velsen, J. F. G. and Leelooijer, K.: "Impairment of a Water Injection Well by Suspended Solids: Testing and Prediction". SPE 23822, 1992
61. Cargnel, R. D. and Luzardo, J. P.: "Particle Size Distribution Selection of CaCO<sub>3</sub> Drill-In Fluids: Theory and Applications". SPE 53937, 1999
62. Oyenevin, M. B., Peden, J. M., Ali Hosseini, and Ren, G.: "Factors to Consider in The Effective Management and Control of Fines in High Permeability Sands". SPE 30112, 1995
63. Porter, K. e.: "An Overview of Formation Damage". JPT, Aug., 1989, pp. 780-786

64. Krueger, R. F.: "An Overview of Formation Damage and Well Productivity in Oilfield Operation". JPT, Feb., 1986, pp. 131-152
65. Amaefule, J. O. and Kersey, D. G.: "Advances in Formation Damage Assessment and Control Strategies". Core Laboratories, Div. of Western Atlas International, Houston, TX, Nov. 1988
66. Economides, M. J. O. and Nolte, K. G.: "Reservoir Stimulation". Schlumberger Education Services, Houston, TX, 1987
67. Keelan, D. K. and Koef, E. H.: "The Role of Cores and Core Analysis in Evaluation of Formation Damage". Soc. Petrol. Eng. JPT, May 1977, pp. 482-490
68. Gruesbeck, C. and Collins, R. E.: "Particle Transport through Perforations". Soc. Petrol. Eng. J., Dec. 1982, pp. 857-865
69. Khilar, K. C. and Fogler, H. S.: "Water Sensitivity of Sandstones". Soc. Petrol. Eng. J., Feb. 1983, V. 23, No. 1, pp. 55-64
70. Sharma, M. M. and Yortsos, Y. C.: "Transport of Particulate Suspensions in Porous Media: Model Formulation". AIChE J., V. 33, No. 10, 1987, pp. 1,636-1,643
71. Sharma, M. M. and Yortsos, Y. C.: "Fines Migration in Porous Media". AIChE J., V. 33, No. 10, 1987, pp. 654-662
72. Sharma, M. M. Yortsos, Y. C. and Handy, L. L.: "Release and Deposition of Clays in Sandstones". Soc. Petrol. Eng. SPE 13562, International Symp. On Oilfield and Geothermal Chem., Phoenix, AR, April 9-11, 1985. pp. 125-135
73. Vitthal, S., Gupta, A. and Sharma, M. M.: "A rule based System for Estimating Clay Distribution, Morphology, and Distribution in Reservoir Rocks". Soc. Petrol. Eng. SPE 16870, Oct. 1987
74. Civan, F. and Knapp, R. M.: "Effect of Clay Swelling and Fines Migration on Formation Permeability". Soc. Petrol. Eng. SPE 16235, March 1987
75. Gabriel, G. A. and Inamdar, G. R.: "An Experimental Investigation of Fines Migration in Porous Media". SPE 12168, 58<sup>th</sup> SPE Annual Meeting, San Francisco, CA, Oct. 1983



76. Egbogah, E. O.: "An Effective Mechanism for Fines Movement Control in Petroleum Reservoirs". Canadian Institute of Mining 84-35-16, Jun. 1984, Paper No. 164
77. Donaldson, E. C. and Baker, B. A.: "Particle Transport in Sandstones". SPE 6905 Presented at the 53rd Annual Fall Technical Conference and Exhibition of the Society of Petroleum Engineers of AIME, held in Denver, Colorado, Oct. 9-12, 1977
78. Davidson, D. H.: "Invasion and Impairment of Formation by Particulates". SPE 8210 Presented at the 54th Annual Fall Technical Conference and Exhibition of the Society of Petroleum Engineers of AIME, held Los Vegas, Sept.. 23-26, 1979
79. Hayward, J. T.: "Cause and Cure of Frozen Drill Pipe and Casing". API Drilling and Production Practice, 1937, pp. 8-20
80. Helmick, W. E. and Longley, A. J.: "Pressure Differential Sticking of Drill Pipe, and How It Can be Avoided". API Drilling and Production Practice, 1957, pp. 55-60
81. Bushnell-Waston, Y. M, and Panesar, S. S.: "Differential Sticking Laboratory Tests Can Improve Mud Design". SPE 22549 Presented at the 66<sup>th</sup> Annual Technical Conference and Exhibition of the SPE, Dallas, U.S.A., TX, October 6-9, 1991
82. Ulio, J. and Chiaramente, J.: "Effect of Invasion on the Comensated Neutron Log (CNL) in Gas and Liquid- Filled Formations". SPE 12137, 1983
83. Holbrook, P.: "The Effect of Mud Filtrate Invasion on the EWR Log-Acase History". SPWLA 26<sup>TH</sup> Ann. Logging Symp., June 17-20, 1985
84. Pheleps, G. D, Peden. J.M. and Stewart, G.: "The Effect of Filtration Invasion and Formation Wettability on Repeat Formation Tester Measurements". SPE 12962, 1974
85. Pheleps, G. D, Peden. J.M. and Stewart, G.: "The Analysis of the Invaded Zone Characteristics and their Influence on Wireline Log and Interpretation". SPE 13287, 1984

86. Fordham, E.J, Allen, D.F., Ladva, H.K.J. and Alderman, N.J."The Principle of a Critical Invasion Rate and its Implications for Interpretation". Presented at the 66<sup>th</sup> Annual Technical Conference and Exhibition of the SPE, Dallas, TX, Oct. 6-9, 1991
87. Dewan, J.T. and Chenevert, M.E.:"Mudcake Build-up and Invasion in Low Permeability Formations; Application to Permeability Determination by measurement while Drilling". SPWLA/CWLS Symposium, Calgary, Alberta, June 13-16, 1993
88. Cannon, D.E and Kienitz, C.:"Interpretation of Asymmetrically Invaded formations with Azimuth; and Radial LWD (Logging while Drilling) Data". 40<sup>th</sup> Annual SPWLA Logging Symposium (Oslo, Norway, 30/5-3/6/1999). Trans. PAP no. G, 1999 (12 PP, 24 refs)
89. Peeters, M. and Gomes, R.:"Invasion in Space and Time". 40<sup>th</sup> Annual SPWLA Logging Symposium (Oslo, Norway, 30/5-3/6/1999). Trans. PAP no. A, 1999 (9 PP, 24 refs)
90. Marshall, D.M. and Coates, G.:"Laboratory MRI Investigation in the Effects of Invert Oil muds on Primary MRI log determinations". SOC Core Annual Int. Symp. (Calgray, can., 9/8-10/1997) Proc. PAP no. SCA-9701, 1997 (11 PP, 11 REFS)
91. Borah, N.M., Mallick, R.k., Choudhri, B. and Rathore, Y.S.:"Mud Filtrate Invasion Profile-its Influence on Wireline Logs and Hydrocarbon Producibility: A case Study". SPE et al India Oil and Gas Conference (New Delhi, India, 4-9/7/1998) Proc pp. 119-133, 1999 (SPE no. 39510,6 Refs)
92. Han, D.H. and Batzle, M.:"Fluid Invasion Effects on Sonic Interpretation". 67<sup>th</sup> Annual Seg. Int. MTG (Dallas, 7-11/2/1997) Expanded ABSTR BIOGR Vol. 1, pp. 298-300,1997 (ISSN 10523812, PAP no. BH<sub>3</sub> 4, 9 REFS)
93. Ravi, K.M., Beirute, R.M. and Covington, R.L.:"Erodability of Partially Gelled Drilling Fluid Filter Cake". SPE 24571 Presented at the 67<sup>th</sup> Annual Technical Conference and Exhibition of the SPE, Washington, DC, Oct. 4-7, 1992



94. Sherwood, J. D.: "Formation of a Cement Filter Cake above a Comactiple Mudcake". Chem. Eng. SCI., Vol. 48, 1985, pp. 2767-2775
95. Bannister, C.E. and Lwson, V.m.: "Role of Cement Fluid Loss in Wellbore Completion". SPE 14433 Presented at the 60<sup>th</sup> Annual Technical Conference and Exhibition of the SPE, Las Vegas, NV, Sept. 22-25, 1985
96. Gruesbeck, C. and Collins, R. E.: "Entrainment and Deposition of Fine Particles in Porous Media". Soc., Petrol. Eng. J., Dec. 1982, pp. 847-855
97. Wojtanowicz, A., K., Krilov, Z. and Langlinalis, J. P.: "Syudy on the Effect of Pore Blocking Mechanisms on Formation Damage". Soc. Petrol. Eng. SPE 16233, Production Operations Symp. Oklahoma City, March 8-10, 1987
98. Yan Bingo, M. B. Oyeneyin, and J. M. Peden.: "Investigation of Pore Blocking Mechanism in Gravel Packs in the Management and Control of Fines Migration", SPE 27342, 1994
99. Van Everdingen, A. F., and Hurst, W., "The Application of the Laplace Transformation to Flow Problems in Reservoirs", TRANS. AIME, 186:305-324, 1949
100. Fraser, L. J., Ried, P., Williamson, D., and Enriquez, F.: "Mechanistic Investigation of the Formation Damaging Characteristics of Mixed Metal Hydroxide Drill-In Fluids and Comparison with Polymer-Base Fluids", SPE 30501 Presented at the SPE Annual Technical Conference and Exhibition held in Dallas, U.S.A., October 22-25, 1995
101. T. Azizi, H. Chen and S. S. Rahman: "Management of Wellbore Stability & Formation Damage by Improved Drilling Mud Design", IADC/SPE 47786 Presented at the 1998 IADC/SPE Asia Pacific Drilling Conference Held in Jakarta, Indonesia, 7-9 September 1998
102. Liu. X. and Civan. F.: "Formation Damage and Skin Factor Due Filter Cake Formation and Fines Migration in the Near-wellbore Region", SPE 27364 presented at the SPE Int. Symposium on Formation Damage Control, Lafayette, LA, Feb. 9-10, 1994

103. Scott Lane, H.: "Numerical Simulation of Mud Filtrate Invasion and Dissipation", SPWLA 34<sup>th</sup> Annual Logging Symposium, June 13-16, 1993.
104. Semmelbeck, M.E., Dewan, J.T. and Holditch, S.A.: "Invasion Based Method Estimating Permeability from Logs", SPE 30581 presented at the SPE ATC&E, Dallas 22-25 Oct. 1995
105. Permadi, P. and Wibowo, W.: "Effects of Non-uniform Skin Distribution on Horizontal Well Inflow Performance", SPE 68952 presented at the SPE European Formation Damage Conf. The Hague, The Netherlands, 21-22 May 2001
106. Menour, H., Al-Majed, A. and Hassan, S.: "Effect of Formation Damage, Length and Reservoir Thickness on the inflow Performance of Horizontal Wells", SPE 59356 presented at the 2000 SPE/DOE Improved Oil Recovery Symp. Tulsa OK, 3-5 April 2000
107. Longeron, D. G., Alfenore, J., and Salehi, N.: "Experimental Approach to Characterise Drilling Mud Invasion, Formation Damage and Cleanup Efficiency in Horizontal Wells with Openhole Completions", SPE 58737 Presented at the 2000 SPE International Symposium on Formation Damage, Lafayette, 23-24 Feb. 2000
108. Zain, Z. M., and Sharma, M. M.: "A Simple Model for Filter Cake Lift-off", Oil and Gas Journal, Nov 1, 1999
109. Ryan, D. F., Brown, S. V., and Burnham, M. P.: "Mud Clean Up in Horizontal Wells: A major Joint Industry Study". SPE 30528 Presented at the SPE Annual Technical Conference & Exhibition held in Dalas, U.S.A., 22-25 October, 1995
110. Bailey, L., Meeten, G., Way, P., and L Allore, F.: "Filtercake Integrity and Reservoir Damage". SPE 39429 Presented at 1998 SPE International Symposium on Formation Damage Control, Lafayette, Feb. 18-19
111. Zulkeffeli, M. Z., and Sharma .M. M.: "Cleanup of Wall-Building Filter cakes". SPE 56635 Presented at Presented at the SPE Annual Technical Conference & Exhibition held in Houston, Texas, 3-6 October, 1999



112. Davison, J.M., Jones, M., Shuchart, C. E., and Gerard, C.: "Oil-Based Muds Reservoir: their Performance and Cleanup Characteristics". SPE 58798 Presented at the 2000 SPE International Symposium on Formation Damage Held in Lafayette, Louisiana, 23-24 Feb. 2000
113. Rana, S. R., and Sharma, M.: "The relative Importance of Solids and Filtrate Invasion on the Flow Initiation Pressure". SPE 68949 Presented at the SPE European Formation Damage Conference held in the Hague, The Netherlands, 21-22 May 2001
114. Civan, F.: "Evaluation and Comparison of Formation Damage Models". SPE 23787, Proceedings of the International Symposium on Formation Damage Control, 26-27 Feb. 1992, Lafayette, LA, pp. 219-236
115. Civan, F.: "A Multi-Purpose Formation Damage Model". SPE 31101, Proceedings of the International Symposium on Formation Damage Control, 14-15 Feb. 1996, Lafayette, LA, pp. 311-326
116. Larsen, H.D.: "Determination the Filtration Characteristics of Drilling Muds- Part I and Part II". The Petroleum Engineer, Sept./Nov. 1938, pp. 42-48, 50-59
117. Arthur, K. G. and Peden, J. M.: "The Evaluation of Drilling Fluid Filter Cake Properties and Their Influence on Fluid Loss". SPE 17617 Presented at the SPE international meeting on Petroleum Engineering, held in Tianjin, China, Nov. 1-4, 1988
118. Jones, P.H. and Babson, E.C.: "Evaluation of Rotary Drilling Muds". API Drilling and Production Practice, 1935, pp. 22-33
119. Hall, C. D., and Dollaride, F. E.: "Effects of Fracturing Fluid Velocity on Fluid Loss Agent Performance". J.Pet.Tech., May, 1964, p.555
120. Beeson, C. M. and Wright, C. C.: "Loss of Mud Solids to Formation Pores". The Petroleum Engineer, Aug. 1952, pp. B40-B52
121. Peden, J. M., Avalos, M. R. and Arthur, K. G.: "The Analysis of the Filtration Under Dynamic and Static Conditions". SPE 12503 Presented at the Formation Control Symposium held in Bakersfield, CA, Feb. 13-14, 1984

122. Simpson, J. P.: "Drilling Fluid Filtration under Simulated Downhole Conditions". SPE 4779, First SPE Formation Damage Control Symposium, New Orleans, L.A., Feb., 1974
123. Simpson, J. P.: "A New Approach to Oil Base Muds for Lower-Cost Drilling". JPT, May 1979. pp. 643-650
124. Bezemer, C. and Havenaar, I.: "Filtration Behaviour of Circulating Drilling Fluids". SPEJ, Dec. 1966, pp. 292-298
125. Fisk, J. V. and Jamison, D.E.: "Physical Properties of Drilling Fluids at High Temperatures and Pressure". IADC/SPE 17200 Presented at the 1988 IADC/SPE Drilling Conference held in Dallas, Texas, Feb. 28-Mar 2, 1988. pp.511-518. Also on SPE Drilling Engineering, Dec. 1989. pp. 314-346
126. Williams, M.: "Radial Filtration of Drilling Muds". Pet. Trans. of AIME. Vol. 136, 1940, pp. 57-69
127. Gates, G. L and Bowie, C. P.: "Correlation of Certain Properties of Oil Well Drilling Fluids with Particle Size Distribution". Unit States Bureau of Mines, R.I. 3645, 1942, PP.1-22
128. Milligan, D. I. and Weintritt, D.J.: "Filtration of Drilling Fluids at Temperature of 300 ° F and Above". API Drilling and Production Practice, 1961, pp. 42-48
129. Schremp, F. W. and Johnson, V. L.: "Drilling Fluid Filter Loss at High Temperature and High Pressures". Pet. Trans. of AIME. Vol. 195, 1952, pp. 157-162
130. Byck, H.T.: " Effects of Temperature on Plastering Properties and Viscosity of Rotary Drilling Muds". Pet. Trans. of AIME. Vol. 136, 1940, pp. 165-173
131. Byck, H. T.: "The Effect of Formation Permeability on the Plastering Behaviour of Mud Fluids". API Drilling and Production Practice, 1940. Also in Oil and Gas Journal, Vol. 39, No. 3, May 30, 1940, pp. 50-51
132. Williams, M. and Cannon, G.E.: "Evaluation of Filtration Properties of Drilling Muds". The Oil Weekly, June 20, 1938, pp. 25-32
133. Peden, J. M., Avalos, M. R. and Arthur, K. G.: "The Analysis of the Dynamic Filtration and Permeability Impairment Characteristics of Inhibited Water



- Based Muds". SPE 10655 Presented at the SPE Formation Control Symposium, held in Lafayette, LA, March 24-25, 1982
134. Dickey, G. D., and Bryden, C. L.: "Theory and Practice of Filtration". Reinhold Publishing Corp., New York, 1946
  135. Wyant, R. E., Reed, R. L. Sifferman, T. R. and Wooten, S. O.: "Dynamic Fluid Loss Measurement of Oil Mud Additives". SPE 14246 Presented at the 60<sup>th</sup> Annual Technical Conference and Exhibition of the Society of Petroleum Engineers held in Las Vegas, NV September 22-25, 1985
  136. Chesser, B. G., Clark, D.E. and Wise, W. V.: "Dynamic and Static Filtrate-Loss Techniques for, Monitoring Filter-Cake Quality Improves Drilling-Fluid Performance". SPE 20439 Presented at the 1990 SPE Annual Technical Conference and Exhibition held in New Orleans, Sept. 23-26, SPE Drilling and Completion, Sept. 1994
  137. Havenaar, I.: "Mud Filtration at the Bottom of the Borehole". Pet. Trans. of AIME. Tech. Note 337, 1956, pp. 312
  138. Bizanti, M.: "Mud Filtration while Drilling". Okla. Univ. et al. Drilling Muds Nat Conf., Proc., Norman, Okla, May, 1986, pp. 44-62
  139. Plank J. P. and Gossen, F. A.: "Visualisation of Fluid Loss Polymer in Drilling Mud Filter Cakes". SPE 19534 Presented at the 64<sup>th</sup> Annual Technical Conference and Exhibition of the Society of Petroleum Engineers held in San Antonio, TX, Oct. 8-11, 1989
  140. Fisk, J. V. and Shaffer, S. S.: "The Filterability of Drilling Fluids". SPE 20438 Presented at the 65<sup>th</sup> Annual Technical Conference and Exhibition of the Society of Petroleum Engineers held in New Orleans. LA, Sept. 23-26, 1990
  141. Warren, B. K. and Smith, T. R.: "Static and Dynamic Fluid-Loss Characteristics of Drilling Fluids in a Full-Scale Wellbore". SPE 26069 Presented at the Western Regional Meeting held in Anchorage, Alaska, U.S.A., May 26-28, 1993
  142. Di Jiao and M.M. Sharma. : "Dynamic Filtration of Invert-Emulsion Muds". SPE 24259, Sept. 1993

143. Fordham, E. J., Ladva, H. K., Hall, C., Baret, J. F. and Sherwood, J. D.: "Dynamic Filtration of Bentonite Muds Under Different Flow Conditions". SPE 18038 Presented at the 63<sup>rd</sup> Annual Technical Conference and Exhibition of the Society of Petroleum Engineers held in Houston, TX, Oct. 2-5, 1988
144. Sharma, S. M., Lall, R.C., Mathur, R. M. and Chilingarian, G. V.: "Effects of Various Drilling Fluid Additives on Water Loss and Permeability of Filter Cakes". Energy Sources, 1980, Vol. 5, Ed. 2, pp. 171-181
145. Bo, M. K., Freshwater, D. C. and Scarlett, B.: "The Effect of Particle Size Distribution on the permeability of Filter Cakes". Trans. Inst. Chem. Eng., Vol. 43, 1965, pp. T228-T232
146. Sawdon, W. A.: "Control of Colloidal Properties is Vital in Mud Conditioning". The Petroleum Engineer, Vol. 62, 1935, pp. 50-56
147. Krubein, W. C. and Monk, G. D.: "Permeability as a Function of the Size Parameters of an Unconsolidated Sand". Pet. Trans. AIME, Vol. 151, 1943
148. Gatlin, C. and Nemir, C. E.: "Some Effects of Size Distribution on Particle Bridging in Lost Circulation and Filtration Tests". JPT, June 1961, pp. 575-578
149. Mahajan, N. C. and Barron, B. M.: "Bridging Particle Size: A Key Factor in the Design of Non-Damaging Completion Fluids". SPE 8792, 4<sup>th</sup> SPE Symposium on Formation Damage Control, Bakersfield, C.A., 28-29, Jan., 1980
150. McCuire, P. L. and McFall, A. L.: "An Investigation of Low Invasion Fluids for Pressure Coring". 5<sup>th</sup> Annual U.S.D.O.E. Symposium on E.O.R., Tulsa, 1979
151. Lawhon, C. P., Evans, W. M. and Simpsom, J. P.: "Laboratory Drilling Rate and Filtration Studies of Emulsion Drilling Fluids". JPT, July 1967, pp. 943-948
152. Black, A. D., Dearing, H. L. and Di Bona, B. G.: "Effects of Pore Pressure and Mud Filtration on Drilling Rate on Permeable Sandstone". J. Petrol. Technol., Sept. 1985, pp. 1671-1681



153. Lautrec, J.D.: "Behaviour of Mud Under Borehole Conditions. SPE 4851, 1974
154. Porter, K. E.: "A Basic Scanning Electron Microscope Study of Drilling Fluids". SPE 8790, 4<sup>th</sup> SPE Symposium on Formation Damage Control, Bakersfield, C.A., 28-29, Jan. 1980
155. Fraser, L. J., Ried, P., Williamson, D. and Enriquez, F.: "Mechanistic Investigation of the Formation Damaging Characteristics of Mixed Metal Hydroxide Drill-In Fluids and Comparison with Polymer-Base Fluids". SPE 30501 Presented at the SPE Annual Technical Conference and Exhibition held in Dallas, U.S.A., October 22-25, 1995
156. Yiedan, Li, Elisabeth Rosenberg, and Argillier, J. F.: "Correlation between Filter Cake Structure and Filtration Properties of Model Drilling Fluids". SPE 28961 Presented at the International Symposium on Oilfield Chemistry held in San Antonio. TX. U.S.A., February 14-17, 1995
157. Argillier, J. F., Annie Audibert, and Daniel Longeron.: "Performance Evaluation and Formation Damage Potential of New Water-Based Drilling Formula". SPE 58484 Presented at the SPE Drilling and Completion, Dec. 1999
158. Darcy, H. P. G.: "Les Fontaines Publique de la Ville de Dijon". Vactor Delmont, Paris, 1856
159. Sperry, D. R.: "The Principles of Filtration". Met.Chem.Eng., Vol. 15, No. 4, 1916, pp. 198-203
160. Ruth, B. F., Montillon, G. H. and Montonna, R. E.: "Studies in Filtration-I and II". J Ind.Eng.Chem., Vol. 25, 1933, pp. 76-82, 153-161
161. Ruth, B. F.: "Studies in Filtration-III. Deviation of General Filtration Equations". J Ind.Eng.Chem., Vol. 27, 1935, pp. 708-723
162. Shuang Jiu Peng, and Peden, J. M.: "Prediction of Filtration under Dynamic Conditions". SPE 23824 Presented at the SPE Ind. Symposium on Formation Damage Control held in Lafayette, Louisiana, February 26-27, 1992

163. Almy, C. and Lewis, W. K.: "Factors Determining the Capacity of a Filter Press". J Ind.Eng.Chem., Vol. 4, July, 1912, pp. 528-532
164. Baker, F. P.: "A Study of the Fundamental Laws of Filtration Using Plant-Scale Equipment". J Ind. Eng. Chem., Vol. 13, 1921, pp. 610-612
165. Weber, H. C. and Hershey, R. L.: "Some Practical Applications of the Lewis Filtration Equipment". J Ind.Eng.Chem., Vol. 18, April, 1926, pp. 314-344
166. Carman, P. C.: "Fundamental Principles of Industrial Filtration". Trans. Inst. Chem. Eng. (London), Vol. 16, 1938, pp. 168-188
167. Hasseen, B. R.: "New Technical Estimates Drilling Filtrate Invasion". SPE 8971, 4<sup>th</sup> SPE Symposium on Formation Damage Control, Bakersfield, C.A., 28-29, Jan. 1980
168. Havenaar, I.: "Mud Filtration at the Bottom of the Borehole". J. Petrol. Technol. (May 1956). p. 64; Trans AIME, Vol. 207. p.312
169. Martins, A.L, Waldmann, A.T, Aragao, A.F, and Lomba, R.F: "Predicting and Monitoring Fluid Invasion in Exploratory Drilling". SPE 86497, SPE Symposium on Formation Damage Control, USA, 18-20 February 2004
170. API "Recommend Practice on the Rheology and Hydraulics of Oil-Well Drilling Fluids" 13D/ Published by American Petroleum Institute, Washington, Third Addition, June 1, 1995
171. API "Recommended Practice Standard Procedure for Oil Based Drilling Fluids" 13B-2/ Published by American Petroleum Institute, Washington, Third Addition, February 1998
172. API "Recommended Practice Standard Procedure for Laboratory Testing Drilling Fluids". Supplement 2 to API Recommended Practice 13I/ Published by American Petroleum Institute, Washington, June 1997
173. Nigel, Evans, et al.: "High Performance Emulsifiers for Synthetic Based Muds", SPE 63101, 2000
174. Hanson, P. M., et al.: "Investigation of Barite "Sag" in Weighted Drilling Fluids in Highly deviated Wells", SPE 20423, 1990



175. Bern, P. A., et al.: "Barite Sag: Measurement, Modelling and Management", SPE/IADC 47784, 1998
176. M-I Drilling Fluid Engineering Manual, 1991
177. Erhu Gao, Martin Booth, and Nail MacBeath. : "Continued Improvements on High-Pressure/High Temperature Drilling Performance on Wells With Extremely Narrow Drilling Windows-Experiences From Mud Formulation to Operational Practices, Shearwater Project". IADC/ SPE 59175, New Orleans, U.S.A., February 2000
178. Di Jio and M.M. Sharma: "Dynamic Filtration of Invert-Emulsion Muds", SPE 24759, 1992
179. Djebbar Tiab and Erle C. Donaldson.: "Petrophysics: Theory and Practice of Measuring Reservoir Rock and Fluid Transport Properties", Gulf Publishing Company, Houston, 1996
180. Guyod, H.: "Fundamental Data for The Interpretation of Electric Logs", Oil Weekly, 115, 38, October 1944
181. Deveton, J. H.: "Log Analysis of Subsurface Geology: Concepts and Computer Methods", New York, John Wily, 1986
182. Unalmiser, S and Funk, J.: "Engineering Core Analysis", Distinguished Author Series, JPT, 106-114, April 1998.
183. Hilchie, D. W.: "The Effect of Pressure and Temperature on The Resistivity of Rocks", D. Phil. Thesis, The University of Oklahoma, 1964
184. Pirson, S.: "Oil Reservoir Engineering", Michigan, MacGraw-Hill, 1958
185. Asquith, G. B.: "Basic Well Log Analysis for Geologists", AAPG, Tulsa, 1982
186. Dixon, J. R. and Marek, B. F.: "Properties of Bimodal Pore Size Distribution on Electrical Properties of Some Middle Eastern Limestone", SPE 20601, 1990
187. Forchheimer, P.: "Hydrolik", Teubner, Leipner and Berlin 116-118, 1914
188. Erle C. Donaldson and Byron A. Baker.: "Particle Transport in Sanstones", SPE 6905

189. Ergun, S.: "Fluid Flow Through Packed Column", Chemical Engineering Progress, 48, 2, 89-94, 1952
190. Dacun Li, Robert K. Svec, Tom W. Engler, and Reid B. Grigg. : "Modelling and Simulation of The Wafer Non-Darcy Flow Experiments", SPE 68822, 2001
191. Jones, S. C.: "Using The Inertial Coefficient,  $\beta$ , to Characterise Heterogeneity in Reservoir Rock", SPE 16949, 1987
192. Noman, R. and Archer, J. S.: "The Effect of Pore Structure on Non-Darcy Gas Flow in Some Low Permeability Reservoir Rocks", SPE, 1987
193. Geertsma, J.: "Estimating The Coefficient of Inertial Resistance in Fluid Flow Through Porous Media", SOC. Pet. Eng., 445-450, Oct. 1974
194. Tek, M. R., Coats, K. H. and Katz, D. L.: "The Effect of Turbulence on The Flow of Natural Gas Through Porous Reservoirs", JPT, 799-806, July 1962.
195. Firoozabadi, A. and Katz, D. L.: "An Analysis of High-Velocity Gas Flow Through Porous Media", JPT, 211-216, Feb. 1979
196. Coles, M. E., and Hartman, K. J.: "Non-Darcy Measurements in Dry Core and the Effect of Immobile Liquid", SPE 39977, Mrch 1998
197. Janicek, J. D. and Katz, D. L.: "Application of Unsteady State Gas Flow Calculations", Proc., U. of Michigan Research Conference, June 20, 1955
198. Liu, X., Civan, F., and Evans, R. D.: "Correlation of The Non-Darcy Flow Coefficient", JCPT 34, No. 10, 50-54, Dec. 1995
199. F. Thauvin and K. K. Mohanty: "Network Modelling of Non-Darcy Flow Through Porous Media", Transport in Porous Media 31, 19-37, 1998
200. Cooper, J. W., Wang, x., and Mohanty, K. K.: "Non-Darcy-Flow Studies in Anisotropic Porous Media", SPEJ, 334-341, Dec. 1999
201. David S. Marshall, Russel Gray and Michael T. Byrn: "Development Practice for Formation Damage Testing", SPE 38154, June 1997
202. David S. Marshall, Russel Gray and Michael T. Byrn: "Return Permeability Comparative Study", SPE 54763, June 1999



203. Chhabra R.P. and Richardson J. F.: "Non-Newtonian Flow in the Process Industries, Fundamentals and Engineering Applications", ISBN 0 7506 3770 6, 1999
204. Bingham, E. C.: "Fluidity and Plasticity". McGraw-Hill Book Co., New York, 1922
205. Govier, G. W. and Aziz, K.: "The Flow of Complex Mixtures in Pipes". Van Nostrand-Reinhold, New York, 1972
206. Zamora, M. and Bleier, R.: "Prediction of Drilling Mud Rheology Using a Simplified Herschel-Bulkley Model" Journal of Pressure Vessel Technology (Transactions of the ASME), August 1977, pp. 485-490
207. Zamora, M. and David, L., Lord: "Practical Analysis of Drilling Mud Flow in Pipes and Annuli". Paper SPE 4976, 1974
208. Hemphill, T., Wellington Campos and Ali Pilehvair: "Yield Power Law Model More Accurately Predicts Mud Rheology". Oil and Gas Journal, 23 Aug. 1993
209. Robertson, R. E. and Stiff, H. A. jr.: "An Improved Mathematical Model for Relating Shear Stress to Shear Rate in Drilling Fluids and Cement Slurries". Society of Petroleum Engineers Journal, Vol. 16, no 1, 1976
210. Casson, N.: "In: Rheology of Disperse Systems". C.C Mill (Ed). Pergamon Press, 1959
211. Adam, T. Bourgoine Jr, Martin, E. Chevenert, Keith. K. Meillheim and F. S. Young Jr.: "Applied Drilling Engineering". Society of Petroleum Engineers, Richardson (Texas), 1986
212. Bailey, W. J. and Weir, I. S.: "Investigation of Methods for Direct Rheological Model Parameter Estimation". J. Pet. Sci. and Eng., 21, Nos. 1-2, pp. 1-13
213. "Drilling Technology Manual". The Robert Gordon University, 2003
214. Jensen, T. B. and Sharma, M. P.: "Study of Friction Factor and Equivalent Diameter Correlations for Annular Flow of Non-Newtonian Drilling Fluids". J. Energy Res. Tech., 109, pp. 200-205
215. Healy, M. J. R.: "The Use of  $R^2$  as a Measure of Goodness of Fit". J. Royal Statistical Soc. A 147, Part 4, pp. 608-609

216. McMordie, W. C., Bennett, R. B., and Bland, R. G.: "The Effect of Temperature and Pressure on Viscosity of Oil Base Muds". SPE 4974, Houston, U.S.A., 1974
217. De Wolfe, R. C., Coffin, G. B., and Byrd, R. V.: "Effects of Temperature and Pressure on Rheology of Less toxic Oil Muds". SPE 11892, Aberdeen, U.K., 1983
218. Politte, M. D.: "Invert Oil Mud Rheology as a Function of Temperature and Pressure". SPE/IADC 13458, New Orleans, U.S.A., 1985
219. Bailey, T.J., Bern, P. A., and McEwan, F.: "Low-Toxicity Oil Muds; A Knowledge of downhole Rheological Behaviour Assists Successful Field Application". SPE Drilling Engineering, 1986, 107
220. Houwen, O. H., and Geehan, T.: "Rheology of Oil-Base Muds". SPE 15416, New Orleans, U.S.A., 1986
221. Gucuyener, I. H.: "A Rheological Model for Drilling Fluids and Cement Slurries". SPE 11487, Manama, Bahrain, 1983
222. Wanneng, S., Jianping, C., and Zhenxue, L.: "Comparison of Rheological Models in High Shear Rate Range and Experimental Relationship between Penetration Rate and High Shear Viscosities". SPE 14858, Beijing, China, 1986
223. Alderman, N. J., Gavigent, A., Guillot, D., and Maitland, G. C.: "High Temperature, High Pressure Rheology of Water Based Muds". SPE 18035, Houston, U.S.A., 1988
224. Davison, J. M., Clary, S., Saasen, A., Allouche, M., Bodin, D., and Nguyen, V-A.: "Rheology of Various Drilling Fluid Systems Under Deepwater Drilling Conditions and the Importance of Accurate Predictions of Downhole Fluid Hydraulics". SPE 56632, Houston, U.S.A., 1999
225. Rommetveit, R., and Bjorkevoll, K.S.: "Temperature and Pressure Effects on Drilling Fluid Rheology and ECD in Vert Deep Wells". SPE/IADC 39282, Bahrain, 1997



226. Romero, J., and Touboul, E.: "Temperature Prediction for Deepwater Wells; A Field Validated Methodology". SPE 49056, New Orleans, U.S.A., 1998
227. Kihan, M. A, Jilani, S. Z, Menouar, H. and Al-Majed, A. A.: " A Non-Destructive Method for Mapping Formation Damage", Elsevier Science B. V. 2001
228. Bryan F. J. Manly.: "Multivariate Statistical Methods", A Primer 2<sup>nd</sup> Addition, 1997
229. David A. Aaker.: "Multivariate Analysis in Marketing: Theory and Application", 2<sup>nd</sup> 1975
230. "Users Guide 2: Data Analysis and Quality Tools", Minitab Statistical Software, 1998
231. Dearing, H. L and Ali, S, A.: "Drill-in fluid Selection Crucial To Well Productivity", Petroleum Engineer International, Jan. 1996, 21-25
232. Ali Ghalambor and M. J. Economides: "Formation Damage Abatement: A Quarter-Century Perspective", SPE no. 58744, Feb. 2000
233. Michael J. Economides, A. Daniel Hill, and Christine Ehlig-Economides: "Petroleum Production systems", 1994
234. Michael G and Curtis H Whitson "Well Performance", 1998
235. Personnel Communication with Dowel Schlumberger Company, Dyce, Aberdeen
236. Joshi, S.D.: "A Review of Horizontal Well and Drainhole Technology", SPE no. 16868, September 1987
237. Brant Bennion, D., Brent Thomas, F. and Ronald F. Bietz: "Formation Damage and Horizontal Wells - A Productivity Killer?", SPE no. 37138, November 1996

## **APPENDIX A**

- Description of Testing Facilities
- Tabular and Graphical Permeability Measurement
- HP-HT Filtration Testing Procedure
- Static and Dynamic Filtration Testing Results for WBM
- Static and Dynamic Filtration Testing Results for OBM
- Initial Permeability Testing Procedure
- Return Permeability Testing Procedure
- HP-HT Fann 70 Viscometer Testing Procedure
- HP-HT Fann 70 Viscometer Readings for WBM and OBM
- Particle Size Distribution Testing Procedure

#### A4.1.1.4 DESCRIPTION OF TESTING FACILITIES

The highlighted major testing equipment items such as dynamic filtration rig, HP-HT Fann-70 Rheometer, formation damage equipment and Malvern Mastersizer Micro Plus were described in chapter 4 and other testing equipment is mentioned below.

**Drilling fluid testing equipment and application**

EQUIPMENT	APPLICATION
Silverson Mixer model (L 4RT-A)	mixing WBM and OBM
Malvern Mastersizer Micro Plus (MAF-5001)	measure particle size distribution
LP-LT Fann-35A Viscometer	measure fluid rheology
Titration Kit	measure chemical properties
pH Meter	measure pH of WBM
Pressurised Mud Balance	measure mud density
Retort Kit	measure water, oil and solids percentage
Electric Stability Tester	measure stability of water in oil emulsion
Roller Oven	measure stability at HP-HT
Density Meter model (DMA 38)	measure density of mud and filtrate
HP-HT Fann-70 Viscometer	measure HP-HT fluid rheology
Modified Dynamic Filtration rig	measure dynamic filtration
Formation Damage Testing Apparatus	measure initial and return permeability
Cannon-Fenske Glass Capillary Viscometer	measure viscosity and density of filtrate
Gas Permeameter Unit model (90101)	measure gas core permeability
Conductivity Meter model (WPA CM35)	measure conductivity of brine
Precision Component Analyser model 6425	measure formation resistivity factor



## A1 LP-LT Fann-35A Viscometer

The direct indicating 6-speed viscometer is a rotational type of instrument powered by an electric motor as shown in Figure A1. Drilling fluid is contained in the annular space between two concentric cylinders. The outer cylinder or rotor sleeve is driven at a constant rotational velocity (rpm). The rotation of the rotor sleeve in the fluid produces a torque on the inner cylinder or bob. A torsion spring restrains the movement of the bob, and a dial attached to the bob indicates displacement of the bob. The steady value of the dial reading measurement is undertaken at rotor speeds of 600, 300, 200, 100, 6, and 3 rpm for fluid to be homogenous. However the fluid rheology can be measured using 6-speed Fann-35 at temperature up-to 180<sup>o</sup>F and only at 14.7-psi pressure using a thermostatically controlled viscometer cup. The equipment has been used for fluid viscosity measurement before and after hot rolling as routine tests. The field engineer use LP-LT Fann 35A Viscometer.

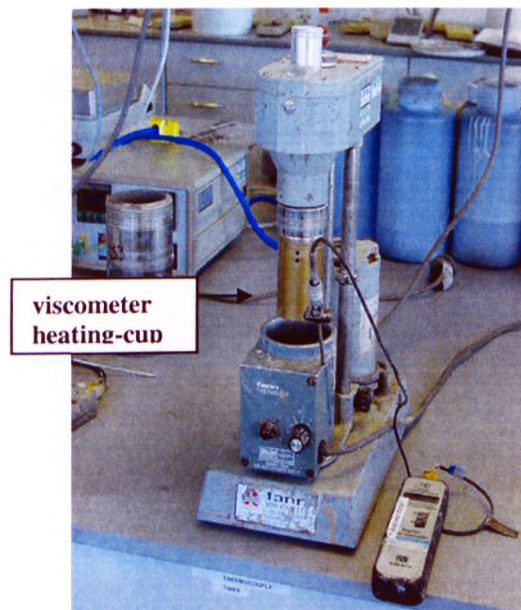


Figure A1 LP-LT Fann-35A Viscometer



### **Testing Procedure**

1. Place agitated mud sample in a thermostatically controlled viscometer cup and adjust surface of mud to scribed line on the rotor sleeve.
2. Heat the mud sample to required temperature.
3. Start the motor by placing the switch in the high-speed position with the gear shift all the way down. Wait for a steady indicator dial value, and record the 600-rpm reading.
4. Change switch to 300, 200, 100, 6, and 3 rpm respectively. Wait for a steady value and record the dial reading.

### **A2 Gas Permeameter Unit (Model No. 90101)**

The Nitrogen Gas Permeameter is an instrument, which has been designed to permit accurate and rapid measurements of gas permeability in core samples. The instrument consists of two mass flow controllers to measure and control flow of injected gas and pressure, and a transducer to monitor generated pressures (Figure A2).

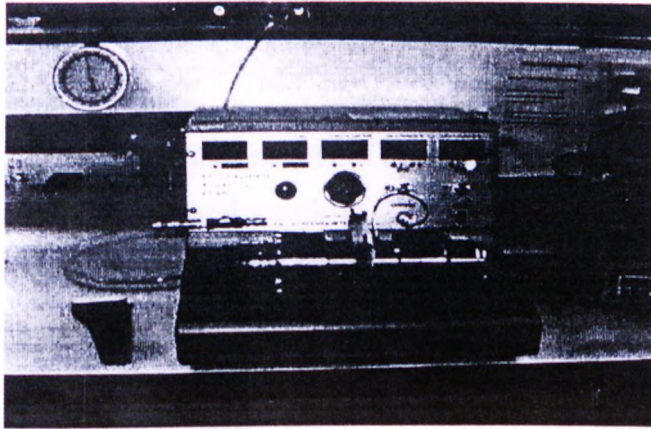


Figure A2 Gas permeameter unit

### **A3 Cannon-Fenske Glass Capillary Viscometer**

The Cannon-Fenske viscometer Figure A3 is an instrument equipped with liquid controlled temperature bath and provides a method for determination of kinematic viscosity of filtrate by measuring the time for a volume of 60 ml filtrate to flow under

gravity through a calibrated glass capillary viscometer at temperatures up to 180°F. The dynamic viscosity can be obtained by multiplying the measured kinematic viscosity by the density of the filtrate.

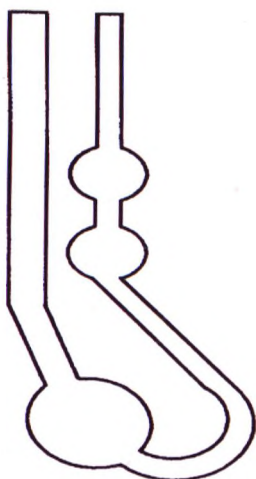


Figure A3 Cannon-Fenske viscometer



Figure A4 Retort kit

#### **A4 Retort Kit**

A retort was used to determine the quantity of liquids such as water, oil, and solids in drilling fluid. A carefully measured sample of mud is placed in a container and heated until the liquid components have been vaporised. The vapours are passed through a condenser and collected in a graduated cylinder, graduated in percent. The volume of liquid, oil and/or water is measured directly in percent Figure A4.

#### **A5 Density Meter**

The density meter model (DMA 38) Figure A5 has been used to measure filtrate and mud density.





Figure A5 Density Meter

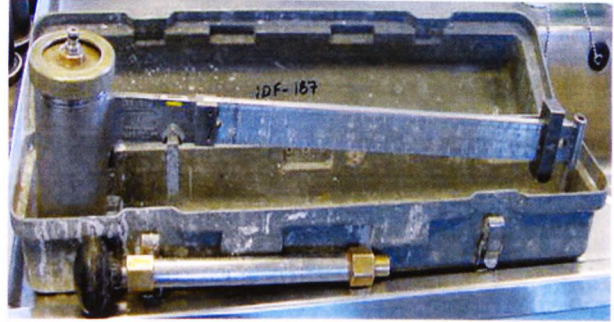


Figure A6 Mud balance

#### **A6 Pressurised Mud Balance**

The mud balance provides a simple method for accurate determination of mud density. The mud balance as shown in Figure A6, principally consists of a base on which rests a graduated arm with cup, lid, knife-edge, rider, built-in spirit level, and counter weight. The constant volume cup is affixed to one end of the graduated arm, whereas counterweight is on the opposite end.

#### **A7 PH Meter**

The recommended method for PH measurement of water based mud is with glass-electrode for accurate values Figure A7.



Figure A7 PH meter

### **A8&A9      Roller Oven**

Fluid stability under high temperature has been tested using a 350 ml pressurised cell. To prevent boiling of the liquid, the cells were pressurised with 100 psi nitrogen through the top valve connection as shown in Figure A8. The cells are rolled in an oven, for at least 16 hours at 300° F as shown in Figure A9. Meanwhile one cell can be used for a static ageing test. The cells are then cooled to room temperature, the rheological, Filtration properties, mud density, and electric stability are measured and compared to the same properties before ageing.

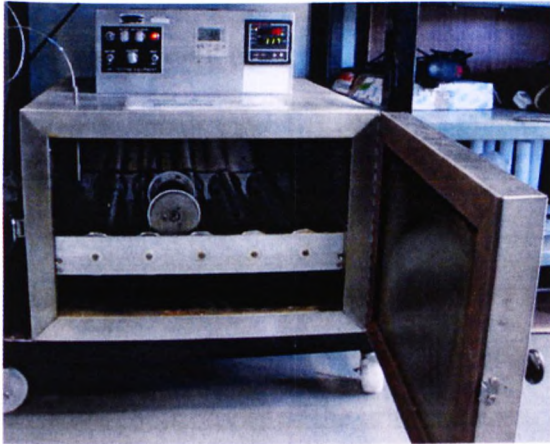


Figure A8 Roller oven



Figure A9 Pressurised cell

### **A10    Electric Stability Tester**

The stability of water in oil emulsion was tested in an emulsion tester as shown in Figure A10, voltage was imposed on the oil-based mud using two electrodes and then gradually increased until initiation of current flow. Inasmuch as current flow is an indication of emulsion breakdown, the relative stability is indicated by voltage at the breakdown point.



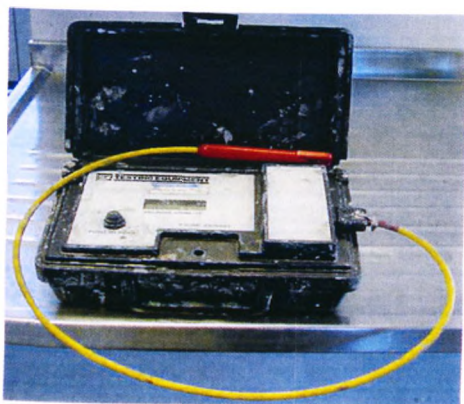


Figure A10 Electric stability tester mixer

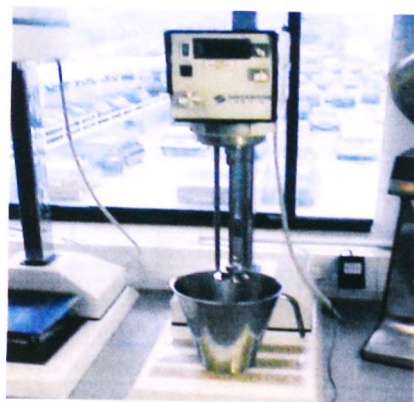


Figure A11 Silverson

### A11 Silverson Mixer

Silverson mixer model (L 4RT-A) Figure A11 used for mixing water and oil based muds.

### A12 Conductivity Meter

Conductivity meter model (WPA CM35) Figure A12 is an instrument used to measure conductivity of the brine solution.



Figure A12 Conductivity meter



Figure A13 Precision Component Analyser

### A13 Precision Component Analyser model 6425

An instrument used to measure resistivity formation factor Figure A13.

### A14 Titration Kit

Chemical titration kit has been used to measure fluid properties such as calcium and chloride contents, alkalinity, etc.

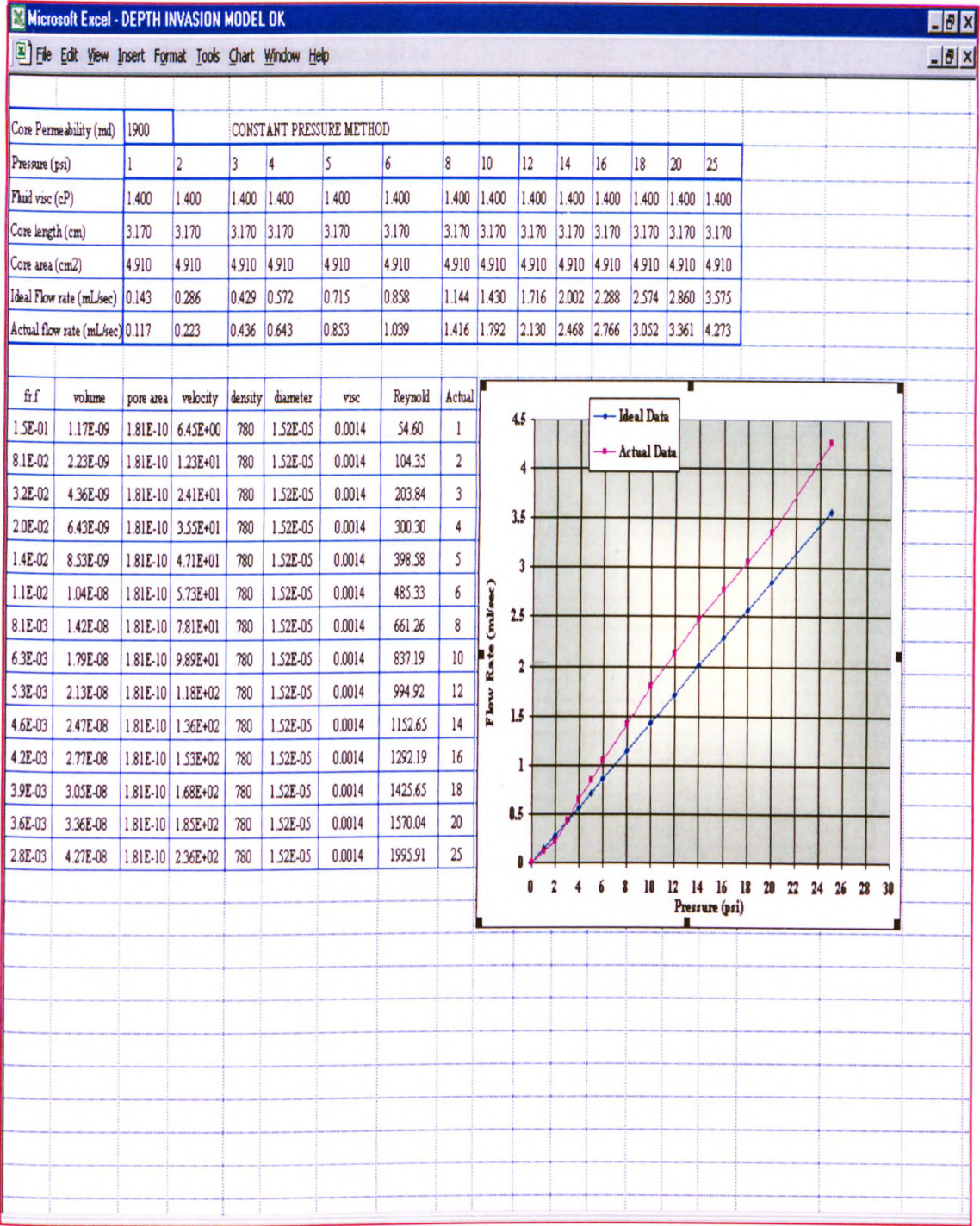


Figure A15 (4.37) Tabular and graphical display for permeability measurement and deviation in linearity in turbulent flow regime



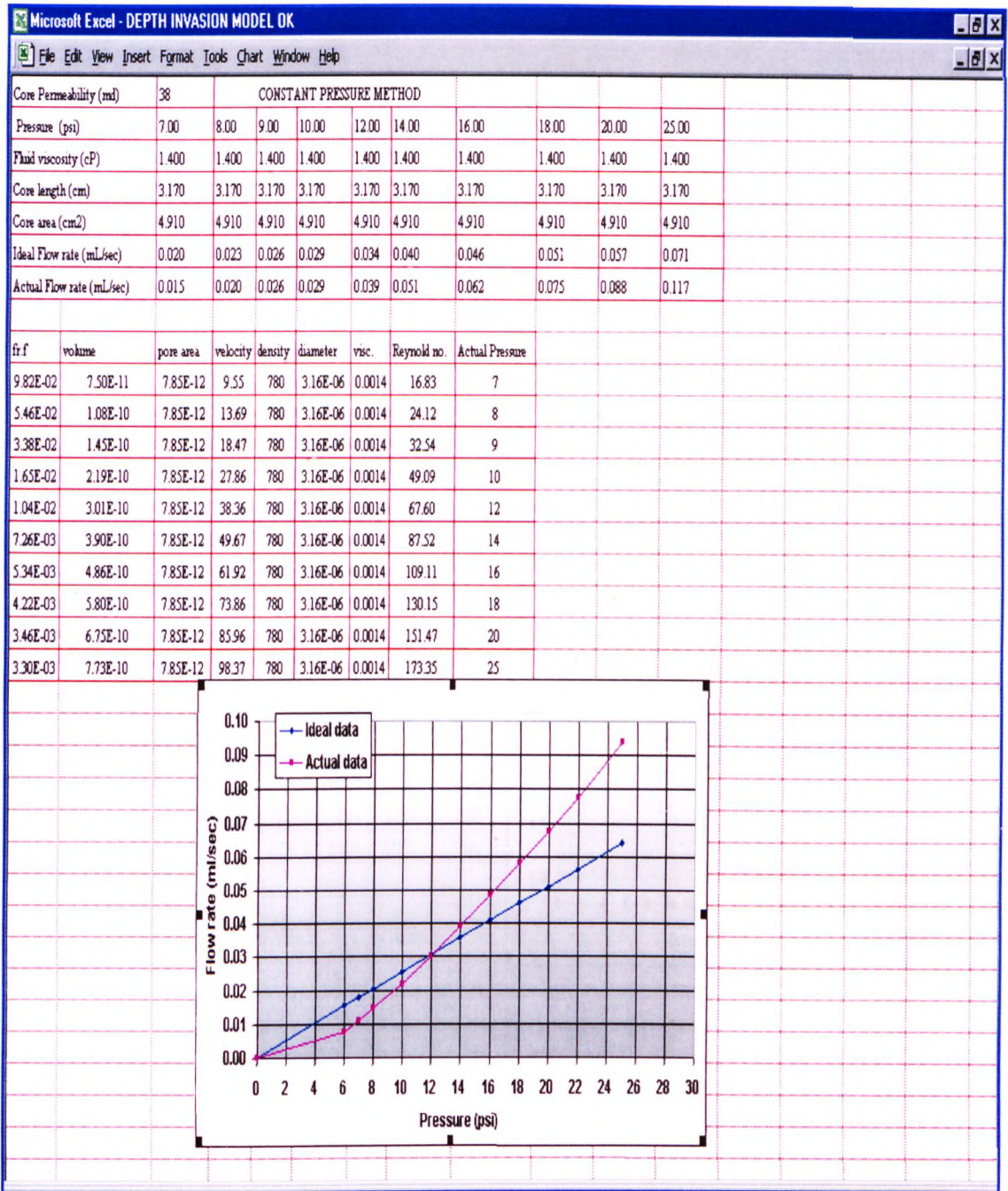


Figure A16 (4.38) Tabular and graphical display for permeability measurement and deviation in linearity in laminar flow regime

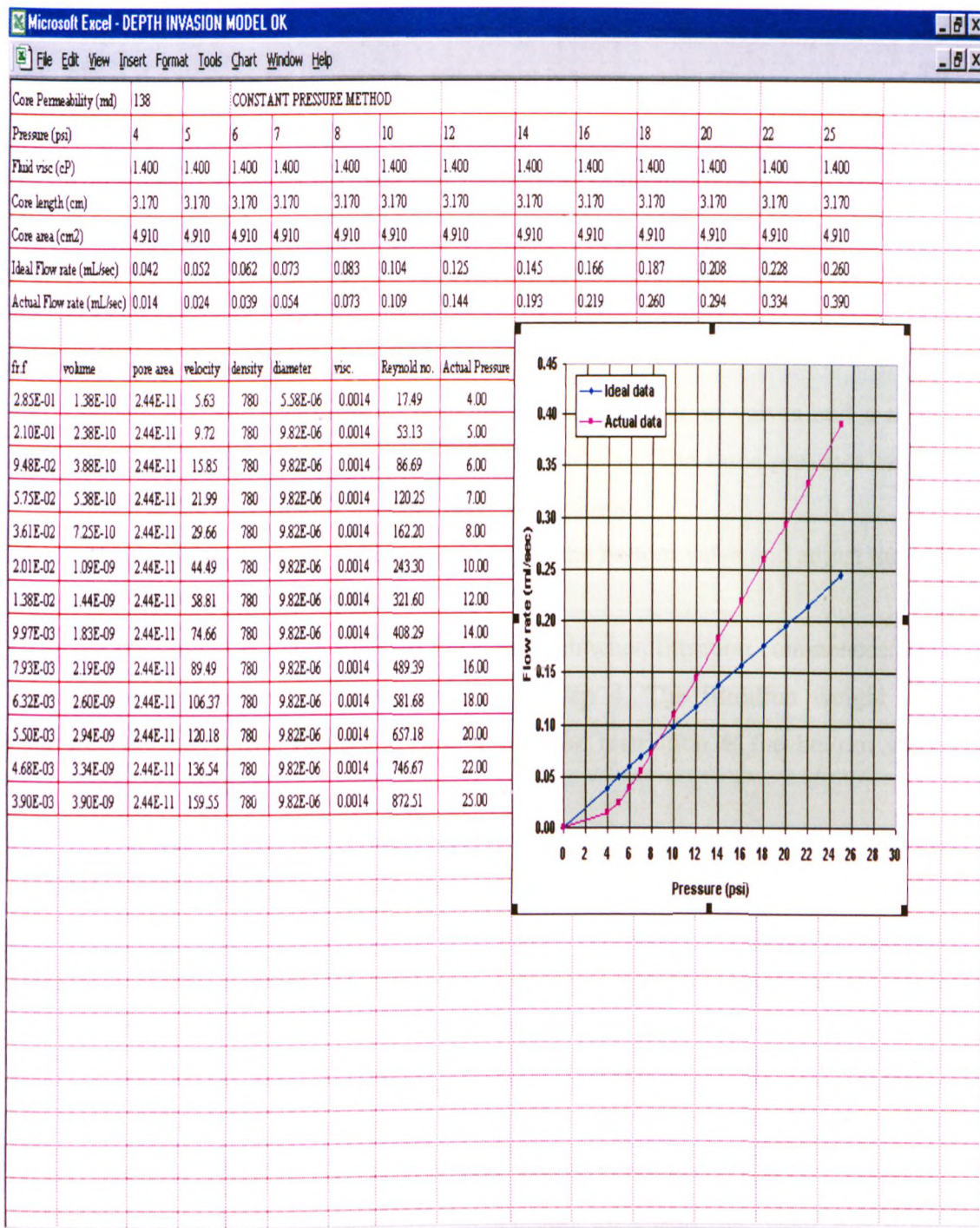


Figure A17 (4.39) Tabular and graphical display for permeability measurement and deviation in linearity in laminar flow regime



#### **A4.2.2 HP-HT filtration Testing Procedure:**

1. Plug heating jacket into a power source for preheat to the test temperature and adjust the thermostat in order to maintain this temperature. Pour a sample of the mud to be tested into a glass beaker and place it on a heating unit at 150 ° F fitted with a magnetic stirrer (to maximise the number of tests to be done).
2. Once the correct temperature is reached pour the mud into the cell and the top cover bolted in position. Place the cell into the heating jacket with both bottom and top valves stems closed. The volume of mud poured into the cell should be fixed for any test carried.
3. Connect the Nitrogen pressure units to the top and bottom valves and apply a pressure of 100 psi from the top unit whilst heating. The same pressure can be applied to the bottom unit with the valve stem closed.
4. Once the correct temperature is reached open the bottom valve and adjust the top valve to the required test pressure.

Open the bottom outlet valve and start the stopwatch when filtration commences. The spurt loss was measured at 20 seconds from step 4. The filtration weight was measured manually with respect to time due to the restriction at the bottom valve when used above 200 ° F.

The first filtration test conducted was stopped after seven hours and up on equilibrium, dynamic filtration was recorded after about two hours. Thereafter the bottom valve was initially closed followed by the top valve and after cooling, the pressure was then carefully released. The top cover was then removed, the mud drained off, the bolts were loosened and the bottom cover and core were then removed. Any excess mud lying on the surface of the cake, especially from the static filtration test, was then gently scraped and the filter cake thickness was measured by caliper. The total weight of the wet filter cake was recorded and it was then placed in a heated oven at 90 ° C for two days to dry out. To ensure the cake was dried completely the oven temperature was then raised to 120 ° C for another day. No

decrease in weight was recorded after this second drying. Finally, the cell was cleaned carefully and dried with pressurised air.

Table A1 (4.14) Effect of pressure and temperature (static filtration experiments) for W B M

TEMP.	150 F			200 F		
TIME	200 psi	500 psi	800 psi	200 psi	500 psi	800 psi
	ml	ml	ml	ml	ml	ml
0.5	0.09	0.25	0.56	0.28	0.67	1.22
5	0.64	1.11	1.4	1.07	1.98	2.42
10	1.07	1.52	2.07	1.55	2.55	3
15	1.5	1.95	2.61	1.93	3.05	3.47
20	1.84	2.24	3.01	2.3	3.52	4.04
25	2.1	2.53	3.33	2.66	3.78	4.36
30	2.31	2.88	3.63	2.98	4.02	4.84
40	2.83	3.46	4.15	3.5	4.77	5.39
50	3.25	3.85	4.61	4.02	5.14	5.95
60	3.59	4.35	5.05	4.52	5.67	6.53
75	4.04	4.89	5.64	5.16	6.38	7.28
90	4.49	5.43	6.24	5.81	7.1	8.03
105	4.86	5.98	6.85	6.3	7.72	8.68
120	5.24	6.54	7.46	6.79	8.35	9.33
135	5.54	6.89	7.87	7.26	8.95	9.93
150	5.84	7.24	8.28	7.74	9.55	10.53
165	6.11	7.55	8.64	8.16	10.08	11.08
180	6.39	7.87	9	8.59	10.62	11.63
195	6.64	8.14	9.27	8.99	11.07	12.11
210	6.89	8.42	9.55	9.39	11.53	12.56

Table A2 (4.15) Effect of pressure and temperature (static filtration experiments) for W B M

TEMP.	250 F			300 F		
TIME	200 psi	500 psi	800 psi	200 psi	500 psi	800 psi
	ml	ml	ml	ml	ml	ml
0.5	0.35	0.9	1.33	0.98	1.68	2.05
5	0.95	1.25	1.85	1.62	3.51	4.44
10	1.39	2.11	3.1	2.28	4.61	5.56
15	1.99	2.75	3.92	2.73	5.51	6.24
20	2.4	3.43	4.48	3.04	6.19	7.09
25	3.02	4.17	5.05	3.46	6.88	7.58
30	3.28	4.8	5.54	3.88	7.45	8.14
40	4	5.75	6.47	4.51	8.5	9.21
50	4.65	6.52	7.4	5.19	9.46	10.18
60	5.25	7.26	8.15	5.83	10.38	11.14
75	5.5	8.26	9.08	6.76	11.51	12.24
90	6.75	9.26	10.01	7.69	12.64	13.34
105	7.35	9.99	10.83	8.42	13.57	14.31
120	7.96	10.72	11.65	9.15	14.51	15.28
135	8.59	11.47	12.4	9.88	15.38	16.23
150	9.22	12.22	13.16	10.61	16.25	17.19
165	9.63	12.85	13.78	11.32	16.98	17.96
180	10.05	13.48	14.4	12.03	17.71	18.74
195	10.35	13.96	14.97	12.69	18.43	19.44
210	10.65	14.45	15.55	13.35	19.15	20.14



Table A3 (4.16) Effect of solids % (static filtration experiments) for WBM  
at 250 F & 500 psi Condition

	9 PPG			11 PPG		13 PPG		
TIME	400 MD	2000 MD	5000 MD	2000 MD	5000 MD	400 MD	2000 MD	5000 MD
0.5	0	0	0	0	0	0	0	0
5	1.75	2.91	3.26	1.15	1.57	2.33	1.93	1.86
10	3.16	4.45	5.07	2.32	2.6	3.4	3.02	2.95
15	4.25	5.6	6.59	3.26	3.26	4.25	3.86	3.79
20	5.22	6.49	7.71	3.93	3.73	4.99	4.42	4.35
25	6.02	7.4	8.55	4.58	4.24	5.55	4.76	4.69
30	6.55	7.88	9.36	5.21	4.55	6.24	4.98	4.91
40	7.65	9.19	10.69	6.23	5.51	7.2	5.31	5.24
50	8.69	10.2	11.94	7.09	6.12	8.06	5.47	5.4
60	9.55	11.17	13.1	7.96	6.81	8.9	5.62	5.55
75	10.93	12.47	14.4	8.98	7.77	9.97	6.7	6.45
90	12.31	13.78	15.8	10.01	8.74	11.04	7.98	7.35
105	13.44	14.95	16.97	10.84	9.55	11.96	8.86	8.15
120	14.58	16.12	18.15	11.67	10.37	12.88	9.7	8.95
135	15.56	17.05	19.17	12.38	11.08	13.67	10.44	9.6
150	16.55	17.99	20.21	13.09	11.79	14.47	11.19	10.25
165	17.45	18.93	21.12	13.75	12.46	15.17	11.85	10.85
180	18.35	19.83	22.04	14.42	13.14	15.88	12.52	11.45
195	19.15	20.63	22.84	14.93	13.64	16.55	13.12	11.95
210	19.95	21.43	23.64	15.39	14.14	17.23	13.72	12.45

Table A4 (4.17) Effect of plugging agent fluid loss (static filtration experiments) for WBM  
at 250 F & 500 psi Condition

TIME	base mud	3%	8%	13% OIL
0.5	0.9	0.81	0.75	0.65
5	1.25	0.95	0.88	0.75
10	2.11	1.51	1.21	0.91
15	2.75	2.15	1.85	1.25
20	3.43	2.83	2.53	1.97
25	4.17	3.57	3.27	2.67
30	4.8	4.2	3.9	3.3
40	5.75	5.15	4.85	4.25
50	6.52	5.92	5.62	5.02
60	7.26	6.66	6.36	5.76
75	8.26	7.56	7.16	6.46
90	9.26	8.46	7.96	7.16
105	9.99	9.21	8.56	7.76
120	10.72	9.96	9.36	8.36
135	11.47	10.62	9.98	8.86
150	12.22	11.29	10.6	9.36
165	12.85	11.89	11.11	9.81
180	13.48	12.49	11.59	10.26
195	13.96	13.01	12.04	10.46
210	14.45	13.53	12.48	11.01

Table A5 (4.18) Effect of viscosifying agent fluid loss (static filtration experiments) for WBM

at 250 F & 500 psi Condition				
	base mud	1 lb/bbl	3lb/bbl.	5lb/bbl
TIME	ml	ml	ml	ml
0.5	0.9	0.77	0.63	0.47
5	1.25	1.12	0.98	0.82
10	2.11	1.98	1.84	1.68
15	2.75	2.62	2.48	2.32
20	3.43	3.3	3.16	3
25	4.17	4.04	3.9	3.74
30	4.8	4.67	4.53	4.37
40	5.75	5.62	5.48	5.32
50	6.52	6.39	6.25	6.09
60	7.26	7.13	6.99	6.83
75	8.26	8.03	7.79	7.63
90	9.26	9.03	8.79	8.43
105	9.99	9.66	9.32	9
120	10.72	10.39	10.04	9.57
135	11.47	11.04	10.64	10.07
150	12.22	11.69	11.19	10.57
165	12.85	12.26	11.69	10.97
180	13.48	12.81	12.19	11.37
195	13.96	13.31	12.59	11.67
210	14.45	13.81	12.99	11.97

Table A6 (4.19) Effect of coating agent fluid loss (static filtration experiments) for WBM

at 250 F & 500 psi Condition				
	base mud	1 lb/bbl	3lb/bbl.	5lb/bbl
TIME	ml	ml	ml	ml
0.5	0.9	0.87	0.79	0.67
5	1.25	4.91	0.9	4.78
10	2.11	9.91	1.76	9.78
15	2.75	14.91	2.4	14.78
20	3.43	19.91	3.08	19.78
25	4.17	24.91	3.82	24.78
30	4.8	29.91	4.45	29.78
40	5.75	39.91	5.4	39.78
50	6.52	49.91	6.17	49.78
60	7.26	59.91	6.91	59.78
75	8.26	8.07	7.73	7.54
90	9.26	8.97	8.55	8.31
105	9.99	9.62	9.19	8.91
120	10.72	10.3	9.83	9.51
135	11.47	10.95	10.4	10.05
150	12.22	11.6	10.98	10.59
165	12.85	12.17	11.53	11.09
180	13.48	12.75	12.08	11.59
195	13.96	13.25	12.53	11.89
210	14.45	13.75	12.98	12.19



Table A7 (4.20) Effect of pressure and temperature (dynamic filtration experiments) for WBM

TEMP.	150 F			200 F		
TIME	200 psi	500 psi	800 psi	200 psi	500 psi	800 psi
	ml	ml	ml	ml	ml	ml
0.5	0.36	0.51	0.74	0.45	0.65	0.98
5	1.23	1.48	1.78	1.54	1.73	2.36
10	1.86	2.18	2.46	2.09	2.64	3.15
15	2.27	2.77	3.01	2.69	3.29	3.81
20	2.57	3.16	3.47	3.2	3.74	4.29
25	2.97	3.6	3.96	3.54	4.2	4.81
30	3.19	3.86	4.25	3.89	4.58	5.3
40	3.73	4.42	4.97	4.56	5.24	6.17
50	4.2	4.95	5.45	5.21	5.9	6.77
60	4.66	5.35	5.95	5.69	6.47	7.39
75	5.23	5.97	6.6	6.48	7.31	8.17
90	5.8	6.6	7.25	7.27	8.16	8.95
105	6.25	7.17	7.85	7.81	8.86	9.71
120	6.69	7.75	8.45	8.35	9.57	10.48
135	7.09	8.22	8.95	8.82	10.12	11.08
150	7.49	8.69	9.45	9.29	10.67	11.68
165	7.89	9.16	9.95	9.76	11.22	12.28
180	8.29	9.63	10.45	10.23	11.77	12.88
195	8.69	10.1	10.95	10.7	12.32	13.48
210	9.09	10.57	11.45	11.17	12.87	14.08

Table A8 (4.21) Effect of pressure and temperature (dynamic filtration experiments) for WBM

TEMP.	250 F			300 F		
TIME	200 psi	500 psi	800 psi	200 psi	500 psi	800 psi
	ml	ml	ml	ml	ml	ml
0.5	0.56	0.83	1.17	0.75	1.15	2.11
5	1.87	2.25	2.75	2.61	3.86	4.84
10	2.55	3.15	3.65	3.71	5.19	5.8
15	3.06	3.92	4.42	4.39	6.24	6.63
20	3.45	4.48	4.98	5.09	6.84	7.6
25	3.76	5.05	5.55	5.66	7.49	8.22
30	4.18	5.55	6.05	6.16	7.98	8.81
40	4.85	6.45	6.95	7.11	9.1	9.95
50	5.35	7.31	7.81	7.96	10.11	10.97
60	5.85	7.95	8.45	8.84	11.22	11.94
75	6.59	9.04	9.54	9.88	12.52	13.31
90	7.33	10.14	10.64	10.92	13.83	14.69
105	7.99	11	11.5	11.72	14.94	15.92
120	8.66	11.87	12.37	12.52	16.06	17.16
135	9.23	12.52	13.14	13.35	16.93	18.11
150	9.8	13.17	13.92	14.19	17.8	19.06
165	10.37	13.82	14.69	14.99	18.67	20.01
180	10.94	14.47	15.47	15.79	19.54	20.96
195	11.51	15.12	16.24	16.59	20.41	21.91
210	12.08	15.77	17.02	17.39	21.28	22.86

Table A9 (4.22) Effect of solids % (dynamic filtration experiments) for WBM

at 250 F &amp; 500 psi Condition

	9 PPG			11 PPG		13 PPG		
	400 MD	2000 MD	5000 MD	2000 MD	5000 MD	400 MD	2000 MD	5000 MD
TIME	ml	ml	ml	ml	ml	ml	ml	ml
0.5	5.48	2.29	14.75	1.96	4.5	1.52	1.41	1.9
5	7.97	4.6	18.72	3.87	5.48	4.28	3.52	3.7
10	9.37	4.77	20.26	4.98	6.32	5.36	4.54	4.71
15	10.58	4.8	21.54	5.85	6.99	6.21	5.43	5.4
20	11.55	8.43	22.75	6.56	7.58	6.89	6.01	6.02
25	12.37	8.46	23.76	7.05	8.11	7.55	6.69	6.56
30	13.13	8.53	24.55	7.52	8.59	8.13	7.19	7.03
40	14.64	8.55	26.05	8.53	9.6	9.19	8.2	7.91
50	15.92	15.42	27.4	9.46	10.4	10.12	9.08	8.76
60	17.02	18.29	28.75	10.23	11.2	10.89	9.87	9.54
75	18.6	20.91	30.42	11.33	12.3	12.01	10.94	10.47
90	20.18	23.53	32.1	12.43	13.4	13.14	12.01	11.41
105	21.45	25.45	33.58	13.33	14.3	14.09	12.85	12.26
120	22.73	27.37	35.07	14.23	15.2	15.04	13.7	13.12
135	23.87	29	36.32	14.95	15.95	15.8	14.47	13.82
150	25.02	30.64	37.57	15.68	16.7	16.69	15.34	14.52
165	26.12	32.29	38.82	16.4	17.45	17.44	16.09	15.27
180	27.22	33.95	40.07	17.13	18.2	18.19	16.85	16.02
195	28.32	35.6	41.32	17.85	18.95	18.96	17.6	16.77
210	29.42	37.26	42.57	18.58	19.7	19.69	18.35	17.52

Table A10 (4.23) Effect of plugging agent fluid loss of (dynamic filtration experiments) for WBM

at 250 F &amp; 500 psi Condition

TIME	base mud	3%	8%	13% OIL
	ml	ml	ml	ml
0.5	0.83	1.34	1.31	0.8
5	2.25	3.14	3.04	2.37
10	3.15	4.08	3.88	3.18
15	3.92	4.69	4.42	3.86
20	4.48	5.17	5.03	4.34
25	5.05	5.64	5.43	4.81
30	5.55	6.02	5.84	5.22
40	6.45	6.82	6.53	5.96
50	7.31	7.52	7.12	6.63
60	7.95	8.07	7.68	7.17
75	9.04	8.97	8.44	7.87
90	10.14	9.87	9.21	8.57
105	11	10.62	9.83	9.14
120	11.87	11.37	10.46	9.71
135	12.52	11.99	11.01	10.16
150	13.17	12.61	11.56	10.61
165	13.82	13.23	12.11	11.06
180	14.47	13.85	12.66	11.51
195	15.12	14.47	13.21	11.96
210	15.77	15.09	13.76	12.41



Table A11 (4.24) Effect of viscosifying agent fluid loss of (dynamic filtration experiments) for WBM

at 250 F & 500 psi Condition				
	base mud	1 lb/bbl	3lb/bbl.	5lb/bbl
TIME	ml	ml	ml	ml
0.5	0.83	1.48	2.11	4.68
5	2.25	2.83	3.22	4.95
10	3.15	3.68	3.95	5.22
15	3.92	4.38	4.53	5.65
20	4.48	4.9	5.05	6.05
25	5.05	5.41	5.44	6.36
30	5.55	5.87	5.69	6.62
40	6.45	6.73	6.4	7.26
50	7.31	7.49	7.06	7.76
60	7.95	8.08	7.64	8.22
75	9.04	9.03	8.44	8.91
90	10.14	9.97	9.24	9.6
105	11	10.77	9.93	10.19
120	11.87	11.57	10.63	10.78
135	12.52	12.17	11.18	11.23
150	13.17	12.77	11.73	11.68
165	13.82	13.37	12.28	12.13
180	14.47	13.97	12.83	12.58
195	15.12	14.57	13.38	13.03
210	15.77	15.17	13.93	13.48

Table A12 (4.25) Effect of coating agent fluid loss of (dynamic filtration experiments) for WBM

at 250 F & 500 psi Condition				
	base mud	1 lb/bbl	3lb/bbl.	5lb/bbl
TIME	ml	ml	ml	ml
0.5	0.83	2.95	4.04	5
5	2.25	4.04	4.54	5.2
10	3.15	5.04	5.13	5.4
15	3.92	5.82	5.52	5.75
20	4.48	6.39	5.9	6.01
25	5.05	6.78	6.29	6.35
30	5.55	7.17	6.56	6.61
40	6.45	8.03	7.25	7.26
50	7.31	8.79	7.83	7.85
60	7.95	9.55	8.61	8.37
75	9.04	10.44	9.28	9.12
90	10.14	11.33	9.95	9.87
105	11	12.13	10.61	10.46
120	11.87	12.94	11.27	11.07
135	12.52	13.6	11.87	11.62
150	13.17	14.26	12.47	12.17
165	13.82	14.92	13.07	12.72
180	14.47	15.58	13.67	13.27
195	15.12	16.24	14.27	13.82
210	15.77	16.9	14.87	14.37

Table A13 (4.26) Effect of shear rate of (dynamic filtration experiments) for WBM  
at 250 F & 500 psi Condition

	80 rpm	120 rpm	160 rpm	200 rpm
TIME	ml	ml	ml	ml
0.5	0.83	1.44	1.98	2.02
5	2.25	3.3	4.07	4.81
10	3.15	4.44	5.07	5.81
15	3.92	5.26	5.87	6.61
20	4.48	6.04	6.66	7.4
25	5.05	6.66	7.34	8.08
30	5.55	7.21	7.8	8.54
40	6.45	8.2	8.72	9.46
50	7.31	9.24	9.6	10.34
60	7.95	10.05	10.4	11.14
75	9.04	11.15	11.53	12.22
90	10.14	12.24	12.57	13.31
105	11	12.95	13.48	14.22
120	11.87	13.65	14.39	15.13
135	12.64	14.35	15.14	15.93
150	13.42	15.05	15.89	16.73
165	14.07	15.75	16.64	17.53
180	14.72	16.45	17.39	18.33
195	15.37	17.15	18.14	19.13
210	16.02	17.85	18.89	19.92



Table A14 (4.27) Effect of pressure and temperature (static filtration experiments) for OBM

TEMP.	150 F			200 F		
TIME	200 psi	500 psi	800 psi	200 psi	500 psi	800 psi
0.5	0.06	0.11	0.14	0.11	0.21	0.29
5	0.067	0.18	0.21	0.18	0.38	0.47
10	0.07	0.26	0.3	0.26	0.56	0.66
15	0.11	0.31	0.37	0.35	0.65	0.75
20	0.16	0.37	0.45	0.45	0.74	0.85
25	0.19	0.47	0.52	0.52	0.79	0.9
30	0.21	0.56	0.62	0.6	0.84	0.95
35	0.25	0.58	0.65	0.67	0.88	0.99
40	0.3	0.61	0.68	0.74	0.93	1.05
45	0.33	0.66	0.74	0.79	0.98	1.1
50	0.36	0.71	0.8	0.85	1.04	1.15
55	0.38	0.76	0.85	0.9	1.08	1.19
60	0.41	0.81	0.91	0.97	1.13	1.24
75	0.48	0.89	0.95	1.08	1.3	1.4
90	0.55	1	1.1	1.21	1.44	1.56
105	0.6	1.08	1.17	1.33	1.58	1.71
120	0.66	1.16	1.26	1.45	1.73	1.85
135	0.72	1.23	1.34	1.55	1.86	1.98
150	0.76	1.3	1.42	1.65	1.99	2.12
165	0.8	1.35	1.5	1.73	2.08	2.23
180	0.84	1.41	1.56	1.83	2.18	2.35

Table A15 (4.28) Effect of pressure and temperature (static filtration experiments) for OBM

TEMP.	250 F			300 F		
TIME	200 psi	500 psi	800 psi	200 psi	500 psi	800 psi
0.5	0.14	0.28	0.37	0.21	0.34	0.45
5	0.29	0.44	0.53	0.47	0.6	0.68
10	0.42	0.59	0.67	0.73	0.85	0.94
15	0.53	0.74	0.82	0.9	1.05	1.11
20	0.67	0.88	0.95	1.05	1.24	1.34
25	0.79	0.99	1.09	1.18	1.34	1.49
30	0.89	1.11	1.22	1.29	1.52	1.62
35	1.02	1.26	1.37	1.44	1.69	1.79
40	1.13	1.39	1.5	1.57	1.85	1.96
45	1.21	1.48	1.6	1.68	1.95	2.05
50	1.28	1.58	1.69	1.76	2.06	2.18
55	1.35	1.69	1.79	1.86	2.16	2.3
60	1.41	1.78	1.88	1.95	2.27	2.41
75	1.59	1.99	1.98	2.14	2.47	2.64
90	1.75	2.18	2.27	2.34	2.7	2.85
105	1.92	2.38	2.46	2.54	2.89	3.06
120	2.08	2.56	2.65	2.72	3.1	3.27
135	2.23	2.74	2.83	2.9	3.29	3.47
150	2.38	2.91	3	3.07	3.48	3.66
165	2.53	3.1	3.18	3.26	3.66	3.85
180	2.66	3.27	3.34	3.41	3.84	4.03

Table A16 (4.29) Effect of filter medium (static filtration experiments) for OBM

		at 250 F & 500 psi Condition		
	filter paper	400 md	2000 md	5000 md
TIME	F.L ml	F.L ml	F.L ml	F.L ml
0.5	0.11	0.28	0.32	0.36
5	0.39	0.44	0.42	0.45
10	0.66	0.59	0.55	0.53
15	0.81	0.74	0.7	0.69
20	0.97	0.88	0.85	0.84
25	1.07	0.99	0.95	0.96
30	1.17	1.11	1.08	1.09
35	1.3	1.26	1.21	1.23
40	1.43	1.39	1.34	1.33
45	1.51	1.48	1.43	1.42
50	1.59	1.58	1.56	1.55
55	1.65	1.69	1.66	1.65
60	1.7	1.78	1.75	1.76
75	1.91	1.99	1.96	1.97
90	2.1	2.18	2.15	2.13
105	2.23	2.38	2.35	2.33
120	2.35	2.56	2.53	2.52
135	2.49	2.74	2.7	2.71
150	2.64	2.91	2.89	2.88
165	2.76	3.1	3.05	3.06
180	2.89	3.27	3.2	3.19

Table A17 (4.30) Effect of solids% (static filtration experiments) for OBM

	6%	13%	20%
TIME	9 ppg	11 ppg	13 ppg
0.5	2.41	0.28	0.07
5	2.47	0.44	0.16
10	2.53	0.59	0.27
15	2.58	0.74	0.43
20	2.63	0.88	0.59
25	2.73	0.99	0.66
30	2.84	1.11	0.74
35	2.89	1.26	0.79
40	2.95	1.39	0.85
45	3.01	1.48	0.94
50	3.07	1.58	1.03
55	3.14	1.69	1.1
60	3.21	1.78	1.18
75	3.43	1.99	1.37
90	3.65	2.18	1.58
105	3.82	2.38	1.69
120	3.99	2.56	1.81
135	4.17	2.74	1.92
150	4.35	2.91	2.03
165	4.5	3.1	2.14
180	4.65	3.27	2.24



Table A18 (4.31) Effect of coating agent fluid loss (static filtration experiments) for OBM  
at 250 F & 500 psi Condition

	base mud	0.25 lb/bbl	1.0 lb/bbl	2.0 lb/bbl	4.0 lb/bbl
TIME	ml	ml	ml	ml	ml
0.5	0.34	0.19	0.34	0.14	0.16
5	1.09	0.93	0.72	0.40	0.47
10	1.53	1.34	1.00	0.56	0.64
15	1.83	1.63	1.22	0.68	0.82
20	2.12	1.91	1.44	0.80	0.99
25	2.37	2.14	1.62	0.96	1.13
30	2.61	2.36	1.80	1.11	1.27
35	2.83	2.54	2.02	1.20	1.37
40	3.04	2.72	2.23	1.28	1.47
45	3.23	2.89	2.33	1.43	1.56
50	3.41	3.06	2.42	1.57	1.65
55	3.56	3.23	2.58	1.63	1.75
60	3.70	3.39	2.73	1.69	1.84
75	4.17	3.87	3.04	1.98	2.12
90	4.63	4.35	3.34	2.27	2.39
105	5.01	4.73	3.59	2.47	2.55
120	5.38	5.10	3.83	2.66	2.71
135	5.74	5.40	4.04	2.86	2.87
150	6.10	5.70	4.24	3.06	3.02
165	6.38	6.00	4.44	3.26	3.18
180	6.65	6.29	4.64	3.46	3.34

Table A19 (4.32) Effect of plugging agent fluid loss (static filtration experiments) for OBM

	base mud	0.25 lb/bbl	1.0 lb/bbl	2.0 lb/bbl	4.0 lb/bbl
TIME	ml	ml	ml	ml	ml
0.5	0.34	0.47	0.16	0.12	0.12
5	1.09	1.23	0.40	0.54	0.34
10	1.53	1.60	0.66	0.75	0.36
15	1.83	1.87	0.87	0.90	0.44
20	2.12	2.13	1.08	1.04	0.51
25	2.37	2.36	1.22	1.14	0.59
30	2.61	2.58	1.36	1.24	0.67
35	2.83	2.76	1.46	1.35	0.73
40	3.04	2.93	1.55	1.45	0.79
45	3.23	3.08	1.67	1.54	0.85
50	3.41	3.22	1.78	1.62	0.91
55	3.56	3.35	1.84	1.70	0.94
60	3.70	3.47	1.90	1.78	0.96
75	4.17	3.84	2.14	2.01	1.05
90	4.63	4.21	2.38	2.24	1.13
105	5.01	4.52	2.60	2.43	1.25
120	5.38	4.82	2.82	2.62	1.37
135	5.74	5.08	2.97	2.79	1.47
150	6.10	5.33	3.12	2.95	1.56
165	6.38	5.53	3.27	3.10	1.66
180	6.65	5.72	3.42	3.25	1.76

Table A20 (4.33) Effect of viscosifying agent fluid loss (static filtration experiments) for OBM  
at 250 F & 500 psi Condition

TIME	base mud	0.25 lb/bbl	1.0 lb/bbl	2.0 lb/bbl	4.0 lb/bbl
	ml	ml	ml	ml	ml
0.5	0.34	0.10	0.32	0.07	0.05
5	1.09	0.49	0.70	0.08	0.07
10	1.53	0.77	0.86	0.27	0.08
15	1.83	1.05	1.03	0.37	0.09
20	2.12	1.33	1.19	0.47	0.09
25	2.37	1.53	1.35	0.57	0.10
30	2.61	1.73	1.50	0.66	0.10
35	2.83	1.91	1.61	0.74	0.10
40	3.04	2.08	1.71	0.82	0.10
45	3.23	2.27	1.85	0.92	0.10
50	3.41	2.46	1.99	1.02	0.10
55	3.56	2.60	2.09	1.08	0.11
60	3.70	2.74	2.18	1.14	0.11
75	4.17	2.96	2.47	1.33	0.14
90	4.63	3.18	2.75	1.52	0.17
105	5.01	3.51	2.96	1.64	0.22
120	5.38	3.84	3.17	1.76	0.26
135	5.74	4.20	3.36	1.87	0.32
150	6.10	4.55	3.54	1.98	0.37
165	6.38	4.82	3.68	2.08	0.40
180	6.65	5.09	3.82	2.18	0.42



Table A21 (4.34) Effect of pressure and temperature (dynamic filtration experiments) for OBM

TEMP.	150 F			200 F		
TIME	200 psi	500 psi	800 psi	200 psi	500 psi	800 psi
0.5	0.03	0.06	0.1	0.11	0.13	0.15
5	0.09	0.1	0.16	0.22	0.28	0.33
10	0.18	0.2	0.27	0.38	0.47	0.51
15	0.3	0.34	0.34	0.52	0.59	0.6
20	0.33	0.43	0.44	0.62	0.7	0.69
25	0.37	0.53	0.56	0.72	0.82	0.8
30	0.4	0.62	0.66	0.8	0.91	0.91
35	0.49	0.7	0.76	0.85	1.02	1.01
40	0.55	0.76	0.82	0.95	1.05	1.06
45	0.68	0.84	0.88	0.98	1.1	1.15
50	0.72	0.93	0.98	1.04	1.14	1.23
55	0.78	0.99	1.05	1.07	1.19	1.29
60	0.84	1.05	1.11	1.09	1.21	1.35
75	0.91	1.14	1.21	1.23	1.39	1.54
90	0.97	1.23	1.31	1.37	1.56	1.73
105	1.01	1.29	1.38	1.47	1.67	1.85
120	1.05	1.35	1.45	1.57	1.78	1.97
135	1.09	1.41	1.52	1.67	1.89	2.09
150	1.13	1.47	1.59	1.77	2	2.21
165	1.17	1.53	1.66	1.87	2.11	2.33
180	1.21	1.59	1.73	1.97	2.22	2.45

Table A22 (4.35) Effect of pressure and temperature (dynamic filtration experiments) for OBM

TEMP.	250 F			300 F		
TIME	200 psi	500 psi	800 psi	200 psi	500 psi	800 psi
0.5	0.23	0.35	0.41	0.33	0.55	0.71
5	0.62	0.71	1.02	0.78	0.94	1.13
10	0.81	0.92	1.29	1.07	1.24	1.35
15	1.01	1.11	1.43	1.36	1.45	1.61
20	1.19	1.3	1.57	1.5	1.61	1.84
25	1.33	1.46	1.7	1.66	1.74	1.96
30	1.5	1.63	1.84	1.82	1.96	2.24
35	1.57	1.75	1.93	2.02	2.12	2.33
40	1.67	1.83	2	2.1	2.35	2.55
45	1.78	1.96	2.1	2.17	2.45	2.65
50	1.88	2.04	2.25	2.27	2.54	2.75
55	1.91	2.14	2.3	2.39	2.74	2.95
60	1.99	2.26	2.35	2.49	2.92	3.07
75	2.18	2.46	2.58	2.75	3.21	3.36
90	2.38	2.66	2.82	3.01	3.49	3.65
105	2.51	2.81	2.99	3.18	3.68	3.85
120	2.64	2.97	3.16	3.36	3.87	4.05
135	2.77	3.12	3.33	3.53	4.06	4.25
150	2.9	3.28	3.5	3.71	4.25	4.45
165	3.03	3.43	3.67	3.883	4.44	4.65
180	3.16	3.59	3.84	4.06	4.63	4.85

Table A23 (4.36) Effect of shear rate (dynamic filtration experiments) for OBM

at 250 F & 500 psi Condition				
TIME	80 RPM	120 RPM	160 RPM	200 RPM
0.5	0.28	0.58	0.67	0.71
5	0.44	0.89	0.97	1.06
10	0.59	1.07	1.22	1.36
15	0.74	1.26	1.4	1.56
20	0.88	1.42	1.57	1.75
25	0.99	1.57	1.69	1.95
30	1.11	1.73	1.81	2.11
35	1.26	1.85	1.92	2.22
40	1.39	1.95	2.06	2.39
45	1.48	2.06	2.18	2.48
50	1.58	2.17	2.29	2.63
55	1.69	2.28	2.37	2.74
60	1.78	2.35	2.49	2.85
75	1.99	2.6	2.74	3.15
90	2.18	2.86	3	3.46
105	2.38	3.05	3.25	3.76
120	2.56	3.24	3.51	4.07
135	2.74	3.43	3.76	4.37
150	2.91	3.59	4.02	4.68
165	3.1	3.78	4.27	4.99
180	3.27	3.94	4.53	5.29

Table A24 (4.37) Effect of solids% (dynamic filtration experiments) for OBM

at 250 F & 500 psi Condition			
TIME	9 ppg	11 ppg	13 ppg
0.5	2.06	0.35	0.25
5	2.49	0.71	0.4
10	2.83	0.92	0.57
15	3.12	1.11	0.72
20	3.37	1.3	0.92
25	3.57	1.46	1.02
30	3.77	1.63	1.23
35	3.86	1.75	1.33
40	4.03	1.83	1.43
45	4.17	1.96	1.5
50	4.31	2.04	1.6
55	4.47	2.14	1.64
60	4.58	2.26	1.7
75	4.86	2.46	1.83
90	5.14	2.66	1.96
105	5.38	2.81	2.09
120	5.62	2.97	2.22
135	5.86	3.12	2.35
150	6.1	3.28	2.48
165	6.34	3.43	2.61
180	6.58	3.59	2.74



Table A25 (4.38) Effect of coating agent fluid loss (dynamic filtration experiments) for OBM

at 250 F & 500 psi Condition					
TIME	base mud	0.25 lb/bbl	1.0 lb/bbl	2.0 lb/bbl	4.0 lb/bbl
	ml	ml	ml	ml	ml
0.5	0.14	0.35	0.51	0.31	0.24
5	0.24	0.83	1.16	0.72	0.57
10	0.44	1.23	1.55	0.97	0.88
15	0.85	1.53	1.82	1.16	1.02
20	1.25	1.82	2.08	1.35	1.16
25	1.52	2.21	2.26	1.49	1.29
30	1.78	2.60	2.43	1.63	1.41
35	2.04	2.79	2.56	1.79	1.57
40	2.29	2.97	2.68	1.95	1.72
45	2.56	3.15	2.80	2.05	1.82
50	2.82	3.33	2.92	2.15	1.91
55	3.06	3.48	3.01	2.26	2.02
60	3.30	3.62	3.09	2.36	2.12
75	3.98	4.07	3.38	2.64	2.34
90	4.66	4.52	3.67	2.91	2.55
105	5.20	4.94	3.93	3.10	2.76
120	5.74	5.35	4.18	3.28	2.97
135	6.29	5.77	4.39	3.51	3.15
150	6.83	6.18	4.59	3.74	3.33
165	7.37	6.60	4.80	3.90	3.52
180	7.90	7.01	5.00	4.06	3.71

Table A26 (4.39) Effect of plugging agent fluid loss (dynamic filtration experiments) for OBM

at 250 F & 500 psi Condition				
TIME	0.25 lb/bbl	1.0 lb/bbl	2.0 lb/bbl	4.0 lb/bbl
	ml	ml	ml	ml
0.5				
5	1.72	0.38	0.28	0.12
10	2.59	0.80	0.66	0.31
15	2.86	1.11	0.91	0.32
20	3.12	1.35	1.06	0.43
25	3.37	1.58	1.20	0.53
30	3.63	1.71	1.31	0.60
35	3.88	1.84	1.41	0.67
40	4.07	1.99	1.61	0.76
45	4.26	2.13	1.81	0.84
50	4.42	2.24	1.90	0.88
55	4.57	2.34	1.98	0.91
60	4.70	2.44	2.08	0.97
75	4.83	2.54	2.17	1.03
90	5.21	2.83	2.38	1.19
105	5.59	3.12	2.59	1.34
120	5.92	3.34	2.78	1.50
135	6.25	3.55	2.97	1.65
150	6.54	3.77	3.16	1.81
165	6.82	3.98	3.35	1.96
180	7.11	4.20	3.54	2.12

Table A27 (4.40) Effect of viscosifying agent fluid loss (dynamic filtration experiments) for OBM  
at 250 F & 500 psi Condition

TIME	0.25 lb/bbl	1.0 lb/bbl	2.0 lb/bbl	4.0 lb/bbl
	ml	ml	ml	ml
0.5	0.17	0.08	0.16	0.12
5	0.66	0.33	0.33	0.15
10	1.04	0.56	0.56	0.22
15	1.36	0.75	0.69	0.31
20	1.67	0.94	0.82	0.39
25	1.89	1.10	0.90	0.45
30	2.10	1.26	0.98	0.51
35	2.31	1.38	1.08	0.56
40	2.52	1.49	1.18	0.61
45	2.68	1.60	1.30	0.66
50	2.83	1.70	1.41	0.71
55	3.03	1.83	1.54	0.75
60	3.22	1.95	1.66	0.78
75	3.65	2.30	1.85	0.94
90	4.08	2.65	2.04	1.10
105	4.46	2.87	2.23	1.26
120	4.83	3.09	2.42	1.42
135	5.21	3.31	2.61	1.58
150	5.58	3.53	2.80	1.74
165	5.96	3.75	2.99	1.90
180	6.33	3.97	3.18	2.06



#### A4.3.2.1 Initial and Return Permeability Testing Procedure:

1. The core is saturated in brine for WBM or base oil for OBM, after first being evacuated to assist in removing air from the pore spaces. Install the core plug on the core holder cell. This consists of an HP/HT cell base plate, rubber Hassler sleeve, a stainless steel pressure ring and a stainless steel locking ring. Tightening the locking ring contracts the pressure ring against the rubber sleeve, which in turn seals the sleeve onto the core Figure A18 (4.50).
2. Mark the cell to indicate which is the top (the brine or oil always flows from bottom to top).
3. Invert and fill the cell with liquid to the top. Fit the top lid, keeping the top valve stem open to allow air and excess liquid to escape. Tighten the grub screws.
4. Place the cell in the jacket with both bottom and top valves stems closed.

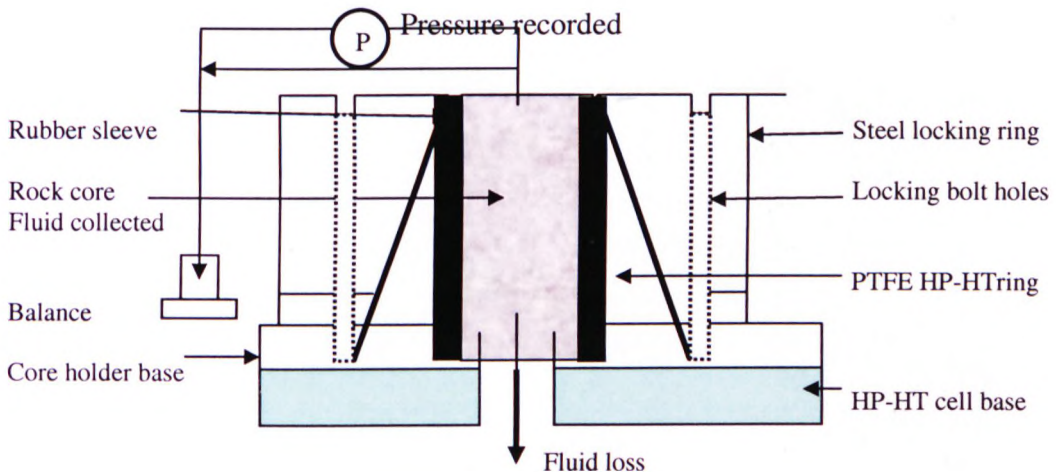


Figure A18 Schematic diagram of the core holder

5. Connect the pressure regulators to the top and bottom valves.
6. Check the closure of the bottom valve stem. Open the pressure valve to the liquid reservoir and bleed 50-100 ml of liquid (oil or brine) through the lower pressure unit to de-air the system.
7. Start the balance programme and the pressure sensor re-zeroed.

8. Open the bottom and top valves, apply pressure to the line and continue flow until a minimum of fifty pore volumes pass through the core and steady flow is achieved.
9. Increase the pressure and repeat step 8 and record as reference point two.
10. Three points in Darcy flow regime can be taken as reference for initial permeability measurement.

The design tool developed in chapter 4 (section 4.1.3.6.4) for quality control flow regimes was used.

**Shut Down Procedure:**

1. Shut off the nitrogen pressure and close both top and bottom valve stems.
2. Bled off the pressure from the liquid reservoir.
3. Remove the top and bottom assemblies.
4. Remove the cell was. Open the top cell and discard all the liquid that flowed through the core.
5. The mud filtration test can be carried out as recommended.

**Core Damage**

After the measurement of the initial permeability of the core plug, place the drilling fluid in the cell and the core can be exposed to the mud under different conditions of temperature, pressure and shear rate.

**Return Permeability Testing Procedure**

1. Depressurise the cell after the mud filtration test with the bottom valve stem remaining closed.
2. Remove the top cover and decantent the excess mud without disturbance to the filter cake. Fill the cell to the top with brine or oil (depending on the type of drilling fluid used).
3. Place the cell in the jacket and close both bottom and top valves stems.
4. Connect the pressure regulators to the top and bottom valves.

5. Check the closure of the bottom valve stem. Open the pressure valve to the liquid reservoir and bleed 50-100 ml of liquid (oil or brine) through the lower pressure unit to de-air the system.
6. Start the balance programme and re-zero the pressure sensor.
7. Open the bottom and top valves, apply pressure to the line and wait for 10 minutes. If the flow starts, continue flowing until the flow rate is steady. Three points in the Darcy flow regime (as above) can be taken as reference for return permeability.
8. Record the flow initiation and cake lift-off pressures.
9. Open the cell and visually observe the filter cake. If the filter cake completely removed then the test completed otherwise remove the cake manually and establish again the return permeability measurement. The shut down procedure can be followed as above.

#### **A4.4.2 HP-HT Fann-70 Rheometer Testing Procedure**

1. Turn the Fann-70 at the main power switch on the console. The pressure gauge and speed display should light.
2. Press the heat/cool start switch until the temperature controller comes on.
3. Start with all parts of the cell, rotor assembly, bob, and bob shaft clean.
4. Ensure that the top of the cell assembly is on its stand with the locking pin in place, preventing the cell from dropping off the stand.
5. Screw the cell baffle snugly into place in the bottom of the coupling, pass the metal rod through the holes in the baffle to tighten it sufficiently.
6. Screw the bob shaft, until the bob is fitted tightly onto it.
7. Screw the bob shaft assembly plus the bob through the hole in the cell baffle into the limit stop at the top of the test cell.
8. Place the rotor assembly into the cell. Lower it gently into place and check that it rotates freely.

9. Place 140 ml of the mud sample into the test cell until it reaches the top of rotor. Ensure that there are no air bubbles in the sample by rotating the rotor in the sample.
10. Place the "O"-ring and backup ring into the cell. The viton O-ring is placed in the groove first followed by the metal backup ring with the bevelled side down.
11. Place the cell under the coupling on the stand. Lift it up and screw it onto the coupling until the threads are hand-tight. The cell can be screwed on tighter with use of a strap wrench.
12. Fill a 20-ml syringe with 16 mls of sample and place a 1-ml syringe with no plunger at the end of it. Place this double syringe into the sample port and inject 15 ml of the sample.
13. Screw on the cap until it is hand tight.
14. Remove the locking pin. Lift the cell carefully from its stand into the hot well with the plugged sample port facing out of the hot well.
15. Close the vent valve and pressurise the cell to the desired pressure and check if there is any leak from the test cell in the heating jacket.
16. If the cell is not leaking the door of the hot well can be closed slowly.
17. Using the speed selector button set the fluid spinning at 200 rpm.
18. Press the start key to commence heating the sample. Once the fluid is at the correct temperature adjust the pressure on the cell and take the desired rheology readings.
19. Keep 500-psi pressure applied on the test cell while heating over 200 °F.
20. Once the test is complete, press the stop key button on the temperature controller to stop the heating process.
21. Press on display key this will start the cooling water process.
22. When test cell has cooled to room temperature, release the pressure on the cell slowly using the pressure release valve. When there is no more pressure on the test cell it can be dismantled safely.
23. Unscrew the coupling lock pin, and disconnect the pressure lines at the port couplings.



24. The cell can now be lifted out of the hot well. Dismantle the cell and clean all the parts thoroughly with detergent.
25. There is risk when dealing with temperature of 300 °F and pressure of 17,000 psi but the design of Fann-70 greatly minimises this risk. However the procedure should be followed carefully.

Table A28 (4.45) HP-HT Fann 70 viscometer reading for W BM							
Temperature	pressure	RPM 3	6	100	200	300	600
150 F	15 psi	4	5	23	38	49	82
	1000 psi	4	5	26	41	53	87
	3000 psi	4	6	27	43	56	92
	5000 psi	4	6	28	44	57	94
	6000 psi	4	6	28	44	58	95
	8000 psi	4	6	29	45	58	96
	10000 psi	4	6	29	46	59	97
	12000 psi	4	6	30	47	59	98
	15000 psi	4	6	30	48	60	100
17000 psi	4	6	31	48	60	101	
200 F	500 psi	3	4	16	24	33	57
	1000 psi	4	5	17	26	34	59
	3000 psi	4	5	18	27	36	60
	5000 psi	4	5	19	27	36	61
	6000 psi	4	5	19	27	37	62
	8000 psi	4	5	19	28	37	62
	10000 psi	4	5	20	29	38	63
	12000 psi	4	5	20	29	38	64
	15000 psi	4	5	20	30	39	65
17000 psi	4	5	21	30	40	67	
250 F	500 psi	3	4	11	16	21	40
	1000 psi	3	4	12	17	22	42
	3000 psi	3	4	13	18	23	43
	5000 psi	3	4	13	19	24	44
	6000 psi	3	4	14	19	24	45
	8000 psi	4	4	15	22	27	47
	10000 psi	4	4	16	22	28	48
	12000 psi	4	4	16	22	28	49
	15000 psi	4	4	16	23	29	50
17000 psi	4	4	17	23	30	52	
300 F	500 psi	3	3	10	14	20	37
	1000 psi	3	3	11	15	20	37
	3000 psi	3	3	11	16	20	37
	5000 psi	3	3	12	17	21	38
	6000 psi	3	3	12	17	21	38
	8000 psi	3	3	13	17	22	39
	10000 psi	3	3	13	18	22	39
	12000 psi	3	4	13	18	22	40
	15000 psi	3	4	14	18	22	41
17000 psi	3	4	15	19	23	42	

Table A29 (4.46) HP-HT Fann 70 viscometer reading for OBM

Temp.	Pressure	RPM 3	6	100	200	300	600
150 F	15 psi	8	9	18	23	29	48
	1000 psi	9	10	20	26	33	51
	3000 psi	10	12	22	32	38	58
	5000 psi	12	13	25	36	44	70
	6000 psi	13	14	26	37	47	75
	8000 psi	15	16	31	43	54	87
	10000 psi	16	17	34	48	59	94
	12000 psi	17	18	37	52	67	106
	15000 psi	18	19	41	58	75	121
	17000 psi	19	20	43	61	79	127
200 F	500 psi	7	8	16	21	25	39
	1000 psi	8	9	20	24	29	42
	3000 psi	8	10	21	25	31	46
	5000 psi	8	10	22	29	34	50
	6000 psi	10	11	22	30	35	54
	8000 psi	10	11	23	33	38	59
	10000 psi	13	14	26	36	44	68
	12000 psi	13	14	29	39	48	76
	15000 psi	13	14	33	45	55	87
	17000 psi	14	15	36	48	60	95
250 F	500 psi	6	8	16	20	22	34
	1000 psi	7	7	17	21	23	36
	3000 psi	7	8	18	21	25	37
	5000 psi	8	10	19	24	29	43
	6000 psi	8	10	21	26	32	46
	8000 psi	8	10	21	26	32	46
	10000 psi	11	12	22	29	34	50
	12000 psi	11	12	23	32	37	57
	15000 psi	13	14	26	35	42	64
	17000 psi	13	14	27	37	45	70
300 F	500 psi	4	6	13	15	19	29
	1000 psi	5	7	14	16	19	30
	3000 psi	5	7	15	18	21	34
	5000 psi	7	8	15	19	21	37
	6000 psi	7	8	16	21	24	37
	8000 psi	7	8	18	21	26	40
	10000 psi	9	10	19	23	29	45
	12000 psi	9	10	20	24	34	49
	15000 psi	11	12	23	31	37	54
	17000 psi	11	12	26	34	43	59

#### **A4.5.2 Particle size Distribution Testing Procedure:**

The Malvern Master-sizer Micro Plus particle size analyser should be operated in accordance with the following procedure:

1. Connect the Malvern Mastersizer Micro Plus to a computer and turn on.
2. The Malvern Mastersizer software includes a row of dialogue boxes at the top of the screen. Setting up the software to the run analysis sample is simply a matter of working through the first four of these dialogue boxes in turn and providing the information requested. Click on the first dialogue box-set-up range, analysis and presentation.
3. Accept default settings (internal-Micro sample dispersion unit).
4. Set up analysis - Enter particle density (SG of sample) and the refractive Index (RI) of the base fluid.
5. Click on second dialogue box - Open a sample file, load a record, and click on ok.
6. Click on third dialogue box - Document sample details and click on ok.
7. Put approximately 500 ml of clean base fluid into a beaker and place under the instrument motor. Lower the motor down into the fluid.
8. On the instrument control panel, press on button and allow the motor to come up to speed. The recommended motor speed is 2000 - 2500 rpm.
9. Click on the fourth dialogue box and follow screen instruction.
10. Collect 0.50 to 1.0 ml of mud sample in a syringe. Add a little sample at a time to avoid saturation - a very small quantity of mud is required. The actual amount will depend on the solids content of the sample.
11. As the sample is added the obscuration will increase until desired value is reached (15-25%) and then press space bar to go on to measure the sample stage.
12. The results in terms of tables and graphs will display and the analysis is now completed.
13. Press the save record button. This automatically saves the results on the recorded file.

## **APPENDIX B**

- Rheological Characterisation Results for WBM and OBM



Table B1 (5.4) Rheological characterisation for WBM									Fluid Rheological Parameters						
									Power Law Model		Bingham Plastic Model		Yield Power Law Model		
									n	K	PV	YP	YP	n	K
Temp.	pressure	Fann	5.1	10.2	170.2	340.4	510.6	1021.2	Regres.Coeff.		Regres.Coeff.		Regres.Coeff.		
150 F	15 psi	(F) SS	20.40	25.50	117.30	188.70	244.80	408.00	0.5525	735	37.9	7.81	3	0.7865	174
		(F) AV	399.20	249.50	68.86	55.39	47.90	39.92	0.99707		0.99166			0.9998	
	1000 psi	(F) SS	20.40	25.50	127.50	204.00	265.20	433.50	0.57877	717	40.5	8.47	3	0.8038	170
		(F) AV	399.20	249.50	74.85	59.88	51.90	42.42	0.99786		0.99954			0.9996	
	3000 psi	(F) SS	21.42	28.05	132.60	214.20	280.50	459.00	0.57526	772	42.9	8.84	2.89	0.7649	228
		(F) AV	419.16	274.45	77.84	62.87	54.89	44.91	0.99796		0.99035			0.9998	
	5000 psi	(F) SS	21.42	28.05	137.70	219.30	285.60	469.20	0.58036	765	43.8	9.05	2.89	0.7703	227
		(F) AV	419.16	274.45	80.84	64.37	55.89	45.91	0.99829		0.99999			0.9997	
	6000 psi	(F) SS	21.42	28.05	137.70	219.30	288.15	474.30	0.58195	763	44.3	8.95	2.89	0.7719	226
		(F) AV	419.16	274.45	80.84	64.37	56.39	46.41	0.99818		0.99032			0.9997	
	8000 psi	(F) SS	21.42	28.05	142.80	224.40	290.70	479.40	0.58634	761	44.7	9.28	2.89	0.7755	225
		(F) AV	419.16	274.45	83.83	65.87	56.89	46.91	0.99665		0.9996			0.9996	
	10000 psi	(F) SS	21.42	28.05	145.35	229.50	293.25	484.50	0.58832	758	45.2	9.48	2.89	0.7787	224
		(F) AV	419.16	274.45	85.33	67.37	57.39	47.41	0.99699		0.99882			0.9995	
	12000 psi	(F) SS	21.42	28.05	147.90	234.60	295.80	489.60	0.59126	750	45.6	9.68	2.89	0.7818	223
		(F) AV	419.16	274.45	86.83	68.86	57.88	47.90	0.9968		0.99821			0.9994	
	15000 psi	(F) SS	21.42	28.05	150.45	238.17	298.35	498.80	0.59482	750	46.6	9.68	2.89	0.7855	222
		(F) AV	419.16	274.45	88.32	69.91	58.38	48.90	0.99679		0.99872			0.9994	
	17000 psi	(F) SS	21.42	28.05	153.00	239.70	300.90	504.90	0.59696	748	47	9.75	2.89	0.7877	221
		(F) AV	419.16	274.45	89.82	70.36	58.88	49.40	0.99695		0.99871			0.9993	

Table B2 (5.5) Rheological characterisation for WBM									Fluid Rheological Parameters						
									Power Law Model		Bingham Plastic Model		Yield Power Law Model		
									n	K	PV	YP	YP	n	K
Temp.	pressure	Fann	5.1	10.2	170.2	340.4	510.6	1021.2	Regres.Coeff.		Regres.Coeff.		Regres.Coeff.		
200 F	500 psi	(F) SS	15.30	20.40	81.60	122.40	163.20	285.60	0.53353	997	26.2	5.19	2	0.70845	191
		(F) AV	299.40	199.60	47.90	35.93	31.94	27.94	0.9957		0.995579			0.99921	
	1000 psi	(F) SS	17.85	22.95	86.70	127.50	168.30	293.25	0.50981	716	26.7	5.83	2.5	0.70839	196
		(F) AV	349.30	224.55	50.90	37.43	32.93	28.69	0.99485		0.995178			0.9993	
	3000 psi	(F) SS	17.85	22.95	91.80	132.60	178.50	300.90	0.51905	707	27.5	6.23	2.5	0.71837	193
		(F) AV	349.30	224.55	53.89	38.92	34.93	29.44	0.99608		0.993381			0.99946	
	5000 psi	(F) SS	20.40	25.50	93.84	132.60	181.05	304.47	0.49403	834	27.6	6.61	3	0.71305	199
		(F) AV	399.20	249.50	55.09	38.92	35.43	29.79	0.99437		0.994088			0.99938	
	6000 psi	(F) SS	20.40	25.50	96.90	134.64	183.09	308.55	0.49736	831	27.9	6.77	3	0.7167	198
		(F) AV	399.20	249.50	56.89	39.52	35.83	30.19	0.99495		0.993492			0.99934	
	8000 psi	(F) SS	20.40	25.50	96.90	137.70	183.60	311.10	0.4994	827	28.2	6.79	3	0.71892	197
		(F) AV	399.20	249.50	56.89	40.42	35.93	30.44	0.99517		0.993509			0.99946	
	10000 psi	(F) SS	20.40	25.50	99.45	142.80	187.68	317.22	0.50492	820	28.8	6.99	3	0.72493	195
		(F) AV	399.20	249.50	58.38	41.92	36.73	31.04	0.9958		0.992728			0.99953	
	12000 psi	(F) SS	20.40	25.50	99.45	144.84	192.27	321.81	0.50853	814	29.3	7.01	3	0.72881	194
		(F) AV	399.20	249.50	58.38	42.51	37.62	31.49	0.99576		0.992784			0.99962	
	15000 psi	(F) SS	20.40	25.50	102.00	147.90	196.86	326.40	0.51289	809	29.8	7.19	3	0.73354	192
		(F) AV	399.20	249.50	59.88	43.41	38.52	31.94	0.99622		0.991951			0.99962	
	17000 psi	(F) SS	20.40	25.50	103.02	149.94	201.45	335.07	0.51771	801	30.6	7.14	3	0.7387	190
		(F) AV	399.20	249.50	60.48	44.01	39.42	32.78	0.99606		0.992576			0.99964	

n = Power law index, dimensionless  
K = Consistency index (cP)  
Pv = Plastic viscosity (cP)  
YP = Yield point (lb/100ft<sup>2</sup>)  
YS = Yield stress (lb/100ft<sup>2</sup>)  
SS = Shear stress (dyne/cm<sup>2</sup>)  
AV = Apparent viscosity (cP)



Table B3 (5.6) Rheological characterisation for WBM									Fluid Rheological Parameters						
									Power Law		Bingham Plastic		Yield Power Law		
									Model		Model		Model		
		n	K	PV	YP	YP	n	K							
Temp.	pressure	Flow	5.1	10.2	170.2	340.4	510.6	1021.2	Regres.Coeff.	Regres.Coeff.		Regres.Coeff.			
250 F	500 psi	(F) SS	12.75	17.85	56.10	81.60	107.10	198.90	0.48182	556	17.9	3.71	1.49	0.6236	216
		(F) AV	249.50	174.65	32.93	23.95	20.96	19.46	0.99064		0.99758			0.9981	
	1000 psi	(F) SS	12.75	17.85	61.20	86.70	112.20	209.10	0.49415	547	18.8	3.93	1.49	0.6398	213
		(F) AV	249.50	174.65	35.93	25.45	21.96	20.46	0.99287		0.99639			0.997	
	3000 psi	(F) SS	15.30	17.85	66.30	91.80	117.30	214.20	0.48029	622	19.1	4.48	2.5	0.7622	98
		(F) AV	299.40	174.65	38.92	26.95	22.95	20.96	0.99215		0.99507			0.9993	
	5000 psi	(F) SS	15.30	17.85	66.30	94.35	119.85	219.30	0.48523	615	19.7	4.47	2.5	0.7676	97
		(F) AV	299.40	174.65	38.92	27.69	23.45	21.46	0.99215		0.99549			0.9994	
	6000 psi	(F) SS	15.30	17.85	68.65	96.90	122.40	224.40	0.49077	610	20.1	4.58	2.5	0.7737	97
		(F) AV	299.40	174.65	40.42	28.44	23.95	21.96	0.99265		0.99484			0.9993	
	8000 psi	(F) SS	17.85	20.40	76.50	109.65	133.11	237.15	0.47651	728	21.1	5.57	3	0.7818	99
		(F) AV	349.30	199.60	44.91	32.19	26.05	23.20	0.9935		0.99234			0.9992	
	10000 psi	(F) SS	17.85	20.40	77.52	110.67	137.70	242.25	0.48143	720	21.7	5.59	3	0.7872	98
		(F) AV	349.30	199.60	45.51	32.48	26.95	23.70	0.99364		0.99266			0.9993	
	12000 psi	(F) SS	17.85	20.40	79.05	112.20	139.23	246.84	0.48465	716	22.1	5.61	3	0.7911	98
		(F) AV	349.30	199.60	46.41	32.93	27.25	24.15	0.99375		0.99281			0.9992	
	15000 psi	(F) SS	17.85	20.40	81.60	114.24	143.82	252.45	0.48065	701	22.6	5.72	3	0.7974	97
		(F) AV	349.30	199.60	47.90	33.53	28.14	24.70	0.99421		0.99246			0.9991	
	17000 psi	(F) SS	17.85	20.40	83.64	117.30	150.96	260.61	0.49655	699	23.5	5.82	3	0.8061	95
		(F) AV	349.30	199.60	49.10	34.43	29.54	25.50	0.99455		0.99249			0.9991	

Table B4 (5.7) Rheological characterisation for WBM										Fluid Rheological Parameters					
										Power Law Model		Bingham Plastic Model		Yield Power Law Model	
										n	K	PV	YP	YP	n
Temp.	pressure	Flow	5.1	10.2	170.2	340.4	510.6	1021.2	Regres.Coeff.	Regres.Coeff.		Regres.Coeff.			
300 F	500 psi	(F) SS	12.75	15.30	51.00	71.40	91.80	178.50	0.46657	531	15.9	3.26	2	0.7203	101
		(F) AV	249.50	149.70	29.94	20.96	17.96	17.47	0.98788		0.99996			0.9995	
	1000 psi	(F) SS	12.75	15.30	56.10	76.50	99.45	183.60	0.48158	523	16.4	3.68	2	0.735	99
		(F) AV	249.50	149.70	32.93	22.46	19.46	17.96	0.99183		0.99665			0.999	
	3000 psi	(F) SS	12.75	15.30	56.10	81.60	102.00	187.17	0.46615	516	16.8	3.8	2	0.7422	98
		(F) AV	249.50	149.70	32.93	23.95	19.96	18.31	0.99276		0.99533			0.9994	
	5000 psi	(F) SS	13.77	16.32	61.20	84.15	107.10	191.25	0.48029	566	17.1	4.26	2.2	0.7459	100
		(F) AV	299.46	159.68	35.93	24.70	20.96	18.71	0.99351		0.99377			0.9992	
	6000 psi	(F) SS	13.77	16.32	61.20	84.15	107.10	191.25	0.48029	566	17.1	4.26	2.2	0.7459	100
		(F) AV	299.46	159.68	35.93	24.70	20.96	18.71	0.99351		0.99377			0.9992	
	8000 psi	(F) SS	13.77	16.32	63.75	86.70	109.14	193.80	0.48499	563	17.3	4.44	2.2	0.7511	99
		(F) AV	299.46	159.68	37.43	25.46	21.36	18.96	0.99444		0.99231			0.999	
	10000 psi	(F) SS	13.77	16.32	65.28	87.72	109.14	196.35	0.48723	561	17.5	4.48	2.2	0.7536	99
		(F) AV	299.46	159.68	38.32	25.75	21.36	19.21	0.99452		0.99172			0.9988	
	12000 psi	(F) SS	15.30	17.85	66.30	89.25	109.65	199.92	0.46805	640	17.7	4.69	2.5	0.7488	102
		(F) AV	299.40	174.65	38.92	26.20	21.46	19.96	0.99297		0.99237			0.9988	
	15000 psi	(F) SS	15.30	17.85	69.87	91.80	112.20	205.02	0.47427	636	18.1	4.85	2.5	0.7558	101
		(F) AV	299.40	174.65	41.02	26.95	21.96	20.06	0.99363		0.99086			0.9984	
	17000 psi	(F) SS	15.30	17.85	73.95	96.90	114.75	209.61	0.48151	631	18.5	5.15	2.5	0.7639	100
		(F) AV	299.40	174.65	43.41	28.44	22.46	20.51	0.99458		0.98801			0.9978	

n = Power law index, dimensionless  
K = Consistency index (cP)  
Pv = Plastic viscosity (cP)  
YP = Yield point (lb/100ft<sup>2</sup>)  
YPS = Yield stress (lb/100ft<sup>2</sup>)  
SS = Shear stress (dyne/cm<sup>2</sup>)  
AV = Apparent viscosity (cP)



Table B5 (5.8) Rheological characterisation for OBM									Fluid Rheological Parameters						
									Power Law Model		Bingham Plastic Model		Yield Power Law Model		
									n	K	PV	YP	YP	n	K
									Regres.Coeff.		Regres.Coeff.		Regres.Coeff.		
Temp.	pressure	Fann	5.1	10.2	170.2	340.4	510.6	1021.2							
150 F	15 psi	(F) SS	40.80	46.41	91.80	118.32	145.35	242.25	0.304551	2278	19.3	10.02	6.89	0.5849 310	
		(F) AV	798.40	454.09	53.89	34.73	28.44	23.70	0.97403		0.99586			0.9967	
	1000 psi	(F) SS	46.41	52.53	100.98	133.11	167.79	260.61	0.299576	2613	20.7	11.65	7.89	0.5849 342	
		(F) AV	908.18	513.97	59.28	39.07	32.83	25.50	0.975959		0.9943			0.9975	
	3000 psi	(F) SS	52.53	58.65	114.24	163.20	195.33	297.84	0.307506	2899	23.9	13.58	9.1	0.6126 338	
		(F) AV	1027.94	573.85	67.07	47.90	38.22	29.14	0.979373		0.99049			0.9987	
	5000 psi	(F) SS	58.65	64.26	127.50	181.56	223.38	357.00	0.317434	3127	29.1	14.41	10.4	0.6513 304	
		(F) AV	1147.70	628.74	74.85	53.29	43.71	34.93	0.974486		0.99541			0.9988	
	6000 psi	(F) SS	64.26	70.38	133.11	190.74	237.15	383.01	0.31049	3456	31.1	15.27	11.4	0.6426 335	
		(F) AV	1257.48	688.62	78.14	55.99	46.41	37.47	0.969123		0.9971			0.9978	
	8000 psi	(F) SS	76.50	81.60	157.08	218.79	274.38	441.66	0.306284	4104	35.7	17.96	14.01	0.682 298	
		(F) AV	1497.00	798.40	92.22	64.22	53.69	43.21	0.968831		0.99714			0.9989	
	10000 psi	(F) SS	81.60	86.70	172.38	242.25	302.43	479.40	0.312791	4327	38.9	19.62	15.02	0.6984 298	
		(F) AV	1596.80	848.30	101.20	71.11	59.18	46.91	0.972533		0.99572			0.9994	
	12000 psi	(F) SS	86.70	91.80	190.74	265.20	339.15	540.60	0.324469	4485	44.4	20.87	16.01	0.7203 298	
		(F) AV	1696.60	898.20	111.98	77.84	66.37	52.89	0.973673		0.9961			0.9995	
	15000 psi	(F) SS	91.80	96.90	209.61	297.84	383.01	617.10	0.339602	4599	51.5	22.15	17	0.7459 288	
		(F) AV	1796.40	948.10	123.05	87.42	74.95	60.38	0.974734		0.99638			0.9995	
	17000 psi	(F) SS	96.90	102.00	218.79	311.61	400.35	647.70	0.338063	4859	54	23.17	18	0.7498 293	
		(F) AV	1896.20	998.00	128.44	91.47	78.34	63.37	0.973738		0.99671			0.9995	
Table B6 (5.9) Rheological characterisation for OBM									Fluid Rheological Parameters						
									Power Law Model		Bingham Plastic Model		Yield Power Law Model		
									n	K	PV	YP	YP	n	K
									Regres.Coeff.		Regres.Coeff.		Regres.Coeff.		
Temp.	pressure	Fann	5.1	10.2	170.2	340.4	510.6	1021.2							
200 F	500 psi	(F) SS	33.15	38.76	81.60	108.12	129.03	198.90	0.315963	1855	15.9	9.13	5.4	0.5702 308	
		(F) AV	648.70	379.24	47.90	31.74	25.25	19.46	0.986599		0.98786			0.9983	
	1000 psi	(F) SS	38.25	43.86	102.00	122.91	147.39	214.20	0.311548	2173	16.8	11.25	6.4	0.5864 316	
		(F) AV	748.50	429.14	59.88	36.08	28.84	20.96	0.993312		0.97428			0.9984	
	3000 psi	(F) SS	42.33	48.45	105.57	127.50	157.08	232.56	0.303079	2423	18.2	11.8	7.1	0.5774 348	
		(F) AV	828.34	474.05	61.98	37.43	30.74	22.75	0.988934		0.98237			0.9985	
	5000 psi	(F) SS	42.33	48.45	109.65	145.35	172.38	256.02	0.325218	2320	20.6	12.2	7.1	0.605 330	
		(F) AV	828.34	474.05	64.37	42.66	33.73	25.05	0.991142		0.98109			0.9994	
	6000 psi	(F) SS	48.45	54.06	114.24	150.96	176.97	274.38	0.307979	2697	21.7	12.95	8.4	0.6145 314	
		(F) AV	948.10	528.94	67.07	44.31	34.63	26.85	0.985295		0.98764			0.9994	
	8000 psi	(F) SS	48.45	54.06	118.32	167.79	195.33	302.43	0.329336	2581	24.6	13.23	8.4	0.6412 298	
		(F) AV	948.10	528.94	69.46	49.25	38.22	29.59	0.986146		0.98703			0.9996	
	10000 psi	(F) SS	66.30	71.40	133.11	181.56	223.38	344.76	0.288895	3718	27.1	16.07	12	0.6425 305	
		(F) AV	1297.40	698.60	78.14	53.29	43.71	33.73	0.972092		0.99446			0.999	
	12000 psi	(F) SS	66.30	71.40	145.35	199.92	246.84	387.60	0.312751	3555	31.3	16.46	12	0.6737 289	
		(F) AV	1297.40	698.60	85.33	58.68	48.30	37.92	0.976871		0.99398			0.9996	
	15000 psi	(F) SS	66.30	71.40	167.79	227.97	278.97	441.66	0.342084	3384	36.4	17.55	12	0.7112 273	
		(F) AV	1297.40	698.60	98.50	66.92	54.59	43.21	0.984693		0.99095			0.9998	
	17000 psi	(F) SS	71.40	76.50	181.56	246.84	307.02	484.50	0.346094	3603	40.2	18.82	13	0.7253 274	
		(F) AV	1397.20	748.50	106.59	72.45	60.08	47.41	0.984279		0.9915			0.9998	
n = Power law index, dimensionless															
K = Consistency index (cP)															
Pv = Plastic viscosity (cP)															
YP= Yield point (lb/100ft <sup>2</sup> )															
YPs= Yield stress (lb/100ft <sup>2</sup> )															
SS = Shear stress (dyne/cm <sup>2</sup> )															
AV = Apparent viscosity (cP)															



Table B7 (5.10) Rheological characterisation for OBM									Fluid Rheological Parameters						
									Power Law		Bingham Plastic		Yield Power Law		
									Model		Model		Model		
									n	K	PV	YP	YP	n	K
Temp.	pressure	Fann	5.1	10.2	170.2	340.4	510.6	1021.2	Regres.Coeff.		Regres.Coeff.		Regres.Coeff.		
250 F	500 psi	(F) SS	32.13	38.25	81.60	100.98	114.24	172.38	0.296569	1907	13.2	9.31	5.1	0.5295	359
		(F) AV	628.74	374.25	47.90	29.64	22.36	16.87	0.9917		0.97661			0.9973	
	1000 psi	(F) SS	36.21	36.21	86.70	105.57	118.32	181.56	0.297176	1985	13.9	9.67	7.1	0.8619	44
		(F) AV	708.58	354.29	50.90	30.99	23.15	17.76	0.986855		0.97598			0.9898	
	3000 psi	(F) SS	36.21	42.33	89.25	105.57	127.50	190.74	0.291817	2143	14.6	10.1	5.89	0.5407	360
		(F) AV	708.58	414.17	52.40	30.99	24.95	18.66	0.988557		0.9816			0.9974	
	5000 psi	(F) SS	42.33	48.45	96.90	122.91	145.35	218.79	0.288872	2480	16.9	11.4	7.1	0.5592	358
		(F) AV	828.34	474.05	56.89	36.08	28.44	21.41	0.985821		0.98555			0.9984	
	6000 psi	(F) SS	42.33	48.45	105.57	133.11	163.20	232.56	0.307642	2405	18.3	12.11	7.1	0.5834	345
		(F) AV	828.34	474.05	61.98	39.07	31.94	22.75	0.99121		0.97808			0.9991	
	8000 psi	(F) SS	42.33	48.45	105.57	133.11	163.20	232.56	0.307642	2405	18.3	12.11	7.1	0.5834	345
		(F) AV	828.34	474.05	61.98	39.07	31.94	22.75	0.99121		0.97808			0.9991	
	10000 psi	(F) SS	54.06	60.18	109.65	145.35	172.38	256.02	0.272541	3206	19.5	13.78	9.4	0.5715	370
		(F) AV	1057.88	588.82	64.37	42.66	33.73	25.05	0.978891		0.98895			0.9985	
	12000 psi	(F) SS	54.06	60.18	118.32	163.20	190.74	288.66	0.297467	3056	22.7	14.19	9.4	0.6041	349
		(F) AV	1057.88	588.82	69.46	47.90	37.33	28.24	0.982481		0.98769			0.9992	
	15000 psi	(F) SS	66.30	71.40	133.11	176.97	214.20	326.91	0.279922	3800	25.3	16.28	12	0.6309	313
		(F) AV	1297.40	698.60	78.14	51.95	41.92	31.99	0.974622		0.99271			0.9993	
	17000 psi	(F) SS	66.30	71.40	139.23	190.74	227.97	357.00	0.29674	3670	28.2	16.41	12	0.6531	301
		(F) AV	1297.40	698.60	81.74	55.99	44.61	34.93	0.976169		0.99305			0.9995	
Table B8 (5.11) Rheological characterisation for OBM															
									Fluid Rheological Parameters						
									Power Law		Bingham Plastic		Yield Power Law		
									Model		Model		Model		
									n	K	PV	YP	YP	n	K
Temp.	pressure	Fann	5.1	10.2	170.2	340.4	510.6	1021.2	Regres.Coeff.		Regres.Coeff.		Regres.Coeff.		
300 F	500 psi	(F) SS	21.93	28.05	66.30	76.50	94.35	145.35	0.330158	1261	11.6	6.75	3.1	0.5125	346
		(F) AV	429.14	274.45	38.92	22.46	18.46	14.22	0.991589		0.97992			0.9951	
	1000 psi	(F) SS	27.03	33.15	71.40	81.60	98.94	150.96	0.298119	1619	11.6	7.79	4.1	0.5056	363
		(F) AV	528.94	324.35	41.92	23.95	19.36	14.77	0.988784		0.98041			0.9951	
	3000 psi	(F) SS	27.03	33.15	76.50	90.27	107.61	172.38	0.322268	1543	13.6	7.87	4.1	0.5346	343
		(F) AV	528.94	324.35	44.91	26.50	21.06	16.87	0.989239		0.98355			0.9959	
	5000 psi	(F) SS	33.15	38.76	76.50	98.94	107.10	186.15	0.292083	1939	14.4	8.53	5.4	0.5399	325
		(F) AV	648.70	379.24	44.91	29.04	20.96	18.21	0.977503		0.98889			0.9951	
	6000 psi	(F) SS	33.15	38.76	81.60	104.55	119.85	190.74	0.305593	1900	14.9	9.08	5.4	0.5574	317
		(F) AV	648.70	379.24	47.90	30.69	21.96	18.66	0.98643		0.98654			0.9977	
	8000 psi	(F) SS	33.15	38.76	90.27	107.61	130.05	205.02	0.321032	1850	16.3	9.39	5.4	0.5766	308
		(F) AV	648.70	379.24	52.99	31.59	25.45	20.06	0.988911		0.98446			0.9976	
	10000 psi	(F) SS	45.90	51.00	94.35	117.81	147.90	227.97	0.275909	2690	17.5	11.26	8	0.5778	305
		(F) AV	898.20	499.00	55.39	34.58	28.94	22.31	0.973074		0.99402			0.9975	
	12000 psi	(F) SS	45.90	51.00	103.02	122.91	170.85	251.43	0.298251	2578	20	11.6	8	0.6069	290
		(F) AV	898.20	499.00	60.48	36.08	33.43	24.60	0.975769		0.99035			0.9976	
	15000 psi	(F) SS	56.10	61.20	117.81	157.08	189.72	274.38	0.284022	3230	21.2	14.58	10	0.616	306
		(F) AV	1097.80	598.80	69.16	46.11	37.13	26.85	0.98217		0.98566			0.9997	
	17000 psi	(F) SS	56.10	61.20	130.05	175.44	217.26	302.43	0.30923	3090	24.1	15.5	10	0.6492	290
		(F) AV	1097.80	598.80	76.35	51.50	42.51	29.59	0.987796		0.97852			0.9999	
n = Power law index, dimensionless K = Consistency index (cP) Pv = Plastic viscosity (cP) YP= Yield point (lb/100ft^2) YPs= Yield stress (lb/100ft^2) SS = Shear stress (dyne/cm^2) AV = Apparent viscosity (cP)															



## **APPENDIX C**

- Rheological Models Validation for WBM and OBM
- Static and Dynamic Results for WBM and OBM

Table C1 (6.6) Comparison between model predictions,experimental and independent test data validation data for WBM

															coefficients	
$\tau_i = \tau_s [-A_c \exp(BT + CP)]$															A=	2.74
															B =	0.0064
															C =	1E-05
Temp	Pressure	S.S 600	prediction	S.S 300	prediction	S.S 200	prediction	S.S 100	prediction	S.S 6	prediction	S.S 3	prediction	% Error		
150	15	408		244.8		188.7		117.3		25.5		20.4				
150	1000	433.50	432.35	265.20	259.41	204.00	199.96	127.50	124.30	25.50	27.02	20.40	21.62	0.48		
150	3000	459.00	441.08	280.50	264.65	214.20	204.00	132.60	126.81	28.05	27.57	21.42	22.05	2.04		
150	5000	469.20	449.99	285.60	269.99	219.30	208.12	137.70	129.37	28.05	28.12	21.42	22.50	2.15		
150	6000	474.30	454.51	288.15	272.71	219.30	210.21	137.70	130.67	28.05	28.41	21.42	22.73	1.99		
150	8000	479.40	463.69	290.70	278.22	224.40	214.46	142.80	133.31	28.05	28.98	21.42	23.18	1.76		
150	10000	484.50	473.06	293.25	283.84	229.50	218.79	145.35	136.01	28.05	29.57	21.42	23.65	1.43		
150	12000	489.60	482.62	295.80	289.57	234.60	223.21	147.90	138.75	28.05	30.16	21.42	24.13	1.09		
150	15000	499.80	497.32	298.35	298.39	238.17	230.01	150.45	142.98	28.05	31.08	21.42	24.87	0.42		
150	17000	504.90	507.36	300.90	304.42	239.70	234.66	153.00	145.87	28.05	31.71	21.42	25.37	0.05		
200	500	285.60	312.38	163.20	187.43	122.40	144.48	81.60	89.81	28.05	19.52	15.30	15.62	4.25		
200	1000	293.25	313.95	168.30	188.37	127.50	145.20	86.70	90.26	22.95	19.62	17.85	15.70	3.27		
200	3000	300.90	320.29	178.50	192.17	132.60	148.13	91.80	92.08	22.95	20.02	17.85	16.01	2.50		
200	5000	304.47	326.76	181.05	196.06	132.60	151.13	93.84	93.94	25.50	20.42	20.40	16.34	2.60		
200	6000	308.55	330.04	183.09	198.03	134.64	152.65	96.90	94.89	25.50	20.63	20.40	16.50	2.40		
200	8000	311.10	336.71	183.60	202.03	137.70	155.73	96.90	96.80	25.50	21.04	20.40	16.84	2.91		
200	10000	317.22	343.51	187.68	206.11	142.80	158.87	99.45	98.76	25.50	21.47	20.40	17.18	2.79		
200	12000	321.81	350.45	192.27	210.27	144.84	162.08	99.45	100.76	25.50	21.90	20.40	17.52	3.04		
200	15000	326.40	361.13	196.86	216.68	147.90	167.02	102.00	103.82	25.50	22.57	20.40	18.06	3.53		
200	17000	335.07	368.42	201.45	221.05	149.94	170.39	103.02	105.92	25.50	23.03	20.40	18.42	3.54		
															Comparison between model predictions and experimental data	
															Average error	2.01
															Comparison between validation test data and model predictions	
																2.38

Table C2 (6.7) Comparison between model predictions,experimental and independent test data validation data for WBM

															coefficients	
$\tau_i = \tau_s [-A_c \exp(BT + CP)]$															A=	2.74
															B =	0.0064
															C =	1E-05
Temp	Pressure	S.S 600	prediction	S.S 300	prediction	S.S 200	prediction	S.S 100	prediction	S.S 6	prediction	S.S 3	prediction	% Error		
250	500	198.90	226.84	107.10	136.10	81.60	104.91	56.10	65.22	17.85	14.18	12.75	11.34	6.75		
250	1000	209.10	227.97	112.20	136.78	86.70	105.44	61.20	65.54	17.85	14.25	12.75	11.40	4.91		
250	3000	214.20	232.58	117.30	139.55	91.80	107.57	66.30	66.87	17.85	14.54	15.30	11.63	3.90		
250	5000	219.30	237.28	119.85	142.37	94.35	109.74	66.30	68.22	17.85	14.83	15.30	11.86	3.93		
250	6000	224.40	239.66	122.40	143.80	96.90	110.84	68.85	68.90	17.85	14.98	15.30	11.98	3.37		
250	8000	237.15	244.60	133.11	146.70	109.65	113.08	76.50	70.29	20.40	15.28	17.85	12.23	0.65		
250	10000	242.25	249.44	137.70	149.67	110.65	115.37	77.52	71.71	20.40	15.59	17.85	12.47	0.57		
250	12000	246.84	254.48	139.23	152.69	112.20	117.70	79.05	73.16	20.40	15.91	17.85	12.72	0.79		
250	15000	252.45	262.23	143.82	157.34	114.24	121.28	81.60	75.39	20.40	16.39	17.85	13.11	1.07		
250	17000	260.61	267.53	150.96	160.52	117.30	123.73	83.64	76.91	20.40	16.72	17.85	13.38	0.54		
300	500	178.50	164.72	91.80	98.83	71.40	76.18	51.00	47.36	15.30	10.29	12.75	8.24	1.67		
300	1000	183.60	165.54	99.45	99.33	76.50	76.56	56.10	47.59	15.30	10.35	12.75	8.28	3.96		
300	3000	187.17	168.89	102.00	101.33	81.60	78.11	56.10	48.55	15.30	10.56	12.75	8.44	4.20		
300	5000	191.25	172.30	107.10	103.38	84.15	79.69	61.20	49.54	16.32	10.77	13.77	8.61	5.22		
300	6000	191.25	174.03	107.10	104.42	84.15	80.49	61.20	50.03	16.32	10.88	13.77	8.70	4.72		
300	8000	193.80	177.55	109.14	106.53	86.70	82.11	63.75	51.04	16.32	11.10	13.77	8.88	4.73		
300	10000	196.35	181.13	109.14	108.68	87.72	83.77	65.28	52.08	16.32	11.32	13.77	9.06	4.27		
300	12000	199.92	184.79	109.65	110.87	89.25	85.47	66.30	53.13	17.85	11.55	15.30	9.24	4.25		
300	15000	205.02	190.42	112.20	114.25	91.80	88.07	69.87	54.75	17.85	11.90	15.30	9.52	4.11		
300	17000	209.61	194.27	114.65	116.56	96.90	89.85	73.95	55.85	17.85	12.14	15.30	9.71	4.66		
															Comparison between model predictions and experimental data	
															Average error	3.38
															Comparison between validation test data and model predictions	
																3.27



Table C3 (6.8) Comparison between model predictions, experimental and independent test data validation data for OBM

Table 65 (a-c) Comparison between model predictions and experimental test data validation data for CGM																						
<div><div><math display="block">\tau_i = \tau_s [-A_c \exp(BT + CP)]</math></div><div><table><tr><th colspan="2">COEFFICIENTS</th></tr><tr><th>A</th><th>1.95</th></tr><tr><th>B</th><th>-3.80E-03</th></tr><tr><th>C</th><th>5.00E-05</th></tr></table></div></div>															COEFFICIENTS		A	1.95	B	-3.80E-03	C	5.00E-05
COEFFICIENTS																						
A	1.95																					
B	-3.80E-03																					
C	5.00E-05																					
Temp	Pressure	S.S 600	prediction	S.S 300	prediction	S.S 200	prediction	S.S 100	prediction	S.S 6	prediction	S.S 3	prediction	% Error								
150	15	242.25		145.35		118.32		91.80		46.41		40.80										
150	1000	260.61	280.84	167.79	168.51	133.11	137.17	100.96	106.43	52.53	53.80	46.41	47.30	1.84								
150	3000	297.84	310.38	195.33	186.23	163.20	151.60	114.24	117.62	58.65	59.46	52.53	52.27	0.22								
150	5000	357.00	343.02	223.38	205.81	181.56	167.54	127.50	129.99	64.26	65.72	58.65	57.77	1.96								
150	6000	383.01	360.61	237.15	216.37	190.74	176.13	133.11	136.65	70.38	69.09	64.26	60.73	2.59								
150	8000	441.66	398.54	274.38	239.12	218.79	194.65	157.08	151.02	81.60	76.35	76.50	67.12	4.89								
150	10000	479.40	440.45	302.43	264.27	242.25	215.13	172.38	166.91	86.70	84.38	81.60	74.18	4.29								
150	12000	540.60	486.77	339.15	292.06	265.20	237.75	190.74	184.46	91.80	93.26	86.70	81.98	4.48								
150	15000	617.10	565.55	383.01	339.33	297.84	276.23	209.61	214.31	96.90	108.35	91.80	95.25	2.72								
150	17000	647.70	625.03	400.35	375.02	311.61	305.28	218.79	236.95	102.00	119.74	96.90	105.27	0.26								
200	500	198.90	198.90	129.03	129.03	108.12	118.32	81.60	91.80	38.76	38.76	33.15	33.15	1.50								
200	1000	214.20	232.25	147.39	139.35	122.91	113.43	102.00	88.01	43.86	44.49	38.25	39.12	0.81								
200	3000	232.56	256.67	157.08	154.00	127.50	125.36	105.57	97.27	48.45	49.17	42.33	43.23	0.75								
200	5000	256.02	283.67	172.38	170.20	145.35	138.55	109.65	107.49	48.45	54.34	42.33	47.78	1.55								
200	6000	274.38	298.21	176.97	178.93	150.96	145.65	114.24	113.01	54.06	57.13	48.45	50.22	1.28								
200	8000	302.43	329.57	195.33	197.74	167.79	160.97	118.32	124.89	54.06	63.14	48.45	55.51	2.18								
200	10000	344.76	364.24	223.38	218.54	181.56	177.90	133.11	138.03	71.40	69.78	66.30	61.34	0.40								
200	12000	387.60	402.54	246.84	241.53	199.92	196.61	145.35	152.54	71.40	77.12	66.30	67.80	0.81								
200	15000	441.66	467.69	278.97	280.61	227.97	228.43	167.79	177.23	71.40	89.60	66.30	78.77	2.31								
200	17000	484.50	516.87	307.02	310.12	246.84	252.45	181.56	195.87	76.50	99.02	71.40	87.05	2.86								

Comparison between model predictions and experimental data

Average error

1.70

Model validation with test data

Average error

2.60

Table C4 (6.9) Comparison between model predictions, experimental and independent test data validation data for OBM

<div> <div> <math>\tau_i = \tau_s [-A_c \exp(BT + CP)]</math> </div> <div> <div>COEFFICIENTS</div> <table> <tr><td>A</td><td>1.95</td></tr> <tr><td>B</td><td>-3.80E-03</td></tr> <tr><td>C</td><td>5.00E-05</td></tr> </table> </div> </div>															A	1.95	B	-3.80E-03	C	5.00E-05
A	1.95																			
B	-3.80E-03																			
C	5.00E-05																			
Temp	Pressure	S.S 600	prediction	S.S 300	prediction	S.S 200	prediction	S.S 100	prediction	S.S 6	prediction	S.S 3	prediction	% Error						
250	500	172.38	187.32	114.24	112.39	100.98	91.49	81.60	70.98	36.25	35.89	32.13	31.55	0.84						
250	1000	181.56	192.06	118.32	115.24	105.57	93.81	86.70	72.78	36.21	36.79	36.21	32.35	1.77						
250	3000	190.74	212.26	127.50	127.35	105.57	103.67	89.25	80.43	42.33	40.66	36.21	35.75	0.64						
250	5000	218.79	234.58	145.35	140.75	122.91	114.57	96.90	88.89	48.45	44.94	42.33	39.51	0.77						
250	6000	232.56	246.61	163.20	147.96	133.11	120.45	105.57	93.45	48.45	47.24	42.33	41.53	1.79						
250	8000	232.56	272.54	163.20	163.53	133.11	133.12	105.57	103.28	48.45	52.21	42.33	45.90	2.63						
250	10000	256.02	301.21	172.38	180.72	145.35	147.12	109.65	114.14	60.18	57.71	54.06	50.73	2.83						
250	12000	268.66	332.89	190.74	199.73	163.20	162.59	118.32	126.15	60.18	63.77	54.06	56.06	3.14						
250	15000	326.91	386.76	214.20	232.05	176.97	188.90	133.11	145.56	71.40	74.09	66.30	65.14	4.28						
250	17000	357.00	427.43	227.97	256.46	190.74	208.77	139.23	161.97	71.40	81.89	66.30	71.99	5.77						
300	500	145.35	154.90	94.35	92.94	76.50	75.66	66.30	58.70	28.05	29.68	21.93	26.09	0.56						
300	1000	150.96	158.82	98.94	95.29	81.60	77.57	71.40	60.19	33.15	30.43	27.03	26.75	1.40						
300	3000	172.38	175.53	107.61	105.32	90.27	85.73	76.50	66.52	33.15	33.63	27.03	29.56	0.96						
300	5000	186.15	193.99	107.10	116.39	98.94	94.75	76.50	73.51	38.76	37.16	33.15	32.67	0.64						
300	6000	190.74	203.93	119.85	122.36	104.55	99.61	81.60	77.28	38.76	39.07	33.15	34.35	0.62						
300	8000	205.02	225.38	130.05	135.23	107.61	110.08	90.27	85.41	38.76	43.18	33.15	37.96	2.27						
300	10000	227.97	249.09	147.90	149.45	117.81	121.66	94.35	94.39	51.00	47.72	45.90	41.95	1.23						
300	12000	251.43	275.28	170.85	165.17	122.91	134.45	103.02	104.32	51.00	52.74	45.90	46.36	1.91						
300	15000	274.38	319.83	189.72	191.90	157.08	156.21	117.81	121.20	61.20	61.27	56.10	53.87	2.37						
300	17000	302.43	353.47	217.26	212.08	175.44	172.64	130.05	133.95	61.20	67.72	56.10	59.53	2.55						

Table C5 (6.11) Regression Coefficients of Static Filtration Experiments (WBM)  
Model Applications for Temperature and Pressure

Temperature (F)	Solids Fraction of Slurry (%)	Differential Pressure (psi)	$a_2$ (min/ml <sup>2</sup> )	$a_1$ (min/ml)	$t_o$ (min)
150	35.13	200	4.19	7.55	2.93
		500	2.98	5.79	1.98
		800	2.29	4.59	0.66
200	35.13	200	2.10	6.54	-1.13
		500	1.52	6.64	-5.63
		800	1.21	5.49	-3.24
250	35.13	200	1.19	4.62	2.08
		500	0.86	3.55	3.49
		800	0.63	2.63	3.15
300	35.13	200	0.57	3.62	-3.09
		500	0.45	2.65	-0.66
		800	0.33	1.92	-2.56

Table C6 (6.12) Regression Coefficients of Static Filtration Experiments (WBM)  
Model Applications for Solids Concentration

Temperature (F)	Solids Fraction of Slurry (%)	Differential Pressure (psi)	$a_2$ (min/ml <sup>2</sup> )	$a_1$ (min/ml)	$t_o$ (min)
250	20.99	500	0.42	2.14	-1.40
250	35.13	500	0.84	3.55	3.49
250	49.85	500	0.65	0.88	-0.84



Table C7 (6.13) Regression Coefficients of Static Filtration Experiments (WBM)  
Model Applications for Permeability (WBM)

Temperature (F)	Permeability (MD)	Solids Fraction of Slurry (%)	Differential Pressure (psi)	$a_2$ (min/ml <sup>2</sup> )	$a_1$ (min/ml)	$t_o$ (min)
250	Filter paper	20.99	500	0.39	0.42	0.63
250	400	20.99	500	0.42	2.14	-1.40
250	2000	20.99	500	0.43	1.97	-1.07
250	5000	20.99	500	0.40	2.10	-1.07

Table C8 (6.14) Regression Coefficients of Static Filtration Experiments (WBM)  
Model Applications for Permeability

Temperature (F)	Permeability (MD)	Solids Fraction of Slurry (%)	Differential Pressure (psi)	$a_2$ (min/ml <sup>2</sup> )	$a_1$ (min/ml)	$t_o$ (min)
250	Filter paper	35.13	500	1.05	3.84	0.75
250	400	35.13	500	0.86	3.55	3.49
250	2000	35.13	500	0.80	3.45	2.74
250	5000	35.13	500	0.82	3.29	-2.70

Table C9 (6.15) Regression Coefficients of Static Filtration Experiments (WBM)  
Model Applications for Permeability

Temperature (F)	Permeability (MD)	Solids Fraction of Slurry (%)	Differential Pressure (psi)	a <sub>2</sub> (min/ml <sup>2</sup> )	a <sub>1</sub> (min/ml)	t <sub>o</sub> (min)
250	Filter paper	49.85	500	0.89	11.04	-10.51
250	400	49.85	500	0.65	2.88	-0.84
250	2000	49.85	500	0.76	3.76	-9.91
250	5000	49.85	500	0.89	3.84	-8.96

Table C10 (6.16) Regression Coefficients of Static Filtration Experiments (WBM)  
Model Applications for Fluid Loss Additives (Coating Materials)

Temperature (F)	Fluid Loss Concentration (lb/bbl)	Solids Fraction of Slurry (%)	Differential Pressure (psi)	a <sub>2</sub> (min/ml <sup>2</sup> )	a <sub>1</sub> (min/ml)	t <sub>o</sub> (min)
250	0	35.13	500	0.77	3.65	3.49
250	1.0	35.13	500	0.96	2.32	4.41
250	3.0	35.13	500	1.31	1.63	5.59
250	5.0	35.13	500	1.47	1.55	7.08

Table C11 (6.17) Regression Coefficients of Static Filtration Experiments (WBM)  
 Model Applications for Fluid Loss Additives (Plugging Materials)

Temperature (F)	Fluid Loss Concentration (%)	Solids Fraction of Slurry (%)	Differential Pressure (psi)	a <sub>2</sub> (min/ml <sup>2</sup> )	a <sub>1</sub> (min/ml)	t <sub>o</sub> (min)
250	0	35.13	500	0.77	3.65	3.49
250	3.0	35.13	500	0.94	3.45	4.80
250	8.0	35.13	500	1.18	2.95	6.31
250	13.0	35.13	500	1.66	1.95	8.63

Table C12 (6.18) Regression Coefficients of Static Filtration Experiments (WBM)  
 Model Applications for Fluid Loss Additives (Viscosifying Materials)

Temperature (F)	Fluid Loss Concentration (lb/bbl)	Solids Fraction of Slurry (%)	Differential Pressure (psi)	a <sub>2</sub> (min/ml <sup>2</sup> )	a <sub>1</sub> (min/ml)	t <sub>o</sub> (min)
250	0	35.13	500	0.77	3.65	3.49
250	1.0	35.13	500	1.02	2.22	4.44
250	3.0	35.13	500	1.25	0.58	6.03
250	5.0	35.13	500	1.63	0.22	8.52



Table C13 (6.19) Regression Coefficients of Static Filtration Experiments (OBM)  
Model Applications for Pressure and Temperature:

Temperature (F)	Solids Fraction of Slurry (%)	Differential Pressure (psi)	$a_2$ (min/ml <sup>2</sup> )	$a_1$ (min/ml)	$t_o$ (min)
150	41.70	200	75.25	55.40	4.53
		500	66.49	46.35	3.60
		800	57.12	37.35	2.39
200	41.70	200	42.35	29.66	2.19
		500	38.26	24.41	-0.97
		800	31.45	21.30	-0.80
250	41.70	200	24.67	18.24	1.04
		500	21.65	15.63	1.23
		800	17.85	13.56	1.30
300	41.70	200	14.58	10.0	0.29
		500	12.63	8.65	1.82
		800	10.76	7.85	2.18

Table C14 (6.20) Regression Coefficients of Static Filtration Experiments (OBM)  
Model Applications for Solids Concentration

Temperature (F)	Solids Fraction of Slurry (%)	Differential Pressure (psi)	$a_2$ (min/ml <sup>2</sup> )	$a_1$ (min/ml)	$t_o$ (min)
250	21.90	500	5.86	65.19	2.21
250	41.70	500	21.25	15.63	2.51
250	55.00	500	37.39	20.43	3.13



Table C15 (6.21) Regression Coefficients of Static Filtration Experiments (OBM)  
Model Applications for Permeability

Temperature (F)	Solids Fraction of Slurry (%)	Permea- bility (md)	Differential Pressure (psi)	$a_2$ (min/ml <sup>2</sup> )	$a_1$ (min/ml)	$t_o$ (min)
250	21.90	400	500	5.86	65.19	2.21
250	21.90	2000	500	11.24	31.07	4.83
250	21.90	5000	500	17.76	25.44	5.01
250	41.70	400	500	21.25	15.63	1.23
250	41.70	2000	500	21.66	16.07	2.86
250	41.70	5000	500	21.48	17.90	3.36

Table C16 (6.22) Regression Coefficients of Static Filtration Experiments (OBM)  
Model Applications for Fluid Loss Additives (Coating Materials)

Temperature (F)	Fluid Loss Concentr- ation (lb/bbl)	Solids Fraction of Slurry (lb/bbl)	Differential Pressure (psi)	$a_2$ (min/ml <sup>2</sup> )	$a_1$ (min/ml)	$t_o$ (min)
250	0	41.70	500	3.71	5.09	-0.95
250	0.25	41.70	500	3.86	6.03	-1.24
250	1.0	41.70	500	8.96	6.22	1.95
250	2.0	41.70	500	10.89	6.76	0.20
250	4.0	41.70	500	12.30	9.86	-0.48

Table C17 (6.23) Regression Coefficients of Static Filtration Experiments (OBM)  
Model Applications for Fluid Loss Additives (Plugging Materials)

Temperature (F)	Fluid Loss Concentra tion (lb/bbl)	Solids Fraction of Slurry (lb/bbl)	Differential Pressure (psi)	$a_2$ (min/ml <sup>2</sup> )	$a_1$ (min/ml)	$t_o$ (min)
250	0	41.70	500	3.71	5.09	-0.95
250	0.25	41.70	500	6.34	6.21	0.75
250	1.0	41.70	500	14.51	7.07	1.17
250	2.0	41.70	500	15.0	11.11	-1.85
250	4.0	41.70	500	47.92	35.21	-2.74

Table C18 (6.24) Regression Coefficients of Static Filtration Experiments (OBM)  
Model Applications for Fluid Loss Additives (Viscosifying Materials)

Temperature (F)	Fluid Lose Concentra tion (lb/bbl)	Solids Fraction of Slurry (lb/bbl)	Differential Pressure (psi)	$a_2$ (min/ml <sup>2</sup> )	$a_1$ (min/ml)	$t_o$ (min)
250	0	41.70	500	3.71	5.09	-0.95
250	0.25	41.70	500	5.13	7.96	-1.24
250	1.0	41.70	500	11.39	11.30	0.69
250	2.0	41.70	500	28.51	21.52	3.97
250	4.0	41.70	500	32.26	25.30	-2.21



Regression Coefficients of Dynamic Filtration Experiments  
(Water based mud)

Table C19 (6.35) Pressure and Temperature Applications

Temperature (F)	Solids Fraction in Slurry (%)	Differential Pressure (psi)	C1 (min/ml)	C2 (min)	C3 (1/ml)	t0 (min)
150	35.13	200	146.8	3780.89	0.038	0.09
		500	70.69	955.28	0.073	1.79
		800	49.66	491.84	0.1	1.73
200	35.13	200	120.66	4143.41	0.028	-0.81
		500	40.17	403.3	0.099	2.22
		800	37.03	396.71	0.09	1.42
250	35.13	200	66.31	1183.49	0.053	-2.49
		500	37.42	597.86	0.06	0.22
		800	23.13	186.16	0.12	1.19
300	35.13	200	29.58	394.91	0.074	0.8
		500	23.31	310.69	0.07	1.27
		800	17.99	197.52	0.08	-1.71

Table C20 (6.36) Solids Applications

Temperature (F)	Differential Pressure (psi)	Solids Fraction in Slurry (%)	C1 (min/ml)	C2 (min)	C3 (1/ml)	t0 (min)
250	500	20.99	18.28	306.66	0.055	0.97
250	500	35.13	37.42	597.86	0.06	0.22
250	500	49.85	60.99	2525.56	0.024	-1

Table C21 (6.37) Permeability and Solids Applications

Temperature (F)	Differential Pressure (psi)	Solids Fraction in Slurry (%)	Permeability (md)	C1 (min/ml)	C2 (min)	C3 (1/ml)	t0 (min)
250	500	20.99	400	18.28	306.66	0.058	0.97
250	500	20.99	2000	21.66	484.29	0.044	0.17
250	500	20.99	5000	26.84	826.41	0.032	-0.58
250	500	35.13	400	37.42	597.86	0.06	0.22
250	500	35.13	2000	28.5	350.36	0.08	2.13
250	500	35.13	5000	58.64	2149.69	0.026	-5.37
250	500	49.85	400	60.99	2525.56	0.024	-1
250	500	49.85	2000	38.03	760.59	0.049	0.41
250	500	49.85	5000	33.06	445.08	0.07	0.66

Regression Coefficients of Dynamic Filtration Experiments (Water based mud)

Table C22 (6.38) Shear Rate Applications

Temperature (F)	Differential Pressure (psi)	Solids Fraction in Slurry (%)	Shear rate (rpm)	C1 (min/ml)	C2 (min)	C3 (l/ml)	t0 (min)
250	500	35.13	80	37.42	597.86	0.06	0.22
250	500	35.13	120	26.74	268.46	0.09	0.64
250	500	35.13	160	38.43	784.85	0.048	0.41
250	500	35.13	200	57.7	2125.69	0.027	-1.46

Table C23 (6.39) Fluid loss Additives Applications (Plugging Agent)

Temperature (F)	Differential Pressure (psi)	Solids Fraction in Slurry (%)	Concentration (%)	C1 (min/ml)	C2 (min)	C3 (l/ml)	t0 (min)
250	500	35.13	0	45.07	957.65	0.044	-0.32
250	500	35.13	3	49.74	846.77	0.055	-0.18
250	500	35.13	8	51.91	797.96	0.065	-0.58
250	500	35.13	13	216.89	18243.35	0.011	7.64

Table C24 (6.40) Fluid loss Additives Applications (Viscosifying Agent)

Temperature (F)	Differential Pressure (psi)	Solids Fraction in Slurry (%)	Concentration (lb/bbl)	C1 (min/ml)	C2 (min)	C3 (l/ml)	t0 (min)
250	500	35.13	0	45.07	957.65	0.044	-0.32
250	500	35.13	1	39.29	540.71	0.07	0.43
250	500	35.13	3	31.88	207.7	0.151	1.26
250	500	35.13	5	152.71	7336.79	0.019	1.67

Table C25 (6.41) Fluid loss Additives Applications (Coating Agent)

Temperature (F)	Differential Pressure (psi)	Solids Fraction in Slurry (%)	Concentration (lb/bbl)	C1 (min/ml)	C2 (min)	C3 (l/ml)	t0 (min)
250	500	35.13	0	45.07	957.65	0.044	-0.32
250	500	35.13	1	28.67	240.77	0.119	2.54
250	500	35.13	3	28.85	122.2	0.182	0.69
250	500	35.13	5	101.77	6065.37	0.014	1.93



Regression Coefficients of Dynamic Filtration Experiments (Oil based mud)

Table C26 (6.42) Pressure and Temperature Applications

Temperature (F)	Solids Fraction in Slurry (%)	Differential Pressure (psi)	C1 (min/ml)	C2 (min)	C3 (1/ml)	t0 (min)
150	37.13	200	1102.65	6684.71	0.16	2.7
		500	416.37	1307.29	0.3	4.82
		800	299.19	761.61	0.36	3.47
200	37.13	200	736.6	5062.77	0.14	3.5
		500	340.28	1202.73	0.28	3.31
		800	237.98	773.95	0.28	0.65
250	37.13	200	437.19	4611.62	0.09	1.59
		500	292.99	2437.53	0.11	1.85
		800	192.38	1019.55	0.18	-2.31
300	37.13	200	302	3388.61	0.08	1.76
		500	221.65	2517.81	0.084	0.02
		800	142.79	930.69	0.14	0.66

Table C27 (6.43) Solids Applications

Temperature (F)	Differential Pressure (psi)	Solids Fraction in Slurry (%)	C1 (min/ml)	C2 (min)	C3 (1/ml)	t0 (min)
250	500	21.9	207.85	2177.39	0.095	2.55
250	500	37.13	292.99	2437.53	0.11	1.85
250	500	52	466.01	4067.33	0.113	3.61

Table C28 (6.44) Permeability and Solids Applications

Temperature (F)	Differential Pressure (psi)	Solids Fraction in Slurry (%)	Permeability (md)	C1 (min/ml)	C2 (min)	C3 (1/ml)	t0 (min)
250	500	21.9	400	207.85	2177.39	0.095	2.55
250	500	21.9	2000	106.85	372.04	0.284	2.68
250	500	21.9	5000	103.51	340.34	0.273	0.5
250	500	37.13	400	313.56	2823.47	0.112	1.81
250	500	37.13	2000	315.14	2853.72	0.109	1.8
250	500	37.13	5000	152.83	222.18	0.67	1.02

Table C29 (6.45) Shear Rate Applications

Temperature (F)	Differential Pressure (psi)	Solids Fraction in Slurry (%)	Shear rate (rpm)	C1 (min/ml)	C2 (min)	C3 (1/ml)	t0 (min)
250	500	37.13	80	292.99	2437.53	0.11	1.85
250	500	37.13	120	309.92	3426.88	0.086	-0.46
250	500	37.13	160	165.89	873.94	0.16	-0.7
250	500	37.13	200	134.84	919.38	0.13	-0.4

## Regression Coefficients of Dynamic Filtration Experiments

(Oil based mud)

Table C30 (6.46) Fluid Loss Additives Applications (Coating Agent)

Differential Pressure (psi)	Solids Fraction in Slurry (%)	Concentration (lb/bbl)	Vsp $\times 10^{*-2}$ (ml/sq.cm)	C1 (min/ml)	C2 (min)	C3 (l/ml)	t0 (min)
500	37.13	0	0.68	37.68	191.82	0.12	3.82
500	37.13	0.25	1.7	86.66	837.67	0.09	0.77
500	37.13	1	2.48	161.32	1344.99	0.119	0.16
500	37.13	2	0.68	245.61	2575.23	0.08	-2.84
500	37.13	4	0.77	310.39	3241.22	0.09	-0.67

Table C31 (6.47) Fluid Loss Additives Applications (Plugging Agent)

Differential Pressure (psi)	Solids Fraction in Slurry (%)	Concentration (lb/bbl)	Vsp $\times 10^{*-2}$ (ml/sq.cm)	C1 (min/ml)	C2 (min)	C3 (l/ml)	t0 (min)
500	37.13	0	0.68	37.68	191.82	0.12	3.82
500	37.13	0.25	8.37	88.17	561.84	0.15	-2.64
500	37.13	1	0.18	160.94	945.85	0.17	2.17
500	37.13	2	0.13	265.55	2346.65	0.1	-0.98
500	37.13	4	0.14	415.54	3330.56	0.11	-2.8

Table C32 (6.48) Fluid Loss Additives Applications (Viscosifying Agent)

Differential Pressure (psi)	Solids Fraction in Slurry (%)	Concentration (lb/bbl)	Vsp $\times 10^{*-2}$ (ml/sq.cm)	C1 (min/ml)	C2 (min)	C3 (l/ml)	t0 (min)
500	37.13	0	0.68	37.68	191.82	0.12	3.82
500	37.13	0.25	0.82	63.97	306.9	0.19	0.56
500	37.13	1	0.38	118.06	527.83	0.19	0.26
500	37.13	2	0.33	241.53	1578.51	0.13	0.39
500	37.13	4	0.27	102.19	16.79	3.19	3.1



The Shear Stress Acted on Filter Cake Surface (Water Based Mud)

Table C33 (6.64) Pressure and Temperature Applications

Temperature (F)	Solids Fraction in Slurry (%)	Differential Pressure (psi)	Shear Stress ( $N/m^2$ )
150	35.13	200	12.33
		500	12.6
		800	12.6
200	35.13	200	8.84
		500	10.09
		800	10.09
250	35.13	200	6.75
		500	6.89
		800	7.9
300	35.13	200	6.95
		500	7.07
		800	7.07
250	20.99	500	5.53
250	49.85	500	17.1

Table C34 (6.65) Shear Rate Applications

Temperature (F)	Solids Fraction in Slurry (%)	Differential Pressure (psi)	Shear Rate (rpm)	Shear Stress ( $N/m^2$ )
250	500	35.13	80	6.89
250	500	35.13	120	7.9
250	500	35.13	160	8.8
250	500	35.13	200	9.61

The Shear Stress Acted on Filter Cake Surface (Oil Based Mud)

Table C35 (6.66) Pressure and Temperature Applications

Temperature (F)	Solids Fraction in Slurry (%)	Differential Pressure (psi)	Shear Stress ( $N/m^2$ )
150	37.13	200	19.85
		500	22.54
		800	22.54
200	37.13	200	16.44
		500	18.8
		800	18.8
250	37.13	200	15.34
		500	15.34
		800	18.21
300	37.13	200	10.37
		500	10.37
		800	12.72
250	21.9	500	10.25
250	52	500	37.63

Table C36 (6.67) Shear Rate Applications

Temperature (F)	Solids Fraction in Slurry (%)	Differential Pressure (psi)	Shear Rate (rpm)	Shear Stress ( $N/m^2$ )
250	500	35.13	80	6.89
250	500	35.13	120	7.9
250	500	35.13	160	8.8
250	500	35.13	200	9.61

## **APPENDIX D**

- “A Productivity Tool for Impact of Filtration on Well Performance in an HP-HT Environment”, SPE/IADC 85335, Presented at the SPE/IADC Middle East Drilling Technology Conference & Exhibition held in Abu Dhabi, UAE, 20-22 October 2003
- “Field Applications of a Productivity Tool for Improved Oil Recovery (IOR)”. Paper Presented at the Second International Symposium on Improved Oil Recovery Conference & Exhibition held in Libya, 12-16 September 2003
- CD The Productivity Tool Package





SPE/IADC 85335

## A Productivity Tool for Impact of Filtration on Well Performance in an HP-HT Environment

Mohamed Belkasem Amish, SPE, The Robert Gordon University, Aberdeen

Copyright 2003, SPE/IADC

This paper was prepared for presentation at the SPE/IADC Middle East Drilling Technology Conference & Exhibition held in Abu Dhabi, UAE, 20-22 October 2003.

This paper was selected for presentation by an SPE/IADC Program Committee following review of information contained in an abstract submitted by the author(s). Contents of the paper, as presented, have not been reviewed by the Society of Petroleum Engineers or the International Association of Drilling Contractors and are subject to correction by the author(s). The material, as presented, does not necessarily reflect any position of the SPE, IADC, their officers, or members. Electronic reproduction, distribution, or storage of any part of this paper for commercial purposes without the written consent of the Society of Petroleum Engineers or the International Association of Drilling Contractors is prohibited. Permission to reproduce in print is restricted to an abstract of not more than 300 words; illustrations may not be copied. The abstract must contain conspicuous acknowledgment of where and by whom the paper was presented. Write Librarian, SPE, P.O. Box 833836, Richardson, TX 75083-3836, U.S.A., fax 01-972-952-9435.

### Abstract

In recent times, the oil industry has shown increasing awareness towards maintaining optimum well productivity through better HP-HT drilling/completion fluids design. However, the mechanisms of drilling fluid filtration and impact on productivity performance are not well understood, especially in an HP-HT environment.

In open hole completions the productivity losses are critical because the near-wellbore damage is not by-passed by perforations.

Furthermore, a satisfactory model for field applications to simulate the near-wellbore damage in terms of well flow performance from laboratory core test analysis still is not available.

In this paper, the results of in-depth experimental research into rheology, filtration and formation damage phenomena and the relationships between them. The experimental data combined with data analysis of static and dynamic filtration models provided the database for the semi-empirical mechanistic models that were developed. These models have been combined and incorporated into a design and evaluation tool - the productivity tool, for predicting the effect of HP-HT drilling fluid filtration on formation productivity.

A number of results have been presented to illustrate how the new tool can be used to evaluate the damage factor of a given fluid, specify the invaded zone skin as well as the depth of invasion, two key parameters that are useful and relevant to optimum fluid selection and management in addition to well test data interpretation.

### Introduction

The most common source of formation damage has proved to be drilling operations<sup>1</sup>. Permeability is a characteristic of the formation, and can be altered by solids and mud filtrate invasion during drilling operations. Drilling fluids are used to

facilitate various drilling processes. Drilling mud filtrate will invade the formation to a greater depth than drilling mud particles. A decrease of the permeability (formation damage), results in a decrease of the well productivity<sup>2,3</sup>. The formation damage depends upon many parameters such as formation characteristics, type, composition, filtration and rheological characteristics of drilling fluid and operating conditions (overbalance pressure, time, etc.).

A key parameter in quantifying formation damage is the skin factor<sup>4</sup>. The skin factor estimated from well test data is used in the flow equations to estimate the production rate in wells that are affected by formation damage.

Generally, when rating performance of various drill-in fluid formulations, the permeability damage evaluation is quantified through oil return permeability measurements and flow-initiation pressures performed on core samples damaged during mud filtration tests<sup>5,6</sup>.

Extensive laboratory studies of formation damage and several modeling efforts for prediction of formation damage have been reported in the literature. Most of the previous studies have focused on formation damage from filtration of WBM and incompressible fluids in LP-LT applications.

Few attempts were made to transfer these laboratory data into a near-wellbore model to evaluate the permeability damage. Liu et al.<sup>7</sup> simulated formation damage by fluid injection and mud filtration while Scott Lane<sup>8</sup> and Semmelbeck et al.<sup>9</sup> simulated filtrate invasion for improving log interpretation, but their impact on well performance was not investigated. Some workers<sup>10,11</sup> studied well performance using representative formation damage, but laboratory tests were not integrated in their studies.

The economic impacts of wellbore formation damage justify a thorough study of this problem in order to find ways to minimize its effect on well performance.

This paper presents a productivity tool for screening different HP-HT drilling fluids (WBM and OBM), which specify the invaded zone skin as well as the depth of invasion, and evaluates the damage factor of a given fluid in terms of inflow performance.

### Productivity Tool Formulation

The productivity tool was constructed to provide a design and analysis package, which can be used to perform the following key functions:

1. To analyse wellbore pressure distribution.
2. To analyse the response of the fluid to static and dynamic



filtration in an HP-HT environment.

3. To characterise the rheology and filtration of the selected fluids in an HP-HT environment.

4. Quantify the level and depth of damage and determine the best operating conditions.

5. Determine the impact of the selected fluid on formation productivity.

6. Screen appropriate HP-HT fluids desired for achieving minimum formation impairment.

In order to perform these functions, the productivity tool incorporates a number of mechanistic models, which have been developed as part of the initial project study, which include:

- Rheology prediction models.
- Static and dynamic filtration prediction models.
- Filter cake build-up on sand face evaluation models.
- Prediction models for filtration pressure drop across sand face and filter cake.
- Formation morphological characteristics.
- Prediction models for depth of solids and filtrate invasion.
- Prediction models for skin factor and flow efficiency.

The models are semi-empirical, which have been developed from the input of selected data generated from extensive experimental studies into filtration and formation damage phenomena. All the analysis carried out on laboratory core tests were conducted under linear flow condition, and upscaled into radial flow condition, to simulate near-wellbore damage caused by particulate and filtrate invasion.

The productivity tool has been used to generate a number of results to clearly illustrate the functionality of its applications (Fig 1-28).

**HP-HT Drilling Fluid Rheology.** The rheological behaviour of the drilling fluid has a major impact on pressure distribution in the wellbore and hence an effect drilling overbalance pressure. Therefore, it is necessary to characterise drilling fluid rheology in HP-HT well applications.

Several studies of the HP-HT rheology of WBM and OBM have been presented in earlier papers<sup>12,13</sup>. Some of these studies which include many mathematical expressions are subjective. Politte<sup>12</sup> presented a multi-term equation with 13 numerical constants to model the viscosity of diesel oil. Houwen et al.<sup>13</sup> presented several equations to model rheological parameters. An API Bulletin<sup>14</sup> presented two equations to calculate pressure and temperature constants.

In this study a different procedure has been adopted. Shear stress has been multiplied by a correction factor that depends on pressure and temperature. Then the rheological behaviour and rheological parameters can be calculated from shear stress prediction at the pressure and temperature of interest. Two prediction models have been developed for WBM and OBM.

The models follow the general format:

$$\tau_i = \tau_s [A_c \exp(AP + BT)] \quad (1)$$

The difference between the models is in respect of the empirical constants ( $A_c$ ,  $A$  and  $B$ ).

Data used to evaluate the empirical constants have been

obtained from selective HP-HT Fann viscometer measurements.

The HP-HT Fann-70 viscometer was used for the measurement of the rheological profiles under different temperature and pressure conditions (150-300 °F and 15-17000 psi respectively). Two common HP-HT drilling fluids have been used namely lignosulphonate WBM and synthetic OBM ( $C_{14}$  -  $C_{16}$  olefin).

The models often used to describe the behaviour of the two fluids are Bingham Plastic<sup>15</sup>, Power Law<sup>16</sup> and Herschel Bulkley models<sup>17</sup>. However in this study the WBM and OBM rheological data are best described by the Herschel Bulkley model.

The main difference between OBM and WBM are the effects of pressure, which are more pronounced for OBM than WBM. For WBM the effect of pressure is very small, but is highly affected by an increase in temperature.

Temperature and pressure affects behaviour and interactions of water or oil, clay, polymers and solids in mud. The effect of increasing the temperature of a liquid is to reduce the cohesive forces while simultaneously increasing the rate of molecular interchange. The former effect tends to cause a decrease of shear stress, while the latter causes it to increase. The net result is that liquids show a reduction in viscosity with increasing temperature.

The effect of increased pressure on OBM is to increase the cohesive forces, which tends to increase the viscosity.

A comparison between the experimental data and HP-HT rheological models prediction has been made and validated with Gulf of Mexico field data Fig (1&2), which shows agreement in range of <6% error.

**Drilling Fluid Filtration.** One of the major functions of a drilling fluid is the control of formation pressure. In order to prevent formation fluids from flowing into the borehole, the hydrostatic pressure of the mud column is usually made to exceed the formation pressure.

Wellbore differential pressure can cause excessive loss of liquid and associated drilling mud solids leading to potential permeability impairment of the formation, and contribute to borehole instability<sup>18,19</sup> and formation damage<sup>20</sup>, especially in the HP-HT environment. Therefore the fluid rheology is unique to drilling fluid filtration property.

As a result of overbalance pressure, the filter cake may form on sand face, through which only filtrate can pass, depending on the relationship between mud particle size distribution and formation pore size.

The process of drilling a well results in alternating periods, of varying duration, of dynamic and static filtration (sequential filtration). Dynamic filtration occurs when the mud is circulated; the cake thickness is the difference between the rate of deposition by filtration and the rate of erosion by circulating mud. The erosion rate of particles is proportional to the shear stress exerted by the circulating mud on the cake surface<sup>21</sup>.

Static filtration occurs when the mud is not circulated, and the cake thickness increases as filtration continues.

The existing static and dynamic filtration<sup>21,22</sup> equations can be modified for HP-HT environment in the form:

(i). Static filtration:

$$t = Y_1 V + Y_2 V^2 \exp. (AP + BT) \quad (2)$$

(ii). Dynamic filtration:

$$t = X_1 V - X_2 (1 - e^{-X_3 V}) \exp. (AP + BT) \quad (3)$$

Equation (3) also can be used to predict dynamic from static filtration data. Since the modified filtration Equations (2) and (3) can predict the filtration coefficients ( $Y_1, Y_2, X_1, X_2$  and  $X_3$ ) therefore the filter cake characteristics such as cake resistance, permeability, porosity, etc. can be computed.

The filtration process was investigated under effect of temperature ranging from 150-300 °F, pressures ranging from 200-1000 psi, solids ranging from 6-20% by volume and shear rate ranging from 80-240 rpm.

The modified HP-HT static and dynamic filtration equations (2) & (3) have been used to predict two filtration mechanisms and dynamic from static filtration data corresponding to each experimental condition. The measured data against model prediction have been plotted in Fig (3). The modified filtration models are shown to be representative of the experimental data based on relative error of less than 5 %.

**Filtration Pressure Drops.** At the start of filtration, the pressure drop,  $\Delta P_T$ , is across the sand face, but as the filter cake builds up more of the pressure drop is dissipated across the filter cake,  $\Delta P_C$ , and less across the sand face,  $\Delta P_f$ , thus.

$$\Delta P_T = \Delta P_f + \Delta P_C \quad (4)$$

Fig (4) shows a comparison between pressure drops from experimental observation and models prediction across filter cake and sand face which shows agreement in range of <7 % error. Fig (5) clearly demonstrates the pressure distribution profile across filter cake and sand face.

**Damage from Drilling Fluid.** Formation damage mechanisms have been studied extensively<sup>23, 24</sup>. However, formation damage from drilling fluid can be characterised by the following factors: thickness of filter cake, depth of solids and filtrate invasion and permeability reduction.

The two main damaging mechanisms which have been studied, are particulate invasion during initial filtration period, and filtrate invasion through filter cake.

**A. Filter Cake Build up.** Filter cake thickness is given by:

$$\frac{dh_c}{dt} = \frac{\rho_f s V - K_r \tau}{(1 - ms)} \quad (5)$$

The shear stress should be calculated from rheological behaviour of the mud Equation (1).

If the mud is not circulated then the shear stress  $\tau = 0$ , therefore the filter cake thickness continues increasing as the static filtration continues. However the filter cake thickness  $dh_c$  can be used for calculating actual wellbore radius.

The static and dynamic filter cake build up has been simulated based on modified filtration equations (2) & (3). Fig (6) shows agreement as a comparison is made between experimental data, model prediction and previously published cake build up model<sup>7</sup> with relative error of 2 %.

**B. Depth of Solids Invasion.** Semi-empirical equations have been developed for predicting the depth of solids invasion. These models depend largely on rheological behaviour of the drilling fluids.

For Herschel Bulkley and Power Law fluid the model has been computed as:

$$L_s = \frac{C_1 \Delta P_f D_p^{(1+n)}}{KV_p^n (C_2 \frac{3n+1}{n})^n} \quad (6)$$

For Bingham Plastic fluid the equation is:

$$L_s = C_3 \Delta P_f \frac{D_p^2}{(C_4 \mu_p V_p + C_5 \tau_y D_p)} \quad (7)$$

As it can be observed from the above models the depth of solids invasion requires the knowledge of the formation morphological characteristics such as permeability, porosity, tortuosity etc.

In order to evaluate the morphological characteristics a number of tests were conducted on selected Clashach sandstone cores with porosity ranges from 0.10 to 0.28 and permeability varying from 40 to 4000 md.

Tortuosity ( $\eta$ ) is the actual flow path and can be computed in laboratory from formation resistivity factor ( $F_R$ ) and porosity thus:

$$F_R = a / \phi^b \quad (8)$$

$$\eta = \phi F_R \quad (9)$$

Then the mean pore throat diameter can then be calculated as:

$$D_p = 4.08 (\eta K / \phi)^{0.5} \quad (10)$$

The relationship between permeability and porosity is plotted in Fig (7). The porosity appears to increase with increasing permeability. A comparison between experimental formation resistivity factor, model prediction and external field data from two Middle Eastern carbonate reservoirs<sup>25</sup> has been plotted in Fig (8). Ranges of porosity from 0.10 to 0.24, permeability ranges from 1 to 387 md and formation resistivity factor ranges from 18 to 76 were used. In general, the model represents the experimental and external data based on a relative error of <7 %. However the coefficients for (Equation 8) has been defined for limestone reservoirs.

The measured mean pore throat diameter against model prediction (equation 10) is plotted in Fig (9). The model prediction was validated with external field data from three sandstones: the Berea, from a quarry in Ohio, and the Noxie and Cleveland sandstones, from near Bartlesville, Oklahoma<sup>26</sup>. The sandstones have ranges of porosity from 0.16 to 0.27, permeability ranges from 300 to 1700 md and a wide range of

pore throat diameter ranges from 6 to 30 microns Fig (10). The pore throat model prediction shows agreement with field data based on relative error of <7%.

X-ray mapping has been used to investigate depth of solids invasion for OBM and WBM and agreement has been found with model prediction with relative error of <6% Figs (11) & (12). Fig (13) shows skin damage increases with increased filtration time and is greater for WBM than OBM.

Fig (14) shows depth of solids invasion and permeability reduction factor for WBM and OBM increases as function of filtration volume from the sand face in linear core scale. Figs (15-17) illustrated effect of rheological behaviour on formation damage characterisation. A comparison has been made between actual fluid rheological behaviour model Herschel-Bulkley and Bingham Plastic model. The figures show that the Bingham model predicts higher formation damage than the actual model. The Herschel-Bulkley model best represents the actual fluid rheology.

Figs (18) & (19) shows the depth of solids invasion comparison between Herschel-Bulkley, Bingham Plastic and Power Law models for OBM and WBM as function of formation permeability. The figures clearly illustrate that the depth of invasion is inversely proportional with permeability for Herschel-Bulkley and Power Law fluids. Meanwhile the depth of invasion is directly proportional with permeability for Bingham Plastic. Therefore in drilling tight reservoirs it is recommended to use Bingham Plastic fluid and in drilling high permeability reservoirs it is recommended to use Herschel Bulkley fluid.

**C. Depth of Filtrate Invasion.** The radius of filtrate invasion can be determined from filtration volume as:

i. Invasion in static condition:

$$r_f = \sqrt{r_w^2 + \frac{2r_w}{\phi} \left( \frac{-Y_1 t}{2Y_2} + \frac{(Y_1^2 + 4Y_2 t)^{1.5}}{12Y_2} - \frac{Y_1^3}{12Y_2} \right)} \quad (11)$$

ii. Invasion in dynamic condition:

$$r_f = \sqrt{r_w^2 + \frac{2r_w t (1 - ms) K_r \tau}{\phi \rho_f s}} \quad (12)$$

All the parameters in equation (11&12) can be computed from sequential filtration experiment and Equations (2&3).

**D. Permeability Damage.** The initial formation permeability damaged in the zone occupied by particulate and filtrate is characterised by permeability reduction (damaged) as a function of core length or distance from wellbore in radial well flow. The permeability damage factor can be described as:

$$C_F = k_d / k_f \quad (13)$$

The permeability alteration ( $k_d$ ) can be computed from the knowledge of overall average permeability and total depth of invasion. Fig (20) shows an increase in permeability reduction factor and depth of solids and filtrate invasion as function of

drilling time for WBM and to a lesser extent for OBM.

Fig (21) shows increased overbalance pressures increases the skin damage as a function of drilling time for WBM.

Fig (22) shows an increase in the depth of filtrate invasion as a function of drilling time for WBM and to a lesser extent for OBM.

### Productivity Evaluation

Well performance is reduced when near-wellbore formation is damaged. A key parameters in quantifying the formation damage or the reduction of the well productivity will be the skin factor or by the calculation of flow efficiency.

The skin factor  $s_d$ , defined as:

$$s_d = (1 - k_f / k_d) \ln (r_w / r_f) \quad (14)$$

Using a well productivity index (PI) usually represents well performance. Therefore, well efficiency due to near wellbore damage can be calculated as:

$$FE = PI_{\text{actual}} / PI_{\text{ideal}} \quad (15)$$

Then the damage factor can be computed from reciprocal of the well flow efficiency.

$$DF = 1 / FE \quad (16)$$

Figs (23-26) illustrate the effects of different parameters such as drilling time, overbalance pressure, temperature and permeability on flow efficiency as a comparison between WBM and OBM.

It is necessary during the fluid design stage to screen different HP-HT fluids also based on higher percentage of the return permeability test. Because may be the depth of invasion is inversely proportional with percentage of the return permeability test Fig (28).

However, during flow back for all the cores damaged with OBM as the flow initiated, the filter cake ruptures (pinholing) and scours any invaded solids and filtrate at lower flow rates. For WBM, during flow back as flow initiated part of cake fails and as flow increases the cake ruptures and is completely removed.

Under all testing parameters, OBM shows very high reversible permeability was achieved >85% Fig (27).

WBM shows that the main effect the formation damage is the overbalance pressure.

One would expect an increase in depth of invasion with increasing differential pressure in the sense that higher pressures would force the mud particles and the filtrate to penetrate deeper into the formation. However, contrary to this expectation, the experimental results indicate at lower pressure the permeability damage increases and as pressure increases from 400 to 650 psi the permeability damage decreases. However, as the pressure increases the permeability damage increases, in line with the expectations.

Fig (28) shows three pressure zones: in the first zone, representing the pressure of 100 to 300 psi, return permeability decreases significantly. This is because at lower pressures the deposition is uncompacted forming loose particles and unconsolidated filter cake. Permeable filter cake



allows filtrate and fine particles to pass resulting in deeper migration. This zone characterised by lower return permeability. In the second zone, as differential pressure increases to 650 psi, the particles form tight bridging, compacted and lower cake permeability, thereby allowing less particles through them to move into formation. This is seen by higher return permeability achieved.

The third zone, representing increases in pressure beyond 650 psi results in deeper particle invasion and lower return permeability.

Therefore there are critical pressure zones for compacted bridging, below or above which permeability damage occurs.

Khan et al.<sup>27</sup> investigated depth of invasion using x-ray mapping and they found minimum depth of invasion occurs at pressures between 300 to 500 psi and below or above this range the depth of invasion increased.

## Conclusions

A productivity tool is presented to simulate impact of drilling fluid filtration on formation productivity in an HP-HT environment. The productivity tool can be used for predicting formation damage mechanisms caused by particulate and filtrate invasion.

The tool can evaluate formation damage in laboratory as linear-flow core tests and can be converted to radial-flow scale for oil field applications.

Input requirements include parameters such as hole geometry, BHA configuration, mud type, composition, rheology data and formation characteristics.

The domain application of this productivity tool is relatively wide since it can be used to investigate the influence of many parameters on the well flow performance.

The tool can be used before drilling as design (planning tool), during drilling and post drilling as evaluation and comparison tool with well test data interpretation.

The productivity tool is capable of being utilised to screen different HP-HT drilling fluids desired for achieving minimum impairment and maximum production capacity, two key parameters which are relevant to optimum fluid selection and management, in addition to well test data interpretation.

## Acknowledgements

The author wishes to acknowledge Dr Babs Oyeneyin and Dr Douglas Morrison both of The Robert Gordon University, and Mr Mike Hodder of M-I Drilling Fluids, UK for their support and permission to publish this paper.

## Nomenclature

$a, b$  = coefficients  
 $A, B$  = pressure and temperature coefficients  
 $A_c$  = constant  
 $C_1, C_2, C_3, C_4, C_5$  = constants  
 $C_F$  = permeability reduction factor  
 $DF$  = damage factor  
 $D_p$  = mean pore throat diameter  
 $dh_c$  = filter cake thickness  
 $FE$  = flow efficiency  
 $F_R$  = resistivity formation factor  
 $k$  = consistency index  
 $k_t$  = erodability coefficient

$k_f$  = formation permeability

$k_d$  = permeability damage

$L_S$  = depth of solids

$m$  = ratio of wet to dry cake

$n$  = Power law index

$P$  = applied pressure

$PI_{\text{actual}}$  = productivity index after formation damage

$PI_{\text{ideal}}$  = productivity index before formation damage

$\Delta P_T$  = total differential pressure

$\Delta P_f$  = pressure across formation

$\Delta P_c$  = pressure across filter cake

$r_f$  = radius of filtrate invasion

$r_w$  = wellbore radius

$s$  = solids concentration

$s_d$  = drilling skin factor

$t$  = time

$T$  = temperature

$V$  = filtrate volume

$V_p$  = velocity in porous medium

$Y_1, Y_2, X_1, X_2, X_3$  = filtration coefficients

## Greek Symbols

$\eta$  = tortuosity

$\mu_p$  = plastic viscosity

$\tau_y$  = yield point

$\tau_s$  = shear stress at standard condition

$\tau_i$  = shear stress at depth of interest

$\phi$  = porosity of formation

$\rho_f$  = density of filtrate

## Acronyms

BHA = bottom hole assembly

LP-LT = low pressure-low temperature

HP-HT = high pressure-high temperature

OBM = oil based mud

md = millidarcy

WBM = water based mud

## References

1. Michael J. Economides, A. Daniel Hill, and Christine Ehlig-Economides: "Petroleum Production systems", 1994.
2. Krueger, R. F.: "An Overview of Formation Damage and Well Productivity in Oilfield Operation", JPT, Feb., 1986, pp. 131-152.
3. Dearing, H. L. and Ali, S. A.: "Drill-in fluid Selection Crucial To Well Productivity", Petroleum Engineer International, Jan. 1996, 21-25.
4. Van Everdingen, A. F., and Hurst, W., "The Application of the Laplace Transformation to Flow Problems in Reservoirs", TRANS. AIME, 186:305-324, 1949.
5. Fraser, L. J., Ried, P., Williamson, D., and Enriquez, F.: "Mechanistic Investigation of the Formation Damaging Characteristics of Mixed Metal Hydroxide Drill-In Fluids and Comparison with Polymer-Base Fluids", SPE 30501 Presented at the SPE Annual Technical Conference and Exhibition held in Dallas, U.S.A., October 22-25, 1995.
6. Davison, J.M., Jones, M., Shuchart, C. E., and Gerard, C.: "Oil-Based Muds Reservoir: their Performance and Cleanup Characteristics", SPE 58798 Presented at the 2000 SPE International Symposium on Formation Damage Held in Lafayette, Louisiana, 23-24 Feb. 2000.
7. Liu. X. and Civan. F.: "Formation Damage and Skin Factor

Due Filter Cake Formation and Fines Migration in the Near-wellbore Region”, SPE 27364 presented at the SPE Int. Symposium on Formation Damage Control, Lafayette, LA, Feb. 9-10, 1994.

8. Scott Lane, H.:”Numerical Simulation of Mud Filtrate Invasion and Dissipation”, SPWLA 34<sup>th</sup> Annual Logging Symposium, June 13-16, 1993.

9. Semmelbeck, M.E., Dewan, J.T. and Holditch, S.A.:”Invasion Based Method Estimating Permeability from Logs”, SPE 30581 presented at the SPE ATC&E, Dallas 22-25 Oct. 1995.

10. Permadi, P. and Wibowo, W.:”Effects of Non-uniform Skin Distribution on Horizontal Well Inflow Performance”, SPE 68952 presented at the SPE European Formation Damage Conf. The Hague, The Netherlands, 21-22 May 2001.

11. Menour, H., Al-Majed, A. and Hassan, S.:”Effect of Formation Damage, Length and Reservoir Thickness on the inflow Performance of Horizontal Wells”, SPE 59356 presented at the 2000 SPE/DOE Improved Oil Recovery Symp. Tulsa OK, 3-5 April 2000.

12. Politte, M. D.:”Invert Oil Mud Rheology as a Function of Temperature and Pressure”, SPE/IADC 13458, New Orleans, U.S.A., 1985.

13. Houwen, O. H., and Geehan, T.:”Rheology of Oil-Base Muds”, SPE 15416, New Orleans, U.S.A., 1986.

14. API Bulletin 13B: Recommended Practice on the Rheology and Hydraulics of Oil-Well Drilling Fluids, API BUL 13D, Third Edition, June 1, 1995

15. Bingham, E. C.:”Fluidity and Plasticity”, McGraw-Hill Book Co., New York, 1922.

16. Govier, G. W. and Aziz, K.:”The Flow of Complex Mixtures in Pipes”, Van Nostrand Reinhold, New York, 1972.

17. Herschel, W. H. and Bulkley, R.:”Measurement of Consistency as Applied to Rubber-Benzene Solutions”, Proceedings of the American Society of Testing Materials, Vol. 26, 1926, pp 621-633.

18. Chenevert, M.E.:”Shale Control with Balanced-Activity Oil Continuous Muds”, JPT, Oct 1970. pp. 1309.

19. Bushnell, Y.M, and Panesar, S. S.:”Differential Sticking Laboratory Tests can Improve Mud Design”, SPE 22549 Presented at the 66<sup>th</sup> Annual Technical Conference and Exhibition of the SPE, Dallas, TX, Oct. 6-9, 1991.

20. Ali Ghalambor and M. J. Economides:”Formation Damage Abatement: A Quarter-Century Perspective”, SPE no. 58744, Feb. 2000.

21. Shuang Jiu Peng, and Peden, J. M.:”Prediction of Filtration Under Dynamic Conditions”, SPE 23824 Presented at the SPE Ind. Symposium on Formation Damage Control held in Lafayette, Louisiana, February 26-27, 1992.

22. Arthur, K. G. and Peden, J. M.:”The Evaluation of Drilling Fluid Filter Cake Properties and Their Influence on Fluid Loss”, SPE 17617. 1988.

23. M. B. Amish and M. B. Oyeneyin and M. H. Hodder” Characterisation of Drilling Fluid Filtration under Downhole Conditions”, under progress

24. Yan Bingo, M. B. Oyeneyin, and J. M. Peden:”Investigation of Pore Blocking Mechanism in Gravel Packs in the Management and Control of Fines Migration”, SPE 27342, 1994.

25. Oyeneyin, M. B., Peden, J. M., Ali Hosseini, and Ren, G.:”Factors to Consider in The Effective Management and Control of Fines in High Permeability Sands”, SPE 30112, 1995.

26. Dixon, J. R. and Marek, B. F.:”Properties of Bimodal Pore Size Distribution on Electrical Properties of Some Middle

Eastern Limestone”, SPE 20601, 1990.

27. Erle C. Donaldson and Byron A. Baker.:” Particle Transport in Sanstones”, SPE 6905. Fluid Hydraulics”, SPE 56632, Houston, U.S.A., 1999.

28. Kihan, M. A, Jilani, S. Z, Menouar, H. and Al-Majed, A. A.:” A Non- Destructive Method for Mapping Formation Damage”, Elsevier Science B. V. 2001.

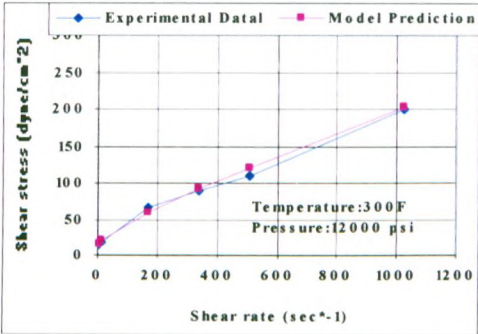


Fig. (1) Comparison experimental and model prediction for WBM

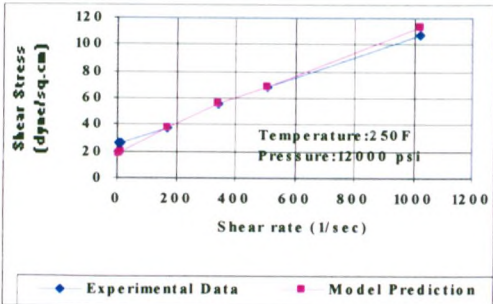


Fig (2) Model validation with external field data for OBM

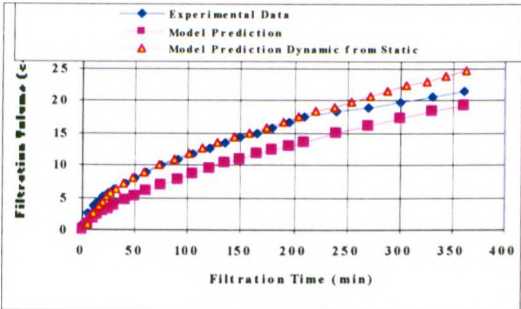


Fig (3) Filtration volume versus time for WBM

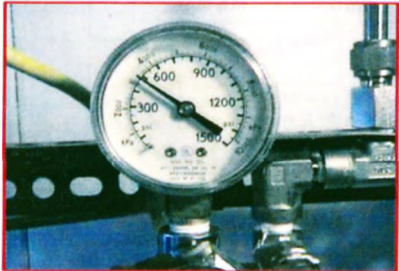


Fig (4a) Pressure drop across filter cake (top gauge)



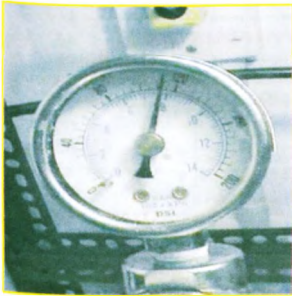


Fig (4b) Pressure drop across sand face (bottom gauge)

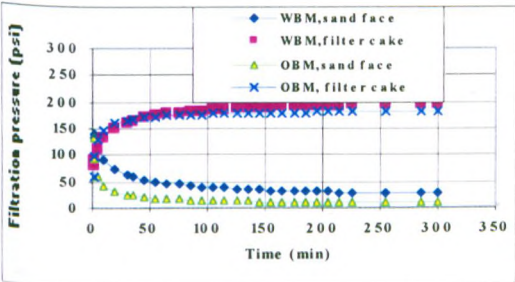


Fig (5) Pressure drop across filter cake and sand face versus time

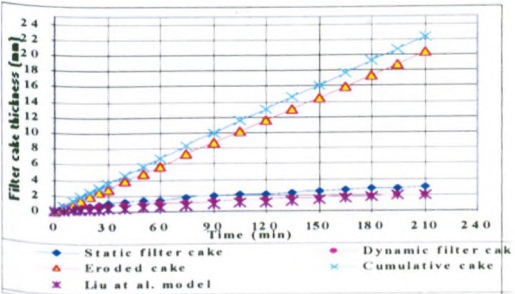


Fig (6) Filter cake build up versus time for WBM

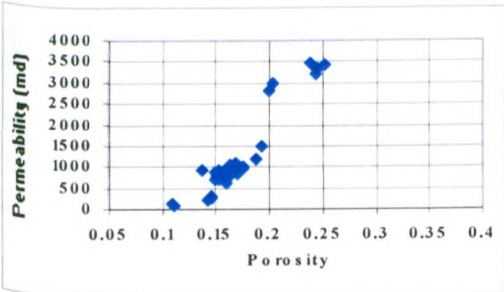


Fig (7) Permeability and porosity relationship

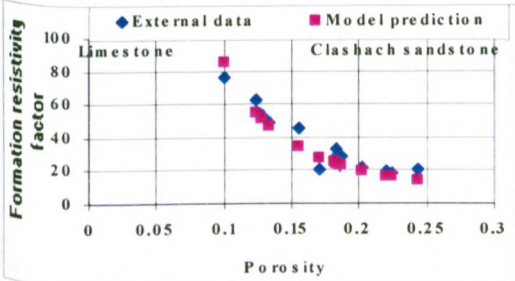


Fig (8) A comparison between external data and model prediction

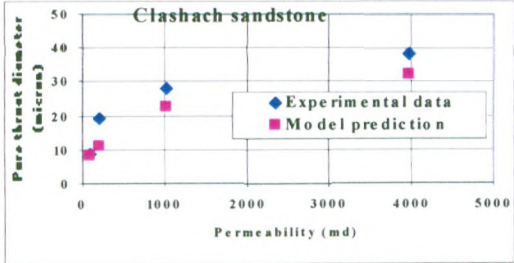


Fig (9) A comparison between experimental data & model prediction

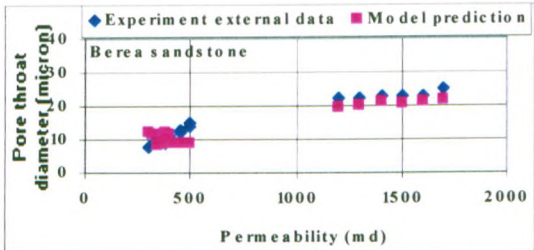


Fig (10) A comparison between field data and model prediction

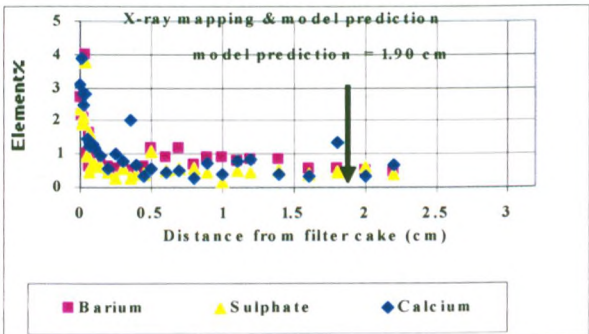


Fig (11) X-ray and model prediction for OBM

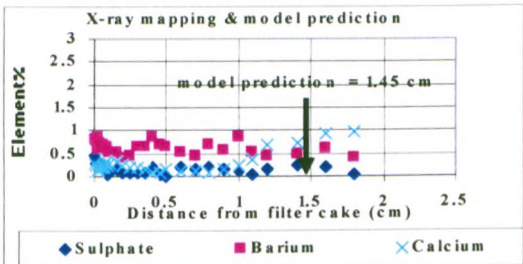


Fig (12) X-ray and model prediction for WBM

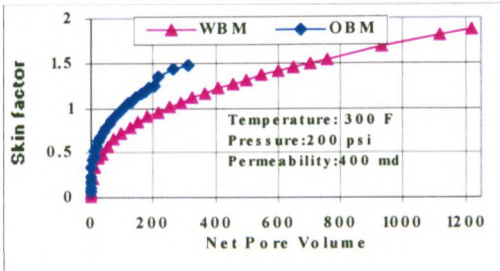


Fig (13) Skin factor versus net pore volume

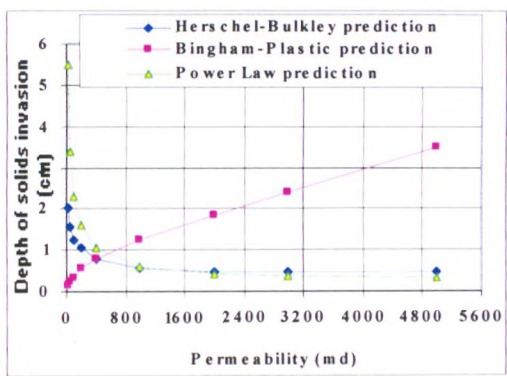
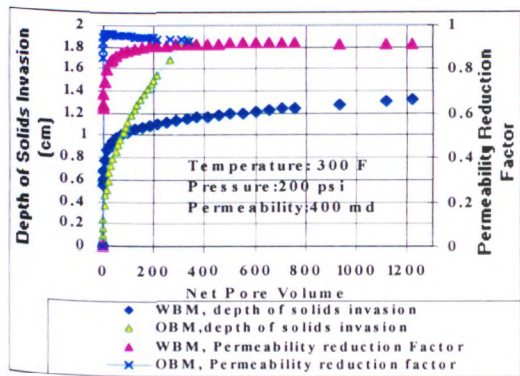


Fig (18) Depth of solids invasion versus permeability for OBM

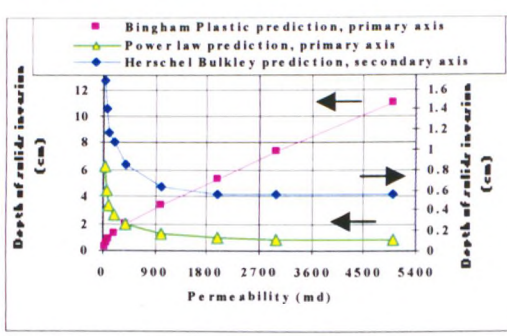
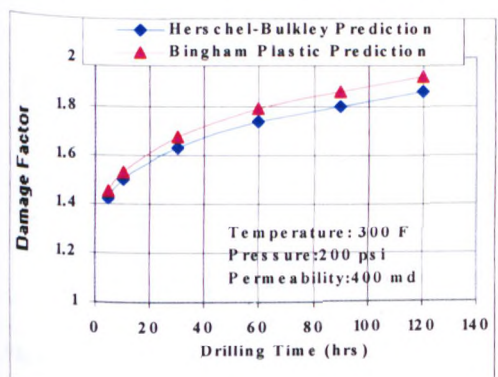


Fig (19) Depth of solids invasion versus permeability for WBM

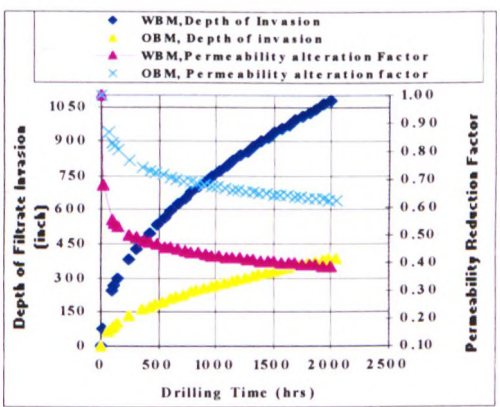
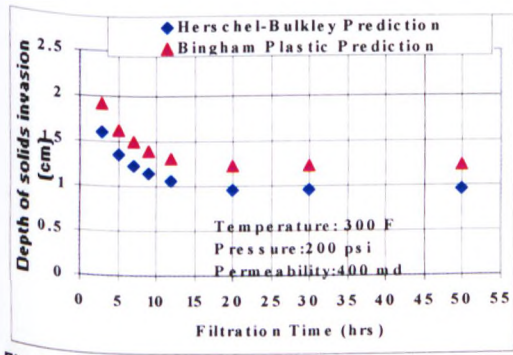
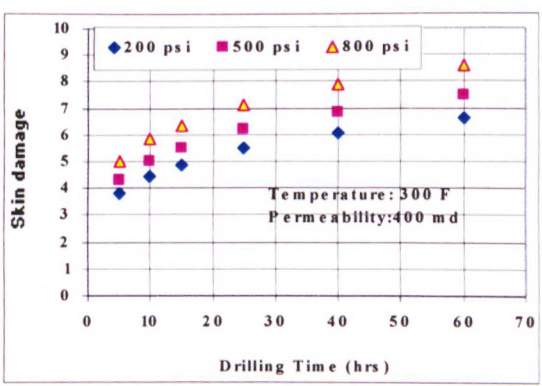
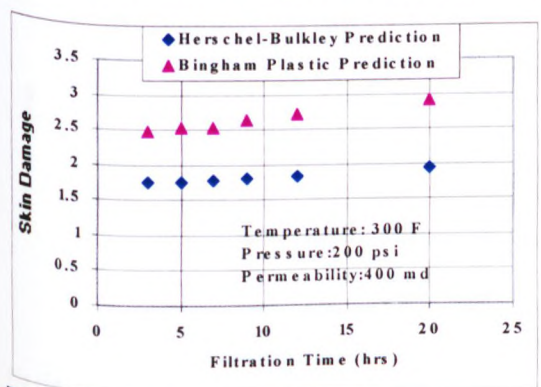


Fig (20) Permeability alteration versus drilling time





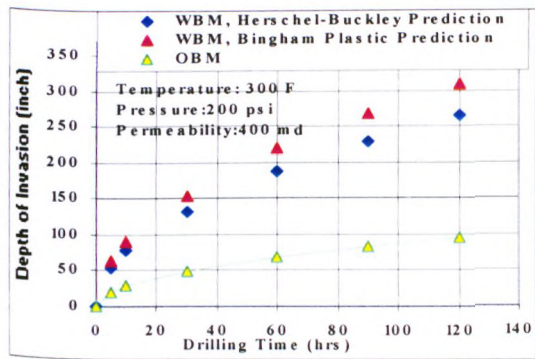


Fig (22) Depth of filtrate invasion versus drilling time

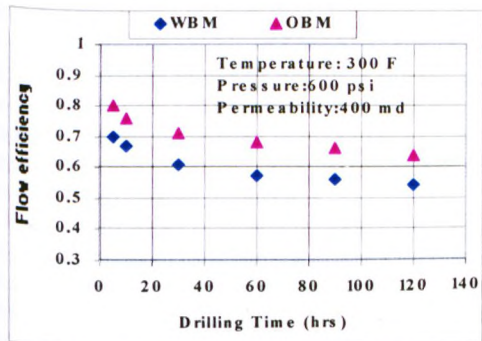


Fig (23) Flow efficiency versus drilling time

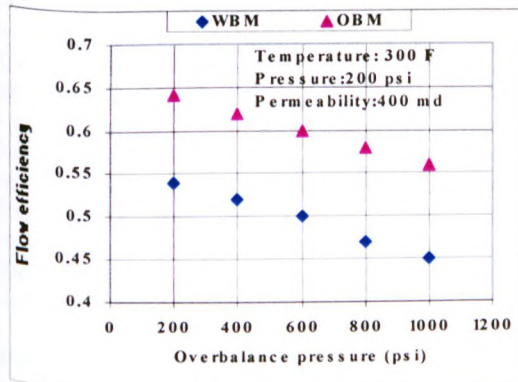


Fig (24) Flow efficiency versus overbalance pressure

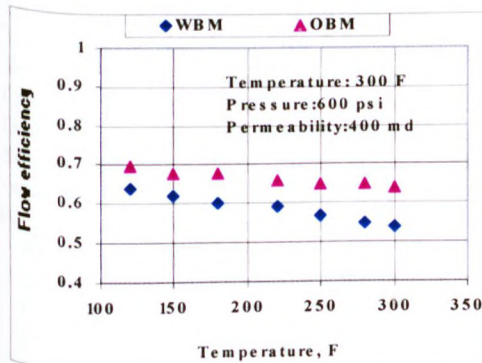


Fig (25) Flow efficiency versus temperature

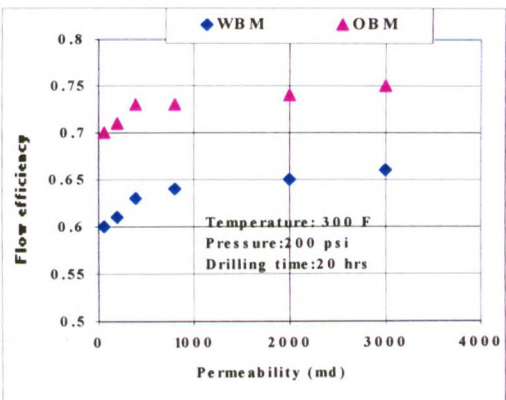


Fig (26) Flow efficiency versus permeability

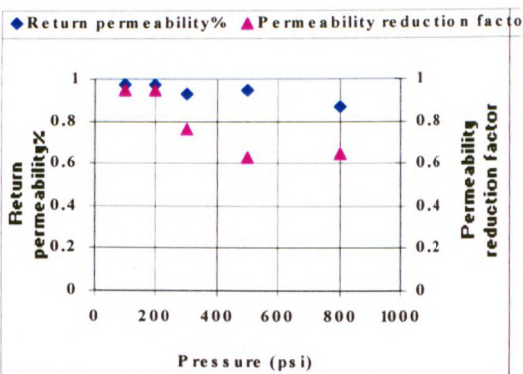


Fig (27) Effect of pressure on formation damage for OBM

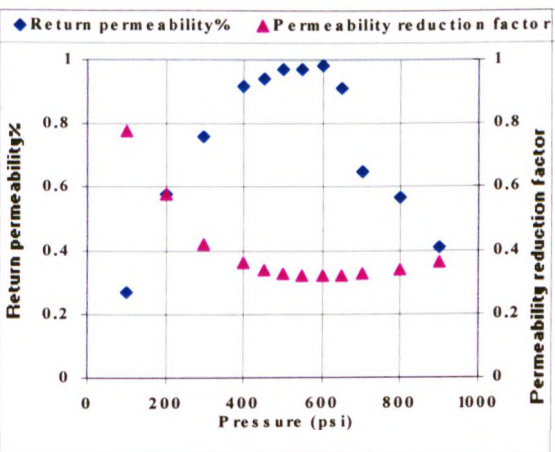


Fig (28) Effect of pressure on formation damage for WBM

# Field Applications of a Productivity Tool for Improved Oil Recovery (IOR)

## Abstract

In recent times, the oil industry has shown increasing awareness towards maintaining optimum well productivity through better high-pressure, high temperature (HP-HT) drilling/completion fluids design. However, the mechanisms of drilling fluid filtration and impact on productivity performance are not well understood under downhole conditions.

In open hole completions, the productivity losses are critical because the near-wellbore damage is not by-passed by perforations. Furthermore, a satisfactory model for field applications to simulate the near-wellbore damage in terms of well flow performance from laboratory core test analysis still is not available.

The results of in-depth experimental data combined with data analysis of static and dynamic filtration models provided the database for the semi-empirical mechanistic models that were developed. These models have been combined and incorporated into a design and evaluation tool - the productivity tool (PRT), for predicting the effect of HP-HT drilling fluid filtration on formation productivity in terms of formation damage in vertical wells.

In this paper, we present applications of the PRT using field data from North African oilfields with both water-based and oil-based muds (WBM and OBM), both selected as suitable for HPHT wells. The PRT shows good agreement with the field measurements.

## Introduction

The most common source of formation damage has proved to be drilling operations<sup>1</sup>. Permeability is a characteristic of the formation, and can be altered by solids and mud filtrate invasion during drilling operations. Drilling fluids are used to facilitate various drilling processes. Drilling mud filtrate will invade the formation to a greater depth than drilling mud particles. A decrease of the permeability (formation damage), results in a decrease of the well productivity<sup>2,3</sup>. The formation damage depends upon many parameters such as formation characteristics, type, composition, filtration and rheological characteristics of drilling fluid and operating conditions (overbalance pressure, time, etc.).

A key parameter in quantifying formation damage is the skin factor<sup>4</sup>. The skin factor estimated from well test data is used in the inflow equations to estimate the production rate in wells that are affected by formation damage.

Generally, when rating performance of various drill-in fluid formulations, the permeability damage evaluation is quantified through oil return permeability measurements and flow-initiation pressures performed on core samples damaged during mud filtration tests<sup>5,6</sup>.

Extensive laboratory studies of formation damage and several modeling efforts for prediction of formation damage have been reported in the literature. Most of the previous studies have focused on formation damage from drilling fluid filtration of water-based mud (WBM) and incompressible fluids in low-pressure, low temperature (LP-LT) applications.

Few attempts have been made to transfer these laboratory data into a near-wellbore model to evaluate the permeability damage.

Liu et al.<sup>7</sup> simulated formation damage by fluid injection and mud filtration while Scott Lane<sup>8</sup> and Semmelbeck et al.<sup>9</sup> simulated filtrate invasion for improving log interpretation, but their impact on well performance was not investigated. Some workers<sup>10,11</sup> studied well performance using representative formation damage, but laboratory tests were not integrated in their studies.

The economic impacts of wellbore formation damage justify a thorough study of this problem in order to find ways to minimize its effect on well performance.

This paper presents applications of the productivity tool using field data for screening different HP-HT drilling fluids (WBM and OBM), which specify the invaded zone skin as well as the depth of invasion, and evaluates the damage factor of a given fluid in terms of inflow performance.

## Function of the Productivity Tool

The productivity tool was constructed to provide a design and analysis package, which can be used to perform the following key functions:

1. To analyse wellbore pressure distribution.
2. To analyse the response of the fluid to static and dynamic filtration in an HP-HT environment.
3. To characterise the rheology and filtration of the selected fluids in an HP-HT environment.
4. Quantify the level and depth of damage and determine the best operating conditions.
5. Determine the impact of the selected fluid on formation productivity.
6. Screen appropriate HP-HT fluids desired for achieving minimum formation impairment.

In order to perform these functions, the productivity tool incorporates a number of mechanistic models, which have been developed as part of the initial project study, which include:

- Rheology prediction models.
- Static and dynamic filtration prediction models.
- Filter cake build-up on sand face evaluation models.
- Prediction models for filtration pressure drop across sand face and filter cake.
- Formation morphological characteristics.
- Prediction models for depth of solids and filtrate invasion.
- Prediction models for skin factor and flow efficiency.

The models are semi-empirical, which have been developed from the input of selected data generated from extensive experimental studies into filtration and formation damage<sup>12,13</sup> phenomena. All the analysis carried out on laboratory core tests were conducted under linear flow conditions, and upscaled into radial flow conditions, to simulate near-wellbore damage caused by particulate and filtrate invasion.

### Productivity Tool Formulation

**Drilling Fluid Rheology.** The rheological behaviour of the drilling fluid has a major impact on pressure distribution in the wellbore and hence an effect drilling overbalance pressure and fluid filtration. Therefore, to adequately predict downhole filtration, it is also necessary to predict downhole rheology.

Several studies of the HP-HT rheology of WBM and OBM have been presented in earlier papers<sup>14,15</sup>. Some of these studies which include many mathematical expressions are subjective. Politte<sup>14</sup> presented a multi-term equation with 13 numerical constants to model the viscosity of diesel oil. Houwen et al.<sup>15</sup> presented several equations to model rheological parameters. An API Bulletin<sup>16</sup> presented two equations to calculate pressure and temperature constants.

In this study, a different procedure has been adopted. Shear stress has been multiplied by a correction factor that depends on pressure and temperature. Then the rheological behaviour and rheological parameters can be calculated from shear stress prediction at the pressure and temperature of interest. Two prediction models have been developed for WBM and OBM.

The models follow the general format:

$$\tau_i = \tau_s [A_C \exp(AP + BT)] \quad (1)$$

Where  $\tau_i$  is the shear stress at depth of interest and  $\tau_s$  the shear stress at standard conditions. The difference between the models is in respect of the empirical constants ( $A_C$ , A and B).

Data used to evaluate the empirical constants have been obtained from selective HP-HT Fann-70 viscometer measurements.

The models often used to describe the behaviour of the two fluids are Bingham Plastic<sup>17</sup>, Power Law<sup>18</sup> and Herschel Bulkley models<sup>19</sup>. However, in this study the WBM and OBM rheological data are best described by the Herschel Bulkley model.

The main difference between OBM and WBM are the effects of pressure, which are more pronounced for OBM than WBM. For WBM the effect of pressure is very small, but is highly affected by an increase in temperature.

Temperature and pressure affects behaviour and interactions of water or oil, clay, polymers and solids in mud. The effect of increasing the temperature of a liquid is to reduce the cohesive forces while simultaneously increasing the rate of molecular interchange. The former effect tends to cause a decrease of shear stress, while the latter causes it to increase. The net result is that liquids show a reduction in viscosity with increasing temperature.

The effect of increased pressure on OBM is to increase the cohesive forces, which tends to increase the viscosity.

**Drilling Fluid Filtration.** One of the major functions of a drilling fluid is the control of formation pressure. In order to prevent formation fluids from flowing into the borehole, the hydrostatic pressure of the mud column is usually made to exceed the formation pressure.

Wellbore differential pressure can cause excessive loss of liquid and associated drilling mud solids leading to potential permeability impairment of the formation, and contribute to borehole instability<sup>20,21</sup> and formation damage<sup>22</sup>, especially in the HP-HT environment. The differential pressure depends on mud weight, fluid rheology and formation pressure.

As a result of overbalance pressure, the filter cake may form on sand face, through which only filtrate can pass, depending on the relationship between mud particle size distribution and formation pore size.

The process of drilling a well results in alternating periods, of varying duration, of dynamic and static filtration (sequential filtration).

Dynamic filtration occurs when the mud is circulated; the cake thickness is the difference between the rate of deposition by filtration and the rate of erosion by circulating mud. The erosion rate of particles is proportional to the shear stress exerted by the circulating mud on the cake surface<sup>23</sup>.

Static filtration occurs when the mud is not circulated, and the cake thickness increases as filtration continues.

The existing static and dynamic filtration<sup>23,24</sup> equations can be modified for downhole pressure and temperature conditions.

(i). Static filtration:

Two prediction models have been developed for WBM and OBM. The models follow the general format:

$$t = Y_1 V + Y_2 V^2 \exp. (AP + BT) \quad (2)$$

Where t is time and V the volume of filtrate. The difference between the models is in respect of the empirical constants ( $Y_1$ ,  $Y_2$ , A and B).

(ii). Dynamic filtration:



Two prediction models have been developed for WBM and OBM. The models follow the general format:

$$t = X_1 V - X_2 (1 - e^{-X_3 V}) \exp. (AP + BT) \quad (3)$$

Equation (3) also can be used to predict dynamic from static filtration data. Since the modified filtration Equations (2) and (3) can predict the filtration coefficients ( $Y_1$ ,  $Y_2$ ,  $X_1$ ,  $X_2$  and  $X_3$ ) therefore the filter cake characteristics such as cake resistance, permeability, porosity, etc. can be computed.

**Filtration Pressure Drops.** At the start of filtration, the pressure drop,  $\Delta P_T$ , is across the sand face, but as the filter cake builds up more of the pressure drop is dissipated across the filter cake,  $\Delta P_C$ , and less across the sand face,  $\Delta P_f$ , thus.

$$\Delta P_T = \Delta P_f + \Delta P_C \quad (4)$$

**Damage from Drilling Fluid.** Formation damage mechanisms have been studied extensively<sup>25, 26</sup>. However, formation damage from drilling fluid can be characterised by the following factors: thickness of filter cake, depth of solids and filtrate invasion and permeability reduction.

The two main damaging mechanisms which have been studied, are particulate invasion during initial filtration period, and filtrate invasion through filter cake.

*A. Filter Cake Build up.* Filter cake thickness is given by:

$$\frac{dh_c}{dt} = \frac{\rho_f s V - K_r \tau}{(1 - ms)} \quad (5)$$

The shear stress should be calculated from rheological behaviour of the mud Equation (1).

If the mud is not circulated then the shear stress  $\tau$  is zero and the filter cake becomes thicker as static filtration continues.

*B. Depth of Solids Invasion.* Solids invasion occurs during initial filtration period. It is primarily a function of mud particle size distribution and the pore throat diameter of the formation. Semi-empirical equations have been developed for predicting the depth of solids invasion. These models are based on pressure drop in pipes and therefore involve the rheological behaviour of the drilling fluid.

For Herschel Bulkley and Power Law fluids the model has been computed as:

$$L_s = \frac{C_1 \Delta P_f D_p^{(1+n)}}{K V_p^n (C_2 \frac{3n+1}{n})^n} \quad (6)$$

For Bingham Plastic fluid the equation is:

$$L_s = C_3 \Delta P_f \frac{D_p^2}{(C_4 \mu_p V_p + C_5 \tau_y D_p)} \quad (7)$$

These equations assume that the rheological properties of the fluid move through the pore are the same as that of the bulk fluid. This assumption becomes increasingly invalid as the pore throat diameter decreases and mud components that affect the viscosity are screened out. In the limiting case, the viscosity is that of the filtrate.

As it can be observed from the above models, the depth of solids invasion requires the knowledge of the formation morphological characteristics such as permeability, porosity, tortuosity etc.

Tortuosity ( $\eta$ ) is the actual flow path and can be computed in laboratory from formation resistivity factor ( $F_R$ ) and porosity thus:

$$F_R = a / \phi^b \quad (8)$$

$$\eta = \phi F_R \quad (9)$$

Then the mean pore throat diameter can then be calculated as:

$$D_p = 4.08 (\eta K / \phi)^{0.5} \quad (10)$$



**C. Depth of Filtrate Invasion.** The radius of filtrate invasion can be determined from filtration volume as:

i. Invasion in static condition:

$$r_f = \sqrt{r_w^2 + \frac{2r_w}{\phi} \left( \frac{-Y_1 t}{2Y_2} + \frac{(Y_1^2 + 4Y_2 t)^{1.5}}{12Y_2} - \frac{Y_1^3}{12Y_2} \right)} \quad (11)$$

ii. Invasion in dynamic condition:

$$r_f = \sqrt{r_w^2 + \frac{2r_w t(1-ms)K_f \tau}{\phi \rho_f s}} \quad (12)$$

All the parameters in equation (11&12) can be computed from sequential filtration experiments and Equations (2&3).

**D. Permeability Damage.** The initial formation permeability damaged in the zone occupied by particulate and filtrate is characterised by permeability reduction (damage) as a function of core length or distance from the wellbore in radial well flow conditions. The permeability damage factor can be described as:

$$C_F = k_d / k_f \quad (13)$$

The permeability alteration ( $k_d$ ) can be computed from the knowledge of overall average permeability and total depth of invasion.

### Productivity Evaluation

Well performance is reduced when near-wellbore formation is damaged. Key parameters in quantifying the formation damage or the reduction of the well productivity will be the skin factor or by the flow efficiency.

The skin factor  $s_d$ , defined as:

$$s_d = (1 - k_f / k_d) \ln (r_w / r_f) \quad (14)$$

Using a well productivity index (PI) usually represents well performance. Therefore, well flow efficiency due to near wellbore damage can be calculated as:

$$FE = PI_{\text{actual}} / PI_{\text{ideal}} \quad (15)$$

Then the damage factor can be computed from the reciprocal of the well flow efficiency.

$$DF = 1 / FE \quad (16)$$

### Productivity Tool Structure

In order to simulate the impact of drilling fluid filtration on well performance in terms of formation damage, a computer package with the models developed above is required. The structure of calculation is described as follows:

1. Input the data required for the models: wellbore parameters (hole geometry, casing size, etc), operating parameters (overbalance pressure, pump rate, etc), drill-in fluid parameters (mud type, rheology, etc) and formation parameters (permeability, porosity, etc).
2. Compute the rheological behaviour at standard conditions and depth of interest.
3. Compute the rheological parameters and calculate the wellbore pressure distribution.
4. Compute the static and dynamic filtration and calculate filter cake properties.
5. Calculate the pressure drop across filter cake and sand face.
6. Quantify level of resultant damage by computing depth of solids and filtrate invasion, average permeability and permeability damage.
7. Evaluate the results of well performance by computing skin factor, ideal and actual productivity index, flow efficiency and damage factor.

Figure 1 shows a flow chart on which the productivity tool has been developed.

### Application of the Productivity Tool

Specific case studies to illustrate the interpretation and practical usefulness of the productivity tool have been carried out using actual field data. The data are collected from four oil companies in North Africa [Table 1] and can be summarised as follows:

1. Seven wells with the total well depth ranging from 10045 ft to 14580 ft.
2. Reservoir sections drilled in 5.87, 6 and 8.50 inch holes.
3. Open hole and cased hole completions.

4. Wellbore pressure ranging from 5000 psi to 12800 psi.
5. Bottom hole temperature ranging from 240 °F to 330 °F.
6. Reservoir permeability ranging from 50 md to 400 md.
7. Oil based and water based drill-in fluids.

The application of the productivity tool has been used in two ways:

1. Evaluation Stage: The PRT simulated results have been evaluated against field data (post drilling):
  - a) Predicted total wellbore pressure distribution versus field data (pump pressure).
  - b) Predicted well performance in terms of formation damage against field measurements (depth of invasion from logging and skin factor from well test data).
2. Planning stage: The PRT has been used for fluid optimisation and selection against different operating parameters such as fluid type, rheology, pressure, etc.

**Evaluation Stage.** Table 2 illustrates the predicted total wellbore pressure distribution versus field data (pump pressure). The prediction shows agreement with field data.

Table 3 shows predicted (depth of invasion and skin factor) against field measurements. The field measurement from well test data gives the total skin and the PRT predicts the drilling skin. However, stochastic analyses have been carried out based on standard assumptions to calculate both the partial completion skin and perforation skin and add them to the drilling skin predicted from the PRT, in order to enable comparison with field test data Table 4 shows agreement between the PRT predicted skin and field measurement.

**Planning Stage.** The input data are from well number (A1) for a 6 inch hole section and the assumption was made to select the best HP-HT drilling fluid to drill this well with minimum formation damage. The fluid rheology and mud composition data for these types of mud have been used from field data of six wells drilled by various oil companies.

Figures 2 to 8 illustrate the effects of different parameters such as rheological behaviour, drilling time, temperature and overbalance pressure on flow efficiency comparing different types of WBM and OBM drill-in fluids.

Three different rheological properties for both OBM and WBM have been used for fluid selection of this particular well (A1).

#### Optimisation Process:

**Effect of Rheological Parameters.** Figures 2 & 3 show that an increase in rheological parameters (yield stress and consistency index) results in an increase in depth of filtrate invasion and hence an increase in damage factor.

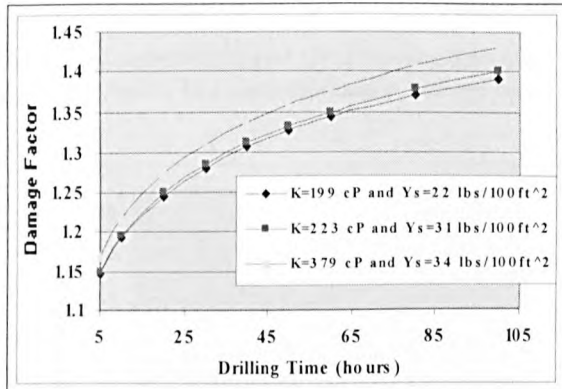


Figure 2 Effect of Rheology on Formation Damage for OBM

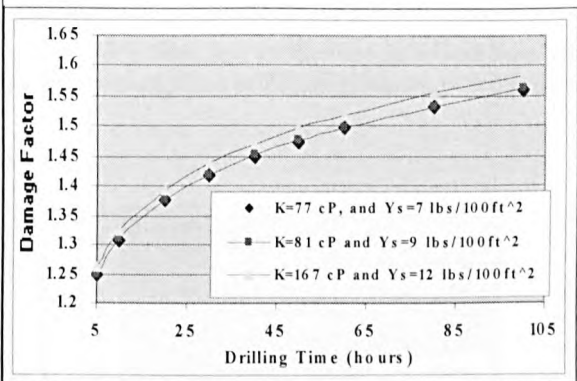


Figure 3 Effect of Rheology on Formation Damage for WBM

**Effect of Rheological Characterisation.** Figure 4 shows the depth of invasion profile for WBM and OBM. The figure also shows the accurate description of the rheological behaviour of the drill-in fluid required to accurately predict the depth of invasion.

Figure 4 illustrates effect of rheological behaviour on formation damage characterisation. A comparison has been made between the actual fluid rheological behaviour models, i.e. Herschel-Bulkley, Power Law and Bingham Plastic models. The figure shows that the Bingham model predicts higher formation damage than the actual model. The Herschel-Bulkley model best represents actual fluid rheology. The depth of invasion was found to be greater for WBM than OBM. Figure 5 shows damage profile using OBM.

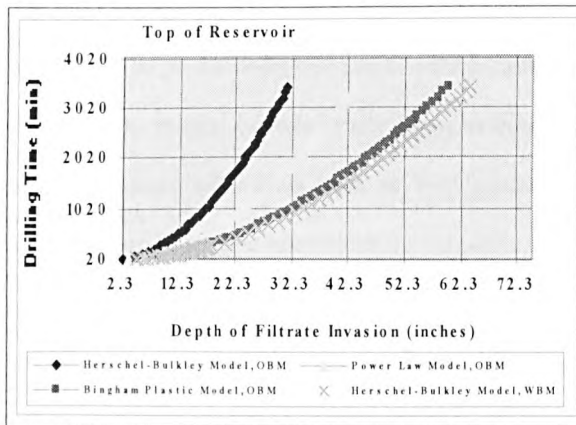


Figure 4 Effect of Rheology Characterisation on Depth of Invasion

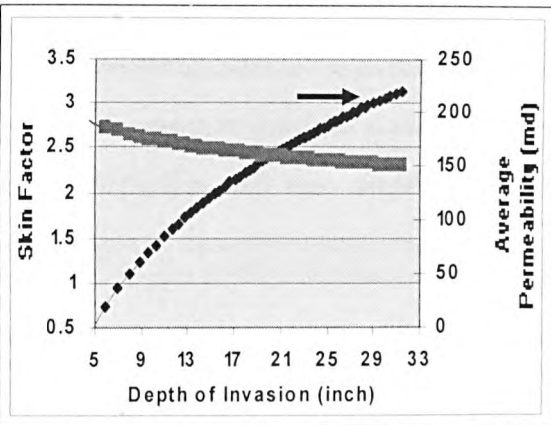


Figure 5 Damage Profile using OBM

**Effect of Drilling Time.** Figure 6 shows an increase in drilling operational time results in an increase in depth of filtrate invasion and hence an increase in damage factor, which is greater for WBM than OBM.

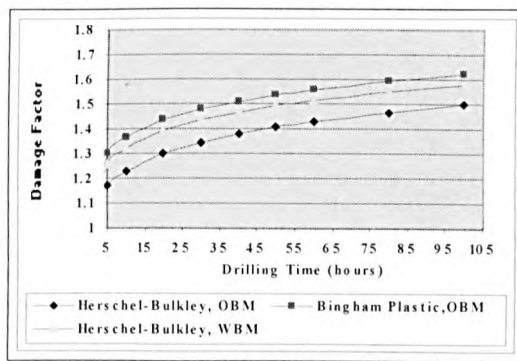


Figure 6 Effect of Drilling Time

**Effect of Wellbore Temperature and Overbalance Pressure.** Figures 7 & 8 show that an increase in bottom hole temperature and overbalance pressure results in a sharp increase in damage factor due to increased depth of filtrate invasion, which is greater for WBM than OBM.

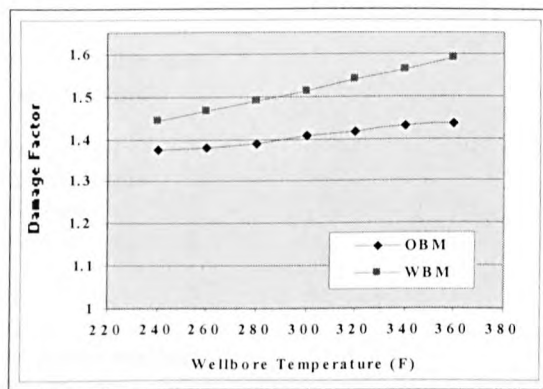


Figure 7 Effect of Wellbore Temperature

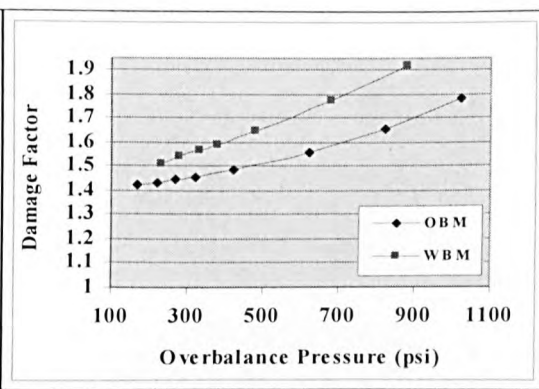


Figure 8 Effect of Overbalance Pressure

Based on the productivity tool simulated analysis, the selection of OBM with rheological parameters [ $n = 0.66$ ,  $K = 199$  cP and  $Y_s = 22$  lb/100ft<sup>2</sup>] to drill this particular well (A1) gives more advantages for well flow performance than for WBM. However, it is necessary during the fluid design stage to screen different HP-HT fluids also based on a higher percentage of the return permeability test. This is because the depth of invasion is may inversely proportional with percentage of the return permeability test<sup>27</sup>.

## Conclusions

The field application of the productivity tool is presented to simulate impact of drilling fluid filtration on formation productivity in an HP-HT environment. The productivity tool can be used for predicting formation damage mechanisms caused by particulate and filtrate invasion.

The tool can evaluate formation damage in laboratory as linear-flow core tests and can be converted to radial-flow scale for oil field applications.

Input requirements include parameters such as hole geometry, BHA configuration, mud type, composition, rheology data and formation characteristics.

The productivity tool can be used to investigate the influence of many parameters on the well flow performance.

The tool can be used before drilling as design (planning tool), during drilling and post drilling as evaluation and comparison tool with well test data interpretation.

The productivity tool is capable of being utilised to screen different HP-HT drilling fluids desired for achieving minimum impairment and maximum production capacity, two key functions which are relevant to optimum fluid selection and management, in addition to well test data interpretation.

## Nomenclature

a, b = coefficients

A, B = pressure and temperature coefficients

$A_c$  = constant

C1, C2, C3, C4, C5 = constants

$C_F$  = permeability reduction factor

DF = damage factor

$D_p$  = mean pore throat diameter

$dh_c$  = filter cake thickness

FE = flow efficiency

$F_R$  = resistivity formation factor

k = consistency index

$k_\tau$  = erodability coefficient

$k_f$  = formation permeability

$k_d$  = permeability damage

$L_s$  = depth of solids invasion

m = ratio of wet to dry cake

n = Power law index

P = applied pressure

$PI_{actual}$  = productivity index after formation damage

$PI_{ideal}$  = productivity index before formation damage

$\Delta P_T$  = total differential pressure

$\Delta P_f$  = pressure across formation

$\Delta P_c$  = pressure across filter cake

$r_f$  = radius of filtrate invasion

$r_w$  = wellbore radius

s = solids concentration

$s_c$  = partial completion skin

$s_d$  = drilling skin factor

$s_p$  = perforation skin

t = time

T = temperature

V = filtrate volume

$V_p$  = velocity in porous medium

$Y_1, Y_2, X_1, X_2, X_3$  = filtration coefficients

$Y_s$  = yield stress

## Greek Symbols

$\eta$  = tortuosity

$\mu_p$  = plastic viscosity

$\tau_y$  = yield point

$\tau_s$  = shear stress at standard condition

$\tau_i$  = shear stress at depth of interest



$\phi$  = porosity of formation  
 $\rho_f$  = density of filtrate

### Acronyms

BHA = bottom hole assembly  
BHT = bottom hole temperature  
Cl/Cls = lignosulphonate mud  
KCl = potassium chloride mud  
PWBM = dispersed polymer mud  
LP-LT = low pressure-low temperature  
HP-HT = high pressure-high temperature  
OBM = oil based mud  
md = millidarcy  
TVD = total vertical depth  
WBM = water based mud

### References

1. Michael J. Economides, A. Daniel Hill, and Christine Ehlig- Economides: "Petroleum Production systems", 1994.
2. Krueger, R. F.: "An Overview of Formation Damage and Well Productivity in Oilfield Operation", JPT, Feb., 1986, pp. 131-152.
3. Dearing, H. L. and Ali, S. A.: "Drill-in fluid Selection Crucial To Well Productivity", Petroleum Engineer International, Jan. 1996, 21-25.
4. Van Everdingen, A. F., and Hurst, W., "The Application of the Laplace Transformation to Flow Problems in Reservoirs", TRANS. AIME, 186:305-324, 1949.
5. Fraser, L. J., Ried, P., Williamson, D., and Enriquez, F.: "Mechanistic Investigation of the Formation Damaging Characteristics of Mixed Metal Hydroxide Drill-In Fluids and Comparison with Polymer-Base Fluids", SPE 30501 Presented at the SPE Annual Technical Conference and Exhibition held in Dallas, U.S.A., October 22-25, 1995.
6. Davison, J.M., Jones, M., Shuchart, C. E., and Gerard, C.: "Oil-Based Muds Reservoir: their Performance and Cleanup Characteristics", SPE 58798 Presented at the 2000 SPE International Symposium on Formation Damage Held in Lafayette, Louisiana, 23-24 Feb. 2000.
7. Liu, X. and Civan, F.: "Formation Damage and Skin Factor Due Filter Cake Formation and Fines Migration in the Near-wellbore Region", SPE 27364 presented at the SPE Int. Symposium on Formation Damage Control, Lafayette, LA, Feb. 9-10, 1994.
8. Scott Lane, H.: "Numerical Simulation of Mud Filtrate Invasion and Dissipation", SPWLA 34<sup>th</sup> Annual Logging Symposium, June 13-16, 1993.
9. Semmelbeck, M.E., Dewan, J.T. and Holditch, S.A.: "Invasion Based Method Estimating Permeability from Logs", SPE 30581 presented at the SPE ATC&E, Dallas 22-25 Oct. 1995.
10. Permadi, P. and Wibowo, W.: "Effects of Non-uniform Skin Distribution on Horizontal Well Inflow Performance", SPE 68952 presented at the SPE European Formation Damage Conf. The Hague, The Netherlands, 21-22 May 2001.
11. Menour, H., Al-Majed, A. and Hassan, S.: "Effect of Formation Damage, Length and Reservoir Thickness on the inflow Performance of Horizontal Wells", SPE 59356 presented at the 2000 SPE/DOE Improved Oil Recovery Symp. Tulsa OK, 3-5 April 2000.
12. M. B. Amish and M. B. Oyeneyin (The Robert Gordon University) and M. H. Hodder (M-I L.L.C.): "Characterisation of Drilling Fluid Filtration under Downhole Conditions", in Progress.
13. M. B. Amish and M. B. Oyeneyin (The Robert Gordon University) and M. H. Hodder (M-I L.L.C.): "Characterisation Mechanisms of Formation Damage", in Progress.
14. Politte, M. D.: "Invert Oil Mud Rheology as a Function of Temperature and Pressure", SPE/IADC 13458, New Orleans, U.S.A., 1985.
15. Houwen, O. H., and Geehan, T.: "Rheology of Oil-Base Muds", SPE 15416, New Orleans, U.S.A., 1986.
16. API Bulletin 13B: Recommended Practice on the Rheology and Hydraulics of Oil-Well Drilling Fluids, API BUL 13D, Third Edition, June 1, 1995.
17. Bingham, E. C.: "Fluidity and Plasticity", McGraw-Hill Book Co., New York, 1922.
18. Govier, G. W. and Aziz, K.: "The Flow of Complex Mixtures in Pipes", Van Nostrand Reinhold, New York, 1972.
19. Herschel, W. H. and Bulkley, R.: "Measurement of Consistency as Applied to Rubber-Benzene Solutions", Proceedings of the American Society of Testing Materials, Vol. 26, 1926, pp 621-633.
20. Chenevert, M.E.: "Shale Control with Balanced-Activity Oil Continuous Muds", JPT, Oct 1970. pp. 1309.
21. Bushnell, Y.M. and Panesar, S. S.: "Differential Sticking Laboratory Tests can Improve Mud Design", SPE 22549 Presented at the 66<sup>th</sup> Annual Technical Conference and Exhibition of the SPE, Dallas, TX, Oct. 6-9, 1991.
22. Ali Ghalambor and M. J. Economides: "Formation Damage Abatement: A Quarter-Century Perspective", SPE no. 58744, Feb. 2000.
23. Shuang Jiu Peng, and Peden, J. M.: "Prediction of Filtration Under Dynamic Conditions", SPE 23824 Presented at the SPE Ind. Symposium on Formation Damage Control held in Lafayette, Louisiana, February 26-27, 1992.
24. Arthur, K. G. and Peden, J. M.: "The Evaluation of Drilling Fluid Filter Cake Properties and Their Influence on Fluid Loss", SPE 17617, 1988.
25. Yan Bingo, M. B. Oyeneyin, and J. M. Peden: "Investigation of Pore Blocking Mechanism in Gravel Packs in the Management and Control of Fines Migration", SPE 27342, 1994.
26. Oyeneyin, M. B., Peden, J. M., Ali Hosseini, and Ren, G.: "Factors to Consider in The Effective Management and Control of Fines in High Permeability Sands", SPE 30112, 1995.

27. M. B. Amish "A Productivity Tool for Impact of Filtration on Well Performance in an HP-HT", in progress.

Table 2 Predicted pump pressure versus field data (pump pressure)  
Pump Pressure (psi)

Well Number	Total Depth (ft)	Hole Section (inch)	BHTemp (°F)	Field Data (Psi)	PRT Prediction (Psi)
A1	13790	8.50	315	2575	2466
	14580	6	330	1780	1670
A2	14500	6	322	1700	1695
B1	13528	5.875	320	2000	2032
	12175	8.50	305	2600	2820
B2	13390	5.875	314	2000	2083
	12245	5.875	280	1500	1566
C1	12370	8.50	290	2850	3000
D1	10045	8.50	240	1950	2092

Table 3 Formation damage predicted against field measurement

Well No.	TVD (ft)	Hole (inch)	BHT (°F)	Depth of Invasion (inches)		Skin	
				Field Data	PRT Prediction	Field Data Total skin	PRT Prediction Drilling skin
A1	14580	6	330	40	34.79	9.00	4.11
A2	14500	6	322	60	77.73	12.0	5.24
B1	13528	5.875	320	60	45.43	10.0	4.00
B2	13390	5.875	314	70	92.73	10.0	5.87
B3	12245	5.875	280	70	90.81	10.0	5.63
C1	12370	8.50	290	60	77.63	9.00	4.48
D1	10045	8.50	240	40	48.69	8.00	3.62

Table 4 Formation damage predicted against field measurement

Well No.	TVD	Mud Type	Field data	PRT prediction		
			Total Skin	Sd	Sc + Sp	Total Skin
A1	14580	OBM	9.00	4.11	3.10	7.21
A2	14500	WBM	12.00	5.24	3.32	8.56
C1	12370	WBM	9.00	4.48	2.84	7.32
D1	10045	WBM	8.00	3.62	2.61	6.23

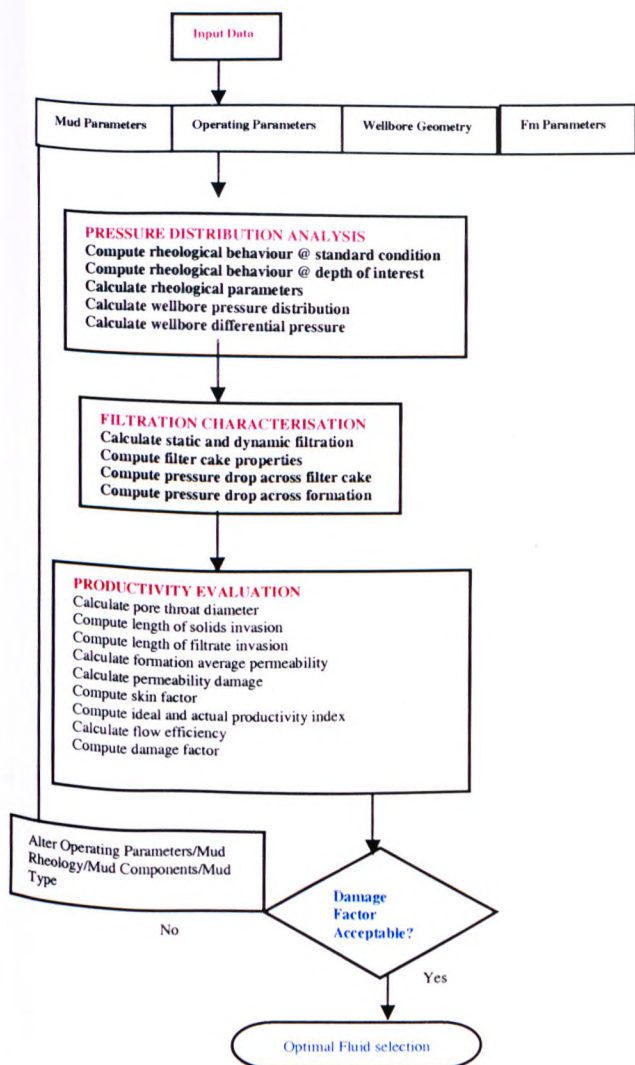


Figure 1 Flow chart

Table 1 Well summary

Co.	Field	Well No.	TVD (ft)	Temp. (°F)	Fluid Type	Hole Section (inch)
1	A	A1	14580	330	OBM	8.50&6
		A2	14500	322	WBM	6
2	B	B1	13528	320	OBM	5.875
		B2	13390	314	WBM	8.50&5.875
3	C	B3	12245	280	WBM	5.875
		C1	12370	290	WBM	8.50
4	D	D1	10045	240	WBM	8.50